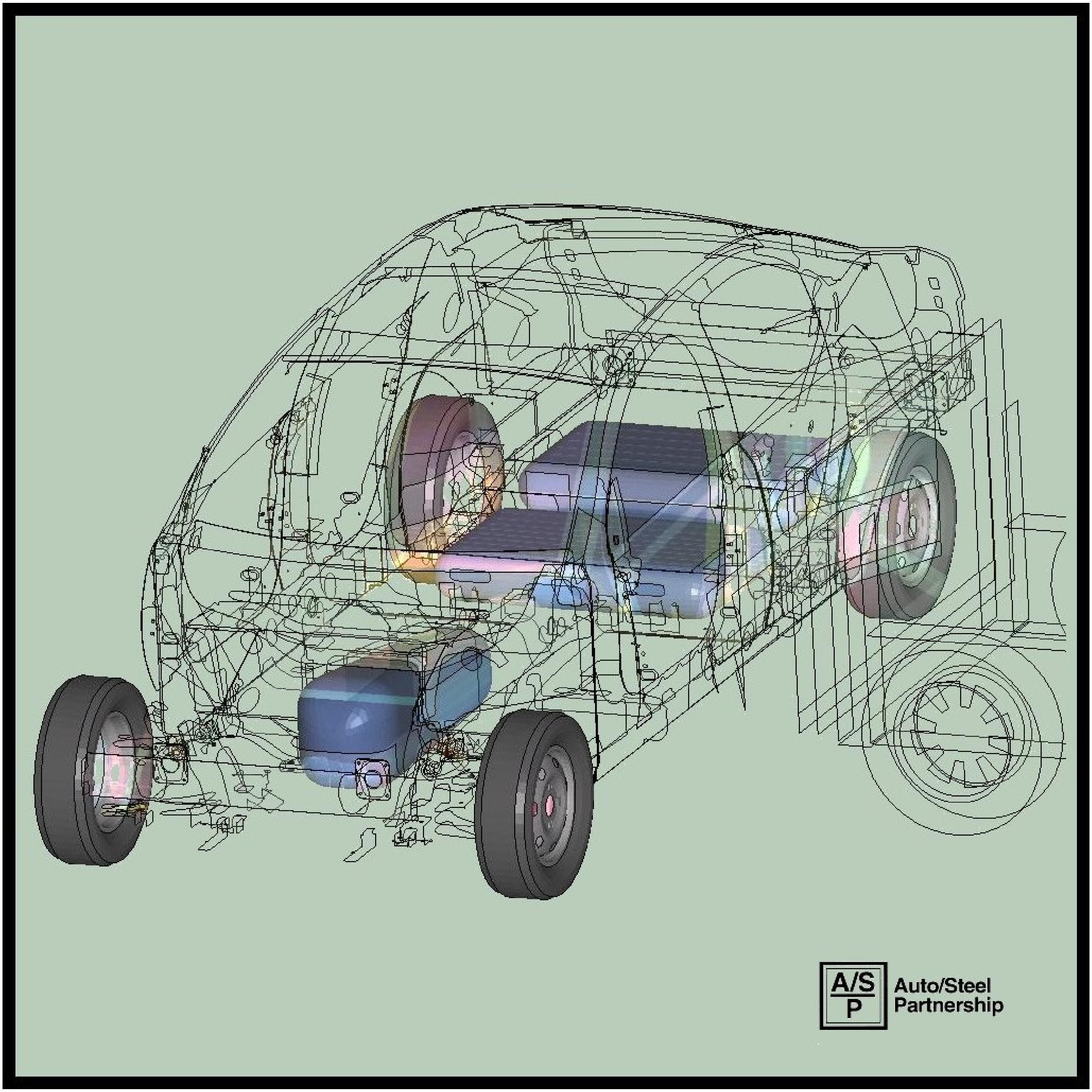

Future Generation Passenger Compartment Phase I Report - Executive Summary

Mass optimization & Fuel Cell packaging study

FGPC Executive Summary

Table of Contents

Future Generation Passenger Compartment (FGPC)

EXECUTIVE SUMMARY

The highlights from the FGPC (Future Generation Passenger Compartment) project are presented in this summary. A detail discussion of each task may be found in its individual report.

1. INTRODUCTION

Initially FGPC was divided into nine tasks but upon request from A/SP Tasks 2.5, 5.5 and 7.5 were added to the project. An individual report is provided for each task, which includes its own appendices.

2. PROJECT BACKGROUND

Various studies conducted by the automotive OEMs (Original Equipment Manufacturers), AISI (American Iron & Steel Institute), IISI (International Iron & Steel Institute) and A/SP (Auto/Steel Partnership) have clearly demonstrated that AHSS (Advanced High Strength Steel) can be effectively utilized in automotive lightweighting, or mass avoidance strategies, to provide the required performance at a lower overall cost. New methodologies and designs must be developed to achieve equal or improved functionality and performance when compared to traditional design, while simultaneously ensuring cost effective manufacturability of the appropriate automotive systems.

Choices pertaining to design, manufacturing and materials are closely related. However, a thorough understanding and documentation of such choices and consequences does not exist today. Addressing this issue, along with bridging other technological "gaps", is a prerequisite for enabling the use of steel in lightweighting automotive structures. Recent technologies anticipate multifunctional and multidisciplinary systems that can use the current and future AHSS in combination with an innovative optimized design.

The USAMP and A/SP strategy for the FGPC program is to propose a new passenger compartment and underbody that can provide the OEMs with an example of AHSS usage in combination with a highly optimized design.

3. PROJECT STRATEGY & FUTURE OPPORTUNITIES FOR NEW DEVELOPMENT

The strategy for Phase I of the FGPC project was to develop a robust design that considered two differing perspectives, near-term or 5-year and long-term or 15-year. Near-term is defined as the knowledge gained from FGPC Phase I used in combination with technology that could be applied to a present vehicle with minor modification. Issues relating to manufacturing, joining and material selection are considered within reach. FGPC Phase II will apply the knowledge gained in Phase I to a donor vehicle selected by USAMP and A/SP.

Near-term material selection was driven by grade/gauge availability and by manufacturing capability. Although these considerations did include an appropriate amount of stretch, it is difficult to apply the specifics of these enabling technology requirements on a design concept. However implementation will be addressed in the FGPC Phase II, the validation phase.

The long-term perspective considers issues such as manufacturing components from materials that are not presently available or in gauges that current design practice would not view as practical. Hence the steel industry will require further research to meet these challenges. For example, though currently unavailable, the optimization indicated that there would be an opportunity to use a 1550MPa grade steel as a Class A surface. There are many approaches that may achieve this outcome such as an exposed hot stamp boron.

The long-term outlook also revised the underbody design to package both traditional diesel and fuel cell powertrains. The diesel option was a conventional front wheel drive configuration. The second option considered packaging a fuel cell and its fuel tanks. Design guidelines were developed for the major components of a fuel cell vehicle, including hydrogen storage tanks, batteries, fuel cell stack and electric drive, to meet established crashworthiness performance criteria.

Using the ULSAB-AVC BIW (Body-In-White) as a baseline model, the FGPC objective was to modify the BIW to accommodate both diesel and fuel cell powertrains and to reduce the BIW mass while still meeting the requirements of the new IIHS Side Impact and Roof Crush regulations.

Strategy:

1. Efficient use of geometry to define the loadpath that meets crashworthiness and stiffness requirements, while absorbing energy through total system topology optimization.
2. Investigate the usage of AHSS materials and manufacturing techniques, such as tailor-welded blanks, to reduce vehicle mass and increase its performance.
3. Reduce the vehicle mass by using topology and shape optimization.

4. RELATIVE MATERIAL COSTS

In order to discourage the use of higher strength steel in parts where it is not required, a cost function was setup to estimate the relative cost of different design configurations. The cost factors defined in Table 1 were used to calculate the relative cost of each design. The cost of each part was calculated by multiplying the mass of the part with the normalized cost factor for the material considered.

MATERIAL NAME	Relative Cost
IF 140/270	1.0
DQSK 210/340	1.104
BH 250/550	1.13
DP 300/500	1.169
HSLA 350/450	1.1948
DP 350/600	1.39
DP 500/800	1.506
Boron 1550	1.805
DP 700/1000	1.584
Mart 1300	1.688

TABLE 1: Relative Material Costs

5. FGPC STRUCTURE, MATERIAL INDEPENDENCY

The strategy implemented by this project concentrated primarily upon multi-disciplinary loadpath optimization, which addressed all the crashworthiness, stiffness and NVH loadcases under consideration. Once the most efficient loadpaths were defined, the second optimization was then allowed to review the gauge and material of each individual component. Thus when considering another material such as composite, aluminum or multi-material vehicle, the knowledge and technology developed by the load path optimization in this project is still valid. However, the FGPC project has demonstrated, the geometry, gauge and the impact of manufacturing, joining and assembly must be considered for each material proposal.

6. FGPC & FUEL CELL OPPORTUNITIES

As part of the long-term perspective of the FGPC project, the vehicle underbody was redesigned to be capable of accommodating both diesel and fuel cell powertrains. As part of Phase I, the Task 2.0: Calibration Baseline evaluated the IIHS Side Impact performance of both diesel and fuel cell powertrains. Although both configurations did not satisfy the IIHS Side Impact target, the fuel cell did provide improved performance over the diesel. This was because fuel cell components provided structural loadpaths during the crash event that improved its performance. Consequently, the remainder of the design optimization focused on the diesel powertrain as the worst-case scenario, with the confidence that the final optimized design could be easily adapted to provide equivalent performance for the fuel cell.

7. **PARTNERSHIP**

This project was managed and executed by ETA with the partnership of EDAG Engineering and Red Cedar Technology.

8. SOFTWARE/HARDWARE

Software:

eta/VPG – FEA Pre/post-processor
eta/DYNAFORM – Metal Forming pre/post-processor
LS/DYNA - Explicit FEA Solver for Crash and Safety Simulation
NASTRAN – Implicit FEA Solver for Linear Static and Modal Simulation
HEEDS – Optimization

Hardware:

16 - CPU Linux cluster
18 - CPU Single PC's interconnection process for Optimization
8 - CPU SGI Altix

9. LESSONS LEARNED

To provide feedback from the experience gained during the course of the FGPC project the following highlights the lessons learned by the FGPC team-members, ETA and its partners.

- B-pillar intrusion should be measured at various heights for the IIHS side impact because the deformation mode may change.
- A cross-member connecting the B-pillars gives the vehicle a robust side impact performance.
- The ideal height for the cross-member is at or slightly above the height of the IIHS side impact bumper.
- Large changes in vehicle curb weight do not significantly degrade the IIHS side impact performance.
- During shape optimization, care should be taken to assure that no connections are lost and that part penetration is minimized.
- Proper loadpaths should be established for the various loadcases before final optimization begins.
- When optimizing for a specific set of loadcases, it is important to consider what other loadcases may be affected because there may be some overlap.
- The optimization should consider as many loadcases as practically possible.
- Unless it is specifically required, for example to evaluate the consequences of styling constraints, the shape optimization should exclude the external A-surfaces of the vehicle and thus avoiding any changes to the styling.
- With respect to material and gauge choice, the initial optimization was free to produce a long-term solution. It was then possible to take the optimization results and produce either a short or long-term solution during the design phase.
- All possible constraints such as the material compatibility for joining need to be specified during the problem setup, so that the final optimized design is manufacturable.

10. CONCLUSION

The optimization methods applied to the FGPC project achieved an 11% mass reduction of the modified parts of the BIW and Door Impact Beams, see Table 2 and 30% mass savings over a conventional in-class vehicle's BIW and IP beam, see Table 3. Table 4 is a comparison of an industry standard vehicle's passenger compartment to FGPC-FCD, the final concept design, which shows a 31% mass reduction.

Based upon these results it is possible to conclude that if the FGPC design methodology is applied to a similar size vehicle a 30% mass reduction is feasible. Furthermore, the resulting design has been shown to be a robust solution that is insensitive to increases in the curb weight. Task 7.5 proved that under the IIHS Side Impact and Roof Crush loadcases, a 350kg increase in curb weight comfortably met the requirements of the test.

MODIFIED PARTS	BASELINE FGPC-BO (kg)	FINAL FGPC-FCD (kg)	MASS SAVINGS (kg)	CHANGE (%)
BIW	130.6	121.0	9.6	7
Doors	12.6	6.4	6.2	49
TOTAL	**143.2**	**127.4**	**15.8**	**11**

TABLE 2: Final Mass Summary For FGPC Project - Modified Parts Only

STRUCTURE	INDUSTRY STANDARD (kg)	FINAL FGPC-FCD (kg)	MASS SAVINGS (kg)	CHANGE (%)
BIW + IP BEAM	310.0	217.6	92.4	30

TABLE 3: Final Mass Summary For FGPC Project - Comparison To Industry Standard

STRUCTURE	INDUSTRY STANDARD (kg)	FINAL FGPC-FCD (kg)	MASS SAVINGS (kg)	CHANGE (%)
Passenger Compartment	246.8	169.3	77.5	31%

TABLE 4: Final Mass Summary For FGPC Project –Comparison To An Industry Standard Passenger Compartment

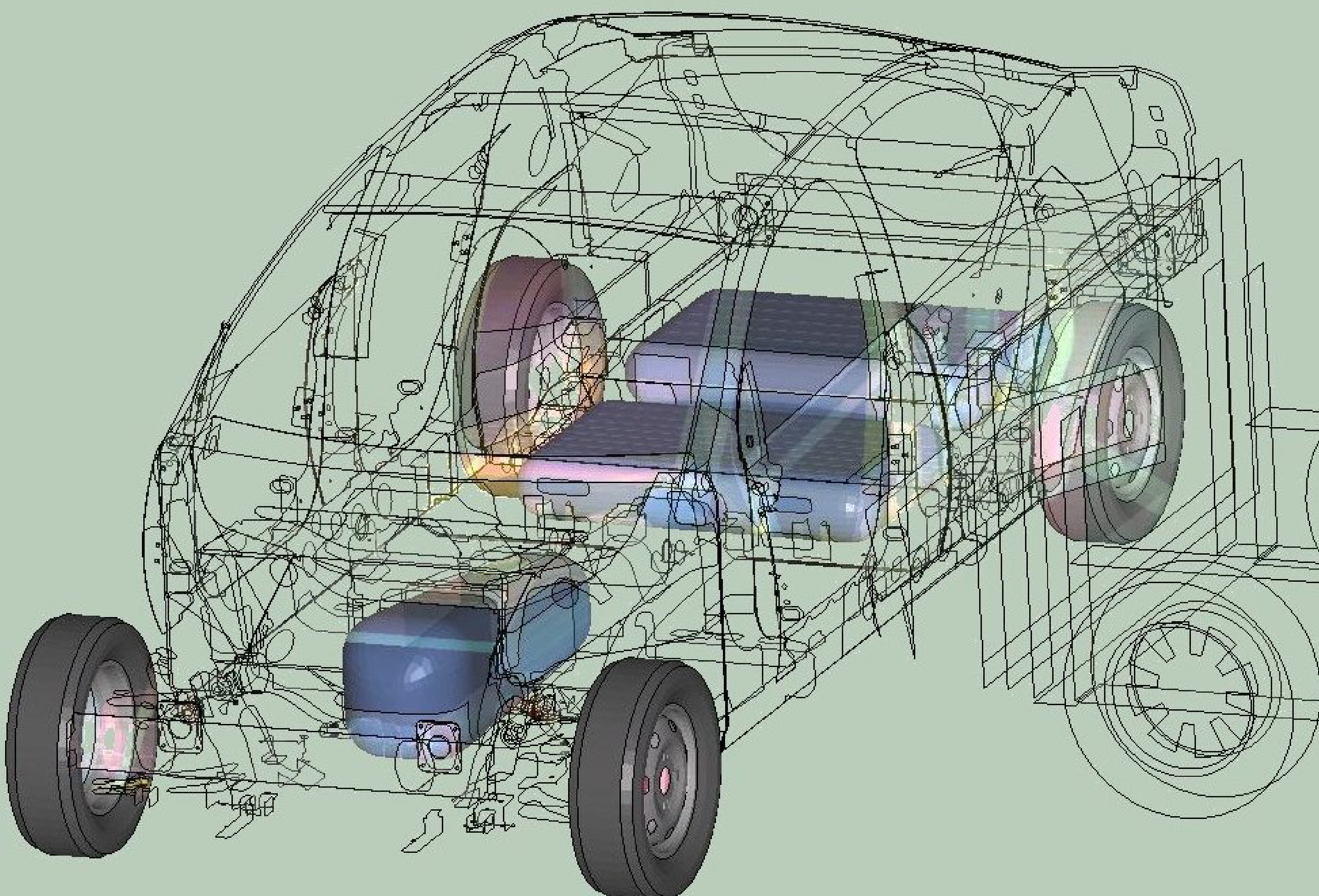

Auto/Steel Partnership

Future Generation Passenger Compartment Task 1.0 - Benchmarking Report

Benchmarking study to determine current vehicle crash/safety design practices & survey of fuel cell technology

Task 1.0 - Benchmarking

Table of Contents

Task 1.0 - Benchmarking

1. INTRODUCTION

This report completes Task 1.0: Benchmarking of the FGPC (Future Generation Passenger Compartment) project. Its purpose is to document the results of a benchmarking study used to determine current crashworthiness design practices and a literature survey used to facilitate an understanding of fuel cell technology.

2. OBJECTIVE

The study will be a benchmarking effort to develop and document integrated solutions that will balance the interaction of materials, manufacturing and performance cost effectively. This study focuses on solutions that will address high volume manufacturing and assembly considering a Dual Powertrain system (traditional diesel drive train and fuel cell).

The benchmarking part of this project is comprised of the following sections:

1. Visits of Project Team members to GM, Ford and DCX “Benchmarking Analysis Centers”
2. Brainstorming Session Summary
3. Appendices:
    a. Appendix 1: Report from Center of Automotive Research (CAR) based on visits to world wide OEM’s, such as Volvo, BMW, Honda, and Nissan
    b. Appendix 2: Fuel Cell Technology for FGPC, including published articles from Automotive Industries, Autotech Daily, Detroit Free Press and BMW Magazine

3. CONCLUSIONS AND GENERAL OBSERVATIONS

The goal of the benchmarking effort is to gather information that would identify the latest technology trends used by world wide OEM’s for crashworthiness in general and specifically IIHS side impact and rollover scenarios. This knowledge will then be used to enhance the design of the FGPC vehicle.

The strength or weakness of a particular design investigated during benchmarking is a relative statement and could only be graded if the design targets and their performance constraints were known. Therefore it is believed that each design has its own philosophy.

Design philosophy is defined as a target that designers would like to achieve for overall vehicle behavior and vehicle components behavior in different proving ground tests and attributes (front crash, side impact, rear crash). Of course the design philosophy or vehicle definition is based on target performance, development cost, vehicle rank, manufacturing, material, styling, etc. Definitions should be known so one can identify whether a particular design is within that design envelope or not. Since the design philosophy and constraints of the benchmarked vehicles are not known, it is not appropriate to judge a design as good or bad. Such a categorization is also not within the scope of this program.

The key question in the crash and safety environment of the auto industry is:

“How should the US, IIHS, ECE, NCAP, ARD and Japanese regulations be met within one vehicle system package with no major architectural changes in the packaging and tooling (to control cost and weight). “

At the same time the challenge to meet all safety issues, reduce the vehicle mass, and make the vehicle fuel efficient for current types of drivetrain and future vehicles with a Hydrogen Fuel Cell drivetrain should be recognized.

Most automakers and their key suppliers predict that hydrogen fuel cell technology would be able to demonstrate commercial feasibility and production validation by 2010, with vehicles ready for public sale by 2015.

OEM's worldwide are developing crash load paths using all available tools to meet FMVSS, ECE, IIHS and NCAP Front, Side and Rear crash requirements. Although crash load paths are similar on all vehicles, each manufacturer has their own strategies for managing the crash energy and load paths.

- For front impact, the trend is to more evenly distribute loads to improve passenger protection, and to be more crash-compatible with vehicles of differing ride heights using energy management and load path mechanisms.
- For side impact, controlling the B-pillar intrusion and deformation mode, by balancing the lower and upper regions of the body structure, is critical. Reinforced B-pillar, rocker, and roof structures are generally needed to meet performance targets.
- For rear crash, similar strategies as used in front impact are under development, using energy management and load path mechanisms within one system to meet all rear crash scenarios.

All benchmarked vehicles in this study have used all of the above techniques to meet the targets. However, some vehicles used layers of steel reinforcement to resist the loads.

It is predicted that in future vehicles, where there are more development strategy leads, the vehicle design will have a different approach to achieve these crash and safety goals.

Overall, it was observed that a few vehicles have incorporated a considerable amount of reinforcement within the body side in the rocker, A-pillar, B-pillar and roof rail sections. It is possible that the original architecture was not designed for some events and they had to reconfigure their design by adding reinforcement to meet the specific targets such as rollover and IIHS side impact.

Other design features that were found to be common in this benchmarking effort include the use of bulkheads, which are used for the prevention of local buckling, and a wider B-pillar section, which provides better resistance in side impact and rollover and better load transformation for vehicle dynamics, and also helps to stiffen the body in torsion. This could reduce the number of reinforcements that are used inside of the B-pillar (weight reduction using geometry). Styling could be an issue in this type of design.

A deep rocker section with multiple layer reinforcements are usually used because it will not allow the section to collapse in FMVSS 214 and ECE side impact, where the barrier hits the rocker section. The rocker is used for the load path for front crash as well.

The FGPC team also observed a deep section in the roof rail from A to C-pillars compared to the smaller section with multiple reinforcements that are used in many vehicles to address rollover, IIHS front and side impact issues.

If all these ideas are used properly, based on design philosophy, it can be called a smart design and if it is used out of its envelope it would be considered over designed.

In summary, for the FGPC project, the strategy to meet the objectives will be:

1. First, the use of geometry to design the load path to meet crashworthiness performance, while absorbing energy using total system topology optimization.
2. Secondly, investigate the usage of HSS materials and manufacturing techniques (e.g. tailor welded blank) that can reduce weight and increase performance.
3. Finally, optimize the mass of the components using topology and shape optimization to reduce weight.

In the design of vehicle components, beading will be used to improve local and overall stiffness and crash modes of body panels.

3.1. VISIT N. AMERICAN OEM'S – GM, FORD AND DCX

The following vehicles were evaluated at the three OEM teardown centers and are described in more detail in the following sections. For reference Table 1 summarizes the available NCAP and IIHS crash ratings.

Model Year	Model	NCAP Frontal		IIHS Frontal Offset	NCAP Side		IIHS Side	Rollover	Visit
		Driver	Passenger		Front	Rear			
2003	Toyota Camry	5	4	G	3	4	P	3	GM
2004	Toyota Prius	5	4	na	4	4	na	4	GM
2003	BMW 330i	4	5	G	3	5	na	4	GM
2004	Hyundai XG350	5	5	G	4	4	na	4	GM
2004	VW Touareg	4	4	na	5	5	na	na	GM
2005	Chrysler 300C	5	5	na	4	5	na	4	Ford
2005	Ford 500	5	5	na	5	5	na	4	Ford
2005	Honda Odyssey	5	5	G	5 *	5	na	4	Ford, DCX
2003	Honda Civic	5	5	G	4	4	na	4	DCX
2003	Honda Pilot	5	5	G	5	5	na	4	DCX
2003	Pontiac Montana	4	4	P	5	4	na	3	DCX
2004	Toyota Sienna	5	5	G	5	5	na	4	DCX

* Safety Concern: Driver door became unlatched and opened, increasing the likelihood of occupant ejection

Numbers in each column represent the number of stars for the rating, e.g. "4" is a 4-star crash rating
For IIHS tests, "G" represents the highest Good rating, and "P" represents the lowest Poor rating

TABLE 1: Available NCAP & IIHS Crash Ratings Summary

3.1.1. GM BENCHMARKING KNOWLEDGE CENTER VISIT

The Team visited the GM benchmarking Knowledge Center to observe the new technology that is used in design, manufacturing and material handling for the vehicles that were displayed at the time of this visit.

A total of twelve vehicles were torn down in different levels. The following are the report and feedback of the team after the visit. The goal was to point out the significant and important findings from each vehicle that stand out in regards to meeting FMVSS, IIHS and ECE performance regulations. From the original group of twelve vehicles, the following five were chosen to study in more detail, since they possess design features relative to this project.

1. 2003 Toyota Camry SE (North American Version)
2. 2004 Toyota Prius
3. 2003 BMW 330i
4. 2004 Hyundai XG350
5. 2004 VW Touareg Wagon

3.1.2. GENERAL OBSERVATIONS

- No Tailor Laser Welded Blanks were seen in BIW in above vehicles
- Some of the vehicles, such as the Hyundai XG350 and VW Touareg, have multiple layers of reinforcements, and apparently they are used for crash and safety issues such as rollover, IIHS front, side and rear crash
- Most of the vehicles had straight longitudinal load-carrying members
- The BMW 330i has a solid one-piece rear seat and solid tunnel and reinforcement, which is good for NVH, rear crash and vehicle torsional stiffness; has solid front seat reinforcements and inner reinforcement provides load path for side impact; and has solid steel MIG-welded hinge pillar that provides door attachment strength for door stop, door check and NVH
- The Toyota Camry has bulkheads inside the rocker to prevent local buckling and has deep solid seat cross-members to address side impact issues; and has a wide B-pillar and reinforcements for better performance on overall attributes
- The Hyundai has multiple side rail reinforcements to prevent local deformation for IIHS side impact and prevent rollover occupant injury; has double reinforcement in B-pillar and rocker sections for IIHS and FMVSS side impact
- The Toyota Prius has a wide roof bow to act as a load-carrying member for side impact
- The VW Touareg has a double rocker section with tubular section in the upper rocker to improve side impact underbody performance; has a large deep section roof side rail section to improve side impact and roof crush performance

FIGURE 1: 2003 BMW 330i

FIGURE 2: BMW 330 - Solid One Piece Rear Seat, No Holes In Seat Back, Solid Tunnel & Reinforcement (Good For NVH, Rear Crash & Vehicle Torsional Stiffness)

FIGURE 3: BMW 330i - Solid Front Seat Reinforcements & Inner-Reinforcement To B-Pillar & Tunnel (Load Path For Side Impact)

FIGURE 4: BMW 330i - Solid Steel, MIG Weld Hinge –Pillar (Door Attachment Strength For Door Drop, Door Check & NVH)

FIGURE 5: 2003 Toyota Camry SE

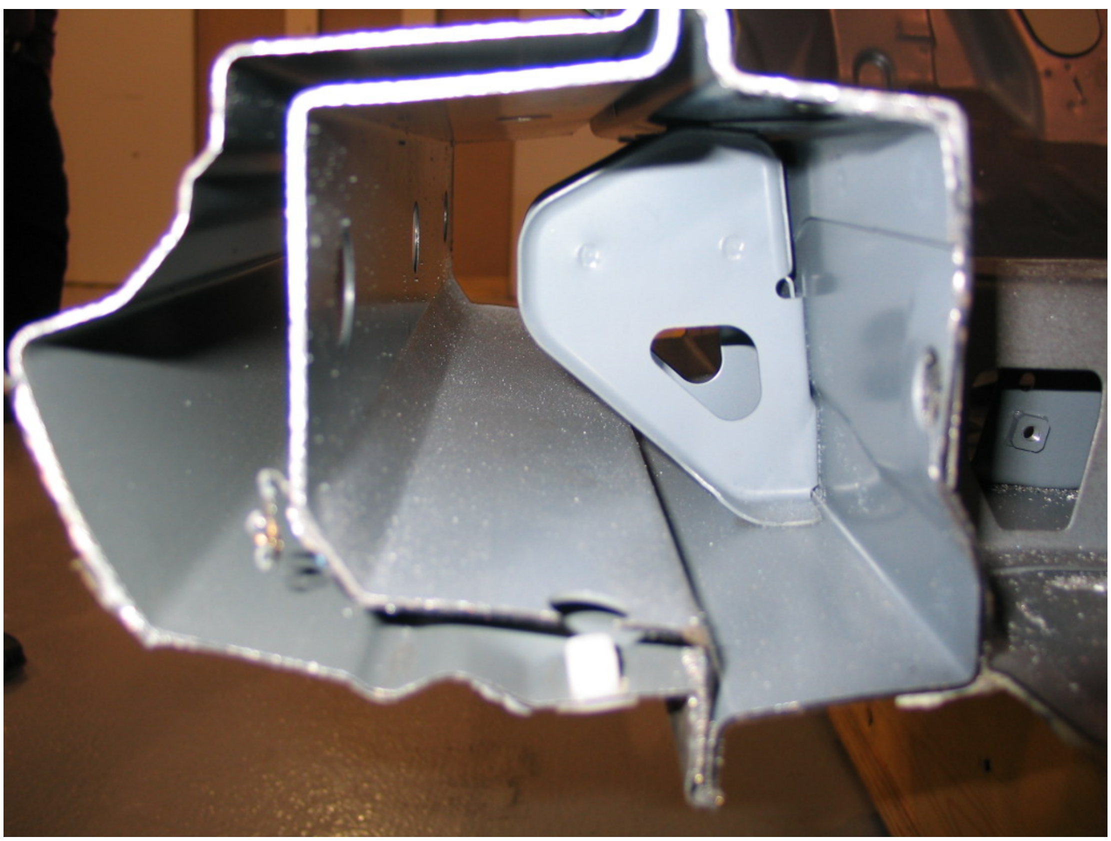

FIGURE 6: Toyota Camry - Local Stiffeners Inside Rocker To B-Pillar Joint
(Bulkheads Are Used For Local Buckling Prevention & FMVSS 214 Side Impact)

FIGURE 7: Toyota Camry - Deep Solid Seat Cross-members To The Tunnel (Side Impact Load Path)

FIGURE 8: Toyota Camry - Tunnel Heavy Reinforcement
(Carry Load From Crash Side To Non-Crash Side With No Buckling)

FIGURE 9: Toyota Camry - Wide B-Pillar, Reinforcement Covering Access Holes
(Large Section Provides Better Performance On Overall Attributes If Packaging & Styling Allows)

FIGURE 10: 2004 Hyundai XG350

FIGURE 11: Hyundai XG350 Vehicle Overview

FIGURE 12: Hyundai XG350 - Side Rail (Cant-Rail) Two Reinforcement A to B-Pillar Section (Prevent Local Deformation For IIHS Side Impact & Prevent Rollover Occupant Injury)

FIGURE 13: Hyundai XG350 - Side Rail (Cant-Rail) Two Reinforcement B to C-Pillar Section (Prevent Local Deformation For IIHS Side Impact & Prevent Rollover Occupant Injury)

FIGURE 14: Hyundai XG350 - B-Pillar Section At Belt Line - Double Reinforcement For IIHS & FMVSS Side Impact

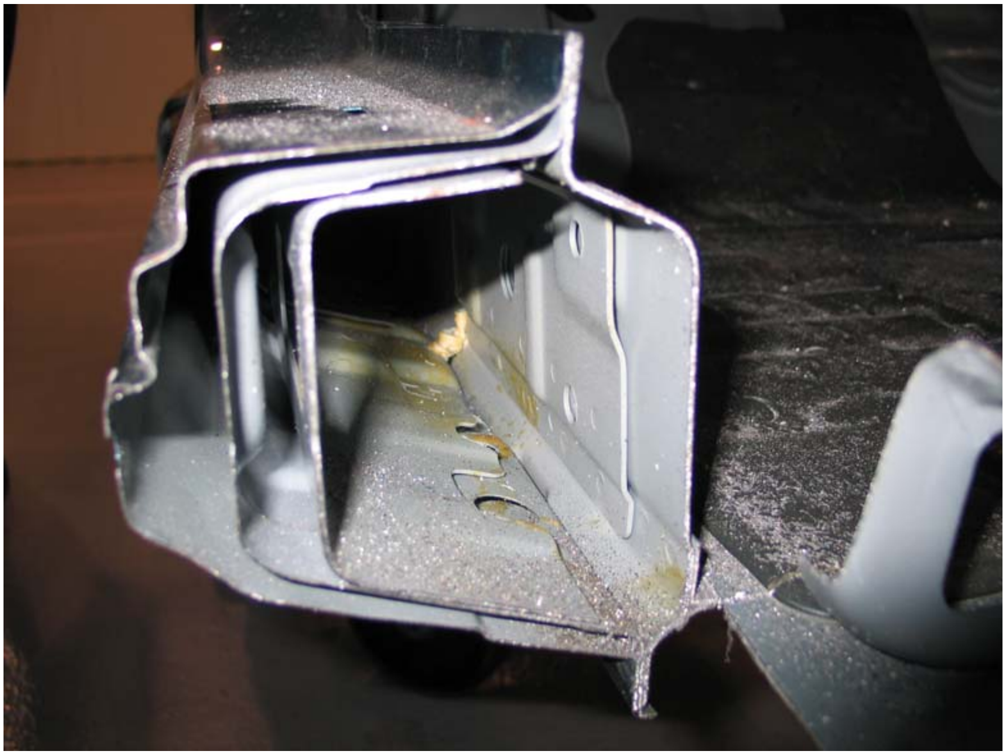

FIGURE 15: Hyundai XG350 - Rocker Section
(Double Reinforcement To Strengthen The Section For FMVSS Side Impact)

FIGURE 16: 2004 Toyota Prius

FIGURE 17: 2004 Toyota Prius BIW

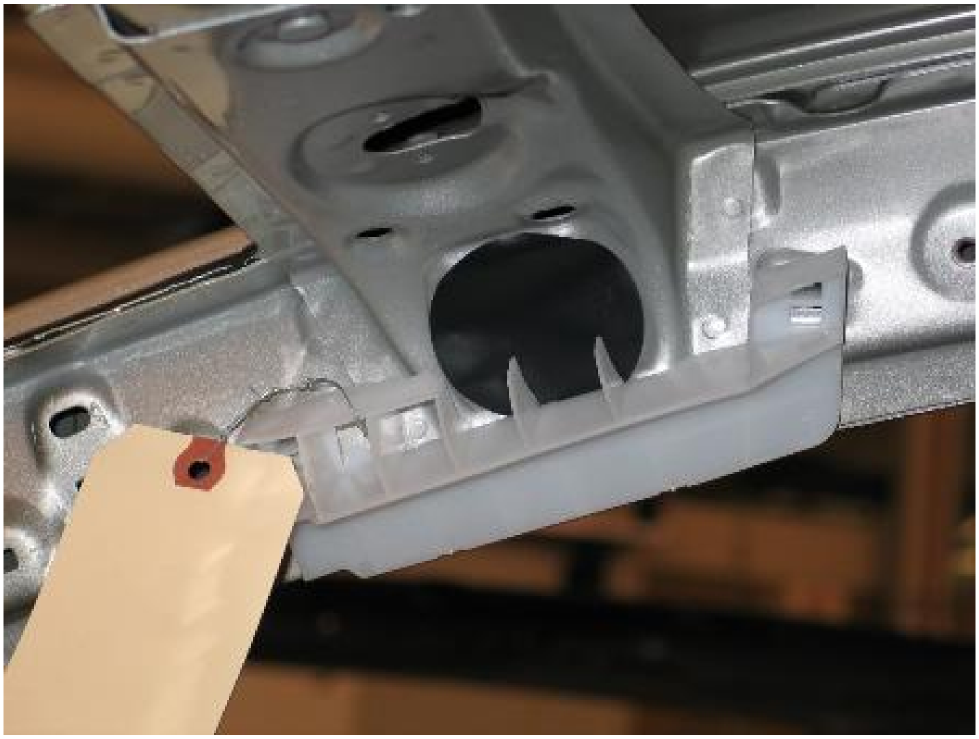

FIGURE 18: Toyota Prius - Wide Roof Bow Cover Whole Side Rail (Load Carrying Member For Side Impact)

FIGURE 19: Toyota Prius - Body-Side C-Pillar Support

FIGURE 20: 2004 VW Touareg Wagon

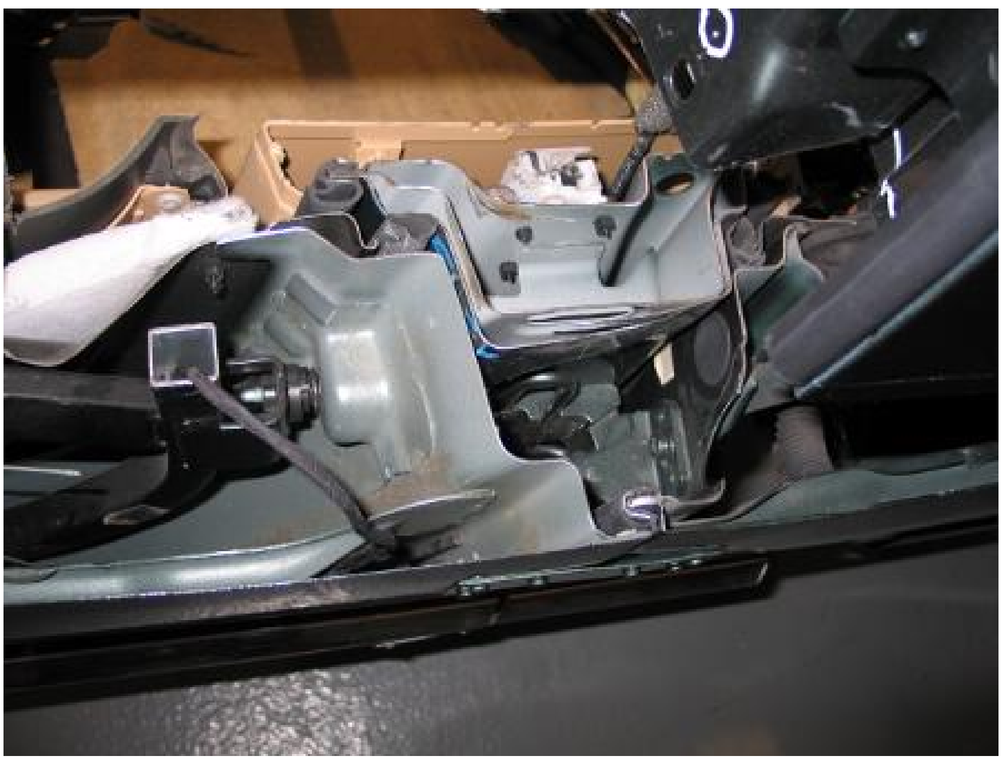

FIGURE 21: VW Touareg B-Pillar Section - Deep Section & Double Reinforcement (Strengthen For FMVSS Side Impact)

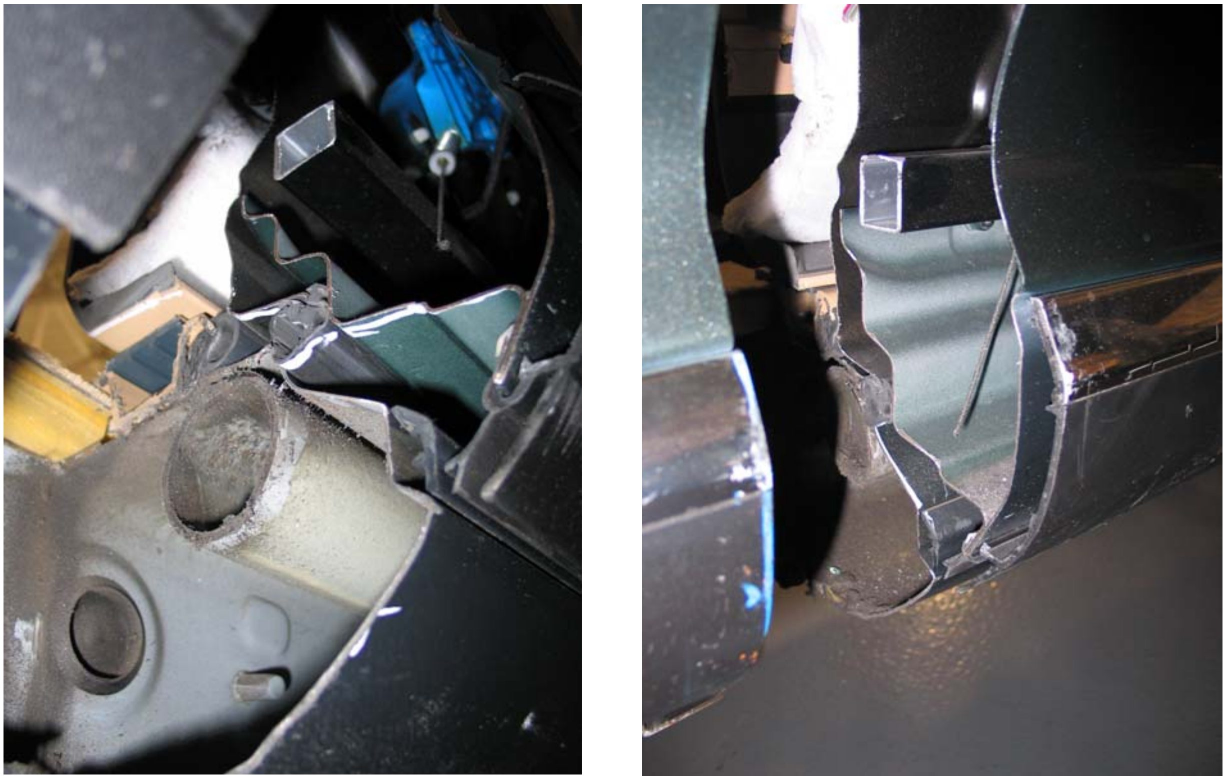

FIGURE 22: VW Touareg - Double Rocker Section (One In body & One In doors)
With Tubular Section In Upper Rocker
(Improve Side Impact Underbody Performance)

FIGURE 23: VW Touareg - Tubular Vertical Beam At Latch Side Of Door

FIGURE 24: VW Touareg - Roof Section Large Section Side Rail
(Improve Side Impact & Roof Crush Performance)

FIGURE 25: VW Touareg - Side Rail, Deep Section & Double Cant-Rail Reinforcement
(Improve Side Impact & New FMVSS 214 Requirements)

FIGURE 26: VW Touareg - Side Rail Section (Improve IIHS Side Impact & Pole Impact)

FIGURE 27: VW Touareg - Side Door Section Belt Line - Belt reinforcement

3.1.3. FORD PRODUCT AND VALUE BENCHMARKING CENTER VISIT

There were approximately 90 vehicles at the Ford Product and Value Benchmarking Center. Many of the vehicles were not completely torn down to BIW, with cutouts in the exterior sheet metal common for viewing the interior structure. The group focused primarily on the following three vehicles:

1. 2005 Chrysler 300C RWD
2. 2005 Ford 500
3. 2005 Honda Odyssey

General Observations

- Design for side impact strength varies by manufacturer, but key is to balance lower and upper regions of body structure
- Sensitivity of changing cutout in base of B-pillar should be investigated
- Many of the Japanese OEMs use beading and roof bows extensively; it is less prevalent in the domestic vehicles
- The Chrysler 300C has curved beams that transmit crash loads from dash panel to rocker, and unsymmetrical deep seat cross-members combine with these curved beams to form key structural joints for underbody strength and for front and side impact

FIGURE 28: Chrysler 300C - Front View Shows Substantial Upper & Lower Rail Sections & Rear Wheel Drive Tunnel

FIGURE 29: Chrysler 300C - Underbody View With Load Path For Front & Side impact (Curved Beams Transmit Crash Loads From Base Of Dash Panel To Rocker, Creating An Effective Triangular Area; Unsymmetrical Deep Seat Cross-members Merge With Curved Beams At Rocker To Form Key Structural Joints For Underbody Strength For Front & Side Impact)

FIGURE 30: Chrysler 300C - Rear Interior Body Structure, Showing Large Cutouts In Base Of B-Pillar

FIGURE 31: Chrysler 300C - Upper Structure Shows Single Roof Bow Just Rearward Of B-Pillar

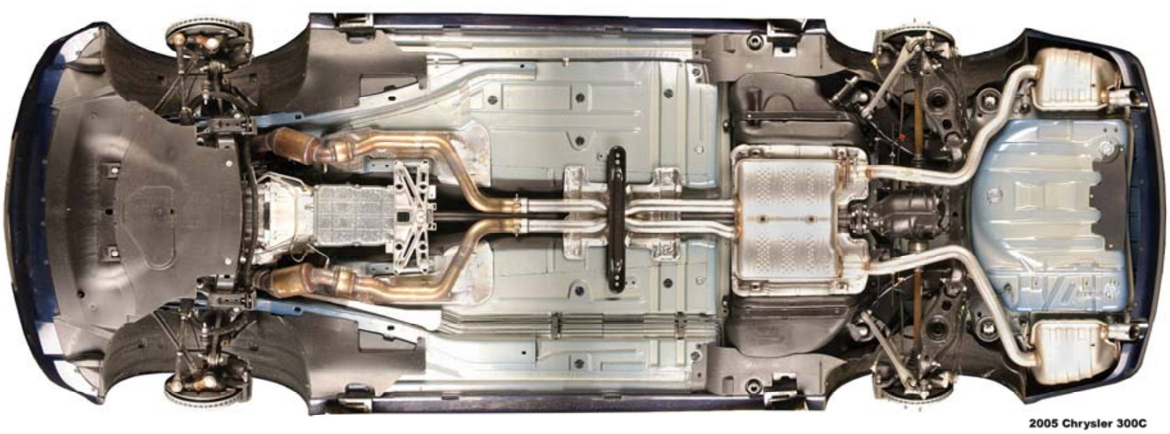

FIGURE 32: Chrysler 300C - Underbody Shows Recessed Exhaust & Chassis Systems For Better Aerodynamics

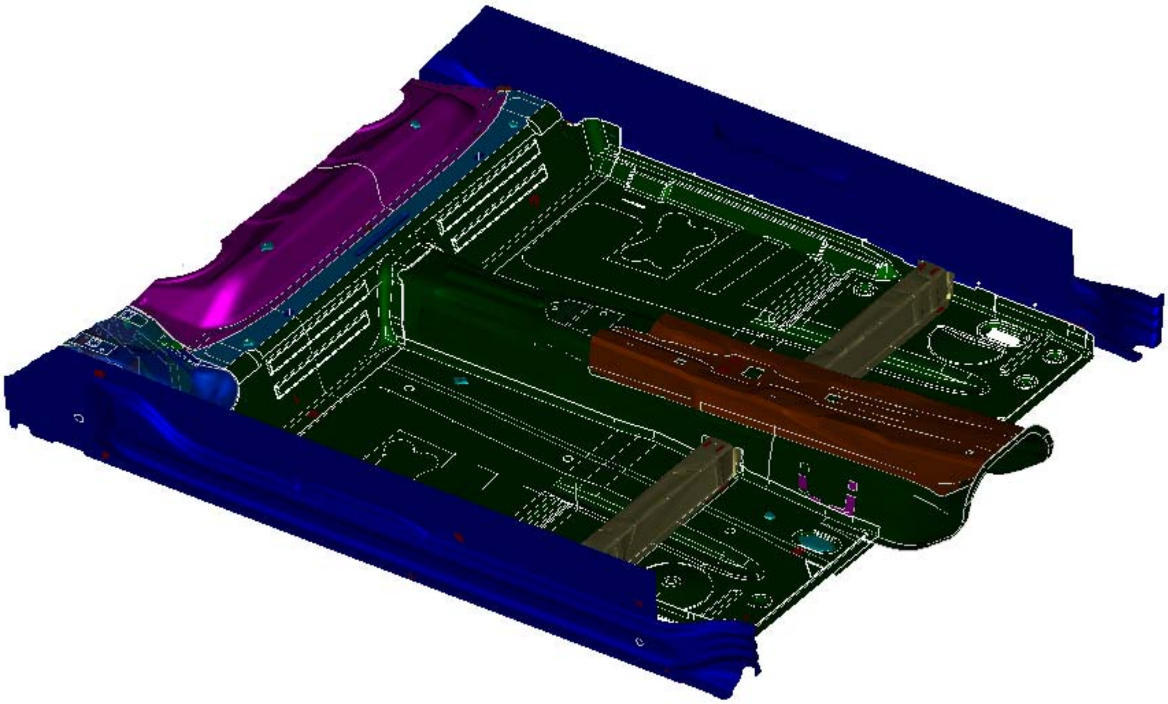

FIGURE 33: 2005 Ford 500 Floorpan Geometry

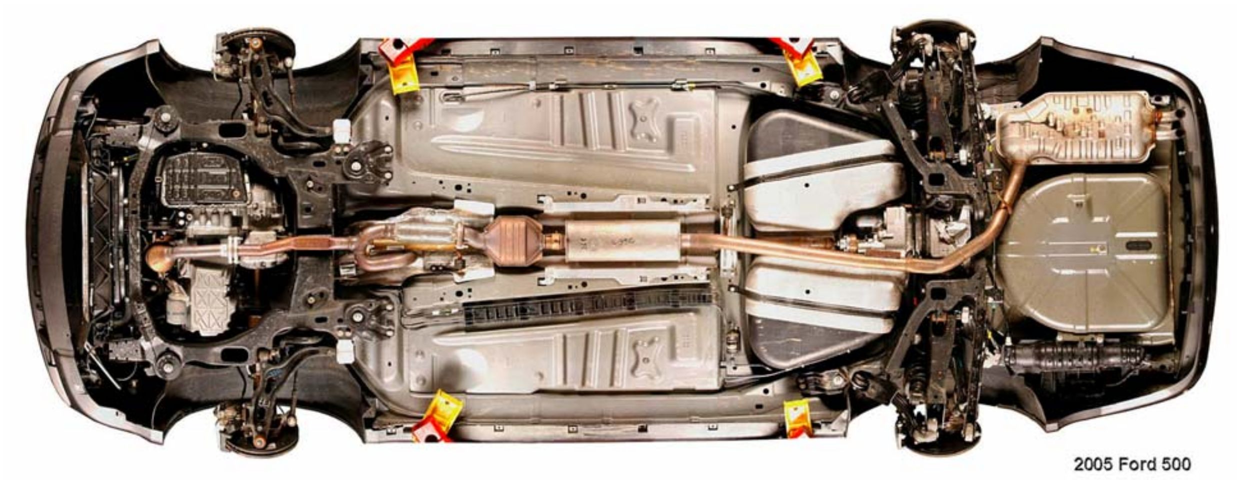

FIGURE 34: Ford 500 - Underbody View of 2005 Ford 500

FIGURE 35: Honda Odyssey - Floorpan & Lower B-Pillars View Facing Forward

3.1.4. DAIMLERCHRYSLER VEHICLE BENCHMARKING CENTER VISIT

The team members visited the Daimler Chrysler Vehicle Benchmarking Center. The group focused primarily on the following vehicles:

1. Honda Civic
2. 2003 Honda Pilot
3. 2003 Pontiac Montana
4. 2004 Toyota Sienna
5. 2005 Honda Odyssey

General Observations

- Honda uses beading extensively for local stiffening
- Honda uses more roof bows than many other vehicles
- Honda's B-pillars have smooth transitions that helps in manufacturability
- The Honda Civic has multiple reinforcements in the B-pillar to roof section, bulkhead in rocker, and double section front seat cross-member for side impact strength; has large IP cross car beam for side impact and steering column shake; has dual parallel front door intrusion beams
- The Honda Pilot has multiple roof bows including large C-ring cross-member to provide stiffness for side impact and NVH
- The Pontiac Montana has less beading than the Honda vehicles
- The Toyota Sienna has a large B-pillar section with multiple reinforcements and rocker section with bulkhead to address side impact issues
- The ACE structure of the Honda Odyssey offers multiple load cells for more robust front crash performance; uses integration of unibody with ladder frame construction to control crash loads; and has standard side curtain airbags providing protection for all thee rows of occupants

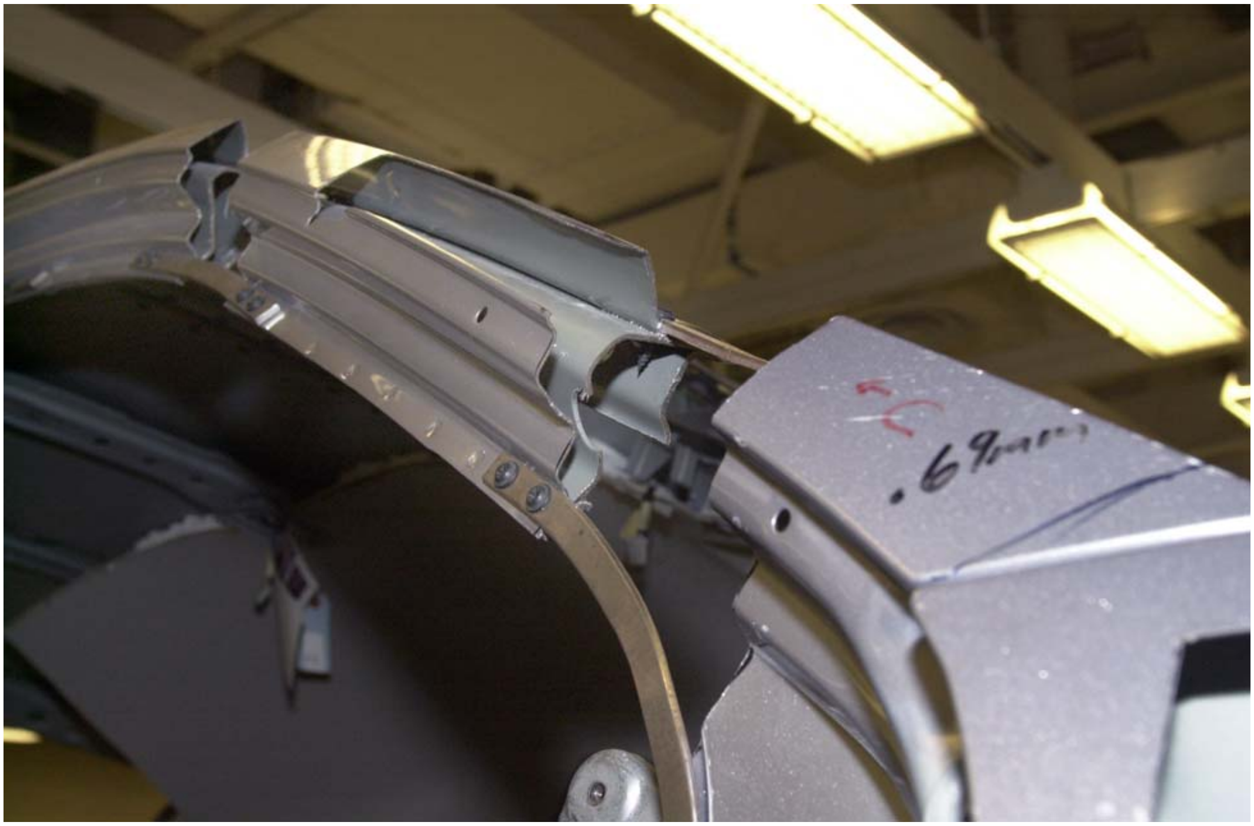

FIGURE 36: Honda Civic: C-Pillar Lower Section, Exterior Panels 0.69mm Thick

FIGURE 37: Honda Civic - C-Pillar Upper/Roof Side Rail Area, Sections Small With Higher Gauge

FIGURE 38: Honda Civic - B-Pillar To Roof Section, Use Of Multiple Reinforcements

FIGURE 39: Honda Civic - Rocker Section With Bulkhead

FIGURE 40: Honda Civic - Large IP X-Car Beam For Side Impact & Steering Column Shake (Steering Column Mounting Bracket Is Steel, Rather Than Magnesium)

FIGURE 41: Honda Civic - Dual Tubular Parallel Front Door Intrusion Beams

FIGURE 42: Honda Civic - Double Section Large Front Seat Cross-member To Tunnel

FIGURE 43: Honda Civic - Tunnel Cross-member

FIGURE 44: Honda Civic – Front-End Sheet Metal, Extensive Use Of Beading

FIGURE 45: 2003 Honda Pilot - B-Pillar Has Nicely Styled Shape With Smooth Transitions

FIGURE 46: 2003 Honda Pilot - B-Pillar To Roof Joint Inside View, Bolted Roof Bow To Side Rail

FIGURE 47: 2003 Honda Pilot - Multiple Roof Bows Including Large Bolted-In C-Ring Cross-member

FIGURE 48: 2003 Pontiac Montana - Lack of Beading Is Evident

FIGURE 49: 2004 Toyota Sienna - One-Piece Body Side Outer Stamping

FIGURE 50: 2004 Toyota Sienna - Large B-Pillar Section Has Tight Radius At Rear Joint With Rocker

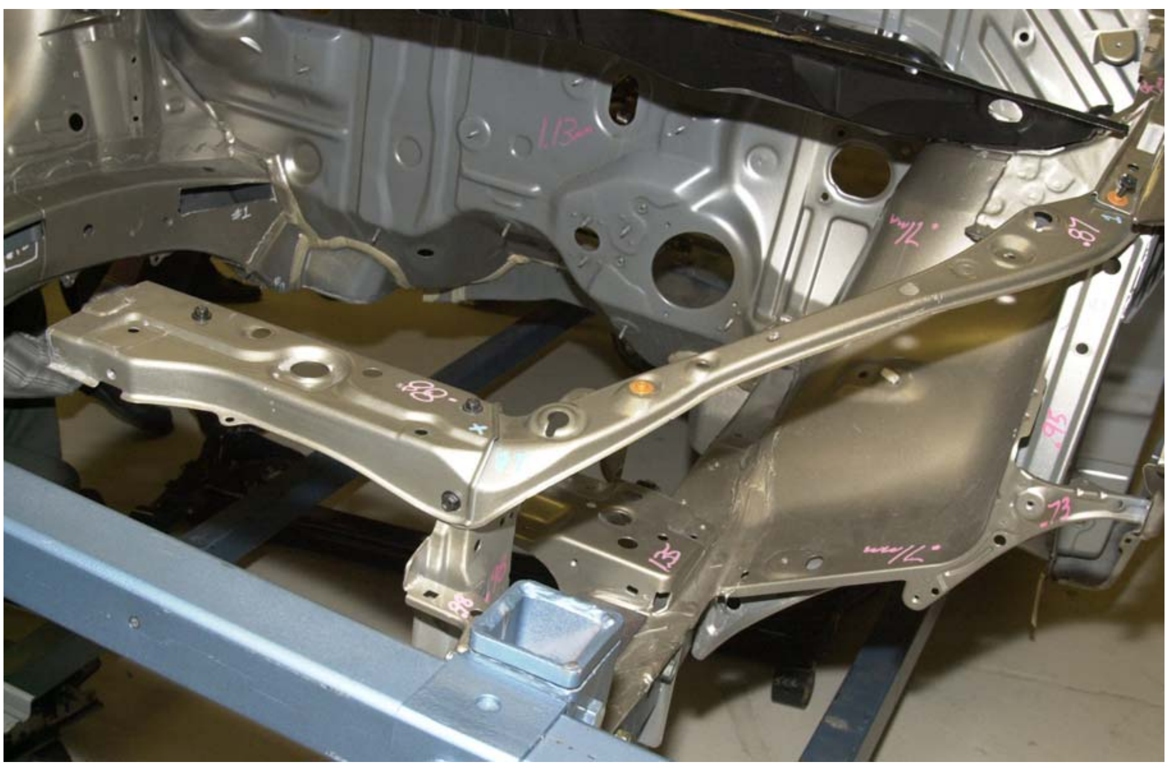

FIGURE 51: 2004 Toyota Sienna - Front End Sheet Metal

FIGURE 52: 2004 Toyota Sienna - Rocker Section With Bulkhead

FIGURE 53: 2004 Toyota Sienna - B-Pillar section, 3 Thickness Weld With Multiple Reinforcements

FIGURE 54: 2004 Toyota Sienna - Check Strap For Hinge Stop

FIGURE 55: 2004 Toyota Sienna - Substantial Body Side Reinforcement B-Pillar To Roof-Stack-up 5T

Figure 56: 2005 Honda Odyssey - Advanced Compatibility Engineering (ACE) Structure

FIGURE 57: 2005 Honda Odyssey - Close-up Of ACE Structure
(Multiple Load Cells For Front Crash Performance)

FIGURE 58: 2005 Honda Odyssey - One-Piece Body Side Outer, Including Wrap-Around To Liftgate (See Next Picture)

FIGURE 59: 2005 Honda Odyssey - Wrap-Around Construction At Liftgate

FIGURE 60: 2005 Honda Odyssey - Front Underbody Construction Showing Transition To Ladder Frame

FIGURE 61: 2005 Honda Odyssey - Rear Underbody Construction Showing Integration Of Unibody With Ladder Frame Including Total Of 9 Cross-members

FIGURE 62: 2005 Honda Odyssey - Floor Structure With Cross-member Tied In To Forward Edge Of B-pillar (Note Lack Of Holes In Floorpan)

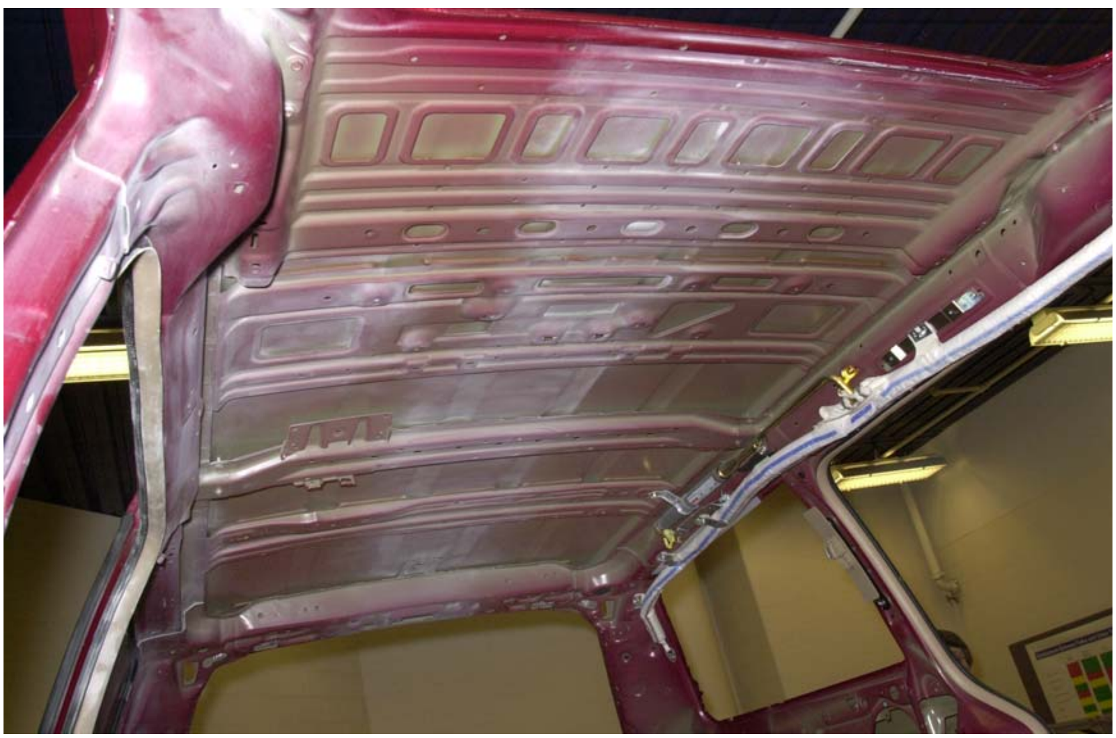

FIGURE 63: 2005 Honda Odyssey - Interior Roof Area With Extensive Use Of Roof Bows

FIGURE 64: 2005 Honda Odyssey - Interior Roof Area With Extensive Use Of Roof Bows

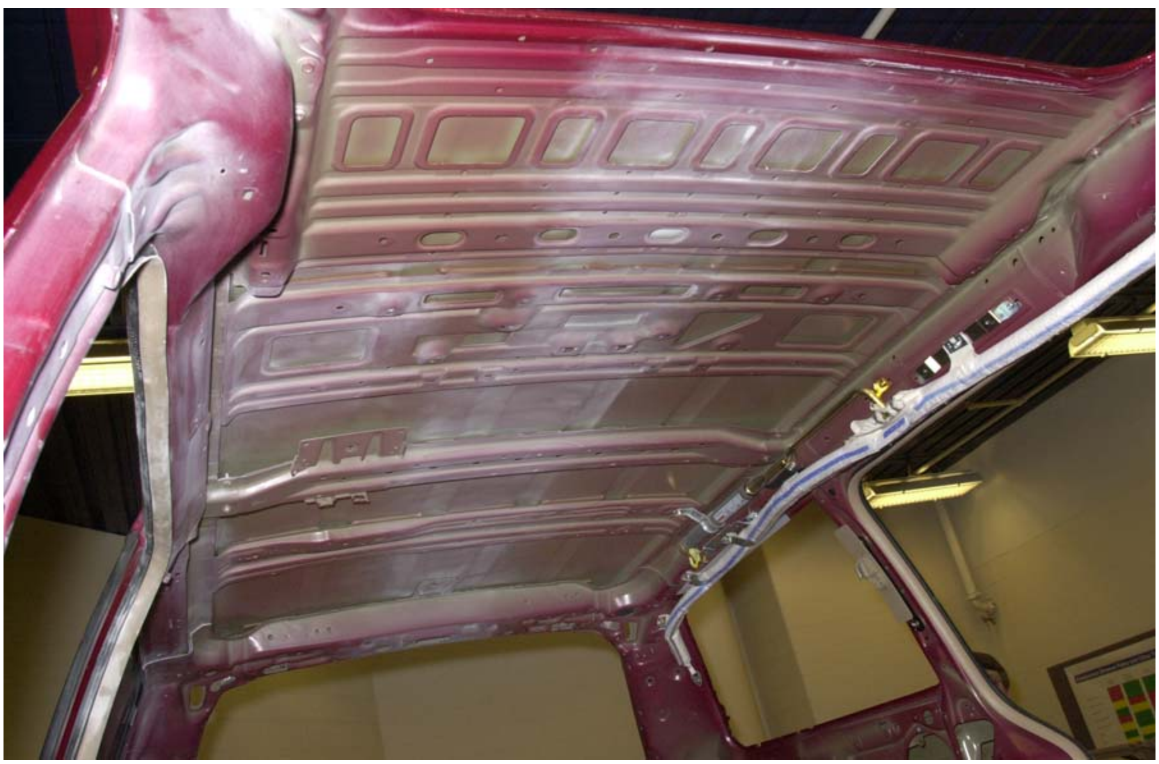

FIGURE 65: 2005 Honda Odyssey - Side Curtain Airbags From A to D-Pillars Providing Protection For All Three Rows Of Occupants

3.2. BRAINSTORMING SESSION SUMMARY

As part of the team meeting on March 4, 2005, a brainstorming session was held to capture the ideas or lessons learned from the cumulative benchmarking activities. Following is a summary from this session.

1. Increase panel stiffness through efficient use of beads (aggressive beads, lighter gauges)
2. Keep an open mind on material selection; consider the use of unconventional (eg stainless steel) or exotic materials. Use the CAE study to determine the ideal properties, then search for a match
3. Should forming strains be included in analysis? The results are estimated to vary by 5-10% and so it was decided to account for this in the final analysis
4. The strategy will first use the geometry to define a load path that meets the performance targets, then a detailed optimization of cross-sectional shape, materials and gauge will be used to reduce the weight. Consideration of manufacturing issues and joining strategy will be made throughout the project
5. Determination of the best topology and loadpath balance will be made to provide feedback to OEM's
6. Joint Policy Board (DOE) will be included in the topology assessment
7. It will be necessary to determine if the gap between the doorframe and B-pillar is sufficient. Refer to the door & seat CAD data to confirm
8. Consideration will be given to dentability performance, joint stiffness and the use of hydroforming
9. Investigate manufacturing technologies that address construction of the Upper B-pillar and door (ie laser braising)
10. Confirm that the outer panels are cosmetic
11. Consider the use of tailor weld blank technology
12. Stainless steel components, such as the rocker section will need to be upgraded (eg Audi A6)
13. Consider improvements to the topology such as adding side reinforcements to the tunnel (eg Chrysler 300C) or using a shear wall bench seat between the B-pillars
14. Once the assignments have been defined, use an integrator representative to act as an enabler for areas such as the doors

APPENDIX A
CENTER FOR AUTOMOTIVE RESEARCH (CAR) REPORT FROM OEM's

In December 2004, the Center for Automotive Research (CAR) published a report for A/SP titled *Body Systems Analysis.* The objective of the study is to identify existing product and process strategies that support the use of advanced high strength steel (AHSS) in automotive body structures, and determine the status of evolving technologies that have a great potential for supporting this AHSS implementation to meet FMVSS, ECE, IIHS and World Global safety requirements.

Four automotive OEM's were investigated:

1. Volvo
2. BMW
3. Honda
4. Nissan

The study focused primarily on Side Impact and Roof Strength, although Front and Rear Impact was also considered. The study found that benchmarking, developing, and documenting proven integrated solutions that will balance the interaction of material, manufacturing, and performance cost effectively is the key to successful implementation.

There is a growing trend for more automakers to concentrate on occupant safety as one of the highest priorities. Although crash load paths are similar on all vehicles, each manufacturer has their own strategies for managing these load paths. Body structures are being designed to better distribute the energy for front impact to protect not only the vehicle's occupants, but also reduce the risk of injury to unprotected road-users by helping to activate the other car's own crumple zones. To accomplish this, Volvo uses an additional low front cross-member in their XC90 (FIGURE A1), while the new Honda Odyssey uses a multiple-cell front structure (FIGURE A2) called Advanced Compatibility Engineering (ACE) to dissipate crash energy over a larger area.

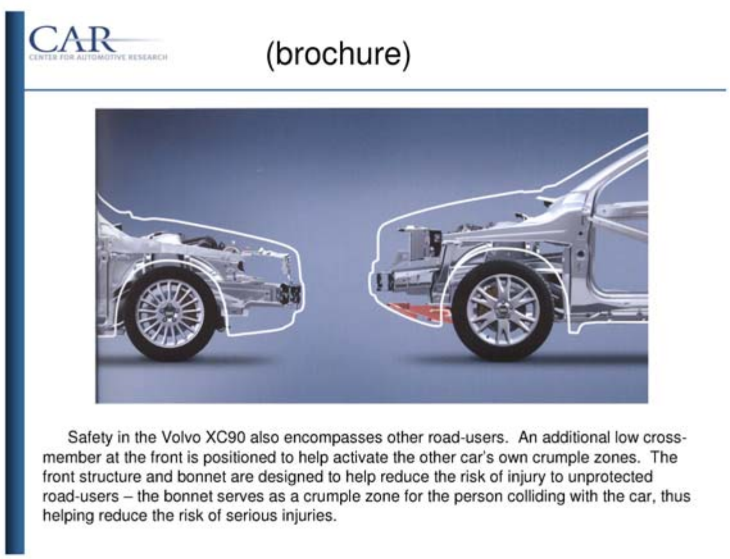

FIGURE A1

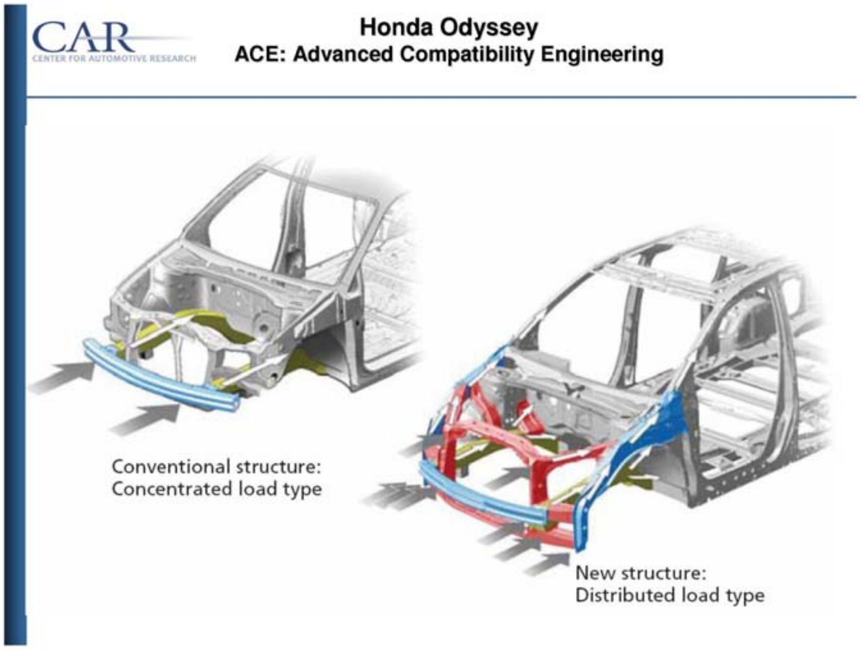

FIGURE A2

For side impact, controlling the B-pillar intrusion and deformation mode, by balancing the lower and upper regions of the body structure, is critical. Reinforced B-pillar, rocker, and roof structures are generally needed to meet performance targets (FIGURE A3).

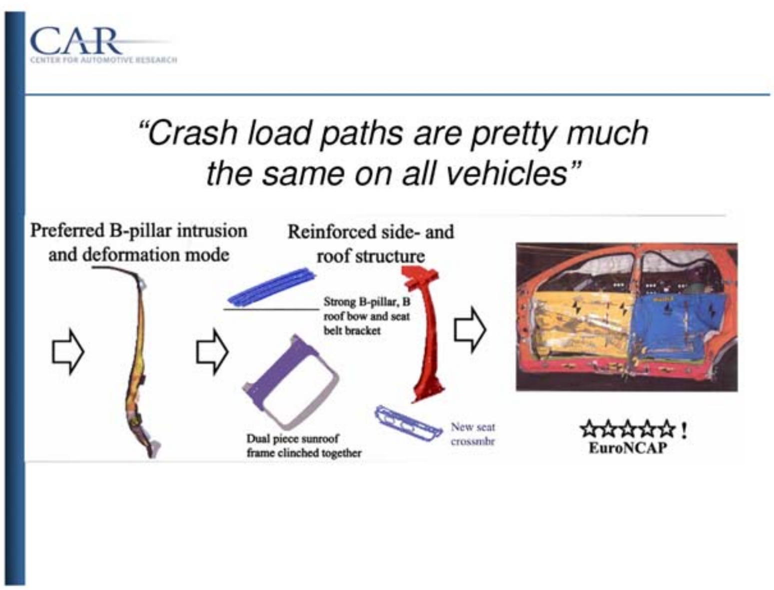

FIGURE A3

Future Generation Passenger Compartment (FGPC)

The use of high strength steel (HSS) in body structure design is becoming more prevalent, primarily to achieve improved safety performance and mass reduction. Volvo's material selection process is to estimate from history where the strength is needed, identify possible material candidates, and evaluate the available materials. For the XC90, high strength and advanced high strength steel are used extensively (FIGURES A4 & A5).

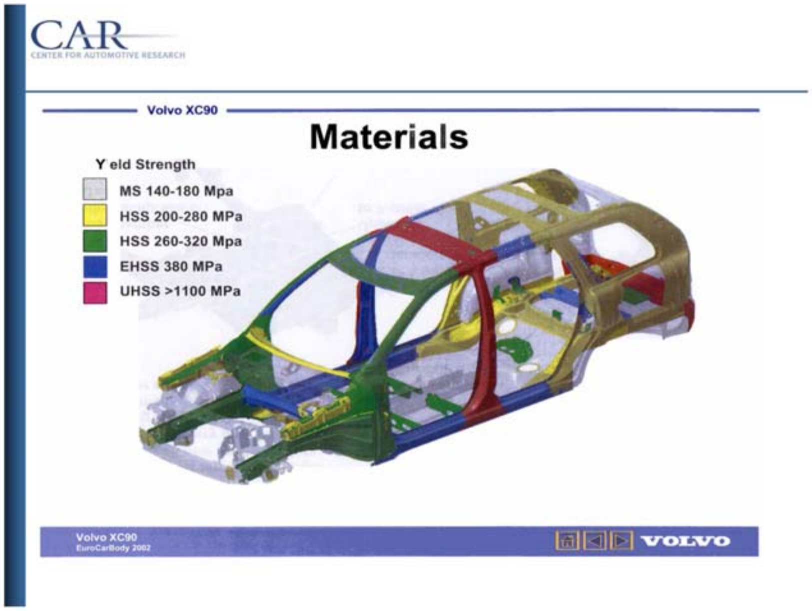

FIGURE A4

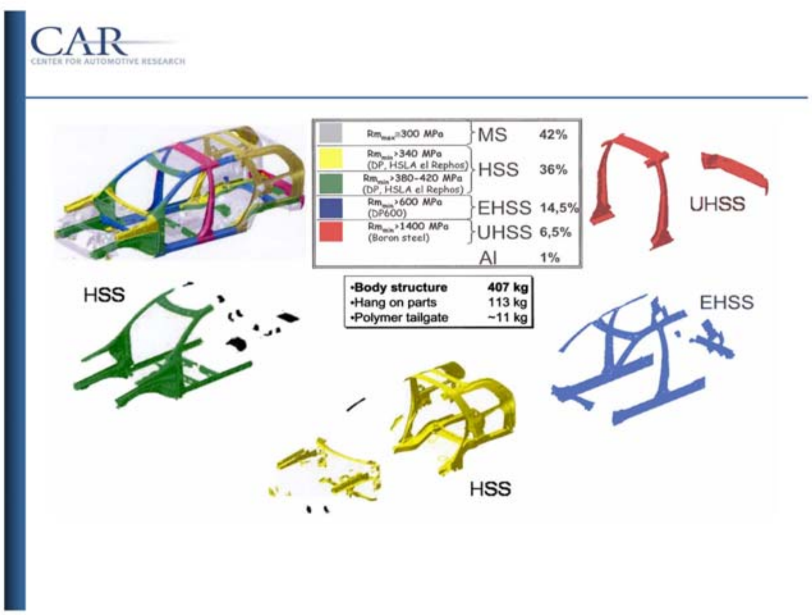

FIGURE A5

To address side impact requirements, Rephos is used for the roof header lower and A-Pillar upper, DP600 for the roof header lower, A-Pillar lower, B-Pillar inner, and rockers, and Boron steel is used for the B-pillar reinforcement, B-Pillar roof bow, and rear seat frame (FIGURE A6). Typical thicknesses for these components range from 1.2mm to 2.0mm. Boron is also used for the door crash beam in the XC90, while DP800 material is used for select applications, such as the S40 door intrusion beam. Mild steel is used for the one-piece body side outer panel with thickness of 0.8mm.

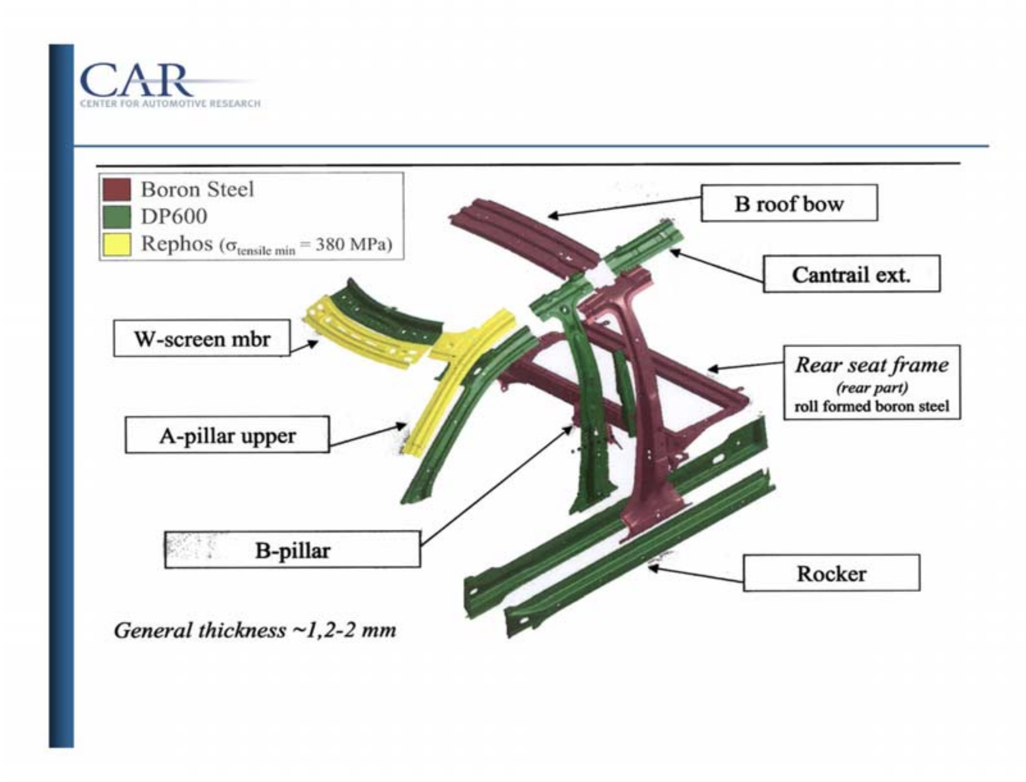

FIGURE A6

Volvo identified several inhibitors in using AHSS (e.g. Boron), including welding and springback concerns that result in expensive processing. The Boron B-Pillar was found to be so stiff that it had to be used as the "master" dimensional panel for the body side. Surface corrosion was also an issue and was addressed by pickling the parts in an acid bath and subsequently oiling the parts to prevent rust.

BMW's priorities in body design and material selection include vehicle performance while attaining a high level of crashworthiness. They have no specific strategy to use HSS; instead they identify the best material on a part-by-part basis, which results in the use of a combination of HSS and aluminum to form a hybrid body structure. The new 3-series vehicle is HSS intensive, which result in an estimated mass savings of almost 20kg. The uses of HSS include DP500 for underbody cross-members and longitudinal rails, DP600 for front seat cross-members, CP800 for B-Pillar, upper A-Pillar, A-Pillar reinforcement and rocker, and TRIP700 for dash panel cross-member and various brackets. BMW also relies heavily on collaboration with steel manufacturers to co-develop materials and processes for HSS. They are also beginning to collaborate more with the university system in Germany to develop advanced material applications.

Honda uses almost 50% HSS in their 2005 Odyssey and have added body reinforcements for better crash performance (FIGURE A7). They identified a key issue on HSS material use to be global availability. Honda also develops their own material standards to ensure worldwide consistency. Honda would not disclose specifically what material is used for particular body components, but they did reveal that they focus on three types of HSS: HSLA, CMn, and DP. Honda has limited experience with TRIP, and has formability concerns with Boron. They use CP in limited applications.

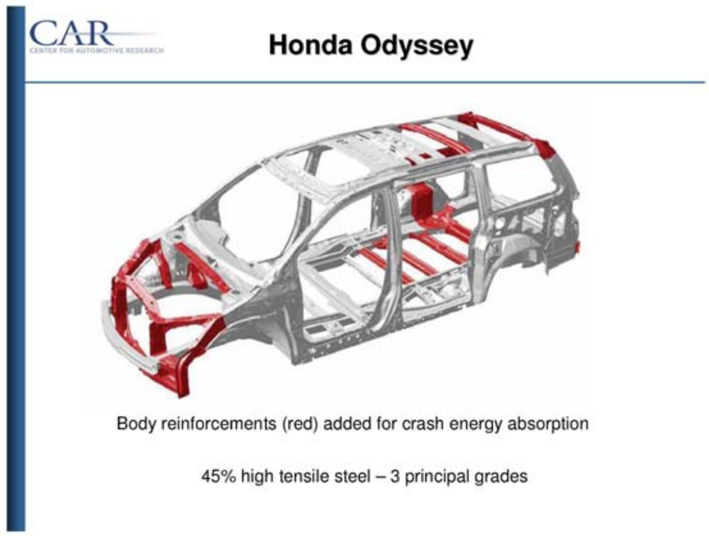

FIGURE A7

Nissan's objectives for use of HSS in body structures are crash management and mass reduction. If necessary, the part design is compromised to accommodate HSS, by using more bending and less forming. About 55% HSS is used in the Micra vehicle (FIGURE A8).

FIGURE A8

The distribution of high strength steels in the Micra is shown in FIGURE A9.

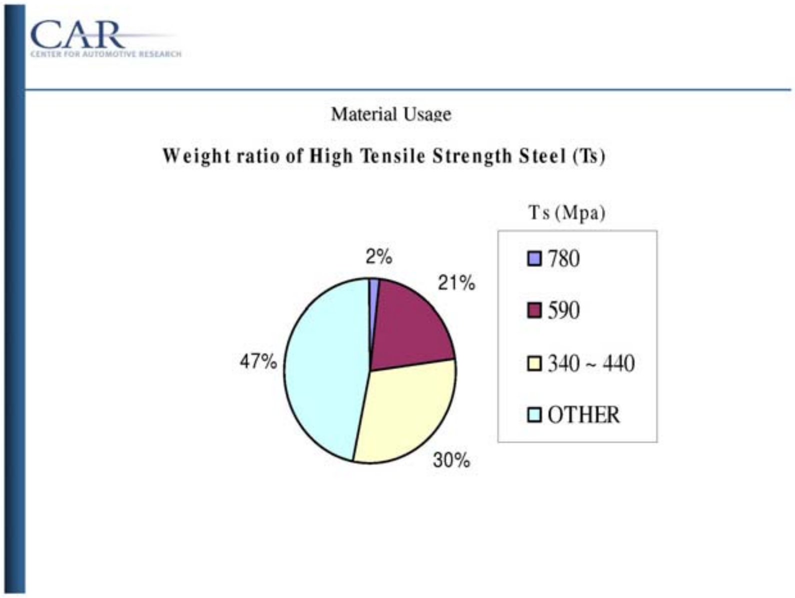

FIGURE A9

Nissan currently uses 500 and 800MPa parts in production. In order to expand the use of new high strength steels, they found that part accuracy, weld-ability, and formability, including springback estimation were issues that needed to be addressed by working together with steel manufacturers.

In summary, many high strength steels are available to the automakers, each with varying tensile strength and elongation to meet the specific design requirements (FIGURE A10).

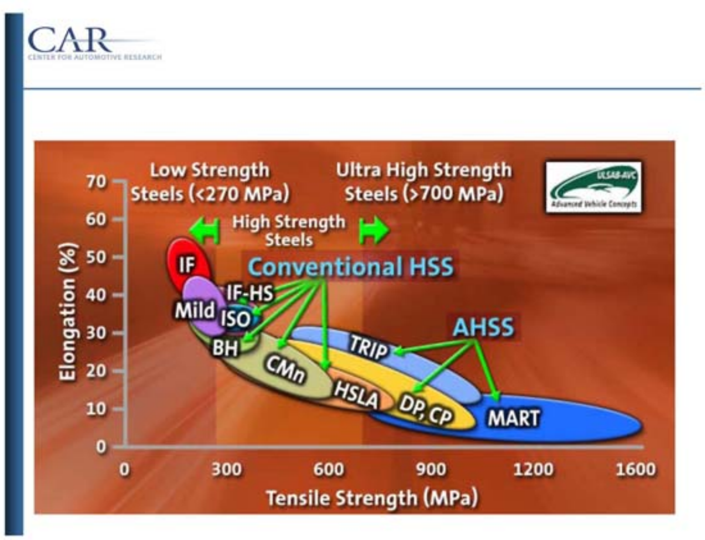

FIGURE A10

APPENDIX B

FUEL CELL TECHNOLOGY FOR FGPC

Use of technological improvements in fuel cell systems is crucial in making fuel-cell powered vehicles attractive enough to encourage mainstream use by consumers. Many buyers will demand that cost, comfort, power, and vehicle range be similar to the vehicles on the market today. Most automakers and their key suppliers predict they would be able to demonstrate commercial feasibility of hydrogen fuel cell technology and production validation by 2010, with vehicles ready for public sale by 2015.

Several trends in fuel cell technology are emerging:

- Power density has been increasing by a factor of 7 times in the last 6 years
- Improvements in durability, reliability, and cold-starting capability
- Cost reduction through material development, systems/components simplifications, and part count reduction
- Use of lightweight, high strength carbon composite storage tanks that hold hydrogen at 10kpsi can boost vehicle range to 300 miles for hydrogen gas and up to 500 miles for liquid hydrogen
- Use of complex metal hydrides with destabilizers to store hydrogen in a solid state, resulting in lower pressure tanks, and easier starting, especially in sub-zero conditions

GM's Sequel vehicle uses improvements in fuel stack design to improve the power density to 1.6kW per liter, with a maximum output of 110kW. The improvements include 1) a new lighter, quieter, and more efficient intake system and 2) a patented, aerospace-inspired jet turbine compressor design that has more dynamic airflow and is lighter, smaller, and less costly.

GM and their HRL Laboratories affiliate are evaluating hydride storage systems. GM and HRL are evaluating many different destabilizers that are needed to lower release temperatures to reasonable levels. The most promising hydride-destabilizer combination is lithium borohydride (LiBH4) with a magnesium hydride destabilizer. A 300 mile vehicle range should be possible if at least a 5% hydrogen to overall hydride system weight ratio is achieved.

Honda allowed an automotive journalist to drive its Honda FCX Fuel Cell vehicle unsupervised for a 3 day span, and he gave it rave reviews. According to the writer, the vehicle performed flawlessly and drives just like a conventional vehicle. The only noticeable difference is that there was a "system check" delay of up to 37 seconds before the vehicle could be driven. The FCX has a top speed of 93mph and cruising range of 190 miles, using an electric motor generating 107hp and 201ft-lb of torque. The dual hydrogen storage tanks are located under the rear seats and are pressurized at 5000psi. Overall length is 164in and weight is 3713lbs, which is 13in shorter and 1300lbs heavier than a Honda Civic coupe.

BMW has been developing hydrogen-powered vehicles for many years. The H2R racecar is powered by hydrogen and holds 9 international speed records. It is powered by liquid hydrogen, with 1 1/8in thick storage tanks, designed from space technology. The H2R holds 24lbs of liquid hydrogen and is high-vacuum insulated. A fleet of 7-series sedans covered a distance of over 100,000 miles, and the Munich airport recently opened Germany's first hydrogen refueling station. The filling process is fully automated, using a special coupling that links the filler neck with the tank nozzle and refueling takes no longer than filling a conventional gasoline or diesel tank.

AUTOMOTIVE INDUSTRIES ARTICLE- FEBRUARY 2005

Automotive Industries published the following article on the GM Sequel vehicle.

COMPONENT LAYOUT

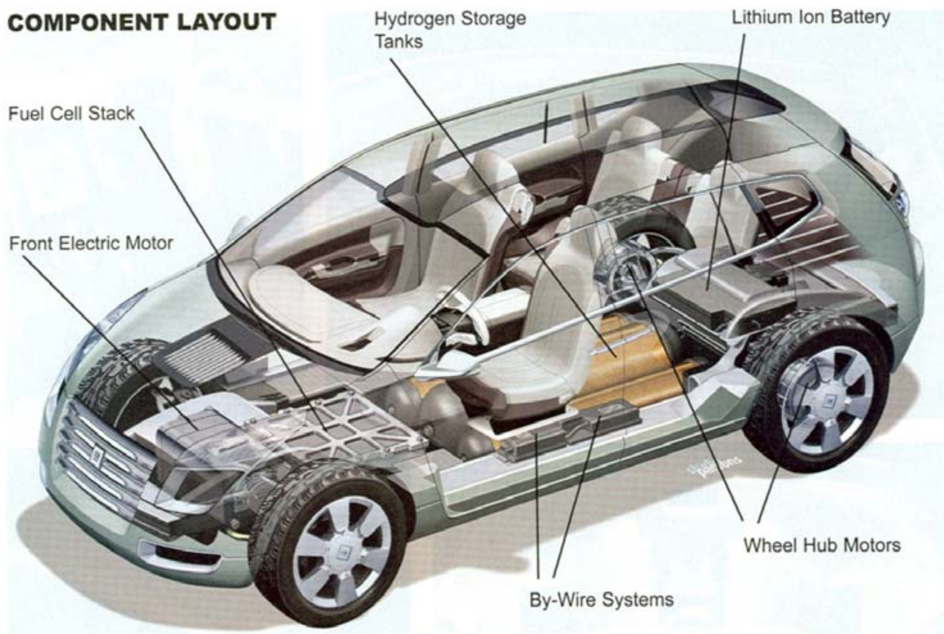

module for the battery sits right behind it. By-wire control modules for the braking, steering and chassis control systems are mounted on top of the frame rails on either side of the hydrogen storage system. An electric traction motor is mounted up front underneath the HVAC control unit, driving the front wheels.

Sequel is powered by GM's newest generation fuel cell stack developed by GM engineers in Honeoye Falls, N.Y. The 73 kW (97 hp) stack is made up of 372 cells and boasts an improved power density of 1.6 kW per liter with a maximum output of 110 kW.

The new stack is smaller than the stack found in HyWire but pumps out 25 percent more power. Technological improvements have allowed GM to eliminate a lot of the hanging-on technology by up-integrating some of those functions into the stack.

The new power module contains the stack, hydrogen and air processing subsystems, cooling system and high-voltage distribution system. The new stack also uses a new air intake system that is lighter, quieter and more efficient than the previous system.

GM switched out the screw-type compressor for a patented, aerospace-influenced jet turbine design. The new compressor offers a more dynamic airflow and is lighter, smaller and costs less than the part it replaces.

Dan O'Connell, head of GM fuel cell production engineering Honeoye Falls, N.Y., says that the smaller stack can operate over a wider range and needs less "care and feeding" than the previous generation.

"As the stacks become more robust they need fewer ancillary components," O'Connell adds, "This not only makes them less complex, but the stacks produce more power out of the same size."

Burns says that the improvements in stack technology have come quite fast.

"We've had a power density increase of a factor of seven times in the last six years," Burns says. "And significant improvements in durability, reliability and cold-start capability."

Burns says that cold-start isn't a question of whether you can do it or not, but whether or not you can do it over and over again throughout the life of the automobile.

"So that becomes the important challenge," Burns adds, "and we're making good progress there."

Burns says that GM has made rapid progress in reducing cost through material development and design improvements and systems and components simplifications, adding that the number of parts has been reduced by a factor of three in the last three years. The latest stack has one-tenth the moving parts of a conventional internal combustion propulsion system.

The three lightweight carbon-composite tanks (a large one in the middle and two smaller ones on each side) are a patented GM design and hold 8 kg (17.6 lb.) of gaseous hydrogen stored at 10,000 psi (compared to 5,000 psi in HyWire). This gives Sequel a range of 300 miles (450 to 500 miles if liquid hydrogen is used).

The carbon-fiber material, supplied by Toray Industries of Tokyo, Japan, provides for a stor-

FIGURE B1

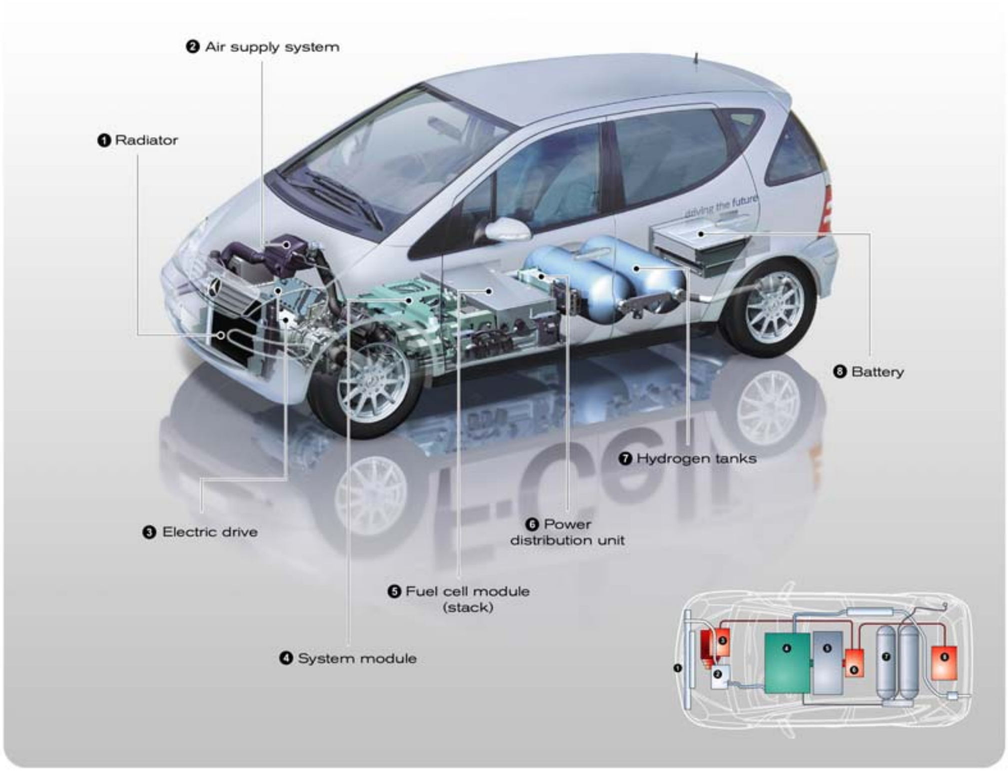

FIGURE B2: GM Sequel Layout

FIGURE B3: GM Sequel Interior

AUTOTECH DAILY ARTICLE- MARCH 2005
Autotech Daily published the following article on GM's efforts relating to hydride storage of hydrogen.

GM STATES CASE FOR HYDRIDE STORAGE OF HYDROGEN
Buoyed by recent advances, General Motors Corp. says complex metal Hydrides may soon be a viable alternative for onboard storage of hydrogen in fuel cell vehicles. Most current prototypes use compressed or liquefied hydrogen. By storing hydrogen in a solid state, fuel tanks wouldn't have to be as highly pressurized as when storing highly compressed gaseous hydrogen. Another benefit: A hydride system likely would be easier to start, notably in sub-zero conditions. But until now, the weight of the metal, high release temperatures and the relatively long time needed to free hydrogen from the hydrides has prohibited such systems. To try to improve these characteristics, GM and its HRL Laboratories LLC affiliate in Malibu, Calif., are teaming complex hydrides with destabilizers. They're currently evaluating more than 140 combinations. Although GM has yet to test any in a vehicle, executives say a hydride system could still be ready by 2010, the same year the company expects to demonstrate a high-volume, commercially feasible fuel cell vehicle.

DESTABILIZERS ARE KEY
The U.S. government has been studying hydrides, in which individual hydrogen atoms bond to a metal matrix, for more than 50 years. The push toward fuel cell vehicles has accelerated research in the last five years into more complex formulas that allow up to 13% hydrogen to be stored by weight of the overall hydride system vs. 1% or 2% for simple hydrides. At least a 5% hydrogen ratio likely is needed to achieve the targeted 300-mpg driving range between fill-ups. About two years ago, GM and HRL (the former Hughes Research Laboratories) began experimenting with destabilizers to try to help lower release temperatures, which can range from about 280°C to 900°C depending on what type of hydride is used. The destabilizers, which also can be hydrides, are mixed with the main metal at a 1:2 ratio to form an alloy that forms a weaker bond with hydrogen. Although adding a destabilizer adds weight, the hydrogen retention percentage is still typically above 5%. Of the 140 different hydride-destabilizer combinations GM and HRL are evaluating, lithium borohhydride ($LiBH_4$) with a magnesium hydride destabilizer has emerged in the last six months as one of the most promising. On its own, $LiBH_4$ can store 13.6% hydrogen by weight, but it requires a 400°C release temperature at 15psi. Adding magnesium reduces the release temperature to 275°C while maintaining a 9% hydrogen storage capacity—with a theoretical capacity of 11.2% with further advances. The target release temperature is 50°C-150°C, which HRL believes will be possible once it finds and tweaks the right hydride-destabilizer blend. GM repurchased a one-third share of HRL in 2001 from Boeing Co. and Raytheon Co., which own the other two thirds of the organization. Raytheon acquired a 50% stake following its 1997 merger with Hughes Aircraft. Hughes Electronics maintained a half ownership until 2000, when it sold its Space and Communications business to Boeing. GM is also looking at ways to reduce the time it takes to release hydrogen from hydrides, which is more dependent on surface area and other factors than it is on temperature. Separately, the company is working with Sandia National Laboratory in Livermore, Calif., to develop lighter, more efficient and cheaper storage tanks to hold the hydrides. Still to be determined is whether hydrogen will be converted from a gas into the hydride on- or off-board. The goal is to be able to refuel a vehicle in the same amount of time it takes to pump gasoline. Another storage option that holds promise is cryo-adsorption. GM describes the process as a cross between liquid and gas storage but with less severe temperature and pressure requirements.

DETROIT FREE PRESS ARTICLE MARCH 2005
The Detroit Free Press published the following articles on the Honda FCX fuel cell vehicle and related technology.

SCIENCE PROJECT: Race is on to improve storage of hydrogen
BY MARK PHELAN
FREE PRESS AUTO CRITIC

LIVERMORE, Calif. -- Behind the locked doors of high-security labs in two of the least likely places you can think of, work to perfect a hydrogen storage system for General Motors' fuel-cell powered cars progresses at a feverish pace.

Storing hydrogen in cars is one of the greatest challenges to getting emissions-free fuel cell cars on the road, GM research and development chief Larry Burns said this week.

The development has two goals: come up with a tank to hold the fuel and develop a way to store the hydrogen chemically rather than as a gas or super-cooled liquid.

Scientists at the U.S. Department of Energy's super-secure Sandia National Laboratory in Livermore, Calif., are working on the storage tanks on a heavily guarded campus ringed by razor wire and guarded by body-armored, heavily armed security staff.

Sandia originated as part of the Manhattan Project to develop the first nuclear bomb in the 1940s. It moved to its current site in Livermore, in California's Central Valley about 30 miles west of San Francisco, in 1956. Today it does work on nuclear weapons and bioterrorism in addition to several hydrogen storage projects with GM.

About 300 miles south, on a Malibu hilltop with a stunning view of the Pacific ocean, another crew of scientists at HRL Laboratories works on ways to convert hydrogen from a flammable, leaky gas to a harmless solid compound.

HRL, formerly known as Hughes Research Laboratories and founded in 1948 by Howard Hughes, is jointly owned by GM, Boeing and Raytheon. HRL's history includes the invention of the laser beam. In addition to GM's fuel-cell research, its present work includes the development of ion propulsion drives for satellites and high-powered lasers for the military.

GM's goal for both its projects is to produce a hydrogen-powered fuel cell car that can go 300 miles on a tank and be refueled as quickly and easily as today's gasoline-burning vehicles, Burns said.

GM is also investigating using highly compressed hydrogen gas or super-cold liquid hydrogen to power the vehicles, but both of those face significant technical and cost challenges, Burns said.

"We like the competitive dynamic" of having people working on several kinds of storage at the same time, he said.

However, GM will have to pick one in the next two or three years if it's going to meet its publicly stated goal of having a fuel cell car ready to go to market in 2010, he said.

Scientists at HRL are testing a wide variety of chemical compounds to see which one works best to store hydrogen, release it to the fuel cell and then store more hydrogen quickly for refueling.

A lot of the work focuses on compounds called metal hydrides, said HRL scientist Leslie Momoda. The tricky part is getting the hydrogen to bond with a metal powder and become solid, then switch back to a gas when the fuel cell needs it.

Another promising line of research called cryo-adsorption uses hydrogen pressurized and refrigerated, but not to the same levels necessary to store gaseous or liquid hydrogen, said James A. Spearot, director of GM's chemical and environmental sciences lab.

VEHICLE DEVELOPMENT: GM's Burns plans fuel cell sales in 2010
BY MARK PHELAN
FREE PRESS AUTO CRITIC

General Motors Corp. research and development boss Larry Burns oversees fuel cell development projects at dozens of sites on several continents. Burns is one of the auto industry's most enthusiastic fuel cell boosters.

He spoke about prospects for the technology during a recent visit to labs in California.

QUESTION: When will GM have a fuel cell vehicle ready for sale?

ANSWER: In 2010, we will have in place a fuel-cell system that's production validated and ready to go head-to-head with internal combustion engines. It will have to produce power for $50 per kilowatt, the same as a gasoline engine. It will have a 300-mile cruising range and a 6,000-hour or 150,000-mile life. That's when we can tell people there's another game in town as well as the internal combustion engine.

Q: That's when you'll have the system ready. When will I be able to walk into a dealership and buy a fuel cell car?

A: I'd be very, very disappointed if you couldn't buy a Chevrolet fuel cell powered vehicle by 2015. Not necessarily from a Chevy dealer in America, though. It could happen somewhere else first. With a fleet, maybe military vehicles, we could do it a lot quicker. We also intend to be the first automaker to sell one million fuel cell vehicles.

Q: Why are you so excited about fuel cells?

A: It's going to be a better car. It'll have better torque, it will be simpler to build and more reliable. This is an enormously exciting time.

FUEL CELL FUELS PROMISE
BY MARK PHELAN
FREE PRESS COLUMNIST

I don't know if the hydrogen fuel cell-powered Honda FCX I drove for a weekend is the wave of the future, but Lord, I hope so.

There's something inspirational about driving nearly 120 miles and producing no noxious emissions.

Carbon monoxide? Zero. Nitrous oxide? Nada. Carbon dioxide? Nyet. Particulates? Mais non, cher.

Just a trickle of lukewarm water from the tailpipe.

The biggest environmental hazard I encountered was the concern that I'd slip and fall when the water froze on my driveway.

The FCX four-door hatchback boasts the first fuel cell any automaker has developed that works in sub-zero temperatures, and I was the first writer to drive the car unsupervised for three days in real-world conditions.

Every automaker that can afford to is working to perfect the hydrogen fuel cell. Total investment in the research probably amounts to hundreds of millions of dollars a year.

That's a huge commitment, but this could be the beginning of the next industrial revolution -- virtually limitless fuel with no harmful emissions. The prospect makes engineers giddy, and they are all convinced that this is the silver bullet that could once and for all take the auto industry out of the environmental debate – if some important hurdles are overcome.

The FCX performed brilliantly, which is to say: just like a conventional car. Turn the key, it starts. Depress the accelerator and it goes.

The electric motor produces 107 horsepower and a muscular 201 pound-feet of torque. That's more torque than a sporty V6-powered Volkswagen Golf GTi, giving the FCX enough oomph that I inadvertently squealed its all-season Yokohama tires several times on Woodward Avenue.

The FCX's top speed is 93mph, and it more than held its own on highways and surface streets in and around Detroit. At 164in long and weighing 3,713lbs, the FCX is about 13in shorter and nearly 1,300 pounds heavier than a Honda Civic coupe.

Driving the FCX to the grocery store or to meet friends for coffee was no different from driving any subcompact hatchback, except it had less environmental impact than throwing away the wrapper from a candy bar.

As exalting as driving the FCX was, the car also comes equipped with an overwhelming irony: The car might run on the most plentiful element in the universe, but I had an eye glued to the fuel gauge all weekend because I was afraid I'd run out.

With its twin tanks full of hydrogen, the FCX has a maximum cruising range of 190 miles. That's less than two-thirds the range automakers figure a car needs to be practical.

Automakers have made huge advances in how their fuel cells work, but they're still stumped about how to store enough hydrogen on board. The Honda's two fuel tanks held hydrogen at 5,000psi and the consensus among automakers is that you need 10,000psi for a workable cruising range. Building tanks to meet that standard and withstand automotive crashes is still prohibitively expensive.

And then the nearest hydrogen filling station was about 2,000 miles away. DTE Energy has a facility in Southfield that creates hydrogen to generate electricity and refuel vehicles, but it's not ready for drive-up customers yet.

The FCX ran smoothly and dependably. It ran a systems check each time I started it. If I'd run the car within the last two or three hours, I received a "ready to drive" message on the dashboard after 10 seconds or less -- about as much time as it takes to put my cappuccino in the cupholder and fasten my seatbelt. After sitting out one sub-20 degree night, the check lasted about 37 seconds. The process took about 18 seconds after I let the car sit in sub-freezing temperatures for more than 24 hours, and the heater provided warm air less than a minute after startup.

From hood to hatch, the drive system consists of an 80-watt (107 horsepower) electric motor, a fuel cell under the passenger compartment floor, two hydrogen tanks under the rear seat and a capacitor to store electricity that sits behind the rear seatback.

In addition to the fuel cell, the FCX also produces electricity with regenerative braking. The capacitor stores electricity from both the fuel cell and the brakes.

The fuel cell generates electricity whenever the FCX is running, and the capacitor steps in when you accelerate hard or drive at high speed.

The FCX runs quietly, and what little noise it makes is more similar to an electric fan than a conventional engine. It's never as nearly silent as a hybrid-electric running in pure electric mode, however.

The FCX's hydrogen gauge predicted a cruising range of about 126 miles when I picked it up. I drove it nearly to the last atom and covered 117.2 miles.

Late on a particularly cold evening, a warning lamp appeared and a dashboard message flashed "power reduced."

That had no obvious effect on the FCX's operation, though, and my final 15 miles were as guilt- and emissions-free as the first mile I drove.

FIGURE B4: Honda FCX Fuel Cell Vehicle

- Top Speed Of 93mph and cruising range of 190 miles, using electric motor generating 107 hp and 201 ft-lb of torque
- The dual hydrogen storage tanks are located under the rear seats and are pressurized at 5000psi
- Overall length is 164in and weight is 3713lbs, which is 13in shorter and 1300lbs heavier than a Honda Civic coupe

FUEL CELL MAKER SETS GOAL

A leading developer of hydrogen fuel cells for automobiles announced a timetable for making the technology more feasible by 2010.

Ballard Power Systems Inc. of Burnaby, British Columbia, said Tuesday it would demonstrate a commercially viable fuel cell stack, which uses hydrogen fuel to generate electricity in vehicles, in five years. Ballard said by 2010 its fuel cell stack would be more durable, cost-effective and better able to start in freezing conditions.

The company said its road map would follow targets set by the U.S. Energy Department and help automakers chart the development of the technology.

"We're showing through our actions and not just words that this technology is real and by 2010 we'll be able to demonstrate its commercial viability," said Dennis Campbell, Ballard's president and CEO.

Fuel cells convert hydrogen and oxygen into water to produce electricity. Unlike batteries that go dead after the reactive chemicals are used up, fuel cells can be replenished with hydrogen and oxygen. The technology has been used in experimental vehicles and as a power supply for some buildings.

Nick Cappa, a DaimlerChrysler AG spokesman on advanced technology, said several steps would need to be taken before the technology could become widely used. DaimlerChrysler has more than 100 fuel-cell vehicles, the auto industry's largest fleet.

"Although it may be feasible for fuel-cell technology to make that leap in 2010, that does not necessarily mean the market is ready for it," Cappa said. "It does not necessarily mean the infrastructure will be there."

General Motors Corp. spokesman Scott Fosgard said the company has spent more than $1 billion on fuel-cell technology and has said it could be commercially viable by 2010.

Ballard is partially owned by DaimlerChrysler and Ford Motor Co., but Campbell said the technology would be "available to all comers" in the auto industry.

BMW MAGAZINE ARTICLE
The following article appeared in BMW magazine regarding the H2R hydrogen powered racecar and the 7-series hydrogen powered production vehicles.

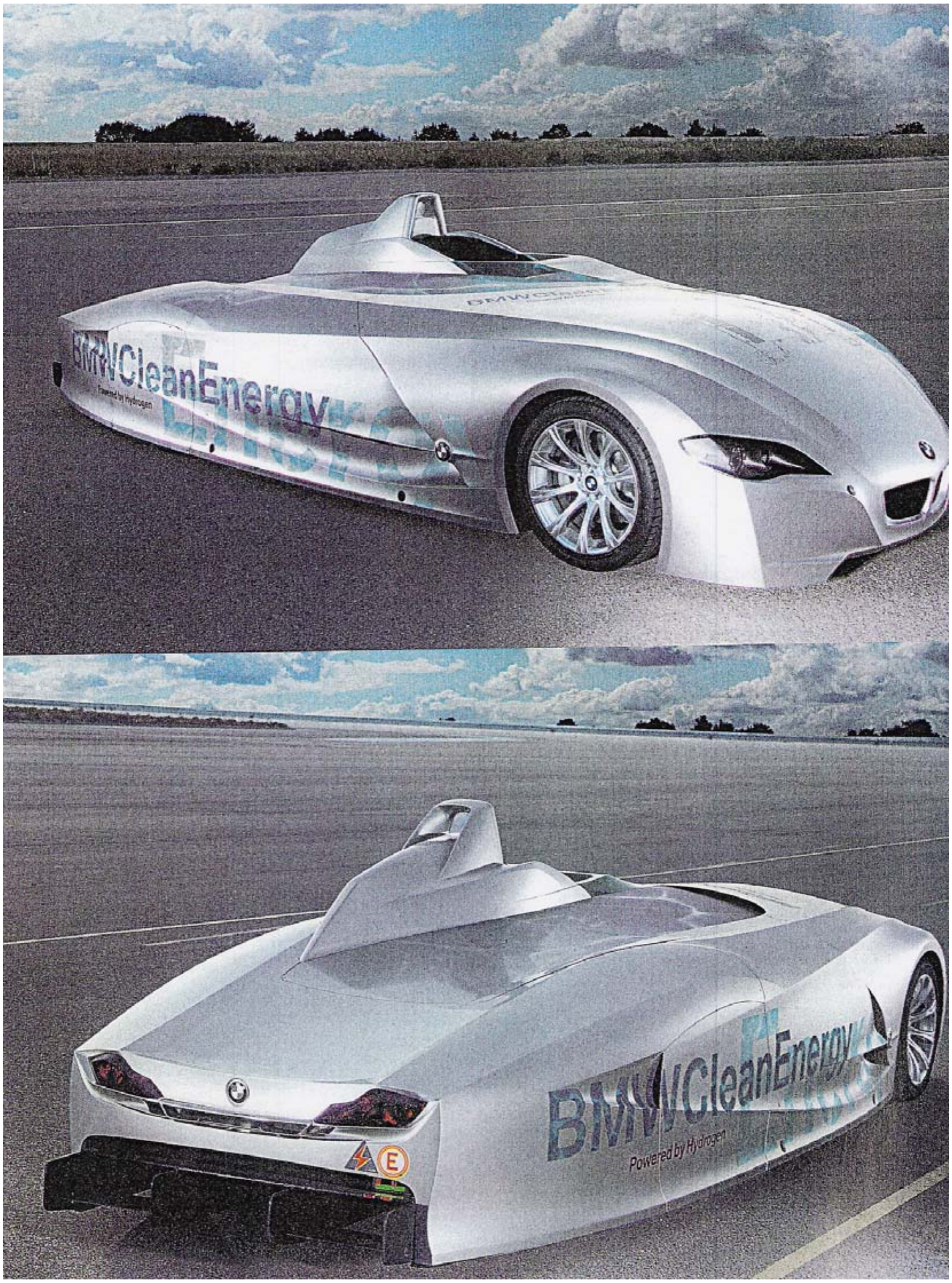

FIGURE B5

The H2R hydrogen-powered racecar breaking records on the test track at Miramas in south France. Burkhard Göschel, BMW Group's head of development (right), waves the checkered flag to indicate that the 300 kilometer-an-hour mark (186 mph) has been exceeded

Text: Michael Seitz

Spontaneously, the engineers and test drivers give vent to all the bottled-up tension – a last-minute triumph. They rush trackside, signaling the record-breaking run to the driver in the silver car: three raised fingers – 302.4 km an hour (187 mph). Fantastic! Even before the BMW H2R turns into the final stretch you feel it coming, as the wind pressure rattles the crash barrier. The low-slung racer shoots past at top speed and instantly disappears in the banked curve of BMW's test track at Miramas in south France. Its 12-cylinder engine burns hydrogen – the fuel of the future. With an output of over 285 hp, the H2R has established no less than nine international records for hydrogen-powered engines.

The experts see hydrogen as the up-and-coming energy source. It is the simplest, oldest and most abundant element in the universe, and our earth has it in virtually unlimited supply (although as a compound – H_2O, or water). To separate hydrogen (H_2) from oxygen (O), electricity – preferably generated by solar, wind or water power – is needed. The hydrogen thus produced can then be transformed into energy by engines or fuel cells.

Re-combining hydrogen with oxygen results in a highly volatile mixture. In the BMW engine, hydrogen combusts in the same, controlled manner as the conventional gasoline/air mixture. But there is one significant difference: under optimal conditions, burning hydrogen gas leaves little other than water vapor as a waste product.

Around the world, people look to a better future with energy produced from hydrogen. This smallest molecule could solve one of our greatest problems: dependence on fossil fuels, and the global warming caused by them, through increasing carbon dioxide levels. No one doubts that fossil reserves such as petroleum, natural gas and coal are running out. Although it's unclear exactly when, one day these sources will be completely gone. At the same time, the world's energy requirements are expanding more rapidly than once anticipated. It makes sense, then, to look for alternatives while there is still time.

BMW has a good deal of specialized experience with hydrogen technology. Sustainable mobility became a BMW concern very early on, and its engineers have

38 BMW Magazine

FIGURE B6

187.4 MPH

conducted research in this field since the late 1970s with great success. Between 2000 and 2002, a fleet of hydrogen-powered BMW 750hL cars covered a distance of some 105,000 miles (which amounts to circling the globe several times – another record). The research vehicles all bear a lower-case "h" for "hydrogen" in their model designation.

The BMW Group will soon be one of only a few manufacturers in the world to offer for sale a series production car powered by hydrogen technology. Hybrid power models will be available within the current 7 Series range. While providing the dynamic ride quality traditionally associated with BMW, they will have the ability to switch between gasoline and hydrogen fuel while on the move, thus making them independent of hydrogen refueling stations, which, as yet, are few and far between.

In the H2R, it is the 6.0-liter, 12-cylinder engine that has made the car a record-breaker. This is essentially the same engine as the one used in BMW's flagship model, the 760i. There is, however, a striking difference in the way the fuel is treated: in the series production engine, gasoline is directly injected into the combustion chambers. The modified hydrogen engine, on the other hand, prepares its mixture in the intake manifold directly in front of the combustion chamber. According to Klaus Borgmann, the head of engine development for the BMW Group, the direct injection of hydrogen is only a matter of time. "In test bench trials, the performance of these engines have jumped twenty percent."

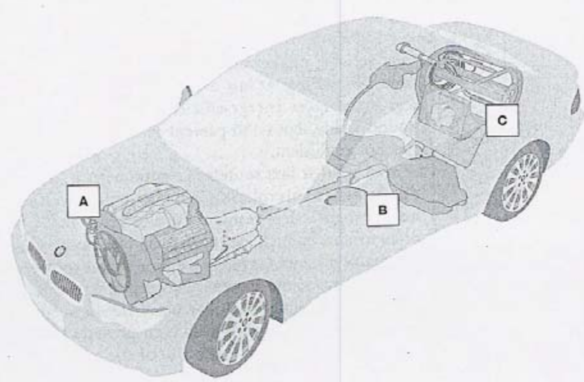

BMW 7 Series with hydrogen-powered engine

A Engine with hybrid drive for hydrogen and gasoline fuel

B Gas tank beneath the rear seat, as in series production models

C Special tank with high vacuum insulation for super-cooled liquid hydrogen

BMW Magazine 39

FIGURE B7

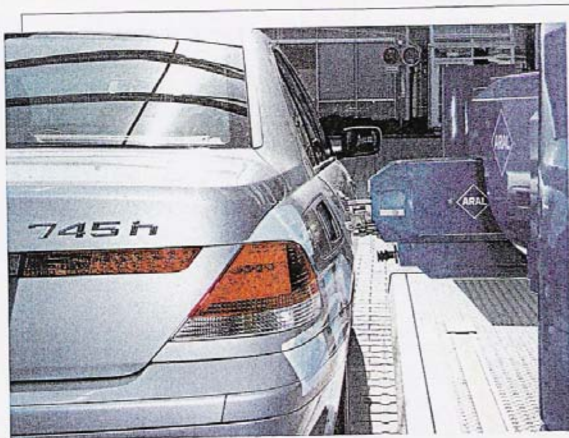

BMW IS ALREADY BUILDING THE FASTEST CARS FOR USE WITH THE FUEL OF TOMORROW

Robotic service: a BMW 745h takes on super-cooled liquid hydrogen at a fully automated refueling station at the Munich airport

Burkhard Göschel, the BMW Group board member responsible for development, also said of a markedly better performance as compared with conventional gasoline engines, "Our objective is to achieve a 50 percent increase in overall efficiency."

With its variable valve control system, the 12-cylinder engine is ideal for burning hydrogen. H_2 ignites more readily and burns more rapidly than gasoline. To avoid backfire from the intake manifold, the closing times of the inlet and outlet valves are synchronized by two BMW innovations: Valvetronic, the highly efficient, fully variable intake valve control system; and VANOS camshaft spacing. At just over 10 oz. per gallon, hydrogen is the most energy-efficient fuel by weight. One pound yields about 150 percent more energy than the gasoline equivalent.

But what at first sounds like good news is, in fact, a disadvantage. This colorless, odorless and tasteless gas is not only lighter than gasoline, but also lighter than air. In order to store enough hydrogen fuel to take a car over an acceptable distance (as set by gasoline engine standards), it must be made more dense. The gas is therefore either compressed or liquefied. Today, buses are already driving around cities and airports with high-pressure hydrogen tanks on their roofs. But the size of the tank, and the immense interior pressure of several hundred bar, make this quite impractical for ordinary cars. That leaves liquefaction. Hydrogen gas turns into liquid at -450° F, reducing its volume to around a thousandth of the original gas.

The special tanks used for this super-cooled hydrogen come from space technology. They were adapted by the BMW engineers to accommodate the features of a car and steadily improved upon for decades. The tank of BMW's record-breaker holds 24 lbs. of liquid hydrogen and is high vacuum-insulated. As with an oversized thermos flask, the 1 1/8-inch-thick special insulating space is the equivalent of 30 ft. of polystyrene casing. Crash tests have demonstrated that a hydrogen tank located at the rear of the vehicle poses no greater hazard than the normal gas tank. Refueling is a simple procedure, as can be seen at Germany's first hydrogen refueling station at the Munich airport. In a fully automated process, a special coupling links the filler neck with the tank nozzle and refueling takes no longer than filling the conventional gasoline or diesel tank.

Meanwhile, back at Miramas on this September Sunday, the record-breaking trials are over. An official from the FIA, motorsport's international governing body, inscribes a total of nine international records for the BMW H2R; some from a running start, others from a standing start. And what does this mean? That BMW is already building the fastest cars for tomorrow's environmentally friendly fuel.

bmwgroup.com/scienceclub
bmw.com/cleanenergy

40 BMW Magazine

FIGURE B8

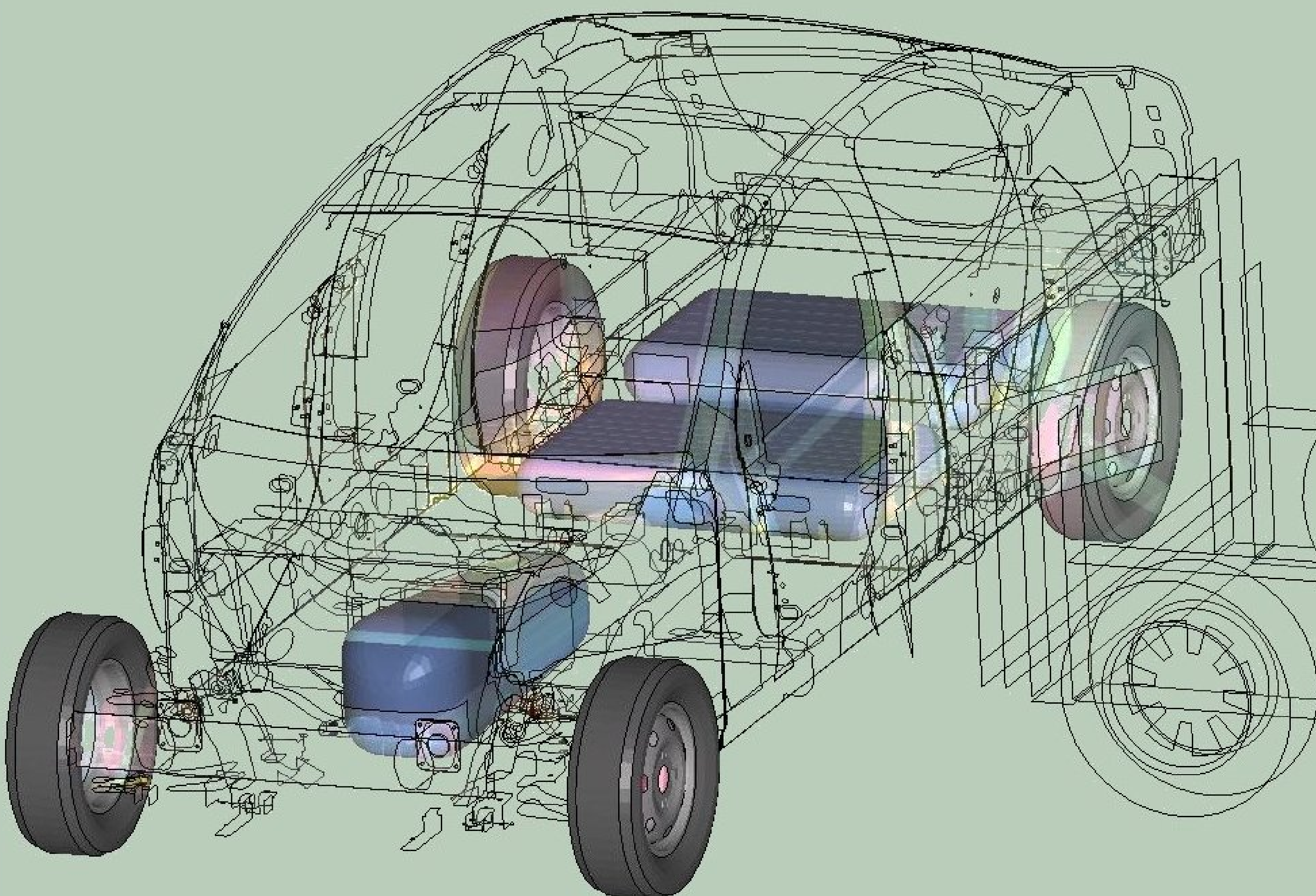

A/S P Auto/Steel Partnership

Future Generation Passenger Compartment
Task 2.0 - Calibration Report

Calibration of the baseline design, repackaging for both Fuel Cell & Diesel Powertrain options & CAE performance assessment

Task 2.0 – Calibration Baseline

Table of Contents

Task 2.0 - Calibration

1. INTRODUCTION

This report completes Task 2.0: Calibration Baseline of the FGPC (Future Generation Passenger Compartment) project. Its purpose is to document the design and packaging effort that provided a baseline configuration for the subsequent CAE assessment of vehicle performance for different crashworthiness scenarios.

A/SP provided the initial vehicle model, which was developed for the ULSAB-AVC program. The model was validated and used as the baseline configuration. Two variations were developed:

- Fuel cell power (FGPC-F)
- Conventional rear wheel drive with diesel engine (FGPC-D)

The following definitions are used throughout this report:

- ULSAB-AVC
  Ultra Light Structure Automobile Body-Advanced Vehicle Concept
- FGPC
  Future Generation Passenger Compartment
- FGPC-D
  Diesel Vehicle
- FGPC-F
  Fuel Cell Vehicle

2. OBJECTIVE

The goal of Task 2: Calibration Baseline is to provide evaluation of the Future Generation Passenger Compartment (FGPC) design for fuel cell and traditional engine configurations for five different crash performance attributes:

- FMVSS 208 Front Crash (US-NCAP)
- IIHS Front Crash
- IIHS Side Impact
- FMVSS 301 Rear Crash
- FMVSS 216 Roof Crush

The objective of this effort is 1) to compare the FGPC vehicle performance with ULSAB-AVC in all the above-mentioned attributes and 2) to compare the performance of the fuel cell and traditional engine configurations for each crash attribute and then use the worst case to evaluate the performance of the vehicle with new underbody design.

3. NEW UNDERBODY FUEL CELL PACKAGING AND DESIGN

A new underbody was designed based on the ULSAB-AVC vehicle platform for FGPC. The new underbody was modified and packaged to allow the vehicle structure to be capable of having two different types of drive train: traditional rear drive diesel engine and fuel cell power. FGPC team members developed fuel cell packaging requirements based on information gathered in the benchmarking phase and from the OEM's (GM, FORD and DCX). These requirements include the mass of fuel cell components, and volume of fuel cell tanks and modules. The packaging and design of the new underbody was targeted in a way that the volumes of the fuel cell storage tanks are maximized and shapes of the fuel cell tank are acceptable to be manufactured today or by 2010. The final design of the fuel cell modules includes two oblong-shaped tanks under rear seat and a conical-shaped fuel cell tank under the modified center tunnel.

The FGPC program vehicle targets were developed based on ULSAB –AVC Performance targets:

1. Front Crash – Meet US-NCAP and IIHS 40% ODB Impact structure performance
2. Rear Crash – Meet FMVSS 301
3. Side Impact – Meet IIHS Dynamic Side Impact
4. Roof Crush – Meet FMVSS216

The scope of the design and packaging effort includes the following tasks:

- Review available space for packaging
- Determine and subsequently maximize volume of fuel cell storage tanks
- Develop alternative body design options
- Review sections of fuel cell storage
- Evaluate possible alternative shapes for fuel storage if applicable
- Study possible concessions in packaging
- Incorporate suspension data (if available)
- Establish material thickness of fuel storage containers

The first portion of the design study was to determine the overall volume of the space that was available for fuel cell storage using the existing ULSAB-AVC vehicle structure.

The packaging of the components for the fuel cell option was determined using dimensions obtained from the FGPC team. These components (fuel cell stack, batteries and electronic box) were positioned in strategic areas and reviewed by the committee members to best determine a viable location. The repositioning of the components in the front engine compartment was the starting point for all components and acceptability would be determined using the analytical front-end crash results.

Multiple fuel cell shapes and sizes were packaged to determine the actual fuel storage area that would be available with the existing structure and possible alternative revisions that could be manufactured were determined. A revision to the tunnel area in size and shape was one option along with other revisions to the existing structure. Some considerations include:

Future Generation Passenger Compartment (FGPC)

- The width of the tunnel remained the same and the joint connections to the rail members did not change. The height of the tunnel was raised, holding the front portion at its present height but raising the rear connection to the rear floor pan and kick-down panel as high as possible; this would impact the middle rear seat passenger (Figure 1).

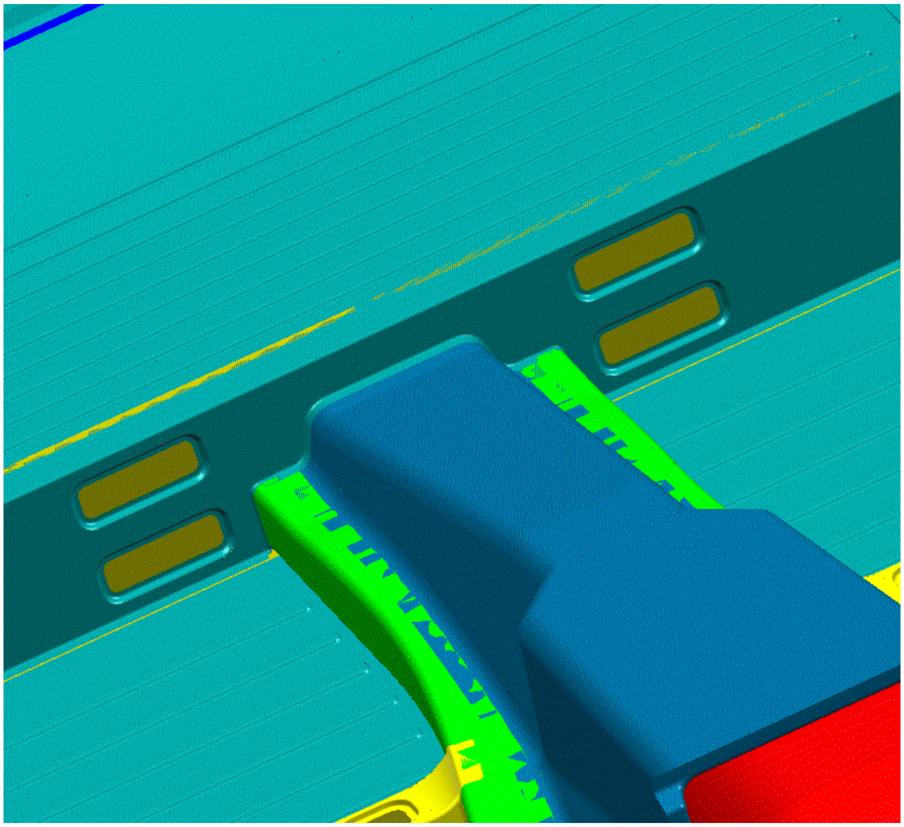

FIGURE 1: Raised Rear Transmission Tunnel

- Alternative shapes other than cylindrical were considered (oblong, conical and irregular). These would be held as possible options and would be packaged with the various revisions to the current structure (Figures 2-4).

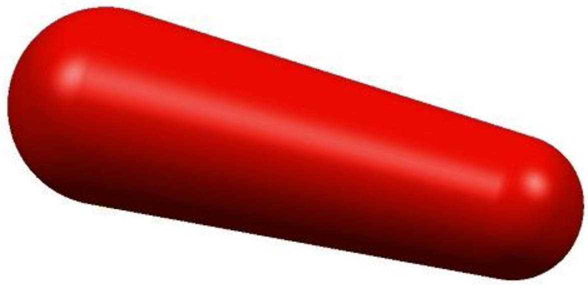

FIGURE 2: Tunnel Fuel Storage - Cone Shape 79,390,000mm³ & 20.65kg

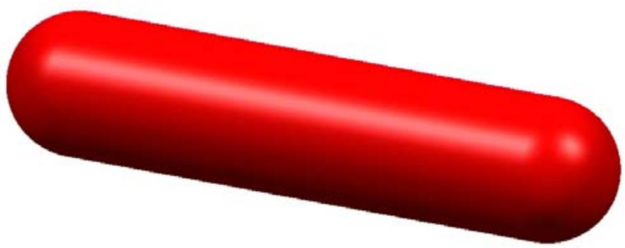

FIGURE 3: Tunnel Fuel Storage - Cylindrical Shape 50,710,000mm³ & 13.18kg

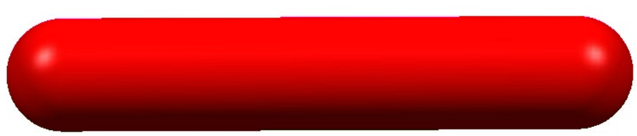

FIGURE 4: Under Rear Seat & Trunk - Cylindrical Shape 23,920,000mm³ & 6.22kg
(Six Tanks Utilized, 3 Under Seat & 3 Under Trunk. Total 143,520,000mm³ & 37.32kg)

- After initial review of the various fuel cell storage alternatives with the team, one fuel cell tank would be considered in the tunnel and cylindrical tanks or oblong tanks would be considered under the rear seat and trunk. After reviewing all the design options, it was decided that an irregular fuel cell shape would be used for the tunnel space to maximize the volume (94,450,000 cmm at 24.56kg) (Figure 5). An oblong shape would be used under the rear seat and the depression for the cushion on the floor in that area would be eliminated in order to maintain maximum height for the fuel cell tank (95,950,000 cmm at 24.96kg) (Figure 6). Another oblong fuel cell tank of duplicate shape and size would be positioned under the trunk floor. Figures 7 - 9 show the fuel tanks position in the vehicle. Brackets were developed to support the fuel cell storage tanks. No revision was made to the trunk floor for packaging the storage tank. While reviewing the fuel tank proposals of Figures 6 & 7, the reader may question the shape of such pressure vessels. However, it should be noted that these are low-pressure vessels and that the FGPC team did gain confirmation of their manufacturability.

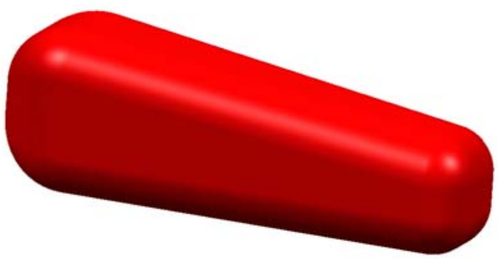

FIGURE 5: Final Front Fuel Tank Shape

FIGURE 6: Final Rear Fuel Tank Shape

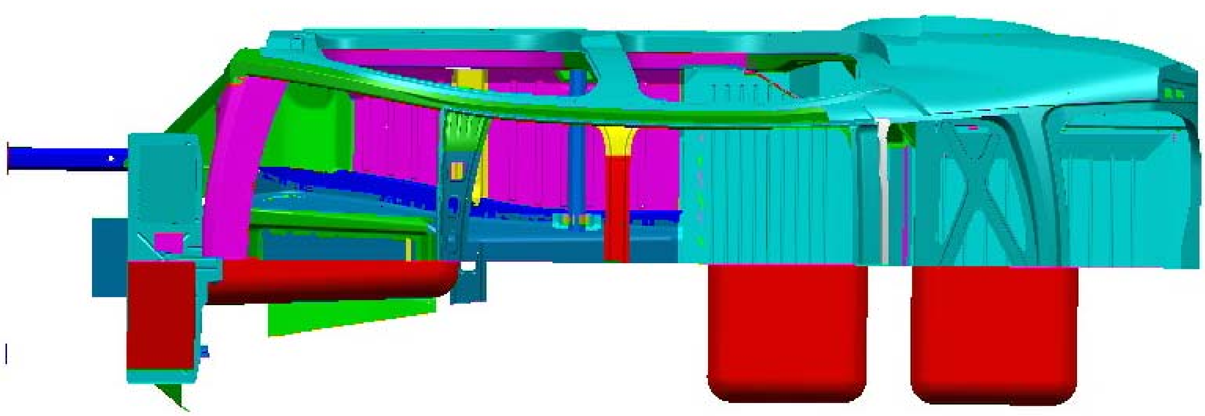

FIGURE 7: Centerline Split Top View Showing Body Structure & Fuel Tanks

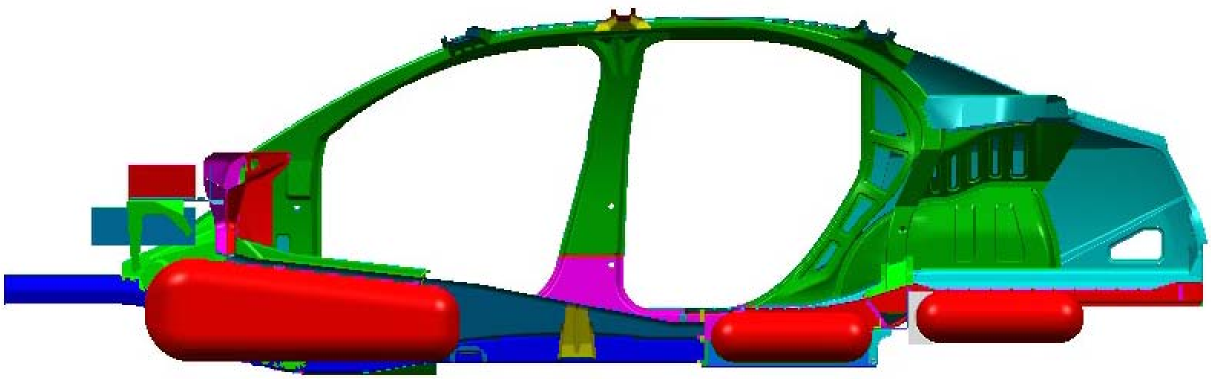

FIGURE 8: Centerline Split Side View Showing Body Structure & Fuel Tanks

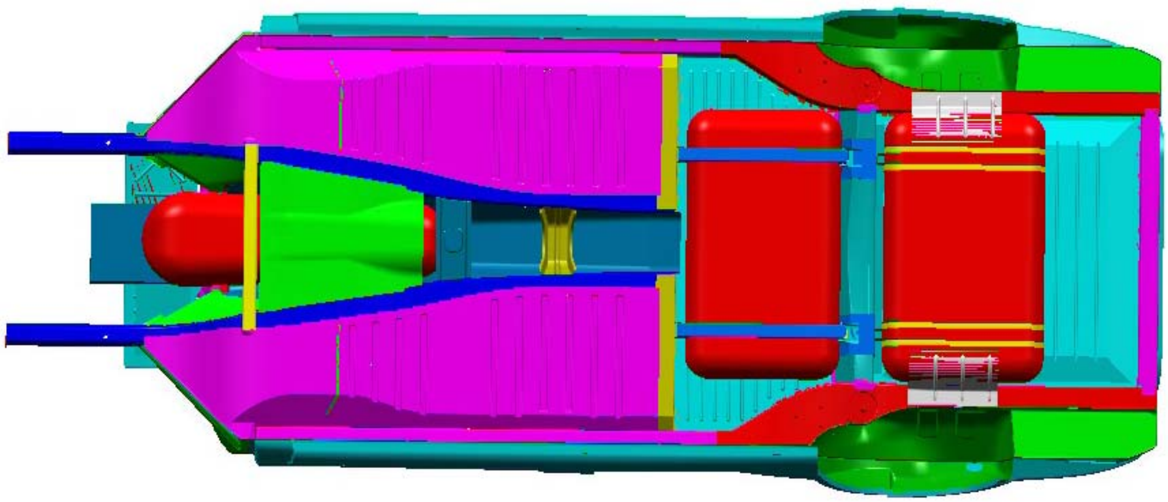

FIGURE 9: Underbody Showing Fuel Cell Tank Locations & Tunnel Fuel Shield

- A possible revision to the rail member was evaluated by straightening its shape from the front seat to the rear running parallel to the centerline of the vehicle. This could possibly obtain additional width at the tunnel between the rails and create more space for fuel cell storage. If feasible, this would change the width of the tunnel and could possibly affect the rear seat passenger's foot clearance (Figure 10).

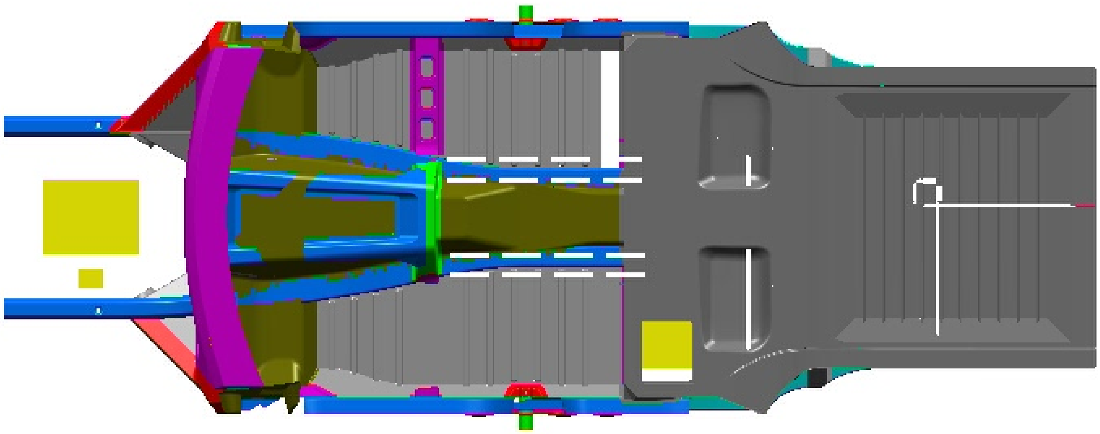

FIGURE 10: Straight Rail Transmission Tunnel

- The fuel cell storage in the rear compartment area (trunk) could only be utilized in the forward area because of the intrusion zone identified from the rear impact analytical run. This would be taken into consideration when attempting to package the fuel cell storage in this location.

The existing ground clearance was a determining factor for the size and location of many of the fuel cells, and was therefore used as a guideline for the packaging of the fuel cells.

To accept the height change and shape through the tunnel area, crossmembers were redesigned and the kick-down area from the front to rear floor was revised (Figure 1).

The crash results showed buckling in the floor pan at the tunnel in the kick-down area. This was possibly due to the kick-down area on the floor and the kick-down reinforcement being revised from the original design. It was agreed to revise this area and to obtain a cross-car vertical wall connection on the floor pan, tunnel, and the reinforcement. The kick-down reinforcement would then revert to a single piece part. The tunnel would also be revised to accommodate this change.

The straightening of the rail members was eliminated from the options due to intrusion into the foot space of the rear seat passenger.

Fuel cell components were packaged under the hood and a front package tray was designed to support these components.

The tubular support extending laterally that was utilized as an attachment point for the rearward portion of the front seat was revised due to the height of the tunnel being raised. The original design crossed over the top of the tunnel but had to be cut off at the tunnel because of the height change (Figure 11). A connecting bracket was placed at either side of the tunnel to accommodate the attachment of this tube. A bracket was designed in the tunnel at this location in an attempt to continue the flow of a cross car support from a side impact.

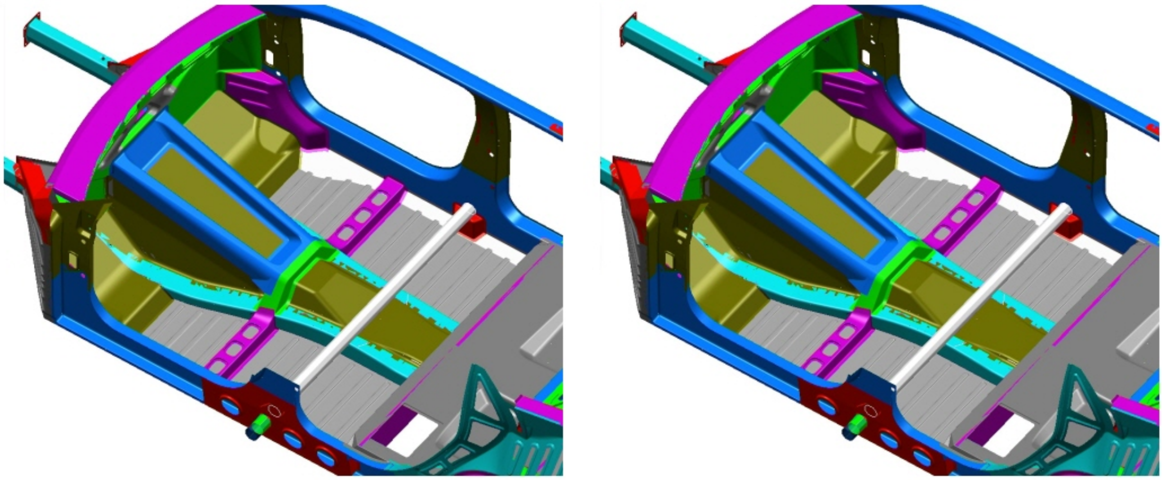

FIGURE 11: Redesigned Cross-member (Left – Original, Right - Revised)

The team wanted the configuration of the top of the tunnel to the rear floor to have the same plane transition, meaning the top of the tunnel would be at the same height as the rear floor at the rear seat area. The step down area on the revised tunnel was changed per the request from the previous meeting. This made the rear kick-down reinforcement two parts compared to one in the original, because of the height of the tunnel. The joint connections to the tunnel were revised to accommodate the change. The front tunnel reinforcement was also revised to agree with the tunnel revision, and it kept its basic shape with minor alterations.

A shield was designed for the tunnel fuel cell trying to incorporate two functions:

- Utilize as a support for the fuel cell tank
- Utilize as a protective barrier

Brackets for the front shield were designed to assist in supporting the shield, and the shield was revised to better accommodate the routing of the fuel cell lines (Figure 9).

To strengthen the upper load path for side impact, a roof bow was designed at the B pillar similar to the roof bow used on the C-Class vehicle. Subsequent analysis results showed the roof bow needed revision, so three separate roof bows were designed:

- Move roof bow rearward to be more inline with the B-pillar from the side view (Figure 12)
- A wider roof bow was positioned strategically at the B-pillar (Figure 13)
- A double roof bow in the area of concern at the B-pillar along the side roof rail (Figure 14)

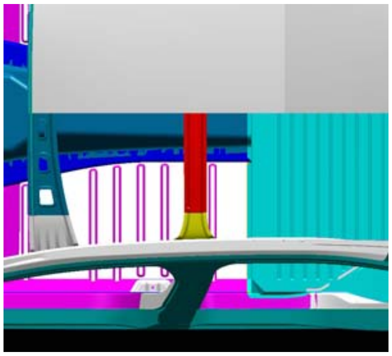

FIGURE 12: Roof Bow At B-Pillar

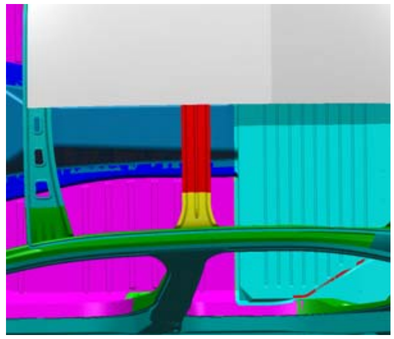

FIGURE 13: Wider Roof Bow

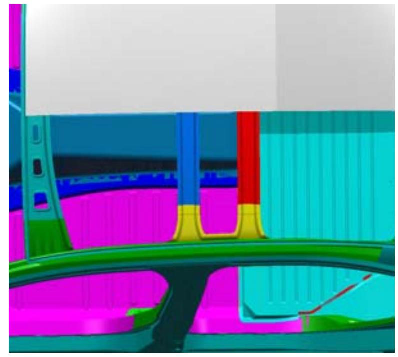

FIGURE 14: Double Roof Bow

The front-end crash results showed intrusion of the motor into the shield and tank. The shortening of the tunnel fuel cell tank will be investigated based on additional information for tank hook-up. The fuel cell motor dimensions were revised slightly to address the front-end crash intrusion. The original volume was maintained but the front of the box was set further rearward.

4. CONCLUSIONS

4.1. FRONT IMPACT

NCAP – Uses Baseline Model

Simulation results for front impact analysis indicate that the performance of FGPC-D case is similar to the ULSAB-AVC model, whereas the FGPC-F performance degraded compared to ULSAB-AVC. The front fuel cell tank contacted the electric motor/gear box causing a higher deceleration pulse, which resulted in lower dynamic crush resistance.

IIHS-ODB – Uses Baseline Model

Simulation results for Offset impact analysis indicate that the performance of FGPC-F vehicle degraded from the ULSAB-AVC model as the fuel cell foot well intrusion is much greater than the FGPC-D model. The reason is because the subframe impacts the fuel cell tank causing an increase in bending of the longitudinal rails.

In summary, the evaluation of the vehicle performance of both drivetrains for NCAP and IIHS case showed that Fuel Cell Engine configuration is the worst case compared with the traditional engine configuration. Also, the vehicle will not meet NCAP flat rigid barrier and IIHS front crash structural performance requirements with the fuel cell powertrain. In the fuel cell configuration, the conical front fuel storage tank will be impacted by the motor/transmission and will cause fuel cell tank structural failure. The IIHS vehicle performance measure was moved from good status to acceptable level; also the fuel cell tank was impacted by front structure components causing failure.

4.2. SIDE IMPACT – USES BASELINE AND MODIFIED MODELS

In IIHS side impact regulation, the vertical range considered for the structural rating extends from the base of the B-pillar interior up to a point that is 540mm above the H-point measurement taken with the seat in the full-rear and full-down position (Reference Figures E2-E3 in Appendix E). The results values from analysis are summarized in Table 1 below.

	BASELINE MODEL (mm)	**MODIFIED MODEL* (mm)**	**REMARKS****
Fuel Cell	85	100	29.4%
Diesel	70	105	50.0%

*Added tunnel & roof bow, modified rear floor cross-member
**Improvements based on Iteration #1

Table 1: Side Impact Results Summary
Distance Between B-Pillar & Seat Centerline (Reference Figure 15)

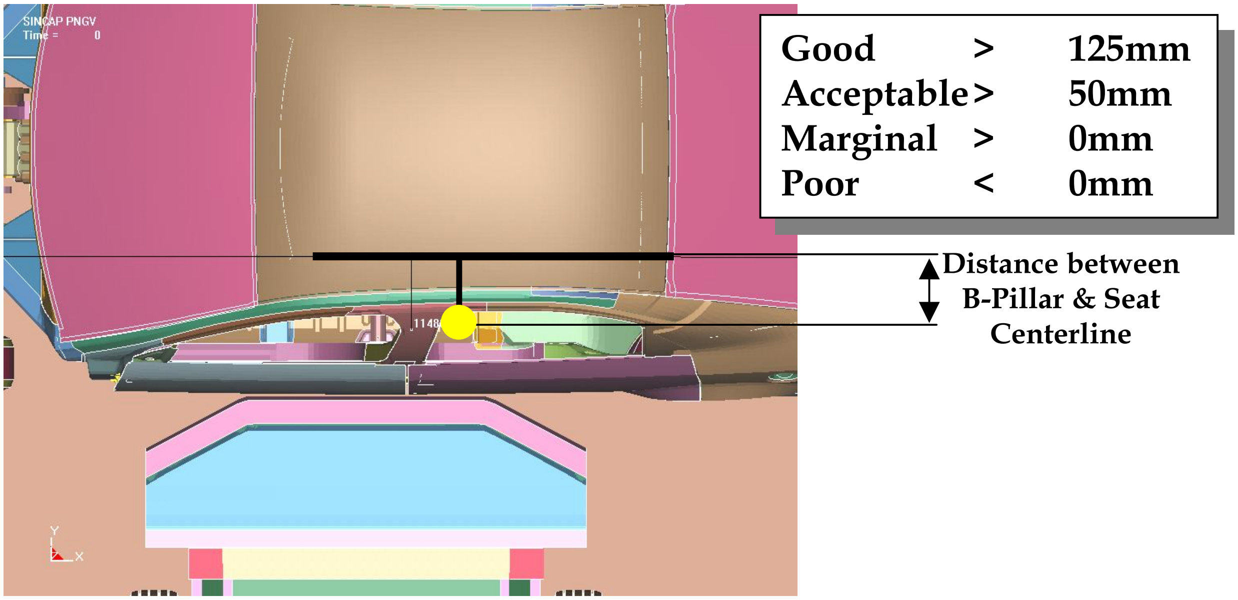

FIGURE 15: Side Impact Measurement Definition

Evaluation of the vehicle side impact performance for each drivetrain configuration showed that both the traditional engine and fuel cell configurations showed weakness. A roof bow was added at the B-pillar to side rail intersection in order to improve the performance of both vehicle configurations that have different mass distributions. The results showed that vehicle performance is below "good" status (125 mm intrusion, see IIHS side impact requirements) for both conditions. However the results showed that vehicle structural performance with the conventional engine is lower than fuel cell powertrain case. The conventional engine configuration is therefore identified as the baseline for the IIHS side impact optimization study, which is Task 3: Optimization of this project.

4.3. REAR CRASH – USES BASELINE MODEL

The worst-case evaluation of the rear crash vehicle performance showed that the fuel cell configuration performs the worst in comparison with the traditional engine design. Analysis results showed that the modified ULSAB-AVC vehicle would meet rear crash FMVSS 301 requirements for both drivetrain cases. The oblong fuel cell and traditional engine fuel tank would survive and there would not be any fuel leakage.

Simulation results for rear impact analysis indicate that both the diesel and fuel cell configurations of the FGPC can withstand the 35 mph rear impact test without fuel tank damage.

The fuel pipe of the diesel model has some plastic (permanent) deformation, but the value is small; only 3 % plastic strain. The diesel fuel tank is well secured.

4.4. ROOF CRUSH – USES BASELINE MODEL

The vehicle would meet roof crush targets for both drivetrains. The worst case would be the heavier vehicle, which would be the fuel cell vehicle, because the force requirement is based on vehicle mass.

5. VEHICLE FINITE ELEMENT MODEL AND ANALYSIS ASSUMPTIONS

5.1. MODEL DESCRIPTION

The original ULSAB-AVC model was used as a baseline and modified to accommodate the fuel cell system configuration and some structural and modeling changes to improve the side impact crash performance. A more detailed description of the modifications is included in Section 2.6.3.2. Figure 16 shows the fuel cell model unique components. A common attribute model philosophy was used so the same model could be used for all the crash analysis types. The full finite element model is shown in Figure 17. The models have an approximately 15~20 mm mesh size throughout.

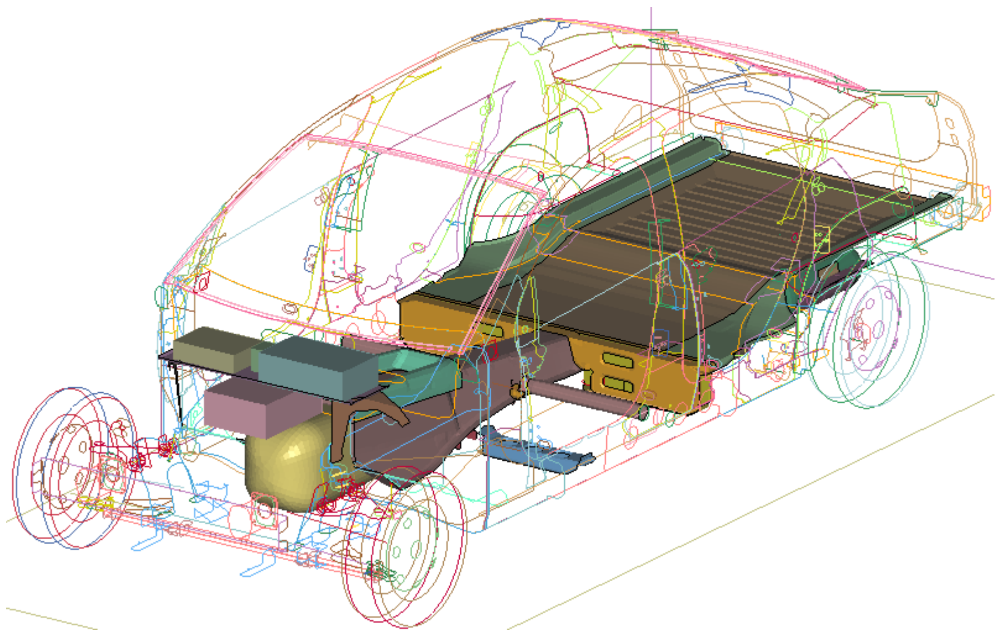

FIGURE 16: Fuel Cell Model Components

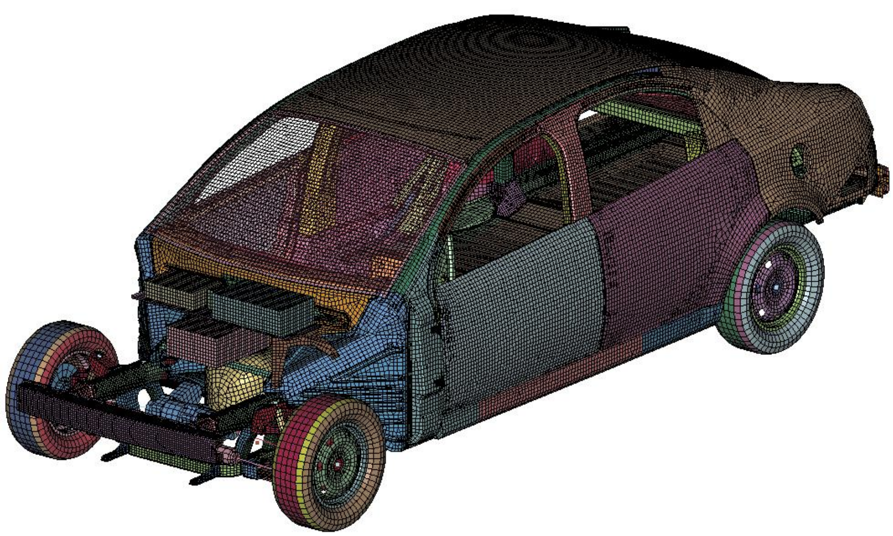

FIGURE 17: Fuel Cell Finite Element Model

Parts modified in both models

- Rear Floor
- Tunnel
- Cross Member Kick–down
- Front Cross Member Support
- Rear Seat Cross Member and Reinforcement-Tunnel.

Parts newly created in both models

- Cross member
- Tunnel and Mounting Bracket Upper/Lower
- Cross member Support Front Seat Rear.

Parts newly created for fuel cell model only

- Front Fuel Cell and Rear Fuel Cell Front/Rear Tanks
- Front Fuel Cell Mounting Brackets
- Front and Rear Fuel Cell Mounting Brackets and Supports
- Battery Tray and Support Bracket
- Battery Center/LH
- Electronic Box
- Fuel Cell Stack

	PART	NODE	SHELL	SOLID	BEAM	DISCRET	MAS	NODAL
Fuel Cell	327	222,111	214,257	1,028	296	92	126,197	7,068
Diesel	319	206,370	199,325	1,028	298	94	122,695	6,842

TABLE 2: Model Statistics (Common Attribute Model)

Figures 18 and 19 show the side impact moving deformable barrier and front impact offset deformable barrier finite element models respectively.

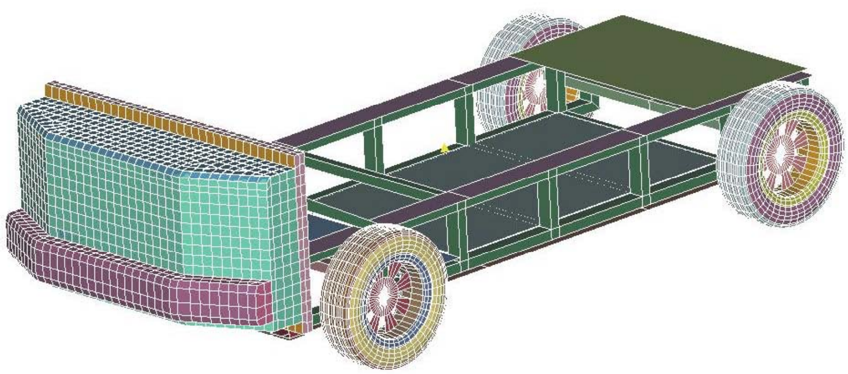

FIGURE 18: Side Impact Moving Deformable Barrier Model

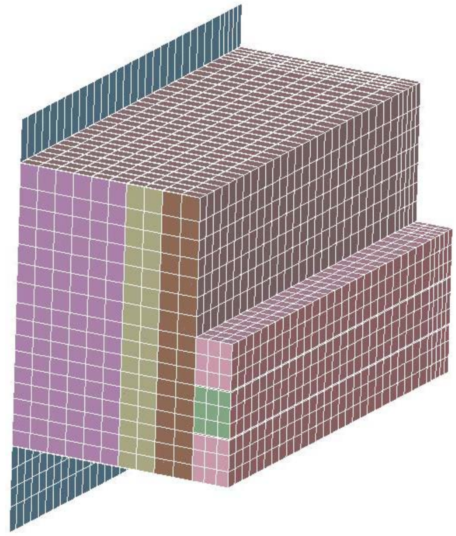

FIGURE 19: Front Impact Offset Deformable Barrier Model

Mass Distribution
The vehicle analytical test mass for the FGPC-D diesel model is defined to be base curb weight (1102 kg) plus occupants (two 50th percentile male dummies), luggage and optional equipment mass (286 kg), for a total mass of 1388 kg. Similarly, the curb weight for the FGPC-F fuel cell model is 1159 kg, and includes three fuel cell storage tanks (75 kg), fuel cell stack (100 kg), battery1 (56 kg), battery2 (12 kg), electronic box (14kg) and electric motor/gearbox (40kg). The total mass for the FGPC-F vehicle is 1445 kg, which is the curb weight plus the occupants, luggage, and optional equipment.

The mass of non-structural components that were not modeled as structural parts was spread out using lumped masses. The strategy for applying these lumped masses was updated after the completion of the Task 2: Calibration Baseline phase of the project, to better reflect the actual mass distribution in the vehicle, and will be described in a subsequent report.

A more detailed summary of mass distribution in the models is shown in Appendix A.

5.2. MASS PROPERTIES
Material properties used in model are included in Appendix B.

5.3. ANALYSIS ASSUMPTIONS
- The rigid barrier for front crash was simulated as a fixed rigid wall in front of the vehicle normal to the longitudinal axis of the vehicle with the friction assumption of 0.80.
- The offset deformable barrier for front crash with an overlap of 40% of the vehicle width was used.
- All welding connections were modeled by rigid connections.
- Airbag tires are used.
- No failure is assumed in the material
- Strain rate effects are considered

6. FRONT CRASH

6.1. NCAP

6.1.1. REGULATIONS

Detailed specifications are described in Appendix C.

6.1.2. LOADS AND BOUNDARY CONDITIONS

The vehicle is impacted to rigid wall with a speed of 35 mph (see Figure 20 and 21). The Baseline model was used in this analysis.

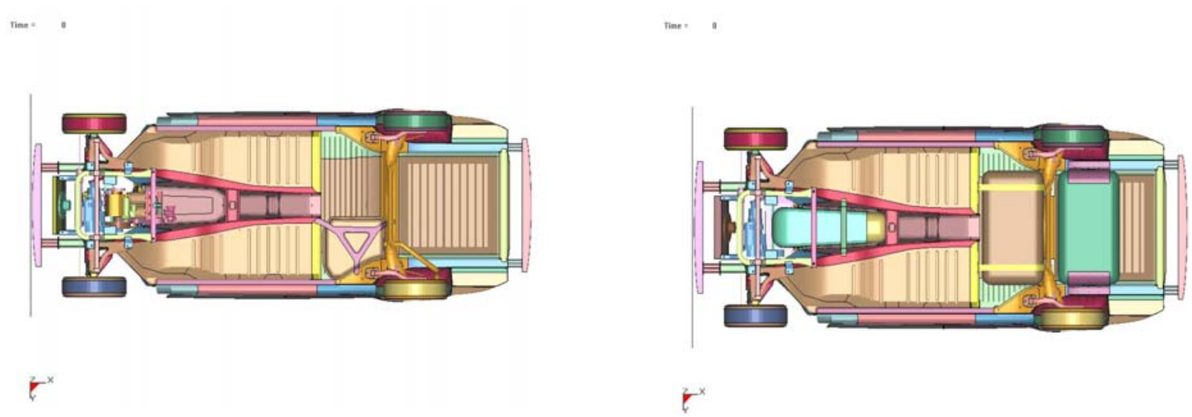

FIGURE 20: NCAP Bottom View Of Undeformed Structure Of Both Vehicles

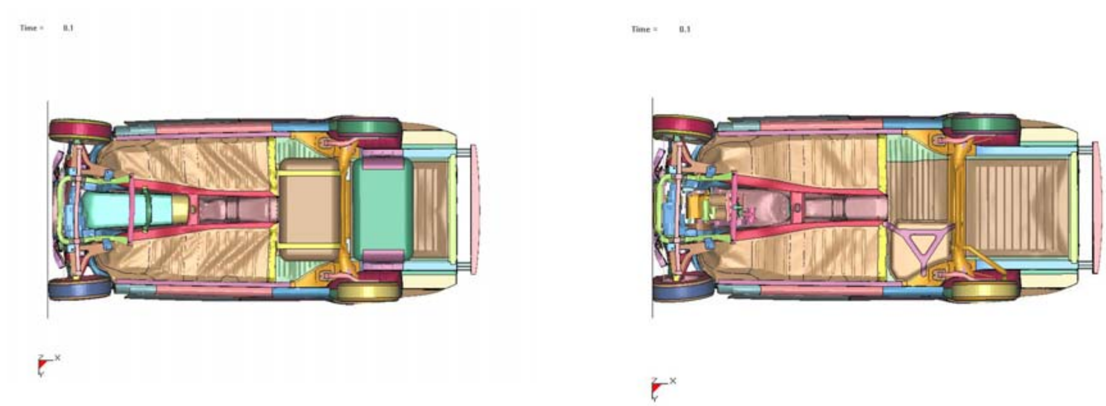

FIGURE 21: NCAP Bottom View Of Deformed Structure Of Both Vehicles

6.1.3. RESULTS

Displacement and velocity measurements in key areas and critical locations were compared to identify the worst case between the two vehicles.

FUEL CELL VEHICLE

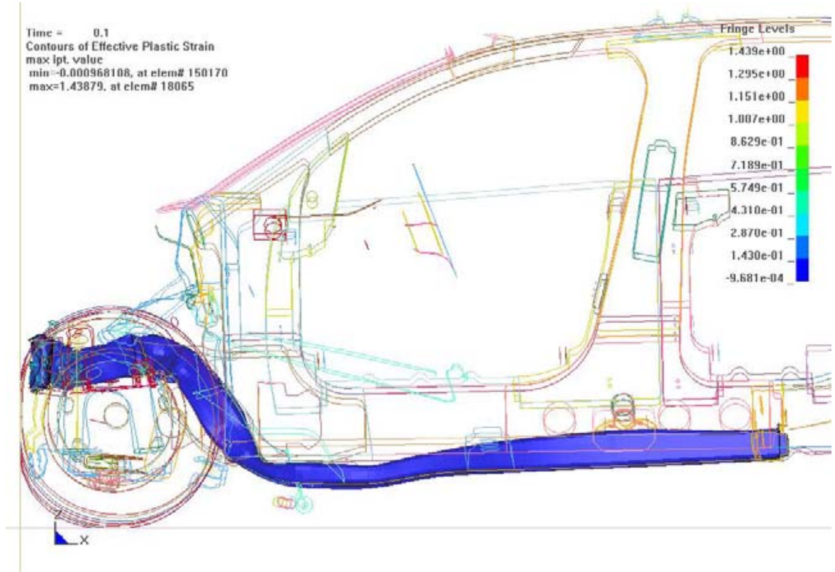

DIESEL ENGINE VEHICLE

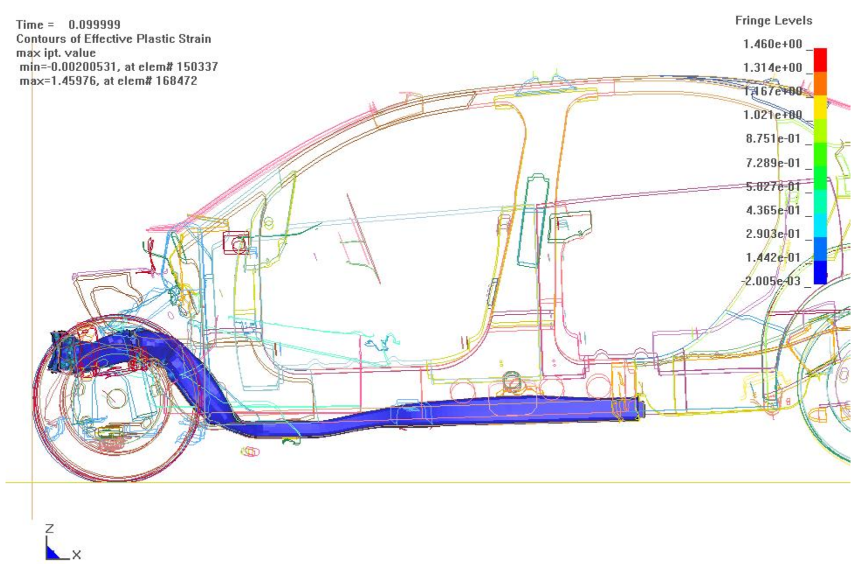

FIGURE 22: Front Longitudinal Member Buckling Mode Comparison

Figure 22 shows a comparison of the deformed shape of the longitudinal members for both vehicles.

Figures 23, 24 and 25 shows displacement, velocity and acceleration vs. time measured at the B-pillar for ULSAB-AVC **(A)**, FGPC with Diesel (FGPC-D) **(B)** and FGPC with Fuel Cell (FGPC-F) **(C)** powertrain configurations respectively.

The displacements of A and B are very close, and C is less (Figure 23) which corresponds with the velocity deceleration in Figure 24, which shows the FGPC-F velocity decreases to zero more quickly. Figure 25 shows higher average acceleration for the FGPC-F between 50-60 msec, and the deceleration occurs earlier than other two vehicle curves.

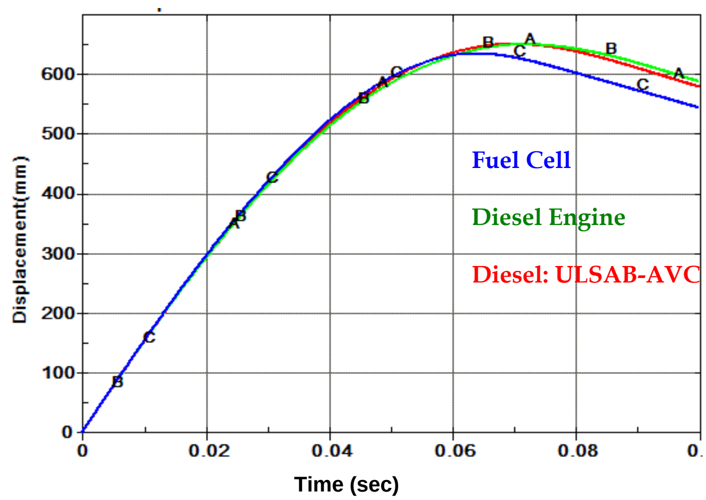

FIGURE 23: B-Pillar Displacement Comparison

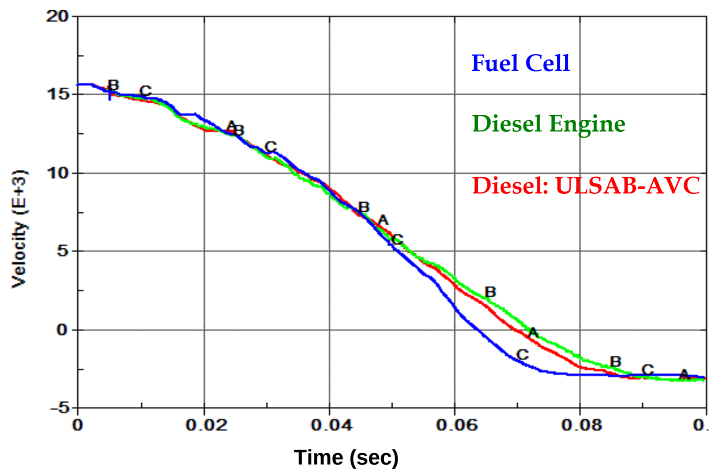

FIGURE 24: B-Pillar Velocity Deceleration Comparison

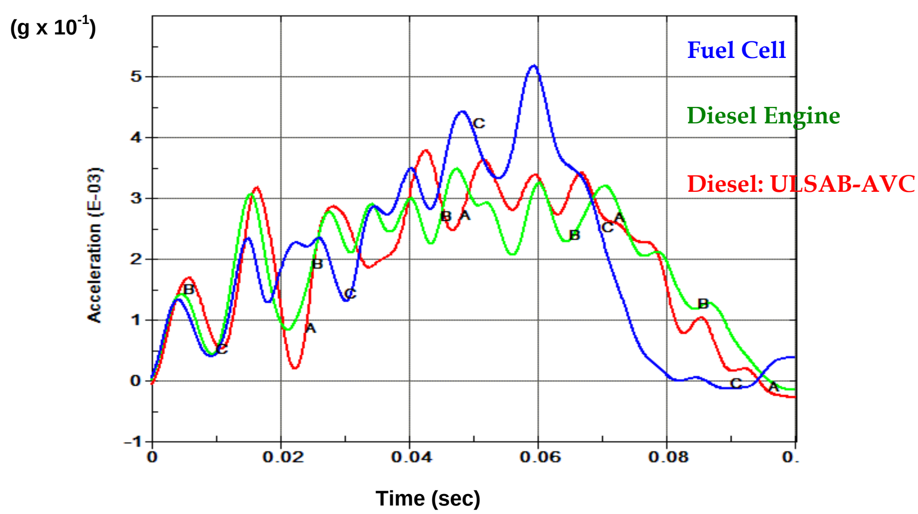

FIGURE 25: B-Pillar Acceleration Comparison

Absorption of kinetic (impact) energy of the vehicle structure, acceleration pulse, dynamic crush and time to zero velocity were measured to evaluate the structural strength for all three-vehicle configurations (TTZV is the time to zero velocity). See Table 3.

	ENERGY (J)	PEAK ACCEL. (g)	DYNAMIC CRUSH (mm)	TTZV (msec)
Diesel-ULSAB-AVC	8091	37036	651	69.9
Diesel-Engine	7866	34.39	651	72.4
Fuel Cell	8065	51.02	635	63.9

TABLE 3: Results Summary for all three configurations

The results of the FGPC-D and ULSAB-AVC are the same, however the fuel cell tank configuration would impact into transmission, causing higher peak acceleration values.

6.2. IIHS FRONT CRASH 40% ODB

6.2.1. REGULATIONS

Detailed specifications are described in Appendix D.

6.2.2. LOADS AND BOUNDARY CONDITIONS

The fuel cell and conventional vehicles are impacted into a deformable barrier with a 40% offset (OBD) at a speed of 40 mph (see Figures 26 and 27). The Baseline model was used in this analysis.

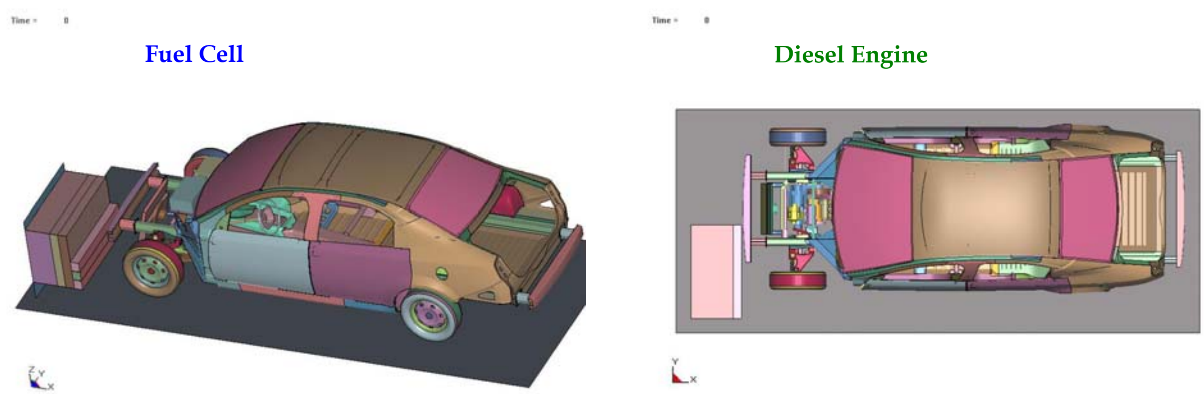

FIGURE 26: IIHS Front Crash - Both Vehicles

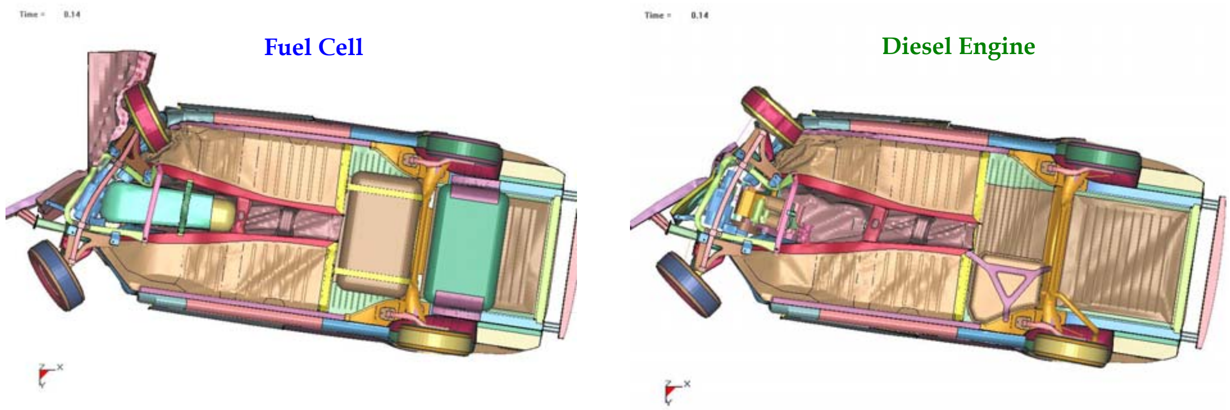

FIGURE 27: IIHS ODB Deformed Shape - Both Vehicles

6.2.3. RESULTS

Displacement measurements in key areas and critical locations were compared to identify the worst case between the two vehicles.

Residual footwell intrusion, steering column rear movement and A-pillar displacement were measured to evaluate the structural strength for all three-vehicle configurations. See Table 4.

40% OFFSET	**TARGET (mm)**	**DIESEL ULSAB-AVC (mm)**	**DIESEL-ENGINE (mm)**	**FUELCELL (mm)**
Max Residual Footwell Intrusion	<150	133	109	145
Steering Column Rear Movement	<80	21	12	13
A-Pillar Displacement	<50	11	3	5

TABLE 4: Results Summary for all three configurations

Figures 28, 29 and 30 show resultant foot well intrusion, steering column movement and A-pillar displacement vs. time measured for ULSAB-AVC **(A)**, FGPC with Diesel (FGPC-D) **(B)** and FGPC with Fuel Cell (FGPC-F) **(C)** system respectively.

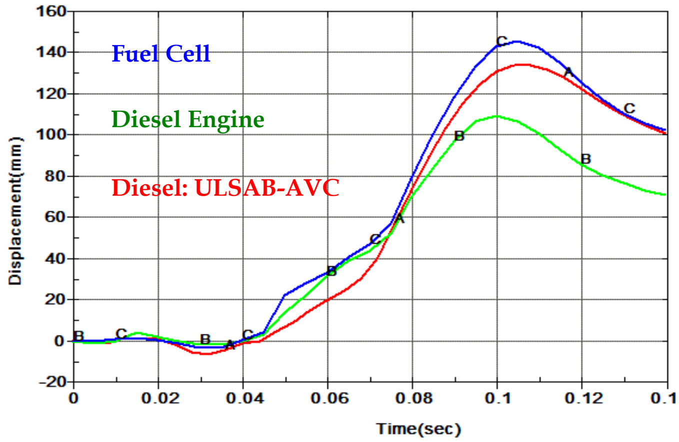

FIGURE 28: Resultant Foot Well Intrusion Comparison

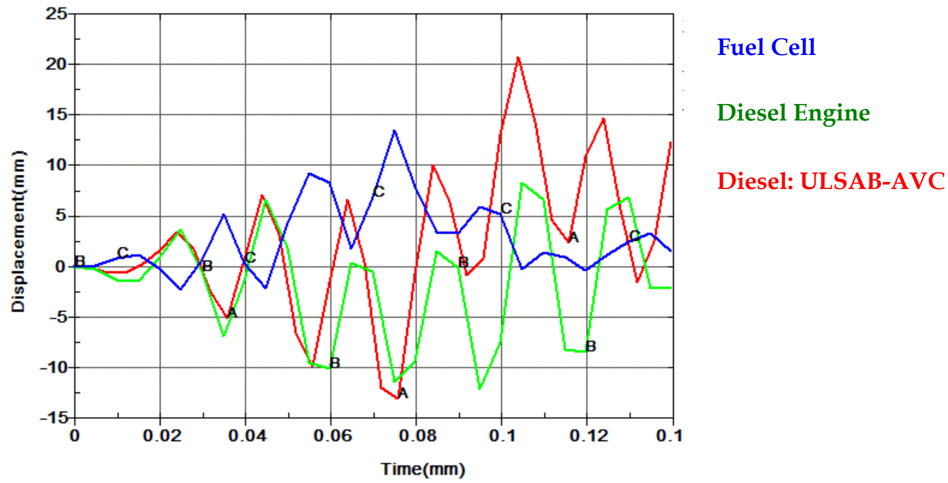

FIGURE 29: Steering Col Rear Movements Comparison

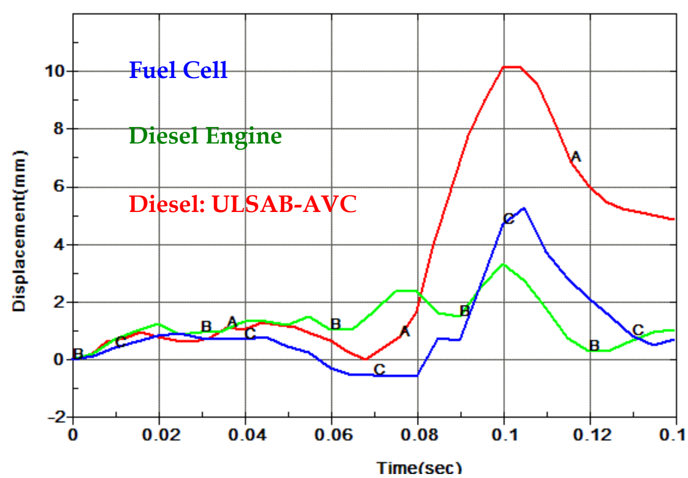

FIGURE 30: A-Pillar Displacement Comparison

The results show that the footwell intrusion, steering column intrusion, and A-pillar displacement of the diesel variation is improved over the ULSAB-AVC diesel variation, due to changes in the tunnel and dash areas.

The footwell intrusion for the fuel cell variation was increased, due to larger mass and the absence of an engine to hold the front rails together.

Figure 31 shows the deformation of the front rail and subframe for the fuel cell variation. The subframe develops a kink, which then contacts the hydrogen storage tank. This issue should be addressed in the future.

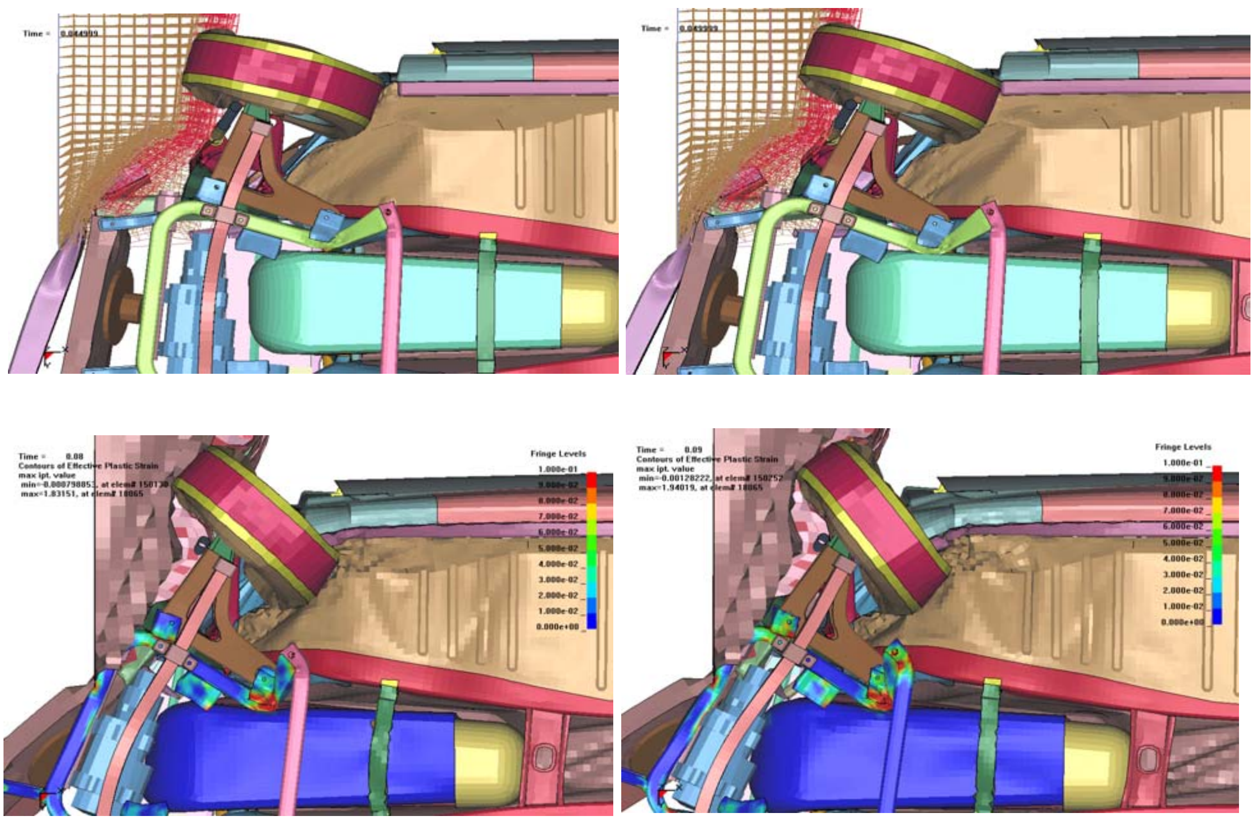

FIGURE 31: Front Rail/Fuel Cell Deformation

7. IIHS SIDE IMPACT

7.1. REGULATIONS

Detailed specifications are described in Appendix E.

7.2. LOADS AND BOUNDARY CONDITIONS

IIHS Moving Deformable Barrier (MDB)

The Moving Deformable Barrier (MDB) was developed and validated. It consists of 34 parts and has a mass of 1500kg, as specified in the IIHS regulations.

The barrier was positioned according to the regulations. The location of the ground plane was calculated from FMVSS 214 model of FGPC-class vehicle of ULSAP-AVC, and the barrier was positioned so that there was 379mm of ground clearance. The distance rearward from the test vehicle's front axle to the closest edge of the deformable barrier (IRD) is 810mm.

The barrier was given an initial velocity of 50kph perpendicular to the vehicle, as specified in the regulations.

Figure 32 shows the Moving Deformable Barrier (MDB) setup for the IIHS Side Impact analysis. Both the Baseline and Modified models were used in this analysis.

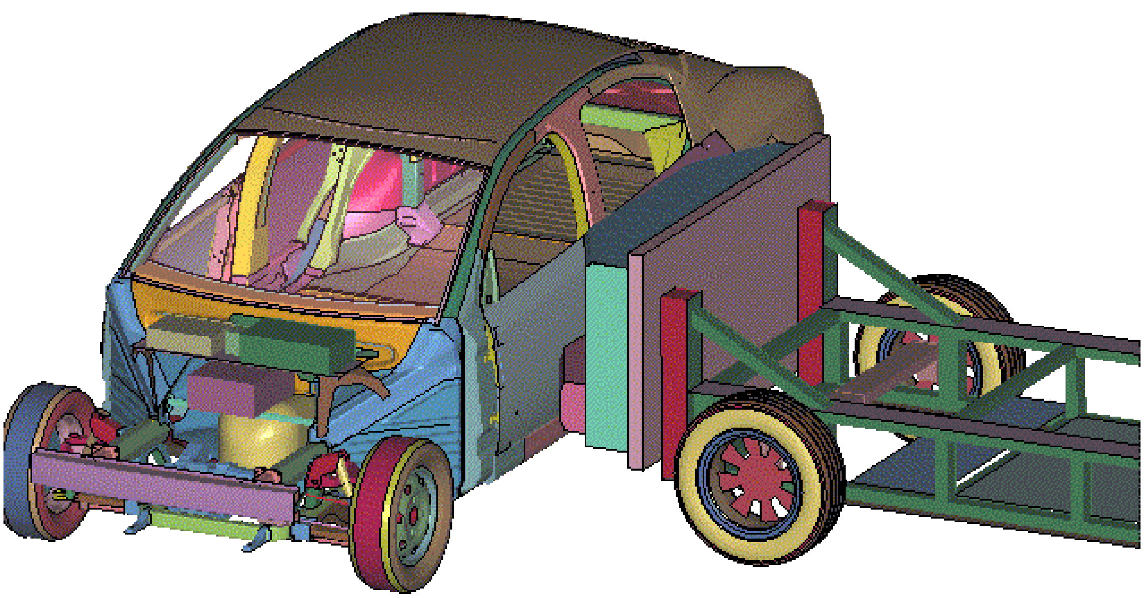

FIGURE 32: Movable Deformable Barrier

7.3. RESULTS

LS/DYNA nonlinear dynamics package is the solver for these simulations.

The following discussion of results refers to the side impact analyses conducted up to 100msec.

The sections from 2.6.4.1 to 2.6.4.4 show the results of fuel cell and diesel models for the IIHS side impact analysis. Two major iterations were performed each for fuel cell and diesel structure. The following sub-cases are representing those performances.

Graphs in the end of this section show the response of the measurement of B-pillar deformation for all iterations in the Concept Phase of this program.

7.3.1. BASELINE MODEL (FGPC-F VEHICLE – FUEL CELL STRUCTURE)

The deformed B-pillar and floor components for the Baseline analysis are shown in Figures 33 to 37. It is seen that the roof side rail section and rear floor structure do not resist incoming barrier loads effectively. The rear floor is seen to collapse downward and impact the fuel tank. The bending mode of roof rail allows the B-pillar structural measuring point to intrude inboard. Reducing this bending mode should reduce the amount of B-pillar intrusion. In summary, the overall IIHS side impact structural performance needs to be improved to address occupant and fuel cell tank protection concerns.

Iteration #2 is run next in an attempt to improve the structural and occupant protection.

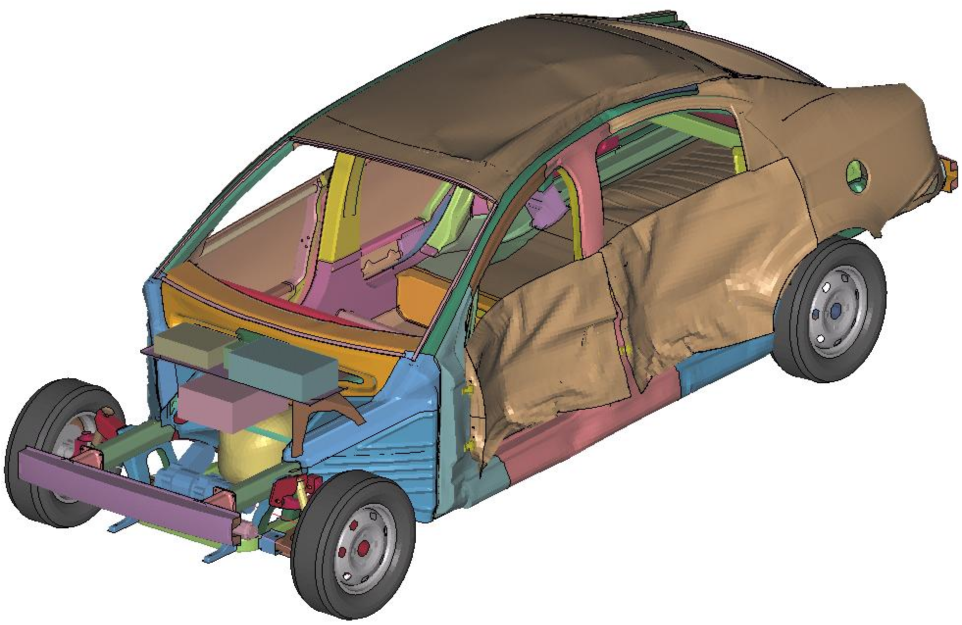

FIGURE 33: FGPC-F Deformed Shape - ISO View

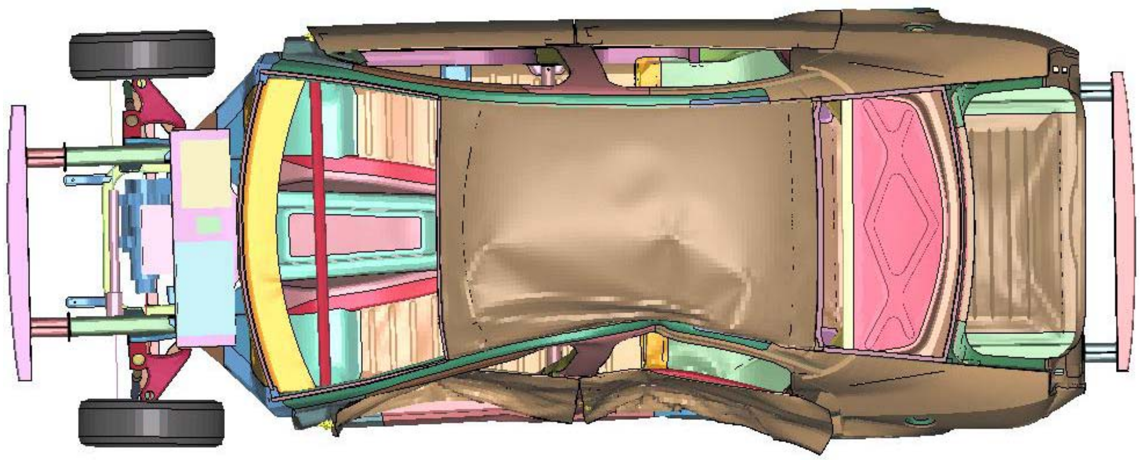

FIGURE 34: Deformation - Top View

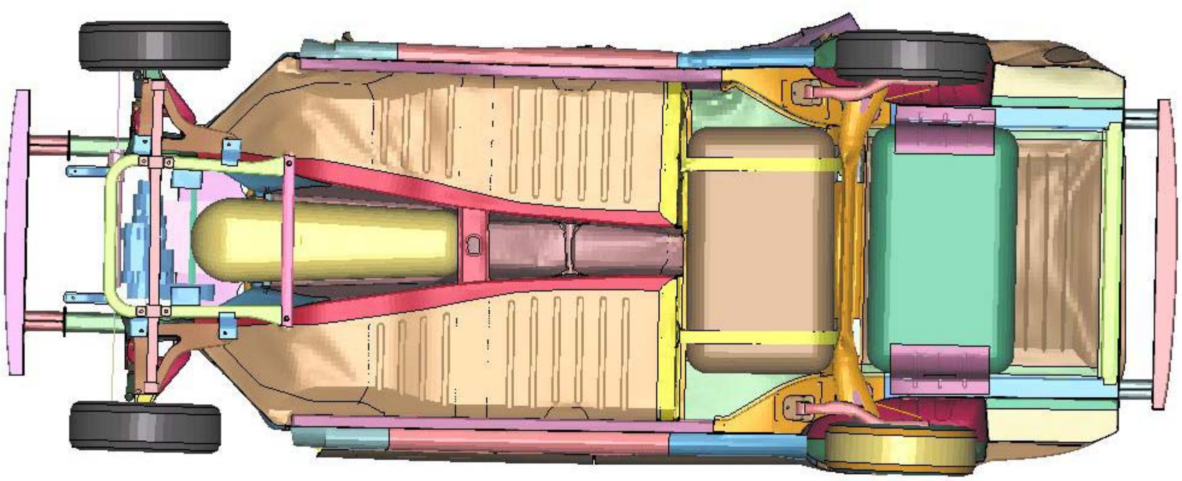

FIGURE 35: Deformation - Bottom View

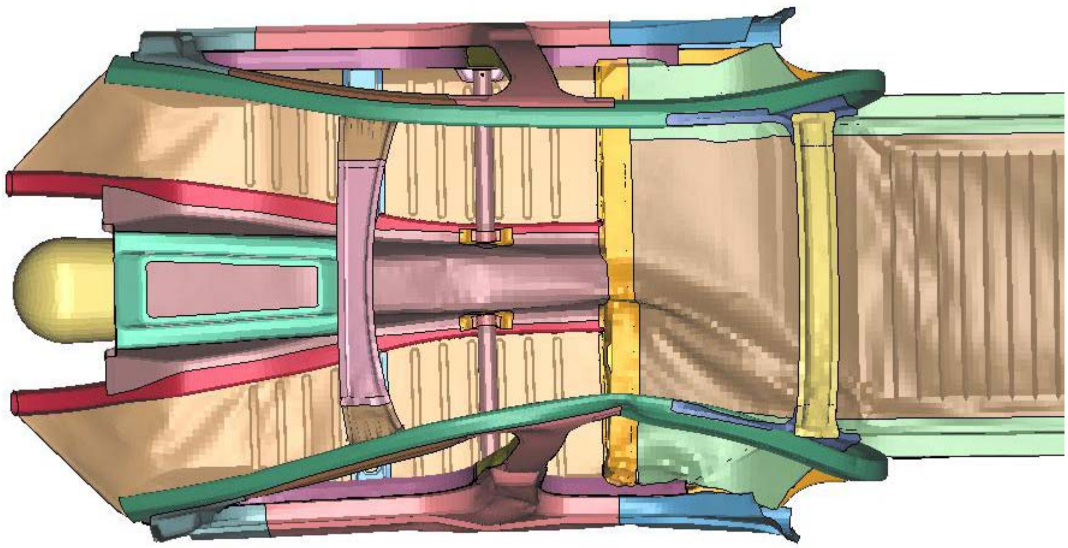

FIGURE 36: Deformation Of Sub-Structure - Inside Top View

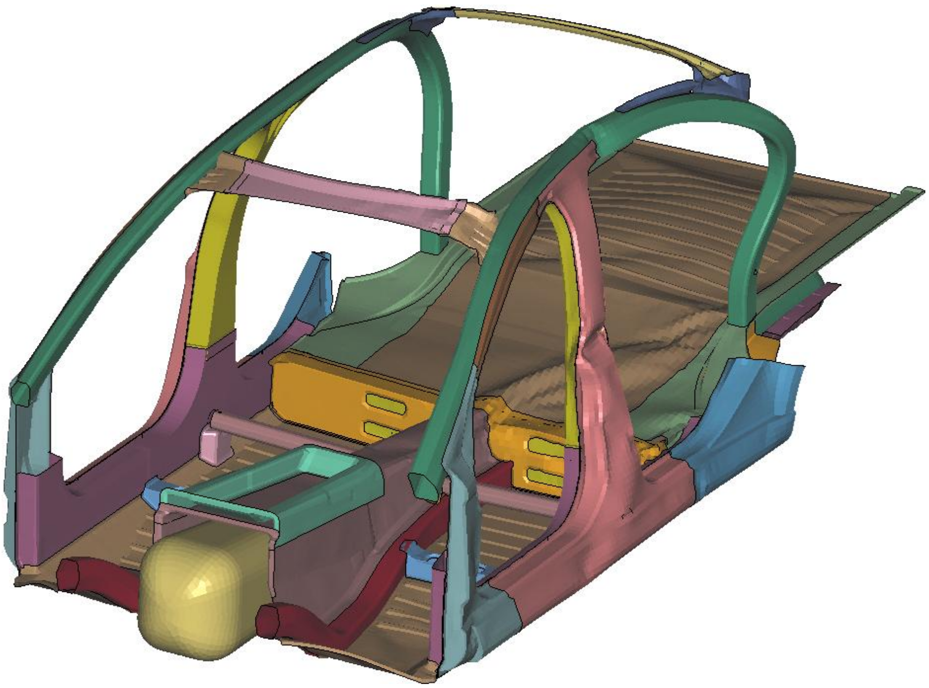

FIGURE 37: Deformation Of Sub-Structure - Inside Iso View

7.3.2. MODIFIED MODEL (FGPC-F – FUEL CELL STRUCTURE)

Design Modification

The first step to improve the vehicle's side impact performance is taken by adding a cross member across the tunnel to avoid tunnel collapse (Figure 38). The cross member in front of the rear floor needs to have an improved section to resist the lateral side impact load since there were limited structural reinforcements at the rear underbody in this region. The rear floor cross-member at the floor kick-down was modified to provide a better load path in the area where the tunnel attaches to the floor (Figure 38).

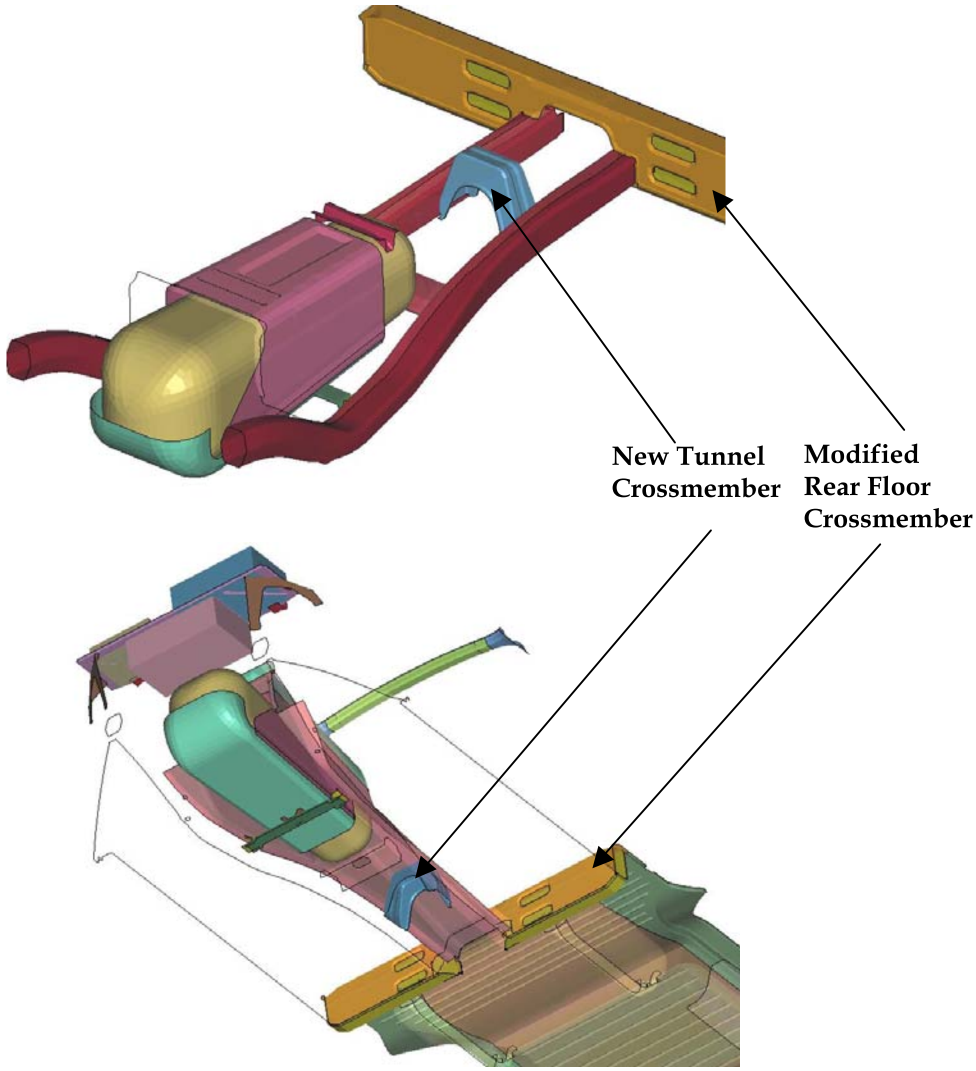

FIGURE 38: Model Modifications

Based on the Baseline model results, the roof rail integrity is another area to be improved to reduce B-pillar intrusion. To address this concern, a new roof bow was designed and connected between the roof side rails (Figure 39).

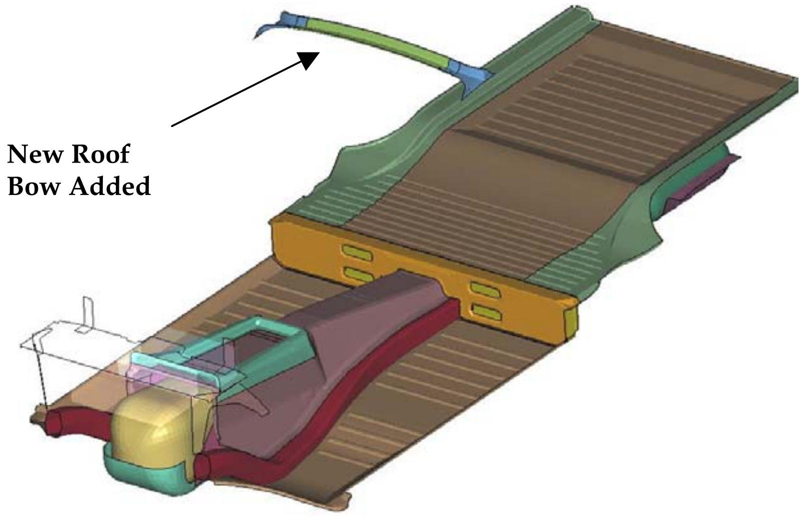

FIGURE 39: Roof Bow Added

Analysis Results
The structural deformations of the vehicle for this iteration are shown in Figure 40 through 44. The figures show that the addition of a roof bow improves the load path by transferring more energy to the B-Pillar and roof side area. This reduces the B-pillar's upper intrusion that results in enhanced vehicle performance. However, the B-pillar bending mode increases due to the vehicle's upper structure getting stronger. This issue will be studied in the optimization phase.

The figures also show that the deformation of the rear floor area is reduced due to the modification of the rear cross-member. The increased section over the tunnel of the cross-member provides a better load path to the non-struck side, so that the rear of the tunnel does not collapse.

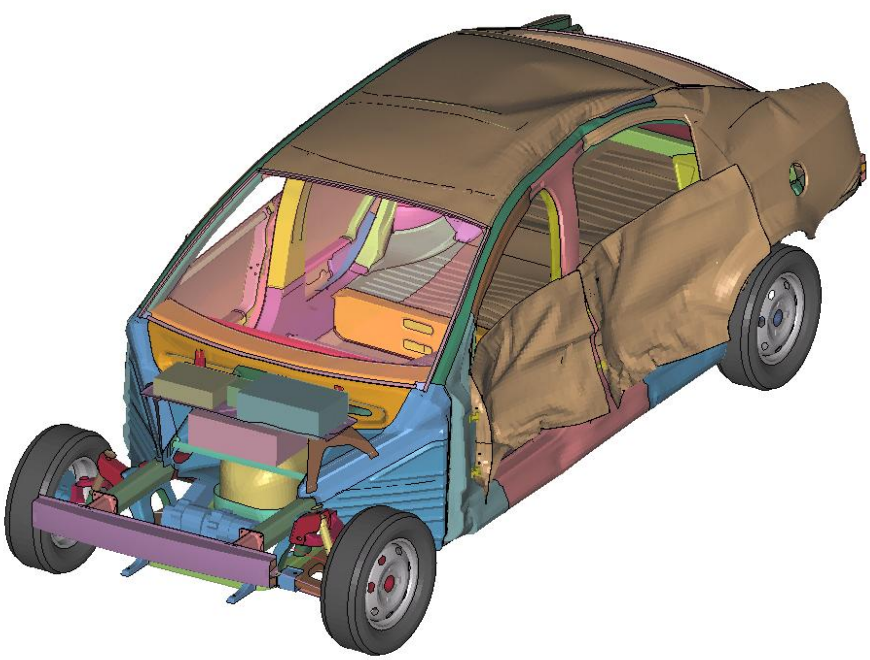

FIGURE 40: Deformation - Iso View

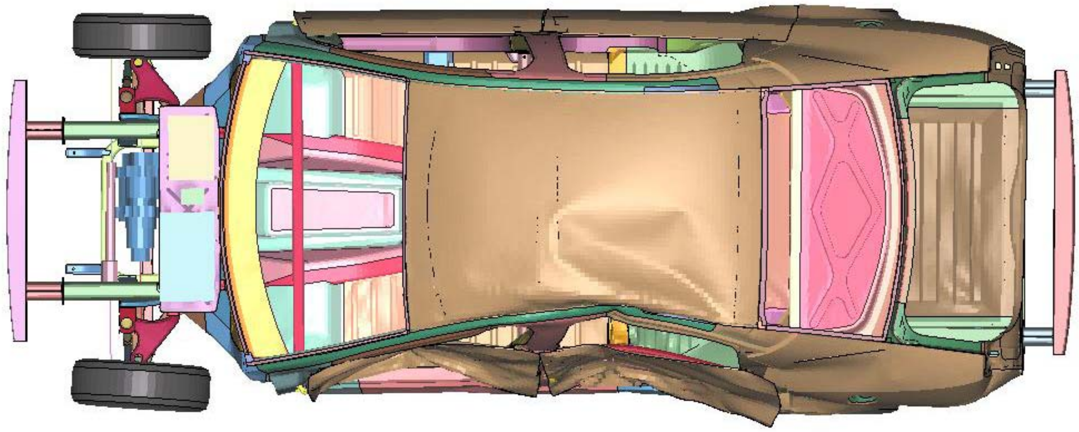

FIGURE 41: Deformation - Top View

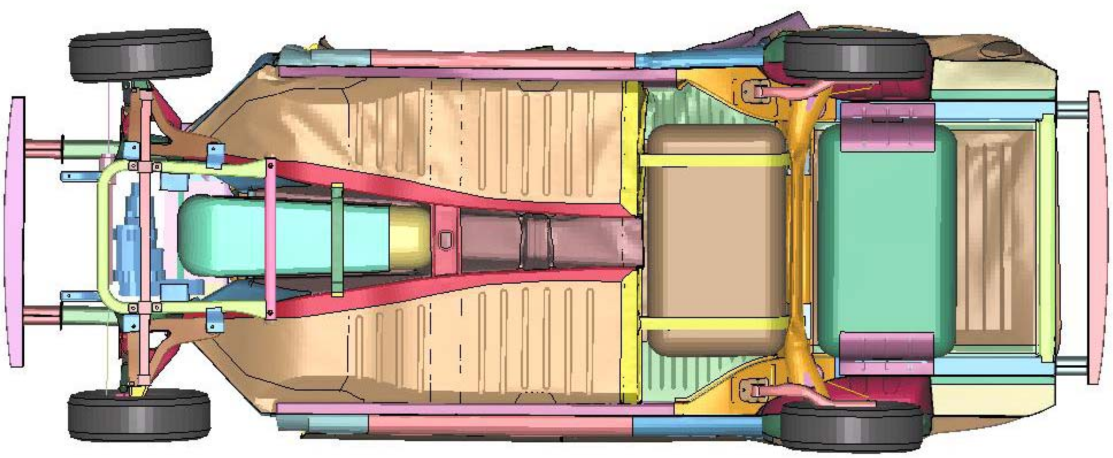

FIGURE 42: Deformation - Bottom View

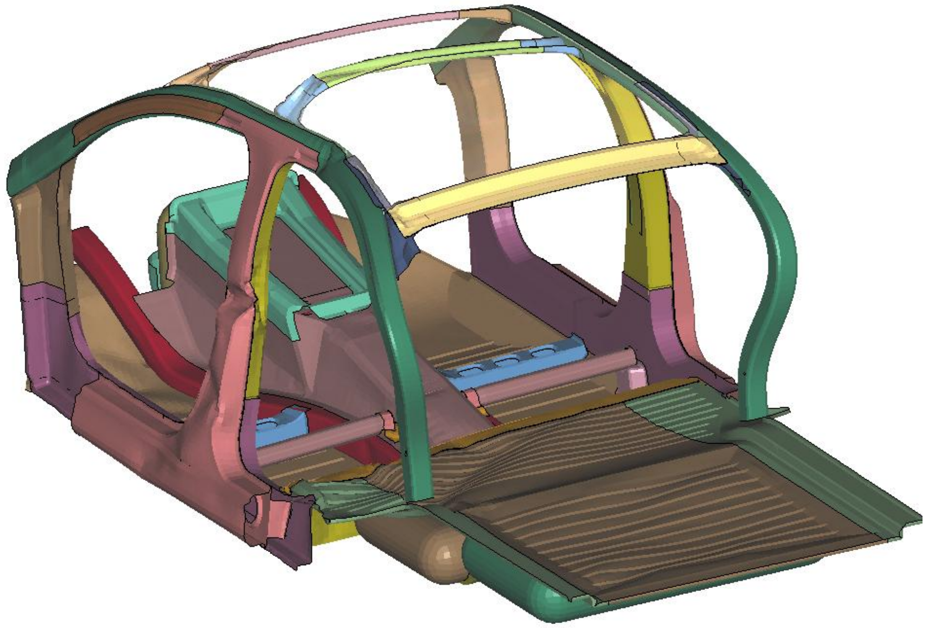

FIGURE 43: Deformation - Inside View From Rear

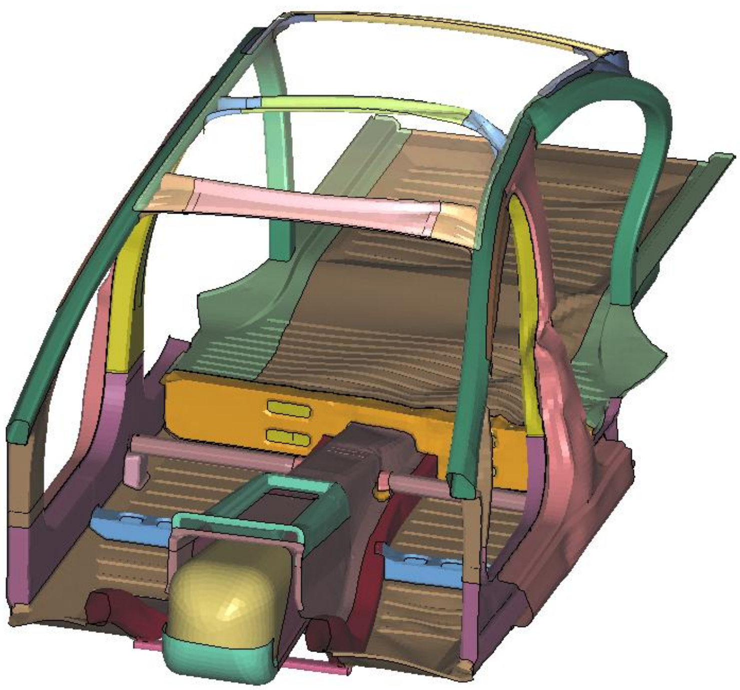

FIGURE 44: Deformation - Inside View From Front

7.3.3. BASELINE MODEL (FGPC-D – DIESEL STRUCTURE)

Design Modification

The vehicle model is the same as the Baseline model of fuel cell structure vehicle with the exception of the unique fuel cell related parts. This iteration will show the effect of replacing a conventional engine with fuel cell system.

Analysis Results

Figures 45 to 49 show different views of the deformed B-pillar and floor structure for Iteration #1 of the diesel structure. The deformation shape of the diesel structure is more severe than the fuel cell structure because there are limited structural components in the rear floor area to replace the stiffness provided by the fuel cell tanks. It is also seen that the roof side rail section and rear floor structure do not resist the applied loads effectively, which is not desired in a side impact. The rear floor collapses downward and the B-pillar deforms, causing the B-pillar structural measuring point to intrude inboard.

Iteration #2 is run next in the same condition as Iteration #2 case of fuel cell structure.

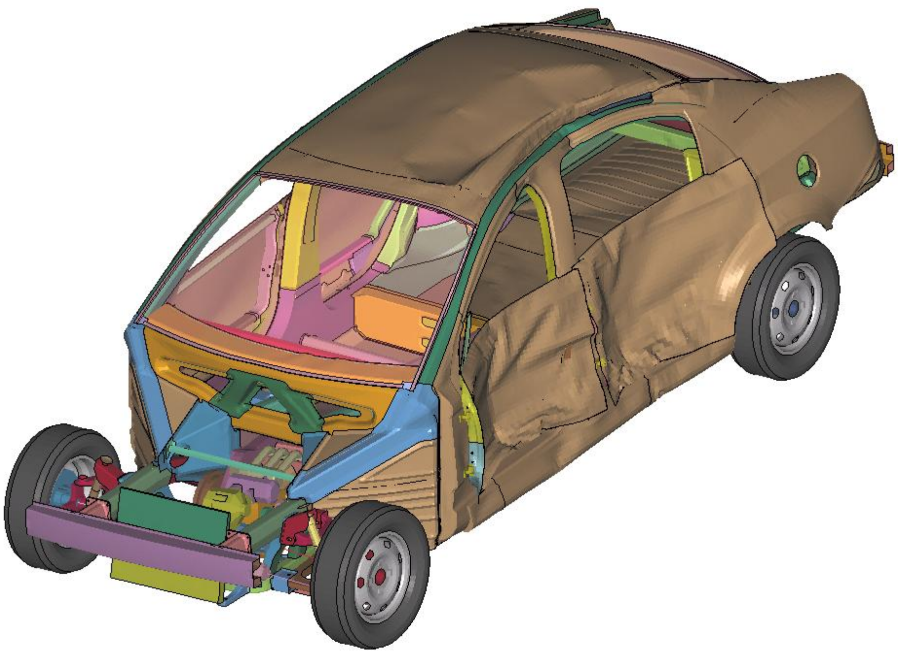

FIGURE 45: Deformation - ISO View

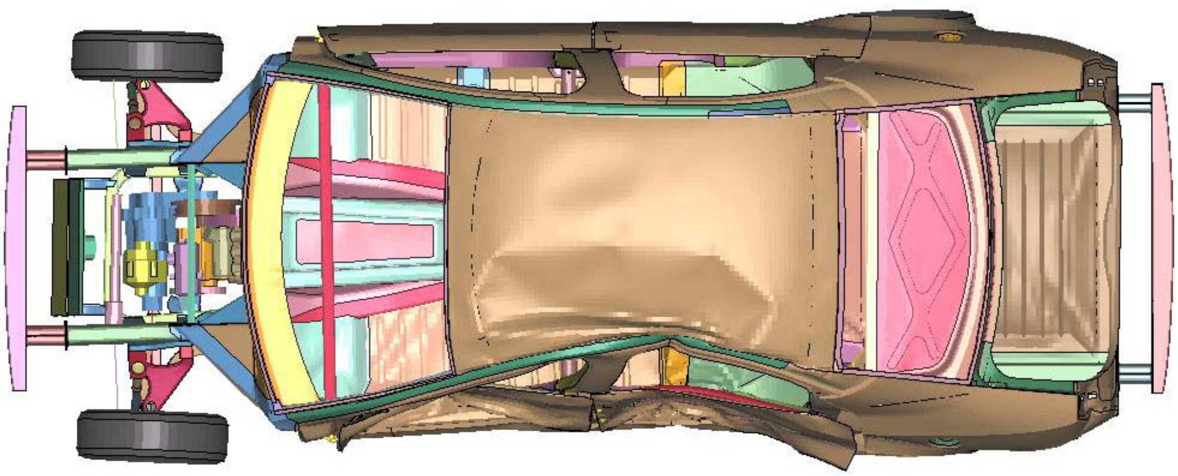

FIGURE 46: Deformation - Top View

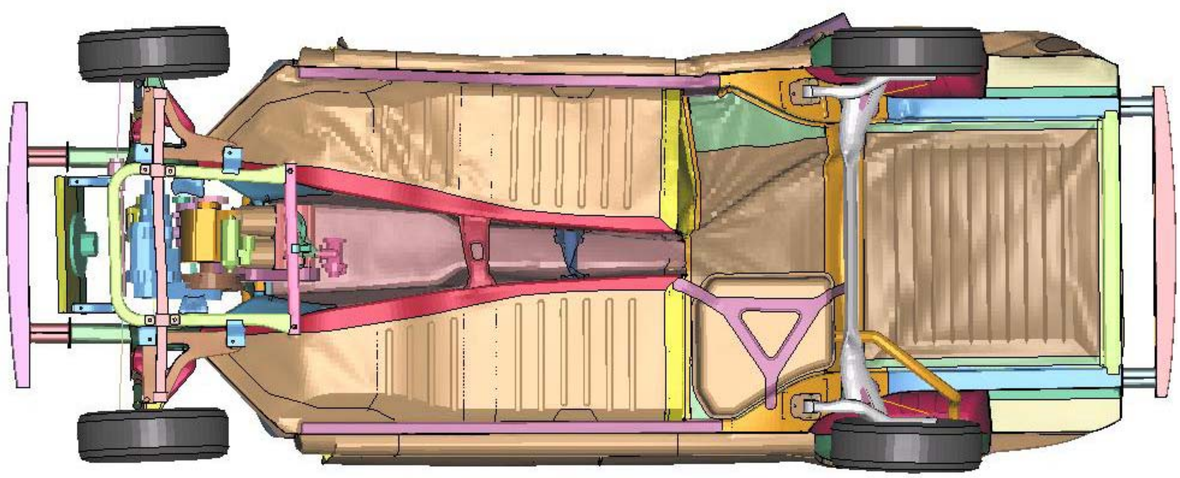

FIGURE 47: Deformation - Bottom View

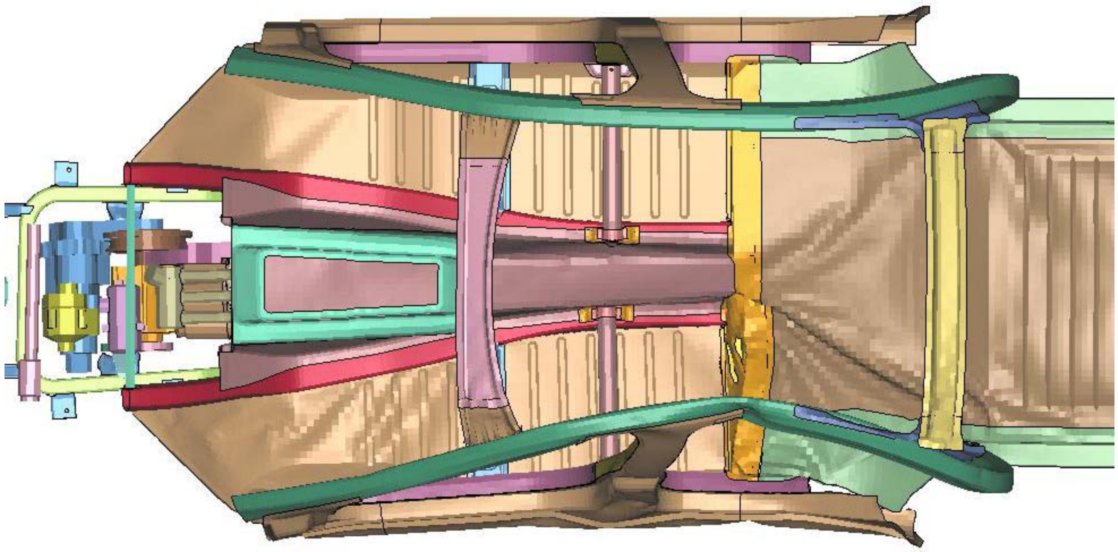

FIGURE 48: Deformation Of Sub-Structure - Inside Top View

FIGURE 49: Deformation Of Sub-Structure - Inside Iso View

7.3.4. MODIFIED MODEL (FGPC-D – DIESEL STRUCTURE)

Design Modification

Structural updates and conditions are same as in fuel cell Modified model.

Analysis Results

The roof constraint system is working and the buckling mode of roof side rail and roof-collapsing mode has been changed. But the positioning and optimizing of the roof bow still need to be determined.

The structural deformations of the vehicle for this iteration are shown in Figures 50 through 54. Figure 56 shows a view of the deformed roof rail and B-pillar for Iteration #2. It is seen that the B-pillar inboard motion is more limited, which is desired in a side impact. The improved deformation pattern comes from a better balancing of the load path from the B-pillar to roof. The response curves of the B-pillar intrusion measuring point show its improvement. Because the roof has less intrusion, there is more space between LH and RH B-pillars. The figure also shows that the rear floor section is deforming significantly due to the lateral force.

Based on the results of this case, an acceptable baseline model for side impact was established.

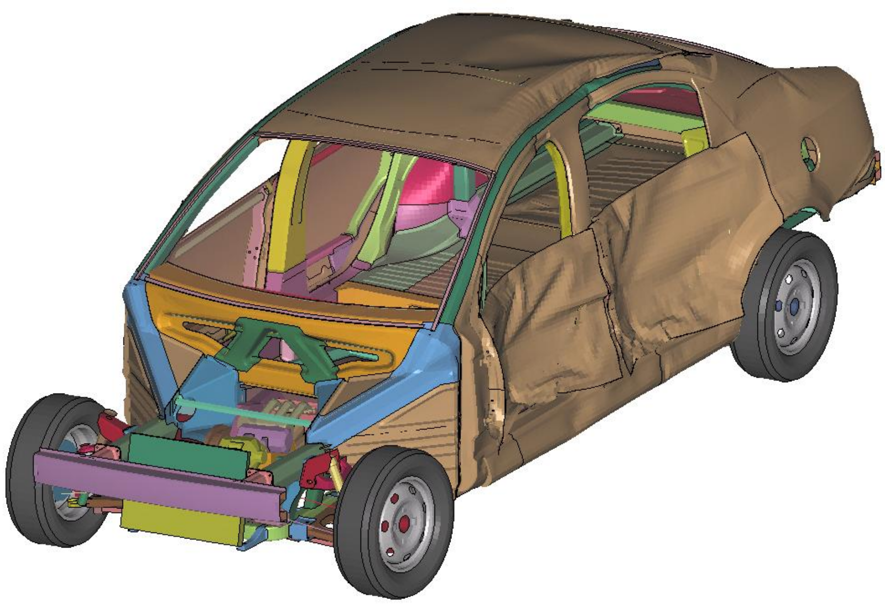

FIGURE 50: Deformation - Iso View

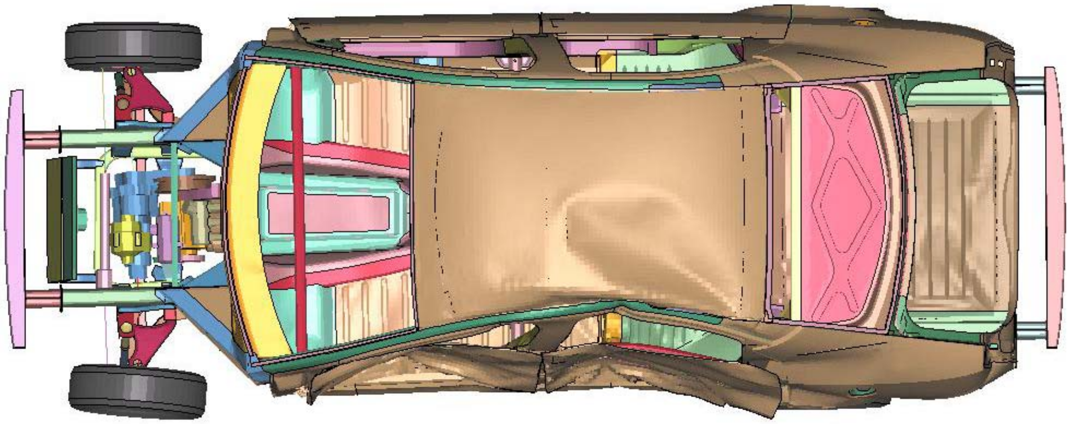

FIGURE 51: Deformation - Top View

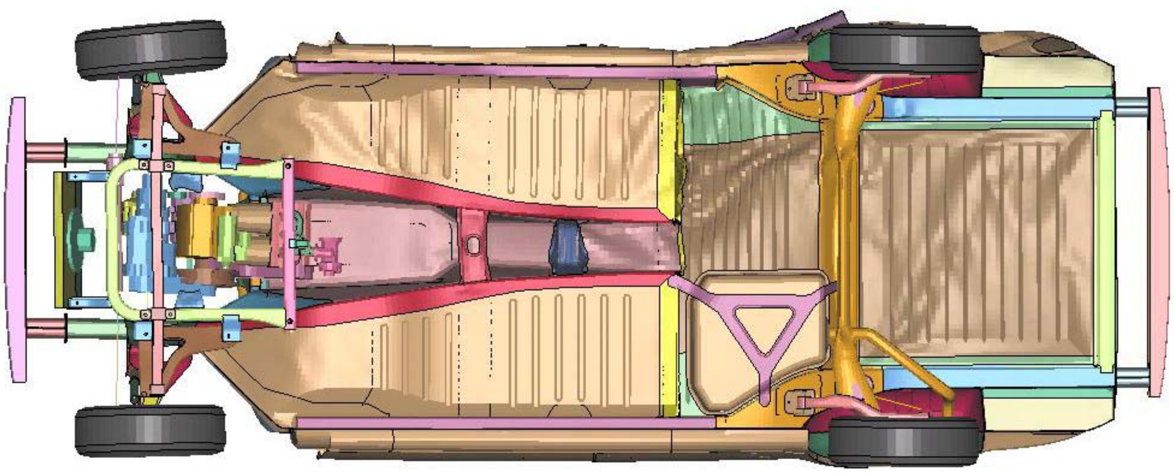

FIGURE 52: Deformation - Bottom View

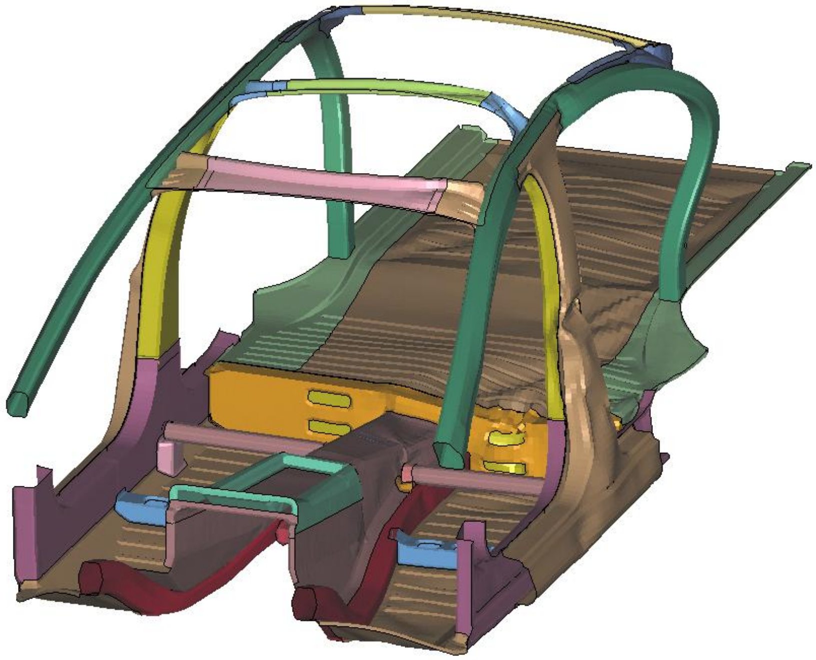

FIGURE 53: Deformation - Inside View ISO

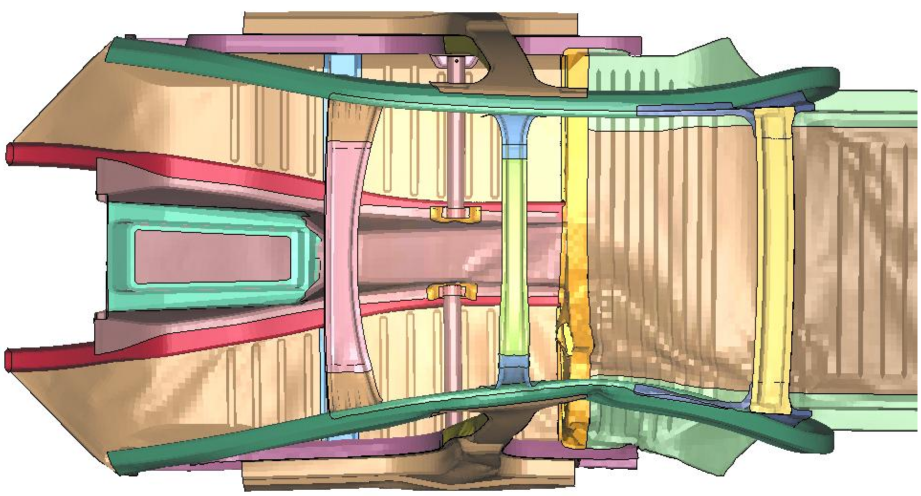

FIGURE 54: Deformation - Inside View Top

8. REAR CRASH (FMVSS301)

8.1. REGULATIONS

Detailed specifications are described in Appendix F.

8.2. LOADS AND BOUNDARY CONDITIONS

The vehicle is impacted by a 1300kg rigid barrier at a speed of 30mph. The Baseline model was used in this analysis.

8.3. RESULTS

Figure 55 shows plastic strain distribution of the fuel tank and fuel lines for the FGPC-F and FGPC-D vehicles. Figure 55 also shows 3% plastic strain in the PGPC-D fuel lines at the marked area in Figure 57. The FGPC-F fuel tank shows no plastic strain, which indicates no permanent deformation.

The buckling mode of the rear longitudinal member for both vehicles is shown in Figure 56. No components contact the hydrogen fuel tank in the FGPC-F vehicle, maintaining an 18 mm gap from the fuel tank to the next closest component.

Rigid wall forces for both vehicles are shown in Figure 58.

FUEL CELL (FGPC-F) **DIESEL ENGINE (FGPC-D)**

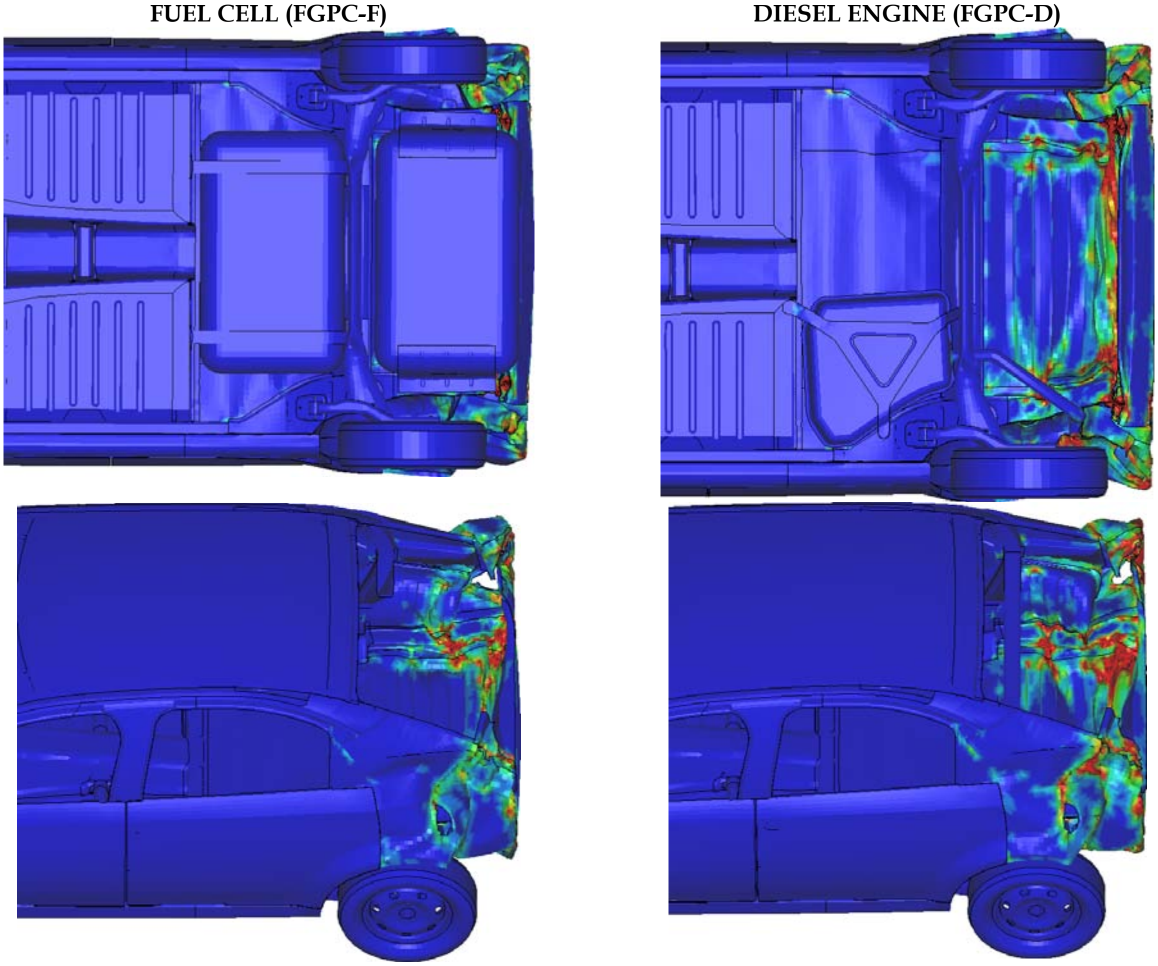

FIGURE 55: FGPC-F & FGPC-D Deformed Shape & Fuel Tank Integrity

FGPC-D FGPC-F

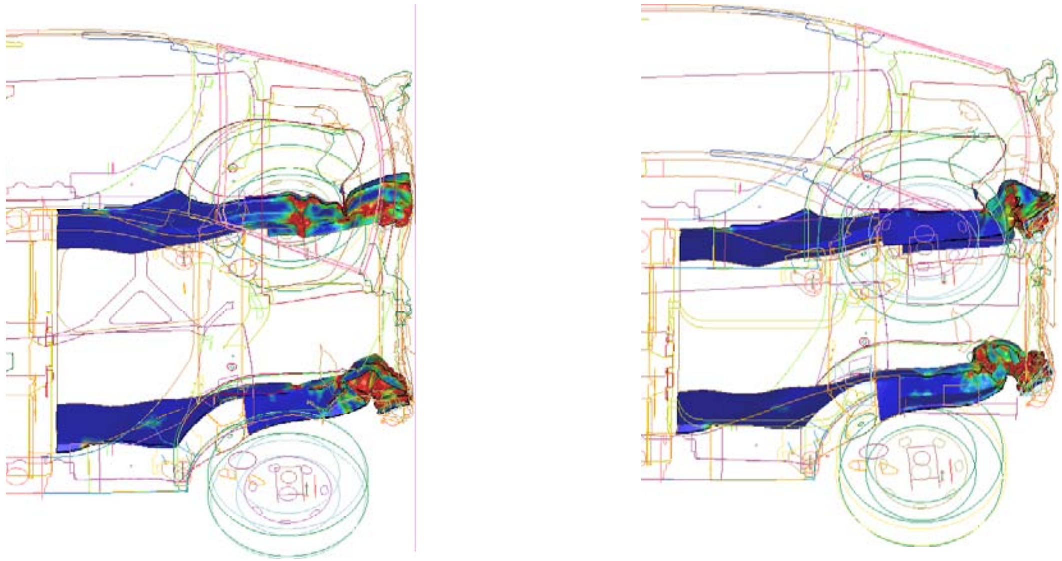

FIGURE 56. Rear Longitudinal Member Buckling Modes

FGPC-D FGPC-F

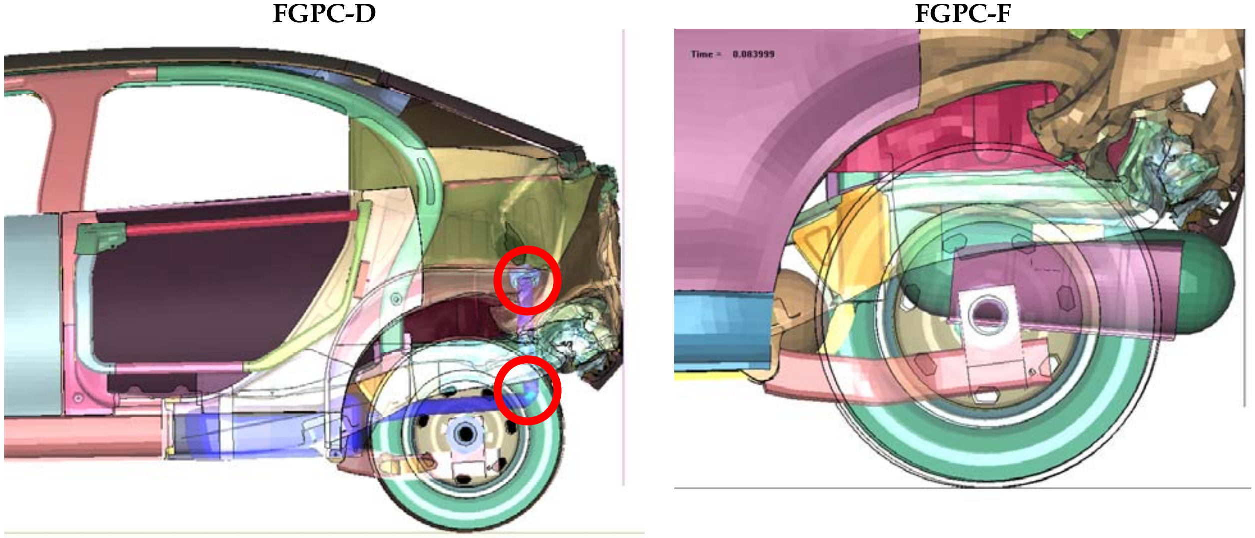

FIGURE 57: Rear Longitudinal Member Buckling Modes

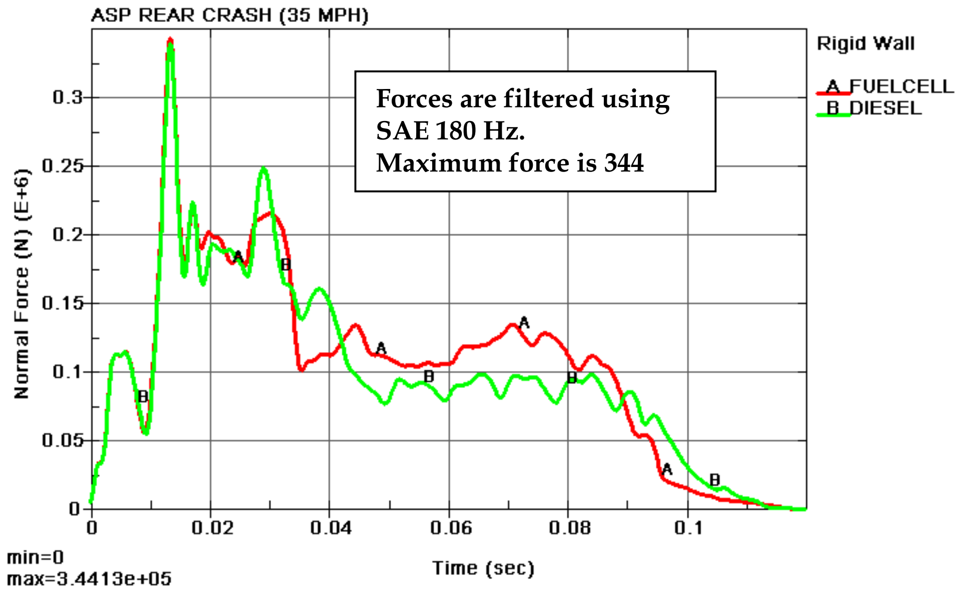

FIGURE 58: Rigid Wall Forces

9. ROOF CRUSH (FMVSS216)

9.1. REGULATIONS

Detailed specifications are described in Appendix G.

9.2. LOADS AND BOUNDARY CONDITIONS

A rigid plate (1829mm X 762mm) moves down on the A-pillar of the vehicle with 50inch/sec velocity (5 inches movement through analysis time of 100msec), as shown in Figure 59. The vehicle boundary condition is fixed at the rocker sill in xyz translation and rotation as shown in Figure 60. The Modified model was used in this analysis.

The analysis speed of 50 inch/sec is made higher than the test speed of 5 inches/120 seconds so that the analysis duration is reasonable. The higher velocity introduces a slight inertial effect into the analysis, which is known to increase the reaction force by a small, but nearly negligible amount.

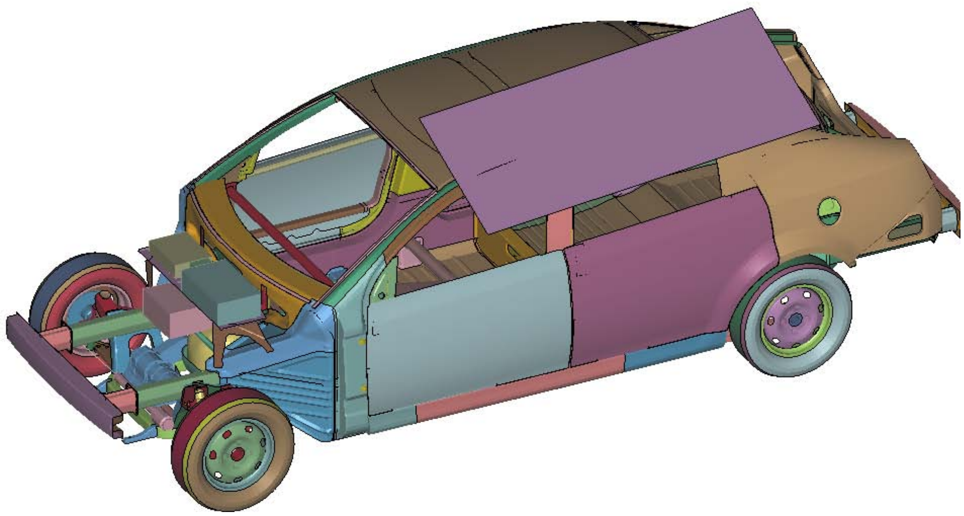

FIGURE 59: Roof Crush Model

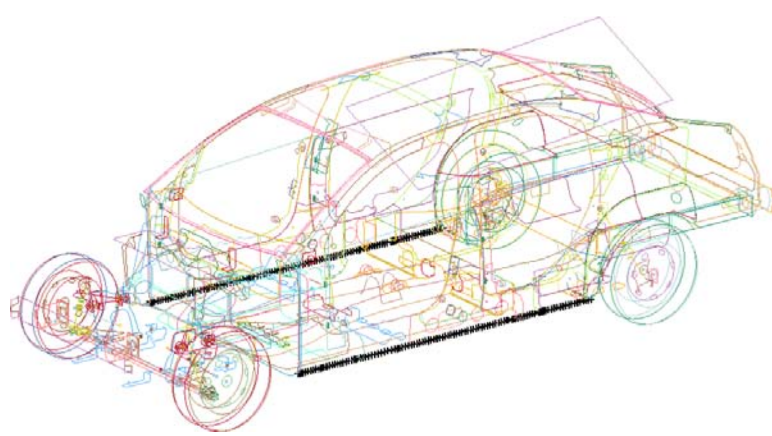

FIGURE 60: Roof Crush Model Boundary Conditions

9.3. RESULTS

Figure 61 shows force vs. displacement curve. FGPC team members set the vehicle target to 2.5 times vehicle curb weight. The results show that FGPC-F, which has 1158.8 kg curb weight, meets the target.

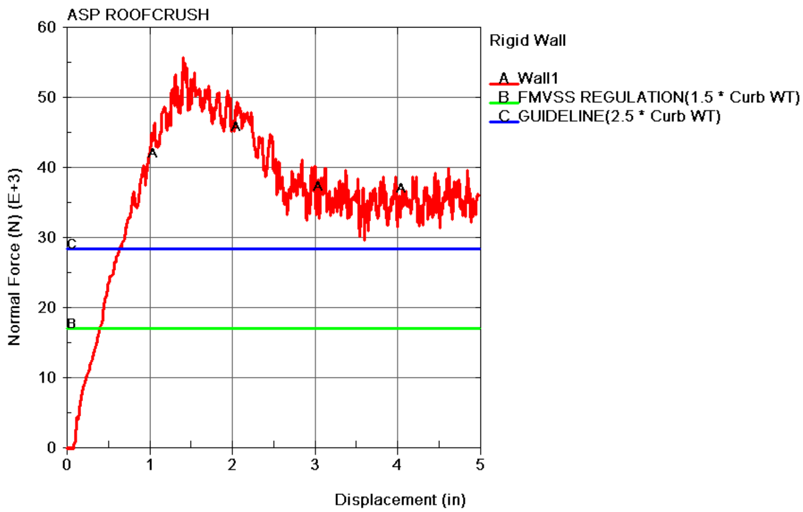

FIGURE 61: Force/Displacement Curve

Figure 62 shows the deformed shape of the vehicle structure. The vehicle body side is buckling at the A-pillar caused by the buckling occurring at the B-Pillar, above the B-Pillar reinforcement.

This vehicle body structure will be used for optimization for both IIHS side impact and roof crush simulations.

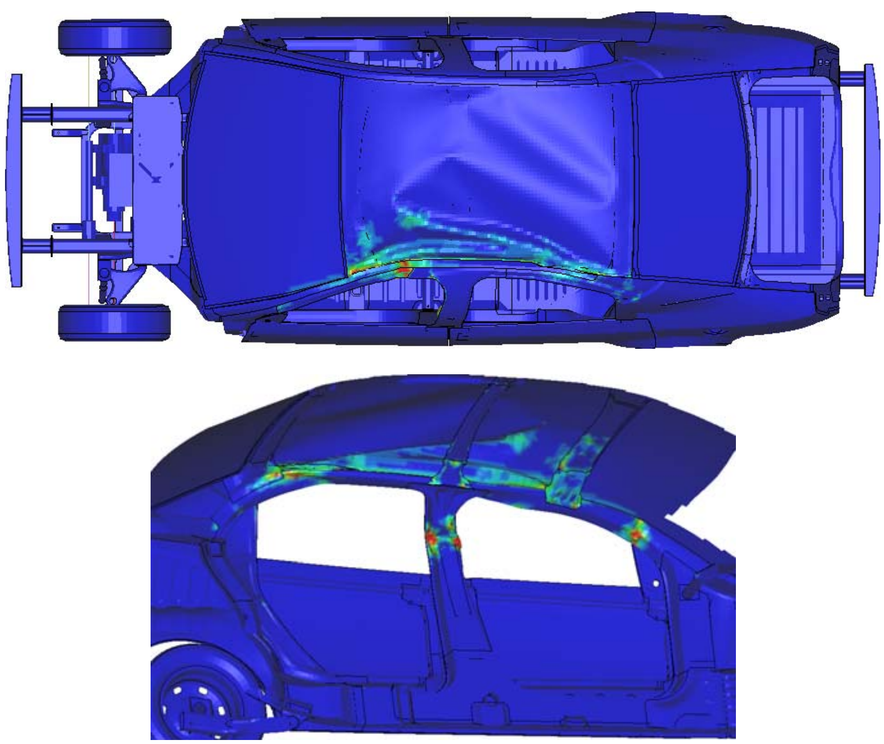

FIGURE 62: Deformed Shapes

APPENDIX A
MASS DISTRIBUTION

ASP MASS

	Original Model	Diesel Model	Fuel Cell Model
	Mass (kg)	Mass (kg)	Mass (kg)
	447.3 Structure Except below 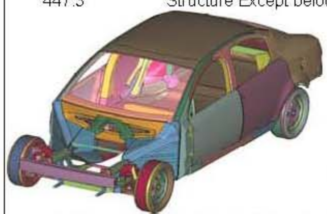	447.3 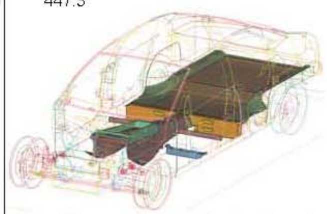	457.7 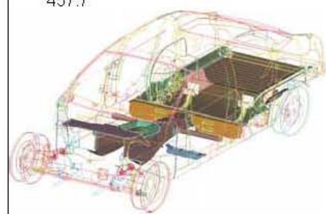
	235 Engine & Attached 	235 Engine & Attached 	
	2 Radiator 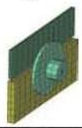	2 Radiator 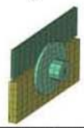	
	8.7 Structural Mass 46.6 Lumped Mass 55.3 Total Mass Fuel Tank 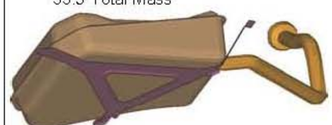	8.7 Structural Mass 46.6 Lumped Mass 55.3 Total Mass Fuel Tank 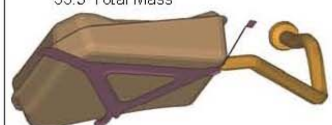	
			222.3 Electronic Box 14 kg Battery1 56 kg Battery2 12.3 kg Fuel Cell stack 100kg Gearbox 40 kg 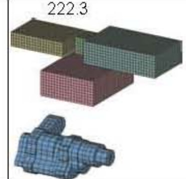
			75 3 X 25 kg, Fuel Cell 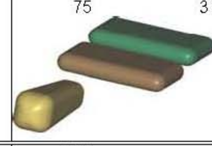
Total Structure mass Total Lumped Mass Total	693 697 1390	693 695 1388	755 690 1445
ETC Common Stucture	Chassis-Front Suspension Structure 46.9 kg Lumped Mass 29.5 kg Total 76.4 kg 	Chassis-Rear Suspension Structure 13.7 kg Lumped Mass 19.4 kg Total 33.1 kg 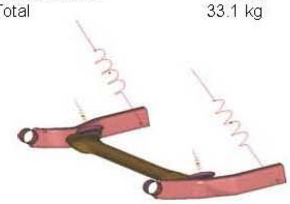	Tires Structure 61.2 kg Lumped Mass 0 kg Total 61.2 kg 

APPENDIX B
MATERIAL PROPERTIES

ASSEMBLY: BIW (Body-In-White)			
PID	**NAME**	**GAUGE (mm)**	**MATERIAL TYPE/GRADE**
57	SUBFRAME_CROSSMEMBER	2.00	HSLA 350/450
11008	Cowl Front	0.80	DP 500/800
11009	Assy Crash Box Bumper Front (x2)	1.10	DP 400/700
11012	Bumper Beam Front Inner	1.00	Mart 1250/1520
11013	Bumper Beam Front Outer	1.00	Mart 1250/1520
11015	Dash	0.65	DP 280/600
11045	Header Front	0.70	IF 300/420
11064	Support Header Front RH	0.70	DP 280/600
11075	Cross-member Back Panel	0.65	DP 280/600
11082	Cross-member Kick-down	0.70	DP 700/1000
11088	Bulkhead Crash Box Dash RH	1.20	DP 700/1000
11116	Assy Reinf Rail Rear Suspension Attach RH	1.30	DP 500/800
11128	Plate Crash Box Rail Front Attach (x2)	3.00	DP 700/1000
11134	Cross-member Support Front Seat Front RH	0.70	TRIP 450/800
11136	Closeout Lower Crash Box Dash RH	0.90	DP 500/800
11138	Closeout Inner Crash Box Dash RH	0.80	DP 400/700
11146	A-Post Inner RH	0.90	DP 700/1000
11153	Cross-member Rear Suspension	1.00	DP 700/1000
11182	Reinf Rail Rear Suspension C-Member RH	1.50	HSLA 350/450
11184	Cross-member Support Front Seat Rear	1.20	Mart 950/1200
11190	Bracket Support Front Seat Rear (x2)	1.20	DP 500/800
11192	Reinf Crash Box Dash RH	1.00	DP 400/700
11194	Reinf Tunnel	0.70	Mart 950/1200
11196	Closeout Outer Crash Box Dash RH	0.80	DP 400/700
11202	Reinf Waist B-Pillar RH	1.50	Mart 1250/1520
11206	Assy Crash Box Bumper Rear (x2)	1.00	HSLA 350/450
11216	Bracket Member Body Side Inner Att Rear RH	1.20	DP 500/800
11226	A-Brace Cowl Front	1.00	DP 500/800
11227	A-Brace Cowl Rear	1.00	DP 500/800
13500	Fuel Tank	1.00	BH 210/340
13501	Fuel Tank Support	1.20	BH 210/340
13502	Fuel Tank Filler Tube	1.20	BH 210/340
31016	Floor Front RH.1	0.65	TRIP 450/800
31036	Wheelhouse Inner RH.1	0.60	DP 500/800
31038	Wheelhouse Outer RH.1	0.60	DP 280/600
31047	Bumper Beam Rear Inner.1	0.80	Mart 1250/1520
31048	Bumper Beam Rear Outer.1	0.80	Mart 1250/1520
31049	Tunnel.1	0.65	DP 300/500
31050	Member Rail Front RH.1	1.50	DP 500/800
31069	Floor Rear.1	0.60	BH 210/340
31074	Back Panel.1	0.60	DP 300/500
31076	Rail Rear RH.1	1.80	DP 700/1000
31124	Support Header Rear RH	0.70	IF 300/420
31126	Header Rear.1	0.70	IF 300/420
31127	Roof.1	0.65	DP 300/500

ASSEMBLY: BIW (Body-In-White) Cont. (Note: New Parts Highlighted in Yellow)			
PID	**NAME**	**GAUGE (mm)**	**MATERIAL TYPE/GRADE**
31130	Member Body Side Inner RH.1	1.00	DP 500/800
31156	Package Tray Upper	0.60	DP 280/600
31157	Package Tray Lower	0.60	DP 280/600
31160	Support Package Tray Lower RH	1.20	IF 300/420
31162	Rocker Inner RH.1	1.50	DP 700/1000
31170	Body Side Outer RH.1	1.50	DP 700/1000
31172	Body Side Inner Rear RH.1	0.70	IF 300/420
31178	Gutter Deck Lid RH	0.70	BH 260/370
31188	Rail Rear Outer Floor Extension RH.1	1.10	DP 500/800
31201	Cross-member Package Tray	1.00	DP 280/600
31208	B-Pillar Inner RH.1	0.70	Mart 950/1200
31212	Extension C-Member Supt Front Seat Rr (x2)	1.20	Mart 950/1200
31214	Support Back Panel.1	0.60	DP 300/500
31222	Reinf B-Pillar Lower RH.1	1.00	DP 700/1000
31336	Wheelhouse Inner RH TWB2.1	1.40	DP 700/1000
31350	Member Rail Front RH TWB2.1	1.30	DP 500/800
31369	Floor Rear TWB2.1	1.10	DP 350/600
31376	Rail Rear RH TWB2.1	1.10	DP 500/800
31436	Wheelhouse Inner RH TWB3.1	1.10	DP 700/1000
31470	Body Side Outer RH TWB2.1	0.70	BH 260/370
31488	Rail Rear Outer Floor Extension RH TWB2	0.60	BH 210/340
31569	Floor Rear TWB4.1	0.70	DP 700/1000
31570	Body Side Outer RH TWB3.1	1.80	DP 700/1000
31670	Body Side Outer RH TWB4	1.20	DP 700/1000
31770	Body Side Outer RH TWB5	0.70	BH 260/370
90017	IP BEAM	2.00	HSLA 350/450
90018	Reinf Waist Outer B-Pillar	0.80	DP 700/1000
400008	Cross-member Support Front Seat Front CTR	1.00	TRIP 450/800
400016	Cross-member tunnel	1.00	TRIP 450/800
400014	PIPE MTG LWR	1.00	TRIP 450/800
400023	ROOF BOW	1.00	TRIP 450/800
400024	GUSSET BRKT	1.00	TRIP 450/800

TABLE B1: BIW - GAUGE & MATERIAL LISTING BY PART

ASSEMBLY: DOORS			
PID	NAME	GAUGE (mm)	MATERIAL TYPE/GRADE
12004	Member Front - Front Door	1.20	IF 260/410
12020	Inner Front - Front Door TWB 1	1.00	Mild 140/270
12026	Mirror Flag - Front Door	1.00	Mild 140/270
12320	Inner Front - Front Door TWB 2	1.20	Mild 140/270
32006	Member Rear - Front Door.1	1.00	IF 260/410
32008	Member Side Intrusion - Front Door (x2).1	1.50	DP 500/800
32010	Member Waist - Front Door (x2).1	1.00	DP 500/800
32028	Outer - Front Door.1	0.60	DP 350/600
32030	Inner Rear - Front Door.1	0.60	Mild 140/270
32032	Outer - Rear Door	0.60	DP 350/600
32034	Inner Front - Rear Door TWB 1	1.00	Mild 140/270
32038	Inner Rear - Rear Door	0.60	Mild 140/270
32040	Member Front - Rear Door	1.20	IF 260/410
32042	Member Rear - Rear Door	1.00	IF 260/410
32044	Member Side Intrusion - Rear Door (x2)	1.50	DP 500/800
32046	Member Waist - Rear Door (x2)	1.00	DP 500/800
32334	Inner Front - Rear Door TWB 2	1.20	Mild 140/270

TABLE B2: DOOR - GAUGE & MATERIAL LISTING BY PART

Steel Grade	YS (MPa)	UTS (MPa)	Total EL (%)	n-value[1] (5-15%)	r-bar	K-value[2] (MPa)
	(flat sheet, as shipped properties)					
BH 210/340	210	340	34-39	0.18	1.8	582
BH 260/370	260	370	29-34	0.13	1.6	550
DP 280/600	280	600	30-34	0.21	1.0	1082
IF 300/420	300	420	29-36	0.20	1.6	759
DP 300/500	300	500	30-34	0.16	1.0	762
HSLA 350/450	350	450	23-27	0.14	1.1	807
DP 350/600	350	600	24-30	0.14	1.0	976
DP 400/700	400	700	19-25	0.14	1.0	1028
TRIP 450/800	450	800	26-32	0.24	0.9	1690
DP 500/800	500	800	14-20	0.14	1.0	1303
CP 700/800	700	800	10-15	0.13	1.0	1380
DP 700/1000	700	1000	12-17	0.09	0.9	1521
Mart 950/1200	950	1200	5-7	0.07	0.9	1678
Mart 1250/1520	1250	1520	4-6	0.065	0.9	2021
	(straight tubes, as shipped properties)					
DP 280/600	450	600	27-30	0.15	1.0	1100
DP 500/800	600	800	16-22	0.10	1.0	1250
Mart 950/1200	1150	1200	5-7	0.02	0.9	1550

YS and UTS are minimum values, others are typical values
Total EL % - Flat Sheet (A50 or A80), Tubes (A5)
[1]n-value is calculated in the range of 5 to 15% true strain.
[2]K-value is the magnitude of true stress extrapolated to a true strain of 1.0. It is a material property parameter frequently used by one-step forming simulation codes.

TABLE B3: Material Properties

APPENDIX C
FRONT CRASH REGULATIONS - NCAP
Scope and Purpose
This standard specifies performance requirements for the protection of vehicle occupant in a crash. The purpose of this standard is to reduce the number of deaths of vehicle occupants and the severity of injuries, by specifying vehicle crashworthiness requirements in terms of forces and accelerations measured on a variety of anthropomorphic dummies in test crashes, and static airbag deployment tests. This standard also specifies equipment requirements for active and passive restraint systems.

Application
Passenger cars, trucks, buses, and multipurpose passenger vehicles with a GVWR of 3,855 kg (8,500 lb) or less and an UVW of 2,495 kg (5,500 lb) or less, except for walk-in van-type trucks or vehicles designed to be sold exclusively to the U. S. Postal Service

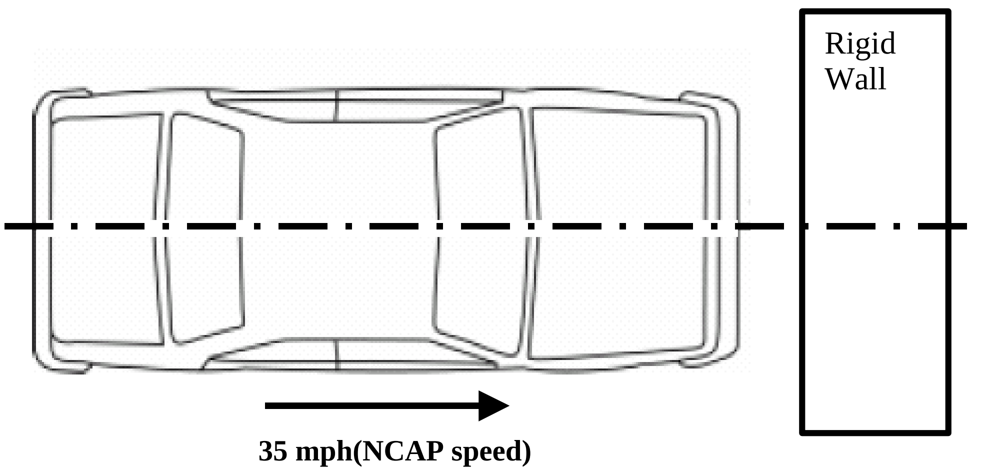

FIGURE C1

APPENDIX D
FRONT CRASH REGULATIONS - IIHS 40% ODB
Offset barrier crash tests are conducted at 40mph (64.4 km/h) and 40 percent overlap. The test vehicle is aligned with the deformable barrier such that the right edge of the barrier face is offset to the left of the vehicle centerline by 10 percent of the vehicle's width (Figure 1). The vehicle width is defined and measured as indicated in SAE J1100 – Motor Vehicle Dimensions, which states, "The maximum dimension measured between the widest part on the vehicle, excluding exterior mirrors, flexible mud flaps, and marker lamps, but including bumpers, moldings, sheet metal protrusions, or dual wheels, if standard equipment."

The vehicle is accelerated by the propulsion system at an average of 0.3 g until it reaches the test speed and then is released from the propulsion system 25 cm before the barrier. The onboard braking system, which applies the vehicle's service brakes on all four wheels, is activated 1.5 seconds after the vehicle is released from the propulsion system.

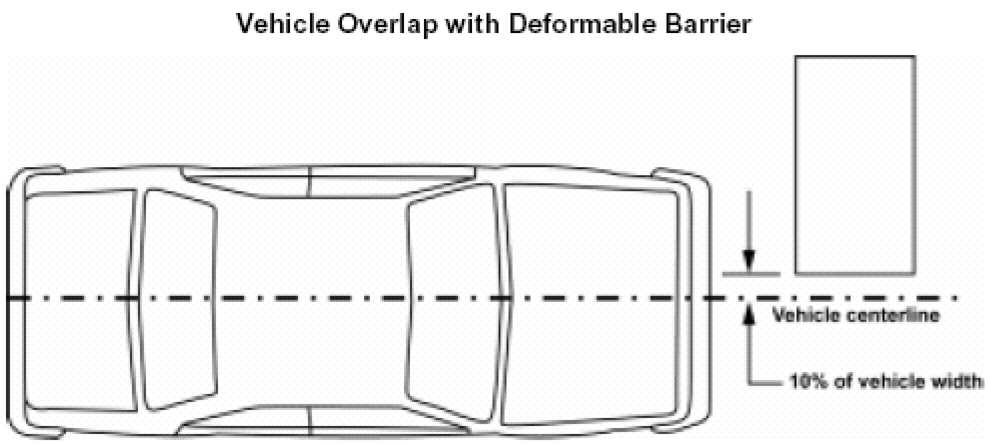

FIGURE D1

Measurement Point Locations
The following are the locations for measuring vehicle intrusion:

Steering column (one point) – The marked reference is the geometric center of the steering wheel, typically on the airbag door. After the crash, this point is measured by folding the airbag doors back into their undeployed position. In most cases, this measurement is probably less than the maximum intrusion into the compartment. However, if the steering column completely separates from the instrument panel (due to shear module separation, for example) during the crash, the steering column postcrash measurement is taken by placing and holding the wheel and column in its approximate maximum dynamic position as recorded on the high-speed film. The film may not always show clearly where the column was during the crash, and in such cases other clues would be needed to reposition the column for measurement. In rare instances, it may not be possible to obtain any meaningful postcrash measurement.

Lower instrument panel (two points) – The left and right lower instrument panel (knee bolster) lateral coordinates are defined by adding 15 cm to and subtracting 15 cm from the steering column reference lateral coordinate, respectively. The vertical coordinate is the same for both left and right references and is defined as 45 cm above the height of the floor (without floormats). If the panel or knee bolster loosens or breaks away in the crash, the postcrash measurements are taken by pressing and holding the panel against the underlying structure.

Brake pedal (one point) – The geometric center of the brake pedal pad (top surface). If the brake pedal is constructed so that it dangles loosely after the crash, the brake pedal is pushed straight forward against the toepan/floorpan and held there to take the postcrash measurement. If the pedal drops away entirely, no postcrash measurement is taken.

Toepan (three points) – The vertical coordinate for all toepan measurement locations is the vertical coordinate of the brake pedal reference. The lateral coordinates of the left, center, and right toepan locations are obtained by adding 15 cm to, adding 0 cm to, and subtracting 15 cm from the brake pedal reference lateral coordinate, respectively. The longitudinal coordinate is measured and a mark is temporarily placed at the locations on the toepan. A utility knife is used to cut a small "v" in the carpet and underlying padding at each point on the toepan. The point of the "v" is peeled back, and the exposed floor is marked and measured. The carpet and padding are then refitted prior to the crash.

Left footrest (one point) – The vertical coordinate for the footrest measurement location is the vertical coordinate of the brake pedal reference. The lateral coordinate of the footrest is obtained by adding 25 cm to the brake pedal reference lateral coordinate. The same procedure described above for cutting the carpet is used to mark and measure the underlying structure. In cases where there is a specific footrest construct at the footrest measurement location, the construct is removed and the underlying structure is marked and measured. The construct is reinstalled prior to the crash.

Seat bolts (typically, four points) – Each of the four (or fewer) bolts that anchor the driver seat to the floor of the vehicle.

A-pillar (one point) – The A-pillar is marked on the outside of the vehicle at the same vertical coordinate as the base of the left front window.

B-pillar (one point) – The B-pillar is marked on the outside of the vehicle at the longitudinal center of the pillar at the same vertical coordinate as the lower A-pillar mark.

APPENDIX E
IIHS SIDE IMPACT REGULATIONS

The IIHS Side Impact regulations state that a 1,500kg moving deformable barrier (MDB) strike the stationary test vehicle on the driver's side at a speed of 50 km/hr and an angle of 90°. The barrier block is made from aluminum honeycomb, and has 379mm ground clearance. The front aluminum mounting plate has been raised 100mm higher off the ground and has been extended 200 mm taller than a standard FMVSS 214 barrier. The longitudinal impact point of the barrier on the side of the test vehicle is dependent on the vehicle's wheelbase. The impact reference distance (IRD) is defined as the distance rearward from the test vehicle's front axle to the closest edge of the deformable barrier when it first contacts the vehicle (Figure E1).

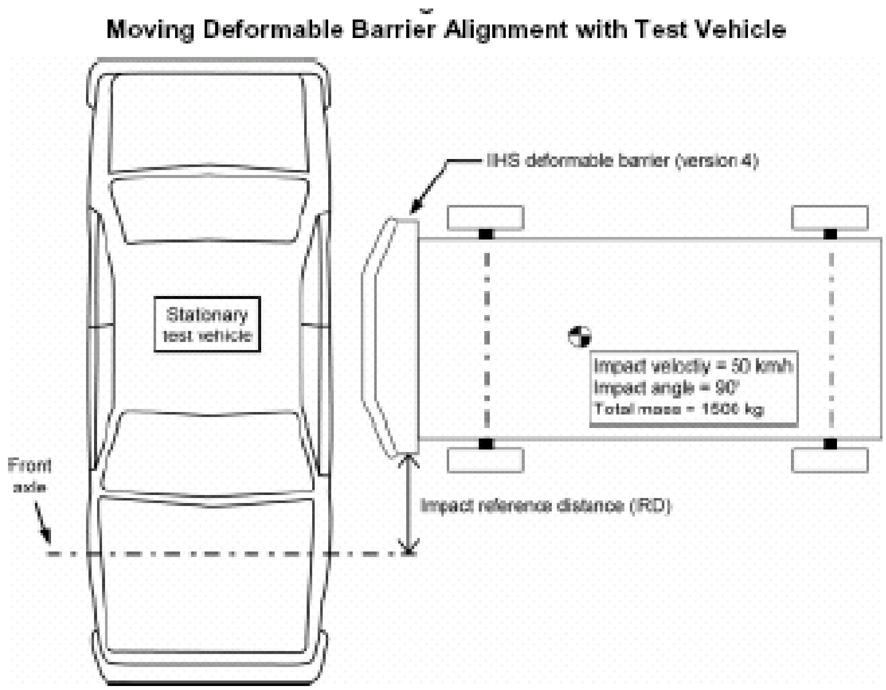

FIGURE E1

The IRD of FGPC vehicle is calculated at 810mm based on regulation.

The studies of FGPC vehicle at this time is only focused on the IIHS structural rating which states that the vertical range considered for the rating extends from the base of the B-pillar interior up to a point that is 540mm above the H-point measurement taken with the seat in the full-rear and full-down position. This corresponds approximately to the shoulder height of a 95th percentile male.

The structural rating requirements are shown in Figures E2 and E3.

Boundary line	Good	Acceptable	Marginal	Poor
B-pillar to driver seat centerline distance (cm)	12.5	5.0	0.0	
Structural failures	Downgrade structural rating by one category			

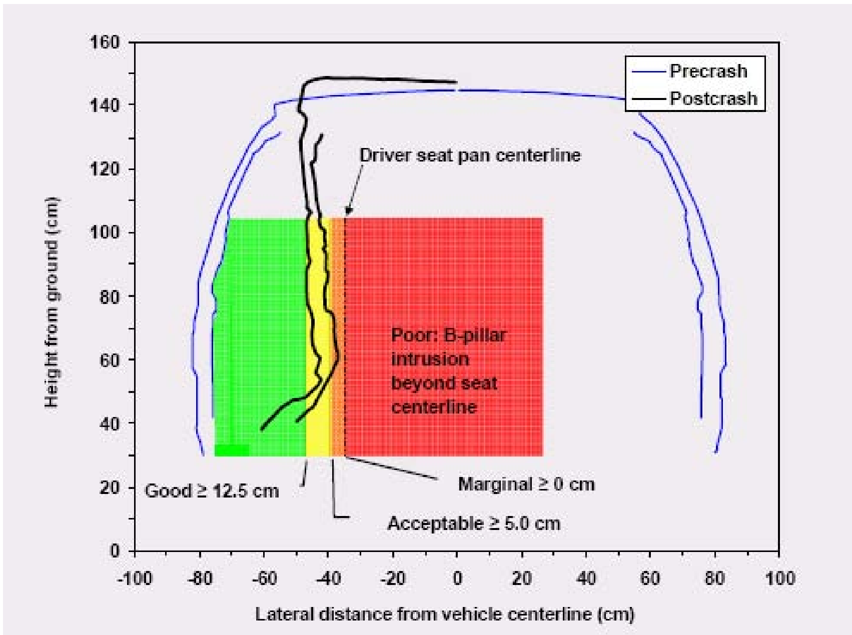

FIGURE E2: Structural Rating (B-Pillar Deformation)

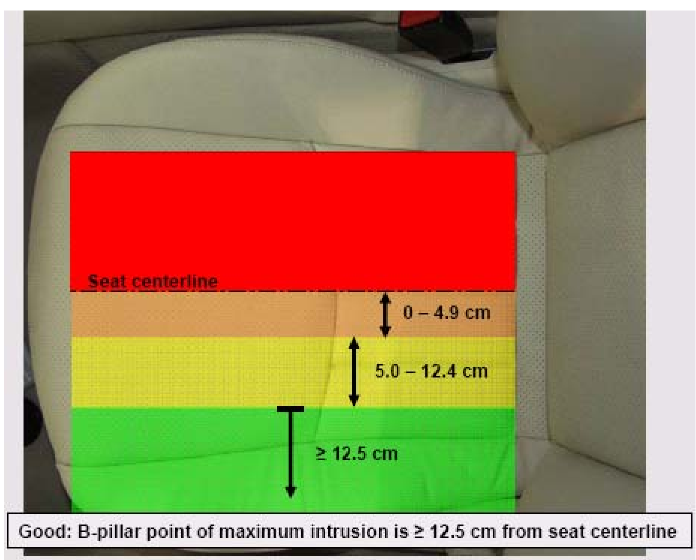

FIGURE E3: Structural Rating (B-Pillar Deformation)

APPENDIX F
REAR CRASH REGULATIONS - FMVSS301
Test requirements
Each passenger car and each multipurpose passenger vehicle, truck, and bus with a GVWR of 10,000 pounds or less shall meet the requirements. When the vehicle is impacted from the rear by a barrier moving at 48 km/h, fuel spillage shall not exceed the limits of the following. Fuel spillage in any fixed or moving barrier crash test shall not exceed 28 g from impact until motion of the vehicle has ceased, and shall not exceed a total of 142 g in the 5-minute period following cessation of motion. For the subsequent 25-minute period, fuel spillage during any 1 minute interval shall not exceed 28 g.

Test conditions
Where a range is specified, the vehicle must be capable of meeting the requirements at all points within the range. The following conditions apply to all tests:

- The fuel tank is filled to any level from 90 to 95 percent of capacity with Stoddard solvent, having the physical and chemical properties of type 1 solvent.
- The fuel system other than the fuel tank is filled with Stoddard solvent to its normal operating level.
- In meeting the requirements, if the vehicle has an electrically driven fuel pump that normally runs when the vehicle's electrical system is activated, it is operating at the time of the barrier crash.
- The parking brake is disengaged and the transmission is in neutral, except that in meeting the requirements of S6.5 when the parking brake is set.
- Tires are inflated to manufacturer's specifications.
- The vehicle, including test devices and instrumentation.

Rear moving barrier test conditions
The rear moving barrier test conditions and the positioning of the barrier and the vehicle is as followings: The barrier and test vehicle are positioned so that at impact

1. The vehicle is at rest in its normal attitude
2. The barrier is traveling at 48 km/h with its face perpendicular to the longitudinal centerline of the vehicle
3. A vertical plane through the geometric center of the barrier impact surface and perpendicular to that surface coincides with the longitudinal centerline of the vehicle

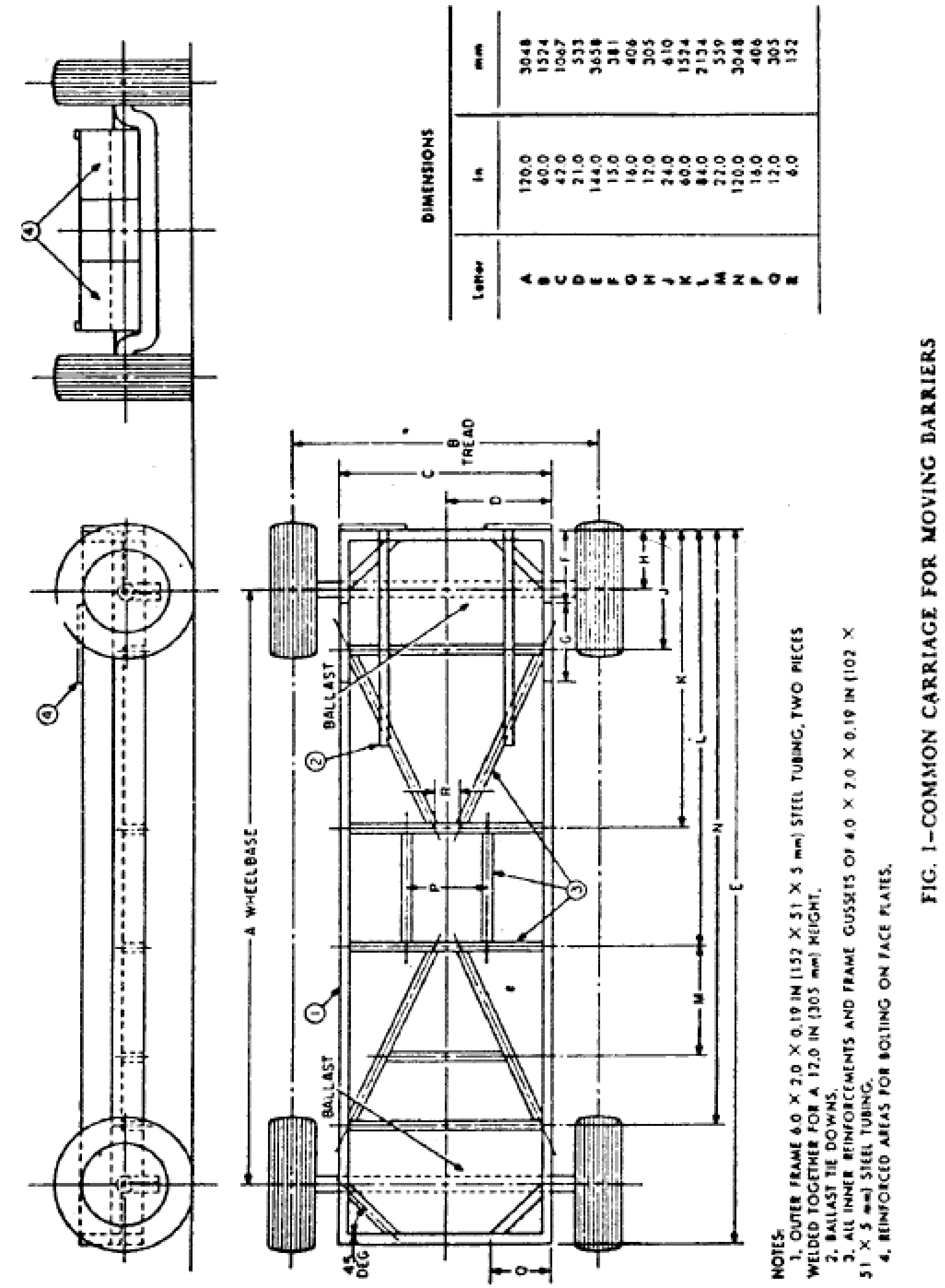
DIMENSIONS
Letter | in | mm
A | 120.0 | 3048
B | 60.0 | 1524
C | 42.0 | 1067
D | 21.0 | 533
E | 144.0 | 3658
F | 15.0 | 381
G | 16.0 | 406
H | 12.0 | 305
J | 24.0 | 610
K | 60.0 | 1524
L | 84.0 | 2134
M | 22.0 | 559
N | 120.0 | 3048
P | 16.0 | 406
Q | 12.0 | 305
R | 6.0 | 152
A WHEELBASE
B TREAD
BALLAST
BALLAST
45 DEG
NOTES:
1. OUTER FRAME 6.0 × 2.0 × 0.19 IN (152 × 51 × 5 mm) STEEL TUBING, TWO PIECES WELDED TOGETHER FOR A 12.0 IN (305 mm) HEIGHT.
2. BALLAST TIE DOWNS.
3. ALL INNER REINFORCEMENTS AND FRAME GUSSETS OF 4.0 × 2.0 × 0.19 IN (102 × 51 × 5 mm) STEEL TUBING.
4. REINFORCED AREAS FOR BOLTING ON FACE PLATES.
FIG. 1—COMMON CARRIAGE FOR MOVING BARRIERS

FIGURE F1

APPENDIX G
ROOF CRUSH REGULATIONS - FMVSS216
Test Device
The test device is a rigid unyielding block with its lower surface formed as a flat rectangle 30 inches X 72 inches.

Test Procedure
Place the sills or chassis frame of the vehicle on a rigid horizontal surface, fix the vehicle rigidly in position, close all windows, close and lock all doors, and secure any convertible top or removable roof structure in place over the passenger compartment.

Orient the test device as shown in Figure 1, so that

1. Its longitudinal axis is at a forward angle (side view) of 5° below the horizontal, and is parallel to the vertical plane through the vehicle's longitudinal centerline;
2. Its lateral axis is at a lateral outboard angle, in the front view projection, of 25° below the horizontal;
3. Its lower surface is tangent to the surface of the vehicle; and
4. The initial contact point, or center of the initial contact area, is on the longitudinal centerline of the lower surface of the test device and 10 inches from the forward most point of that centerline.

Apply force in a downward direction perpendicular to the lower of the test device at a rate of not more than one-half inch per second until reaching a force of 1 ½ times the unloaded vehicle weight of the tested vehicle or 5,000 pounds, whichever is less. Complete the test within 120 seconds. Guide the test device so that throughout the test it moves, without rotation, in a straight line with its lower surface oriented as specified in 1 through 4.

A test device shall not move more than 5 inches, when it is used to apply a force of 1 ½ times the unloaded vehicle weight or 5,000 pounds, whichever is less, to either side of the forward edge of vehicle's roof in accordance with the procedure. Both the left and right front portions of the vehicle's roof structure shall be capable of meeting the requirements, but a particular vehicle need not meet further requirements after being tested at one location.

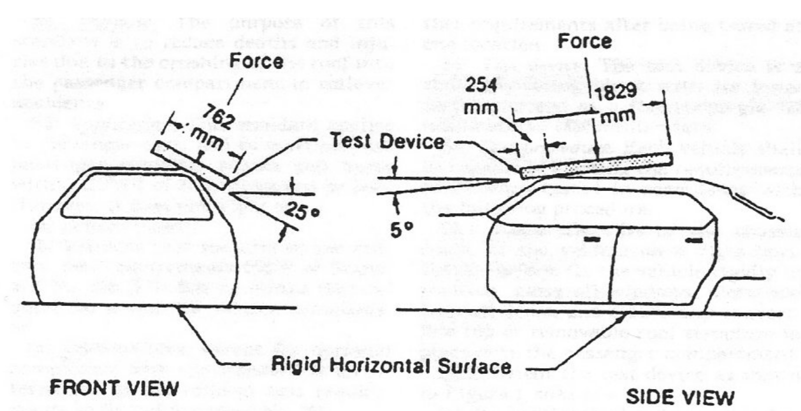

Figure 1.—Test Device Location And Application To The Roof

FIGURE G1

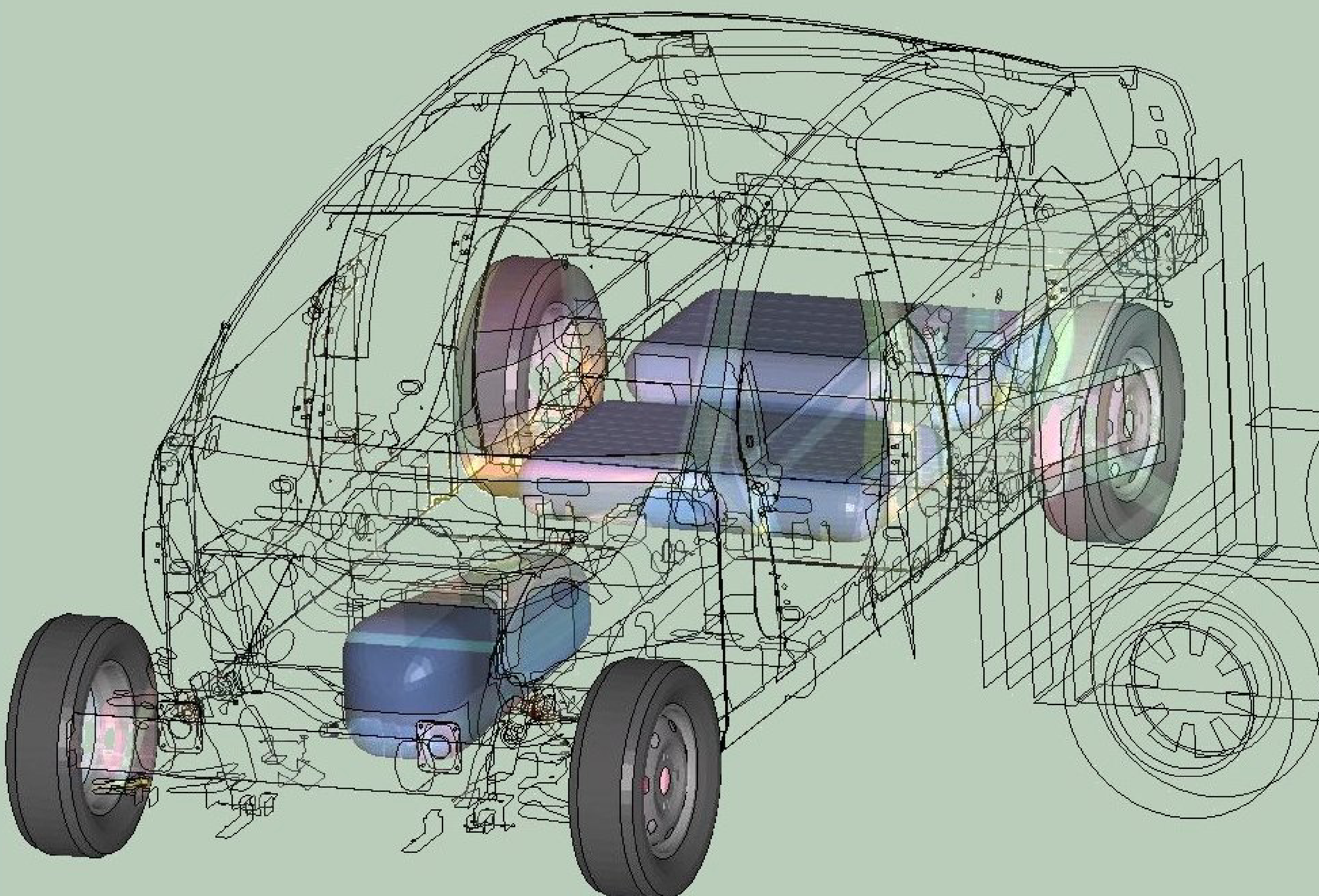

Auto/Steel Partnership

Future Generation Passenger Compartment
Task 2.5 - Mass Redistrubition Report

Mass redistribution of the FGPC baseline model

Task 2.5 – Mass Redistribution

Table of Contents

Task 2.5 – New Mass Redistribution

1. INTRODUTION

This report completes Task 2.5: New Mass Redistribution of the FGPC (Future Generation Passenger Compartment) project. Its purpose is to document changes that were made in the mass distribution of the ULSAB-AVC (Ultra Light Steel Auto Body Advanced Vehicle Concept) CAE model to more accurately simulate the IIHS Side Impact.

2. OBJECTIVE

The objective of this task is to:

- Evaluate the mass distribution of the ULSAB-AVC, which was the foundation of the FGPC vehicle.
- Modify the FGPC model mass distribution to be more representative of a production vehicle.

3. BACKGROUND

The ULSAB-AVC vehicle was the starting point for the FGPC project. In Task 2.0: New Mass Redistribution of the project, the vehicle passenger compartment was modified and packaged to allow the vehicle to be capable of having 2 different types of drive trains: diesel engine and fuel cell. The vehicle was evaluated for front crash, rear crash, roof crush, and IIHS Side Impact. The ULSAB-AVC model mass distribution was carried over for these studies.

It was then decided to add an additional Task 2.5 **"New Mass Redistribution"** to reallocate the mass in a more realistic manner. Task 2.5 represents an additional effort to study and redistribute the lumped masses in the vehicle, add new front seats and occupant masses, and rerun the IIHS side impact simulation. Mass distribution upgrades were performed on the baseline diesel vehicle structure, which is the worst case for IIHS Side Impact.

4. ULSAB-AVC VEHICLE LUMPED MASS STUDY

ULSAB-AVC Vehicle Lump Mass Distribution

The ULSAB-AVC diesel vehicle structure provided to ETA has been taken for this study. The total mass of this vehicle was 1390kg, including 693kg of structural mass and 697kg of lumped mass. The model had 697kg of mass distributed throughout the vehicle in 128,000 individual lumped masses. Figure 1 and Figure 2 show the initial distribution of individual lumped mass.

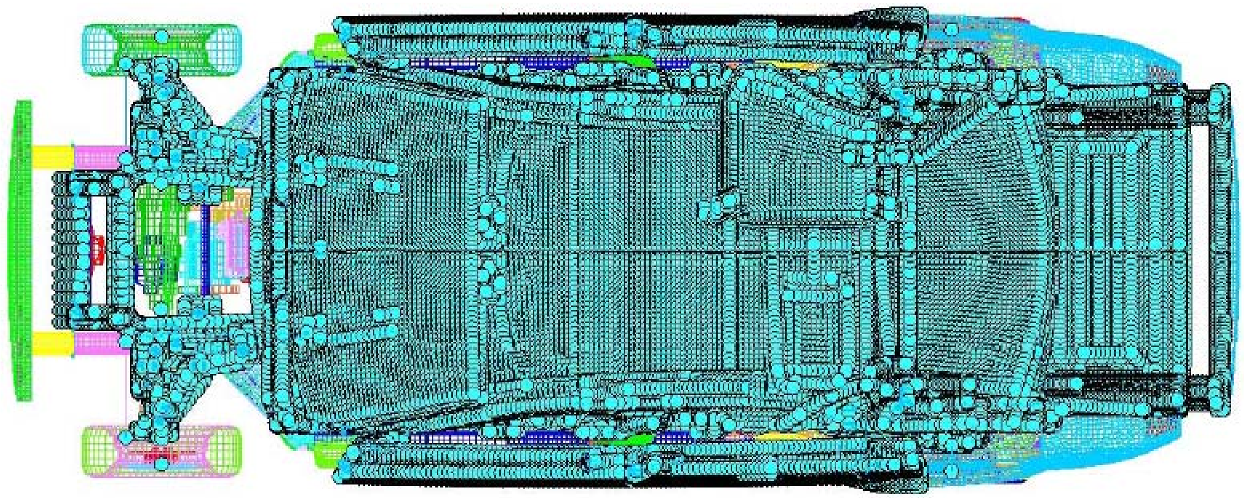

FIGURE 1: Initial Lumped Mass Distribution

47,000 of the 128,000 lumped masses have the same value 2.22E-06kg, as shown in Figure 2.

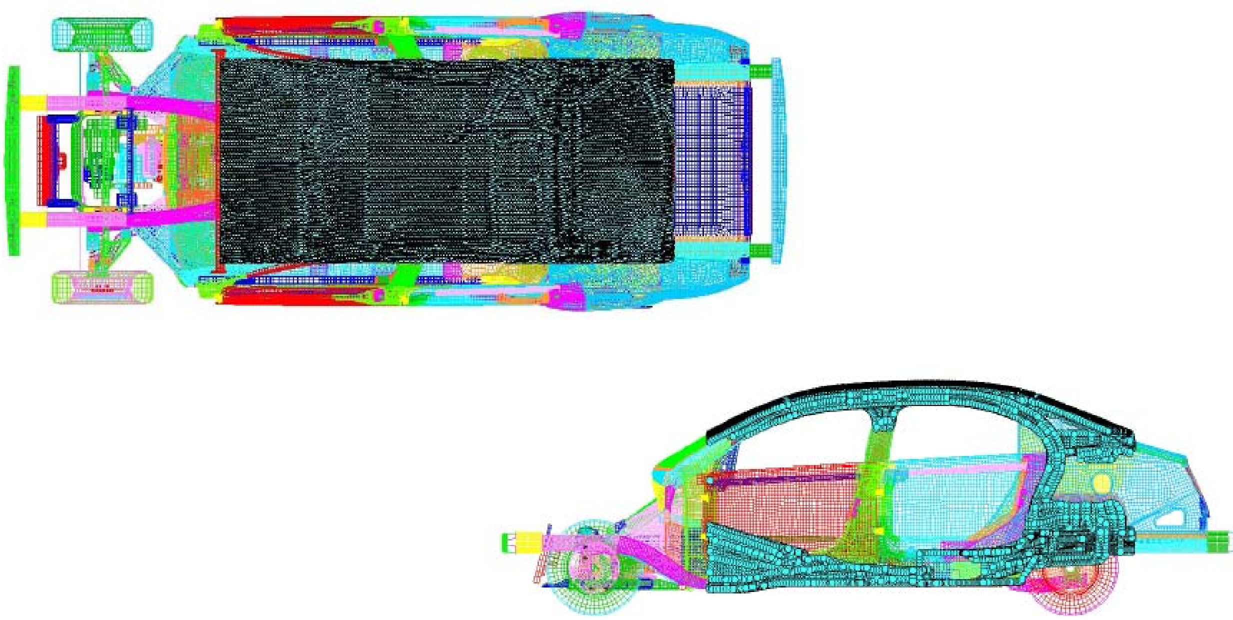

FIGURE 2: 47,000 Lumped Masses of 2.22E-06kg

The chassis-front suspension (Figure 3) had a total mass of 76.4kg, which included structural mass of 46.9kg and lumped masses of 29.4kg.

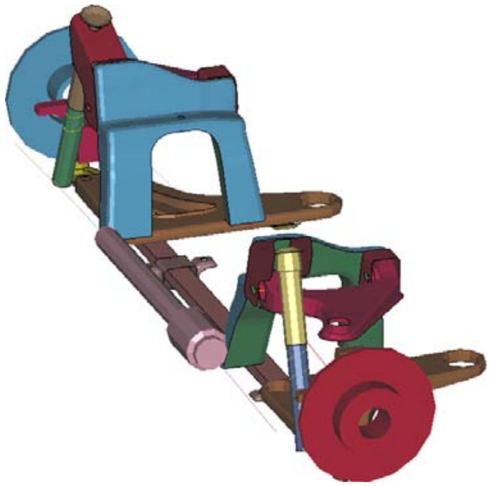

FIGURE 3: Front Suspension

The chassis-rear suspension (Figure 4) had a total mass of 33.1kg, which included structural mass of 13.7kg and lumped masses of 19.4kg.

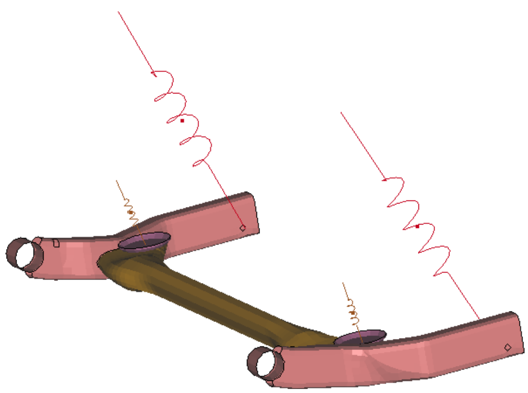

FIGURE 4: Rear Suspension

The fuel tank assembly (Figure 5) had a total mass of 55.3kg, which included structural mass of 8.7kg and lumped masses of 46.6kg.

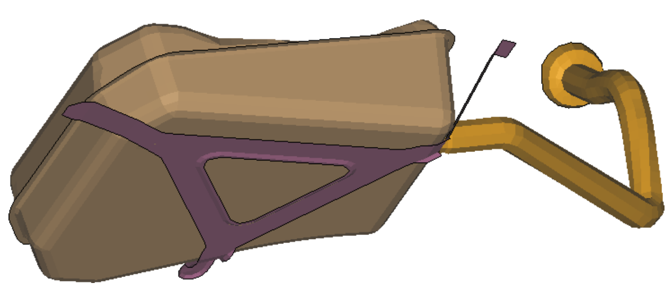

FIGURE 5: Fuel Tank Assembly

The radiator assembly (Figure 6) had a total mass of 11kg, which included structural mass of 2kg and lumped masses of 9kg.

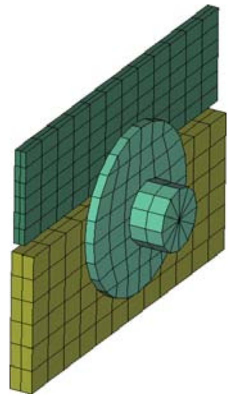

FIGURE 6: Radiator Assembly

The engine and attachments (Figure 7) had a total mass of 235kg.

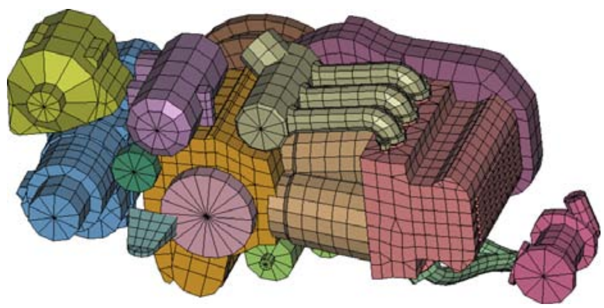

FIGURE 7: Engine & Attachments

The doors and package shelf (Figure 8) had the lumped masses of 61.1kg.

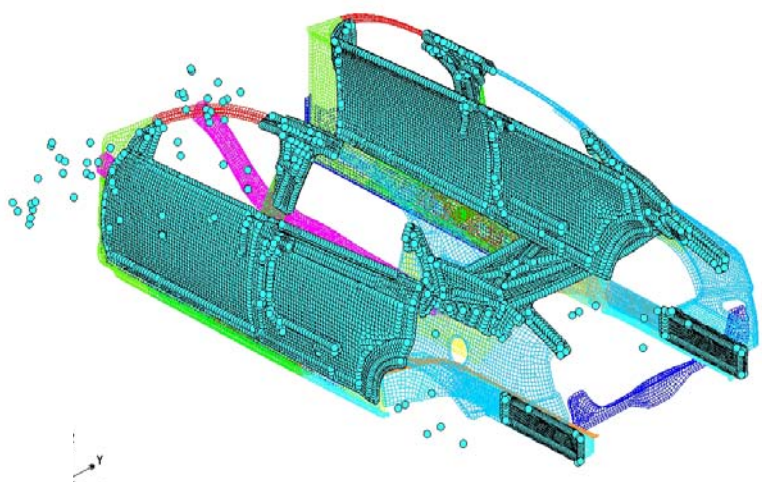

FIGURE 8: Doors & Package Shelf

A part-by-part check found that several structural parts had the most mass attached to them, as shown in Figure 9.

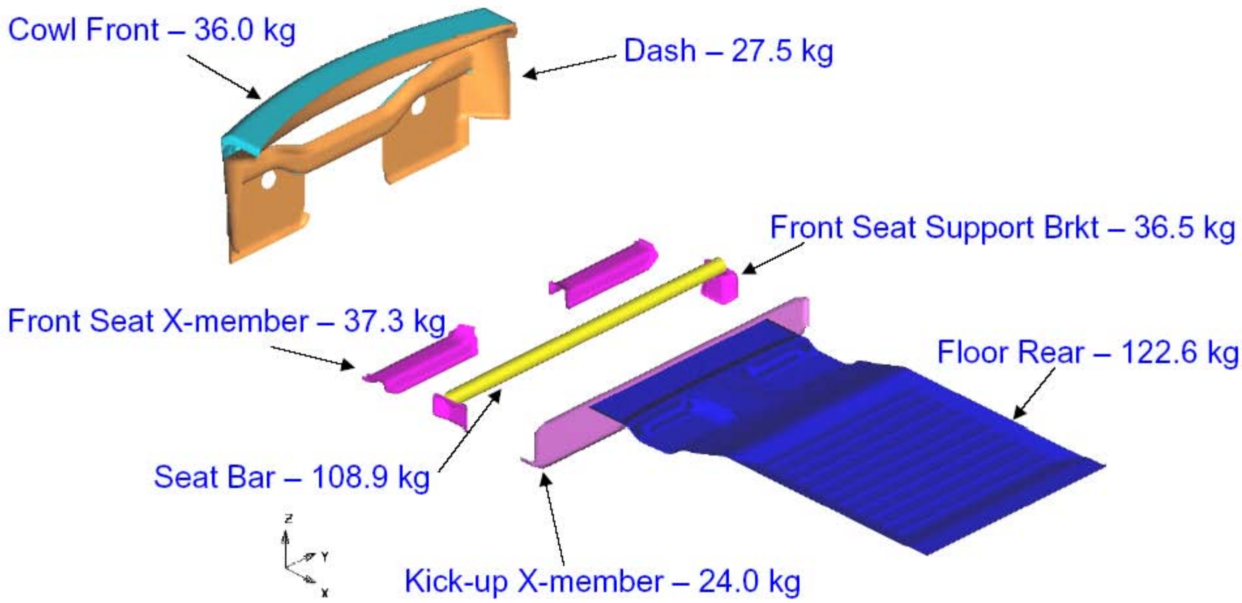

FIGURE 9: ULSAB-AVC Parts With Most Mass Attached

The mass of the front seats and occupants appears to be lumped into the Front Seat Cross-Member, Seat Bar, and Kick-Up Cross-member. ETA recommended that mass be removed and replaced with a donated seat model, and that the occupant mass be attached directly to seat.

5. FGPC VEHICLE LUMPED MASS REDISTRIBUTION

It was decided by A/SP to remove most of the 128,000 lumped masses that were carried over from the ULSAB-AVC model, and replace them with a smaller number of masses representative of components found in production vehicles. The exceptions were the front suspension, rear suspension, fuel tank, dash, cowl, and rear floor because it was thought that these masses were realistic (Figure 10). This left a total of 185kg to be deleted and re-distributed, as shown in Figure 11.

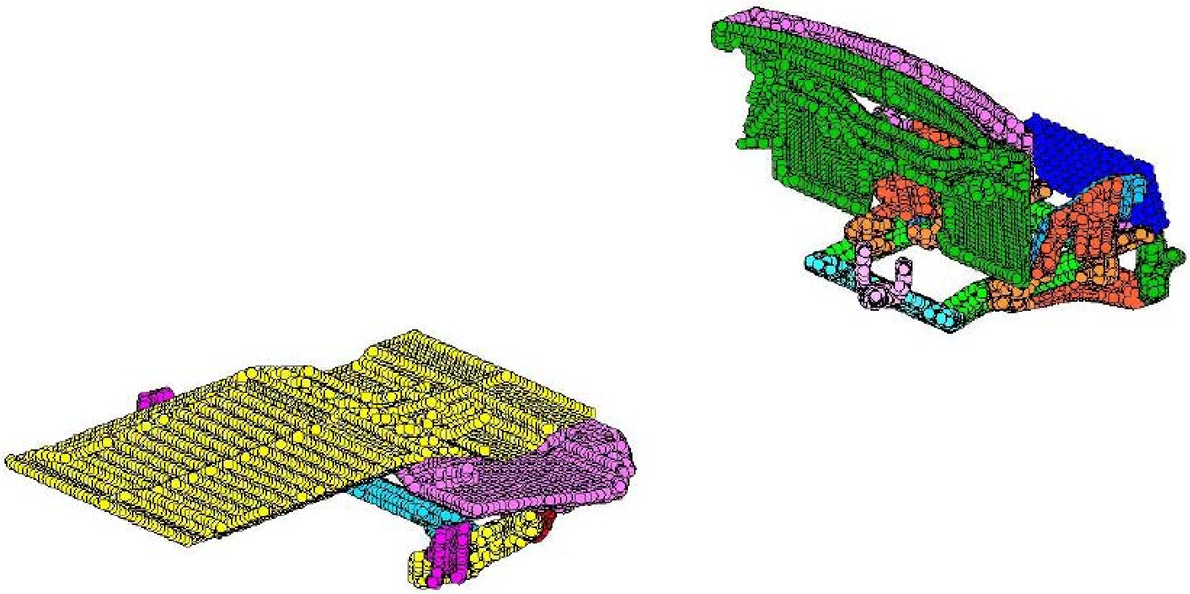

FIGURE 10: Masses Carried Over From ULSAB-AVC

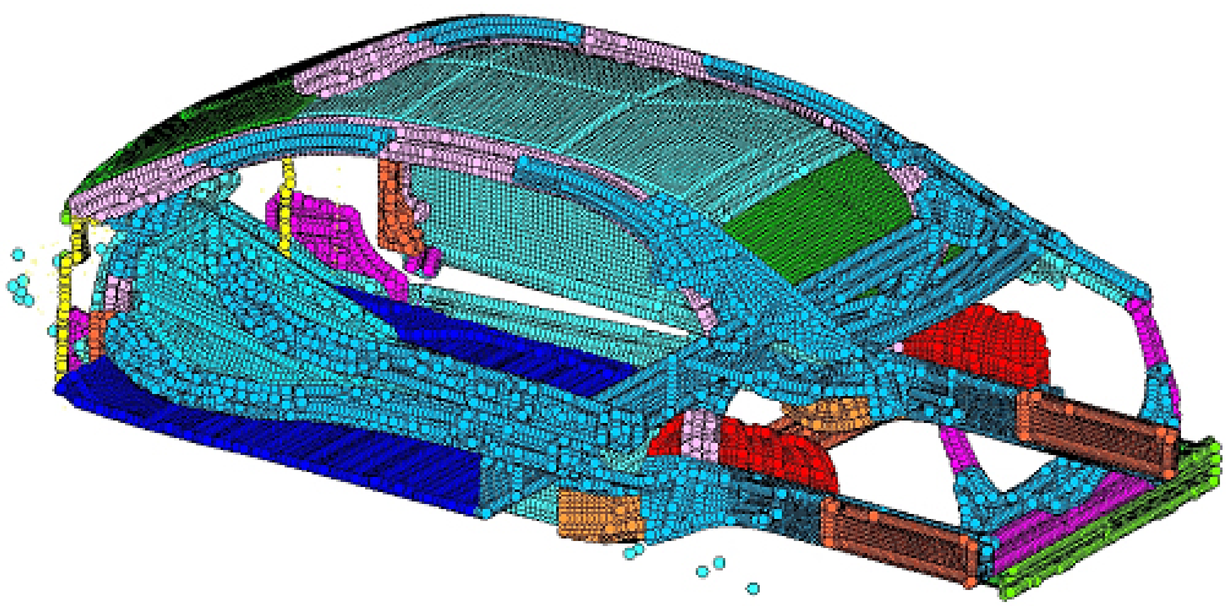

FIGURE 11: 185kg Mass to Be Deleted & Redistributed

In re-distributing the 185kg, the front and rear suspensions had an additional 35kg lumped mass added over what was in the ULSAB-AVC model (Figure 12).

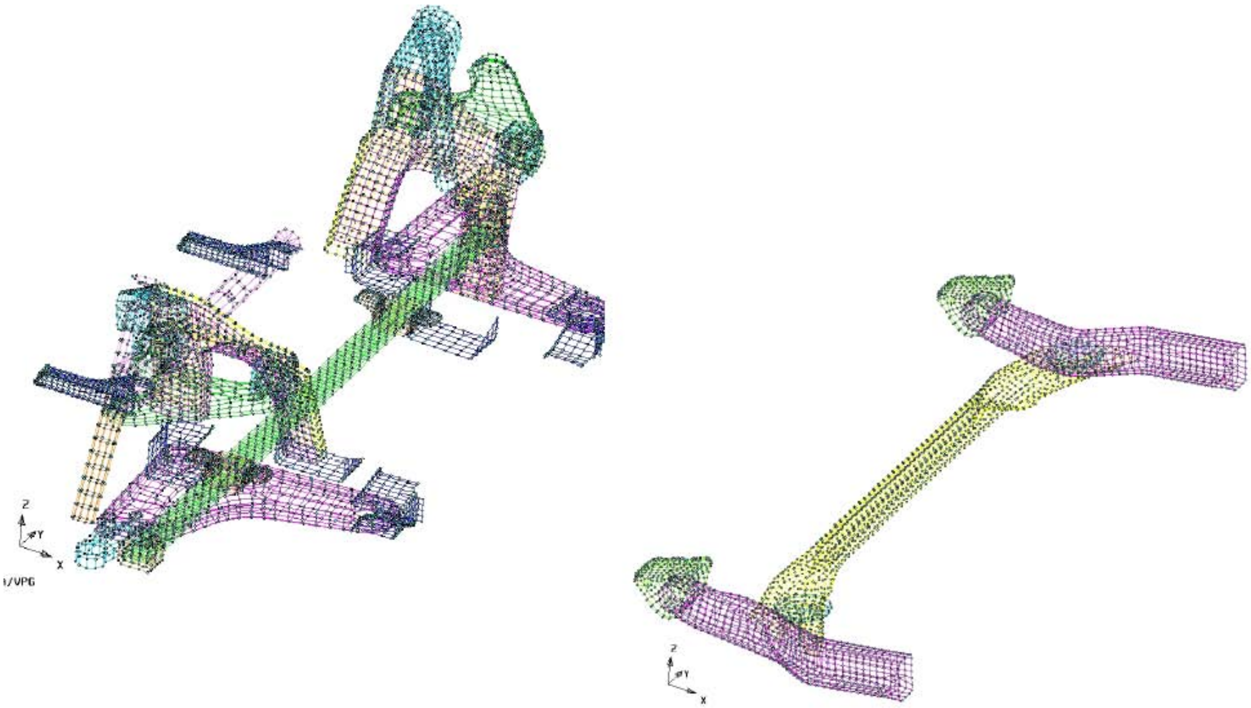

FIGURE 12: Front/Rear Suspensions - 35kg Additional Mass

35kg was added to the engine, increasing its mass from 235kg to 270kg. The fuel tank lumped masses were kept the same as ULSAB-AVC, since it represented 10 gallons of fuel (Figure 13).

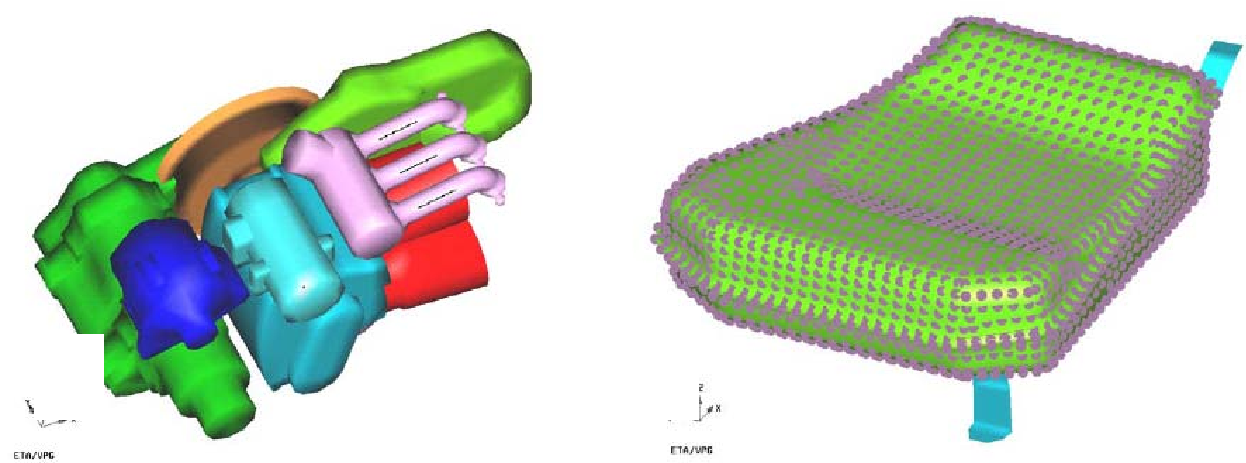

FIGURE 13: 35kg Added To Engine, Fuel Tank Same As ULSAB-AVC

Seat models from the ETA archives were modified and added to the vehicle. The seat masses were adjusted to 30kg per front seat, and the mass of 2 45kg occupants was attached, as shown in Figure 14.

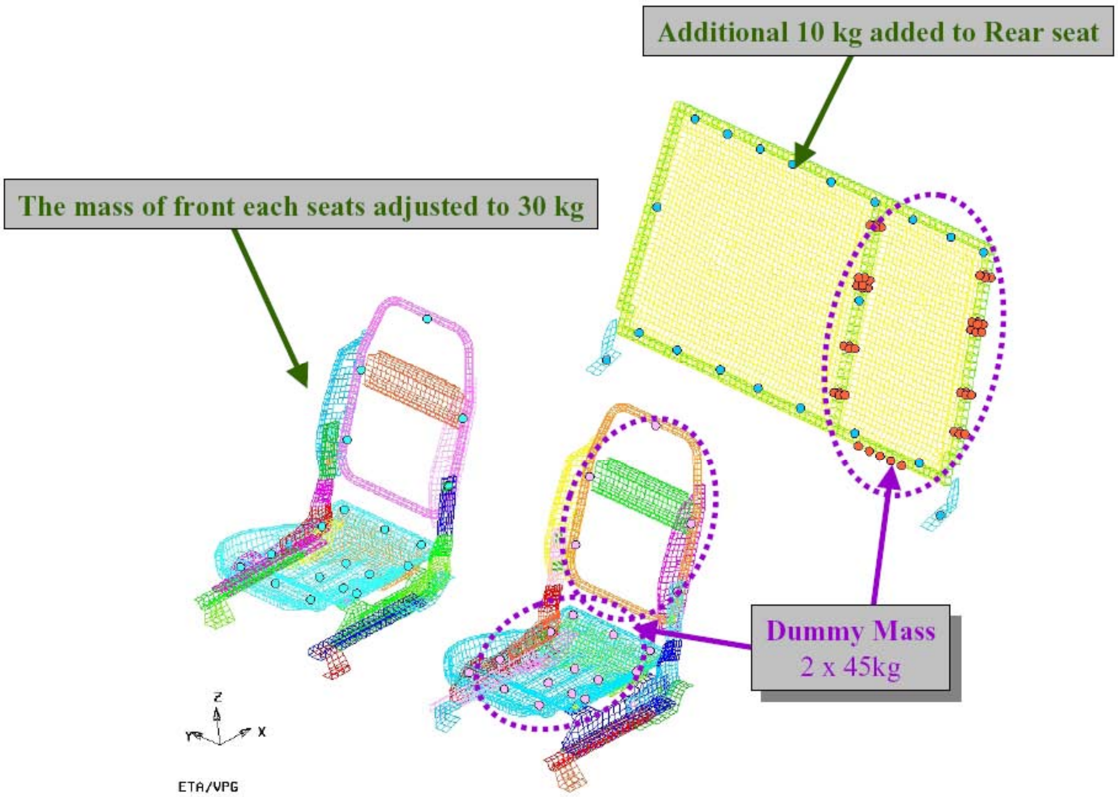

FIGURE 14: Seat Models Added To Vehicle

Finally, mass was added to represent the radiator, bumpers, door hardware, fenders, hood and deck lid, as shown in Figure 15.

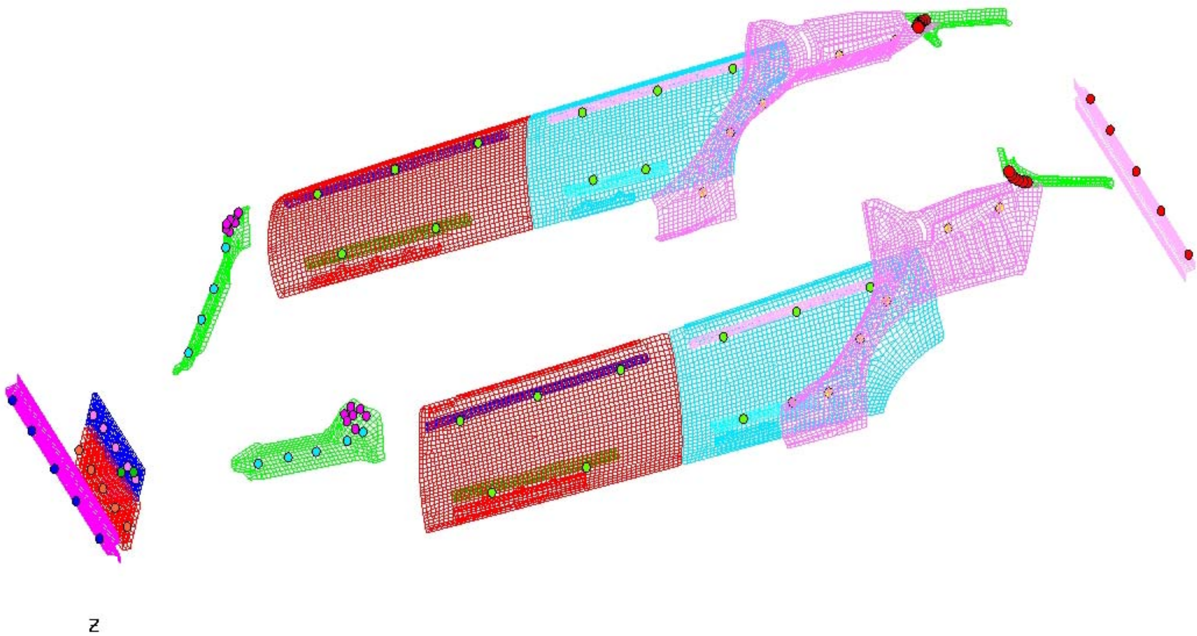

LOCATION	ADDITIONAL MASS (kg)	REMARKS
Radiator	5	Motor, fan
Front Bumper	5	Front fascia
Rear Bumper	5	Rear fascia
4 Doors	20	Trim, Hardware
Front Fender	5	
Rear Fender	5	
Hood	15	
Deck Lid	15	

FIGURE 15: Additional Vehicle Mass

The final lumped mass distribution is shown in Figure 16. The final IIHS simulation mass was 1351kg, as with the ULSAB-AVC. This represented a curb weight of 1102kg, with 90kg for 2 occupants and 159kg for luggage and optional equipment.

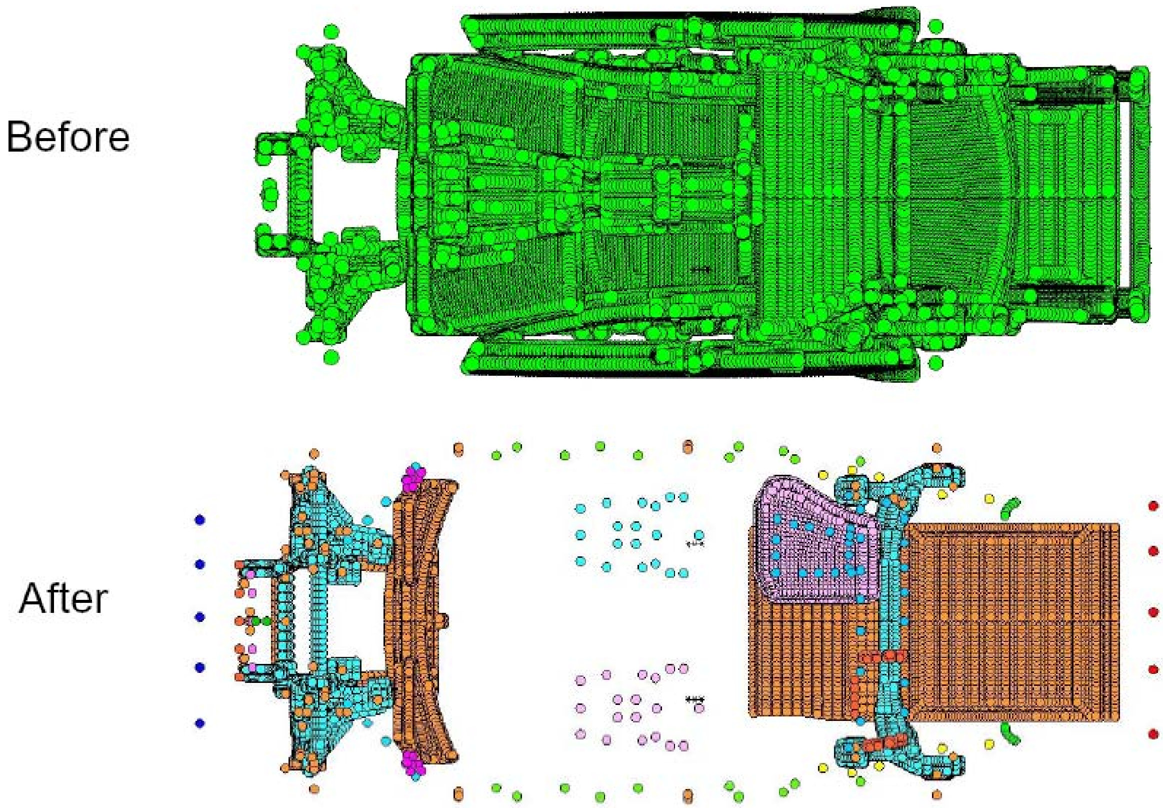

FIGURE 16: Lumped Mass After Redistribution

6. IIHS SIDE IMPACT ANALYSIS

The IIHS side impact was run with the new mass distribution. The result is shown in Figure 17. The modified mass distribution had very little effect on the B-pillar intrusion, changing it only 0.5mm.

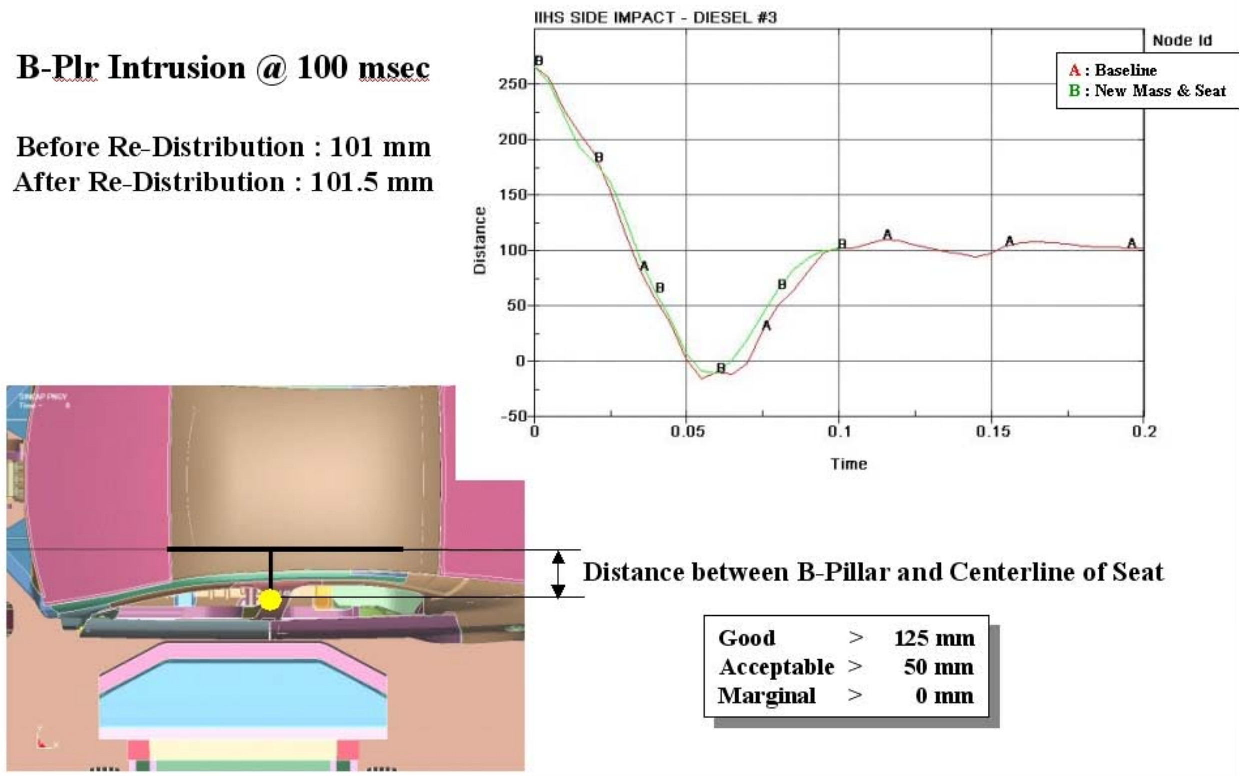

FIGURE 17: Side Impact Result - New Mass Distribution

7. CONCLUSION

The lumped mass of the FGPC vehicle was re-distributed in a more realistic manner than the ULSAB-AVC model, from which it was derived. The effect on the IIHS side impact was minimal.

For future tasks, it was decided to remove the masses that were added to represent the door hardware, and replace it with the 61kg that was in the ULSAB-AVC model, since it was more evenly distributed.

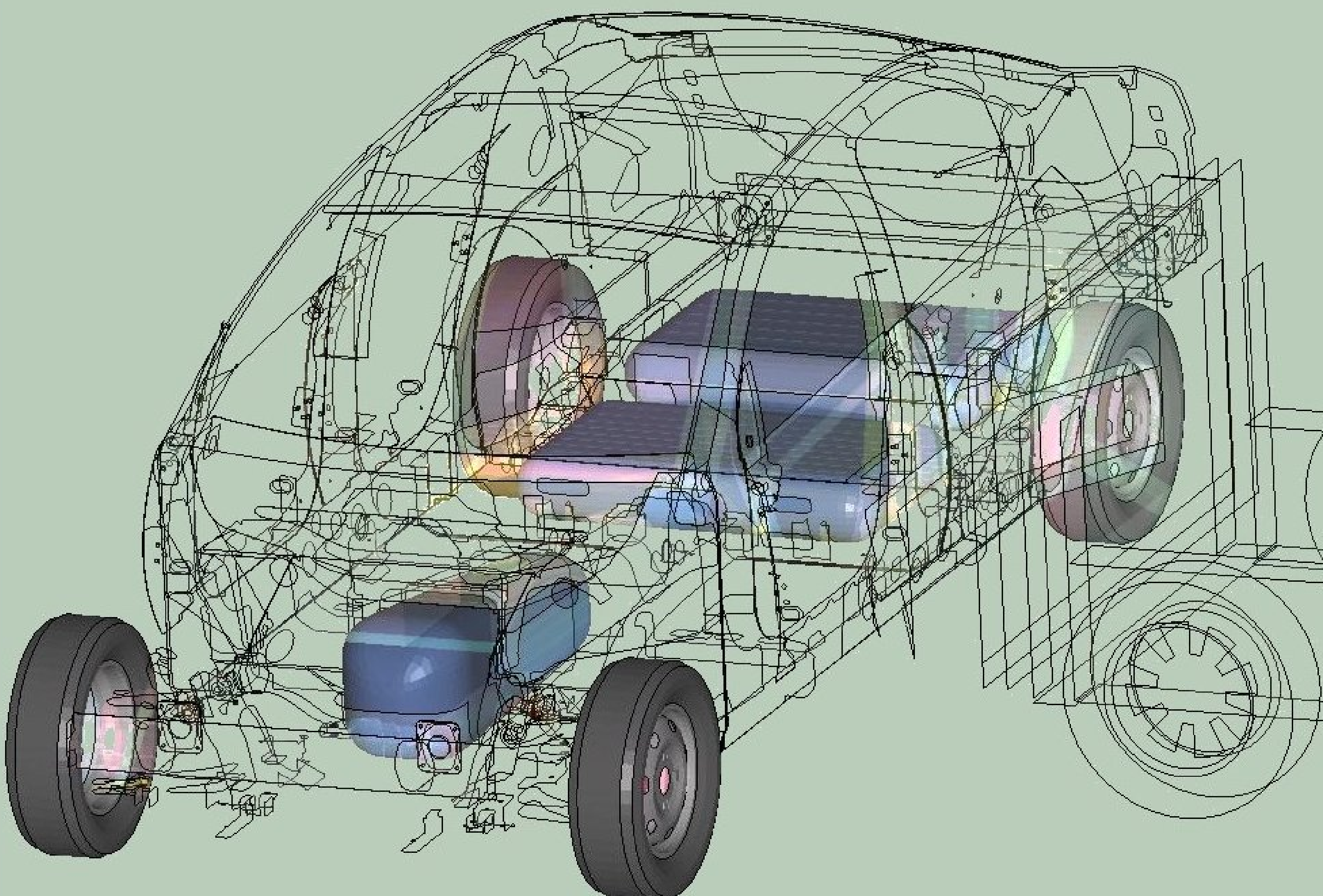

Auto/Steel Partnership

Future Generation Passenger Compartment Task 3.0 - Optimization Report

Multi-disciplinary loadpath, shape, gauge & material optimization to develop the new passenger compartment design concept

Auto Steel Partnership

Task 3.0 - Optimization

Table of Contents

Task 3.0 - Optimization

1. INTRODUCTION

This report completes Task 3.0: Optimization of the FGPC (Future Generation Passenger Compartment) project. Its purpose is to document the process used for identifying the optimal mass design for shape, thickness and material variables, which satisfies the side impact and roof crush targets. Two sub-tasks were defined for Task 3. Part 1 is to identify an optimized load path configuration by finding the optimal placement of load-carrying members and the gauge thickness of parts in the passenger compartment. Part 2 is to refine the design by finding the optimal shape, thickness and material for the parts in the passenger compartment, based on the concept developed in Part 1. For all optimization studies, the front wheel drive diesel engine design is used for the analyses, since its performance was poorest in the baseline analyses.

2. OBJECTIVE

The objective of this task is to minimize the mass of the design while meeting the targets for the side impact and the roof crush loadcases. The mass savings are to be achieved by changing the shape, thickness and material of the passenger compartment components.

3. OPTIMIZATION APPROACH USED

The optimization process is divided into two parts. In the first part of the optimization process, the optimal load paths for the side impact and the roof crush load cases are sought. Once the topology of the structure is known via load path optimization, the final shapes of the parts can be designed, knowing that the placement of the members is already near optimal for the load transfer. The second part of the optimization process is to refine the design by simultaneously modifying the shape, material and thickness of each component. The setup and results from both parts of the optimization are reported in the following sections.

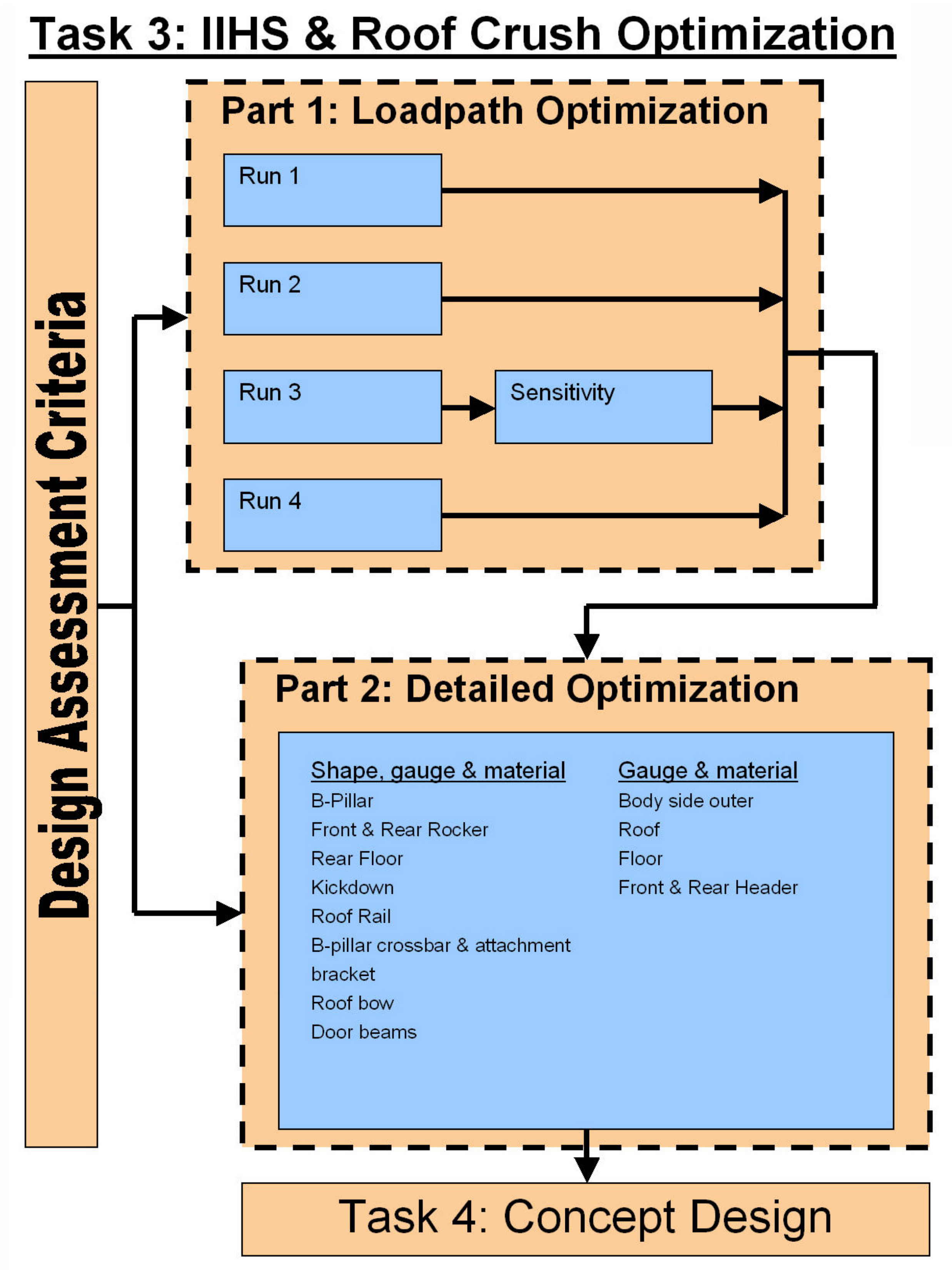

FIGURE 1: Flowchart Of The Optimization Approach

4. BASELINE DESIGN

All results from the optimization runs are compared with the baseline design. The baseline design is the modified model resulting from the completion of Task 2: Calibration Baseline. Unless noted otherwise, wherever mentioned the baseline design refers to this modified ULSAB-AVC front wheel drive diesel engine design. The baseline design did not meet the FMVSS Side Impact requirement that the survival space be greater than 125mm. The survival space for the baseline design is 101mm. Figures 2 & 3 show the deformed baseline model from the side impact analysis and the roof crush analysis respectively.

FIGURE 2: Side Impact Analysis – Baseline Design Deformed Shape

FIGURE 3: Roof Crush Analysis – Baseline Design Deformed Shape

5. PART 1 - DESIGN TOPOLOGY OPTIMIZATION

Three cross-members were studied for identifying their optimal location during the topology optimization: the front seat cross-member, the roof bow and the B-Pillar crossbar. In addition to the location of these cross-members, the thicknesses of the primary parts in the passenger cabin were also varied. Considering thickness in the topology optimization is very important for finding the most mass efficient load path. Without varying the thickness, the load capacity of the other members is not varied, which results in a sub-optimal solution for the topology optimization.

The Roof Rail and the B-Pillar in the baseline design were divided into 3 parts each to allow for different thickness values in different regions of these parts. The division is shown in Figures 4 & 5. The reason for this division is to explore and identify areas in these parts that contribute the most (or the least) to the performance of the design. The materials for all the components in this part of the optimization were not changed relative to the baseline.

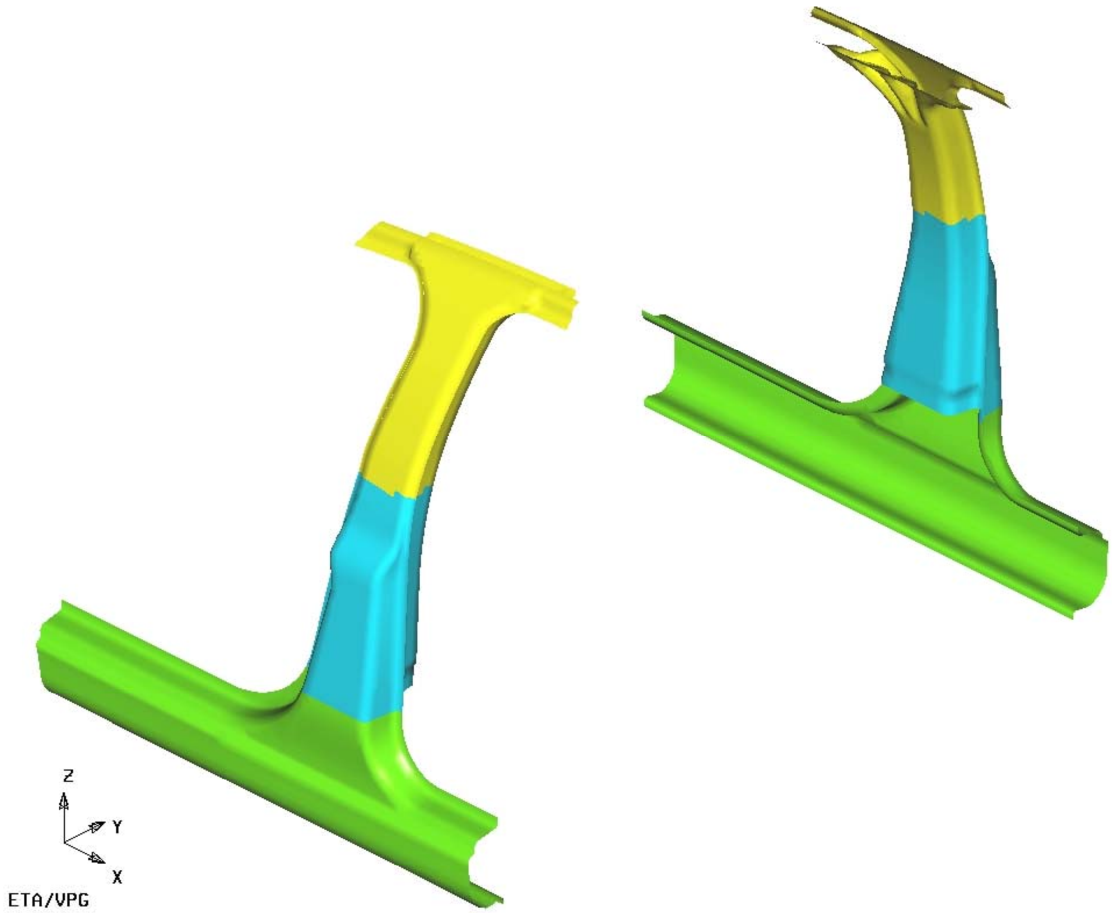

FIGURE 4: B-Pillar - Divided Into Three Sections, Able To Change Gauge Independently

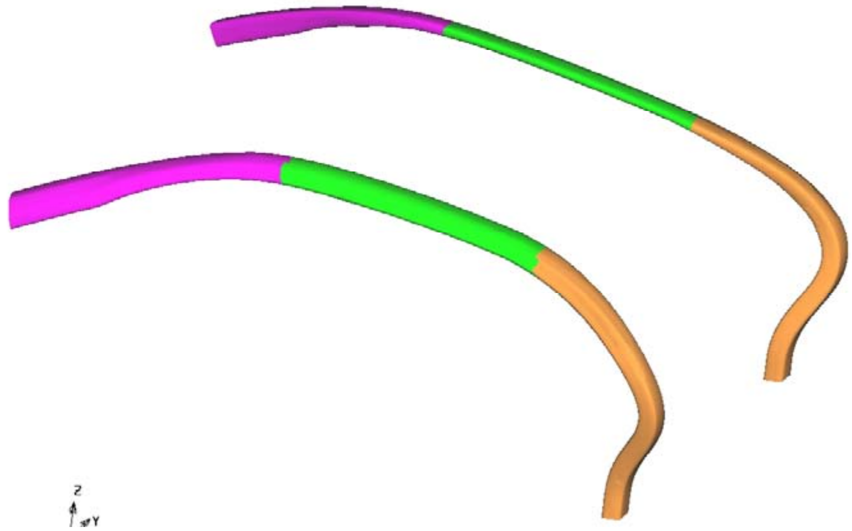

FIGURE 5: Roof Rail - Divided Into Three Sections, Able To Change Gauge Independently

5.1. CROSS-MEMBER REPRESENTATION

The varying cross-members (roof bow, front seat cross-member, and the B-Pillar crossbar) were modeled with beam elements. This representation was used for all the analyses in Part 1 optimization. All the other parts remained unaltered. The beam representation is justified here, as the objective of the study is to find the overall load path, without focusing on the local deformations in these parts. Using a beam representation reduces the modeling effort of the various configurations of these designs. A hollow rectangular closed beam section was used for the roof bow and the front seat cross-member. A hollow circular section was used to represent the B-Pillar crossbar. The dimensions of the beam sections were calculated to give the same inertia properties as the baseline shell section. Figure 6 shows the beam representation.

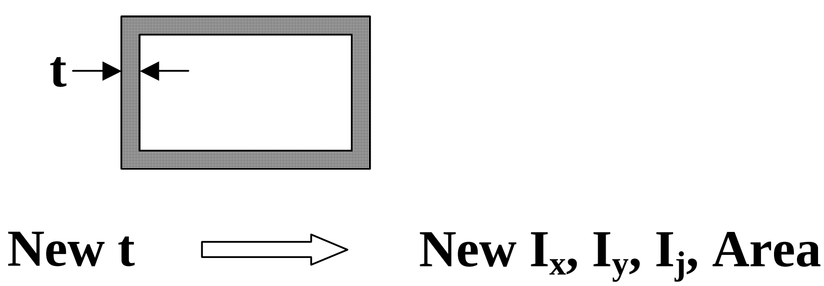

FIGURE 6: Cross-Member Beam Representation - Inertia Properties Used For Beam Sections Are Calculated Based On New Thickness Value.

The size of the cross-member is varied by updating the inertia properties of the section definition. The section properties are calculated using the same cross-sectional dimensions as determined above, but with a new thickness value.

5.2. EVALUATION OF DESIGN PERFORMANCE

During optimization, the software creates a new design by assigning values to all design variables and then executing the analyses required to assess the performance of the design. Three responses were used to assess the performance of each design, as defined in the optimization statement: the mass, the survival space during side impact, and the roof crush force. The discussion below describes how these measurements are calculated for each design.

5.3. MASS

The mass of only the parts being designed is used as a performance measure during all the optimization runs. The sum of the masses for all the designed parts is the value that is optimized during the optimization run.

5.4. SURVIVAL SPACE

The survival space measures the performance of the design for the IIHS side impact analysis. The survival space is measured as the normal distance between an XZ-plane passing through the middle of the driver seat to the closest point on the inner B-Pillar/Rocker. The measurement is shown in Figure 7 & 8. The IIHS side impact regulations consider a value greater than 125mm as good. This value will be used for the target survival space during the optimization run.

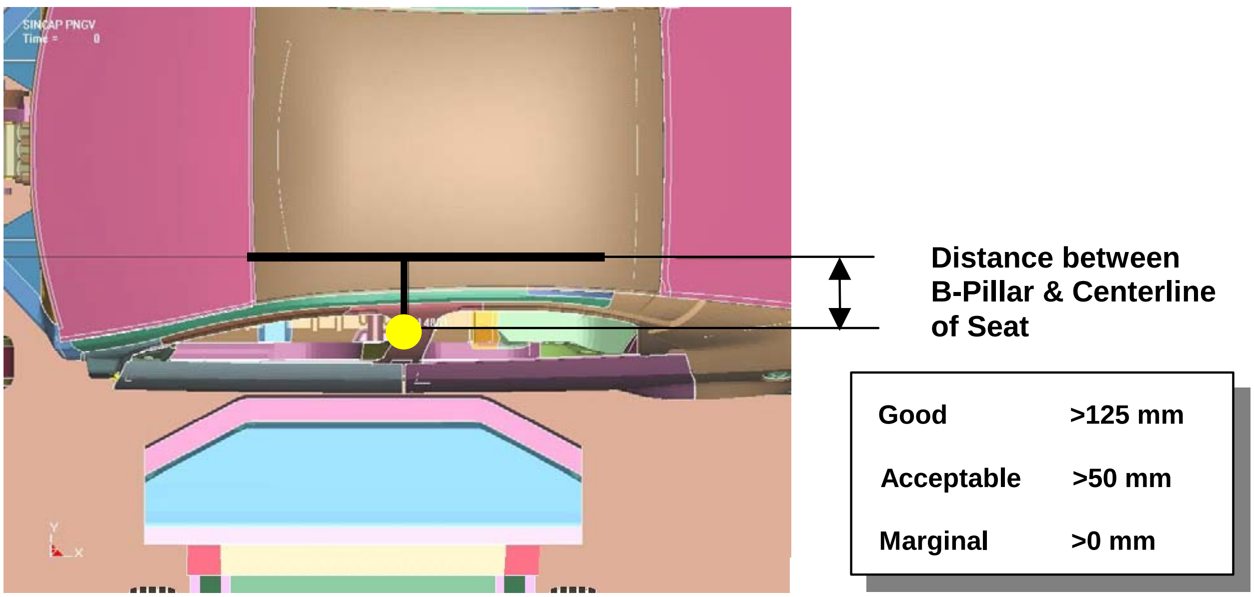

FIGURE 7: Side Impact Survival Space

The distance between the B-Pillar and the centerline of the seat at the end of the side impact analysis is called the survival space. A value greater than 125mm is considered good and has been set as the minimum value for this constraint during the optimization studies.

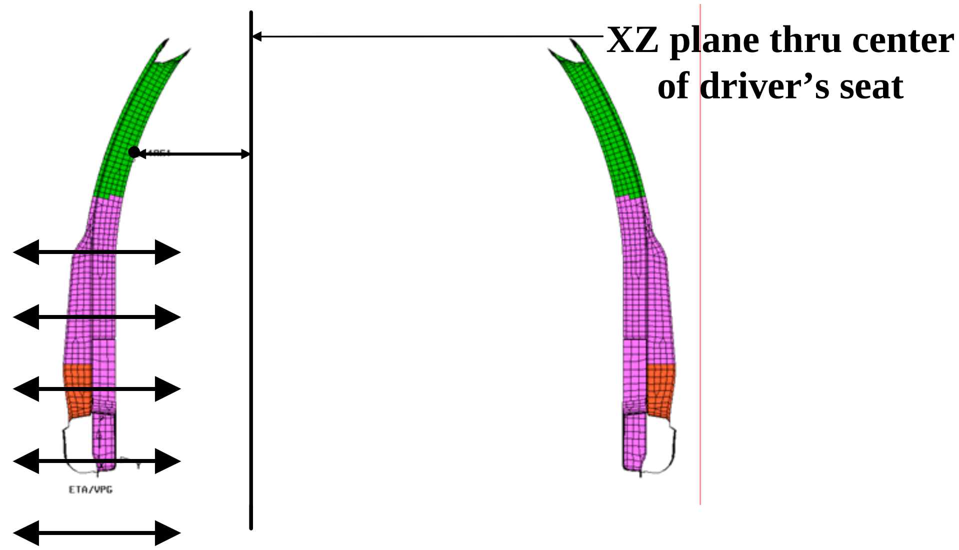

*FIGURE 8: Survival Space - Measured At Multiple Locations,
Worst (Smallest) Quoted As Survival Space Value*

5.5. ROOF CRUSH FORCE

The roof crush force measures the force capacity of the passenger cage in case of roll over. The target is to maintain the force above (2.75 * curb weight of the vehicle). The target force for the baseline design is 31250N. Since we are trying to minimize the mass of the design, this value will be used for the target during optimization. The roof crush force value used during optimization is the minimum roof crush force that is measured after the point at which this force initially exceeds the target force. If the force never passes the target force, the maximum force value is used instead. The baseline roof crush force curve is shown in Figure 9.

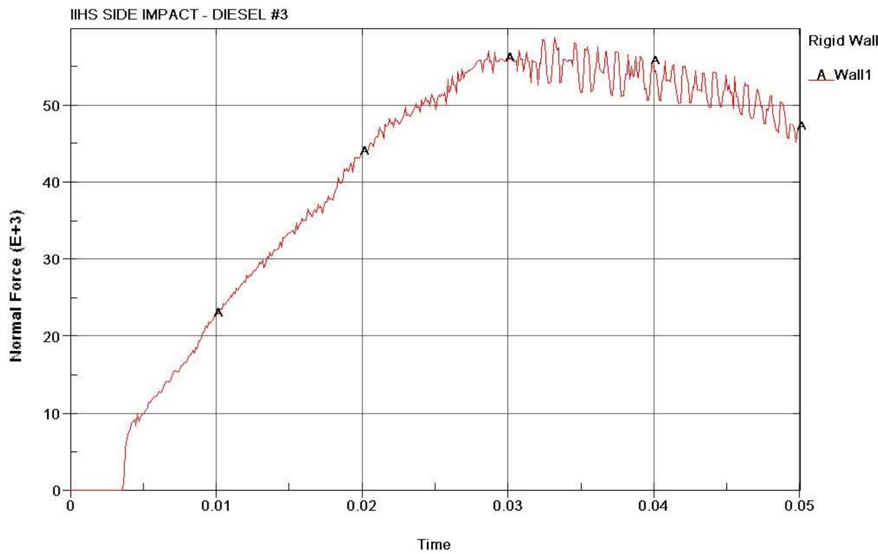

FIGURE 9: Roof Crush Force - Baseline Design

5.6. TOPOLOGY OPTIMIZATION RUNS

Three different optimization runs were setup for identifying the optimal topology for the passenger compartment structure. The different runs included features identified in the benchmarking part of the project. The main difference between the three runs is in the cross-members that were allowed to be varied within each run. The details of each run are given in the following sections.

6. TOPOLOGY OPTIMIZATION – RUN1

The objective of this run is to optimize the location for the roof bow and the front seat cross-member in addition to the thickness of the parts in the passenger compartment for a minimum mass design. Each design in this run has only one roof bow and one front seat cross-member. The optimization statement for the run is:

Minimize:
Mass of the design
Subject to:
Roof crush force ≥ 31250N (2.75 * curb weight)
Survival space ≥ 125mm
By varying:
Fore/aft location of the roof bow
Fore/aft location of the front seat cross-member
Size of the Roof Bow
Size of the Front Seat Cross-member
Size of the Roof Rail Section 1
Size of the Roof Rail Section 2
Size of the Roof Rail Section 3
Size of the B-Pillar Section 1
Size of the B-Pillar Section 2
Size of the B-Pillar Section 3
Size of the Inner Rocker
Size of the B-Pillar Crossbar
Size of the Floor Kick-down
Size of the Front Header
Size of the IP Beam

A total of 15 design variables were considered. Two variables (location of roof bow and location of Front seat cross-member) are discrete and the other 13 variables are continuous. All the design variables are shown in Figure 10.

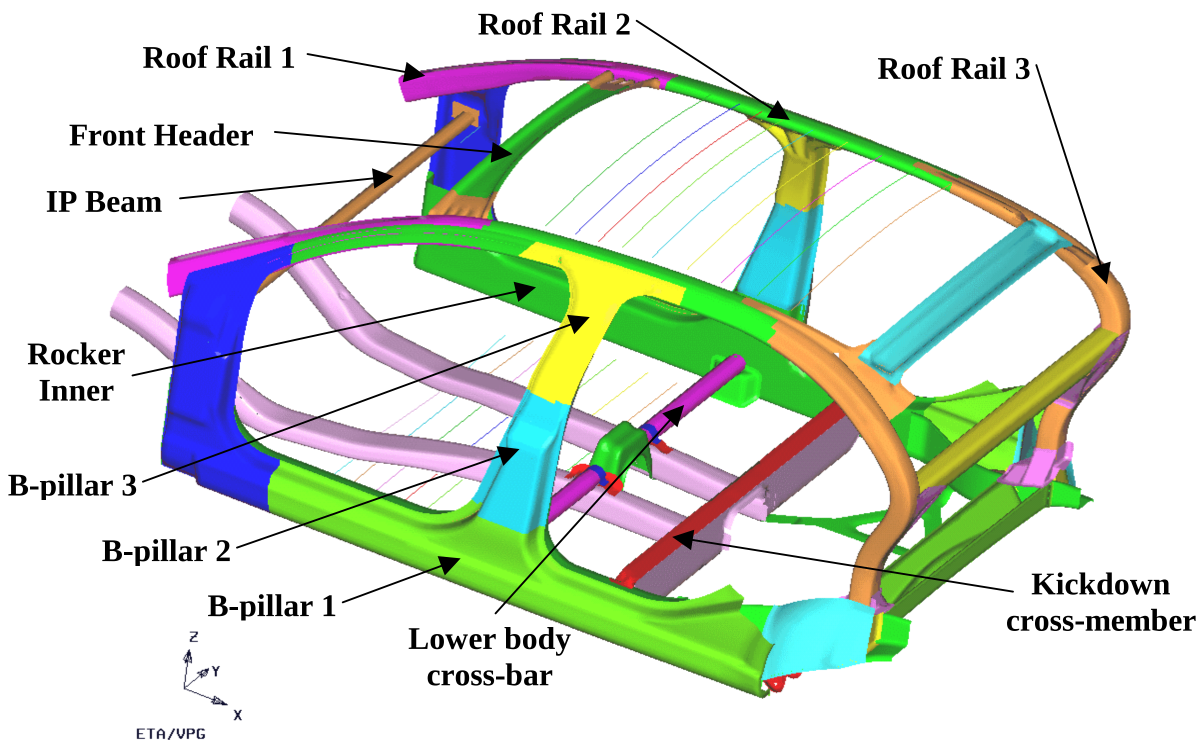

FIGURE 10: Optimization Run1 - Design Variables

Figure 11 shows all the possible locations for the roof bow during the first optimization run. Each design generated during an optimization could have only one of the possible 10 locations. Similarly, Figure 12 shows all 8 possible locations for the front seat cross-member. Again, only one of these 8 cross-members can be active in a given design.

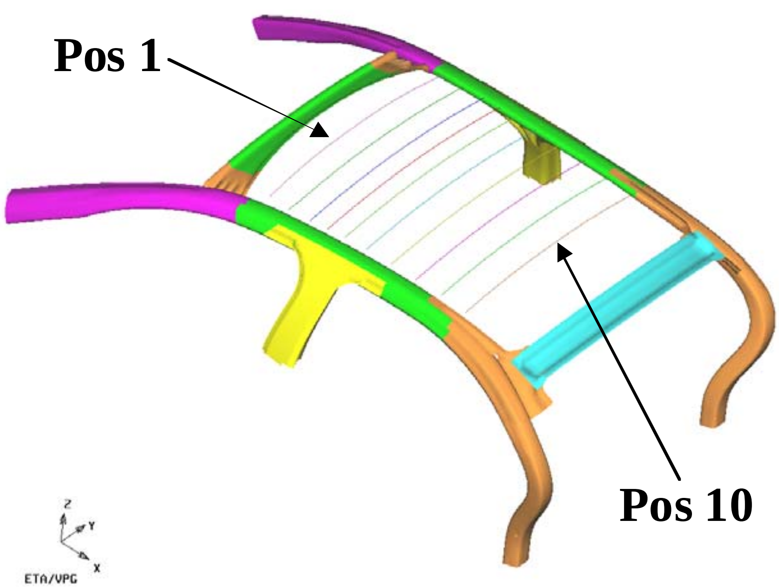

FIGURE 11: Optimization Run1 - Discrete Roof Bow Locations

Each design can only have one of the 10 roof bows shown. The roof bows are numbered 1 through 10, with the positions 1 and 10 as labeled. Position 1 is towards the front of the vehicle.

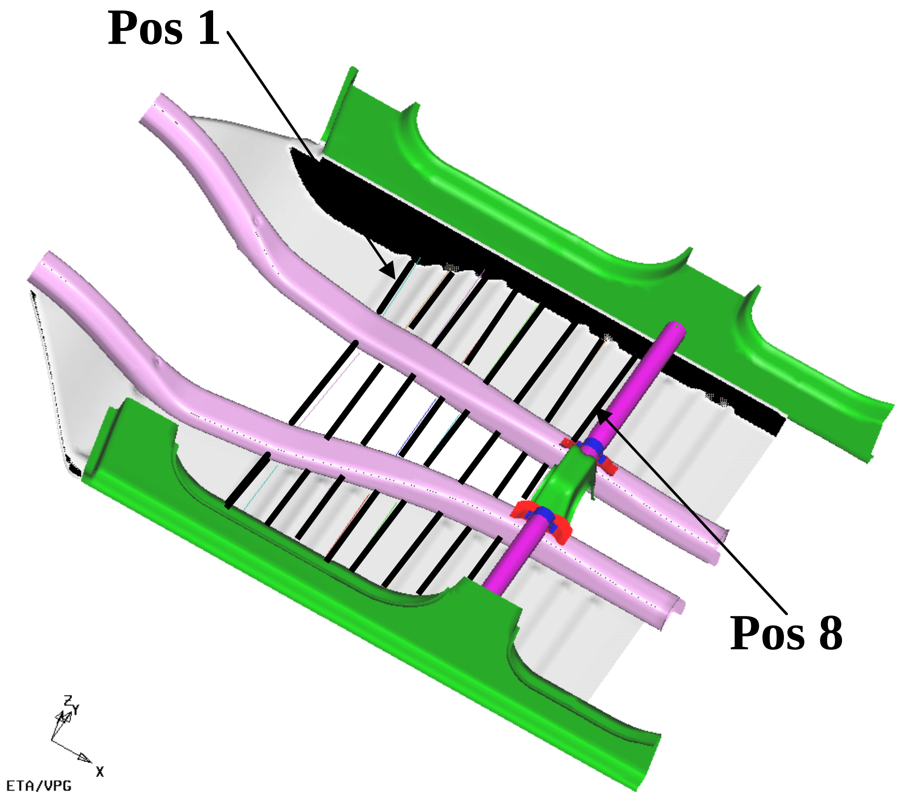

FIGURE 12: Optimization Run1 - Discrete Front Seat Cross-member Locations

Eight discrete locations were created for the front seat cross members during the first design optimization run. Each design can have only one of the eight front seat cross-members shown. The cross members are numbered 1 through 8, with the positions 1 and 8 as labeled. Position 1 is towards the front of the vehicle.

6.1. RESULTS

The optimization reduced the mass of the designed parts by 12.5%, from 58.49 to 51.17kg. Both the survival space and the roof crush force constraints were satisfied; the survival space value was 128mm (>125mm) and the minimum rigid wall force value was 31259N. It should be noted that the baseline design did not meet the survival space constraint. So in addition to satisfying the constraints, the optimization was able to reduce the mass of the designed parts by 12.5%.

VARIABLE NAME	BASELINE	MINIMUM	MAXIMUM	OPTIMIZED
Roof Bow Position	5	1	10	8
Roof Bow Thickness	1.0	0.02	1.5	0.094
Front seat Xmember Position	4	1	8	8
Front seat Xmember Thickness (mm)	1.0	0.02	1.5	0.02
Roof Rail 1 Thickness (mm)	1.0	0.5	2.0	1.13
Roof Rail 2 Thickness (mm)	1.0	0.5	2.0	1.37
Roof Rail 3 Thickness (mm)	1.0	0.5	2.0	0.5
B-Pillar 1 Thickness (mm)	1.80	1.0	2.5	1.24
B-Pillar 2 Thickness (mm)	1.80	1.0	2.5	1.255
B-Pillar 3 Thickness (mm)	1.80	1.0	2.5	1.36
Rocker Thickness (mm)	1.50	1.0	2.0	1.0
Front Header Thickness (mm)	0.7	0.3	1.5	1.022
Cross-Bar Thickness (mm)	1.20	0.75	1.6	0.8775
Kick-down Thickness (mm)	0.7	0.3	1. 5	1.03
IP Beam Thickness (mm)	2.0	1.0	3.0	1.0

TABLE 1: Optimized Values For Variables Studied.
Minimum & Maximum Values Included For Comparison

The optimal positions for the roof bow and the front seat cross member from this run are shown in Figures 13 & 14 respectively. As can be seen the optimal position for the roof bow identified is just behind the B-Pillar, while the optimal position for the front seat cross-member identified is the last position allowed towards the end of the car. Note, that Roof Bow Position 8 with a gauge of 0.094mm was the optimal solution. When defining the Part 2 optimization it was decided to keep the roof bow and allow the shape of the roof rail to vary. This resulted in a significant increase in the roof bow's gauge to 0.95mm. Figures 15 & 16 show the deformed model for the side impact and the roof crush analyses respectively. Figure 17 shows the plot of the rigid wall force for the roof crush analysis. As can be seen from these plots, the optimal design satisfies the constraint targets for the survival space and the roof crush force. Table 1 compares the variable values for the optimal design from this run to the values for the baseline model.

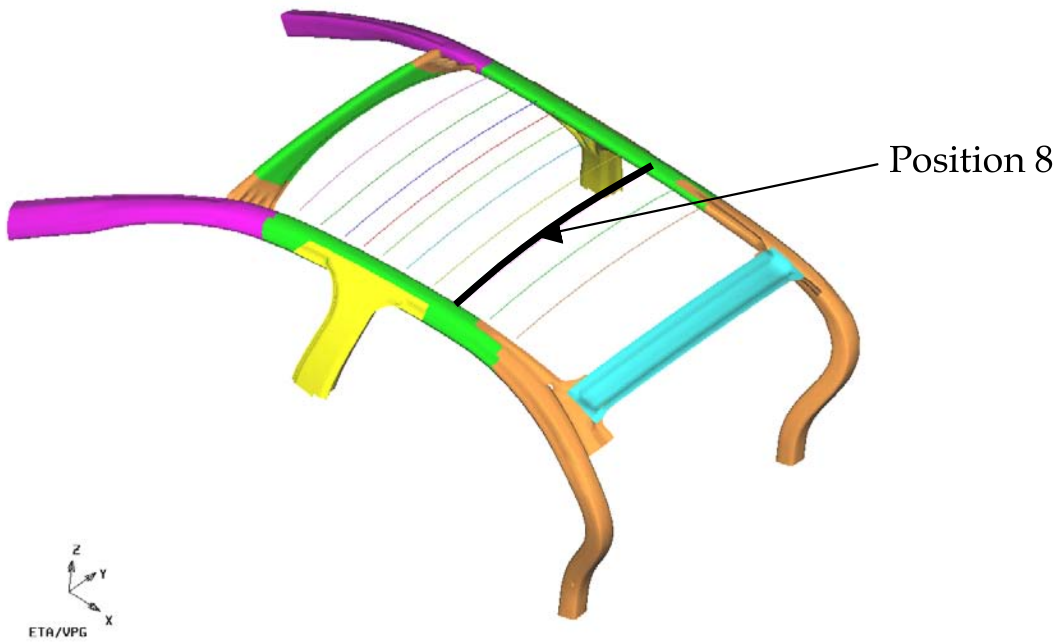

FIGURE 13: Optimization Run1 - Optimal Roof Bow Location

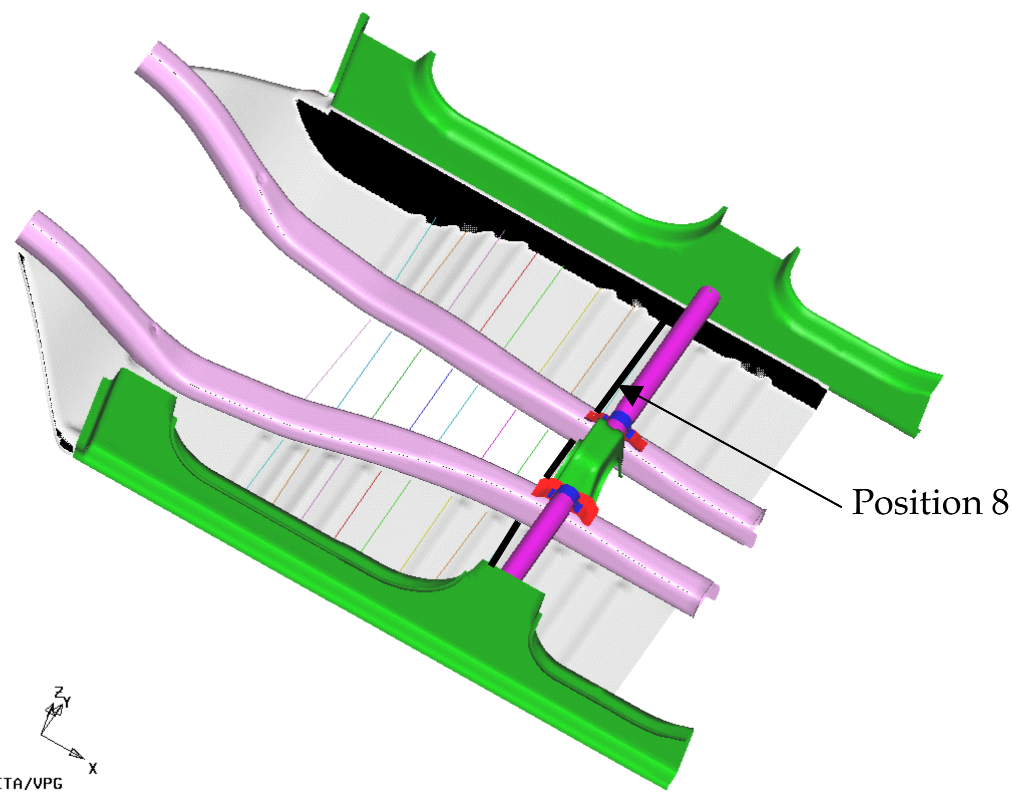

FIGURE 14: Optimization Run1 - Optimal Front Seat Cross-member Location

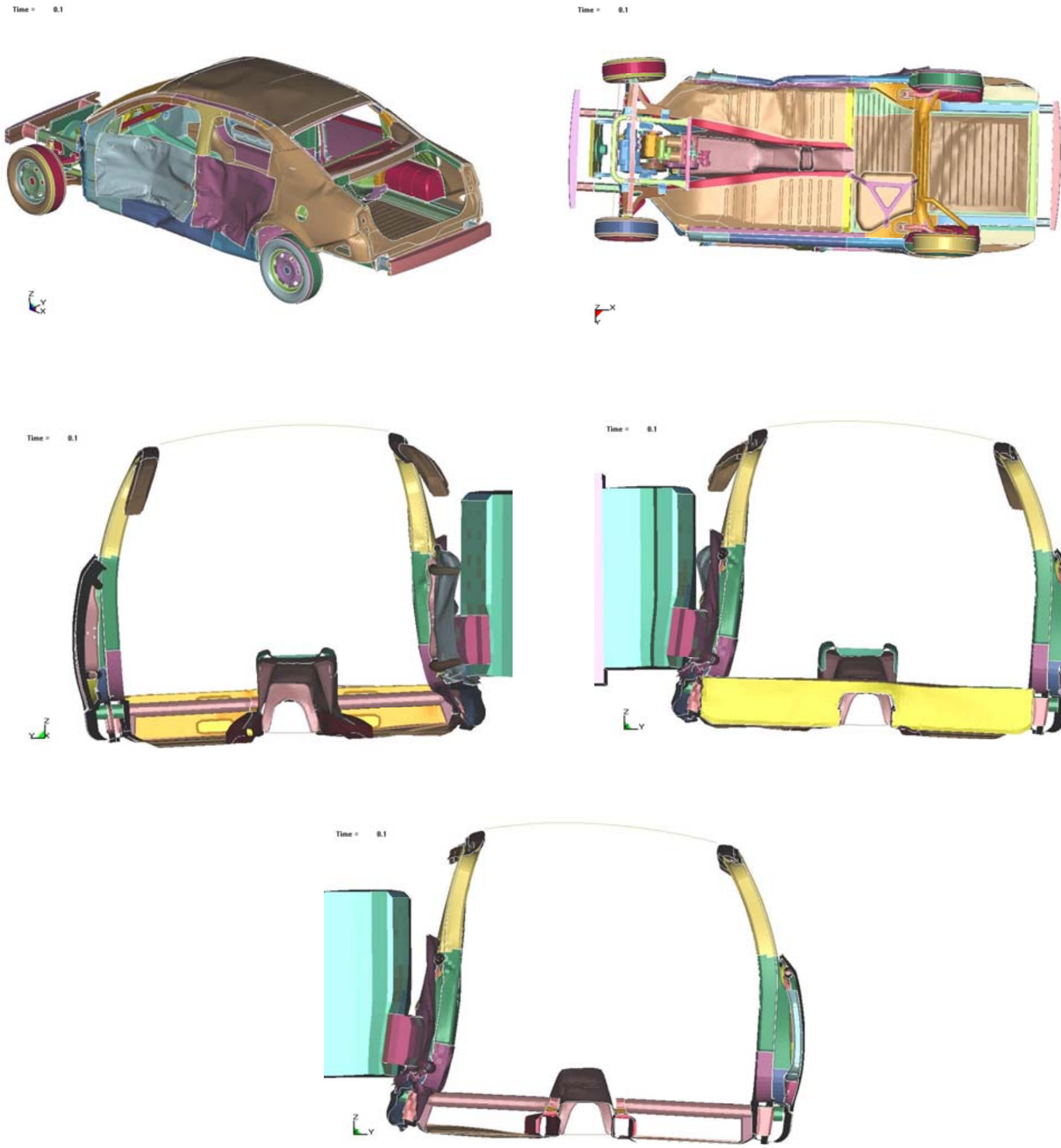

FIGURE 15: Side Impact Analysis – Optimal Run1 Design Deformed Shape

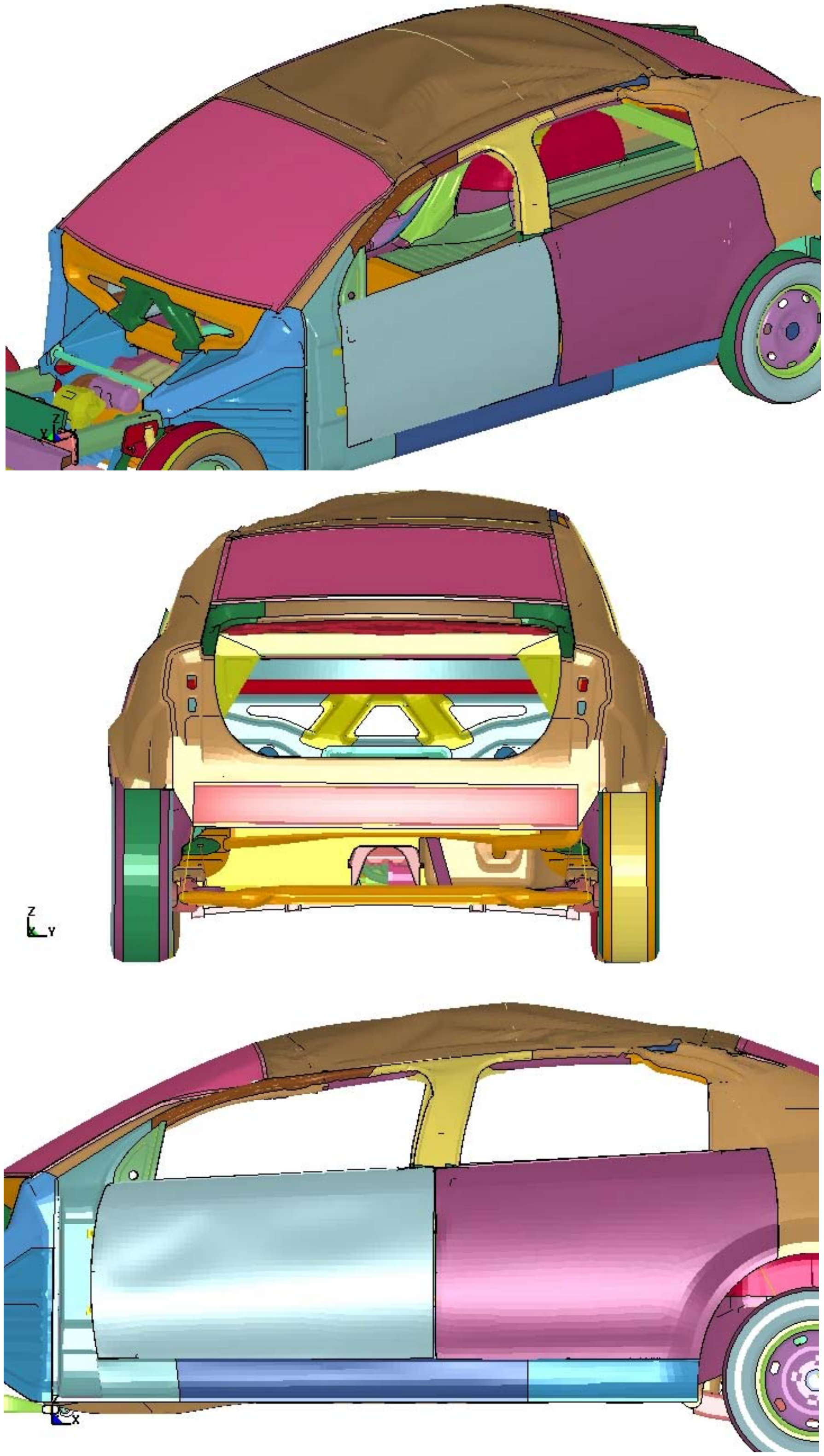

FIGURE 16: Roof Crush Analysis – Optimal Run1 Design Deformed Shape

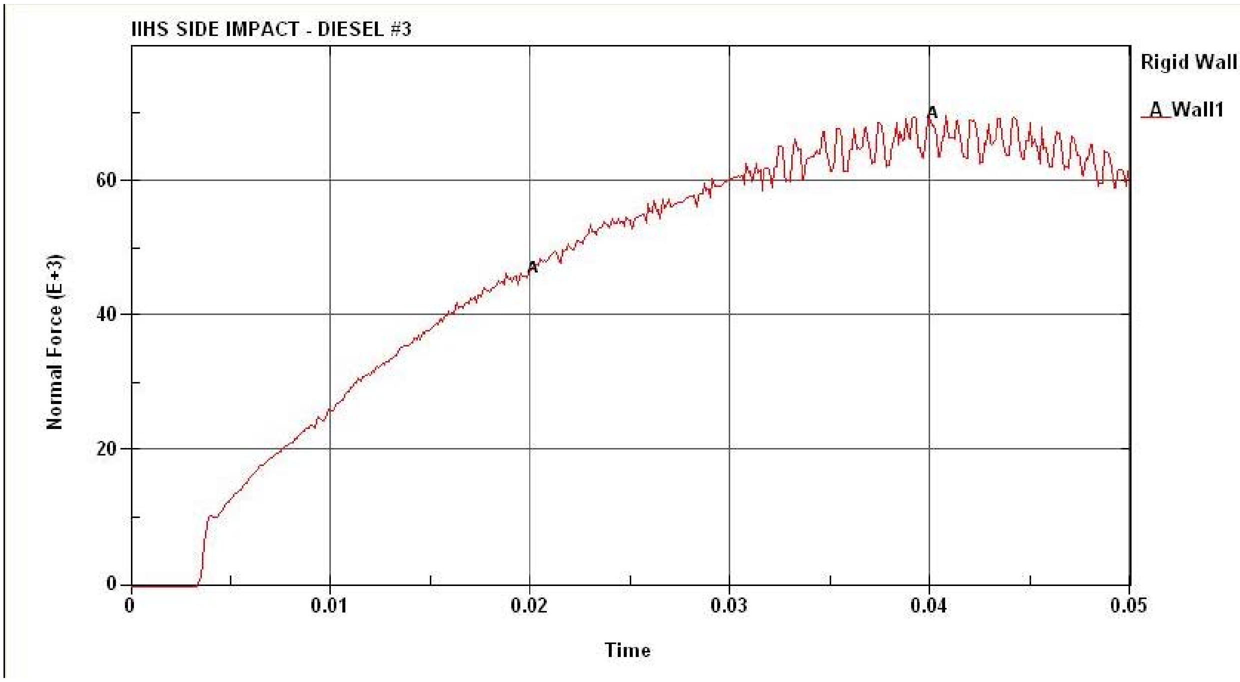

FIGURE 17: Rigid Wall Force – Optimal Run1 Design

6.2. CONCLUSIONS

- The front seat cross member is not required for the considered load cases as the optimal position was very near to the B-Pillar crossbar.
- The optimal location of the roof bow is behind the B-Pillar instead of being in the middle of the B-Pillar as in the baseline design. The optimal roof bow position was near the location where the Roof Rail was buckling in the baseline design
- The back section of the Roof Rail does not play an important role in the side impact and roof crush performance. The optimization reduced the thickness of this section to the minimum value allowed.
- Lower load path members including the kick-down and the crossbar play a very significant role in the side impact performance. The optimization took mass out of the B-Pillar and increased the mass in these parts.
- The B-Pillar section at the bottom is the thickest and the gauge decreases toward the top of the car.

7. TOPOLOGY OPTIMIZATION – RUN2

This run allows each design to have multiple roof bows and front seat cross-members at the same time, unlike Run1 where only one roof bow and one front seat cross-member could exist in a given design. The objective of this run is to find the optimal number, position and size of the roof bows and the front seat cross-members in addition to the thickness of the parts in the passenger compartment for a minimum mass design.

The front seat cross-member locations used for this run are the same as Run 1. The roof bow locations used for this run are shown in Figure 18. The roof bows 1 through 10 are the same as Run1. In addition to these 10 roof bows, another 4 pairs of roof bows were also added to the set of roof bows used in this optimization study. As shown in the figure, the new roof bows added are diagonal instead of straight across the Roof Rail as in the roof bows from Run 1. Roof bow 11 connects the A-pillar from one side of the vehicle to the B-Pillar on the other side of the vehicle. Roof bow 12 connects the B-Pillar to the C-Pillar. Roof bow 13 connects the B-Pillar to the Roof Rail midway between the B-Pillar and the C-Pillar. Finally, roof bow 14 connects from the midway point between B-Pillar and C-Pillar on the Roof Rail to the C-Pillar. The diagonal roof bows were added to allow a different path for the load transfer across the top of the vehicle. All the roof bows and front seat cross-members are present in each design. The size of each member determines whether a particular cross-member is considered active in the design or can be ignored.

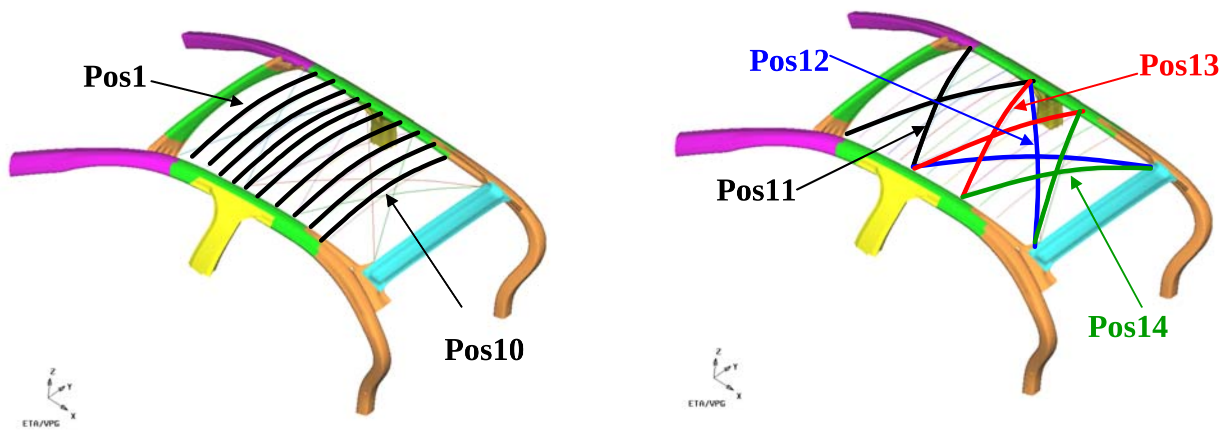

FIGURE 18: Optimization Run2 - Discrete Roof Bow Locations

All 14 roof bows shown are included in every design evaluated. The thickness of each roof bow indicates whether it is treated as active or inactive during post-processing. Position 1 is towards the front of the vehicle.

The optimization statement for the second run is:

Minimize:
Mass of the design
Subject to:
Roof crush force ≥ 31250N (2.75 * curb weight)
Survival space ≥ 125mm
By varying:
Size of the 14 Roof Bows (14 independent variables)
Size of the 8 Front Seat Cross-members (8 independent variables)
Size of the Roof Rail Section 1
Size of the Roof Rail Section 2
Size of the Roof Rail Section 3
Size of the B-Pillar Section 1
Size of the B-Pillar Section 2
Size of the B-Pillar Section 3
Size of the Inner Rocker
Size of the B-Pillar Crossbar
Size of the Floor Kick-down
Size of the Front Header
Size of the IP Beam

A total of 33 design variables were considered. All 33 variables are continuous. All the design variables are shown in Figure 19.

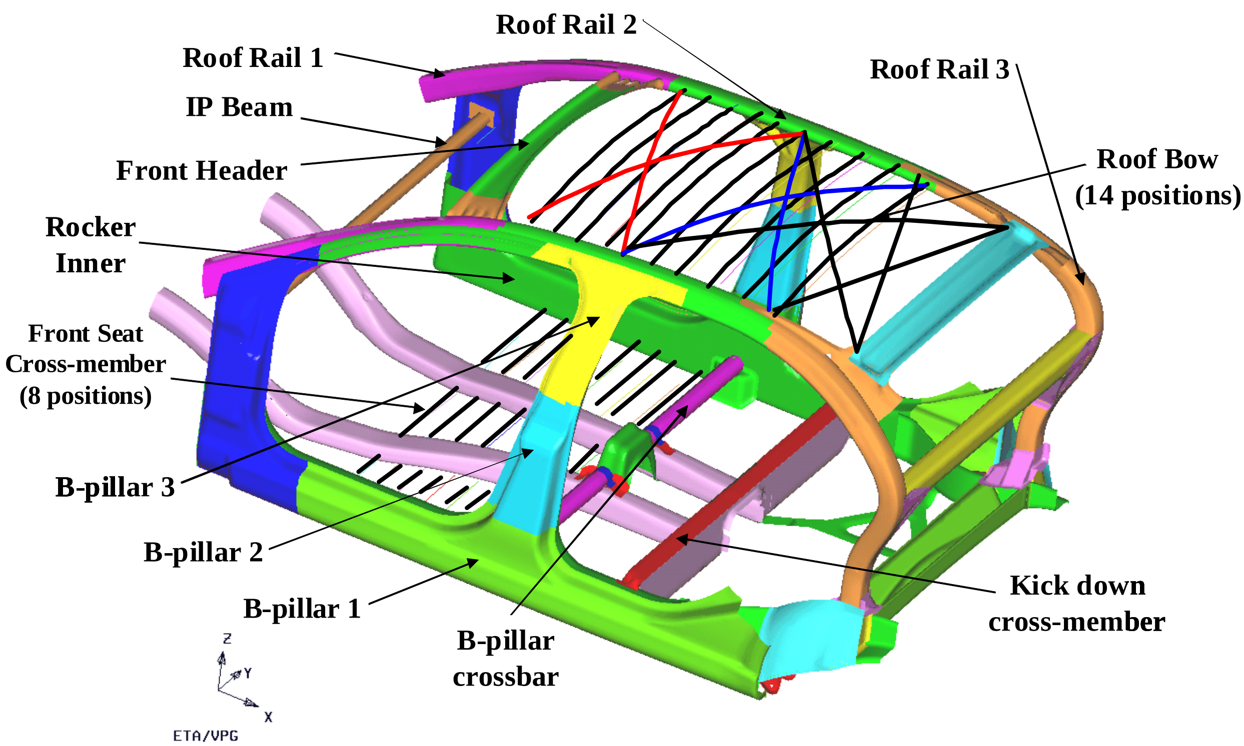

FIGURE 19: Optimization Run2 - Design Variables

The roof bows and the front seat cross members are being designed for size and not location in this analysis. All the roof bows and the front seat cross members shown in the figure are present in each design.

7.1. RESULTS

The optimization reduced the mass of the designed parts by 3.7%, from 58.49 to 56.3kg. Both the survival space and the roof crush force constraints were satisfied. A total of 316 evaluations were performed in the optimization run. At this point of the investigation it became clear that the concept being developed from this run was converging toward the same concept as the topology optimization in run1. As a result it was decided to terminate the run before complete convergence and proceed with the other optimization studies. Figures 20 & 21 show the locations of the roof bows and the front seat cross-members that are active in the design respectively. During post processing, only the roof bow and the front seat cross members with thickness greater than 0.5mm are considered active.

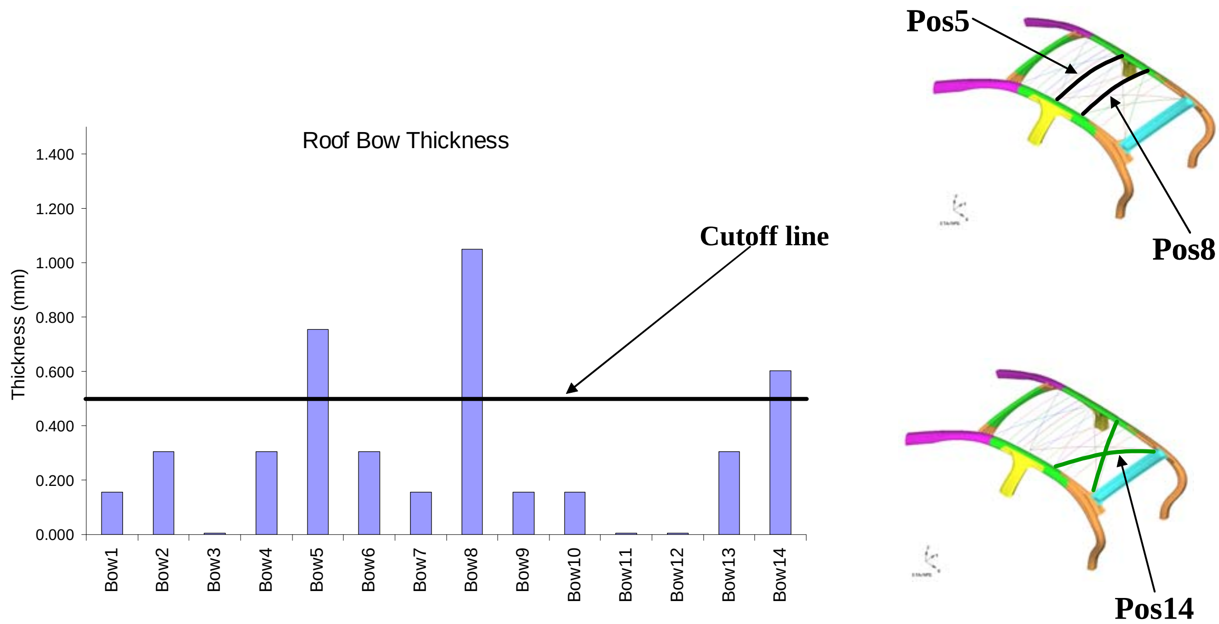

FIGURE 20: Optimization Run2 –Thickness Of Each Discrete Roof Bow Location

The cutoff line is drawn at thickness of 0.5mm. Only roof bows with thickness above 0.5mm are considered active. The three roof bows active in the design are also shown.

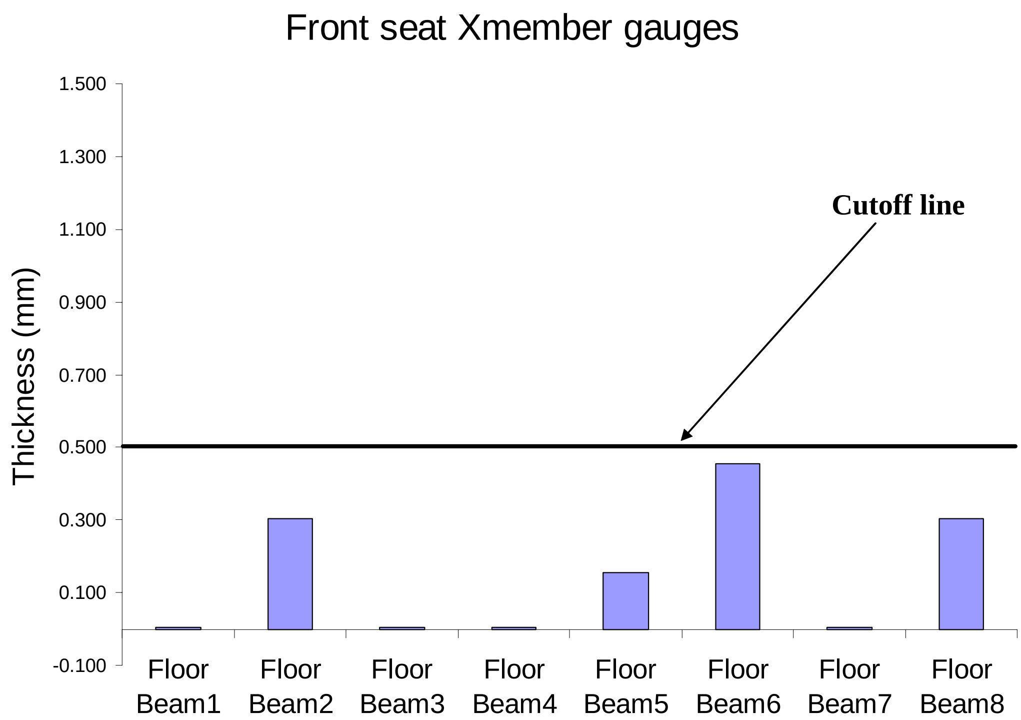

FIGURE 21: Optimization Run2 –Thickness Of Each Discrete Front Seat Cross-member Location

The cutoff line is drawn at thickness of 0.5mm. As can be seen from the graph, no front seat cross members are active in this design.

Figures 22 & 23 show the deformed model for the side impact and the roof crush analyses, respectively, for the optimized design from Run2. Figure 24 shows the plot of the rigid wall force for the roof crush analysis. As can be seen from these plots, the optimal design satisfies the constraint targets for the survival space and the roof crush force. Tables 2 & 3 compare the variable values for the optimal design from this run to the values for the baseline model.

The roof bow position 8 (the optimal location from Run1) is also active in this run. Two other roof bows are also marginally active, but will be ignored in the sequel because this design was not fully optimized (i.e., the optimization run was not converging). The floor beams are all inactive, giving the same trend as the Run1 where the floor beam reduced in thickness to a very small value and moved very close to the crossbar. The thickness comparison of the other parts being varied is shown in Figure 25. As can be seen, almost all the thickness values are the same as the optimized design from Run1.

NAME	BASELINE (mm)	MINIMUM (mm)	MAXIMUM (mm)	CURRENT (mm)
Roof Bow 1 Thickness		0.005	1.5	1.55E-01
Roof Bow 2 Thickness		0.005	1.5	3.04E-01
Roof Bow 3 Thickness		0.005	1.5	5.00E-03
Roof Bow 4 Thickness		0.005	1.5	3.04E-01
Roof Bow 5 Thickness	1.0	0.005	1.5	7.53E-01
Roof Bow 6 Thickness		0.005	1.5	3.04E-01
Roof Bow 7 Thickness		0.005	1.5	1.55E-01
Roof Bow 8 Thickness		0.005	1.5	1.05E+00
Roof Bow 9 Thickness		0.005	1.5	1.55E-01
Roof Bow 10 Thickness		0.005	1.5	1.55E-01
Roof Bow 11 Thickness (A - B)		0.005	1.5	5.00E-03
Roof Bow 12 Thickness (B - C)		0.005	1.5	5.00E-03
Roof Bow 13 Thickness (B - mid BC)		0.005	1.5	3.04E-01
Roof Bow 14 Thickness (C - mid BC)		0.005	1.5	6.03E-01
Front Seat Xmember 1 Thickness		0.005	1.5	5.00E-03
Front Seat Xmember 2 Thickness		0.005	1.5	3.04E-01
Front Seat Xmember 3 Thickness		0.005	1.5	5.00E-03
Front Seat Xmember 4 Thickness	1.0	0.005	1.5	5.00E-03
Front Seat Xmember 5 Thickness		0.005	1.5	1.55E-01
Front Seat Xmember 6 Thickness		0.005	1.5	4.54E-01
Front Seat Xmember 7 Thickness		0.005	1.5	5.00E-03
Front Seat Xmember 8 Thickness		0.005	1.5	3.04E-01

TABLE 2: Roof Bow & Front Seat Cross-member Gauges Prior To Premature Run2 Termination

NAME	BASELINE (mm)	MINIMUM (mm)	MAXIMUM (mm)	CURRENT (mm)
Roof Rail 1 Thickness	1.0	0.5	1.5	1.1
Roof Rail 2 Thickness	1.0	0.5	1.5	1.3
Roof Rail 3 Thickness	1.0	0.5	1.5	0.5
B-Pillar 1 Thickness	1.8	1.0	2.5	1.3
B-Pillar 2 Thickness	1.8	1.0	2.5	1.3
B-Pillar 3 Thickness	1.8	1.0	2.5	1.3
Rocker Thickness	1.5	1.0	2.0	1.1
Front Header Thickness	0.7	0.3	1.25	0.775
Crossbar Thickness	1.2	0.75	1.6	1.09
Kick-down Thickness	0.7	0.3	1.25	0.3
IP Beam Thickness	2.0	1.0	3.0	2.8

TABLE 3: Gauges Of All Remaining Parts Prior To Premature Run2 Termination

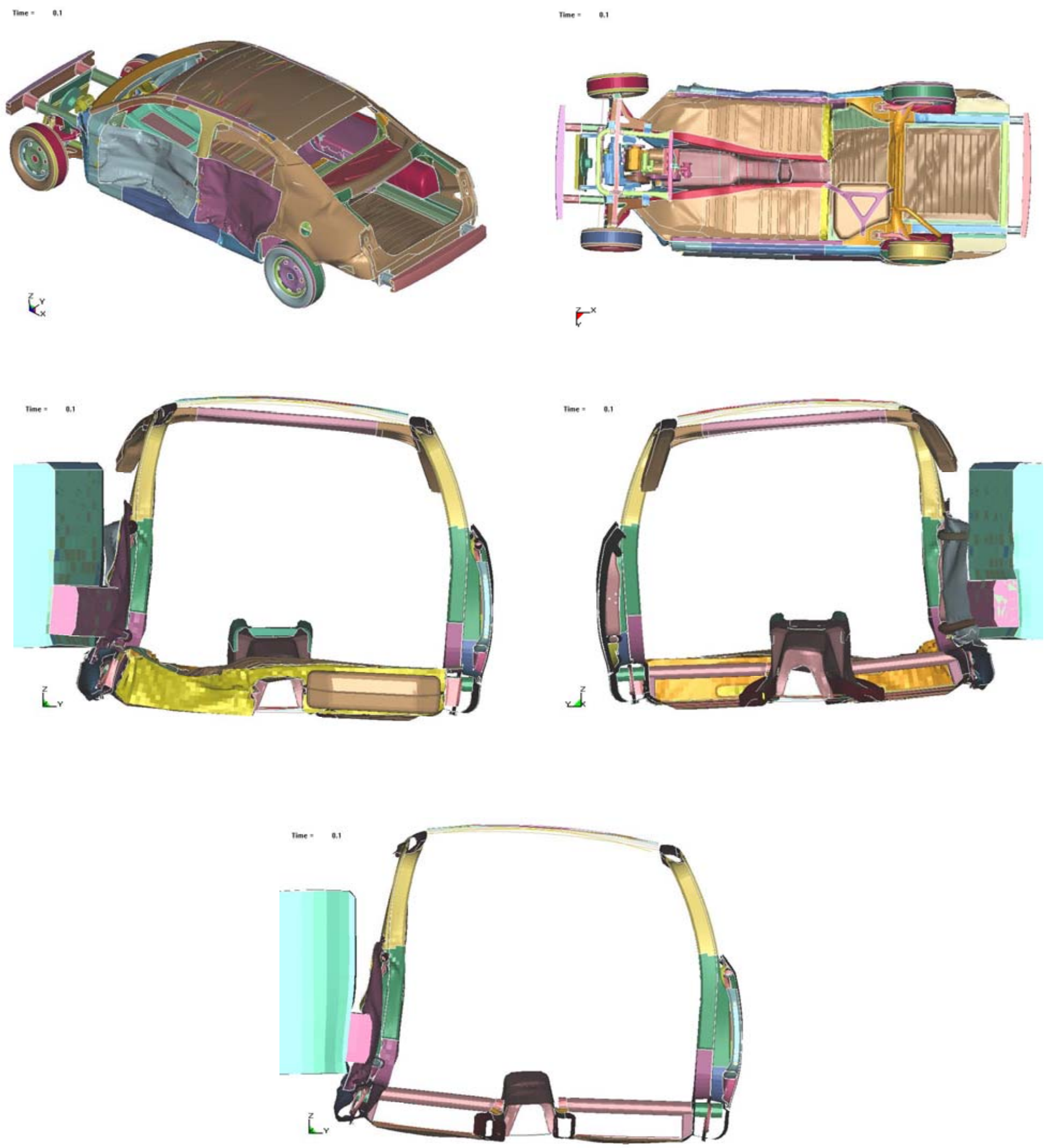

FIGURE 22: Side Impact Analysis – Optimal Run2 Design Deformed Shape

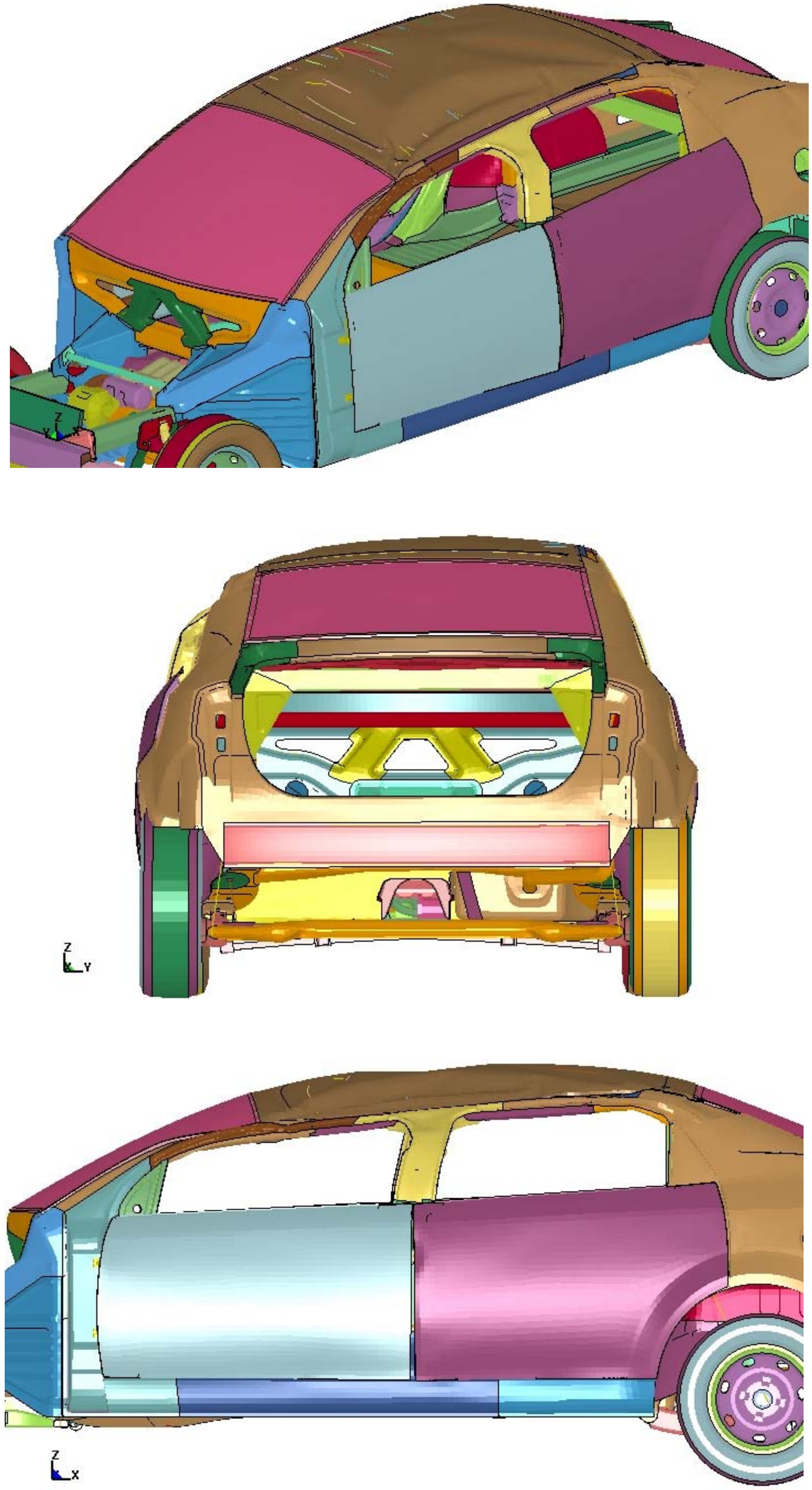

FIGURE 23: Roof Crush Analysis – Optimal Run2 Design Deformed Shape

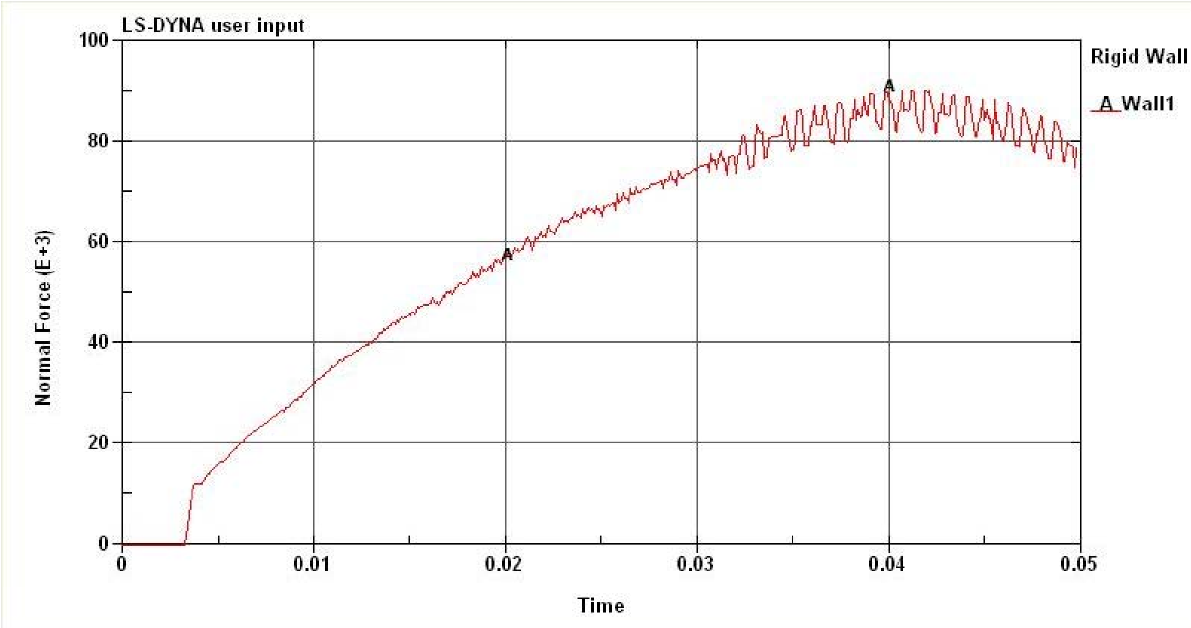

FIGURE 24: Rigid Wall Force – Optimal Run2 Design

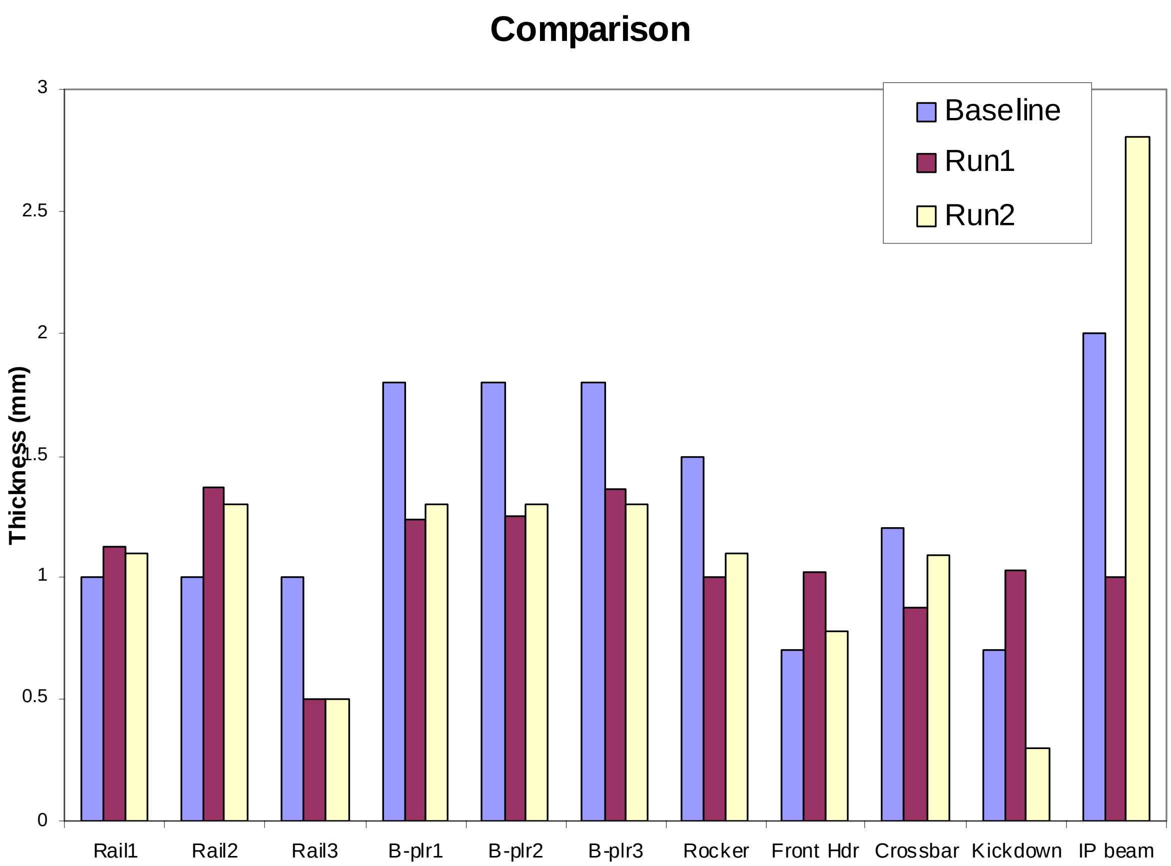

FIGURE 25: Designed Parts Of Baseline, Run1 & Run2 - Thickness Comparison

7.2. CONCLUSIONS

- The optimal load path from this run is very similar to the optimal load path from Run1 in Section 6.
- The front seat cross members contribute very little to the performance of the design in the roof crush and side impact scenarios
- The roof bow location from Run1 is still the most important; however this run also has roof bows at the middle of the B-Pillar and another towards the back of the rails
- The B-Pillar mass can be reduced by increasing the stiffness in the top (Roof Rail + roof bow + headers) and the bottom (B-Pillar crossbar) of the passenger compartment design
- The back section of the Roof Rail does not play an important role in the side impact and roof crush performance. The optimization reduced the thickness of this section to the minimum value allowed.

8. TOPOLOGY OPTIMIZATION – RUN3

After analyzing the results of the first two optimization studies, it was decided to perform another topology optimization study. The optimization run was setup to study the impact of changing the B-Pillar crossbar height on the design performance. The modeling approach for the B-Pillar crossbar was the same as for the roof bows and the front seat cross-member in the first two runs; it was modeled with beam elements. The objective of this run is to find the optimal location and size of the B-Pillar crossbar in addition to the thickness of some of the parts in the passenger compartment for a minimum mass design.

The optimization statement for the run is:

Minimize:
Mass of the design
Subject to:
Survival space ≥ 125mm
By varying:
Location (height) of the B-Pillar crossbar
Size of the B-Pillar Crossbar
Size of the B-Pillar Section 1
Size of the B-Pillar Section 2
Size of the B-Pillar Section 3
Size of the Inner Rocker
Size of the Floor Kick-down
Size of the Front Header

A total of 8 design variables were considered. The thickness of the upper load path members (3 sections of the Roof Rail and the IP-beam) was set to the optimal value from the topology optimization Run1. The upper load path members were not varied, as this optimization was primarily to identify the optimal location of the B-Pillar crossbar and the mass savings that result for the side impact analysis. The roof crush run was not included in the optimization, as the upper load path members were not being varied. The optimal design from this run was analyzed for roof crush to make sure that the design changes to the lower load path members did not compromise the performance in the roof crush analysis. The location of the crossbar was a discrete design variable while all other 7 variables were continuous. All the design variables are shown in Figure 26.

Eleven possible locations for the crossbar were modeled as shown in Figure 27. Each design could only have one of these eleven crossbars active. The position 2 crossbar is at the centerline of the baseline B-Pillar crossbar location. The 11 locations of the crossbars are evenly distributed between the bottom and the top location. The coordinates of the top and bottom crossbar locations are given in the figure.

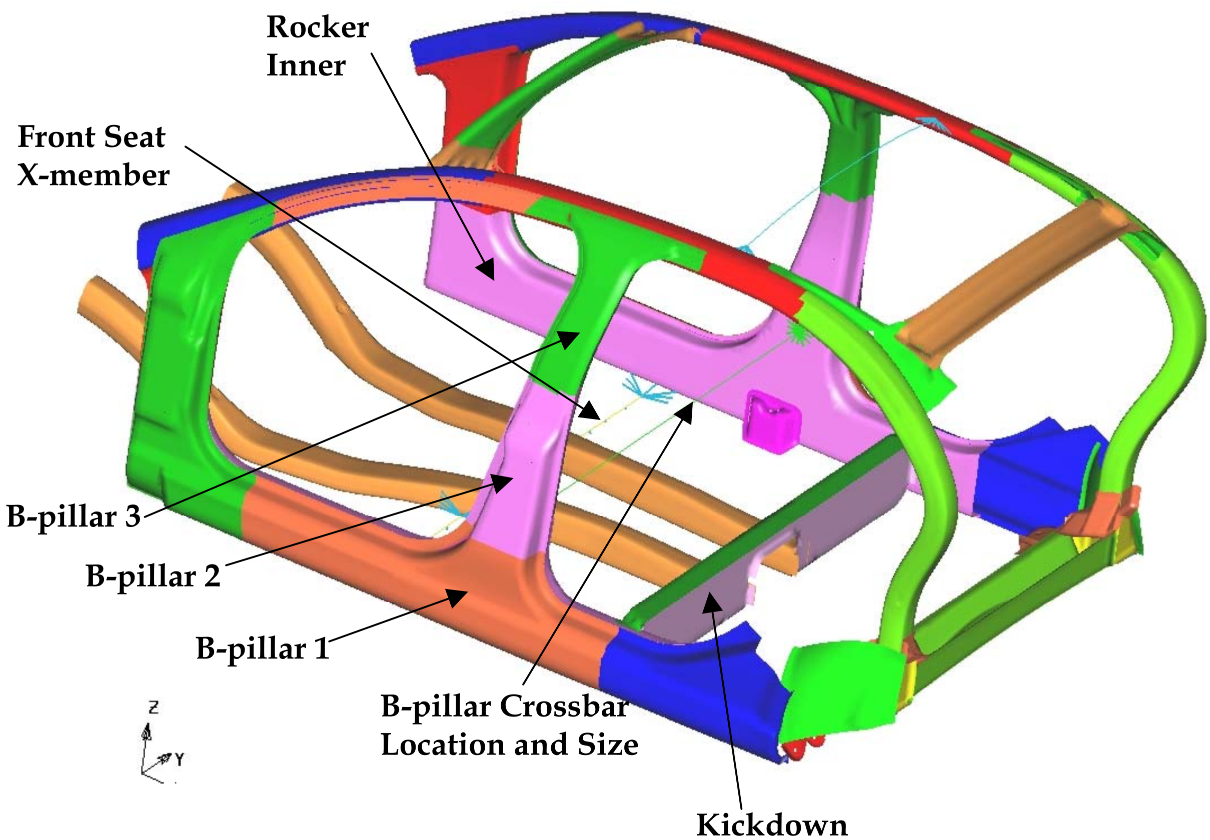

FIGURE 26: Optimization Run3 - Design Variables

All labeled variables were designed for size. The B-Pillar crossbar was also designed for location.

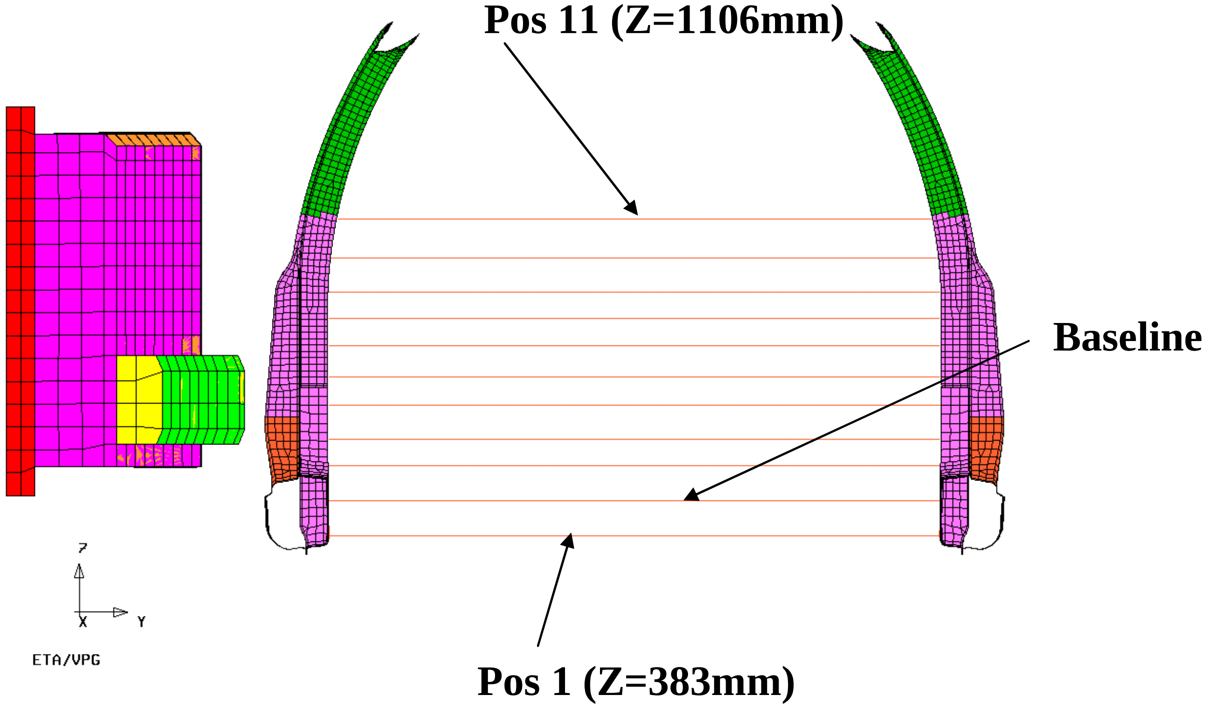

FIGURE 27: Optimization Run3 - Discrete B-Pillar Crossbar Locations

Each design could have only one of the eleven crossbars shown. The crossbars are numbered 1 through 11, with the positions 1 and 11 as shown. Position 1 is towards the bottom of the vehicle.

8.1. RESULTS

The optimization reduced the mass of the designed parts by 23%, from 58.49 to 45kg. Both the survival space and the roof crush force constraints were satisfied. In addition to satisfying the constraints, the optimization was able to reduce the mass of the designed parts by 23%. Figures 28 & 29 show the deformed model for the roof crush and the side impact analyses respectively. Figure 30 shows the plot of the rigid wall force for the roof crush analysis. As can be seen from these plots, the optimal design satisfies the constraint targets for the survival space and the roof crush force. Table 4 compares the variable values for the optimal design from this run to the values for the baseline model.

NAME	BASELINE	MINIMUM	MAXIMUM	BEST	CHANGE
Crossbar Position	2	1	11	9	+7
Front Seat Cross-member Thickness (mm)	1.0	0.1	1.5	0.1	-90%
B-Pillar 1 Thickness (mm)	1.8	1.0	2.5	1.0	-44.4%
B-Pillar 2 Thickness (mm)	1.8	1.0	2.5	1.0	-44.4%
B-Pillar 3 Thickness (mm)	1.8	1.0	2.5	1.0	-44.4%
Rocker Thickness (mm)	1.5	1.0	2.0	1.0	-33%
Cross-bar Thickness (mm)	1.2	0.75	1.8	1.0	-16.67%
Kick-down Thickness (mm)	0.7	0.3	1.25	0.3	-57.14%

TABLE 4: Run3 Optimization - Design Variable Values

As can be seen from Table 4, the crossbar position is much higher than in the baseline design. Also with a higher crossbar, the optimization was able to reduce the thickness of most parts to the lowest allowed values. The crossbar thickness is the only variable that did not go to the minimum value. The gauge thickness reductions are enabled primarily because the higher crossbar carries the majority of the load in the side impact analysis.

The location of the crossbar from the optimized design is not very intuitive. The expected optimal location would be somewhere close to the middle of the impact zone from the barrier. However, after closer examination it was realized why the crossbar was at a higher location. The B-Pillar design tapers inwards towards the top of the car. This means that the crossbars at locations higher than 6 are shorter in span length and hence lighter than the crossbars that are lower. Since the objective is to minimize the mass of the system, the optimization identified the position 9 as the optimal position since it is slightly lighter, even though the intrusion measures are better at other lower locations.

8.2. CONCLUSIONS

- The location of the B-Pillar crossbar has a very significant effect on the side impact performance
- At the optimal location, all the other lower load path members (B-Pillar, kick-down, rocker, front seat cross member) are moved to the lowest allowed gauge value
- A higher location of the crossbar allows significant reductions in mass of the passenger compartment

FIGURE 28: Side Impact Analysis – Optimal Run3 Design Deformed Shape

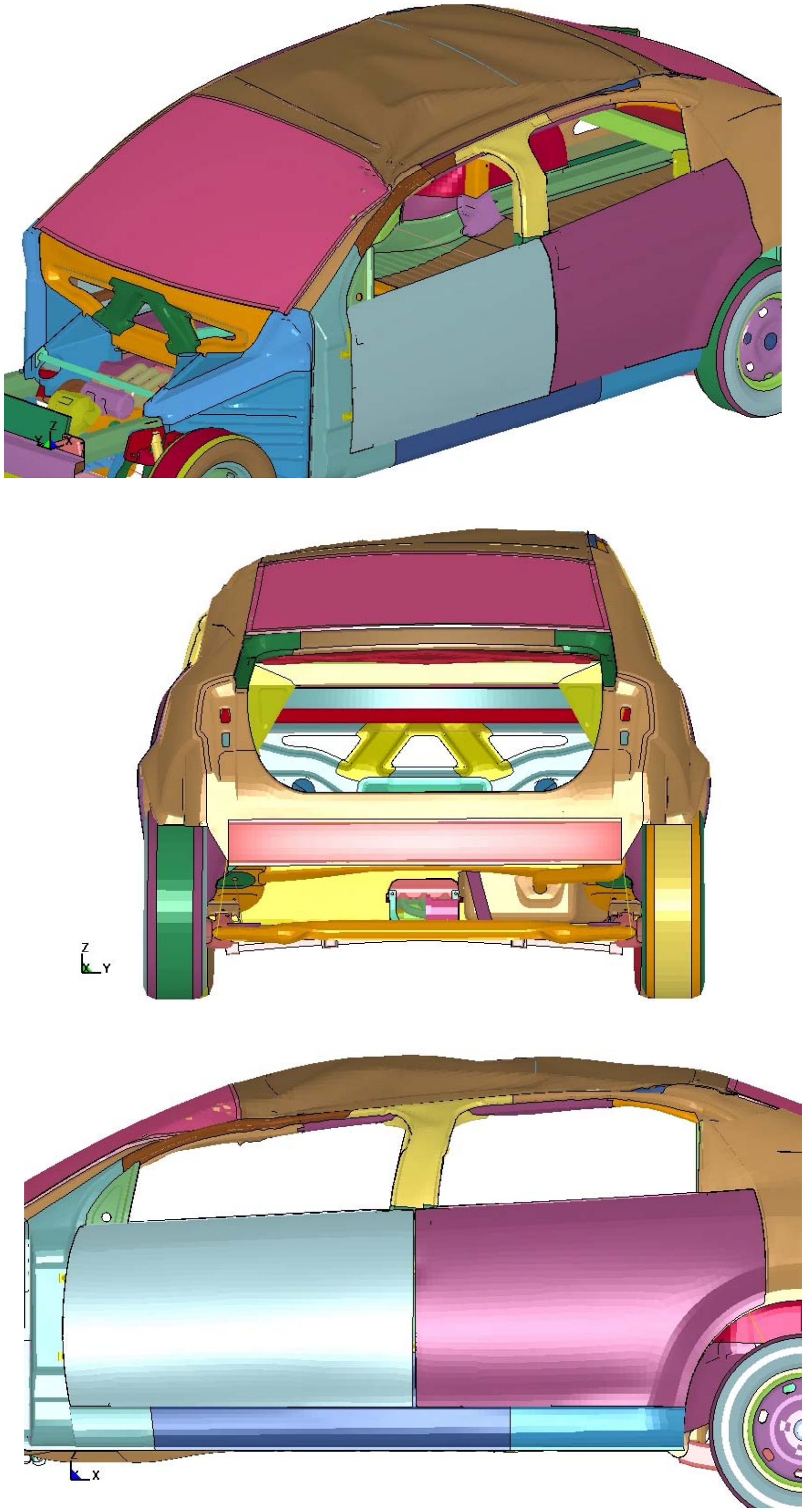

FIGURE 29: Roof Crush Analysis – Optimal Run3 Design Deformed Shape

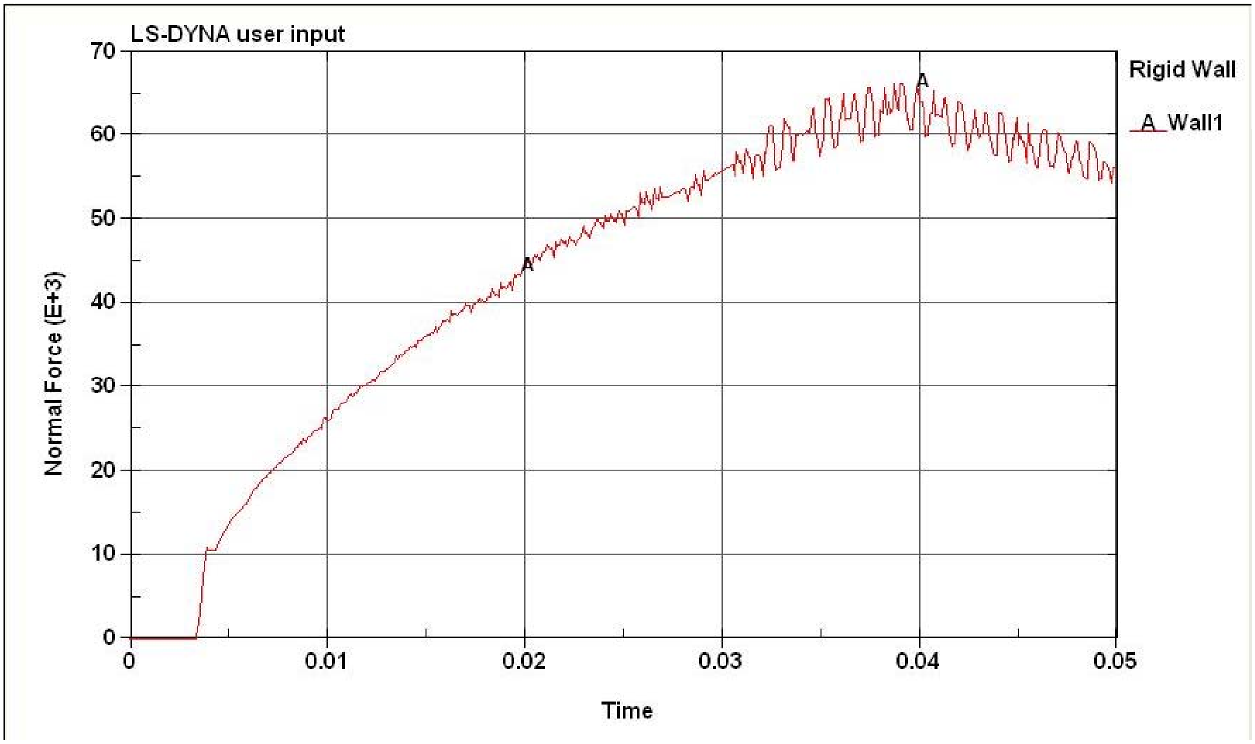

FIGURE 30: Rigid Wall Force – Optimal Run3 Design

8.3. THE NEXT STEP

Based on the above observations and also the fact that it was not feasible to place the B-Pillar crossbar at the optimal location found by the optimization, it was decided to perform a sensitivity study. The objective of this study was to find the effect of the location of the crossbar on the survival space, keeping everything else in the design constant. The intent was to use the results of the study to identify a more practical location of the crossbar without completely losing the mass benefits achieved through raising the crossbar.

9. SENSITIVITY STUDY

In this study, the optimal design from Run3 was used as the baseline. The study was focused on only the location of the crossbar, as the previous optimization result already showed that with a higher crossbar the thickness of all other parts could be reduced to the minimum allowed values. The study was then setup to run this design eleven times, once for each location of the crossbar. The survival space was measured for each of these designs and plotted against the location of the crossbar. Figure 31 shows the sensitivity of the survival space to the location of the crossbar. As can be seen, locations 5-10 satisfy the constraint for the survival space. However, as the crossbar is moved lower along the B-Pillar, there is a sharp reduction in performance. From the results of the study, it was decided to use Position 4 as the final position for the crossbar for the future optimization runs. This position was considered the highest feasible position for a contemporary vehicle design. It was also decided to design the brackets connecting the crossbar to the B-Pillar such that they can transfer more moment and load into the crossbar, thereby raising the "effective" height of the crossbar.

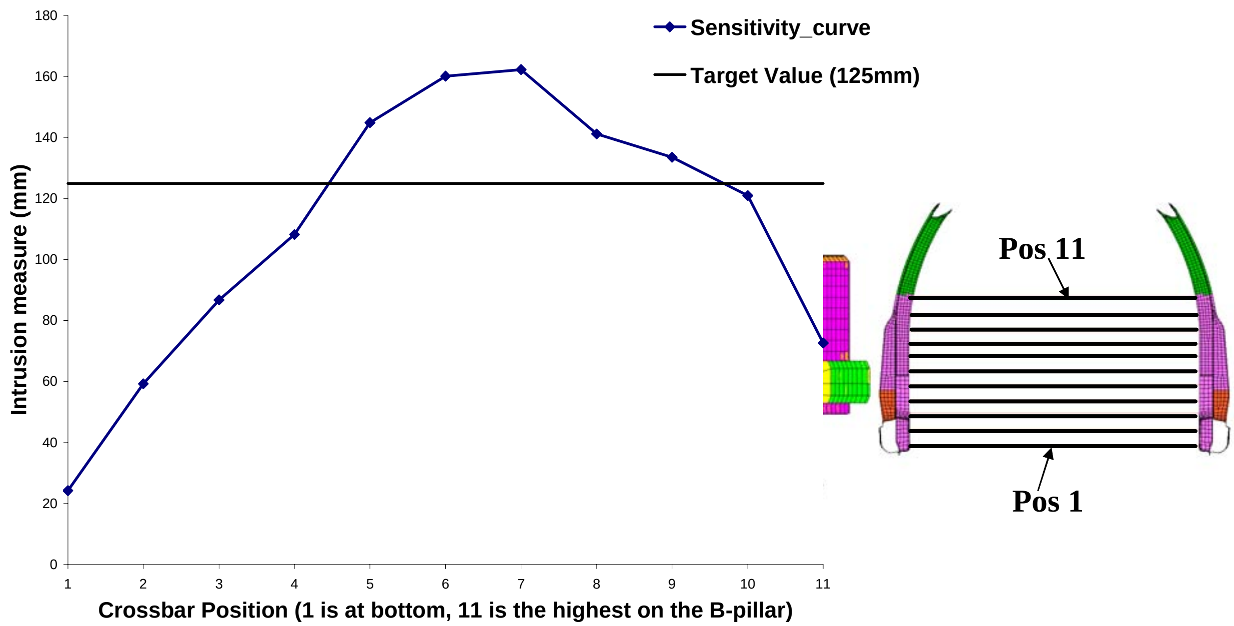

FIGURE 31: Survival Space Sensitivity To Crossbar Location – Optimal Run3 Design

10. TOPOLOGY OPTIMIZATION – RUN4

The curb weight of the vehicle used for the optimization in the first three runs is 1154kg. This weight was viewed as being too light for a production vehicle of this class. There were concerns that the optimal topology identified for this model might not work for a heavier design. To investigate this, another topology run was setup with the vehicle curb weight increased to 1424kg, an increase of about 30%. The same optimization setup as the first topology run was used, but with the heavier model. The objective of this run was to optimize the location for the roof bow and the front seat cross-member in addition to the thickness of the parts in the passenger compartment for a minimum mass design. Each design in this run had only one roof bow and one front seat cross-member. The optimization statement for the run was:

Minimize:
    Mass of the design
Subject to:
    Roof crush force ≥ 38404N (2.75 * curb weight)
    Survival space ≥ 125mm
By varying:
    Fore/aft location of the roof bow
    Fore/aft location of the front seat cross-member
    Size of the Roof Bow
    Size of the Front Seat Cross-member
    Size of the Roof Rail Section 1
    Size of the Roof Rail Section 2
    Size of the Roof Rail Section 3
    Size of the B-Pillar Section 1
    Size of the B-Pillar Section 2
    Size of the B-Pillar Section 3
    Size of the Inner Rocker
    Size of the B-Pillar Crossbar
    Size of the Floor Kick-down
    Size of the Front Header
    Size of the IP Beam

A total of 15 design variables were considered. Two variables (location of roof bow and location of Front seat cross-member) were discrete and the other 13 variables were continuous. All the design variables are shown in Figure 10 from Run1.

Figure 11 shows all the possible locations for the roof bow during the optimization run. Each design generated during optimization could have only one of the possible 10 locations. Similarly, Figure 12 shows all 8 possible locations for the front seat cross-member. Again, only one of these 8 cross-members could be active in a given design.

10.1. RESULTS

Since there was no baseline design for this weight structure, no weight savings are provided. The purpose of this run was to compare the optimal topology for a heavier curb weight to the optimal topology for a lighter vehicle. Figures 32 & 33 show the deformed model for the roof crush and the side impact analyses respectively. Figure 34 shows the plot of the rigid wall force for the roof crush analysis. As can be seen from these plots, the optimal design satisfies the constraint targets for the survival space and the roof crush force. Figures 35, 36, 37 & 38 show the comparison of the best design from this run with the design from Run 1. Table 5 compares the variable values for the optimal design from this run to the values for the optimal design from Run 1. Table 6 compares the response values of the designs from the Runs 1 and 4. As can be seen from the results, the topology is very similar to the topology from Run1. The thickness of the parts is slightly different; however the overall distribution of mass between the various components follows the same pattern. Based on this result, the future optimization runs can be performed on the 1100kg model.

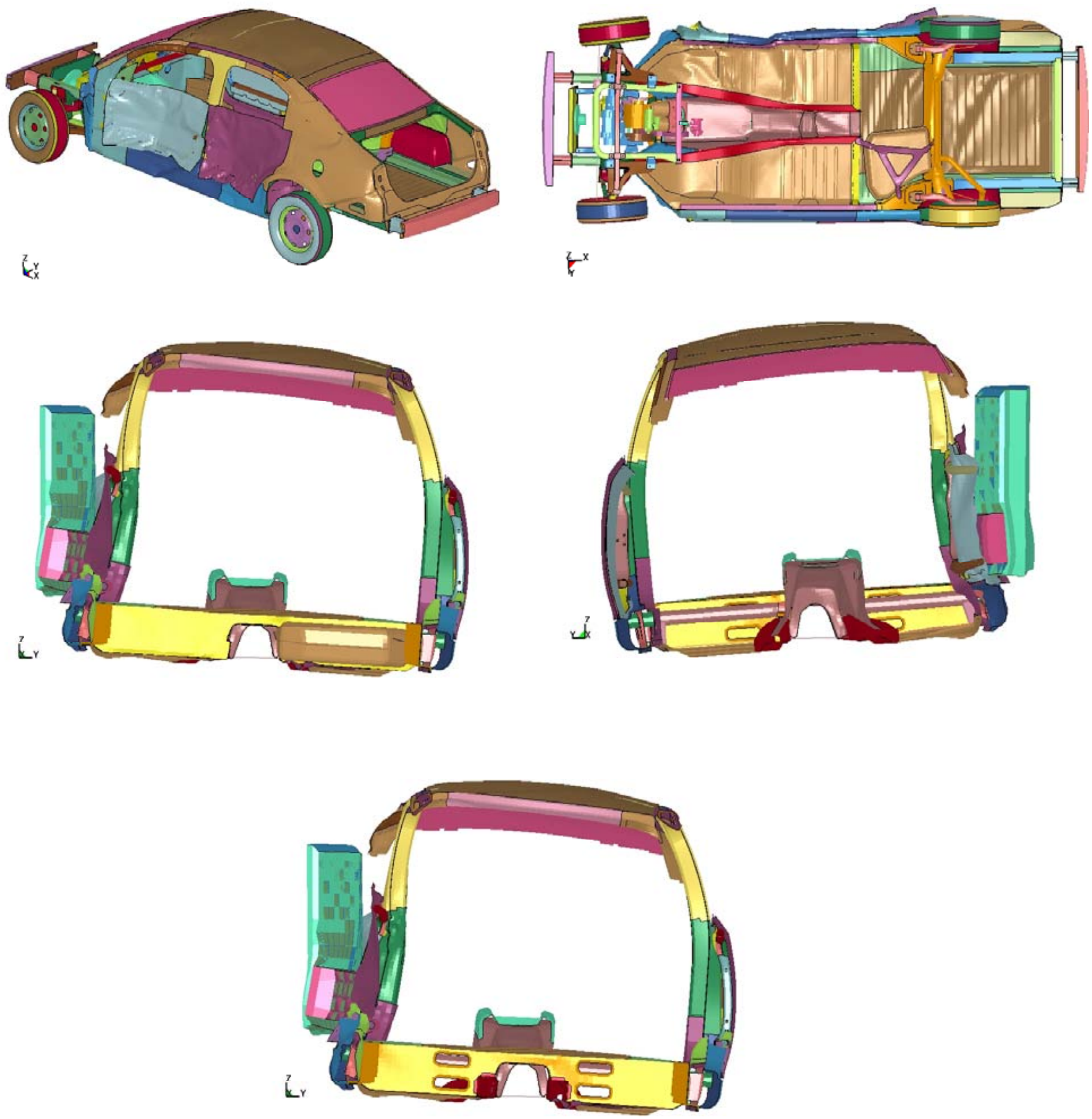

FIGURE 32: Side Impact Analysis – Optimal Run4 Design Deformed Shape

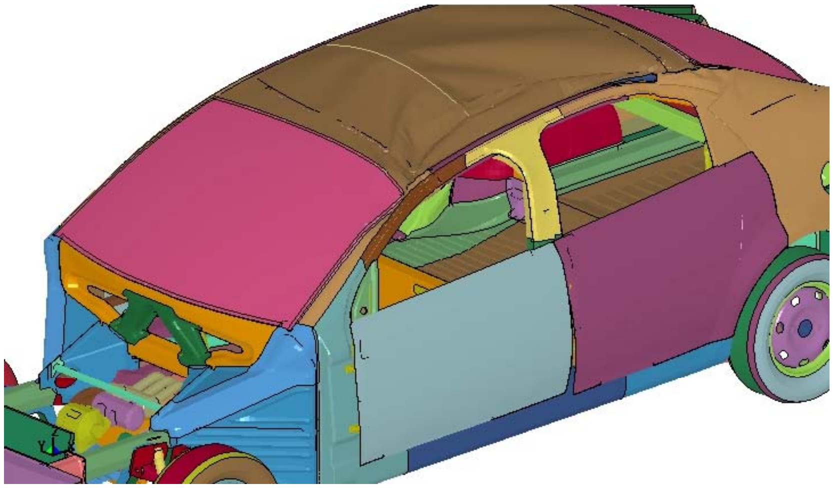

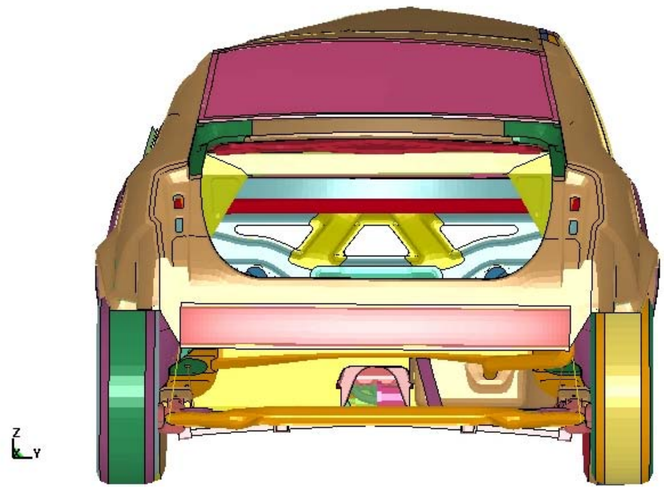

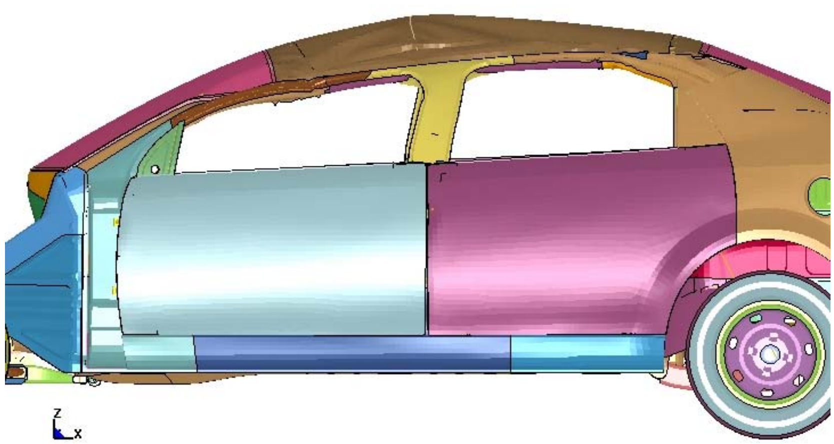

FIGURE 33: Roof Crush Analysis – Optimal Run4 Design Deformed Shape

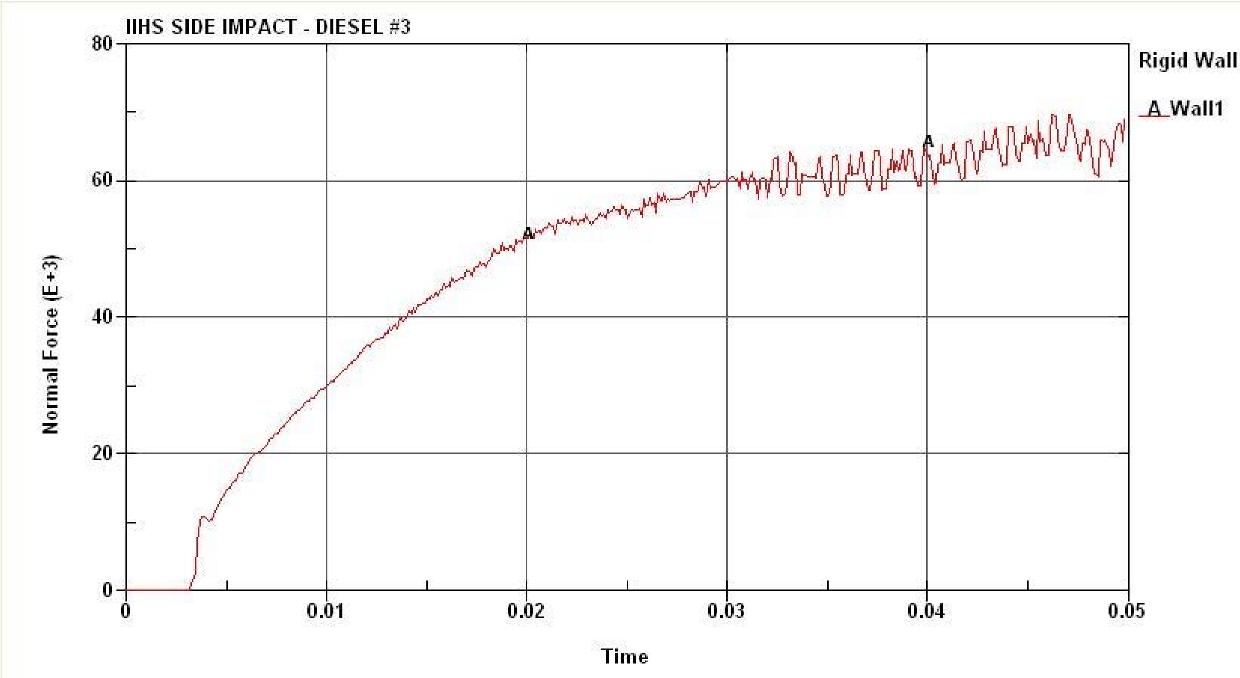

FIGURE 34: Rigid Wall Force – Optimal Run4 Design

Another interesting result from this study was that the percentage increase in structural weight to handle the additional curb weight of the vehicle is only a fraction of the percentage increase in curb weight. The designed parts in the final design from this run weighed 6% more than the same parts from the optimized design of Run1. The increase in curb weight between those two runs is 30%. Moreover, the survival space for the best design in this run is much higher than the required target, which indicates that some more mass can be taken out of the designed parts. This would reduce the increase in structural mass even further.

10.2. CONCLUSIONS

- An increase of 30% in the curb weight only required a 6% increase in the passenger compartment structural mass to meet the side impact and roof crush requirements
- The load paths do not change significantly by moving to a heavier vehicle. This is noted from the fact that the mass distribution between the various passenger compartment members is almost identical to the 1100kg optimal design

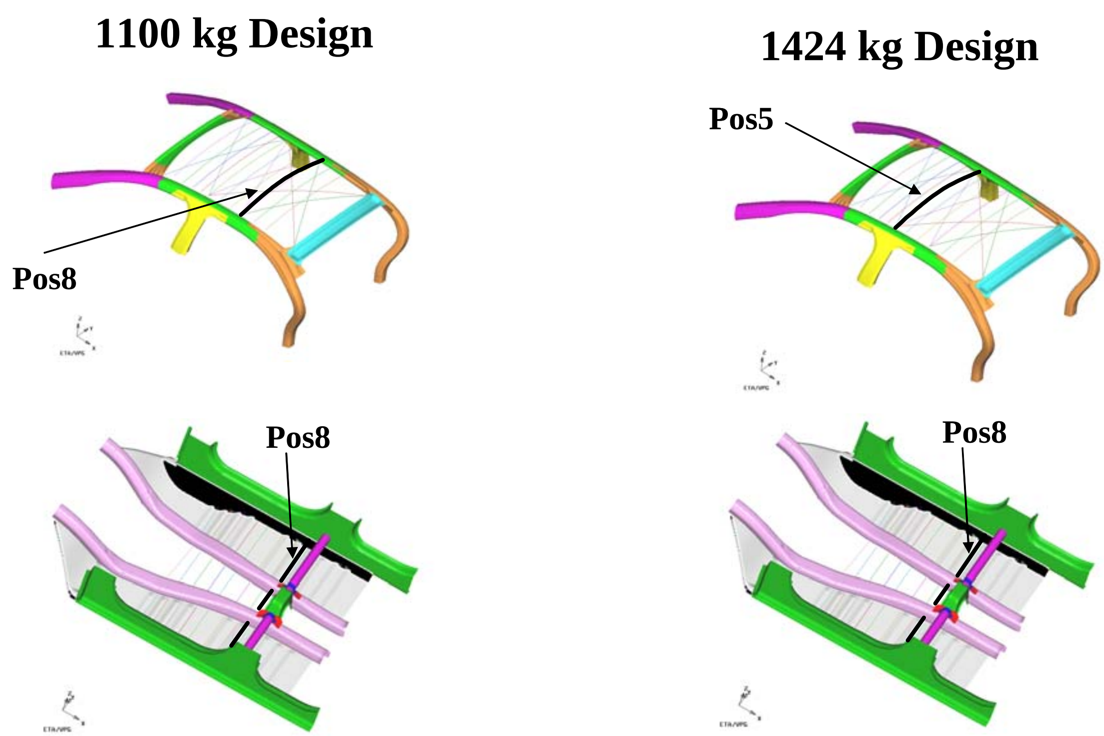

FIGURE 35: Roof Bow & Roof Rail Locations – Run1 (1100kg) & Run4 (1424kg) Optimization Models

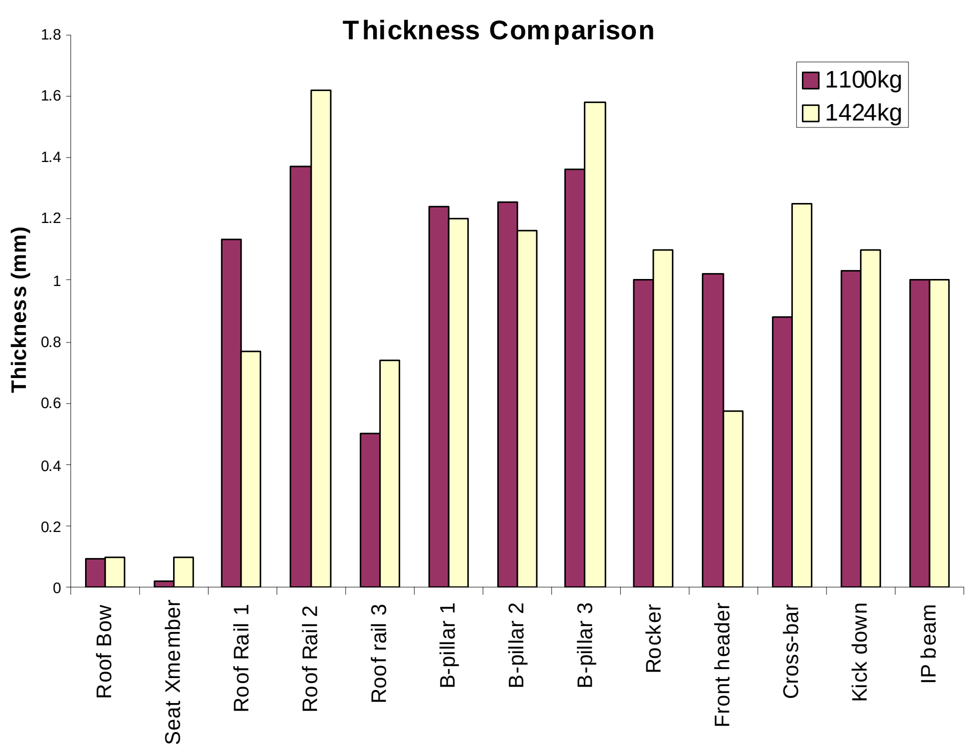

FIGURE 36: Gauge Comparison – Run1 (1100kg) & Run4 (1424kg) Optimization Models

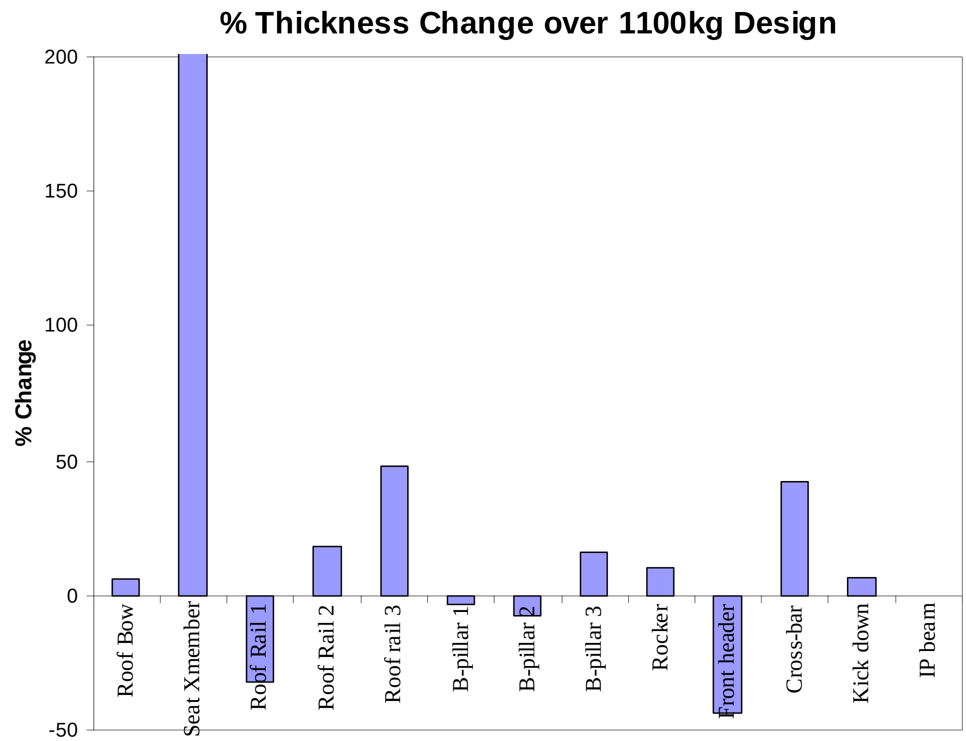

FIGURE 37: Percentage Change In Gauge – Run4 (1424kg) Normalized to Run1 (1100kg)

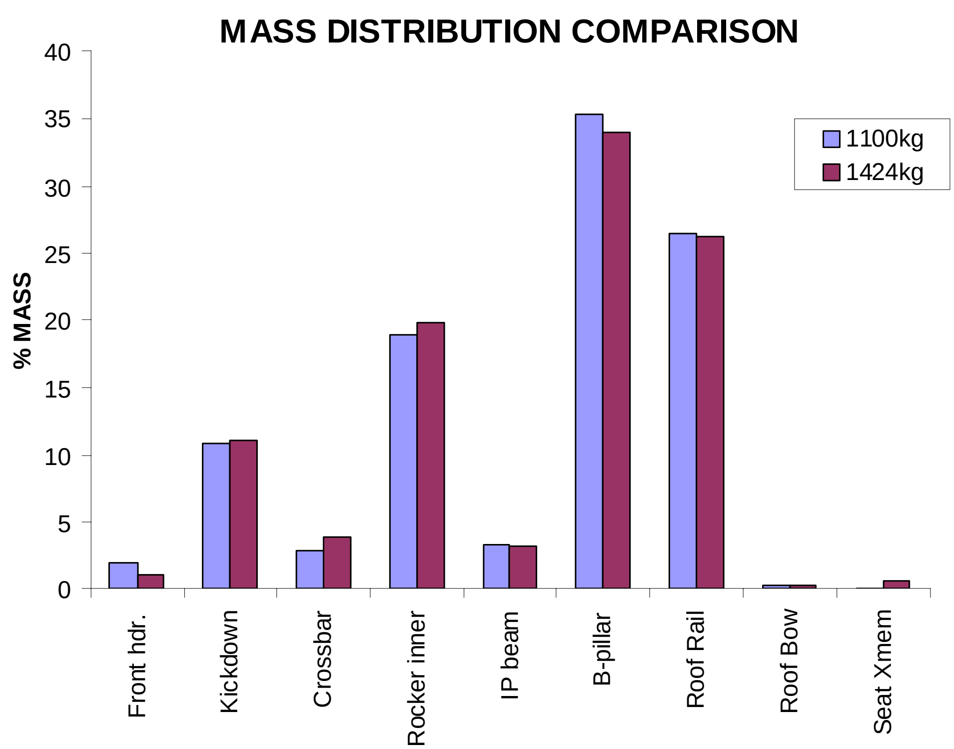

FIGURE 38: Part Mass Distribution Comparison – Run1 (1100kg) & Run4 (1424kg) Optimization Models

NAME	1100 kg	1424 kg
Roof Bow Position	8	5
Front Seat Xmember Position	8	8
Roof Bow Thickness (mm)	0.094	0.1
Front Seat Xmember Thickness (mm)	0.02	0.1
Roof Rail 1 Thickness (mm)	1.13	0.77
Roof Rail 2 Thickness (mm)	1.37	1.62
Roof Rail 3 Thickness (mm)	0.5	0.74
B-Pillar 1 Thickness (mm)	1.24	1.2
B-Pillar 2 Thickness (mm)	1.255	1.16
B-Pillar 3 Thickness (mm)	1.36	1.58
Rocker Thickness (mm)	1.0	1.1
Front Header Thickness (mm)	1.022	0.576
Cross-bar Thickness (mm)	0.8775	1.25
Kick-down Thickness (mm)	1.03	1.1
IP Beam Thickness (mm)	1.0	1.0

TABLE 5: Gauge Summary – Run1 (1100kg) & Run4 (1424kg) Optimization Models

NAME	MODEL	TYPE	DIRECTION	BASELINE	CHANGE
Mass of Designed Parts	1100kg	Objective	Minimize	51.17kg	
	1424kg	Objective	Minimize	54.3kg	+6.26%
Intrusion (measured for the side impact)	1100kg	Constraint	> 125mm	128mm	Satisfied
	1424kg	Constraint	> 125mm	130mm	Satisfied
Minimum Rigid Wall Force (measured for the roof crush)	1100kg	Constraint	>31251.0N	31259.0N	Satisfied
	1424kg	Constraint	> 38404.0N	38425.7N	Satisfied

TABLE 6: Design Response Comparison - Run1 (1100kg) & Run4 (1424kg) Optimization Models

10.3. PART 1 OPTIMIZATION CONCLUSIONS

- 3 total runs were performed for determining the optimal topology
- 1 additional run was performed for a higher curb weight to study the effect of the increased weight on the optimal load path configuration
- An increase in curb weight does not have a significant effect on the optimal load path configuration
- The optimal position of the roof bow is just behind the B-Pillar
- The front seat cross member is not important for the considered load cases. However, it is an important part for other load cases (e.g., pole impact). As a result, the baseline front seat member design will be retained for Part 2 optimization
- A higher B-Pillar crossbar location is better for the side impact performance
- A gusset bracket design will be used for connecting the crossbar to the B-Pillar. The intent is to raise the effective height of the crossbar.

11. PART 2 - DETAILED SHAPE, THICKNESS & MATERIAL OPTIMIZATION

The results from the three topology optimization runs were assimilated to create one design concept, which encompasses the good features of the optimized designs from the topology study. The following features were incorporated into the design:

1. Single roof bow located just behind the B-Pillar.
2. The baseline front seat cross-member was included in the design. Even though the topology runs showed that the front seat cross-member did not contribute significantly with the optimal topology, it was included due to its impact on other analyses like the pole impact.
3. The B-Pillar crossbar was included with the mid-axis located at the position 4 from the topology Run 3.

The objective of this run is to optimize the shape, thickness and material of important parts (identified in the topology optimization part) in the passenger cage compartment to minimize the mass of the system, while maintaining the survival space and rigid wall force constraints.

The optimization statement for the run is:

Minimize:

Mass of the design
Relative cost of the design

Subject to:

Roof crush force ≥ 31250N (2.75 * curb weight)
Survival space ≥ 125mm

By varying:

Shape, Thickness and Material of:

B-Pillar sections
Front Rocker
Rear Rocker
Floor Kick-down
Roof Rail sections
B-Pillar crossbar and attachment bracket
Roof bow
Door beams

Thickness and Material of:

Body side outer parts
Roof
Floor
Front Header
Rear Header

There are a total of 120 design variables for this problem setup. There are 61 shape variables, 39 thickness variables and 20 material variables. All the material variables are discrete; all the other variables are continuous. Each part with a designable material chooses from a unique choice of materials decided upon by the team for the optimization setup. Figure 39 shows all the parts being designed for shape in this optimization setup. The details of the design variables are provided in the next section. Each part being designed is discussed separately and all the variables are explained. The connection strategy for all the parts being designed for shape with the rest of the model is discussed at the end of the section.

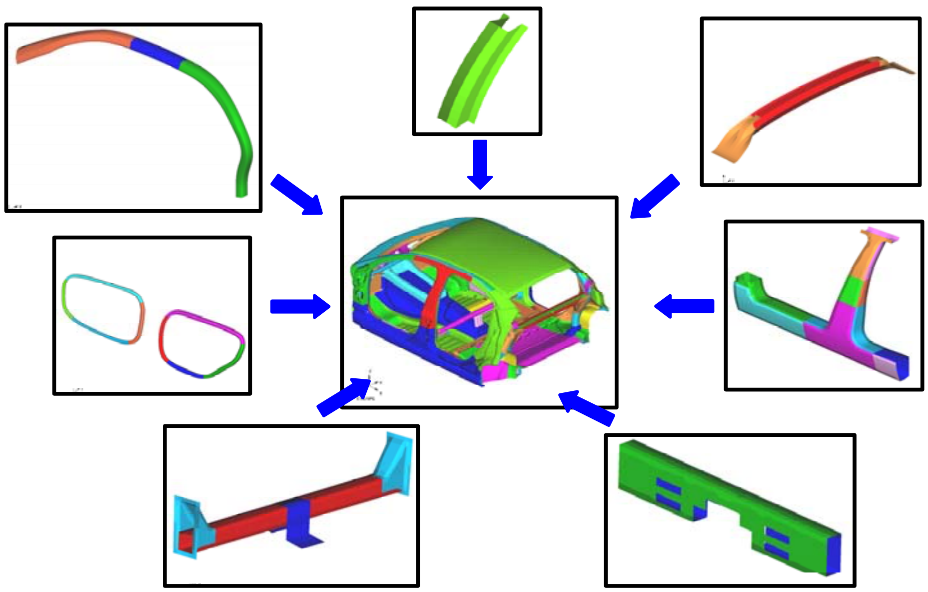

FIGURE 39: Shape Variables

Parts that are being designed for shape are those enclosed in the boxes. The static part of the model, not changed for shape, is also shown. The varying parts are connected to the non-varying parts automatically during the optimization.

11.1. B-PILLAR & ROCKER ASSEMBLY

The B-Pillar and the rocker were designed for shape, thickness and material during the optimization process. Figure 40 shows the parameterized model for the B-Pillar and the rocker. The cross-sectional shape of the B-Pillar and the rocker was not varied, only the size of the cross-sections for the B-Pillar and the rocker was designed. The flanges from the baseline design were not modeled for simplicity. The heights of the three sections of the B-Pillar were also varied, as shown in Figure 41. The allowed design space for the B-Pillar and the rocker is shown in Figure 42 with respect to the baseline design. The B-Pillar is divided into 6 different sections. Both the inner and the outer B-Pillar have three different sections along the height of the B-Pillar. The rocker section was separated into the front rocker and the rear rocker. Each of the front and rear rockers are further divided into the inner and outer sections. The heights of the three sections of the B-Pillar were also designed. The thickness of each section in the B-Pillar and rocker was allowed to vary between 0.6 and 2.0mm. The material choices allowed for the B-Pillar and rocker were: IF 140/270, DQSK 210/340, BH 250/550, DP 300/500, HSLA 350/450, DP 350/600, DP 500/800, DP 700/1000, Mart 1300 and Boron 1550.

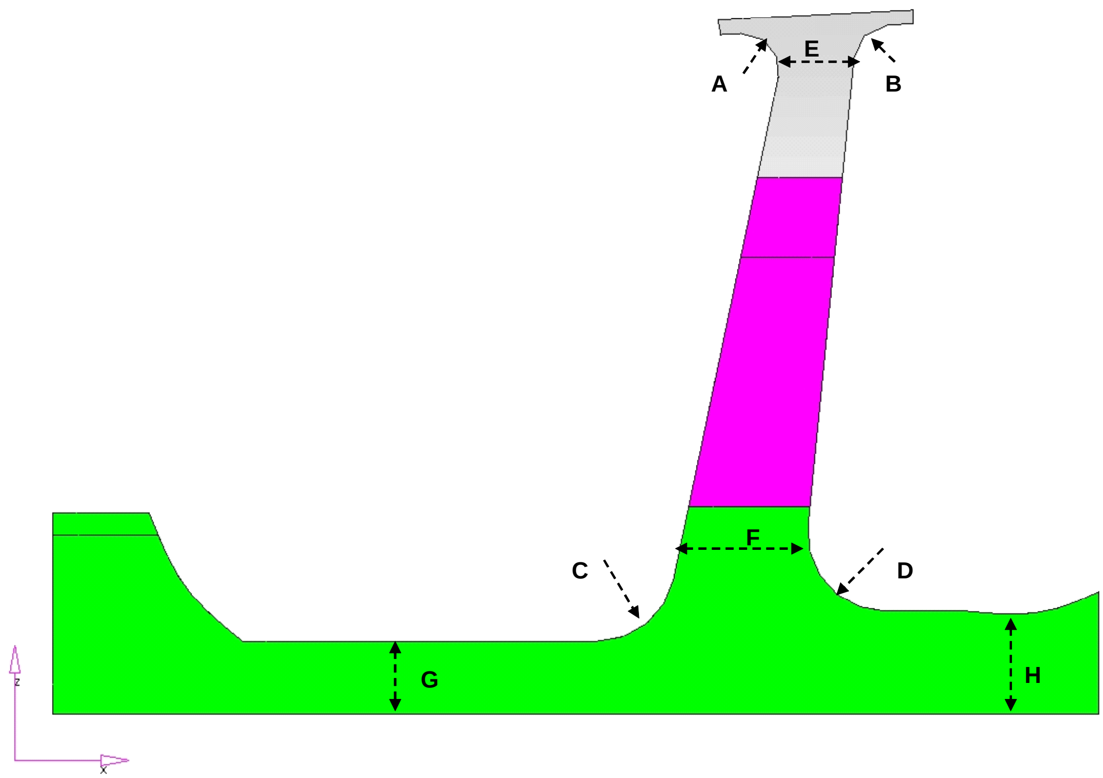

FIGURE 40: Shape Variables - B-Pillar & Rocker Assembly

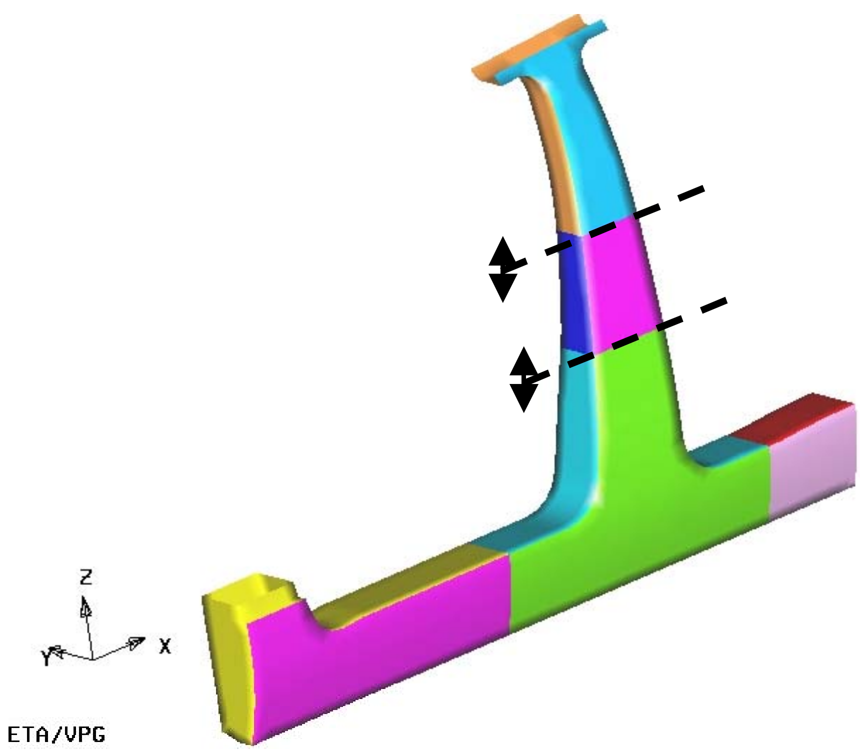

FIGURE 41: Section Height Variables - B-Pillar

The other two shape variables that control the length of each section of the B-Pillar along the height. Also shown are the 10 different sections being designed for thickness, as indicated by the different colors.

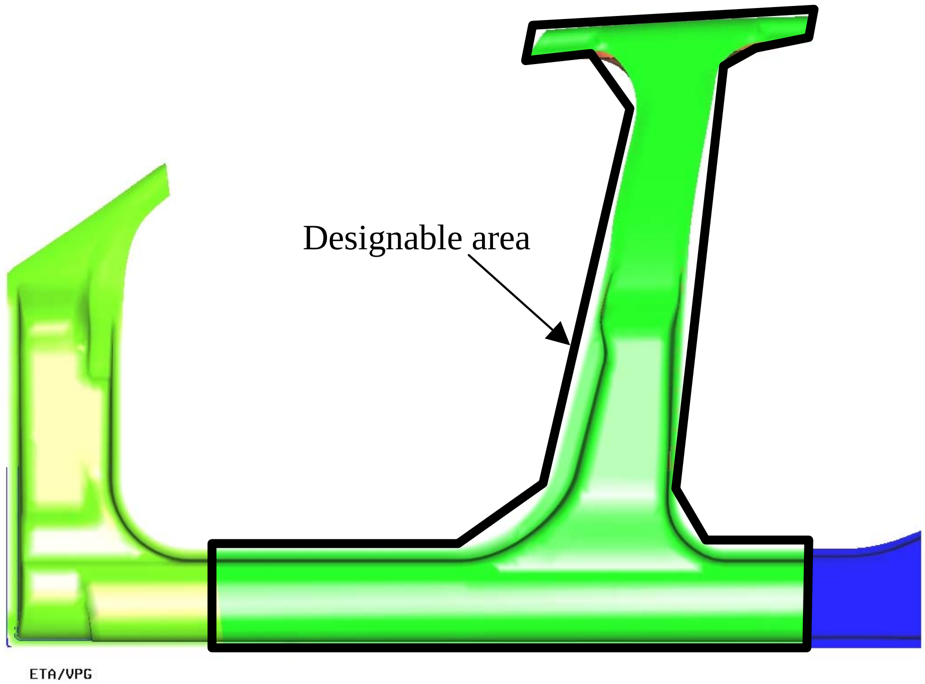

FIGURE 42: Baseline design - B-Pillar & Rocker Assembly

The dark boundary on the figure shows the envelope within which the shape can be varied during optimization. There were a total of 22 variables designed for the B-Pillar and the rocker: 10 shape variables, 10 thickness variables and 2 material variables.

11.2. ROOF RAIL

The Roof Rail was designed for shape, thickness and material during the optimization run. The Roof Rail design allows 3 different sections along the length of the rail. The lengths of the rail sections were also designed. The rail design is modeled as an extrusion along the baseline Roof Rail path. There were 9 different cross-sections controlling the shape of the rail along its length. The shape of the rail was varied by changing the shape of these cross-sections. The shape of each cross-section was varied independently, allowing a varying rail shape along its length. Figure 43 shows the modeling concept for the rail. The section shown in Figure 44 was used for defining the shape of the cross-sections 1, 2, 3, 7, 8, and 9. The section shown in Figure 45 was used for defining the shape of cross-sections 4, 5, and 6. The cross-sections 4, 5 and 6 had a smaller number of variables to allow for a better connection between the B-Pillar and the Roof Rail. In addition to the cross-sectional shape of the rail, the lengths of the three rail sections were also varied during the optimization, as shown in Figure 46.

The cross-sections in the front two rail parts were allowed to vary in perimeter by 20% from the baseline design perimeter. The last section was allowed to vary in perimeter by 50%. The thickness of each of the three sections was allowed to vary independently. The thickness was allowed to vary between 0.6 and 2.0mm. All three sections had the same material however. The material choices for the Roof Rail were: IF 140/270, DQSK 210/340, BH 250/550, DP 300/500, HSLA 350/450, DP 350/600, DP 500/800, and DP 700/1000.

There were a total of 36 variables being designed for the Roof Rail design: 32 shape variables, 3 thickness variables and 1 material variable. The 9 cross-sections shown determine the shape of the rail.

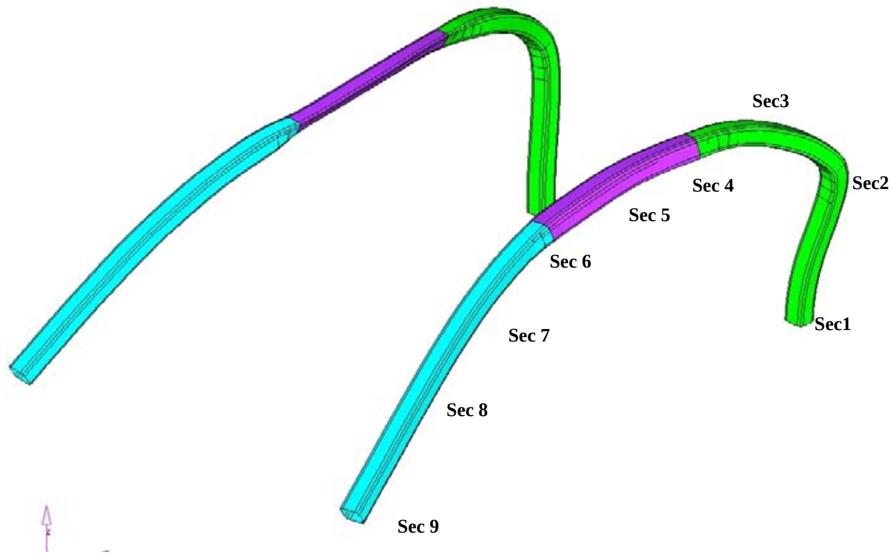

FIGURE 43: Roof Rail Parameterization - Location Of Cross-Sections

The red arrows define the vector along which the control points can move to change the shape of the cross-section.

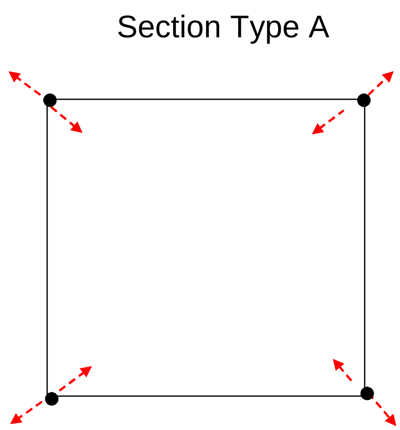

FIGURE 44: Shape Variables - Roof Rail Cross-Sections 1, 2, 3, 7, 8 & 9

The red arrows define the vector along which the control points can move to change the shape of the cross-section.

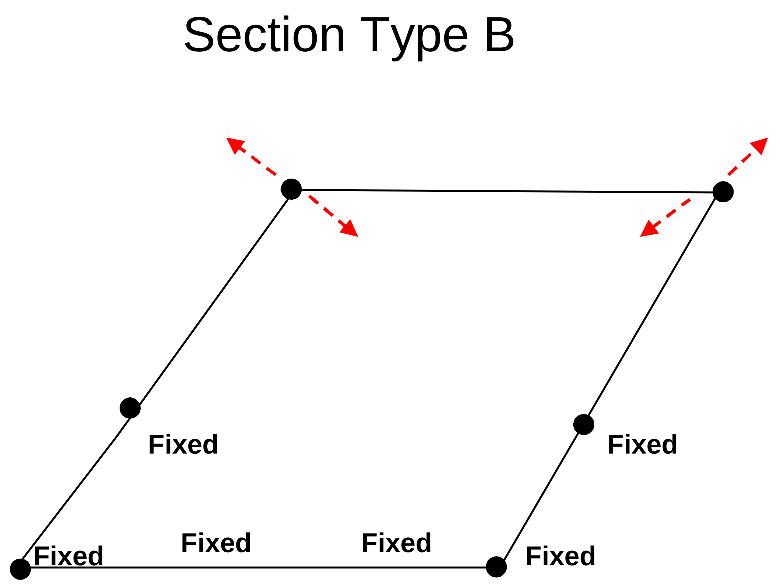

FIGURE 45: Shape Variables - Roof Rail Cross-Sections 4, 5, & 6

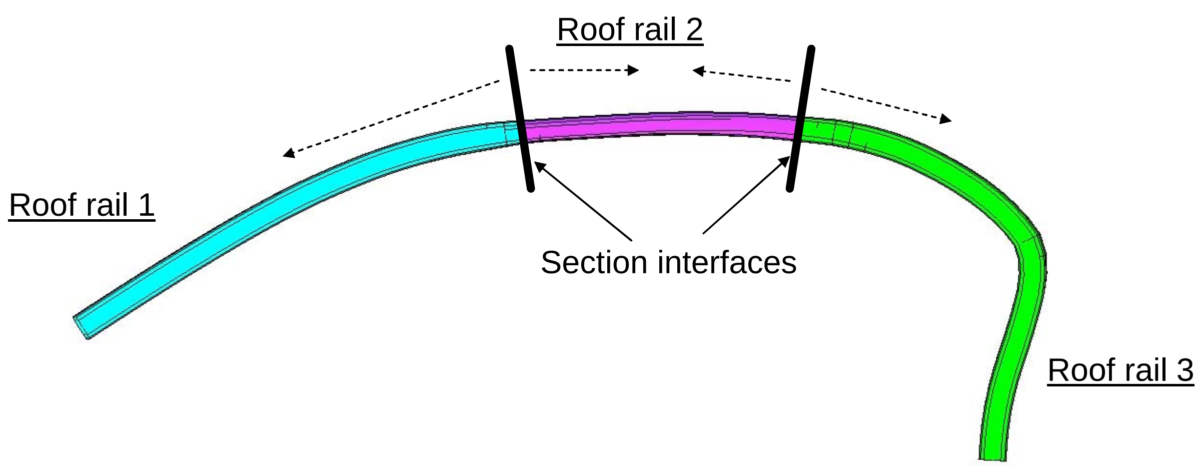

FIGURE 46: Section Interface & Gauge Variables – Roof Rail (Three gauge variables shown in Blue, Purple & Green)

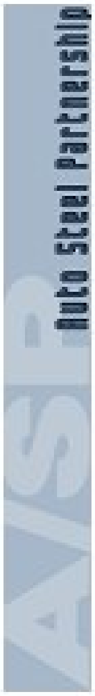

11.3. ROOF BOW

The roof bow was also designed for shape, thickness and material. The basic shape concept of the roof bow and the connecting brackets is shown in Figure 47. The cross-sectional shape of the roof bow being designed is shown in Figure 48. The roof bow is connected to the Roof Rail through a bracket. The shape of the bracket follows the shape of the roof bow. The thickness of the roof bow and the bracket was allowed to vary between 0.6 and 2.0mm. The material choices allowed for the roof bow and the bracket were:
IF 140/270, DQSK 210/340, BH 250/550, DP 300/500, HSLA 350/450, DP 350/600, DP 500/800, DP 700/1000, Mart 1300 and Boron 1550.

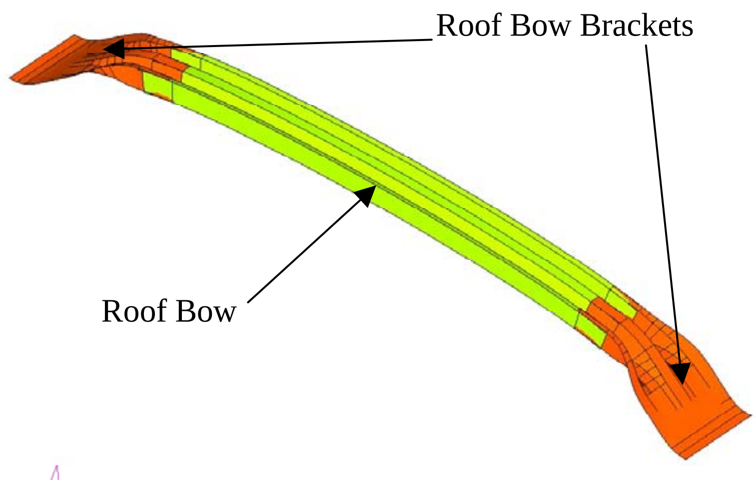

FIGURE 47: Roof Bow Assembly - Roof Bow & Connecting Brackets

The thickness of both these parts was designed independently in the optimization study.

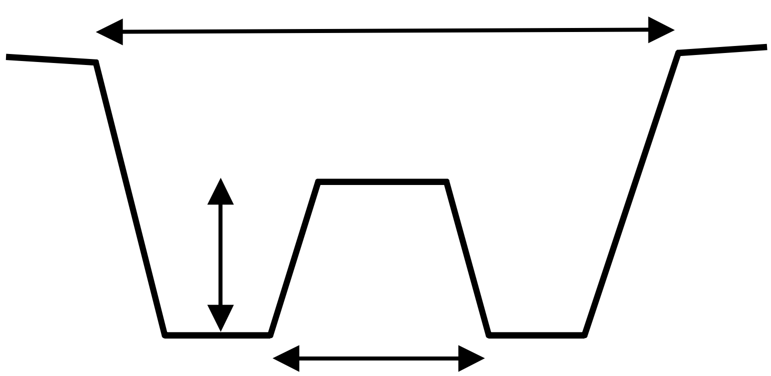

FIGURE 48: Shape Variables - Roof Bow

There were a total of 7 variables being designed for the roof bow and bracket parts: 3 shape variables, 2 thickness variables and 2 material variables.

11.4. FLOOR KICK-DOWN

The floor kick-down area was designed for shape, thickness and material. The shape being designed was primarily the cross-sectional size of the kick-down area. The cross-section was allowed to increase in size towards the top of the vehicle and also towards the back of the vehicle. The design concept and the cross-sectional variables are shown in Figure 49. The thickness of the kick-down was allowed to vary between 0.6 and 2.0mm. The material choices allowed for the kick-down part were: IF 140/270, DQSK 210/340, BH 250/550, DP 300/500, HSLA 350/450, DP 350/600, DP 500/800, DP 700/1000, Mart 1300 and Boron 1550.

There were a total of 6 variables for the floor kick-down: 3 shape variables, 2 thickness variables and one material variable.

11.5. B-PILLAR CROSSBAR

The B-Pillar crossbar and bracket were designed for shape, material and thickness during the optimization study. The crossbar was modeled parametrically to have a rectangular cross-sectional shape. The crossbar assembly is shown in Figure 50. The width and height of the crossbar cross-section are the shape design variables for the crossbar. This is shown in Figure 53. The crossbar bracket that attaches the crossbar to the B-Pillar was also designed for shape. The bracket concept used is shown in Figure 52. The bracket concept was developed to be able to raise the effective height of the crossbar. This shape should transfer a higher moment into the crossbar, allowing more load transfer through the lower load path of the design. The various connection points of the crossbar assembly are shown in Figure 51. The thickness of the crossbar and the bracket are allowed to vary between 0.6 and 2.0mm. The material choices allowed for these two parts are: IF 140/270, DQSK 210/340, BH 250/550, DP 300/500, HSLA 350/450, DP 350/600, DP 500/800, DP 700/1000, Mart 1300 and Boron 1550. The new crossbar design was attached to the tunnel through a bracket. Figure 28 shows the design for the bracket and the connection.

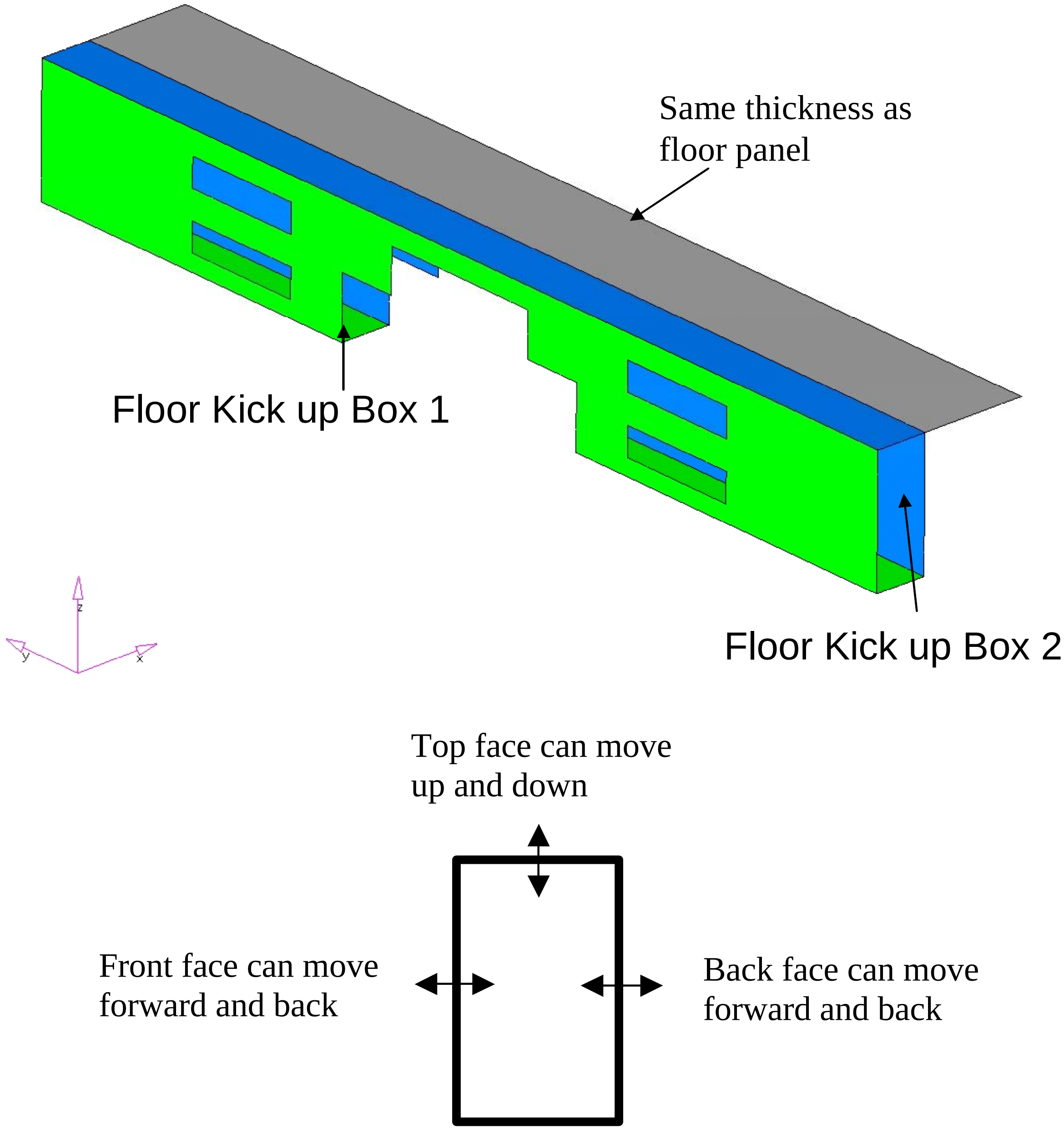

FIGURE 49: Floor Kick-down Assembly & Cross-Sectional Shape

The two different parts of the kick-down region being designed for thickness are also shown. The arrows on the cross-section indicate the dimensions being designed to change the shape of the kick-down.

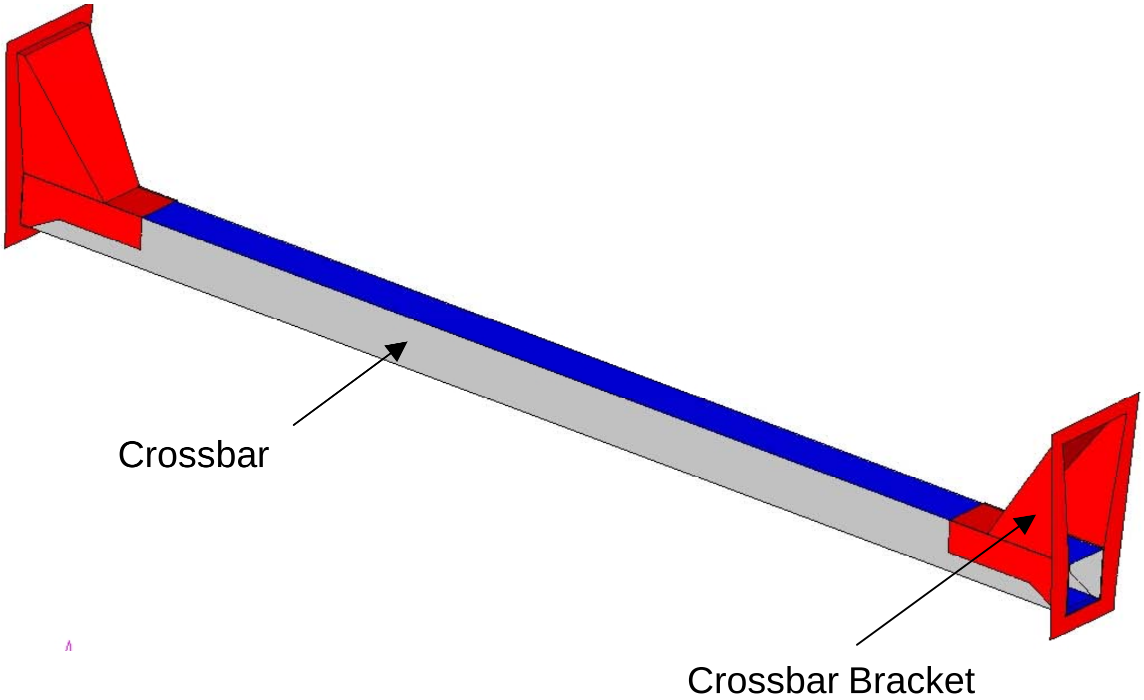

FIGURE 50: Crossbar Assembly

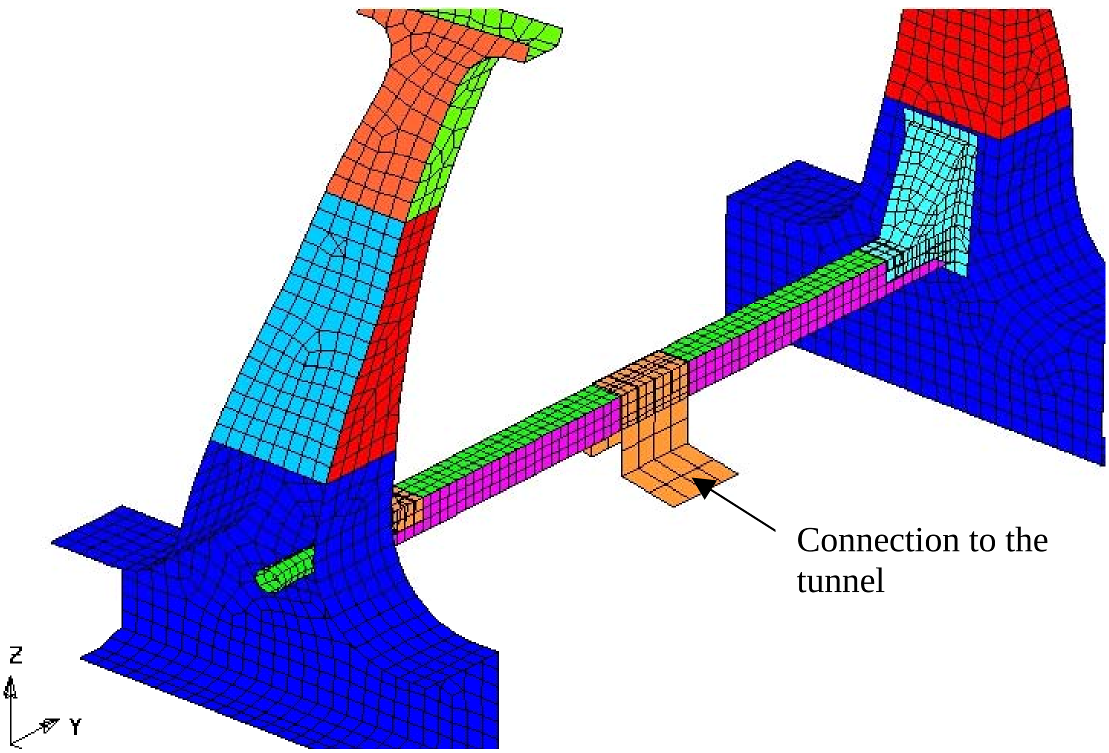

FIGURE 51: Crossbar To Tunnel Connection Bracket

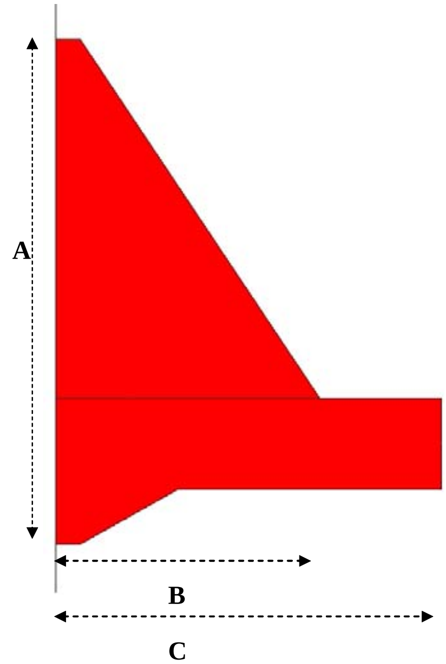

FIGURE 52: Shape Variables – Crossbar Bracket

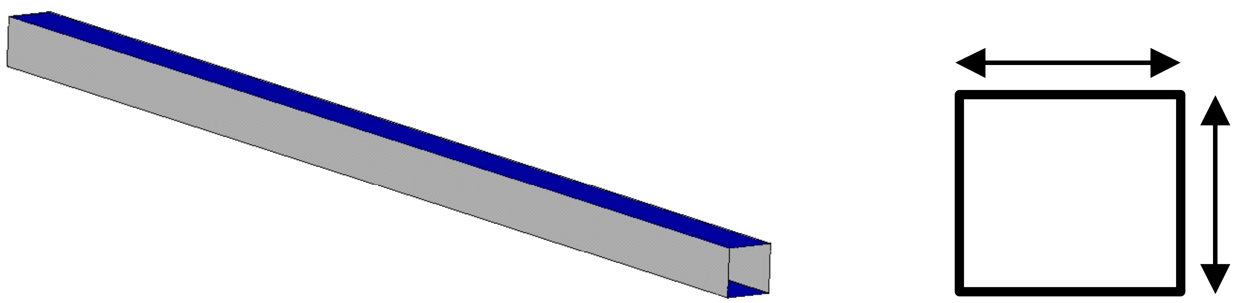

FIGURE 53: Shape Variables – Crossbar Cross-section

The arrows on the cross-sectional shape indicate the variables. The height and the width of the cross-section were treated as the variables for the crossbar shape.

There were a total of 9 variables being designed for the crossbar and the bracket: 5 shape variables, 2 thickness variables and 2 material variables.

11.6. B-PILLAR REINFORCEMENT

The reinforcement was designed for shape, thickness and material in the optimization study. The thickness of the reinforcement was allowed to vary between 0.6 and 2.0mm. The part was allowed to have any material from the following set: IF 140/270, DQSK 210/340, BH 250/550, DP 300/500, HSLA 350/450, DP 350/600, DP 500/800, DP 700/1000, Mart 1300 and Boron 1550.

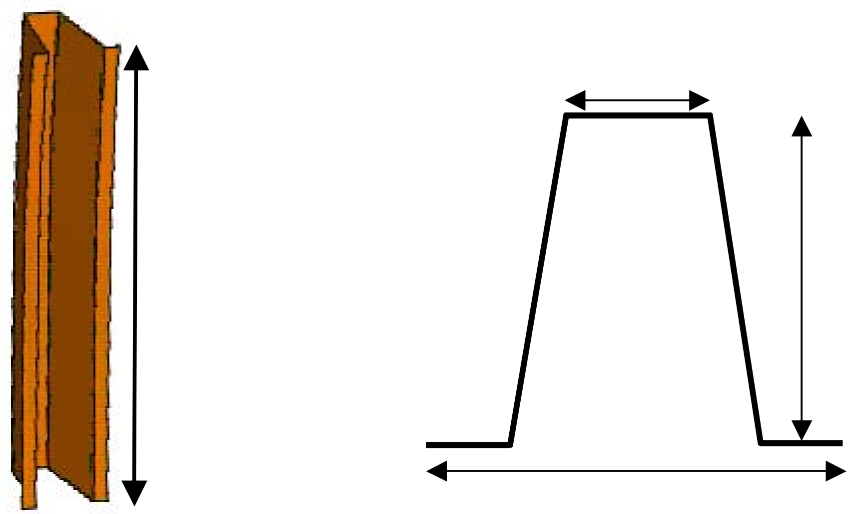

FIGURE 54: Shape Variables – B-Pillar Reinforcement

The cross-sectional shape is also shown, with the arrows indicating the dimensions that were varied to change the shape of the reinforcement.

The shape of the part and the variables are shown in Figure 54. The shape variables designed for the reinforcement are the cross-sectional shape and the length.

There are a total of 5 design variables in the reinforcement: 3 shape variables, 1 thickness variable and 1 material variable.

11.7. SIDE INTRUSION DOOR BEAMS

The door beams were designed for shape, material and thickness during the optimization study. The shape of the door beams was modeled in the similar fashion as the Roof Rail. 4 cross-sections were defined along the length of the door beam where shape can be varied independently. A rectangular shaped cross-section was designed for the door beams. The shape of the cross-section could be varied along the length of the beam due to the 4 independent sections being designed for both the front and the rear door beams. The height and width of the cross-section were varied at each of the 4 spots. The shape of the front door beams and the rear door beams was varied independently. Figure 55 shows the overall design concept and the design variables for the cross-sectional shape.

The thickness of the 4 sections in the front door beams and the rear door beams was also varied independently. The thickness was allowed to vary between 0.8 and 2.0mm. The door beams are allowed to have any material from the following set: IF 140/270, DQSK 210/340, BH 250/550, DP 300/500, HSLA 350/450, DP 350/600, DP 500/800, DP 700/1000, Mart 1300 and Boron 1550.

There were a total of 25 design variables in the door beams: 16 shape, 8 thickness and 1 material variable.

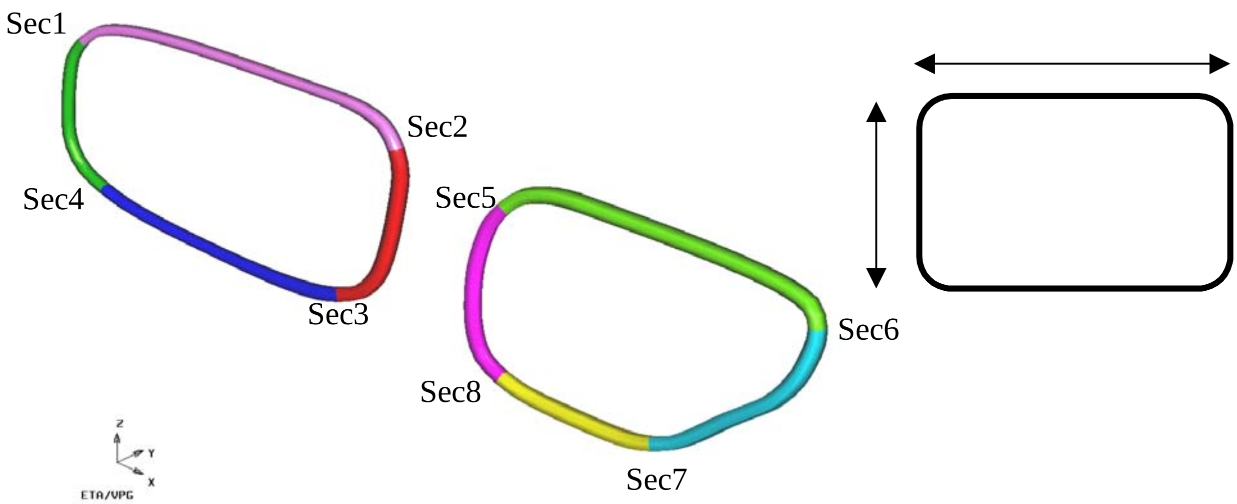

FIGURE 55: Door Beam Parameterization - Location & Shape Variables Of Cross-Sections

In addition to the parts described above, some parts were designed for thickness and material only. The shape of these parts was not modified. These add another 14 variables to the problem; 7 thickness variables and 7 material variables. The parts designed for just thickness and material are: Front header, rear header, roof, front floor, rear floor, body side outer front, body side outer rear parts. Their thickness was allowed to vary between 0.6 and 2.0mm and they were given the following material choices:

- Roof
  IF 140/270, DQSK 210/340, BH 250/550, DP 300/500, HSLA 350/450, DP 350/600
- Floor
  IF 140/270, DQSK 210/340, BH 250/550, DP 300/500, HSLA 350/450, DP 350/600
- Headers
  IF 140/270, DQSK 210/340, BH 250/550, DP 300/500, HSLA 350/450, DP 350/600, DP 500/800, DP 700/1000
- Body Side Outer (front)
  IF 140/270, DQSK 210/340, BH 250/550, DP 300/500, HSLA 350/450, DP 350/600, DP 500/800, DP 700/1000
- Body Side Outer (Back)
  IF 140/270, DQSK 210/340, BH 250/550, DP 300/500, HSLA 350/450, DP 350/600

11.8. MATERIAL COST FACTOR

In order to discourage use of higher strength steels in parts where it is not needed, a relative cost function was setup to estimate the relative cost of different design configurations. The cost factors defined in Table 7 were used for calculating the relative mass of each design. The cost of each part was calculated by multiplying the mass of the part with the normalized cost factor for the material being used for that part. During the optimization more importance was placed on minimizing mass. The mass was assigned twice as much importance as cost. This means that a cost increase of $1 is justified if that results in a 2kg mass saving.

MATERIAL NAME	Relative Cost
IF 140/270	1.0
DQSK 210/340	1.104
BH 250/550	1.13
DP 300/500	1.169
HSLA 350/450	1.1948
DP 350/600	1.39
DP 500/800	1.506
Boron 1550	1.805
DP 700/1000	1.584
Mart 1300	1.688

TABLE 7: Relative Cost Factors Of materials Used

11.9. SUBSYSTEM MODELS

The shape optimization has a total of 120 design variables. Therefore, to increase computational efficiency, the analysis was performed using smaller subsystem models. This strategy gains tremendous time savings over the use of a full system model. Although the optimization analyses were performed on the smaller subsystem models, to assure adequate coupling, some analyses were performed using the full system model.

Different levels of sub-models were created for the optimization. Since a majority of the variables are in the Roof Rail and the B-Pillar assembly, two sub-models were built for these parts: one for the Roof Rail and one for the B-Pillar/rocker assembly. Figures 56 & 57 show the subsystem models for the Roof Rail and the B-Pillar respectively. In addition to these sub-models, another sub-model was used that had all the parts being designed. This higher level sub-model is shown in Figure 58. The figures show the area where the boundary conditions from the full system model are applied.

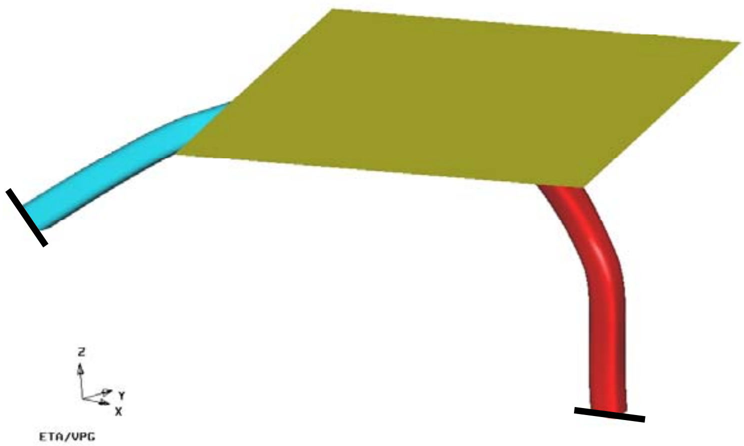

FIGURE 56: Roof Rail Sub-Model - Dark Lines At End Of Roof Rail Indicate Interface Boundary

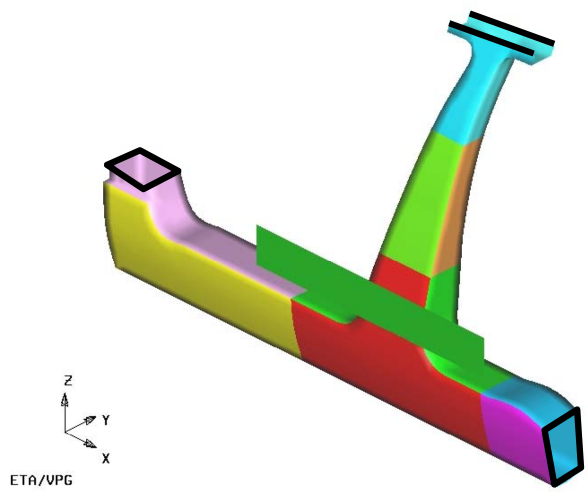

FIGURE 57: B-Pillar Sub-Model - Dark Lines At End Of Roof Rail Indicate Interface Boundary

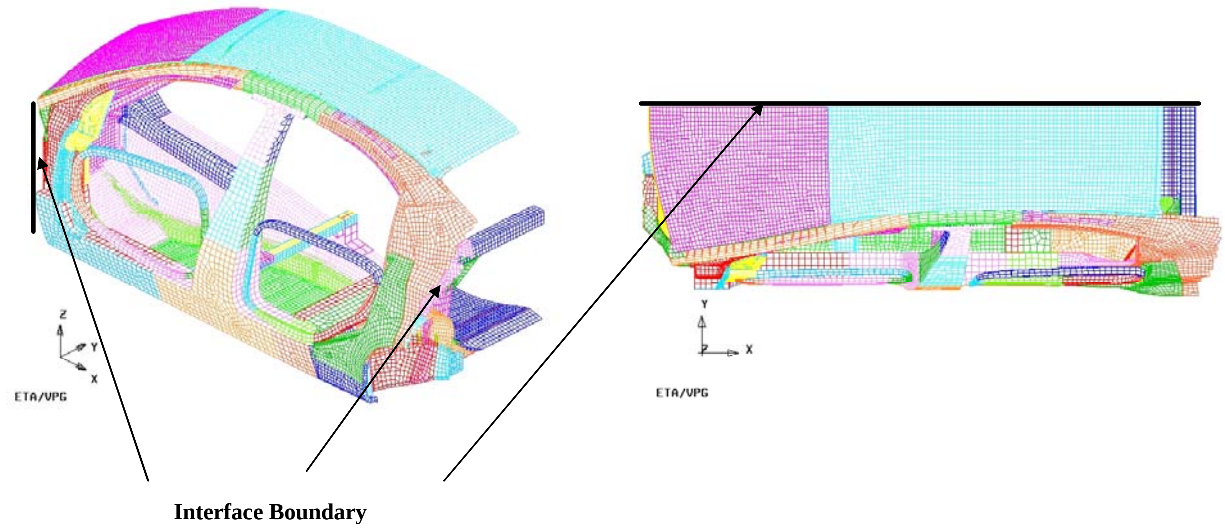

FIGURE 58: Highest Level Sub-Model - Dark Lines At End Of Roof Rail Indicate Interface Boundary

11.10. CONNECTING PARTS

Since the shape of some of the parts was changed during the optimization, the connection of these parts to the static parts of the model needed to be dynamic. New CAD data was created and meshed for all the parts being designed for shape during each and every design evaluation. Two connection strategies were used for different parts: spot-welds and tied contact definitions. The following section describes the connections for the various parts. A welding code was written to facilitate the automatic welding of parts in batch mode during the optimization.

11.11. SPOT WELDS

The rocker was connected to the static part of the A-pillar and the C-Pillar through spot-welds.
The Roof Rail was connected to the A and the C pillar through spot-welds also.
The Roof Rail was connected to the roof through dynamic spot welds.
The Roof Rail was connected to the B-Pillar using spot welds also.
The roof bow and the Roof Rail connections were also created using spot-welds.
The floor kick-down and the tunnel connection have spot welds.
The floor kick-down connection to the rocker was via spot welds.
These welds were re-created automatically every time a new design needs to be evaluated.

11.12. TIED CONTACT DEFINITION

The B-Pillar was connected to the crossbar bracket by a tied contact definition.
The crossbar was connected to the crossbar bracket through a tied contact definition also.
The connection between the crossbar and the crossbar-tunnel attachment bracket was via a tied contact definition.

11.13. RESULTS

The optimization reduced the mass of the designed parts by 33.5kg. This resulted in a reduction of 22% over the baseline design (from 152 to 118.5kg). The relative cost measure was also reduced by 19% (from 215 to 174.7kg). The roof crush and the side impact targets were met for this design. The details of the design are provided in the following sections.

11.13.1. ROOF RAIL

The optimized design of the Roof Rail is 41% lighter than the baseline design. The shape of the rail was changed significantly when compared to the baseline. The large variability (50% and 20%) in the perimeter change allowed during the optimization resulted in a shape, which did not fit well with the rest of the vehicle. The thickness of all the three sections was reduced from the baseline value of 1.0mm. The middle section of the rail has a larger section, which is aligned normal to the roof crush loading plane. The section towards the back of the Roof Rail is reduced to a very small section, which is along the same lines as the results from the other optimization runs. Figures 59 & 60 show the comparison of the cross-sectional shape of the optimized rail to the baseline rail at two different points along the length of the rail. The material used for the optimized design is the same as the material used for the baseline design.

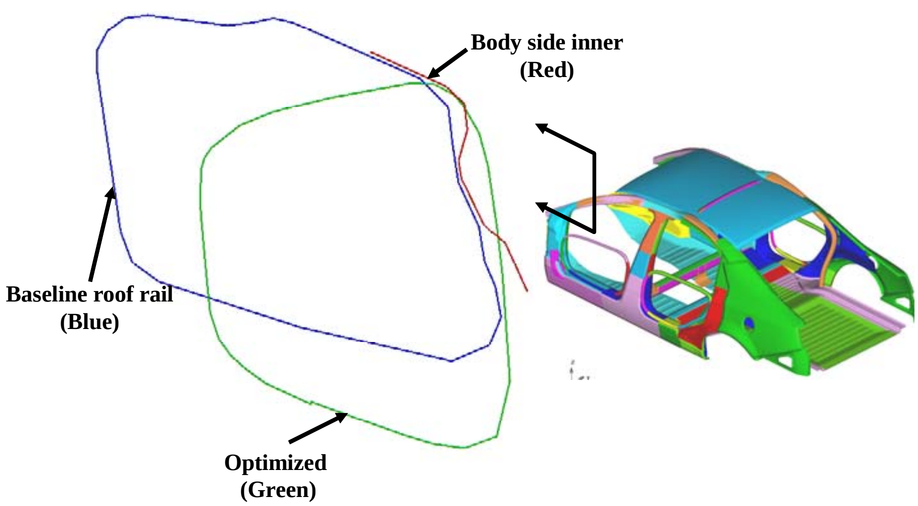

FIGURE 59. Front Roof Rail Cross-Sectional Shape Comparison –Baseline & Optimized

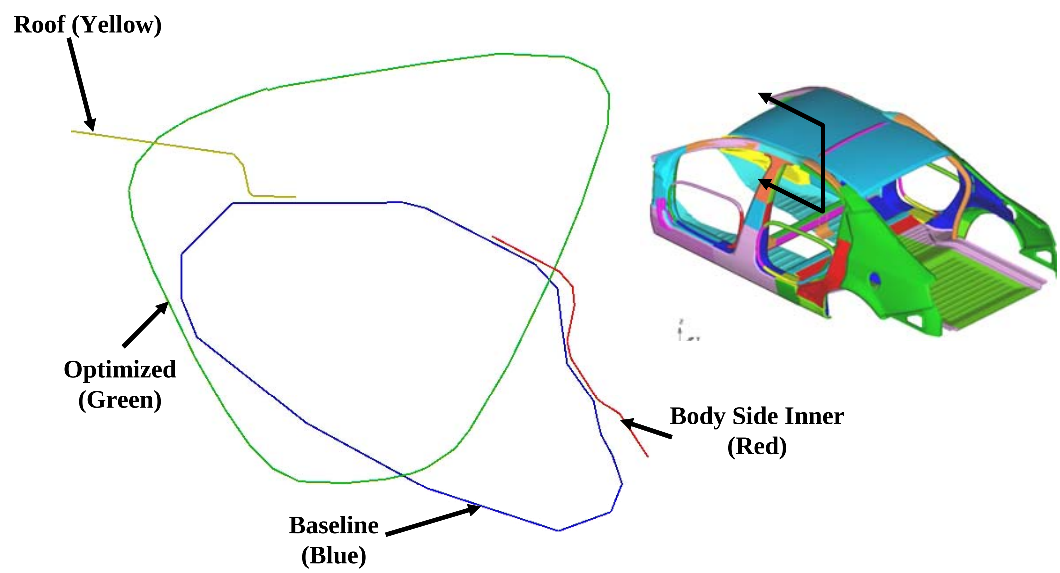

FIGURE 60: Mid Roof Rail Cross-Sectional Shape Comparison –Baseline & Optimized

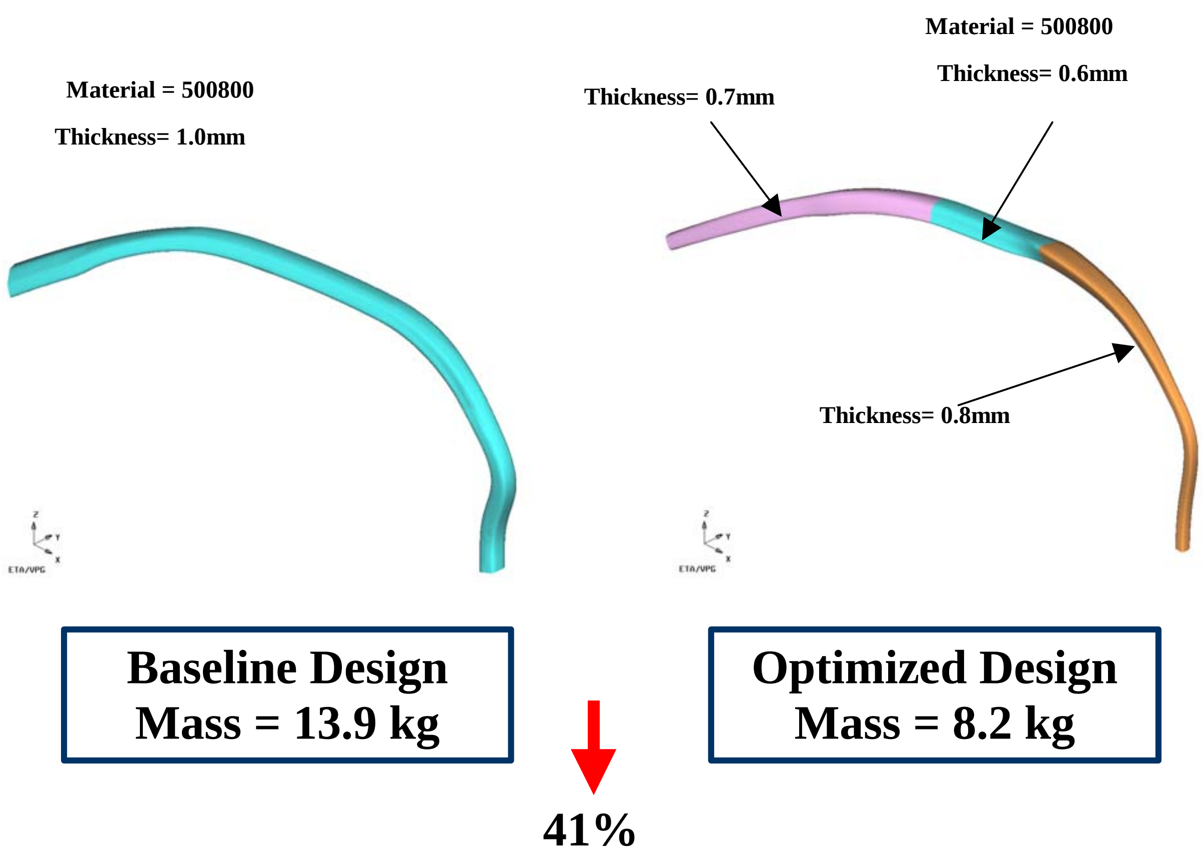

FIGURE 61: Comparison Of Optimized Roof Rail To Baseline Design, Mass Reduced By 41%

11.13.2. ROOF BOW

The optimization process increased the mass of the roof bow by 50% compared to the baseline design. The material of the optimized design was however reduced in grade from DP 500/800 to DP 350/600. The thickness of the parts was also reduced. The increase in weight is due to the increase in the cross-sectional size of the new roof bow.

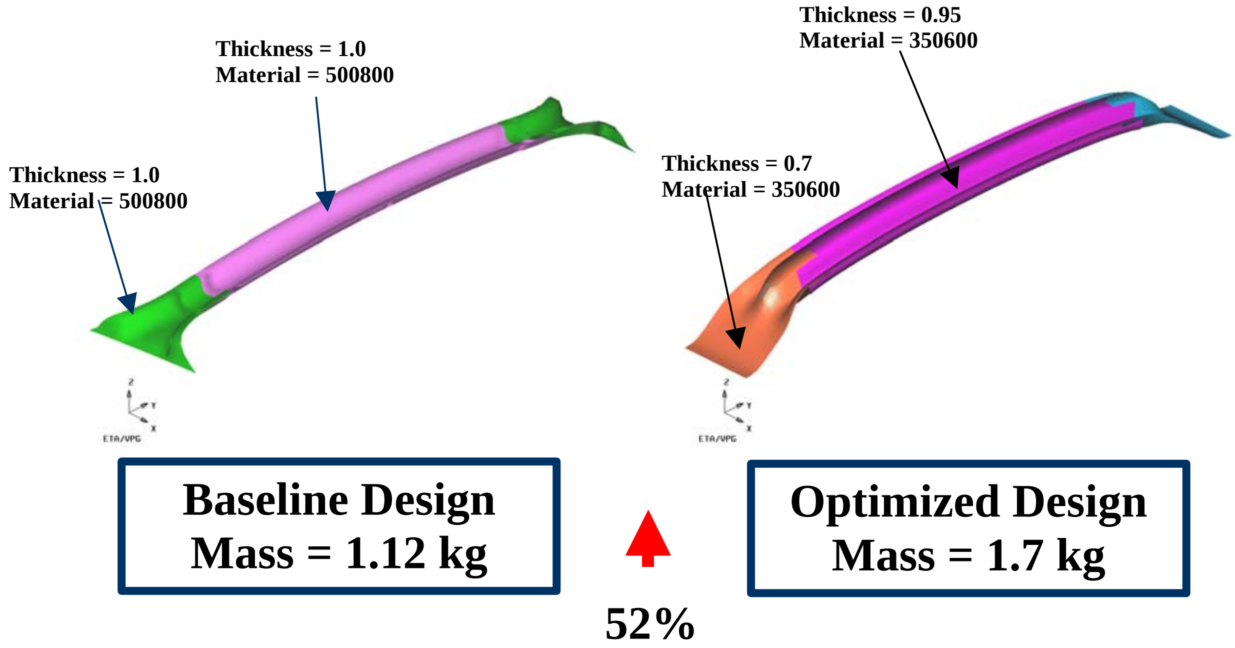

FIGURE 62: Comparison Of Optimized Roof Bow To Baseline Design, Mass Increased By 52%

11.13.3. B-PILLAR CROSSBAR

The B-Pillar crossbar optimized design massed up significantly. The mass of the design was increased by 2.2kg, an increase of about 54%. The material for the crossbar was pushed to the highest grade material allowed (Boron 1550). The cross-sectional size of the crossbar is the largest size allowed during the optimization. The increases are consistent with the results of the topology runs, which indicated the requirement of a stiff crossbar for increased mass savings.

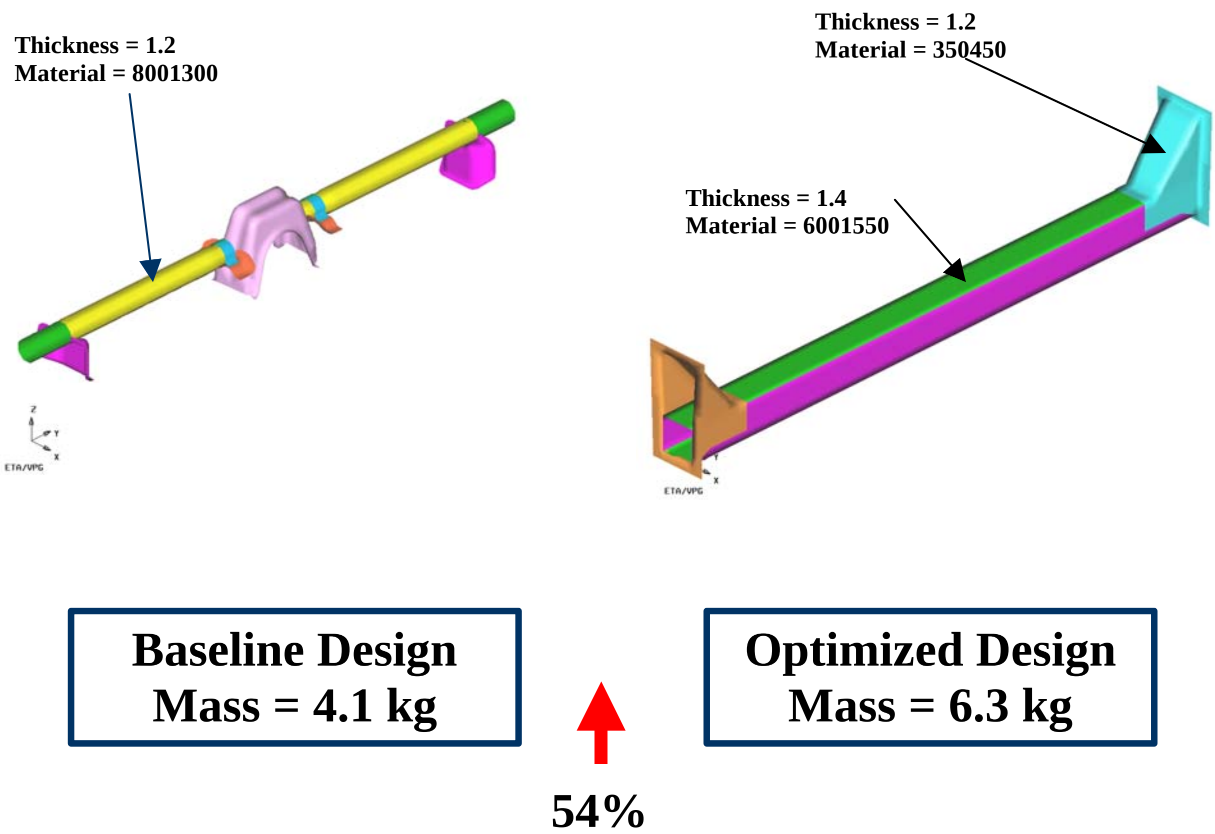

FIGURE 63: Comparison Of Optimized B-Pillar To Baseline Design, Mass Increased By 54%

11.13.4. FLOOR KICK-DOWN

The main changes in the kick-down design were the increase in thickness and the cross-sectional size. The width of the cross-section was moved to the largest allowed size during the optimization. The height of the cross-section was increased with respect to the baseline. However, it did not move to the maximum value. The material of the part remained unchanged from the baseline.

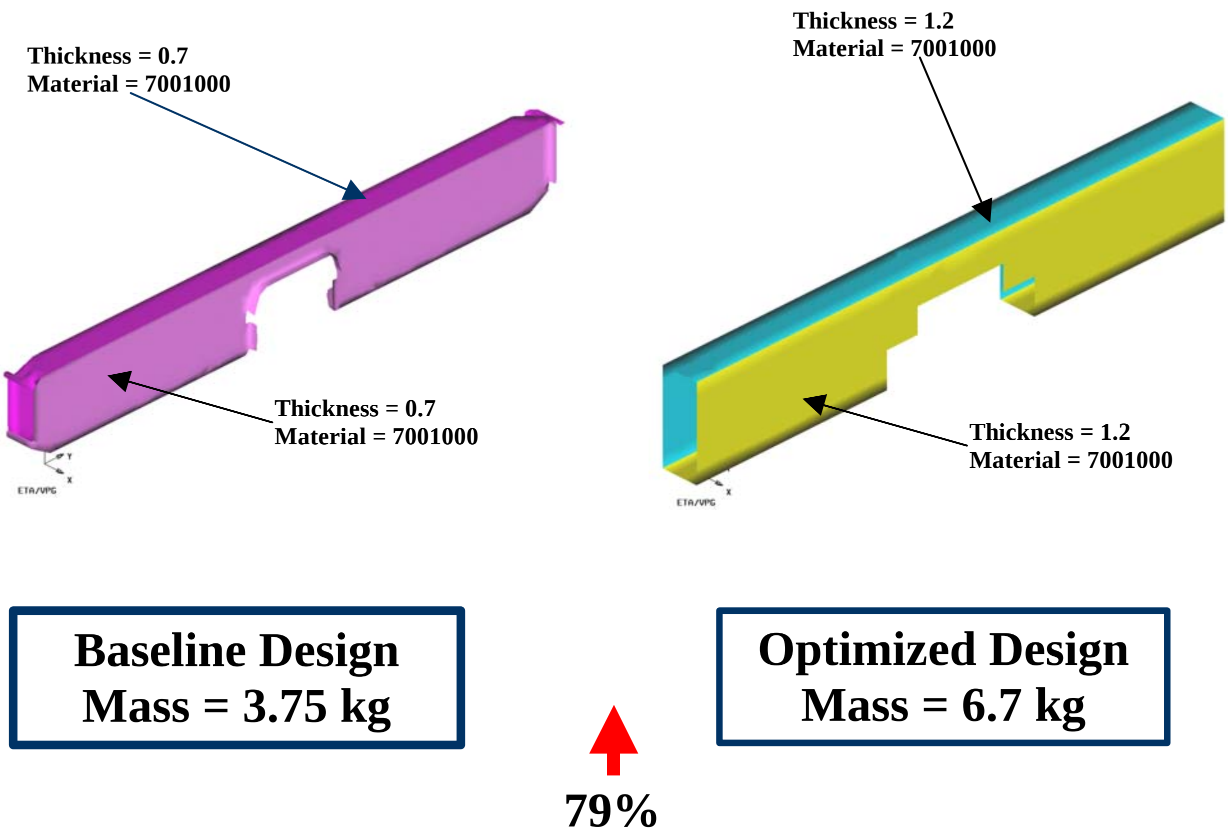

FIGURE 64: Comparison Of Optimized Floor Kick-down To Baseline Design, Mass Increased By 79%

11.13.5. DOOR BEAMS

There was a significant reduction in the mass of the door beams. The thickness of all the sections was reduced to the lowest allowed value of 0.8mm. The material of the door beams was also moved to a lower grade (from DP 500/800 to HSLA 350/450). The mass was reduced by 7.2kg, a reduction of 57%. The cross-sectional size of the door beams was also reduced compared to the baseline design.

Thickness = 1.0, 1.2, 1.5
Material = 500800

Thickness = 0.8
Material = 350450

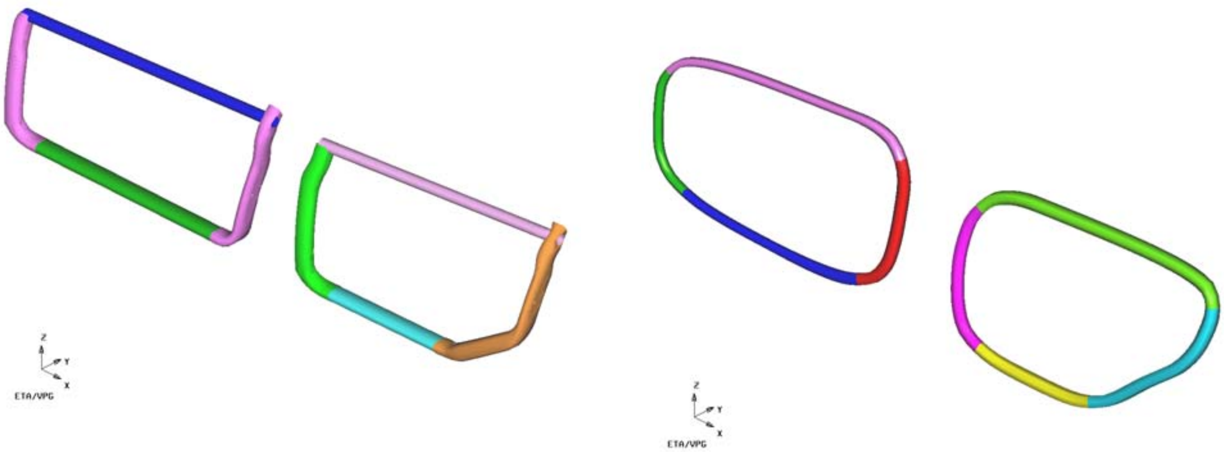

Baseline Design
Mass = 12.58 kg

Optimized Design
Mass = 5.38 kg

57%

FIGURE 65: Comparison Of Optimized Door Beam To Baseline Design, Mass Reduced By 57%

11.13.6. B-PILLAR

The optimized B-Pillar design is 24.7kg lighter than the baseline design. The material savings are primarily from the reduction in the gauge. The material of the B-Pillar and rocker was upgraded to the strongest material allowed in Boron 1550. Since the parametric model did not model the flanges, the overall cross-sectional shape of the B-Pillar sections is larger than the baseline sections. The sections will be updated accordingly for the final shape and thickness optimization to not exceed the size of the baseline sections.

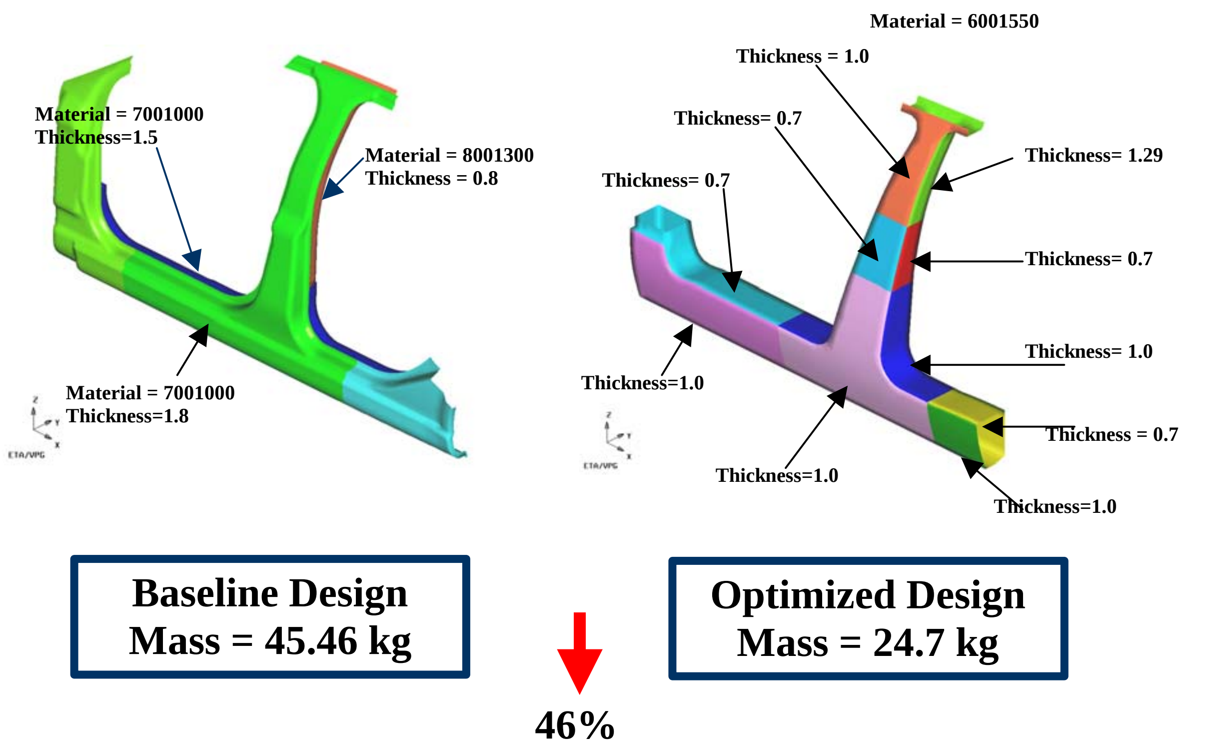

FIGURE 66: Comparison Of Optimized B-Pillar/Rocker Assembly To Baseline Design, Mass Reduced By 46%

11.13.7. B-PILLAR REINFORCEMENT

The main change in the reinforcement was the increase of the span length of the reinforcement. The material was downgraded from Boron 1550 to DP 700/1000. The thickness of the part remained unchanged. Due to increase in the length of the part, the mass increased by 16%.

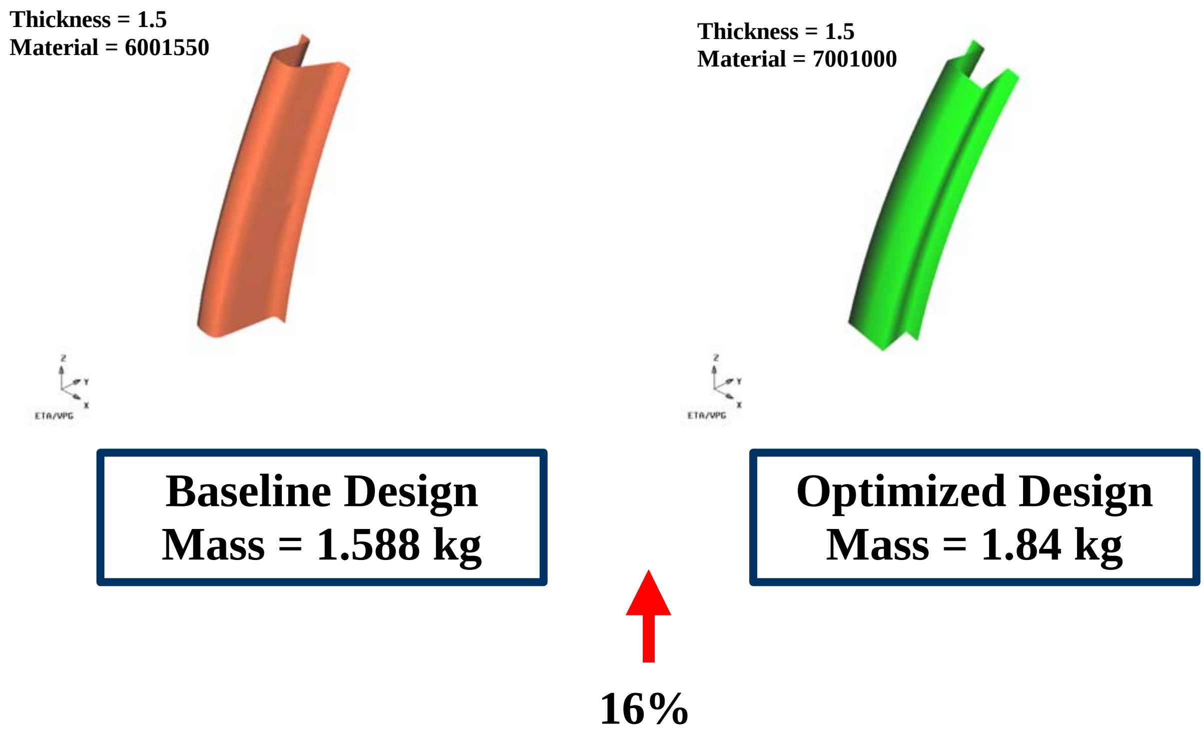

FIGURE 67: Comparison Of Optimized B-Pillar Reinforcement To Baseline Design, Mass Increased By 16%

Figures 68 & 69 show the deformed model of the optimized design for the side impact and roof crush. Figure 70 shows the rigidwall force curve for the optimal design found by the optimization during the Part 2 study.

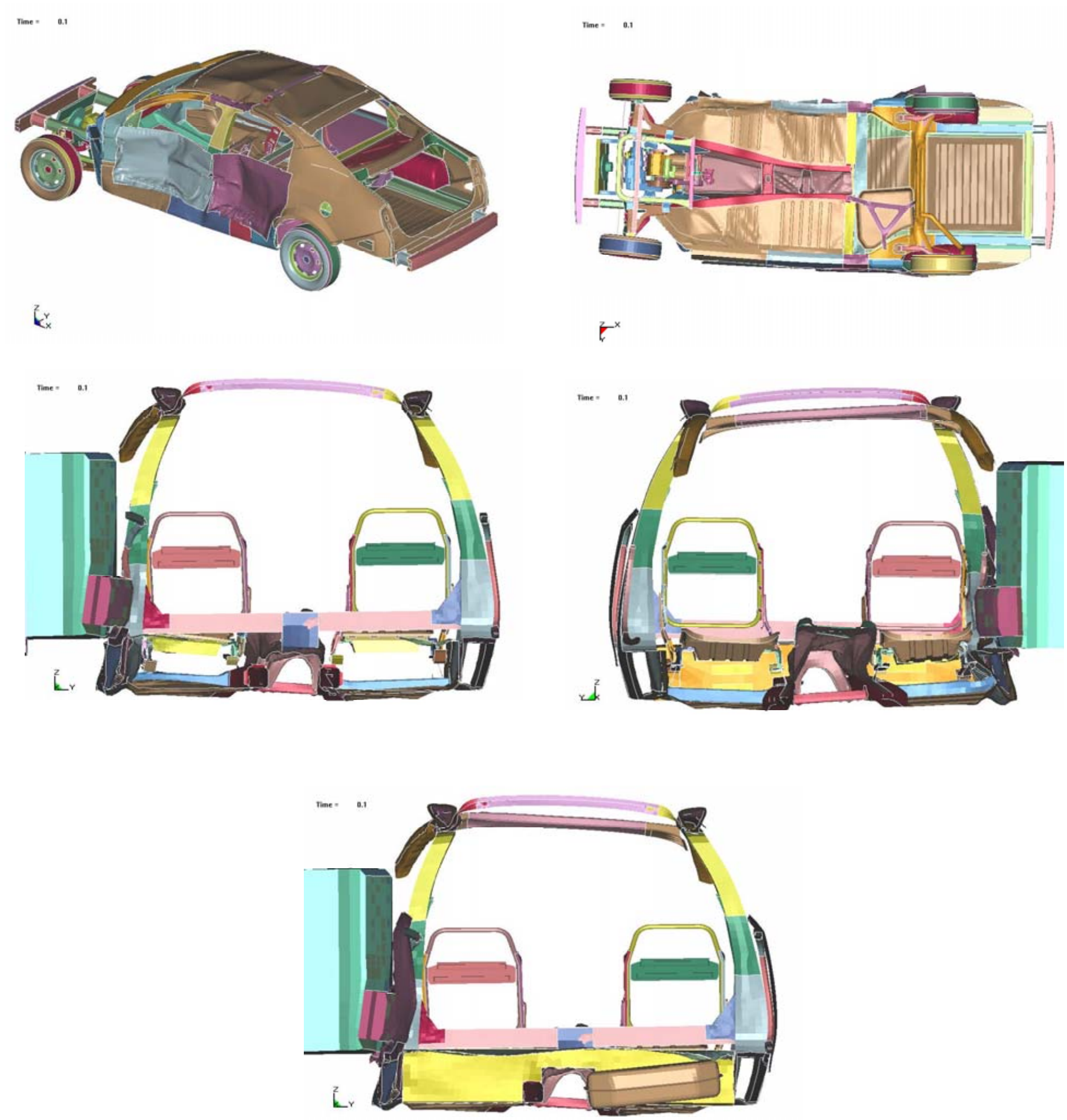

FIGURE 68: Side Impact Analysis – Deformed Shape Of Best Design From Part 2 Optimization

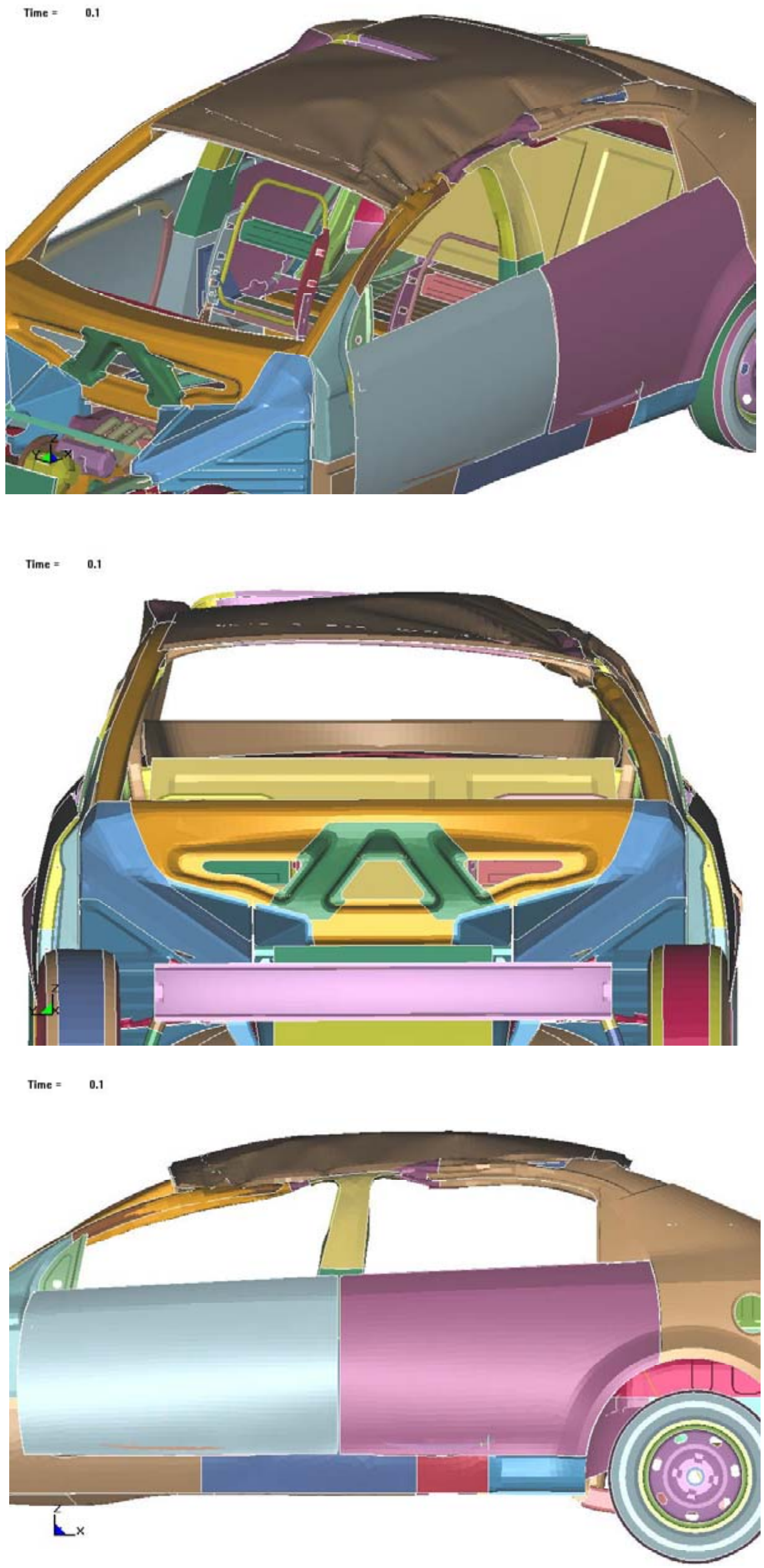

FIGURE 69: Roof Crush Analysis – Deformed Shape Of Best Design From Part 2 Optimization

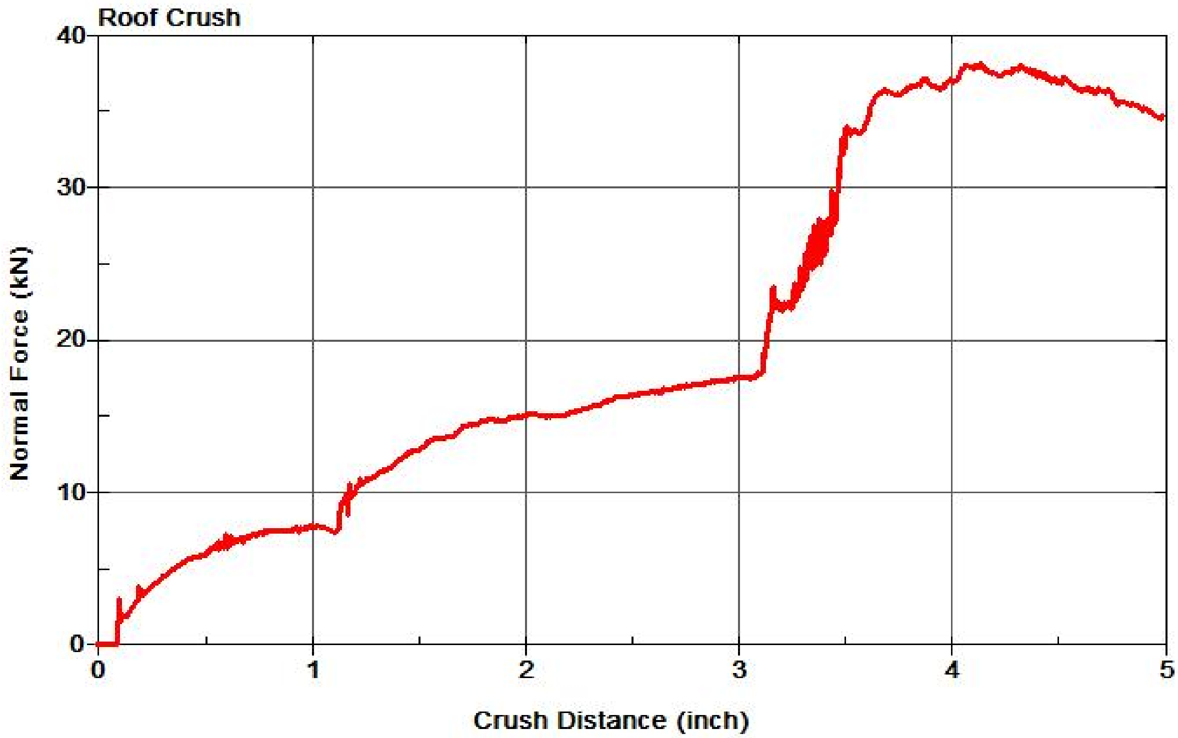

FIGURE 70: Rigidwall Force For Optimal Design From Part 2 Optimization

11.14. TASK 3.0 CONCLUSIONS

- The mass of the designed parts was reduced by 22% when compared to those of the baseline design
- Due to the drastic changes in the Roof Rail shape, certain approximations to the shape will be made such that it mates well with the roof and the rest of the structure
- The B-Pillar and the B-Pillar crossbar for the optimized design use the highest grade material allowed (Boron 1550)
- A final design will be created based on the shape, material and thickness suggested by the optimization. This design will then be used for a final design optimization study, where only the thickness and material of the major passenger compartment parts will be designed

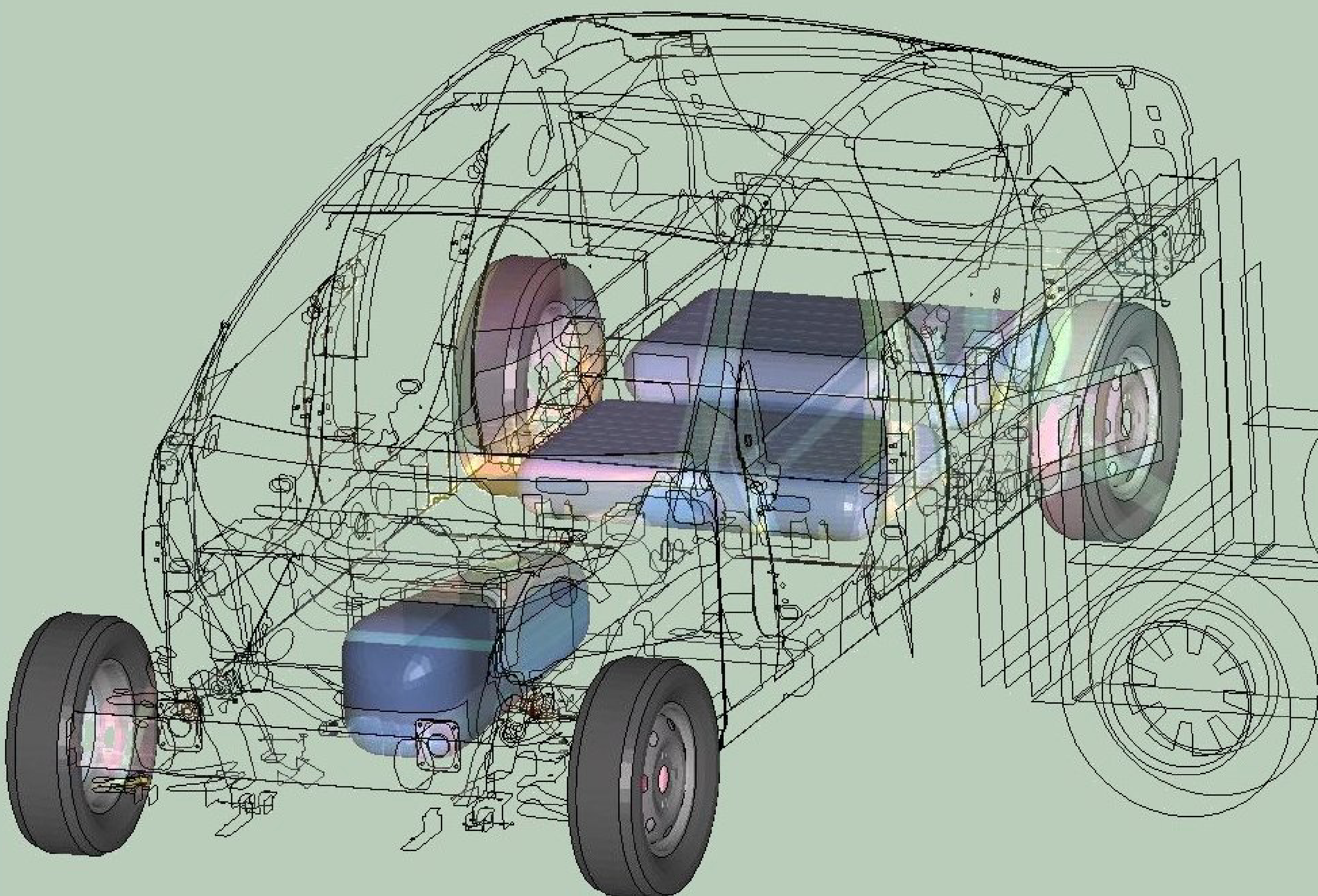

A/S P Auto/Steel Partnership

Future Generation Passenger Compartment
Task 4.0 - Concept Design Study

Integration of the initial optimized FGPC design into a viable production design concept

Task 4.0 - Concept Design

Table of Contents

Task 4.0 - Concept Design

1. INTRODUCTION

This report completes Task 4: Concept Design of the FGPC (Future Generation Passenger Compartment) project. Its purpose is to document the choices made to best integrate the Task 3: Optimization results into a production viable design concept. The design changes were executed on the Task 2: Calibration Baseline version of the FGPC, which had previously modified the baseline FGPC to accommodate both diesel and fuel cell powertrains.

2. OBJECTIVE

To integrate the design directions and recommendations from the Task 3: Optimization into the current concept design stage.

Task 4: Concept Design will take the Task 2: Calibration Baseline design and while considering manufacturability, joining strategy, assembly process and cost reduction incorporate as many of the optimization's mass reduction suggestions as possible.

3. DESIGN CONCEPTS

Four design concepts were considered. Each concept addressed the impact of the Task 3: Optimization, while considering issues such as the use of roll formed versus stamping, ease of assembly, reduction in laser welding, the use of spot-welding and structural adhesives and improvements in structural integrity. Consideration was also given to the simplification of many components and the elimination of non-essential parts.

3.1. VEHICLE CONCEPT A

Concept A used the existing stamping processes defined in the original ULSAB-AVC. Guided by the Task 3: Optimization, the major design change proposed by this concept was an increase in rocker height of 32mm at the front door and 22mm at the rear. This created a constant height rocker, 22mm above the original. To investigate the impact of this on occupant accessibility an additional benchmarking study of current "in-class" production vehicles was performed. The results of the study are discussed later in this section. The lower portion of the Outer Rocker defines part of the exterior styling of the vehicle and so was left unchanged. To create a larger cross-section, the B-Pillar Inner was revised from the occupant sight line down to the bottom of the B-Pillar. The Kick-down was moved rearward 38.75mm and increased in height by 28mm, creating a larger box-section. The front of the Rear Floor was raised to match the Kick-down, tapering downwards to meet the existing seat depression defined in the Task 2: Calibration Baseline redesign.

In Task 2: Calibration Baseline, a Roof Cross-member was added to improve FGPC's side impact performance. Task 3: Optimization identified this feature as an important structural component and determined its most effective location and cross-sectional geometry. However, the resulting proposal interfered with the rear passenger's headroom. Guided by the optimization, it was therefore necessary to modify the size and depth of the cross-section in order to minimize this intrusion.

The original ULSAB-AVC used a Cross-member Support Rear that was part of the seat attachment. Task 3: Optimization repositioned this component to a higher position on both B-Pillars. A bracket was also added to the top of the transmission tunnel providing additional support for the cross-member.

3.2. VEHICLE CONCEPT B

Concept B revised the detailed design of the Rocker, addressing concerns regarding the occupant's accessibility. For each door opening the front portion of the rocker was maintained at the original height, providing a lower step height for the passengers. From the front of each seat backward, the rocker height was tapered upwards toward the B-Pillar for the front seat and the wheel arch for the rear. This compromise maximized both passenger accessibility and the structural benefit of a taller rocker section.

3.3. VEHICLE CONCEPT C

Concept C followed the majority of the concepts presented in Concept A; increased section size of the B-Pillar, revised Kick-down and Cross-member Support Rear positions and the addition of a Cross-member Roof. The Rocker Inner was changed from a stamped to a roll formed component, while maintaining the existing seal flange height. Mating components were updated to reflect this change. The assembly process and joining strategy were also reviewed.

During the review of Concept C the results of the rocker height benchmarking study were presented to the design team; see Table 1. The study considered the upper rocker flange height for variety of current "in-class" production vehicles. It showed that the increase in rocker height proposed by Task 3: Optimization was within the boundaries of current practice. Concept C was revised to reflect the increased rocker height, creating Concept D.

3.4. VEHICLE CONCEPT D

Concept D is derived from Concept C integrating all of its prior design modifications. The major change, based upon the benchmarking study, was the increase in rocker height proposed by the Task 3: Optimization. The section height was increased by 22mm relative to the lower flange across its entire length. The upper rocker flange is now 396mm from ground level compared to the original 374mm. Mating components affected by the new rocker height were revised to accommodate this change.

Concept D was selected as the Task 4: Concept Design.

ROCKER HEIGHT BENCHMARKING COMPAIRISON

This Benchmark was conducted on 2006 "in-class" production vehicles.

ROCKER HEIGHT BENCHMARKING STUDY							
VEHICLE	UPPER FLANGE HEIGHT FROM GROUND (mm)		LOWER FLANGE HEIGHT (mm)	ROCKER SECTION HEIGHT (mm)		UPPER FLANGE VARIATION FROM ULSAB-AVC (mm)	
	FRONT	REAR		FRONT	REAR	FRONT	REAR
ULSAB-AVC	374	374	182	192	192	-	-
Honda Civic	350	370	200	150	170	-24	-4
Volvo S40	365	365	170	195	195	-9	-9
Chevy Cobalt	368	368	200	168	168	-6	-6
Toyota Corolla LE	375	375	235	140	140	1	1
Ford Focus	380	-	190	190	-	6	-
Pontiac G6	405	405	220	185	185	31	31
Dodge Caliber SE	420	435	225	195	210	46	61
Nissan Sentra	Not available						
VW Jetta	Not available						

TABLE 1: Rocker Height Benchmarking

4. DETAILED REVIEW OF CONCEPT D COMPONENTS

4.1. ROCKER INNER (31162/3)

The Rocker Inner design used by the ULSAB-AVC was a stamped TWB (Tailor Welded Blank). The revised design now uses a constant gauge roll formed section, which incorporates both the front and rear door seal flanges. The depth of the rocker has been increased by 22mm relative to the lower flange across its entire length. The upper rocker flange is now 396mm from ground level compared to 374mm for the original ULSAB-AVC design. The front portion of the Rocker Inner is now part of the A-Post Inner and the center section is now part of the B-Pillar Inner. The Body Side Inner Rear has been updated to accommodate these changes.

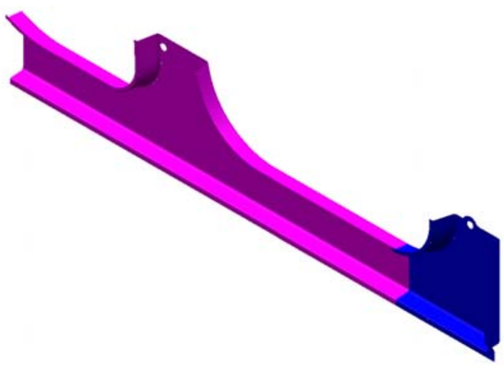

FIGURE 1: Rocker inner (31162/3) (Stamped TWB) (31162/3) ULSAB-AVC

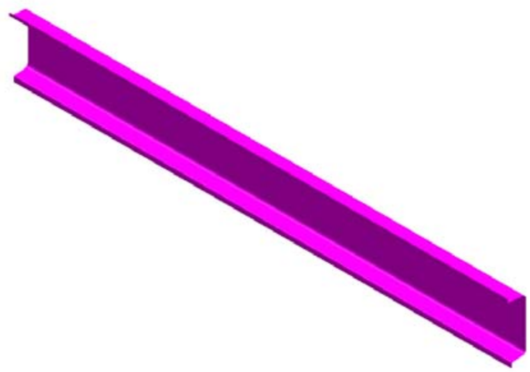

FIGURE 2: Concept D Rocker Inner (Roll formed)

4.2. A-POST INNER (11146/7)

Changes to the A-Post Inner are a direct result of the revisions to the Rocker Inner. The forward portion of the Rocker Inner is now part of the A-Post Inner. The A-Post Inner is now a TWB built up from two pieces, the upper section having the thickest gauge. The transition between the two gauges is located along a line that matches the joint between the original ULSAB-AVC Rocker Inner and the original A-Post Inner. The new A-Post Inner is welded to the inboard side of the new roll formed Rocker Inner.

FIGURE 3: A Post Inner (11146/7)
ULSAB-AVC

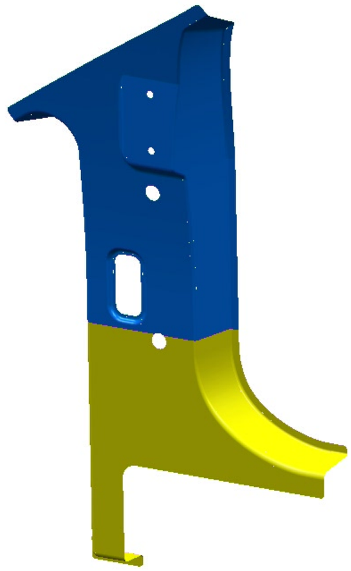

FIGURE 4: Concept D
A Post Inner (TWB) (11146/7)

4.3. B-PILLAR INNER (31208/9)

4.4. B-PILLAR BULKHEAD (41008/9) (NEW PART)

To create a larger cross-section, the B-Pillar Inner was revised from the occupant sight line down to the bottom of the B-Pillar. The original ULSAB-AVC B-Pillar design joined the Rocker Inner just above the horizontal seal flange. The revised design uses a longer B-Pillar which connects directly to the roll formed Rocker Inner. The B-Pillar Inner is no longer a single piece but is instead a TWB. It uses two gauges; the upper section is the thickest. Task 3: Optimization determined the location of the split line for the TWB. The upper joint wraps around the Roof Rail. The lower joint wraps around the inboard side of the roll formed Rocker Inner.

An internal B-Pillar bulkhead was added to provide additional reinforcement for the side impact loadcase. It is positioned horizontally at the same height as the Cross-Member Support Rear (11184/5).

FIGURE 5: B-Pillar Inner (31069/7)
ULSAB-AVC

FIGURE 6: Concept D
B-Pillar Inner (TWB) (31069/7)

FIGURE 7: Concept D
B-Pillar Bulkhead (41008/9) (new part)

4.5. REAR FLOOR (31069)

The Task 2: Calibration Baseline previously raised the rear seat depression, lifting the rear passenger's H-point by 38.5mm. This change was made to accommodate the diesel and fuel cell powertrain options. Task 3: Optimization also increased the Kick-down height by 28mm to improve side impact performance. The Rear Floor was modified to match these revisions. From the front of the Rear Floor, which matched the new Kick-down height, it was angled downward toward the revised seat depression position. The Rear Floor's TWB was also simplified from a 3-piece to a 2-piece blank following the suggestions of the Task 3: Optimization.

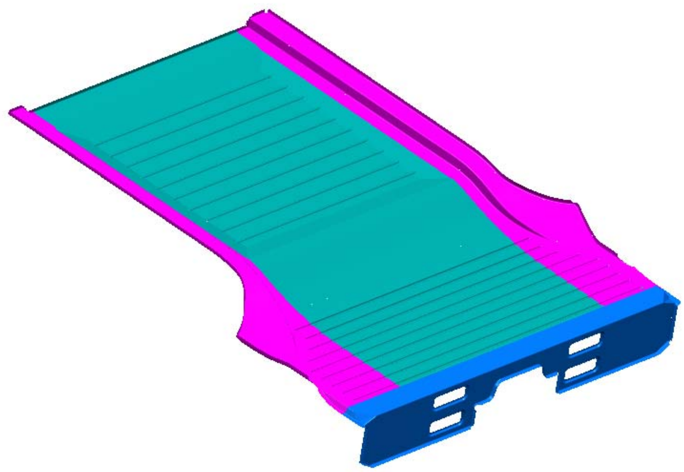

FIGURE 8: Task 2 Redesign Rear Floor (TWB) (31069)

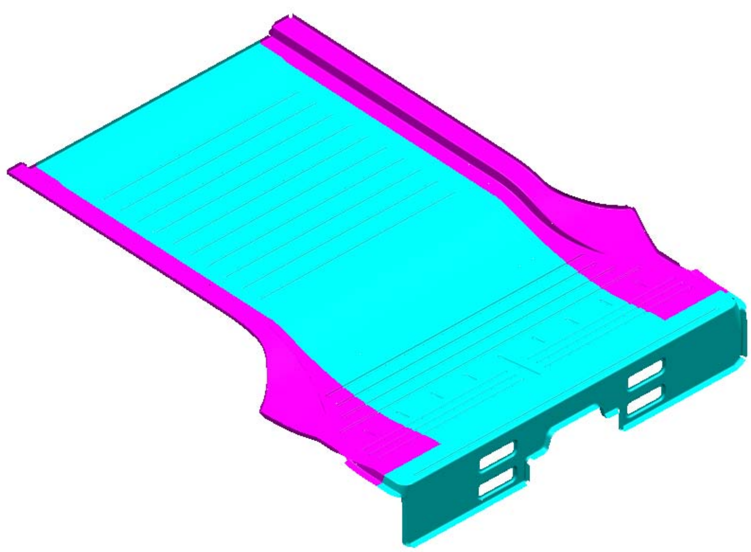

FIGURE 9: Concept D Rear Floor (TWB) (31069)

4.6. CROSS-MEMBER KICK-DOWN (11082)

As suggested by Task 3: Optimization, the Kick-down Cross-member was moved rearward 38.75mm and its height increased by 28mm. The original ULSAB-AVC Kick-down used a large flange to join it to the Front Floor. The design team raised concerns about forming such a large flange. The Concept D design used a smaller flange and extended the Front Floor to accommodate both the shorter flange and the new rearward position of the Kick-down.

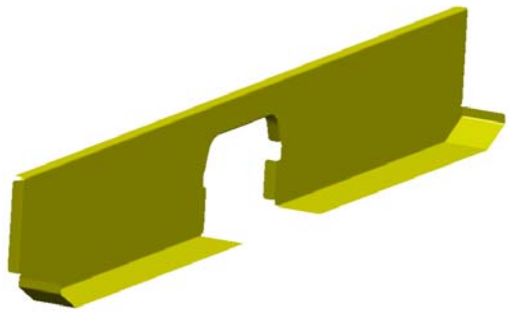

FIGURE 10: Task 2 Redesign Cross-member Kick-down (11082)

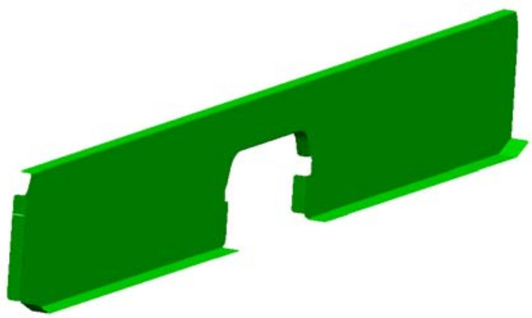

FIGURE 11: Concept D Cross-member Kick-down (11082)

4.7. CROSS-MEMBER ROOF (41004)

4.8. CROSS-MEMBER ROOF BRACKET (41006/7)

The original ULSAB-AVC did not have a Roof Cross-member. However, Task 3: Optimization identified this feature as an important structural component and so considerable effort was made to follow these recommendations. The exact location of the Roof Cross-member was shown to play a significant role in the side impact performance. This position then interfered with the rear passenger's headroom and therefore size and depth of the cross-member's section was modified to minimize this intrusion. A new bracket was also developed to join the Roof Cross-member to the Body Side Outer.

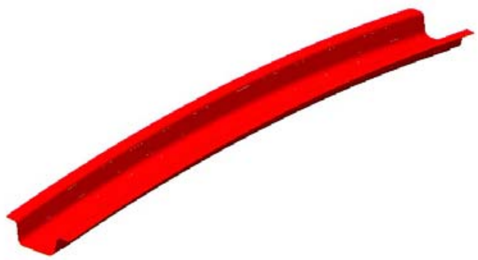

FIGURE 12: Task 2 design
Cross-member Roof (roll formed) (41004)

FIGURE 13: Concept D
Cross-member Roof (roll formed) (41004)

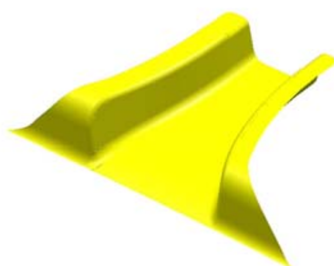

FIGURE 14: Task 2 design
Cross-member Roof Bracket (41006/7)

FIGURE 15: Concept D
Cross-member Roof Bracket (41006/7)

4.9. CROSS-MEMBER SUPPORT REAR (11184)

4.10. CROSS-MEMBER SUPPORT REAR BRACKET OUTER (41002/3) (NEW)

4.11. CROSS-MEMBER SUPPORT REAR BRACKET CENTER (41001) (NEW)

4.12. CROSS-MEMBER SUPPORT REAR BRACKET INNER (41001) (NEW)

The Cross-member Support Rear was called the Cross-member Support Front Seat Rear in the original ULSAB-AVC. The original version of this cross-member was an octagonal tube, placed across the vehicle and joined to both Rocker Inners. For Task 2: Calibration Baseline, it was revised to a square section tube and attached at a higher position on both B-Pillars. The Task 3: Optimization recommended a larger cross-section, increasing it to 80mm square. The Concept D design, using the guidance provided by the optimization, revised the design to 60mm diameter circular cross-section. The design team felt that this size tube would maintain the required side impact performance while providing a more convenient packaging solution. Integrating the cross-member into the front seats was also considered as a possible packaging option for this proposal. The B-Pillar mounting brackets for the cross-member were designed with significant gusseting. This increased the effective height of the cross-member while minimizing its impact on packaging.

FIGURE 16: ULSAB – AVC
Cross-member Support Front Seat Rear (11184)

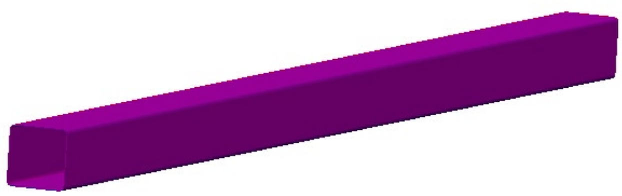

FIGURE 17: Task 2 design
Cross-member Support Front Seat Rear (11184)
Square

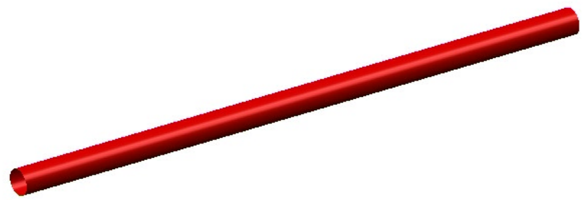

FIGURE 18: Concept D
Cross-member Support Rear: (11184)
Round

FIGURE 19: Concept D (new part)
Cross-member Support Rear Bracket Inner
Common Part (41012)

FIGURE 20: Concept D (new part)
Cross-member Support Rear Bracket Outer:
Common Part (41002)

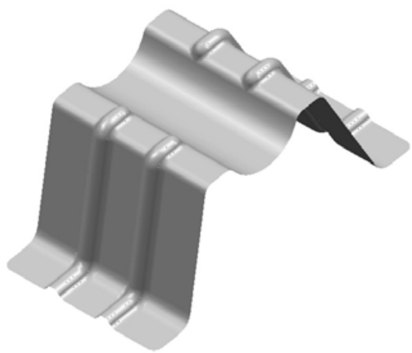

FIGURE 21: Concept D (new part)
Cross-member Support Rear Center Bracket: (41001)

4.13. B-PILLAR REINFORCEMENT (11202/3)

Task 3: Optimization identified the B-Pillar Reinforcement as an important structural component. Though the B-Pillar Outer Reinforcement (32230/1) was eliminated, the B-Pillar Inner Reinforcement was given a deeper section and extended length. The revised design also allowed the B-Pillar Inner Reinforcement to be a roll formed part.

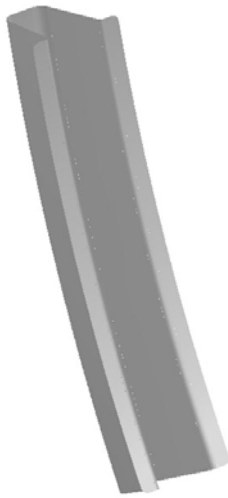

FIGURE 22: ULSAB-AVC
Reinforcement Waist B-Pillar Inner (11202/3)

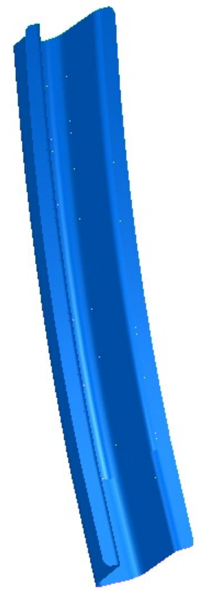

FIGURE 23: Concept D
Reinforcement Waist B-Pillar Inner (11202/3)
Roll formed

4.14. BODY SIDE OUTER (31170/1)

The Body Side Outer was revised to reflect changes made to its mating components. Its TWB was also simplified from 5 to 4 individual pieces and from 4 to 3 material gauges. Reviewed by the design team, this was considered the best compromise between cost and ease of assembly.

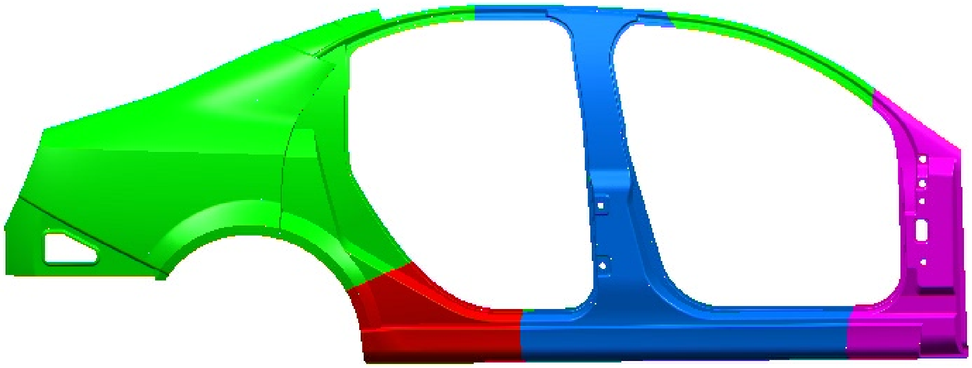

FIGURE 24: (TWB) ULSAB-AVC
Body Side Outer (31170/1)

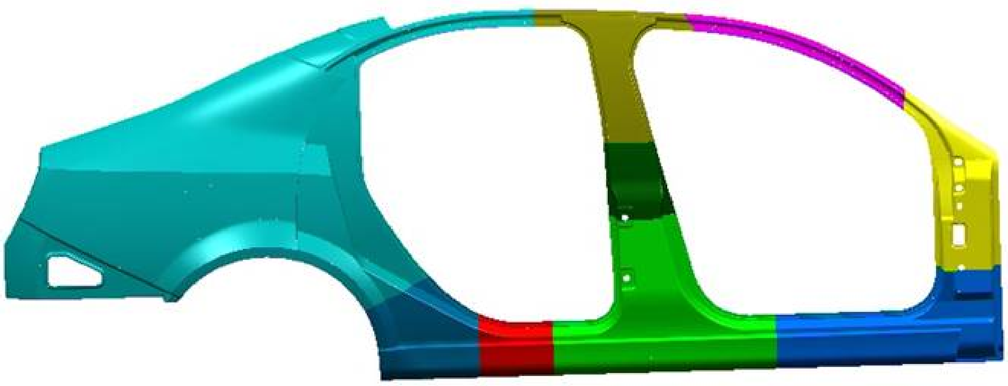

FIGURE 25: Optimization results (TWB)
Body Side Outer (31170/1)

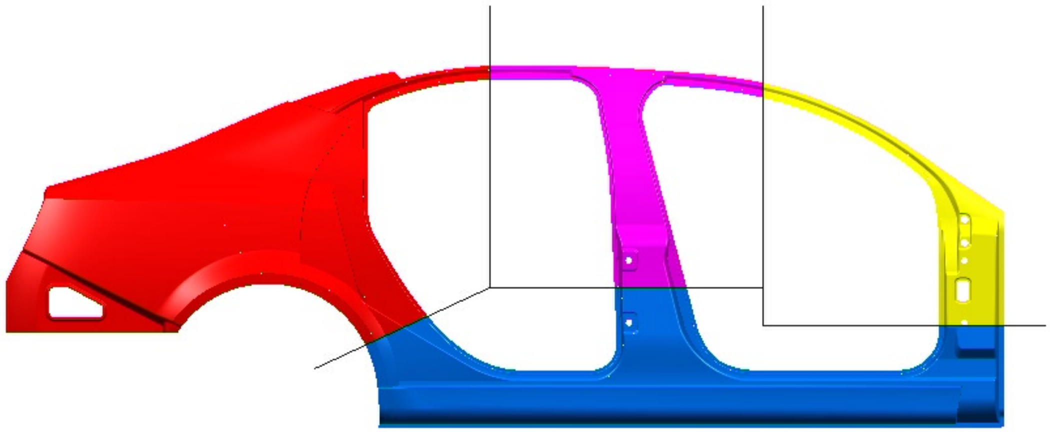

FIGURE 26: Concept D (TWB)
Body Side Outer (31170/1)

4.15. FRONT FLOOR (31016/7)

The Front Floor to Rocker Inner Joint was revised from the vertical flange used on the ULSAB-AVC to a horizontal flange that connects to the bottom of the Rocker Inner. The length of the floor was also increased to accommodate the revised position of the Kick-down.

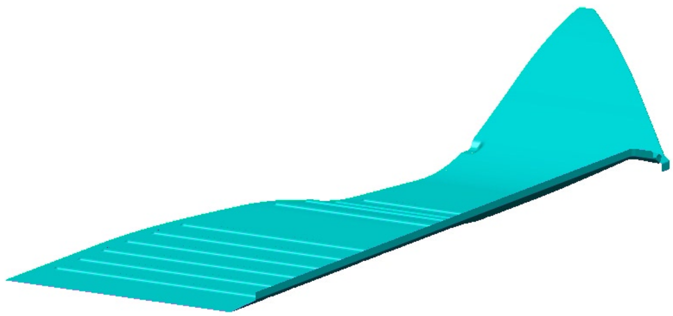

FIGURE 27: ULSAB – AVC
Front Floor (31016/7)

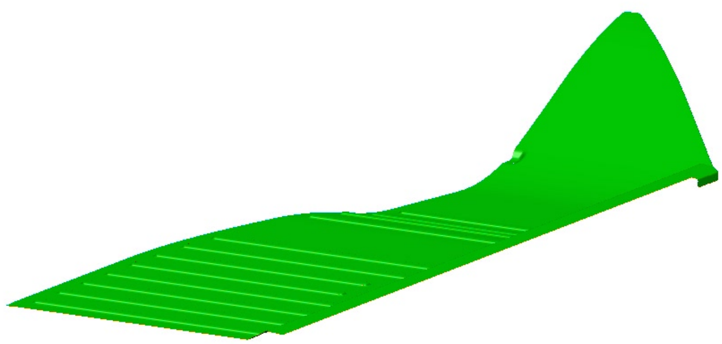

FIGURE 28: Concept D
Front Floor (31016/7)

4.16. COMPONENT REVSIONS

Design changes had previously been made in Task 2: Calibration Baseline to accommodate both the Fuel Cell and Diesel powertrain variants. However, further changes to the following components were necessary to integrate Concept D. The revisions were made to adapt to the redesigned major components and their mating components or to ease the assembly process by avoiding interferences or obstructions.

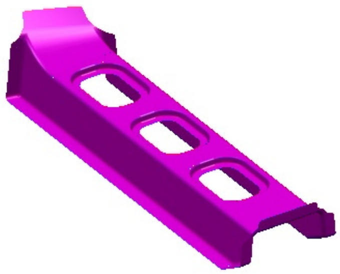

FIGURE 29:
11134/5 Cross-member Support Front Seat Front

FIGURE 30:
11136/7 Closeout Lower Crash Box Dash

FIGURE 31:
11130/1 Member Body Side Inner

FIGURE 32:
11196/7 Close out Outer Crash Box Dash

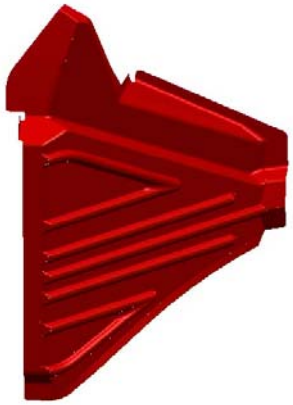

FIGURE 33:
11196/7 Closeout Outer Crash Box Dash

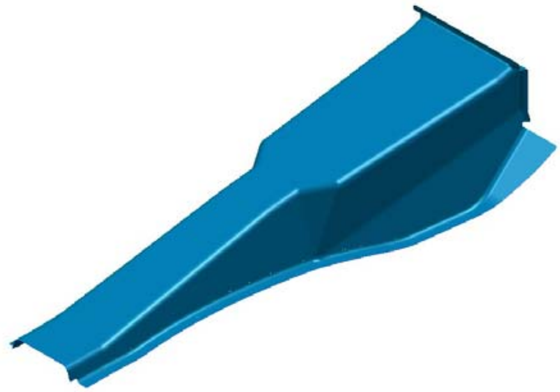

FIGURE 34: Task 2redesign
31049 Tunnel Concept D

FIGURE 35:
31172/3 Body Side Inner

FIGURE 36:
11196/7 Reinforcement Crash Box Dash

4.17. NEW ADDED DESIGNED COMPONENTS

These are new components created for Concept D

FIGURE 37:
41012 Cross-member Support Rear Bracket Inner: Common Part

FIGURE 38:
41009/9 B-Pillar Bulkhead

FIGURE 39:
41004 Cross-member Roof

FIGURE 40:
41006/7 Cross-member Roof Bracket

FIGURE 41:
41002 Cross-member Support Rear Bracket Outer

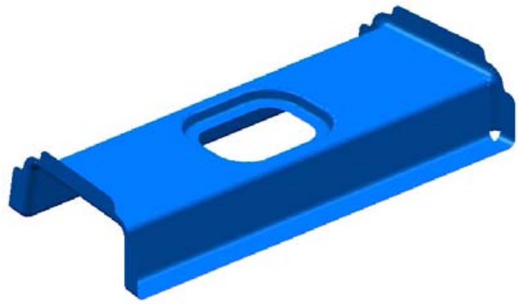

FIGURE 42:
41010 Cross-member Tunnel Lower Task 2 Design

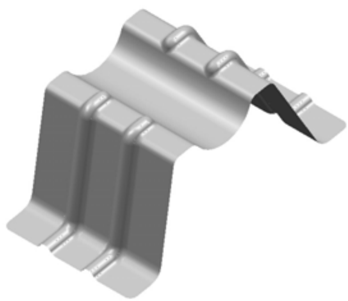

FIGURE 43:
41001 Cross-member Support Rear Center Bracket

4.18. ELIMINATED COMPONENTS

These are components, inherited from ULSAB-AVC, that were eliminated for Concept D

FIGURE 44:
31230/1 Reinforcement Waist B-Pillar Outer

FIGURE 45:
31222/3 Reinforcement B-Pillar Lower

FIGURE 46:
31212 Extension C Member Support Front Seat Rear

FIGURE 47:
11083 Cross-member Tunnel

FIGURE 48:
11190 Bracket Support Front Seat Rear

4.19. DOOR CLOSURES

4.19.1. HYROFORMED DOOR REINFORCEMENTS

The Door Reinforcements were modified to accept changes in the Rocker, B-Pillar, Body Side Inner Rear and the Body Side Outer. Their basic shape was consistent with the original designs. However, revisions were made to adapt to these localized design changes.

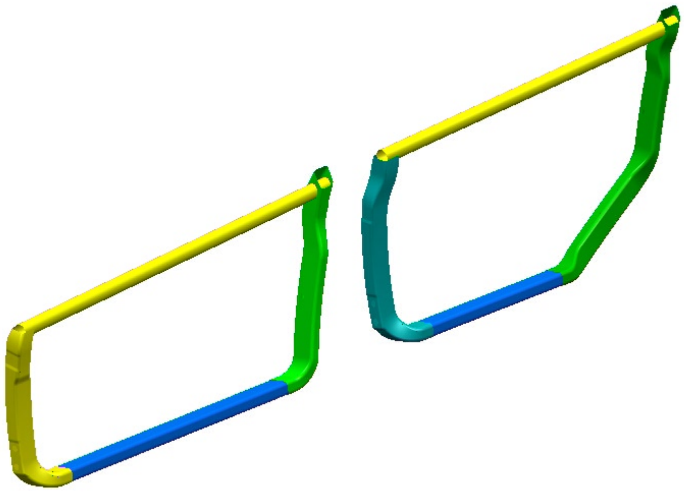

FIGURE 49:
Front and Rear door tubular structure ULSAB – AVC

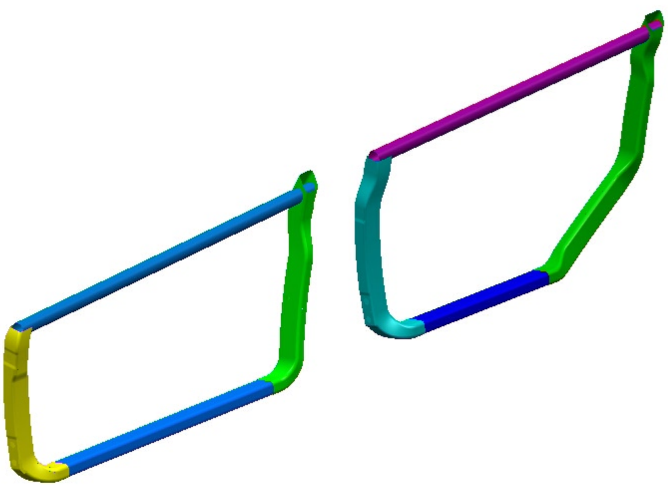

FIGURE 50:
Front and Rear door tubular structure Concept D

4.19.2. INNER AND OUTER DOOR PANELS

The Inner Door Panels were modified to accommodate revisions to the door opening. The bottom of the Outer Door Panel creates a portion of the Door Inner Panel and so was revised to reflect changes in the Rocker. These changes did not affect the exterior of the panel. All the Inner Panels were extended to meet the updated position of the hydroformed Door Reinforcements. The resulting weight gain in the Inner Panels was offset slightly by the decreased length of the Door Reinforcements.

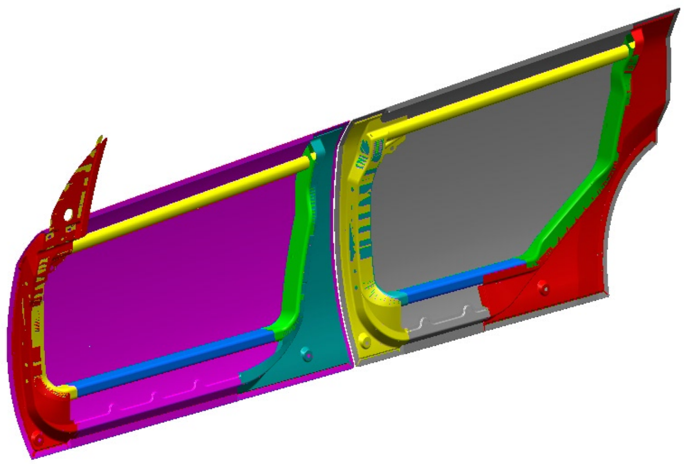

FIGURE 51:
Front and Rear Door Inner Panels ULSAB – AVC

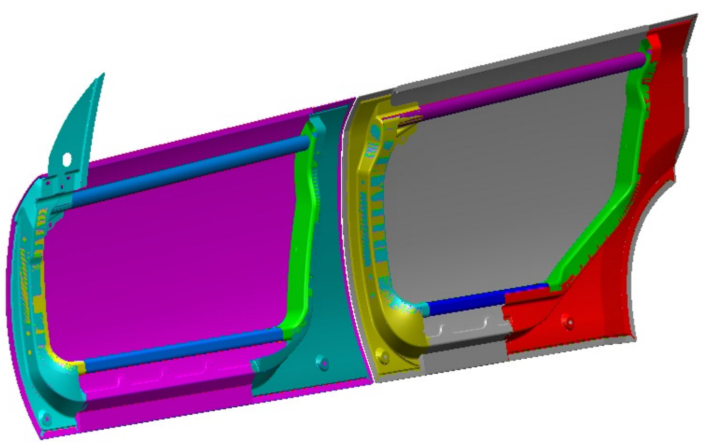

FIGURE 52:
Front and Rear door Inner Panels Concept D

5. WELDING: CONSIDERATIONS FOR LASER WELDING

5.1. PROCESS BASICS

The process uses a 21mm x 1mm weld, which approximates the strength of a conventional resistance spot weld. Similar to traditional resistance welding, the laser stitch weld is positioned in the center of the flange. However, it offers several advantages over continuous laser welding; less heat is added to the flanges, the material is therefore cooler and so there is less risk of wrinkling. Stitch welding also allows better clamping between the "stitches," which compensates for any panel irregularities.

5.2. LASER WELDING COMPONENTS

The laser system has three major components; the laser source, PFO (Primary Focusing Optics) and a robot that positions the PFO. The laser source is connected to the PFO by a fiber optic cable. The PFO itself is mounted on an industrial robot. Both the laser and the robot are controlled by a dedicated software system. Standard focal lengths of the PFO are fixed at 180, 350 and 500mm.

5.3. SAFETY CONSIDERATIONS

Due to safety concerns, the use of laser radiation is highly regulated in the industrial environment. The laser welding process is performed in an enclosed "light tight" enclosure. Operators and maintenance personnel are forbidden from entering the enclosure while the laser is activated because severe burns and blindness can result from even low-level laser radiation. Therefore transporting parts through the enclosure can create a significant challenge in a high volume production environment.

5.4. PROCESS LIMITATIONS

Precise positioning of the PFO is required. The PFO must be held within ±2mm and within 6° of normal to the material. Accessibility of the laser beam and its path must also be considered. It is not recommended that the PFO weld vertically because spatter may fall onto the lens and burn it. Air jets are used to protect the lens but they are not considered 100% effective. Current practice typically limits the PFO to 30° from horizontal. The air jets can also introduce Oxygen into the weld creating sparks and burn through.

It is not recommended that laser and traditional resistance welding be combined in the laser enclosure. Sparks and weld spatter from resistance welding could damage the PFO and so it should be performed outside the enclosure.

Due to the high clamping forces required, laser welding galvanized parts can be difficult. Trapped gasses from the coating can also create holes in the weld.

To achieve good weld quality, the gap between the parts should not exceed 0.1mm (0.004"). Laser welding is a non-contact process. If the parts do not fit with 0.1mm they must be clamped together. There are no electrode shanks to clamp the parts. If the gap is too large it may result in "burn through" creating a hole in the outer part. No additional material is added to fill any gaps.

An important consideration is the focal length of the lens. It is desirable to select a focal length suitable for all the welds in a single process. Each change in focal length requires an additional PFO. Although a single laser source can run many PFO units, multiple PFOs in the same process is both problematic and expensive.

5.5. PART DESIGN CONSIDERATIONS

Flanges must be large enough to accommodate the 21mm x 1mm stitch weld. Welding tight radius corners is discouraged. A minimum flange width of 15mm is recommended. This provides adequate clamping and material to melt between the parts. Welds should not be closer than 8mm to any edge. The beam path must also be considered. It should have a clear path, unobstructed by any additional features of the part.

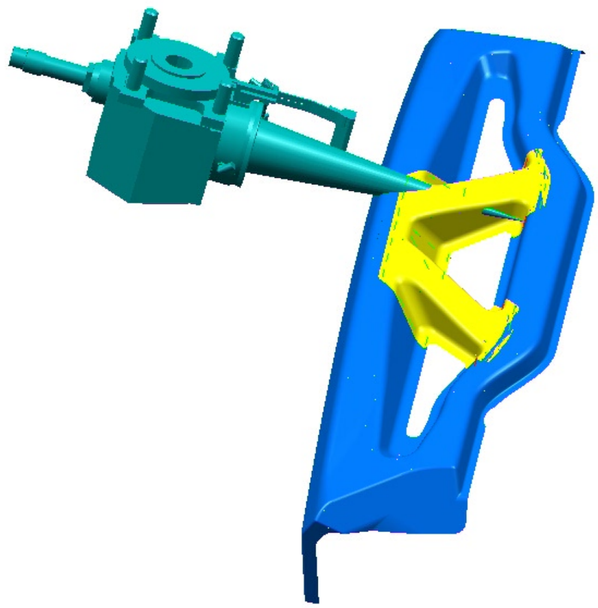

FIGURE 53: Obstructed Beam Path

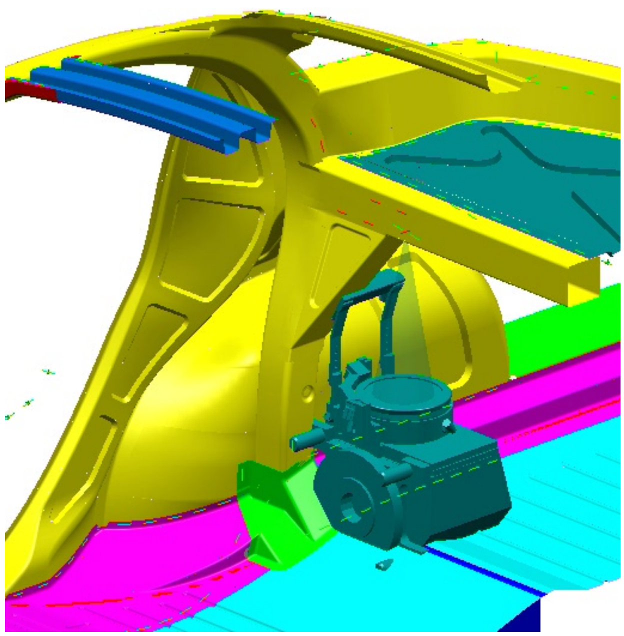

FIGURE 54: Beam Pointing Up
Bad Condition

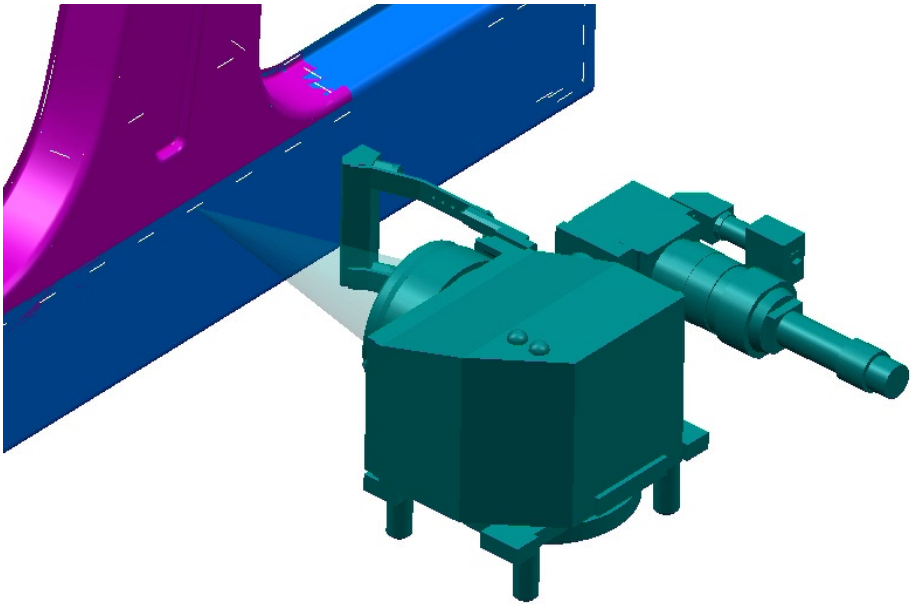

FIGURE 55: Stitch Weld Operation

6. ASSEMBLIES

6.1. JOINING PROCESS

The joining process used by Concept D was derived from the original ULSAB-AVC vehicle. Changes resulted from revisions made to the Rocker Inner. The original assembly placed the Rocker Inner as part of the Underbody Assembly (AVC 36128). Instead for Concept D, the Rocker Inner became part of the Body Side Inner Assembly (37126). This change improved the stability of the Body Side Inner when loading it on to the Underbody Assembly (37125). It also improved access to the Underbody Assembly and assisted the welding operation. The assembly process is called out as Assembly Body Structure Stage 1 (37120A). The Wheelhouse Outer was removed from the Body Side Inner Assembly. This change provided the welding laser's PFO better access to the Rear Underbody Assembly and Wheelhouse Inner, which would have been obstructed by the Wheelhouse Outer. Instead, the Wheelhouse Outer is joined in a second operation at the same station called Assembly Body Structure Stage 2 (37120B).

The joining process used a combination of laser stitch welding, spot welding and structural adhesives. As discussed previously, due to safety concerns, the entire laser welding process for each sub-assembly must be preformed in a totally enclosed environment. All required laser-welding operations for each sub-assembly must be completed before transition to the next station. Spot welding cannot be performed in the laser enclosure and so must be completed separately. All adhesives, whether used in combination with spot or laser welding, must be applied prior to welding. Certain adhesives can be applied to the surface that will be spot-welded. However, it is not possible to apply adhesive to any surface that will be laser welded. Instead the adhesive must be applied between the laser-welded stitches.

An additional sub-assembly (37138) was created to accommodate additional new components.

6.2. FRONT END ASSEMBLY

6.2.1. FGPC 17137 ASSEMBLY COWL FRONT

<u>**Total Welds**</u>
31 Laser (651mm**)**

<u>**Joining Process**</u>
Laser weld 1 > 2

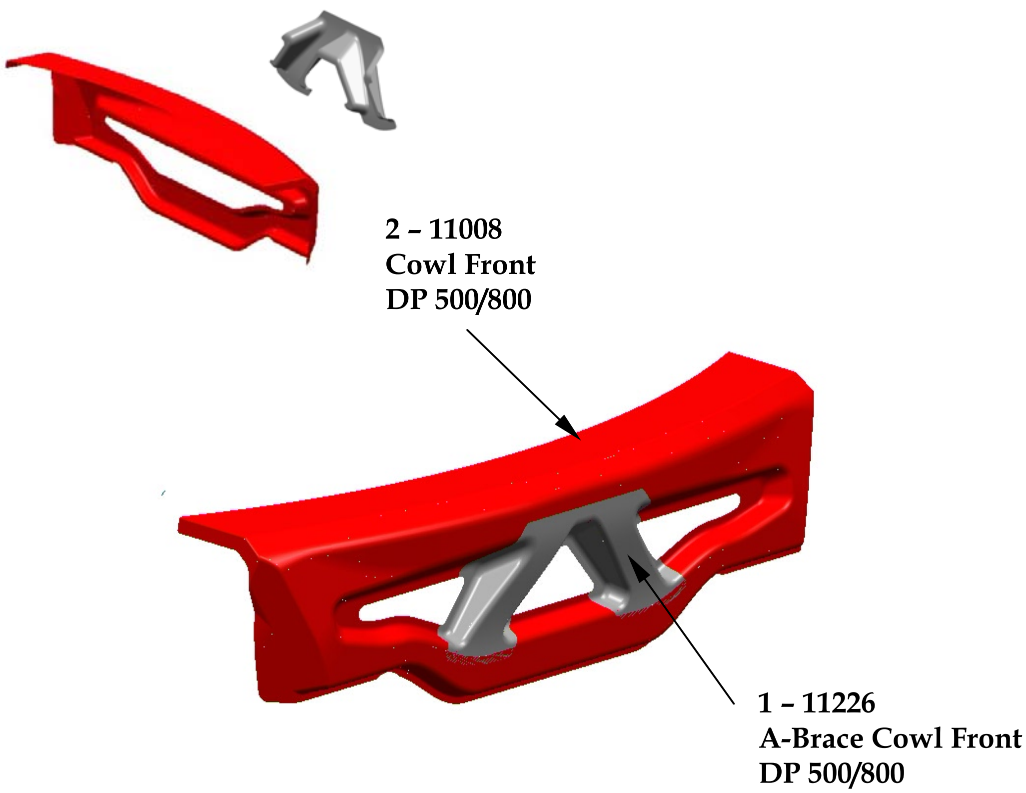

FIGURE 56: 17137 Assembly Cowl front

6.2.2. FGPC 17136 ASSEMBLY DASH

Total Welds
25 Laser (525mm)

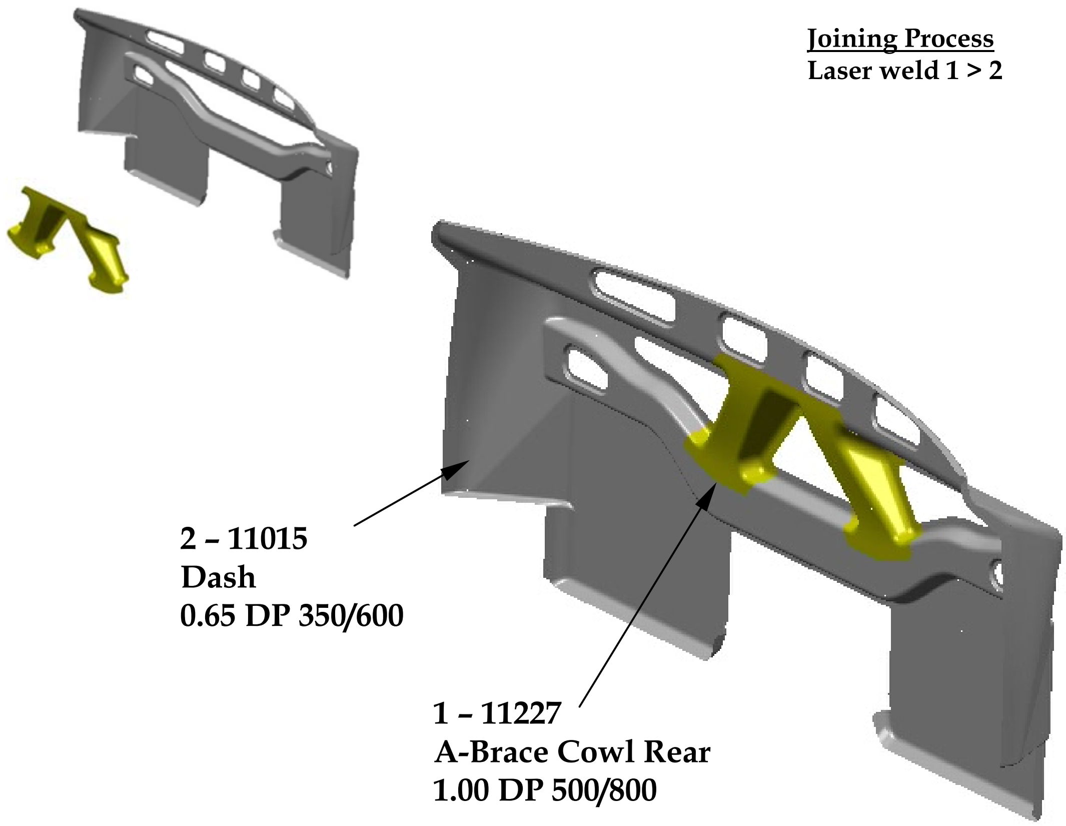

FIGURE 57: 17136 Assembly Dash

6.2.3. 37130 ASSEMBLY RAIL FRONT

<u>Total Welds</u>
128 Laser (2688mm)

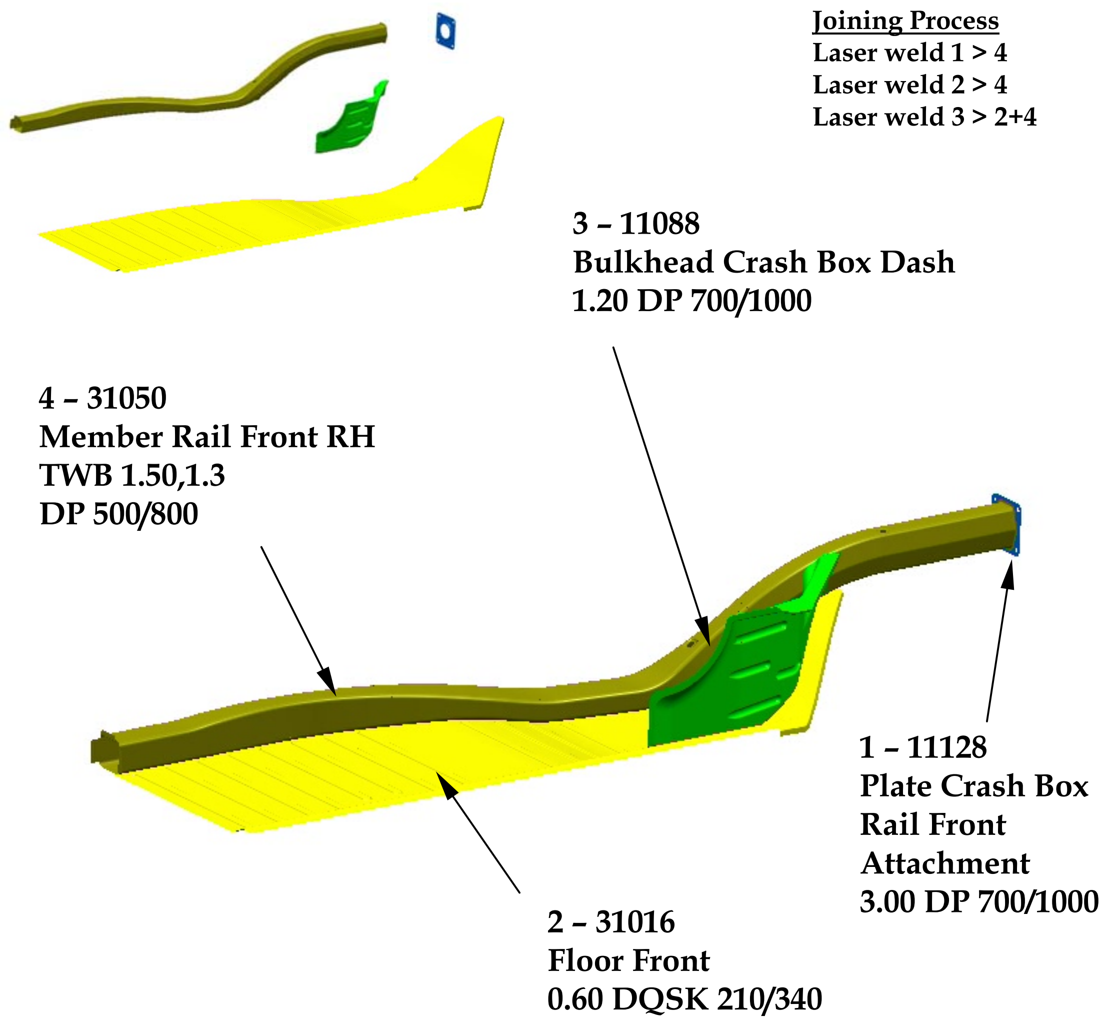

FIGURE 58: 37130 Assembly Rail Front RH
Right Hand (RH) Assembly shown

6.2.4. FGPC 37129 ASSEMBLY TUNNEL

<u>Total Welds</u>
22 Spot
Adhesive (3070mm)

<u>Joining Process</u>
Adhesive 1 > 2
Spot weld 1 > 2

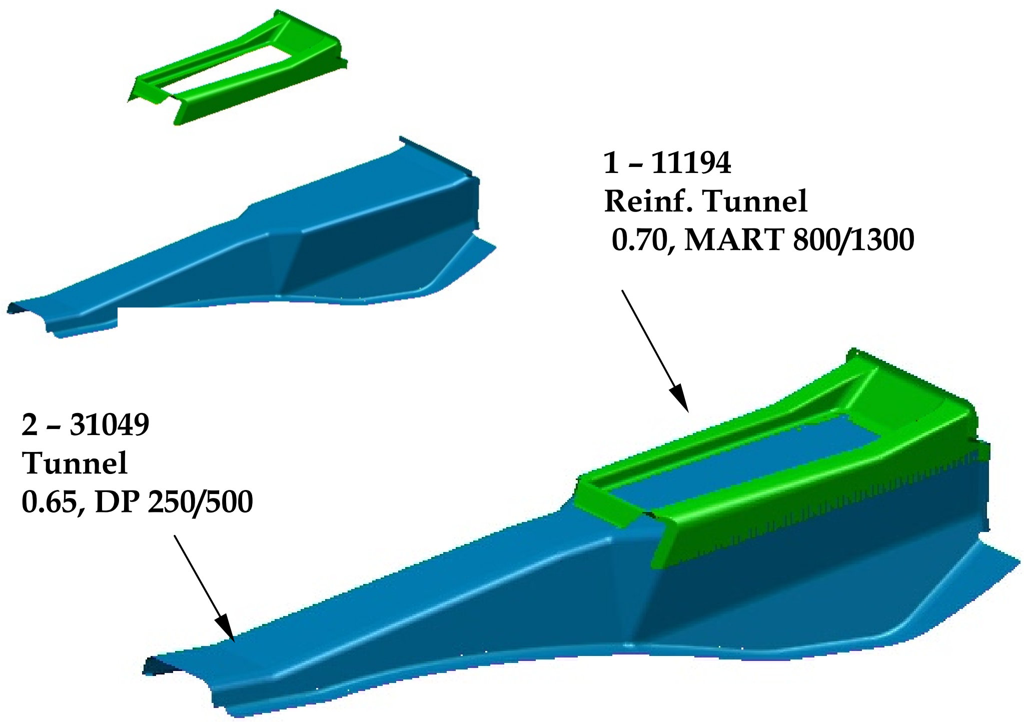

FIGURE 59: 37129 Assembly Tunnel

6.3. TUNNEL AND UNDER BODY ASSEMBLY

6.3.1. FGPC 37132 ASSEMBLY RAIL REAR

Total Welds
54 Spot

Joining Process
Spot weld 1 > 4
Spot weld 2 > 1+4
Spot weld 3 > 4

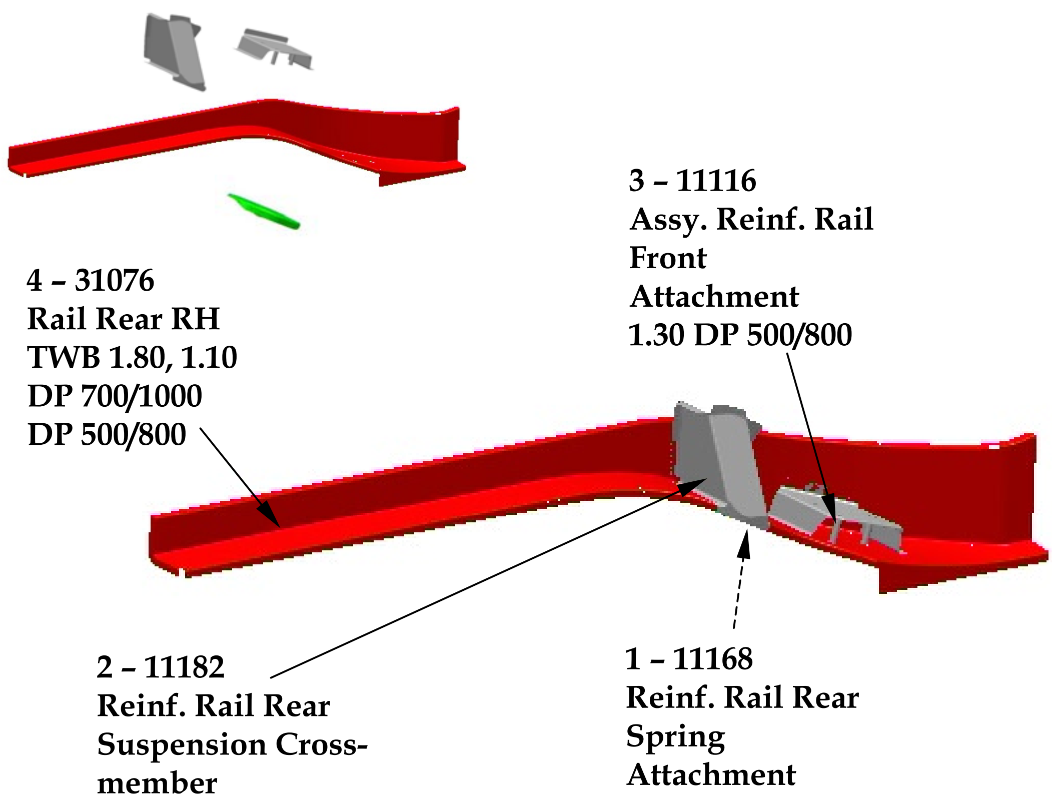

FIGURE 60: 37132 Assembly Rail Rear RH
Right Hand (RH) Assembly shown

6.3.2. FGPC 37128 ASSEMBLY UNDER BODY LADDER

<u>Total Welds</u>

76 Laser (1596mm)
76 Spot
6 Adhesive Patches (1670mm)

<u>Joining Process</u>
Adhesive 1 > 5+6+9
Laser weld10 > 5+6
Laser weld 9 > 5+6
Laser Weld 1 > 5+6+9
Adhesive 2 > 5+6+9
Spot weld 1 > 5+6
Spot weld 2 > 5+6
Spot weld 7 > 3+4
Spot weld 8 > 3+4

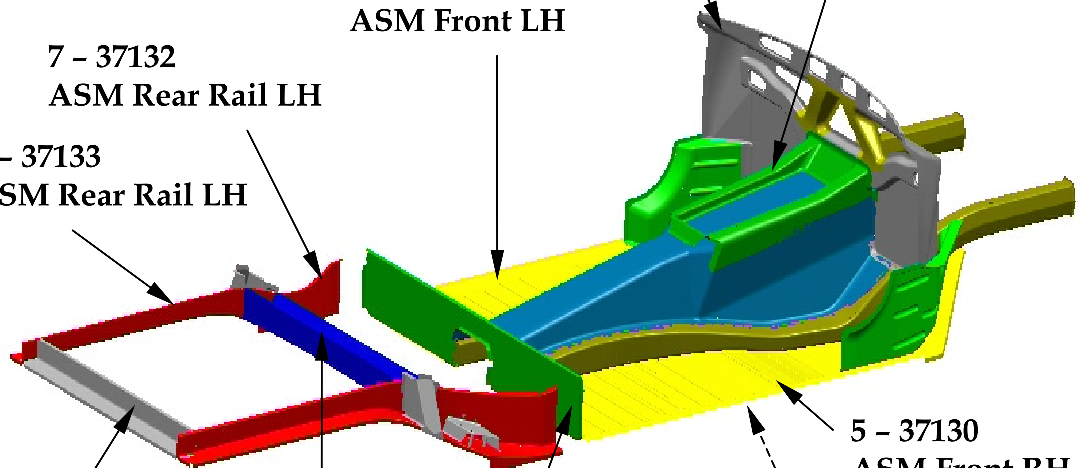

FIGURE 61: 37128 Assembly Underbody Ladder

6.3.3. FGPC 37125 ASM UNDERBODY STAGE 2

Total Welds

136 Laser (2856mm)
195 Spot
9 Adhesive Patches (8180mm)

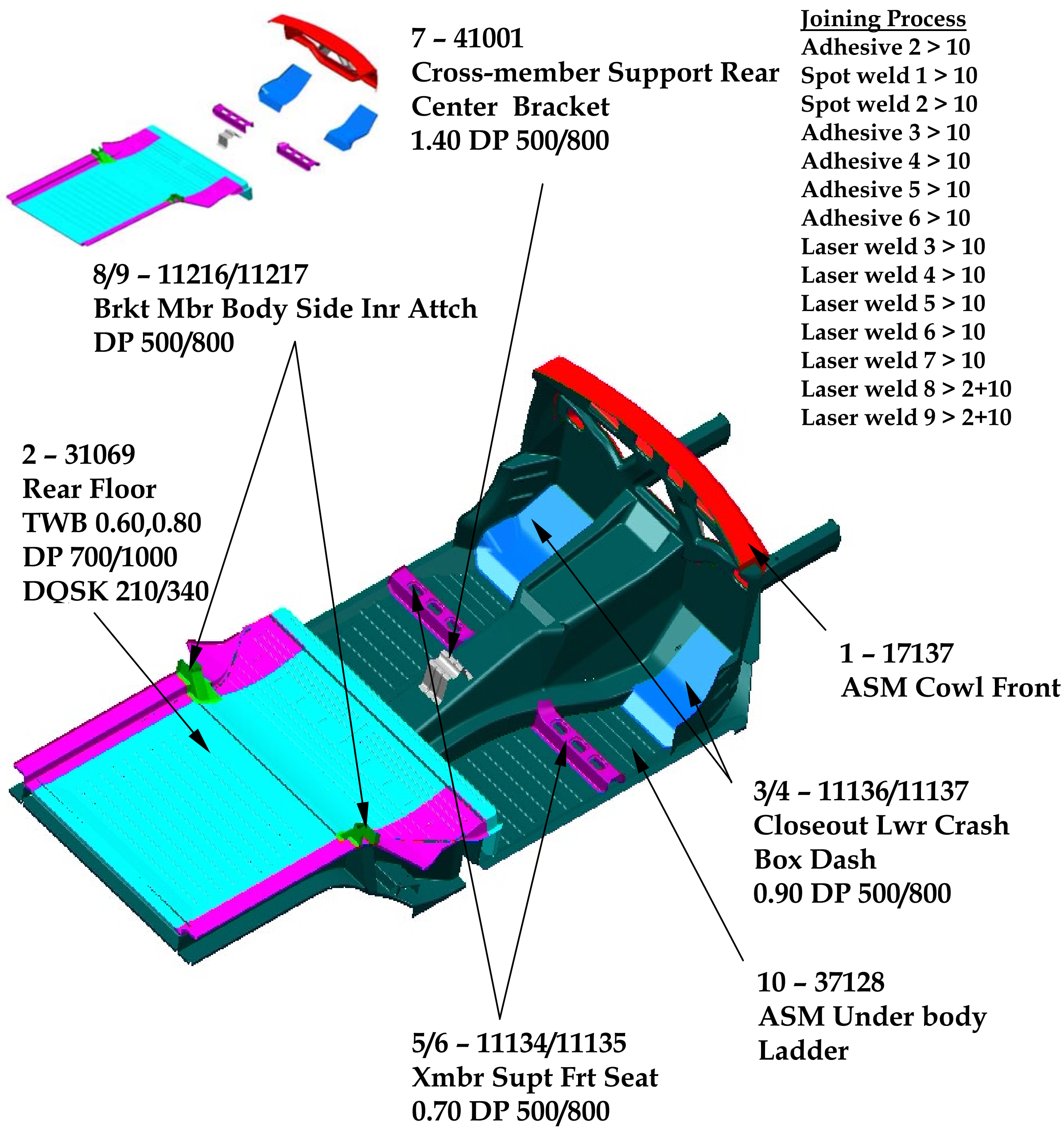

FIGURE 62: 37125 ASM Underbody Stage 2

6.3.4. FGPC 37124 ASM UNDERBODY STAGE 3

Total Welds
184 Laser (3864mm)

Joining Process
Laser weld 1 > 7
Laser weld 2 > 7
Laser weld 3 > 1+7
Laser weld 4 > 2+7
Laser weld 5 > 7
Laser weld 6 > 7

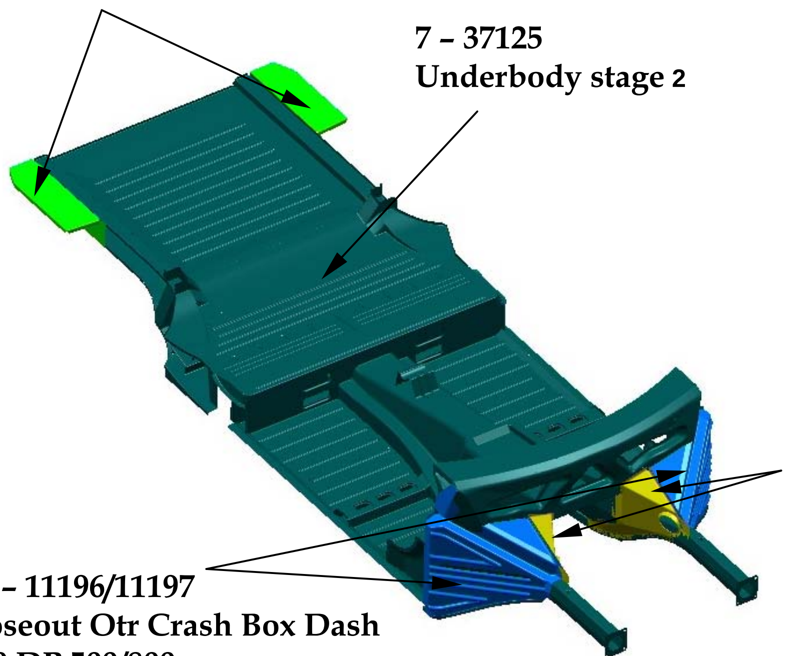

FIGURE 63: 37124 ASM Underbody Stage 3

6.4. FGPC 37126 ASSEMBLY BODY SIDE INNER

<u>Total Welds</u>
354 Laser (7434mm)

<u>Joining Process</u>

Laser weld 1 > 4	Laser weld 8 > 5	Laser weld 14 > 5	Laser weld 2 > 4
Laser weld 12 > 11	Laser weld 10 > 5	Laser weld 3 > 4	Laser weld 5 > 4
Laser weld 14 > 5	Laser weld 6 >4	Laser weld 7 > 4	Laser weld 13 > 4
Laser weld 9 >7+5+11			

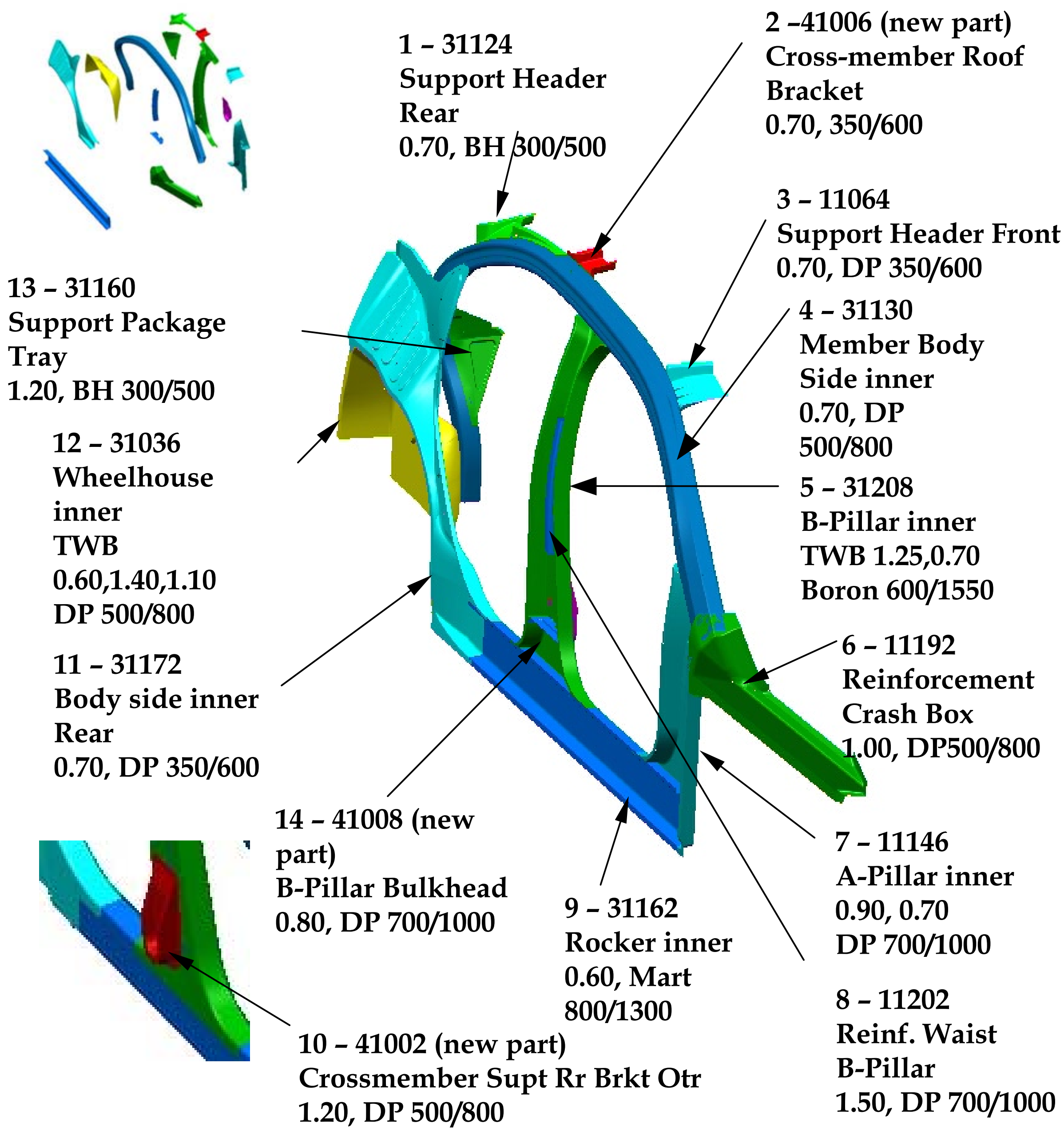

FIGURE 64: 37126 Assembly Body Side Inner (Right Hand (RH) Assembly shown)

6.5. FGPC 37138 ASSEMBLY CROSS-MEMBER SUPPORT REAR

<u>Total Welds</u>
6 MIG (150mm)

<u>Joining Process</u>
MIG weld 1 > 2

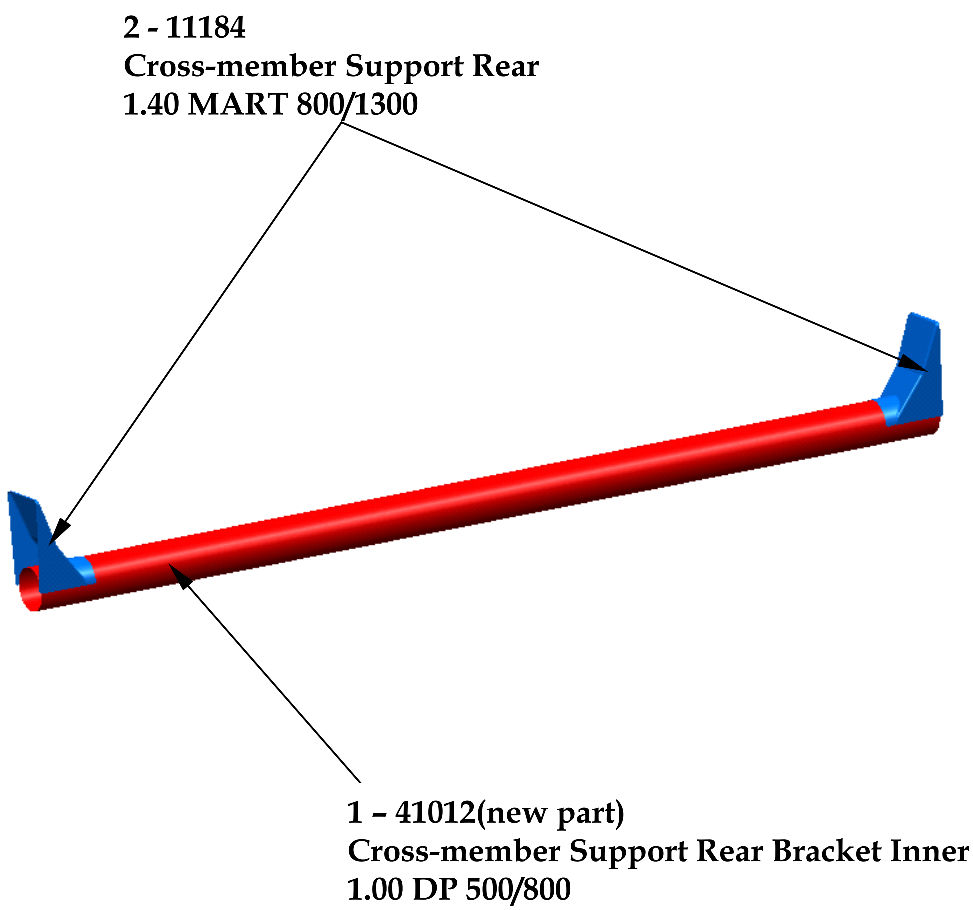

FIGURE 65: 37138 Assembly Cross-member Support Rear

6.6. FGPC 37120A ASM BODY STRUCTURE

6.6.1. FGPC 37120A ASM BODY STRUCTURE STAGE 1

Total Welds

360 Laser	(7932mm)	62 Spot	
2 Adhesive Patches	(506mm)	18 MIG	(330mm)

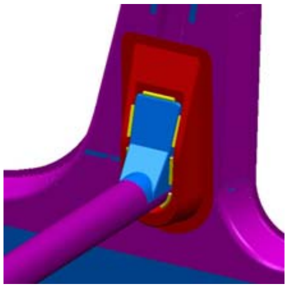

View A
MIG welded

Joining Process

Adhesive 1 > 10
Adhesive 2 > 10
Laser weld 1 > 10
Laser weld 2 > 10
Laser weld 7 > 1+2
Laser weld 8 > 9 +1 +2
Laser weld 9 > 7+1+2+7
Laser weld 3 > 1+2
Laser weld 4 > 1+2
Laser weld 5 > 1+2
Spot weld 1 > 10
Spot weld 2 > 10
MIG weld 6 >1+2

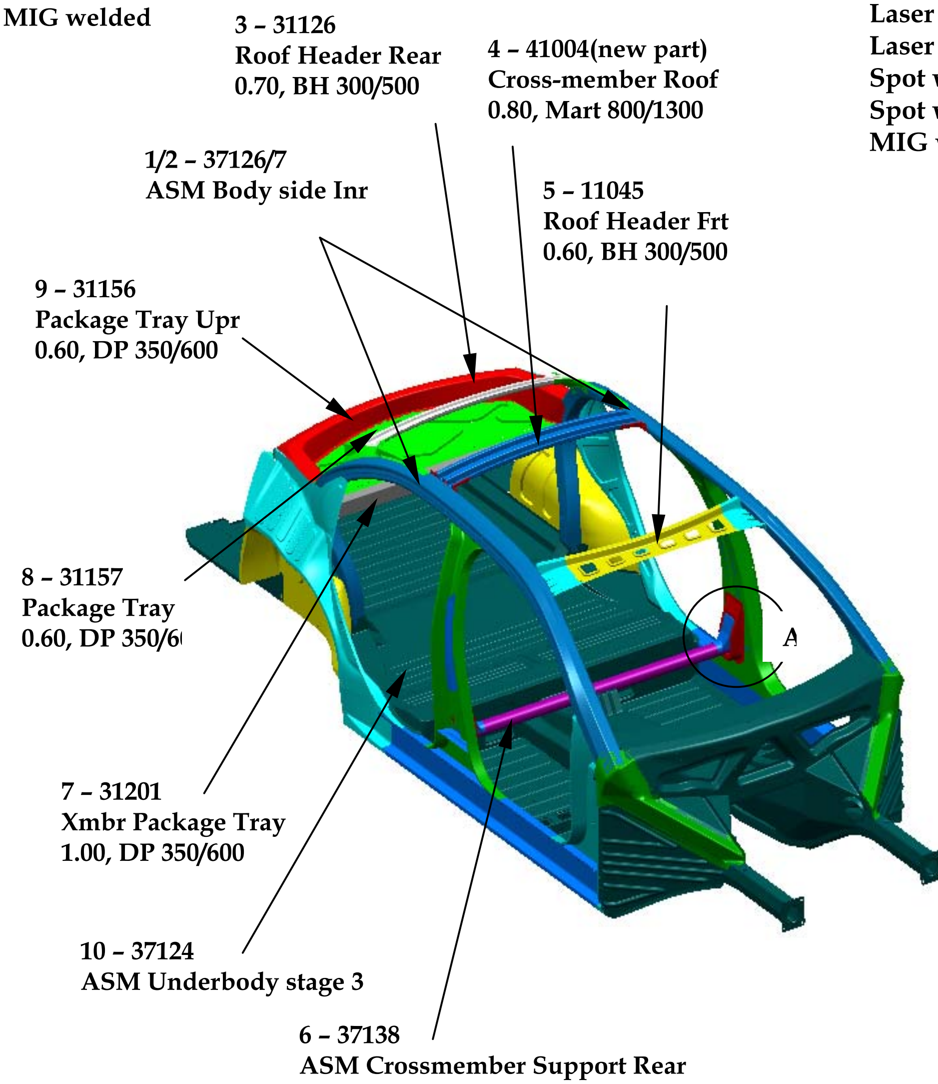

FIGURE 66: 37120A ASM Body structure stage 1

6.6.2. FGPC 37120A ASM BODY STRUCTURE STAGE 2

Total Welds
32 Laser welds (672mm)

Joining Process
Laser weld 1 > 2

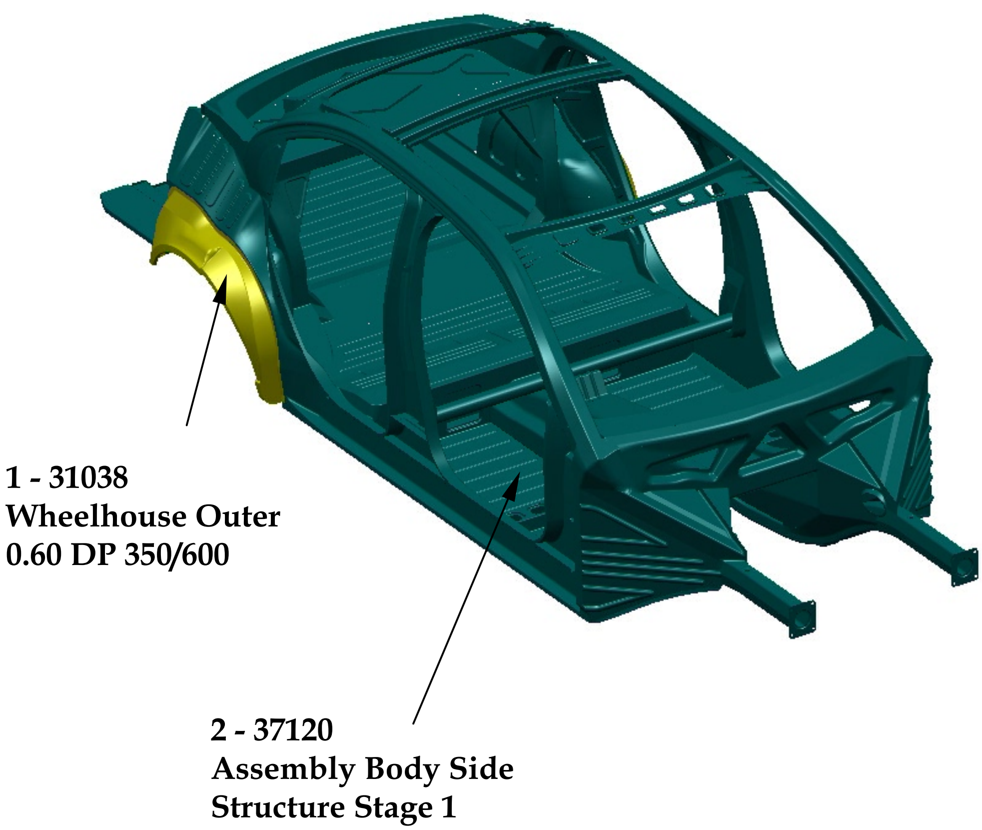

FIGURE 67: 37120B ASM Body structure stage 2

6.7. 37122 ASSEMBLY BODY SIDE OUTER

<u>Total Welds</u>
24 Spot

<u>Joining Process</u>
Spot weld 1 > 2

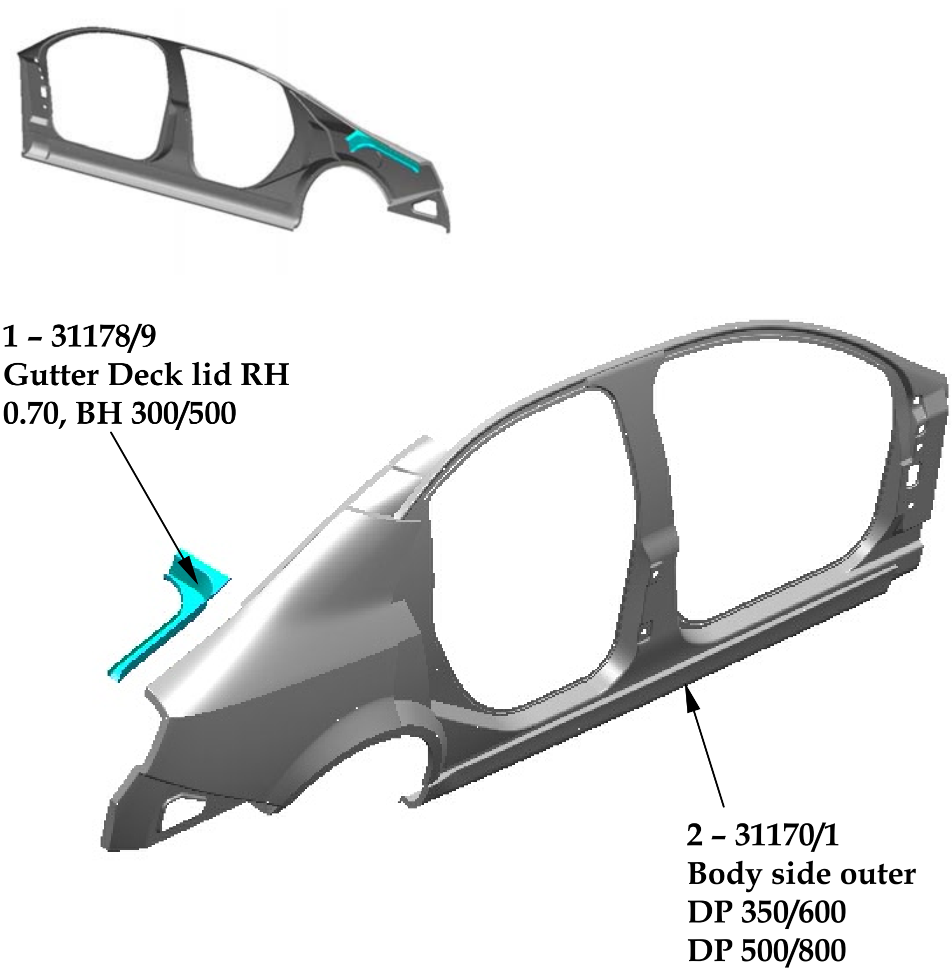

FIGURE 68: 37122 Assembly Body Side Outer
Right Hand (RH) Assembly shown

6.8. FGPC 37121 ASSEMBLY BACK PANEL

Total Welds
68 Spot

Joining Process
Spot Weld 1 > 2

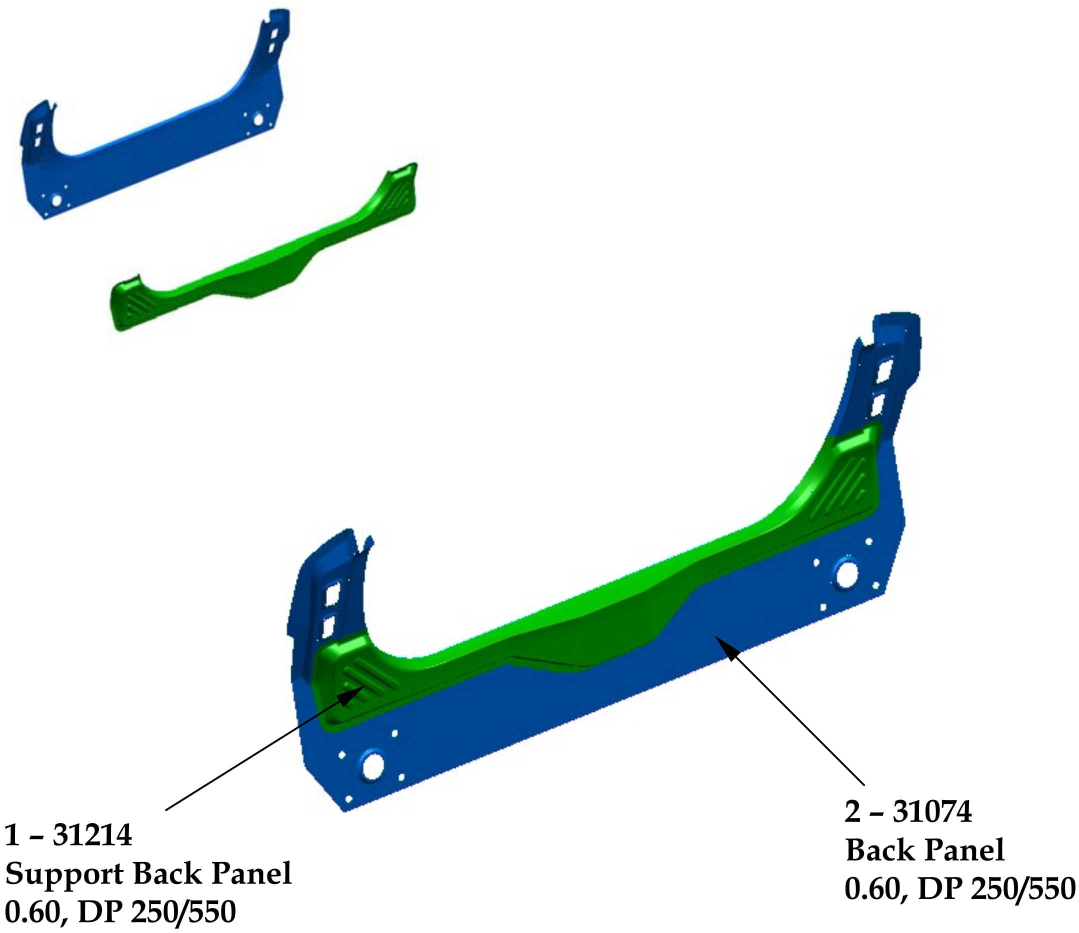

FIGURE 69: 37121 Assembly Back Panel

6.9. FGPC 37119 BODY STRUCTURE COMPLETE

Total Welds

222 Laser (4662mm)
306 spot
2 Adhesive Patches (1800mm)

Joining Process
Laser weld 4 > 3
Laser weld 5 > 3
Laser weld 1 > 4+5
Laser weld 2 >3+4+5
Spot weld 4 > 3
Spot weld 5 > 3
Spot weld 1 > 3

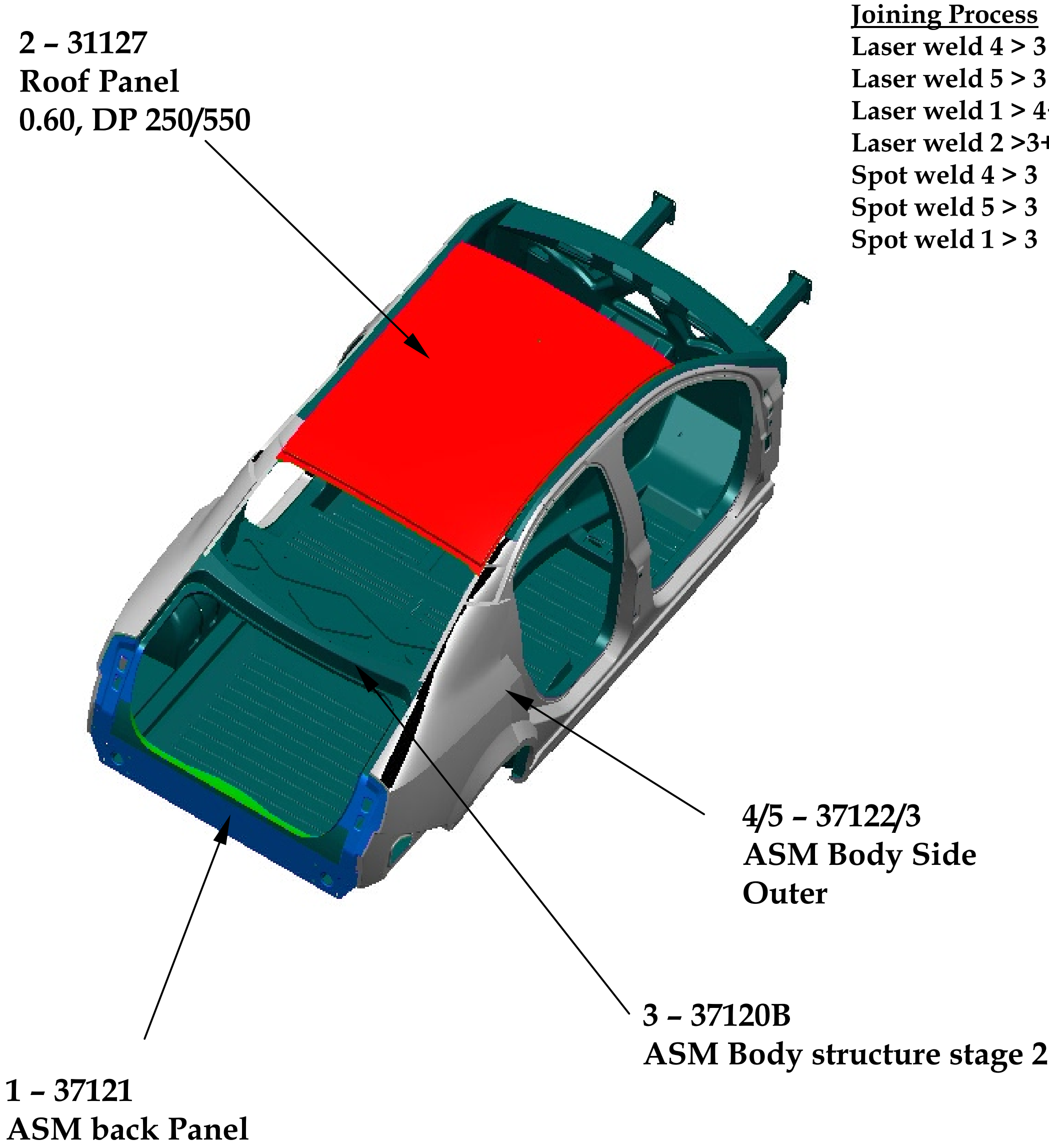

FIGURE 70: 37119 Body Structure Complete

6.10. WELDS AND ADHESIVES

ASSEMBLY	JOINT METHOD	TOTAL LENGTH
17136	25 Laser welds	525mm
17137	31 Laser welds	651mm
37119	222 Laser welds	4662mm
	306 Spot welds	-
	2 Adhesive patches	1800mm
37120A	360 Laser welds	7560mm
	62 Spot welds	-
	2 Adhesive patches	506mm
	18 MIG welds	330 mm
73120B	32 Laser welds	672mm
37121	68 Spot welds	-
37122	24 Spot welds	-
37124	184 Laser welds	3864mm
37125	136 Laser welds	2856mm
	195 Spot weld	-
	9 Adhesive patches	8180mm
37126	354 Laser welds	7434mm
37128	76 Laser welds	1596mm
	76 Spot welds	-
	6 Adhesive patches	1670mm
37129	22 Spot welds	-
	3 Adhesive patches	3070mm
37130	128 Laser welds	2688mm
37132	54 Spot welds	-

JOINT TYPE	ULSAB-AVC		FGPC	
	Total	Length (mm)	Total	Length (mm)
Laser welds		99735	1516	31836
Spot welds	814	-	807	-
Adhesive patches		1606	22	15220
MIG welds	-	-	18	330

TABLE 2: Joint Summary

WELD SUMMARY

The above summarizes the use of adhesives, laser and spot welding for both the ULSAB-AVC and FGPC vehicles. The most significant difference is the reduction in the total length of laser welding. This is primarily due to the use of stitch rather than continuous welding. Stitch welding decreases the amount of heat input into the material, thus reducing the risk of wrinkling. Stitch welding also addresses concerns regarding material clamping. Although many parts feature beads and dimples to improve their panel stiffness, maintaining the correct gap during the welding process is a major concern. Stitch welding allows for additional clamping and fixtures to be placed between the welds.

7. GAUGE AND MASS PARTS LIST

Gauge and mass listed by Part Number for both the ULSAB-AVC baseline and the FGPC Concept D. New or deleted parts are as indicated. Note, the design of some parts was revised, affecting the part's mass without any changes to its gauge.

PART NUMBER	NAME	ULSAB-AVC		Optimized Concept D	
		Gauge (mm)	Mass (kg)	Gauge (mm)	Mass (kg)
11008	Cowl Front	0.80	4.416		4.416
11015	Dash	0.65	4.381		4.381
11045	Header Front	0.70	0.686	0.60	0.586
11064/5	Support Header Front R&L	0.70	0.462		0.462
11075	Crossmember Back Panel	0.65	0.832		0.832
11082	Crossmember Kick-up	0.70	2.002	1.20	3.220
11083	Crossmember Tunnel	0.70	0.602		Deleted
11088/9	Bulkhead Crash Box Dash R&L	1.20	4.752		4.860
11116	Assembly Reinf Rail Rear Suspension Attach R&L	1.30	0.910		0.910
11128	Plate Crash Box Rail Front Attachment (x2)	3.00	0.600		0.600
11134/5	Crossmember Support Front Seat Front R&L	0.70	1.134		1.142
11136/7	Closeout Lower Crash Box Dash R&L	0.90	2.322		2.322
11138	Closeout Inner Crash Box Dash RH	0.80	1.072		1.622
11139	Closeout Inner Crash Box Dash LH	0.80	1.040		1.622
11146/7	A-Post Inner R&L	0.90	2.304		2.060
	Taylor blank for Concept C and D			0.90	
				0.70	1.110
11153	Crossmember Rear Suspension	1.00	2.640		2.640
11168	Reinforcement Rail Rear Spring Attachment R&L	1.20	0.288		0.288
11182/3	Reinf Rail Rear Suspension Crossmember R&L	1.50	1.530		1.530
11184	Crossmember Suppport Rear	1.20	2.568	1.40	2.795
11190	Bracket Support Front Seat Rear (x2)	1.20	0.576		Deleted
11192/3	Reinf Crash Box Dash R&L	1.00	2.340		2.360
11194	Reinforcement Tunnel	0.70	2.394		2.394
11196/7	Closeout Outer Crash Box Dash R&L	0.80	4.688		4.678
11202/3	Reinforcement Waist B-Pillar R&L	1.50	1.770		1.420
11216	Bracket Member Body Side Inner Attach Rear R&L	1.20	0.792		0.792
11224/5	Bracket C-Member Instrument Panel Attachment R&L	1.20	0.264		0.264
11226	A-Brace Cowl Front	1.00	0.980		0.980
11227	A-Brace Cowl Rear	1.00	0.820		0.820
31016/7	Floor Front R&L	0.65	8.918	0.60	9.020
31036/7	Wheelhouse Inner R&L	0.60	2.712		2.712
		1.40	1.932		1.932
		1.10	1.320		1.320
31038	Wheelhouse Outer RH	0.60	1.134		1.134
31039	Wheelhouse Outer LH	0.60	1.146		1.146
31049	Tunnel	0.65	5.252		6.640
31050/1	Member Rail Front R&L	1.50	3.690		3.690
		1.30	13.208		13.480
31069	Floor Rear	0.60	7.932	0.60	3.460
		1.10	3.135	0.80(Mid)(Frt)	13.260
		1.10	2.882		
		0.70	2.002		
31074	Back Panel	0.60	2.172		2.172
31076/7	Rail Rear R&L	1.80	6.336		6.336
		1.10	2.816		2.816
31124/5	Support Header Rear R&L	0.70	0.672		0.672
31126	Header Rear	0.70	0.938		0.938
31127	Roof	0.65	8.905	0.60	8.70

Future Generation Passenger Compartment (FGPC)

PART NUMBER	NAME	ULSAB-AVC Gauge (mm)	ULSAB-AVC Mass (kg)	Optimized Concept D Gauge (mm)	Optimized Concept D Mass (kg)
31130/1	Member Body Side Inner R&L	1.00	14.140	0.70 (Frt)	
				0.80(Mid)	
				0.70 (Rr)	
				0.7 (All)	9.200
31156	Package Tray Upper	0.60	2.316		2.316
31157	Package Tray Lower	0.60	2.208		2.208
31160/1	Support Package Tray Lower R&L	1.20	1.704		1.704
31162/3	Rocker Inner R&L	1.50	3.630	0.70(Frt)	
		0.70	5.054	0.60(Mid)	
				0.70 (Rr)	
				0.60	4.880
31170	Body Side Outer RH	1.50	3.645	0.90(31670)	
		0.70	0.280	1.00(b)	
		1.80	9.108	1.00(c)	
		1.20	2.148	1.10(d)	
		0.70	5.649	1.10(31170)	
				1.00(31470)	
				0.90(g)	
				0.70(h)	
				0.70(j)	
				1.0 Ctr Upr	1.710
				1.25 Ctr Lwr	8.757
				0.7 Rear	5.601
				1.0 Frt	1.371
31171	Body Side Outer LH	1.50	3.645	0.90(31670)	
		0.70	0.280	1.00(b)	
		1.80	9.108	1.00(c)	
		1.20	2.148	1.10(d)	
		0.70	5.649	1.10(31170)	
				1.00(31470)	
				0.90(g)	
				0.70(h)	
				0.70(j)	
				1.0 Ctr Upr	1.710
				1.25 Ctr Lwr	8.757
				0.7 Rear	5.662
				1.0 Frt	1.371
31172/3	Body Side Inner Rear R&L	0.70	5.110	0.70	5.900
31178/9	Gutter Deck Lid R&L	0.70	0.770		0.770
31188/9	Rail Rear Outer Floor Extension R&L	1.10	1.826		1.826
		0.60	0.756		0.756
31201	Crossmember Package Tray	1.00	2.540		2.540
31208/9	B-Pillar Inner R&L	0.70	2.982	1.25(Upr)	2.780
				0.70(mid)	2.780
31212	Extension C-Member Supt Front Seat Rr (x2)	1.20	0.456		Deleted
31214	Support Back Panel	0.60	1.068		1.068
31222/3	Reinforcement B-Pillar Lower R&L	1.00	2.860		Deleted
31230/1	Reinforcement Waist B-Pillar Outer R&L	0.80	0.240		Deleted
32702/3	Applique-Roof Side Rail R&L	0.50	N/A		N/A
XXXXX	Brackets Reinforcements and Hinges (5.042Kg)				N/A
	IP Beam		3.400		3.400
ADDED PARTS					
41004	Crossmember Roof			0.80	1.400
41006/7	Crossmember Roof Bracket R&L			0.70	0.296
41001	Crossmember Support Rear Center Bracket			1.40	0.522
41002/3	Crossmember Support Rear Bracket Outer			1.20	1.336
41008/9	B-Pillar Bulkhead			0.80	0.240
41010	Crossmember Reinf Tunnel Lower			1.00	0.485
41012	B-Pillar Bulkhead Cover			1.00	0.304

TOTAL MASS BODYSIDES & UNDERBODY (kg)	**225.300**		**211.395**

PART NUMBER	NAME	ULSAB-AVC		Optimized Concept D	
		Gauge (mm)	Mass (kg)	Gauge (mm)	Mass (kg)
Front Door Tubular Structure					
12004/5	Hinge Tube Front Door R&L	1.20	1.296	0.80	0.858
32006/7	Latch Tube Front Door R&L	1.00	1.240	0.80	0.992
32008/9	Lower Tube Front Door R&L	1.50	2.580	1.20	2.002
32010/1	Outer Belt Reinforcement - Front Door R&L	1.00	1.600	1.00	1.572
TOTAL MASS (kg)			**6.716**		**5.424**
Rear Door Tubular Structure					
32040/1	Hinge TubeRear Door R&L	1.20	1.488	0.60	0.750
32042/3	Latch Tube Rear Door R&L	1.00	1.700	0.60	1.026
32044/5	Lower Tube Rear Door R&L	1.50	1.560	0.80	0.822
32046/7	Outer Belt Reinforcement -Rear Door R&L	1.00	1.480	0.60	0.884
TOTAL MASS (kg)			**6.228**		**3.482**
Front Door Panels					
32030/1	Inner Rear -Front Door	0.60	1.596		1.720
32028/9	Outer - Front Door	0.60	7.584		7.712
12020/1	Inner Front - Front Door	1.00	1.000		0.992
		1.20	0.768		0.766
TOTAL MASS (kg)			**10.948**		**11.190**
Rear Door Panels					
32038/9	Inner Rear - Rear Door	0.60	2.124		2.100
32032/3	Outer - Rear Door	0.60	7.440		7.640
32034/5	Inner Front - Rear Door	1.00	0.860		0.900
		1.20	0.816		0.878
TOTAL MASS (kg)			**11.240**		**11.518**

TABLE 3: Gauge & Mass Listing By Part No

8. MATERIAL TYPE PART LIST

Material choices listed by Part Number for both the original ULSAB-AVC, the revised ULSAB-AVC and the FGPC Concept D. New or deleted parts as indicated.

PART NUMBER	NAME	ULSAB-AVC			UPDATED TO			TWB	DESIGN OPTIMIZED		
		Material Type	Grade (MPa) Yield Strength	Grade (MPa) Tensile Strength	Material Type	Grade (MPa) Yield Strength	Grade (MPa) Tensile Strength		Material Type	Grade (MPa) Yield Strength	Grade (MPa) Tensile Strength
11008	Cowl Front	DP	500	800							
11015	Dash	DP	280	600	DP	350	600		DP	350	600
11045	Header Front	IF	300	420	BH	300	500		BH	300	500
11064/5	Support Header Front R&L	DP	280	600	DP	350	600		DP	350	600
11075	Crossmember Back Panel	DP	280	600	DP	350	600		DP	350	600
11082	Crossmember Kick-up	DP	700	1000							
11083	Crossmember Tunnel	HSLA	350	450					Deleted	Deleted	Deleted
11088/9	Bulkhead Crash Box Dash R&L	DP	700	1000							
11116	Assembly Reinf Rail Rear Suspension Attach R&L	DP	500	800							
11128	Plate Crash Box Rail Front Attachment (x2)	DP	700	1000							
11134/5	Crossmember Support Front Seat Front R&L	DP	500	800							
11136/7	Closeout Lower Crash Box Dash R&L	DP	500	800							
11138/9	Closeout Inner Crash Box Dash RH	DP	400	700	DP	500	800		DP	500	800
11138/9	Closeout Inner Crash Box Dash LH	DP	400	700	DP	500	800		DP	500	800
11146/7	A-Post Inner R&L	DP	700	1000							
11153	Crossmember Rear Suspension	DP	700	1000							
11168	Reinforcement Rail Rear Spring Attachment R&L	HSLA	350	450							
11182/3	Reinf Rail Rear Suspension Crossmember R&L	HSLA	350	450							
11184	Crossmember Support Rear	MART	950	1200					MART	800	1300
11190	Bracket Support Front Seat Rear (x2)	DP	500	800					Deleted	Deleted	Deleted
11192/3	Reinf Crash Box Dash R&L	DP	400	700	DP	500	800		DP	500	800
11194	Reinforcement Tunnel	MART	950	1200	MART	800	1300		MART	800	1300
11196/7	Closeout Outer Crash Box Dash R&L	DP	400	700	DP	500	800		DP	500	800
11202/3	Reinforcement Waist B-Pillar R&L	MART	1250	1520	BORON	600	1550		DP	700	1000
11216	Bracket Member Body Side Inner Attach Rear R&L	DP	500	800							
11224/5	Bracket C-Member Instrument Panel Attachment R&L	HSLA	350	450							
11226	A-Brace Cowl Front	DP	500	800							
11227	A-Brace Cowl Rear	DP	500	800							
31016/7	Floor Front R&L	TRIP	450	800	DP	500	800		DQSK	210	340
31036/7	Wheelhouse Inner R&L	DP	500	800							
		DP	700	1000							
		DP	700	1000							
31038	Wheelhouse Outer RH	DP	280	600	DP	350	600		DP	350	600
31039	Wheelhouse Outer LH	DP	280	600	DP	350	600		DP	350	600
31049	Tunnel	DP	300	500	DP	250	550		DP	250	550

PART NUMBER	NAME	ULSAB-AVC			UPDATED TO			DESIGN OPTIMIZED			
		Material Type	Grade (MPa)		Material Type	Grade (MPa)		TWB	Material Type	Grade (MPa)	
			Yield Strength	Tensile Strength		Yield Strength	Tensile Strength			Yield Strength	Tensile Strength
31050/1	Member Rail Front R&L	DP	500	800							
		DP	500	800							
31069	Floor Rear	BH	210	340	DQSK	210	340	Side	DQSK	210	340
		DP	350	600				Frt/Mid	DP	700	1000
		DP	350	600							
		DP	700	1000							
31074	Back Panel	DP	300	500	DP	250	550		DP	250	550
31076/7	Rail Rear R&L	DP	700	1000							
		DP	500	800							
31124/5	Support Header Rear R&L	IF	300	420	BH	300	500		BH	300	500
31126	Header Rear	IF	300	420	BH	300	500		BH	300	500
31127	Roof	DP	300	500	DP	250	550		DP	250	550
31130/1	Member Body Side Inner R&L	DP	500	800							
31156	Package Tray Upper	DP	280	600	DP	350	600		DP	350	600
31157	Package Tray Lower	DP	280	600	DP	350	600		DP	350	600
31160/1	Support Package Tray Lower R&L	DP	300	420					BH	300	500
31162/3	Rocker Inner R&L	DP	700	1000					MART	800	1300
		DP	700	1000							
31170/1	Body Side Outer RH	DP	700	1000				Ctr Upr	DP	500	800
		BH	260	370	BH	300	500	Ctr Lwr	DP	500	800
		DP	700	1000				Rear	DP	350	600
		DP	700	1000				Frt	DP	350	600
		BH	260	370	BH	300	500				
31171	Body Side Outer LH	DP	700	1000				Ctr Upr	DP	500	800
		BH	260	370	BH	300	500	Ctr Lwr	DP	500	800
		DP	700	1000				Rear	DP	350	600
		DP	700	1000				Frt	DP	350	600
		BH	260	370	BH	300	500				
31172/3	Body Side Inner Rear R&L	IF	300	420	BH	300	500		DP	350	600
31178/9	Gutter Deck Lid R&L	BH	260	370	BH	300	500		BH	300	500
31188/9	Rail Rear Outer Floor Extension R&L	DP	500	800							
		BH	210	340	DQSK	210	340		DQSK	210	340
31201	Crossmember Package Tray	DP	280	600	DP	350	600		DP	350	600
31208/9	B-Pillar Inner R&L	MART	950	1200	MART	800	1300		BORON	600	1550
31212	Extension C-Member Supt Front Seat Rr (x2)	MART	950	1200	MART	800	1300		Deleted	Deleted	Deleted
31214	Support Back Panel	DP	300	500	DP	250	550		DP	250	550
31222/3	Reinforcement B-Pillar Lower R&L	DP	700	1000					Deleted	Deleted	Deleted
31230/1	Reinforcement Waist B-Pillar Outer R&L	DP	700	1000					Deleted	Deleted	Deleted
32702	Applique-Roof Side Rail R&L	MILD	140	270	IF	140	270		IF	140	270

ADDED PARTS											
41004	Crossmember Roof	DP	500	800					MART	800	1300
41006/7	Crossmember Roof Bracket R&L								DP	350	600
41001	Crossmember Support Rear Center Bracket								DP	500	800
41002/3	Crossmember Support Rear Bracket Outer R&L								DP	500	800
41008/9	B-Pillar Bulkhead								DP	700	1000
41010	Crossmember Reinf Tunnel Lower								DP	500	800
41012	B-Pillar Bulkhead Cover								DP	500	800

PART NUMBER	NAME	ULSAB-AVC			UPDATED TO			DESIGN OPTIMIZED			
		Material Type	Grade (MPa)		Material Type	Grade (MPa)		TWB	Material Type	Grade (MPa)	
			Yield Strength	Tensile Strength		Yield Strength	Tensile Strength			Yield Strength	Tensile Strength
Front Door Tubular Structure											
11204/5	Hinge Tube Front Door R&L	IF	260	410	HSLA	350	450		HSLA	350	450
32006/7	Latch Tube Front Door R&L	IF	260	410	HSLA	350	450		HSLA	350	450
32008/9	Lower Tube Front Door R&L	DP	500	800							
32010/1	Outer Belt Reinforcement - Front Door R&L	DP	500	800							
Rear Door Tubular Structure											
32040/1	Hinge TubeRear Door R&L	IF	260	410	HSLA	350	450		HSLA	350	450
32042/3	Latch Tube Rear Door R&L	IF	260	410	HSLA	350	450		HSLA	350	450
32044/5	Lower Tube Rear Door R&L	DP	500	800							
320467	Outer Belt Reinforcement -Rear Door R&L	DP	500	800							
Front Door Panels											
32030/1	Inner Rear -Front Door	MILD	140	270	IF	140	270		IF	140	270
32028/9	Outer - Front Door	DP	350	600							
12020/1	Inner Front - Front Door	MILD	140	270	IF	140	270		IF	140	270
		MILD	140	270	IF	140	270		IF	140	270
Rear Door Panels											
32038/9	Inner Rear - Rear Door	MILD	140	270	IF	140	270		IF	140	270
32032/3	Outer - Rear Door	DP	350	600							
32034/5	Inner Front - Rear Door	MILD	140	270	IF	140	270		IF	140	270
		MILD	140	270	IF	140	270		IF	140	270

TABLE 4: Material Listing By Part No

9. CONCLUSIONS

This report documented the modifications made to the original pre-optimization geometry in order to implement the recommendations of the Task 3.0: Optimization. Initially four concept designs were created based upon consideration of the optimization, manufacturing feasibility, joining strategy, assembly process and cost reduction. The most significant issue addressed by each of the concepts was the detailed design of the Rocker. The Task 3: Optimization had increased the depth of the Rocker section, which increased the step height for both front and rear passengers. A benchmarking study of current "in-class" production vehicles revealed that the increased Rocker height was acceptable. Based upon this study, Option D was chosen as the most viable design. The report then gave a detailed review of Concept D including a detailed description of the revised components, the joining strategy used to reduce the total amount of laser welding and the assembly process.

Concept D as described in this report will be used as the Concept Design. Task 5: Design Check will validate the Concept Design's performance against the following loadcases:

- IIHS Front Crash 40% ODB (Offset Deformable Barrier)
- Side Pole Impact (FMVSS214 NEW)
- IIHS Side Impact
- Roof Crush
- Door Intrusion
- Rear Crash
- Modal & Static Stiffness
  - Normal Modes (Free-Free)
  - Static Torsion & Bending Stiffness

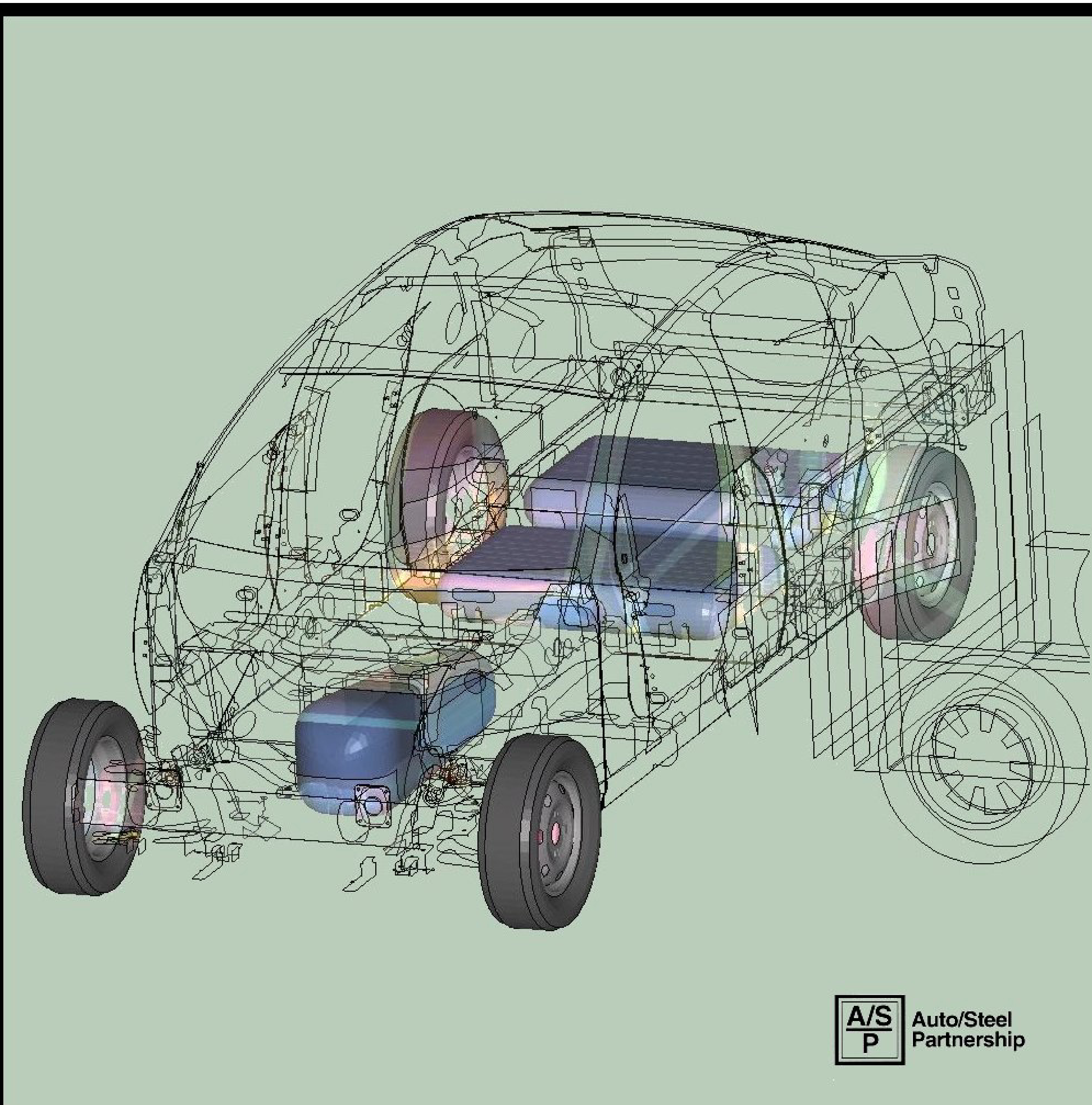

Future Generation Passenger Compartment
Task 5.0 - Concept Design Analysis Check

Design concept's performance assessment under all loadcases considered

Task 5.0 - Concept Design Analysis Check

Table of Contents

Task 5.0 - Concept Design Analysis Check

1. INTRODUCTION

This report completes Task 5.0: Concept Design Analysis Check of the FGPC (Future Generation Passenger Compartment) project. Its purpose is to document the performance of the FGPC Task 4.0: Concept Design under the loadcases listed below. This study was used to confirm that the performance of the concept design did not degrade from the baseline design.

- IIHS Front Crash 40% ODB (Offset Deformable Barrier)
- Side Pole Impact (FMVSS214 NEW)
- IIHS Side Impact
- Roof Crush
- Door Intrusion
- Rear Crash
- Modal & Static Stiffness
    - Normal Modes (Free-Free)
    - Static Torsion & Bending Stiffness

2. NAMING CONVENTION

Throughout this report the various FGPC design levels will be identified in the following manner:

- FGPC-BO (FGPC-Before Optimization)
  Task 2.0: Calibration Baseline - ULSAB-AVC PNGV modified to accommodate both Diesel and Fuel Cell powertrains. This is the FGPC Baseline.

- FGPC-AO (FGPC-After Optimization)
  Task 3.0: Optimization - the optimized FGPC Baseline.

- FGPC-ACD (FGPC-After Concept Design)
  Task 4.0: Concept Design - the optimization results integrated into a production viable vehicle.

3. OBJECTIVE

The objective of this task is to compare the performance of the FGPC-ACD to FGPC-BO for each loadcase.

4. REGULATIONS

Detailed specifications are described in Appendices A through F.

5. IIHS FRONT CRASH 40% ODB

5.1. TARGET

IIHS Front Crash 40% ODB impact is an analysis check loading case. The full regulations are in Appendix A. The target, established here by the FGPC team, considers design changes that may affect the safety cage structural integrity such as door operability and body structure deformation. Based on this strategy the following targets have been set for this loadcase:

- Rocker cross-sectional forces
  Section forces should meet or exceed those of the FGPC-BO.
- Door open-ability
  Doorframe deformation should not exceed FGPC-BO levels.

5.2. LOADS AND BOUNDARY CONDITIONS

The vehicle impacts a deformable barrier, offset 10% from centerline (40% overlap), at 40mph. See Figures 1 & 2.

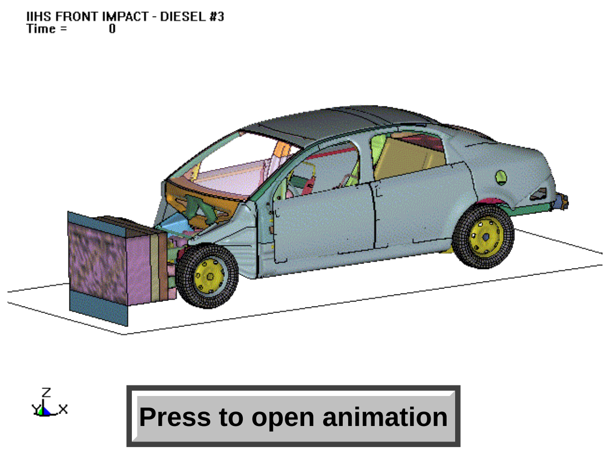

FIGURE 1: IIHS Side Impact Model (ISO View)

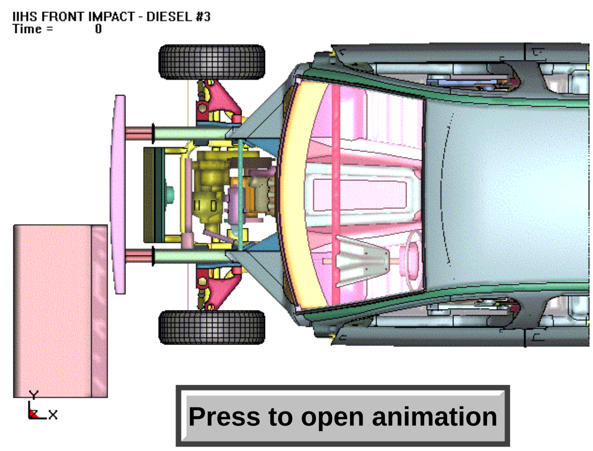

FIGURE 2: IIHS Side Impact Model (Top View)

Rocker cross-sectional forces and door open-ability were used to evaluate the vehicle's performance. The Door open-ability was measured in three locations: Top, Middle and Bottom. See Figure 3.

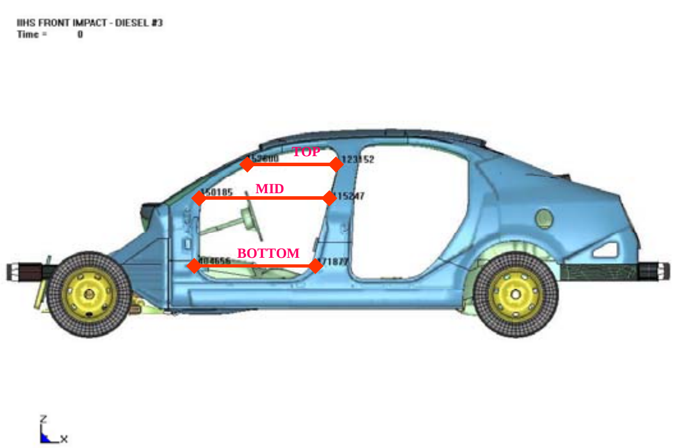

FIGURE 3: Door Open-Ability Measurement Points

5.3. RESULTS

Table 1 and Figures 4 & 5 summarize the Rocker cross-sectional forces and Door open-ability for both the FGPC-BO and FGPC-ACD.

MODELS	MASS (kg)	DOOR OPEN-ABILITY (mm)			ROCKER X-SECTIONAL FORCE (kN)
		TOP	MID	BOTTOM	
FGPC - BO	1351.1	2.5	8.2	17.0	121.5
FGPC - ACD	-23.8	15.1	126.7	169.0	41.7

TABLE 1: IIHS Front Impact 40% OBD for FGPC-BO & FGPC-ACD

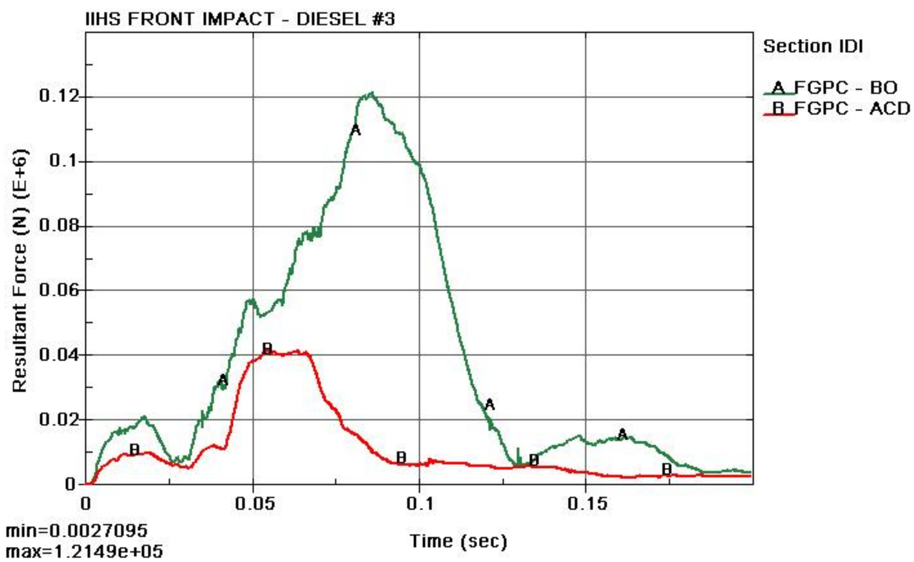

FIGURE 4: Rocker Cross-Sectional Forces for FGPC-BO & FGPC-ACD

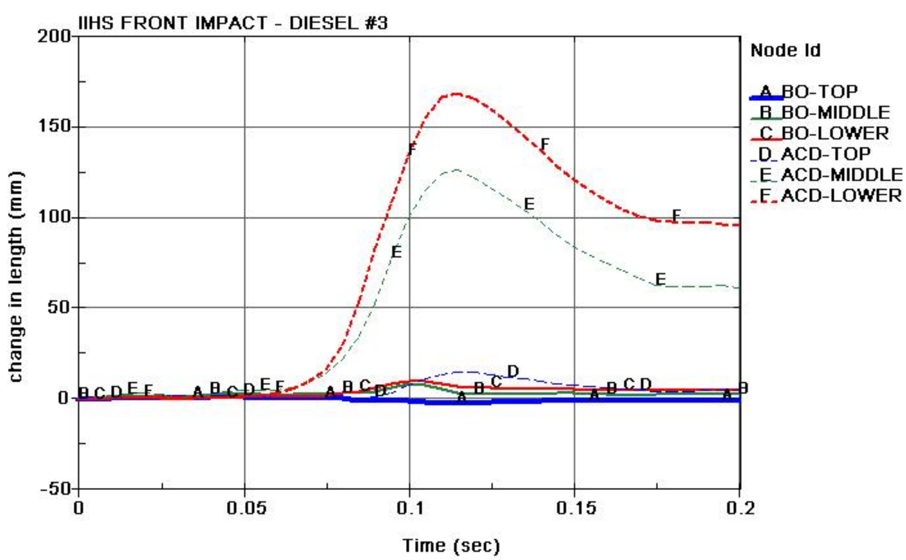

FIGURE 5: Door Open-Ability for FGCP-BO & FGPC-ACD
Measured at Top/Middle/Lower Positions

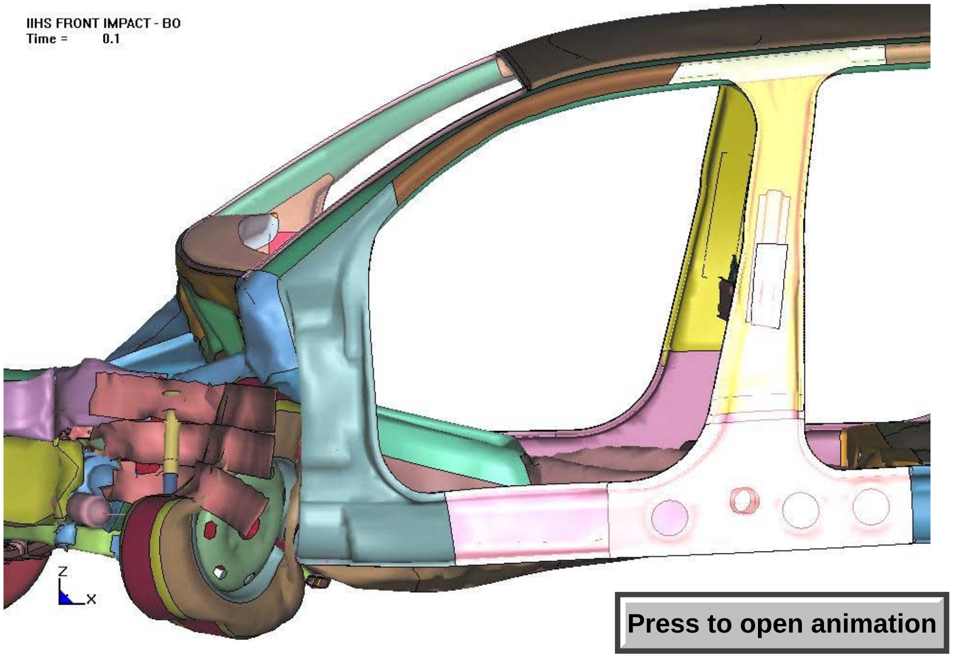

FIGURE 6: IIHS 40% ODB – FGPC-BO Rocker Deformation

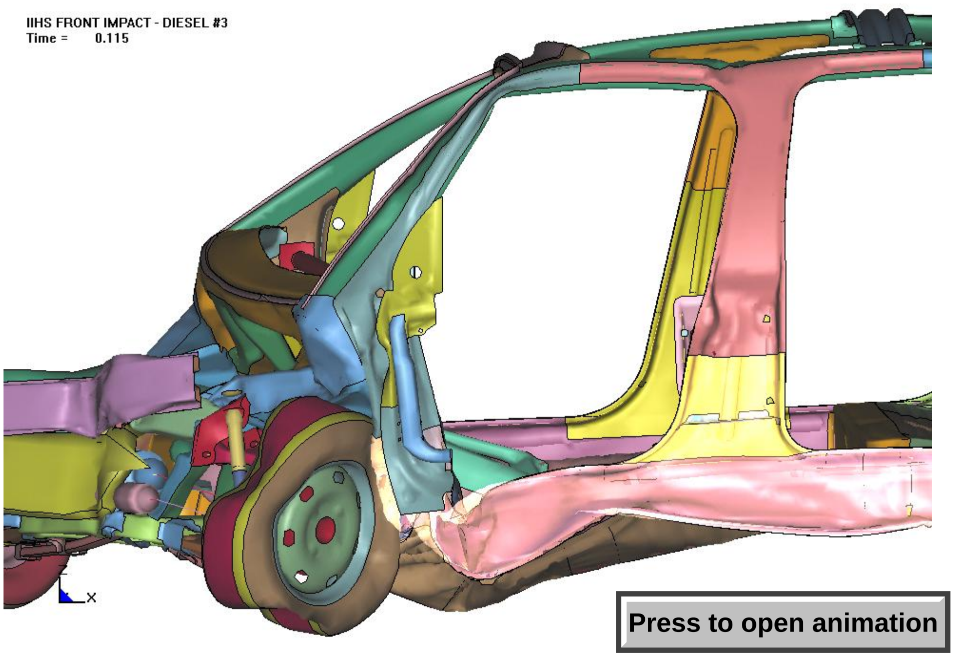

FIGURE 7: IIHS 40% ODB – FGPC-ACD Rocker Deformation

5.4. CONCLUSION

FGPC-ACD did not maintain the performance of FGPC-BO. This load condition was not used as an optimization constraint, allowing it to reduce the Rocker Inner gauge from 1.5 to 0.6mm. This has weakened the lower passenger compartment, the Rocker and A-Pillar, therefore reducing the strength of the doorframe, compare Figures 6 & 7. Further modification will be required to make the FGPC meet the target.

6. SIDE POLE IMPACT (FMVSS214 NEW)

6.1. TARGET

FMVSS214 New Pole Impact sets limits on occupant injury criteria, with no structural performance requirements. Since no occupant models are used in this study, the maximum structural intrusion into the passenger compartment was measured instead. This is similar to the IIHS Side Impact target. The maximum intrusion in the pole impact occurs on the Front Door Inner, while the side impact intrusion is measured at the B-Pillar.

Therefore the target is to meet or exceed the performance of the FGPC-BO, which had a maximum intrusion of 7mm inboard of the driver's seat centerline.

6.2. LOADS AND BOUNDARY CONDITIONS

The vehicle is propelled at 20mph into a 10in diameter pole at an angle of 75 degrees to its longitudinal axis, as shown in Figure 8. The pole is lined up with the center of the occupant's head. It should noted that the seats in the FGPC are designed to be stationary with adjustable driver controls and so the head position will remain constant regardless of occupant size.

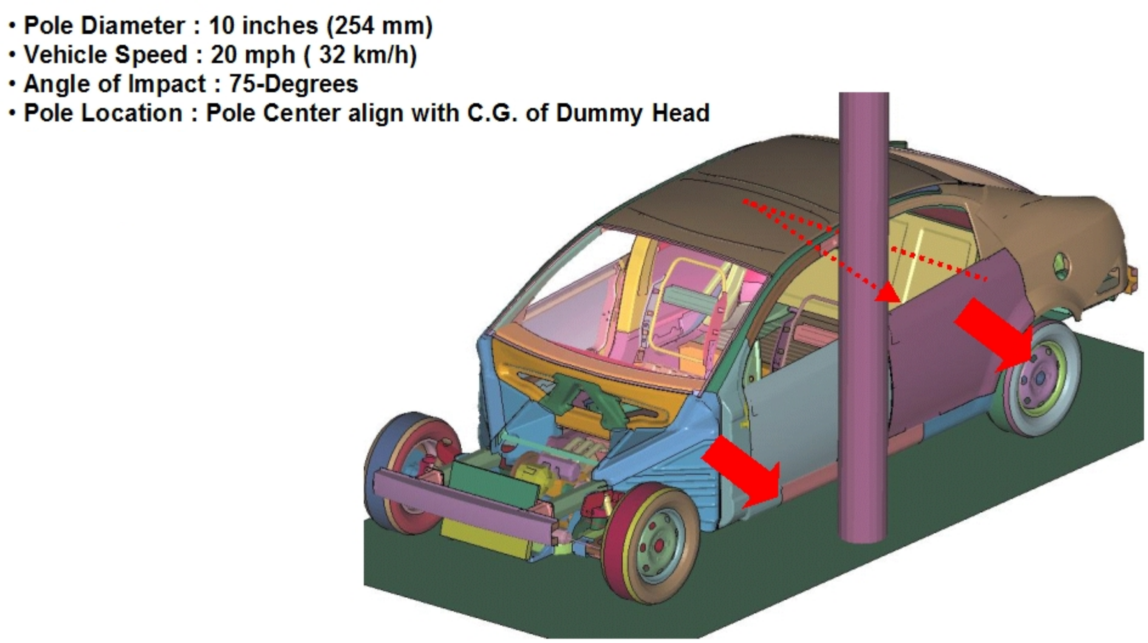

FIGURE 8: Pole Impact Set-Up

6.3. RESULTS

Figure 9 shows the maximum intrusion of the front door relative to the center of the driver's seat. The maximum intrusion of the FGPC-ACD model was 120mm past the seat centerline, compared to 7mm for FGPC-BO.

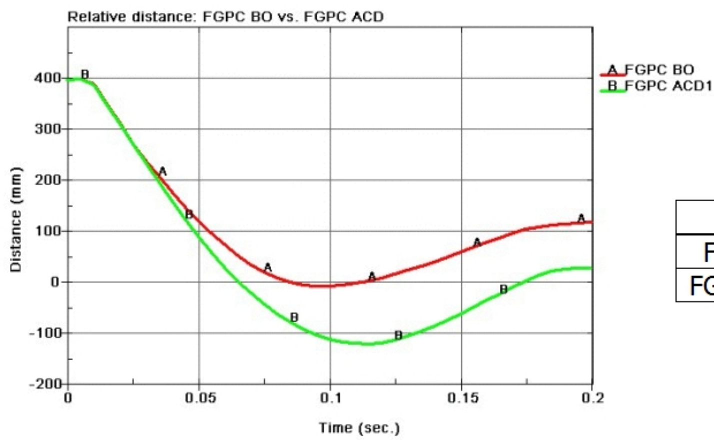

	Min. Distance (mm)
FGPC BO	-7
FGPC ACD1	-120

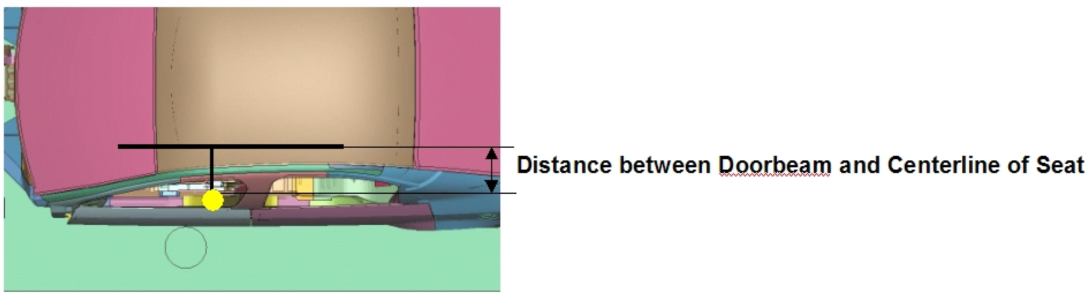

FIGURE 9: Intrusion of Front Door into Passenger Compartment

Figures 10 through 13 compare the deformed shapes for both the FGPC-ACD and FGPC-BO vehicles.

Press to open animation

Press to open animation

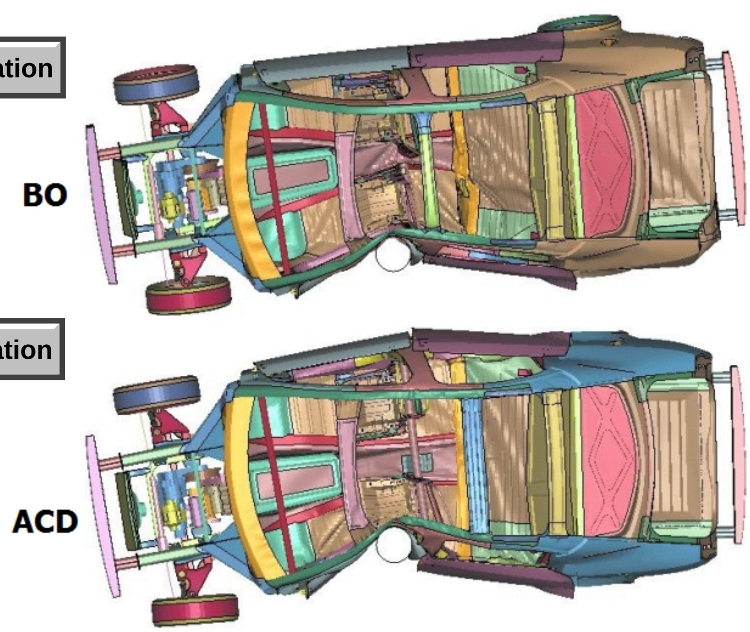

FIGURE 10: Deformed Shape FGPC-BO vs FGPC-ACD (Top View)

Press to open animation

BO

Press to open animation

ACD

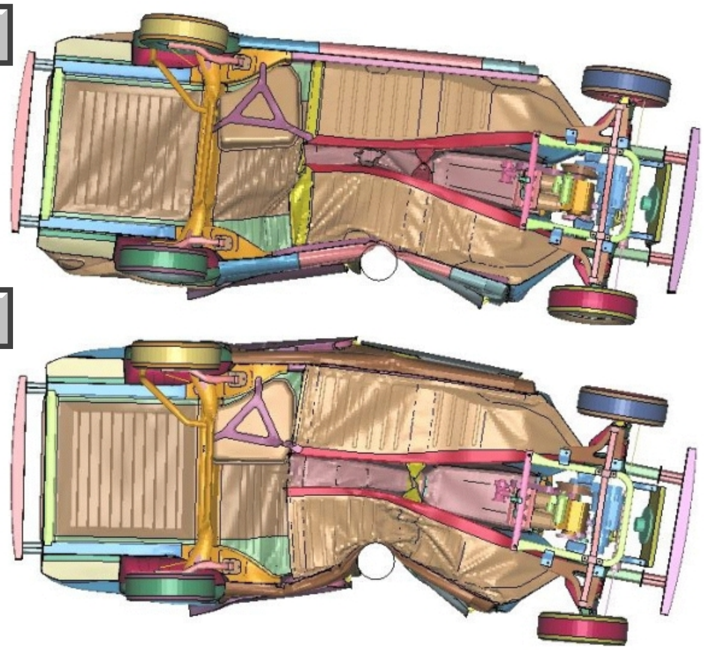

FIGURE 11: Deformed Shape FGPC-BO vs FGPC-ACD (Bottom View)

BO

ACD

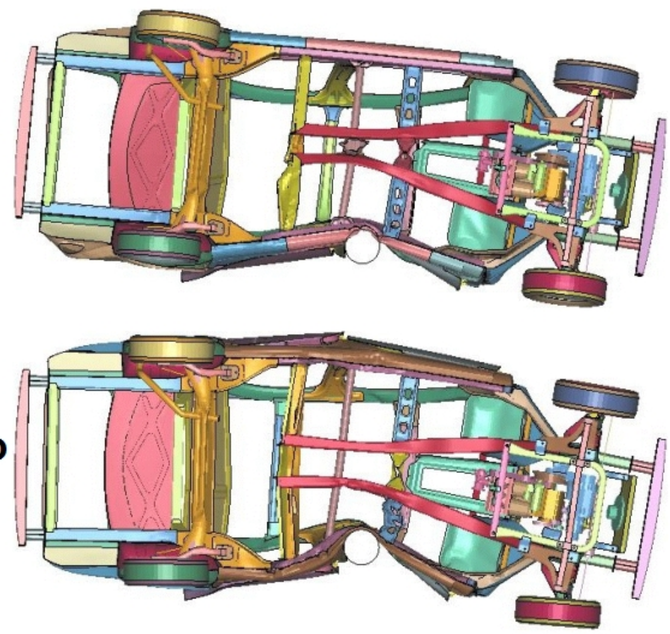

FIGURE 12: Deformed Shape FGPC-BO vs FGPC-ACD (Bottom View Without Floors)

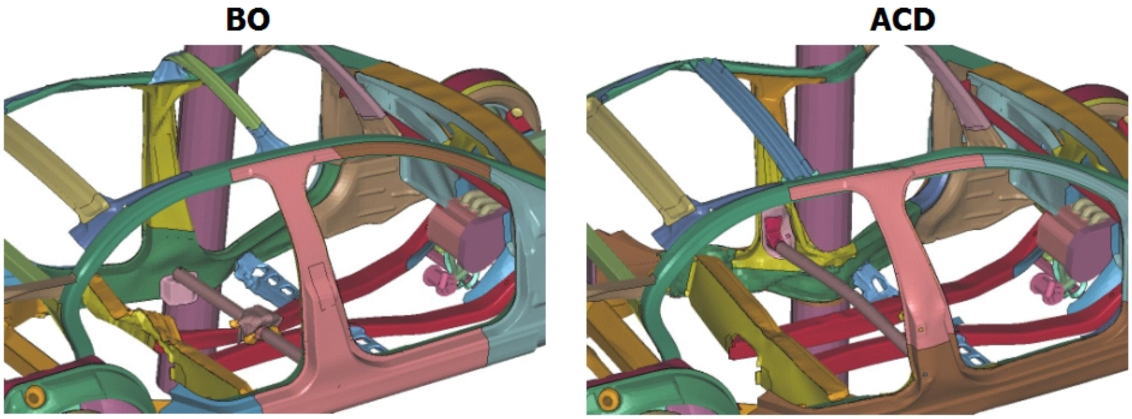

FIGURE 13: Deformed Shape FGPC-BO vs FGPC-ACD (ISO View)

The previous figures show that for the FGPC-BO, the Seat Cross-member transferred the load from the Rocker to the Tunnel. However, for the FGPC-ACD design, the Seat Cross-member is above the Rocker and so it transferred the load directly to the non-struck side of the vehicle. The Rocker therefore has less support between the Kick-down Cross-member and the Front Seat Cross-member, which allows more pole intrusion into the passenger compartment.

6.4. CONCLUSION

FGPC-ACD did not satisfy the FMVSS214 New target, failing to meet the performance achieve by FGPC-BO. It will therefore necessary to carry out additional analysis iterations until FGPC-ACD meets or exceeds the performance achieved by FGPC-BO.

7. IIHS SIDE IMPACT

7.1. TARGET

The regulations for IIHS Side Impact include occupant injury criteria. However, the FGPC project is only concerned with the vehicle structure. Therefore the FGPC team used a target that maintains the IIHS survival space requirement of not less than 125mm. See Figure 17.

7.2. LOADS AND BOUNDARY CONDITIONS

A 1500kg MDB (Moving Deformable Barrier) was positioned so that there was 379mm of ground clearance. The rearward distance from the test vehicle's front axle to the closest edge of the deformable barrier, known as the IRD (Impact Reference Distance), was 810 mm. The barrier impacted the vehicle with an initial velocity of 50kph. See Figure 14.

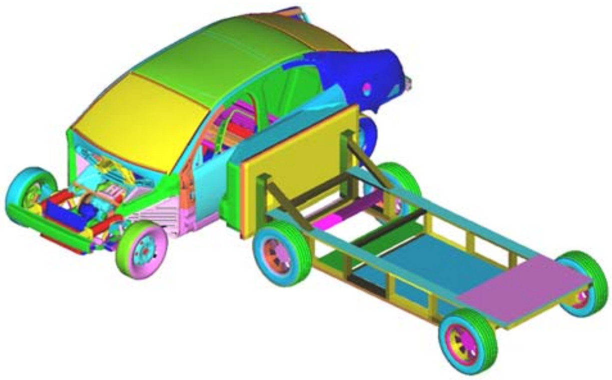

FIGURE 14: IIHS Side Impact Analysis

7.3. RESULTS

7.3.1. FGPC-ACD Baseline

Comparisons of the B-Pillar and Seat Cross-member deformations for FGPC-BO, FGPC-AO and FGPC-ACD are shown in Figure 16. Note the variation in Seat Cross-member size and position between the three designs. For clarity they are also shown separately in Figure 15. FGPC-AO uses an 80 x 80mm square section cross-member, where as FGPC-ACD employs a 60mm diameter tubular section.

The FGPC-ACD Cross-member kinked on the driver's side resulting in increased B-Pillar deformation compared to FGPC-BO. The B-Pillar intrusion (survival space) measurements are shown in Figure 17. The survival space was reduced to 83.7mm, which is below the target of 125mm. Its performance was also inferior to FGPC-BO, 103mm and FGPC-AO, 125mm.

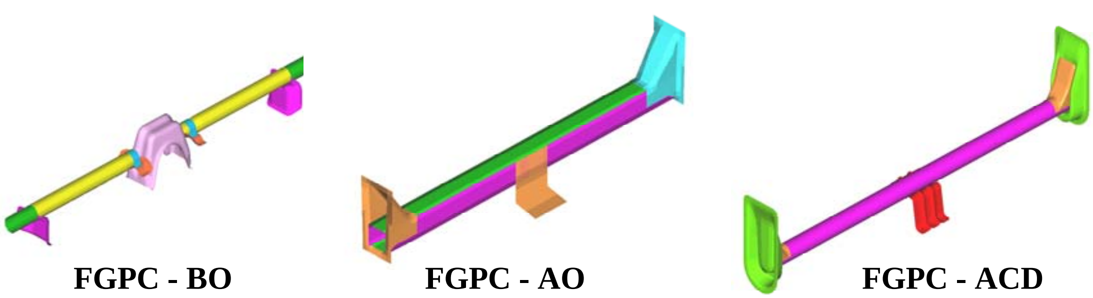

FIGURE 15: Seat Cross-Member - FGPC-BO, FGPC-AO & FGPC-ACD

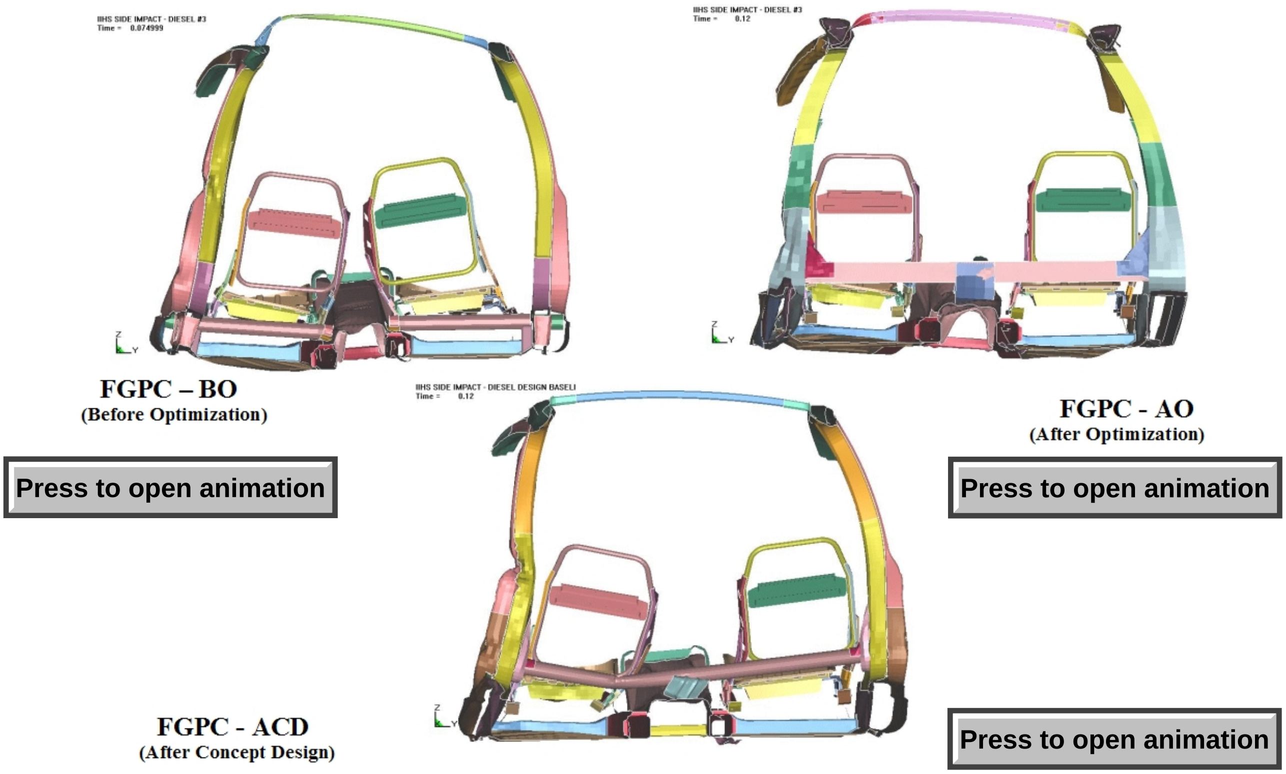

FIGURE 16: B-Pillar & Seat Cross-Member Deformation Comparison

B-Pillar Intrusion

FGPC - BO:	**103.0 mm**
FGPC - AO:	**124.3 mm**
FGPC – ACD Baseline:	**83.7 mm**
FGPC – ACD Final:	**124.7 mm**

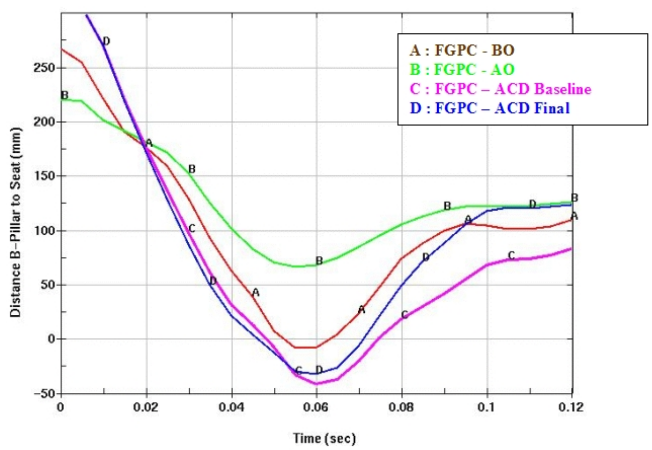

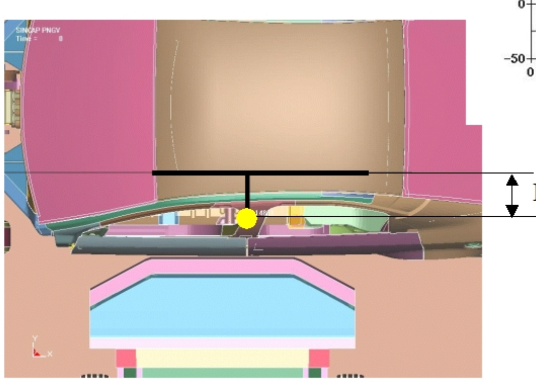

Distance between B-Pillar and Centerline of Seat

Good	>	125 mm
Acceptable	>	50 mm
Marginal	>	0 mm

FIGURE 17: IIHS Side Impact B-Pillar Intrusion

7.3.2. FGPC-ACD Iteration Study

An iteration study was performed to determine why the IIHS Side Impact performance of the FGPC-ACD was inferior to the FGPC-AO, which had previously met the requirements. The FGPC-AO geometry had been simplified for the topology optimization and so the geometry, material and gauge choices for FGPC-ACD required some revision due to manufacturing, joining and assembly considerations.

A summary of the iteration changes made and their effect on side impact performance are listed in Table 2.

SIMULATION	CONFIGURATION	B-PILLAR TO SEAT CENTER DISTANCE (mm)
Original baseline (FGPC-ACD)	Seat penetrates cross-member	82.8
Modified baseline	No penetration between seat and cross-member	83.7
Iteration #1	Original baseline + Removed seat and tunnel connections to cross-member	99.4
Iteration #2	Iteration #1 + Removed bulkhead/side outer lower 1.25→1.0mm	49.7
Iteration #3	Iteration #2 + Cross-member thick 1.4→2.0mm, fixed seat penetration	52.6
Iteration #4	Iteration #3 + Reconnect seats to cross-member	96.6
Iteration #5	Iteration #4 + Added B-Pillar outer reinforcement	102.4
Iteration #6	Iteration #4 + Cross-member reconnected to tunnel	87.7
Iteration #7	Iteration #2 + Increased cross-member diameter from 60 to 80mm	78.2
Iteration #8	Iteration #4 + Replaced bulkhead	111.5
Iteration #9 (FGPC-ACD Final)	Iteration #8 + Side outer lower to original 1.25mm thickness	124.7
Iteration #10	Iteration #8 + Up-gauged cross-member material Mart1300→Boron1550	117.2
TARGET		**>125mm**

TABLE 2: IIHS Side Impact Analysis Iterations

Analysis determined that the most significant differences with respect to side impact performance were:

- Changing the Seat Cross-member from an 80 x 80mm square section tube to a 60mm diameter circular section.
- Changing the Seat Cross-member material from Boron 1550 to Mart 1300.
- Changing the Body-side Outer Lower material from Boron 1550 to DP780.

Iteration #9, which changed the gauge of the 60mm diameter Seat Cross-member from 1.4 to 2.0mm and released its connection to the Tunnel, met the required performance target. Iteration #9 is therefore considered FGPC-ACD Final. Refer to Figure 17. The deformed shape of FGPC-ACD Final is shown in Figure 18.

Press to open animation

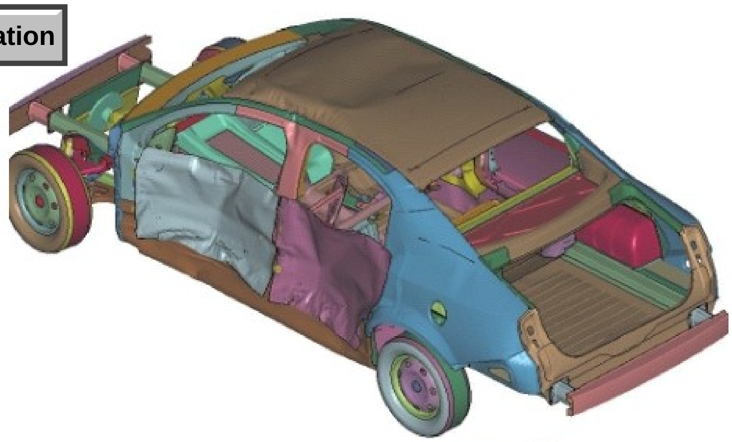

Press to open animation

Press to open animation

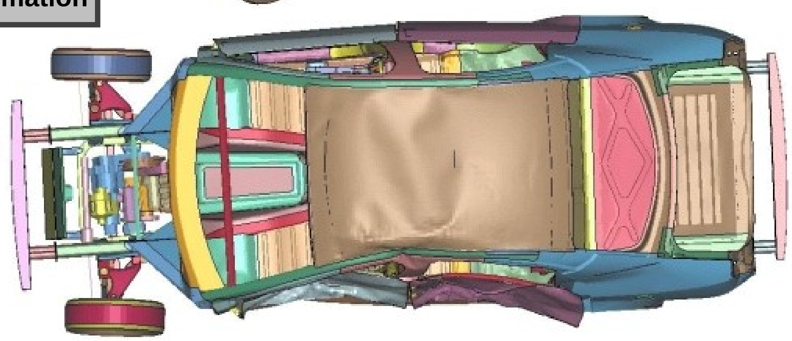

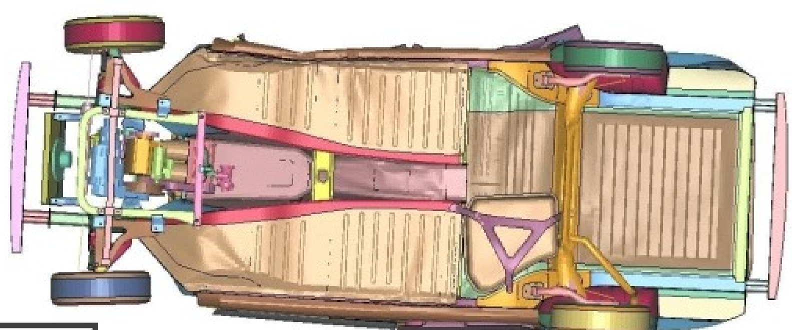

Press to open animation

FIGURE 18: Deformed Shape of FGPC-ACD Final (Iteration #9)

Comparison of the FGPC-ACD Baseline and FGPC-ACD Final deformed shapes is given in Figure 19. The revised Seat Cross-member now bends without kinking, thus reducing the lower B-Pillar intrusion to the target level.

Press to open animation

Press to open animation

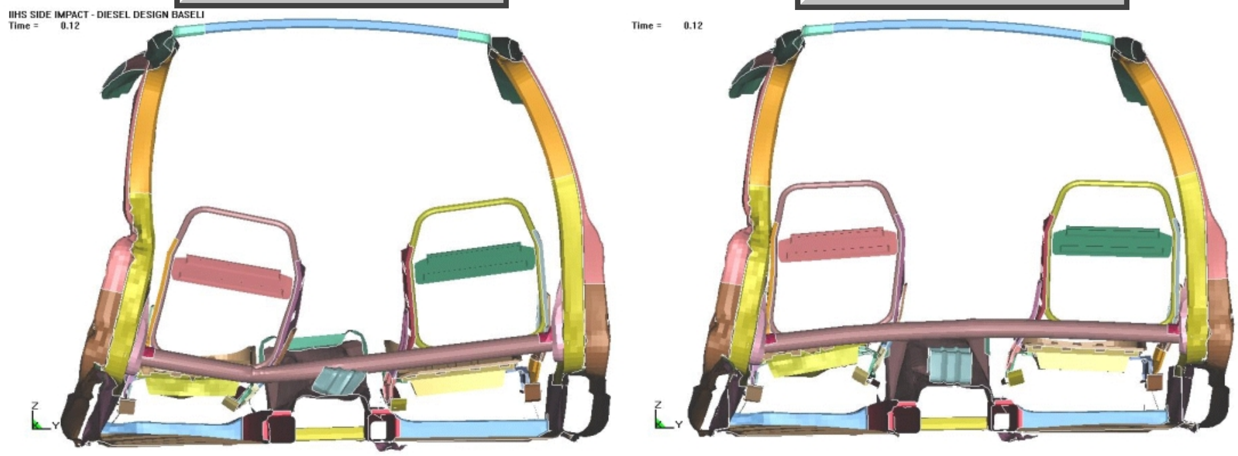

FGPC - ACD Baseline

FGPC – ACD Final

FIGURE 19: FGPC-ACD Baseline & FGPC-ACD Final
B-Pillar Deformation Comparison

7.4. CONCLUSION

FGPC-ACD Baseline model did not meet the IIHS Side Impact requirements. An iteration study showed that by reducing the Seat Cross-member section its performance had suffered. Increasing the Cross-member’s gauge from 1.4 to 2.0mm allowed FGPC-ACD Final to met the target IIHS Side Impact performance of 125mm.

8. ROOF CRUSH (FMVSS216)

8.1. TARGET

The FGPC team set the Roof crush resistance target as a deflection of 127mm or less under a loading of 2.75 x the unloaded vehicle weight. Note this target exceeds the loading set by FMVSS216, which requires the same deflection for a loading of 1.5 x the unloaded vehicle weight.

8.2. LOADS AND BOUNDARY CONDITIONS

A rigid plate (1829 x 762mm) is pushed onto the A-Pillar at a velocity of 50in/sec (5in over the 100msec analysis time). See Figure 20. Note the analysis speed of 50in/sec is higher than the regulation's 5in/120sec. This was done to increase computational efficiency. The higher velocity does introduce a slight inertial effect into the analysis, which is known to increase the reaction force by a small, but nearly negligible amount. Both Rockers were fixed in all degrees of freedom (translations in and rotations about x, y and z). See Figure 21.

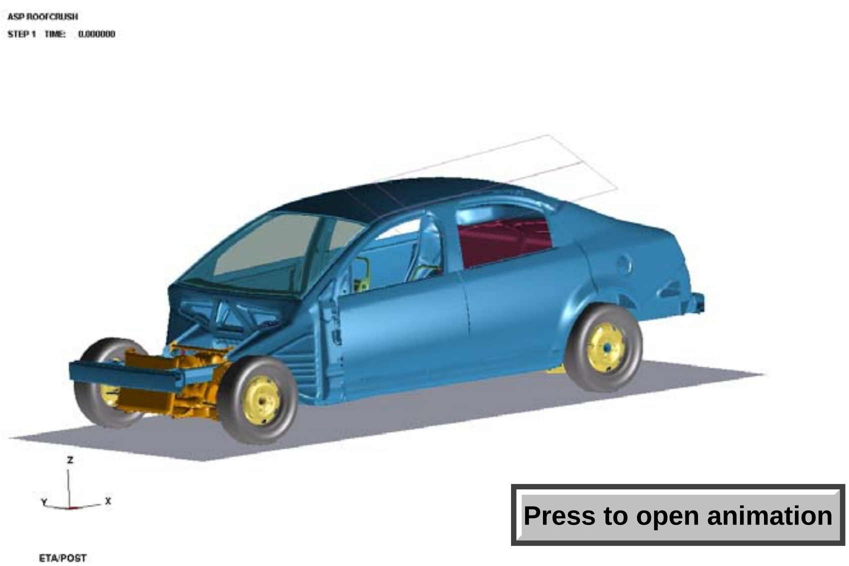

FIGURE 20: Roof Crush Model

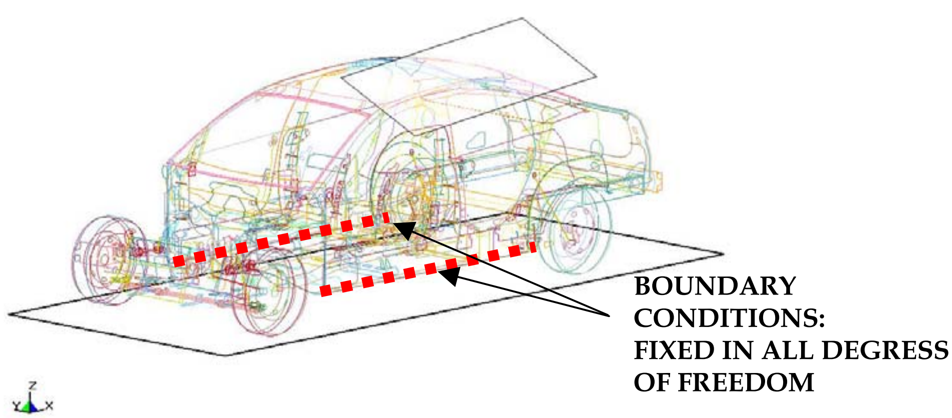

FIGURE 21: Roof Crush Model – Boundary Conditions

8.3. RESULTS

FGPC-ACD performs well under the FMVSS216 load case. Results are shown in Figure 22.

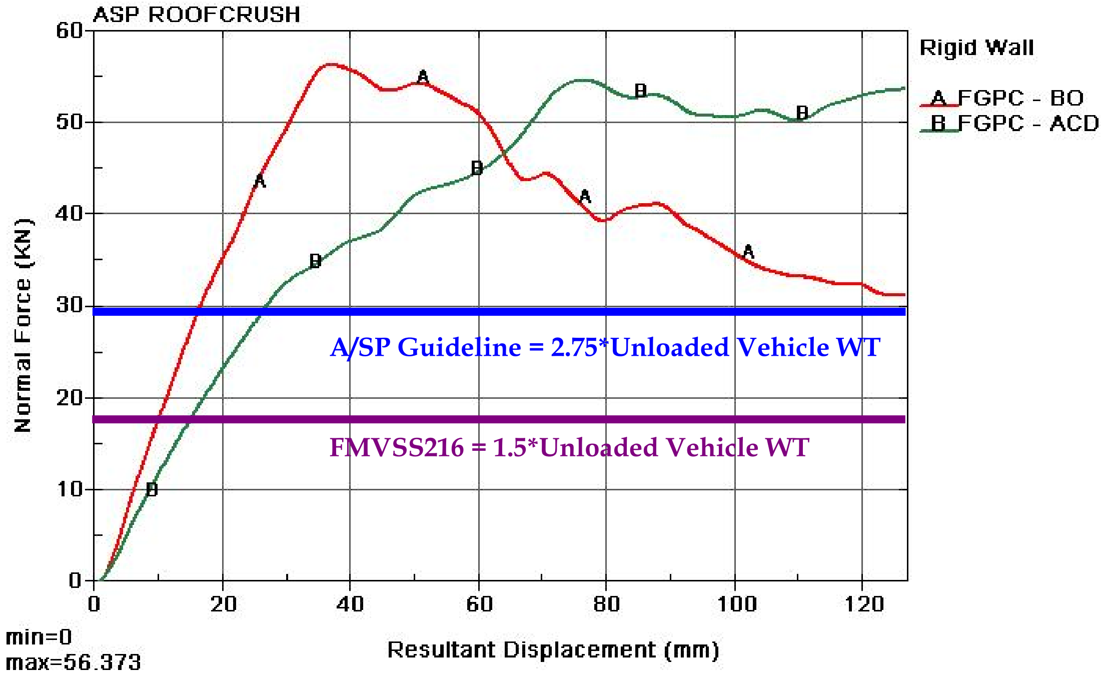

FIGURE 22: Roof Crush Results for FGPC-BO & FGPC-ACD

Figures 23 & 24 show the plastic strain of the FGPC-ACD. The deformation mode is similar to the FGPC-BO. Buckling at the B-Pillar reinforcement causes the body side crumpling at the A-pillar.

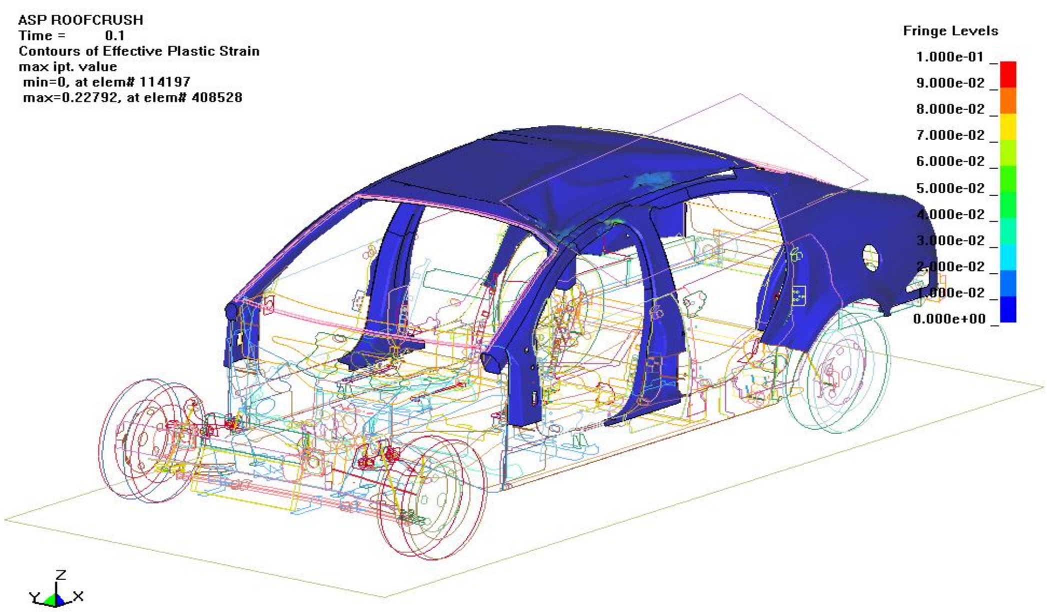

FIGURE 23: Plastic Strain – Deformed Shape (ISO View)

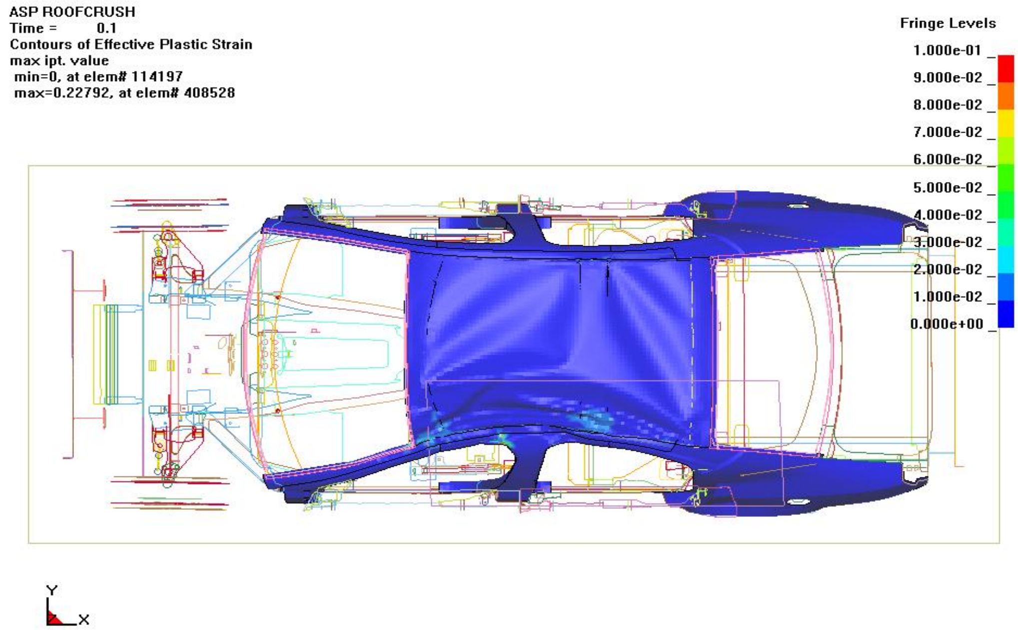

FIGURE 24: Plastic Strain – Deformed Shape (Top View)

8.4. CONCLUSION

FGPC-ACD satisfies the FMVSS216 requirements. The structure also meets the A-SP (Auto/Steel Partnership) recommendation of 2.75 x the unloaded vehicle weight.

9. DOOR INTRUSION (FMVSS214)

9.1. TARGET

FGPC team set the target at 10% above FMVSS 214 requirements, which are listed below:

- Initial crush resistance
  The average force required to deform the door shall not be less than 2250lb over the first 6in of barrier displacement.
- Intermediate crush resistance
  The average force required to deform the door shall not be less than 3500lb over the first 12in of barrier displacement.

9.2. LOADS AND BOUNDARY CONDITIONS

The barrier is a rigid cylinder 12in diameter and 25in high. The longitudinal axis of the cylinder is positioned vertically at the mid-point of the line 5in (127mm) above the lowest point on the door. The bottom of the barrier is inline with this point. The external circumference of the cylindrical barrier is spaced 5mm from the outer door skin.

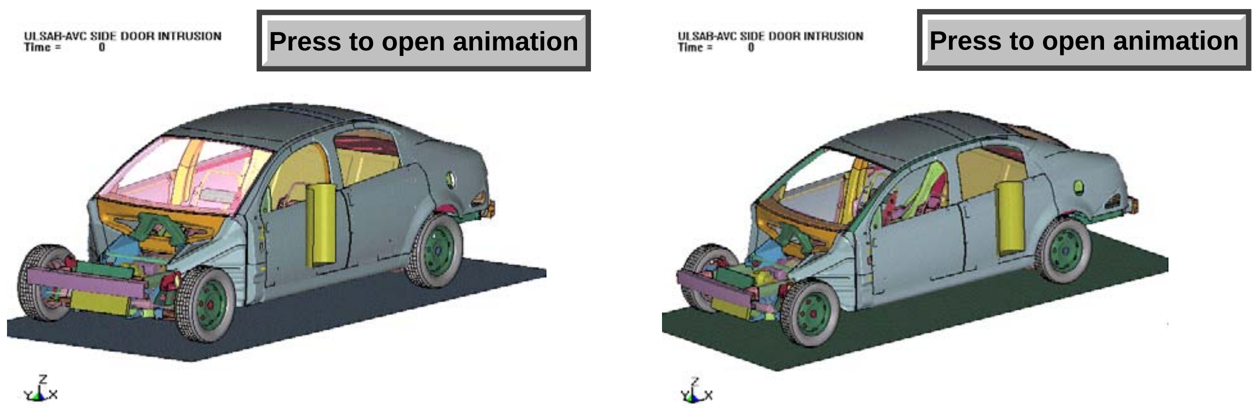

FIGURE 25: Door Intrusion Models (Front & Rear Door)

The front and rear of both Rockers are fixed in all directions. The bottom of the non-impacted Rocker is also fixed in all directions.

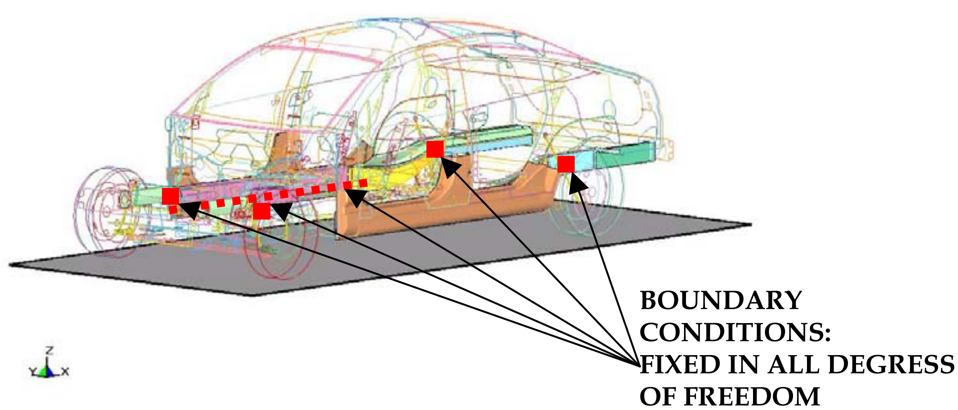

FIGURE 26: Side Door Intrusion – Boundary Conditions

9.3. RESULTS

FGPC-ACD performs well under the FMVSS214 loadcase for both front and rear doors. Figures 27 & 28 show the Barrier Force vs Barrier Displacement for the front and rear doors respectively. Integration of these plots gives the Energy vs Barrier Displacement, Figures 29 & 30, again for both front and rear doors. The average forces at 6in and 12in displacements are calculated from the energy vs displacement plots. Tables 3 & 4 give the average forces for both the front and rear door.

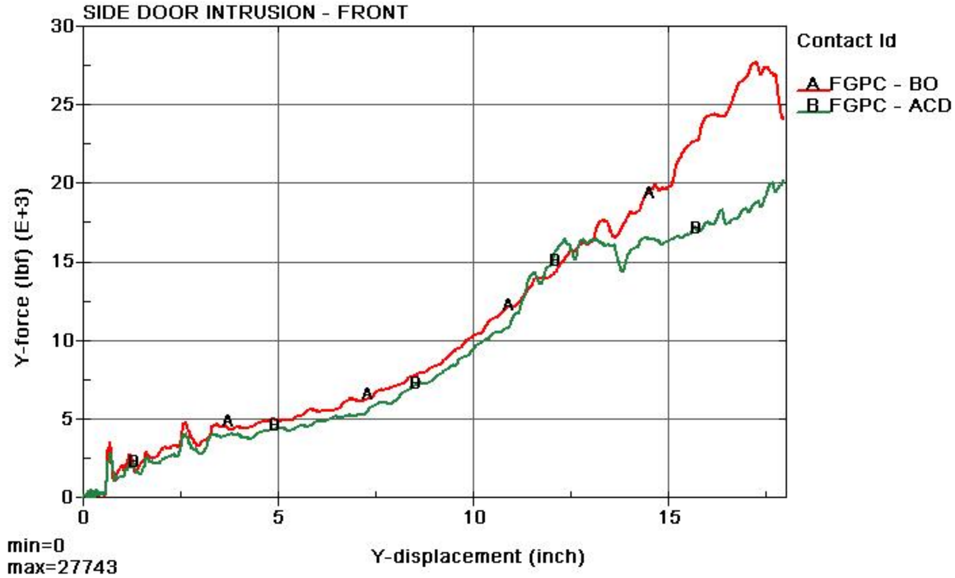

FIGURE 27: Front Door - Barrier Force (lb-f) vs Barrier Displacement (inch) for FGPC-BO & FGPC-ACD

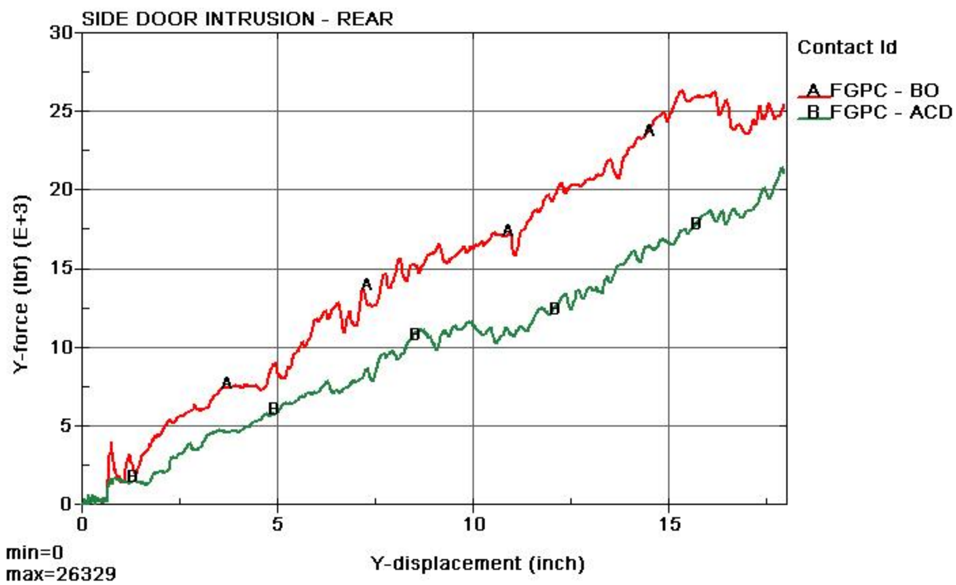

FIGURE 28: Rear Door - Barrier Force (lb-f) vs Barrier Displacement (inch) for FGPC-BO & FGPC-ACD

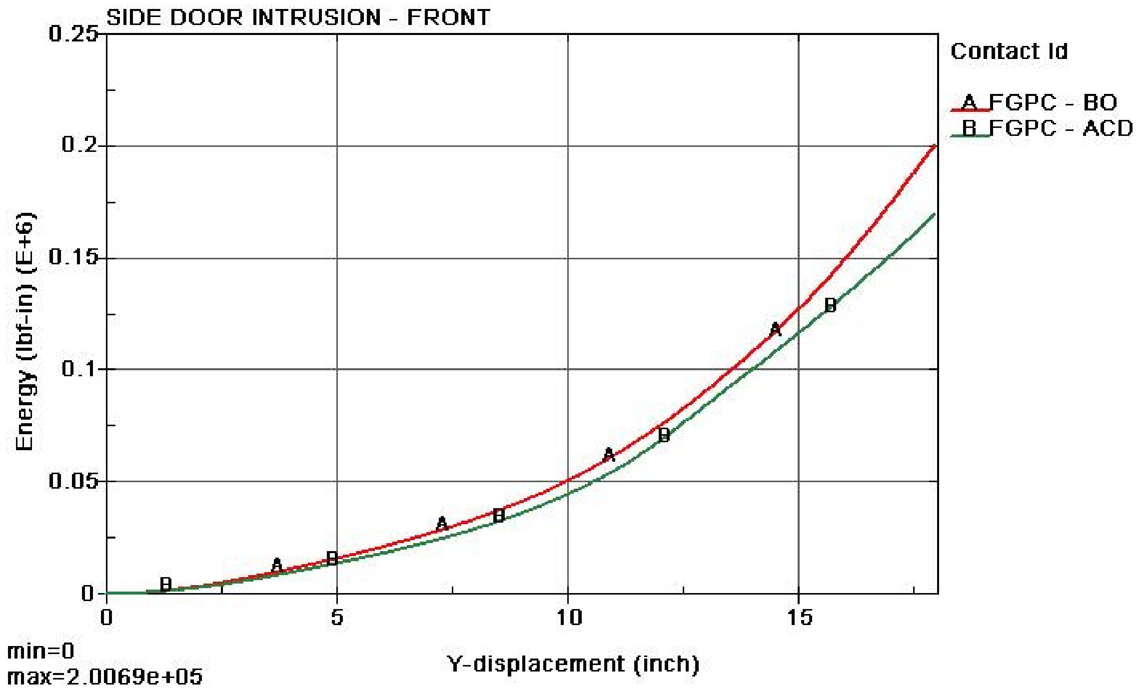

FIGURE 29: Front Door - Energy (lbf-inch) vs Barrier Displacement (inch) for FGPC-BO & FGPC-ACD

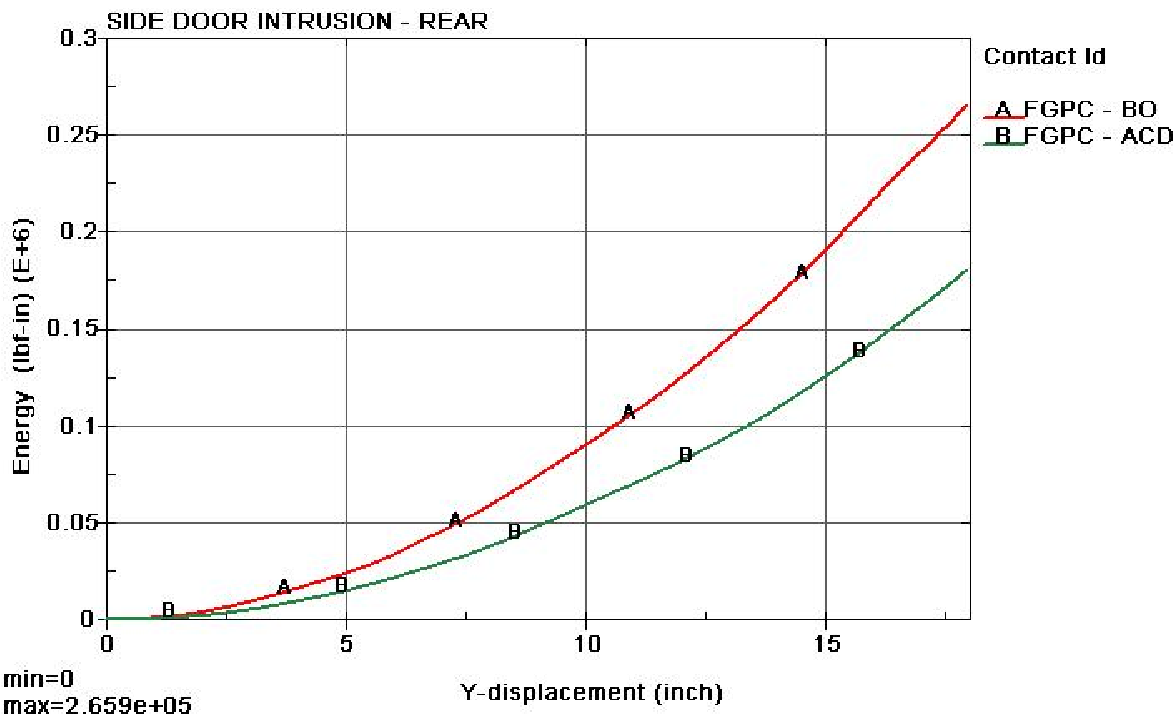

FIGURE 30: Rear Door - Energy (lbf-inch) vs Barrier Displacement (inch) for FGPC-BO & FGPC-ACD

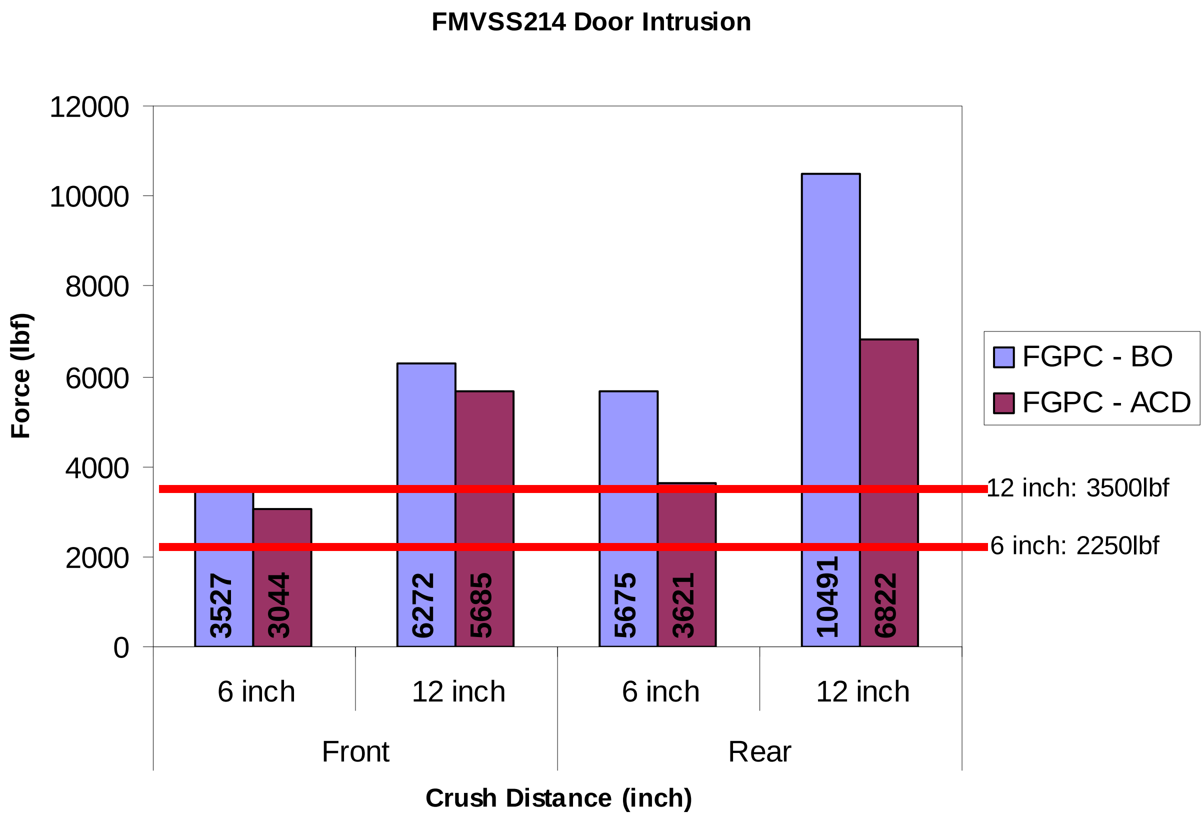

FIGURE 31: Door Intrusion for FGCP-BO & FGPC-ACD

BARRIER SIZE	ULSAB-AVC (lbf)	FGPC-ACD (lbf)	FMVSS214 (lbf)
6 inch	3527	3044	2250
12 inch	6272	5685	3500

TABLE 3: Front Door

BARRIER SIZE	ULSAB-AVC (lbf)	FGPC-ACD (lbf)	FMVSS214 (lbf)
6 inch	5675	3621	2250
12 inch	10491	6822	3500

TABLE 4: Rear Door

9.4. CONCLUSION

FGPC–ACD satisfies the requirements of FMVSS214 and the ASP internal targets (10% above FMVSS 214).

10. REAR CRASH (FMVSS301)

10.1. TARGET

The same target as FMVSS301, which requires maintenance of fuel tank integrity.

10.2. LOADS AND BOUNDARY CONDITIONS

A rigid wall impacts the rear of the vehicle at a constant velocity of 35mph. The vehicle is free to move upon impact. See Figure 32.

FIGURE 32: Rear Crash Model

10.3. RESULTS

No major design changes were made to the rear of the vehicle and so the FGPC-ACD performed as well as the FGPC-BO. Figure 33 shows the deformed shape of the FGPC-ACD at 0.1s, the maximum deformation. The figure clearly shows that the fuel tank integrity was maintained without any deformation. For comparison the deformed shape of FGPC-BO is given in Figure 34.

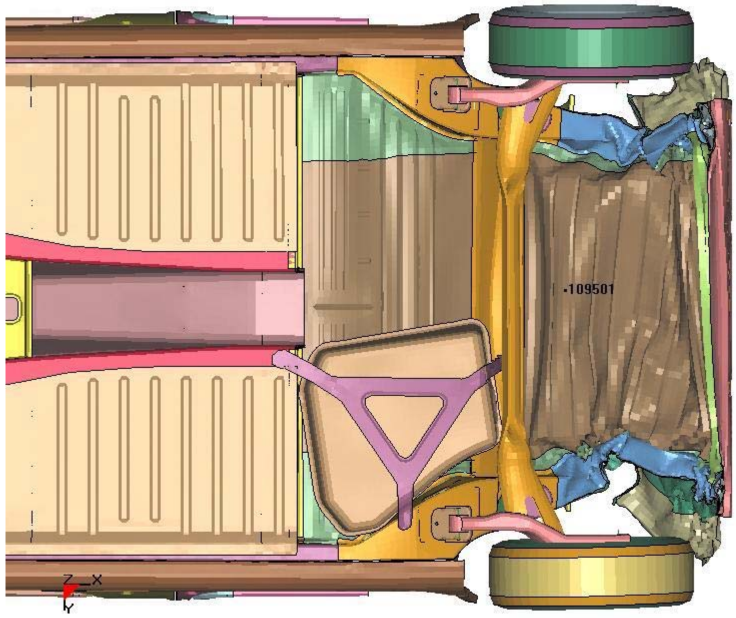

Press to open animation

FIGURE 33: Rear Crash Deformed Shape – FGPC-ACD (Bottom View)

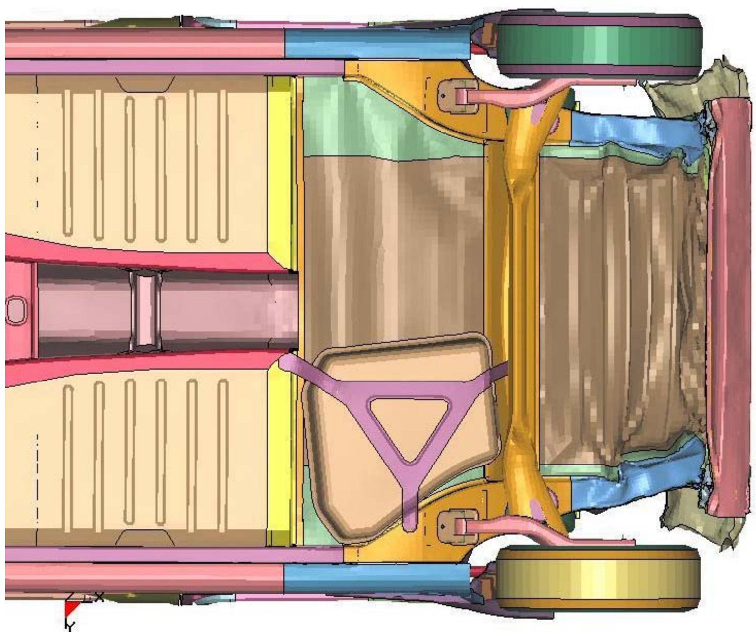

Press to open animation

FIGURE 34: Rear Crash Deformed Shape – FGPC-BO (Bottom View)

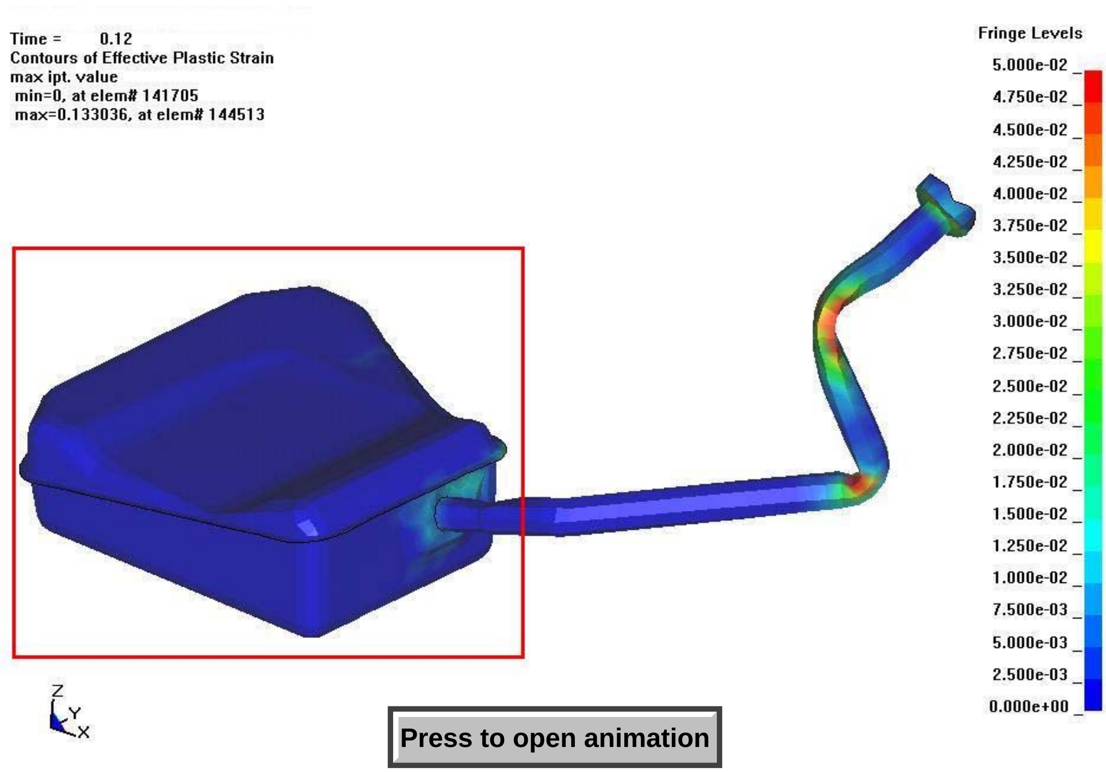

FIGURE 35: Fuel Tank at 5% Plastic Strain

10.4. CONCLUSION

Due to small changes in the rear floor geometry, FGPC-ACD has absorbed more energy. Although less force is transferred to the occupants this does create a risk that the fuel tank's integrity could be jeopardized. However, Figures 33 & 34 clearly show that this did not happen. Note Figure 35 does show a small plastic deformation of the fuel tank filler tube.

11. MODAL AND STATIC STIFFNESS

11.1. TARGET

The target for a trimmed BIW vehicle was 40Hz but since the trimmed body mass and CG was not fully defined the FGPC team decided to use targets for the BIW based upon the ULSAB-AVC performance.

- Modal Modes — Bending – 57Hz
  Torsion – 56Hz
- Stiffness — Bending – greater than 12000N/mm
  Torsion – greater than 13000Nm/deg

11.2. NORMAL MODES (FREE-FREE)

A normal modes analysis was performed on the BIP (Body-In-Prime) model. The torsional and bending modes were extracted and compared to the target values. The mode shapes are shown in the following figures, Figures 36 & 37 show the torsional mode at 54Hz and Figures 38 & 39 show the bending at 61Hz.

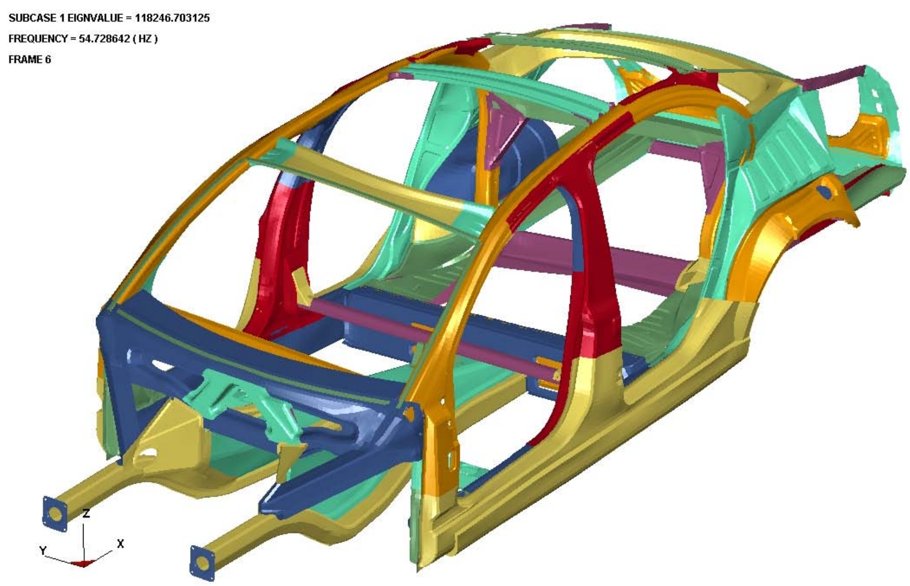

FIGURE 36: Torsion mode (ISO View)

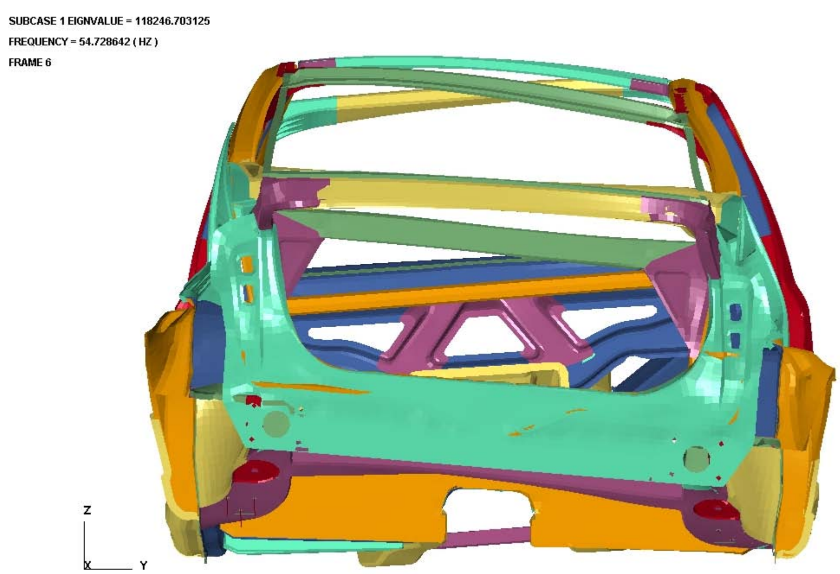

FIGURE 37: Torsion Mode (Rear View)

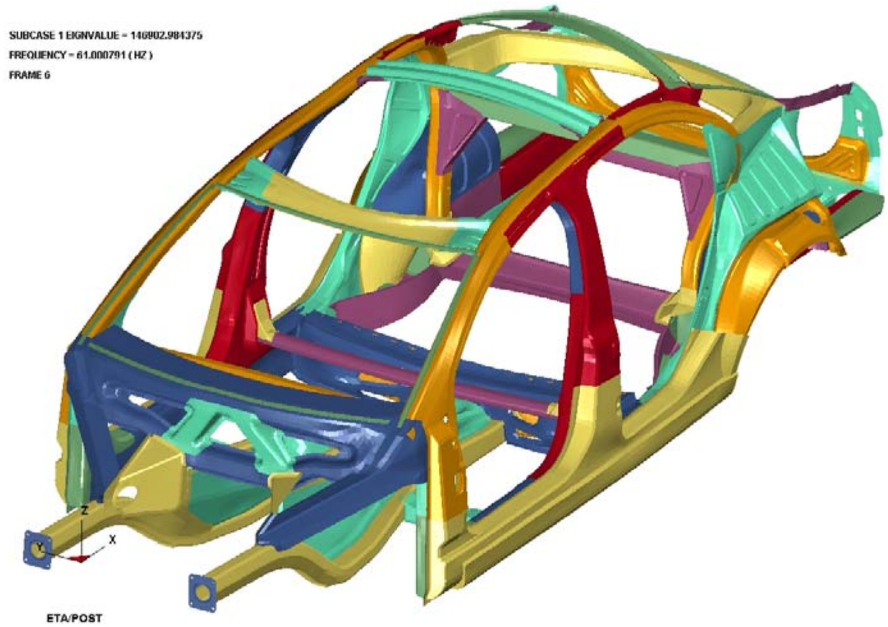

FIGURE 38: Bending Mode (ISO View)

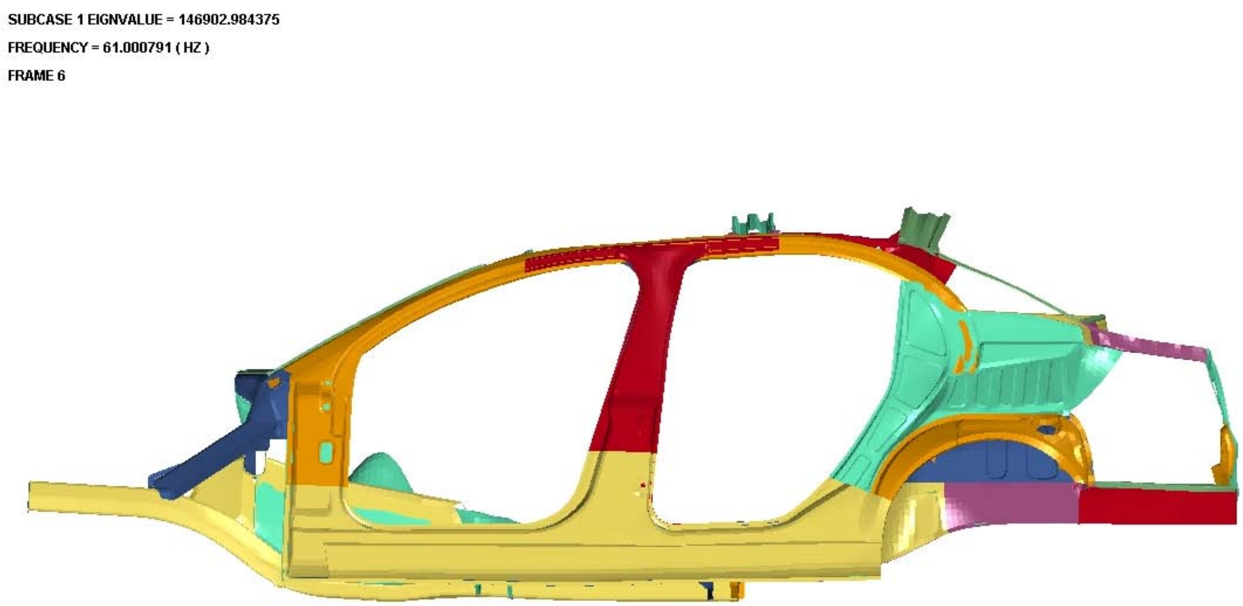

FIGURE 39: Bending Mode (Side View)

Figures 40 & 41 shows the strain energy plots for the Upper and Lower Package Tray joints, indicating potential for improvement.

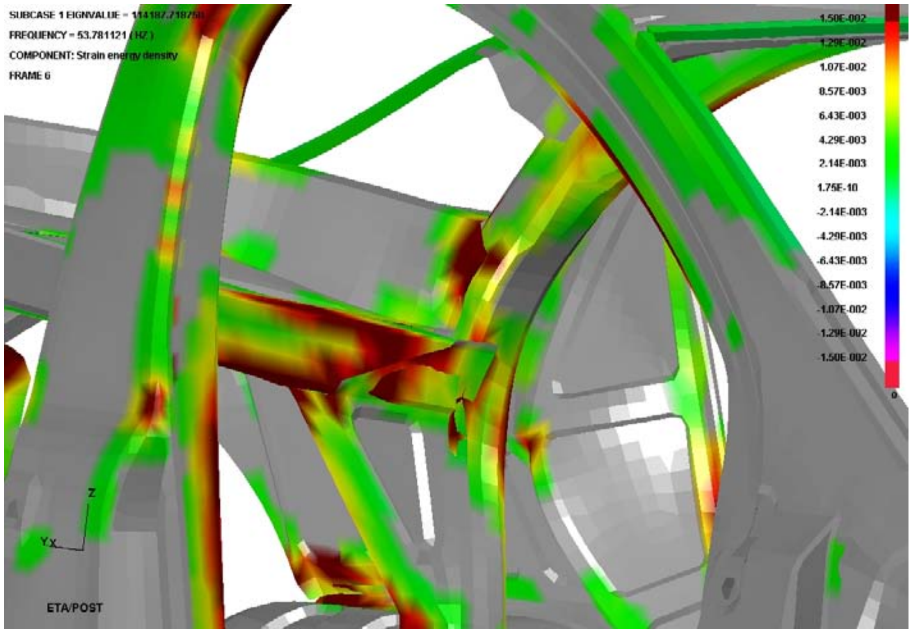

FIGURE 40: Torsion Mode Strain Energy Plot – Package Tray Area Upper Joint

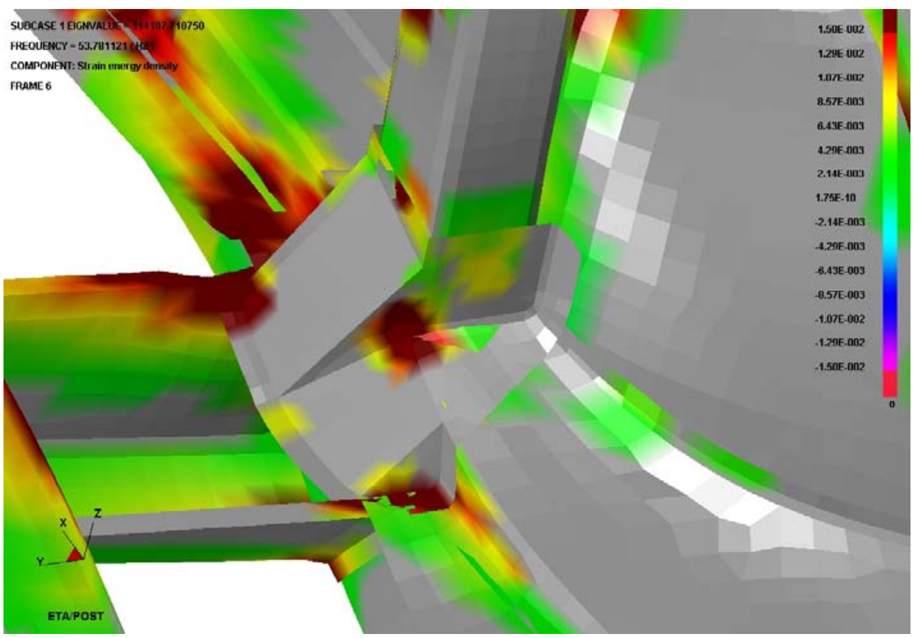

FIGURE 41: Torsion Mode Strain Energy Plot – Package Tray Area Lower Joint

After reviewing the initial results, design modifications were made to more evenly distribute the load around the Package Tray, resulting in improved performance without any mass penalty. Figure 42 shows the current design, Figure 43 the revision.

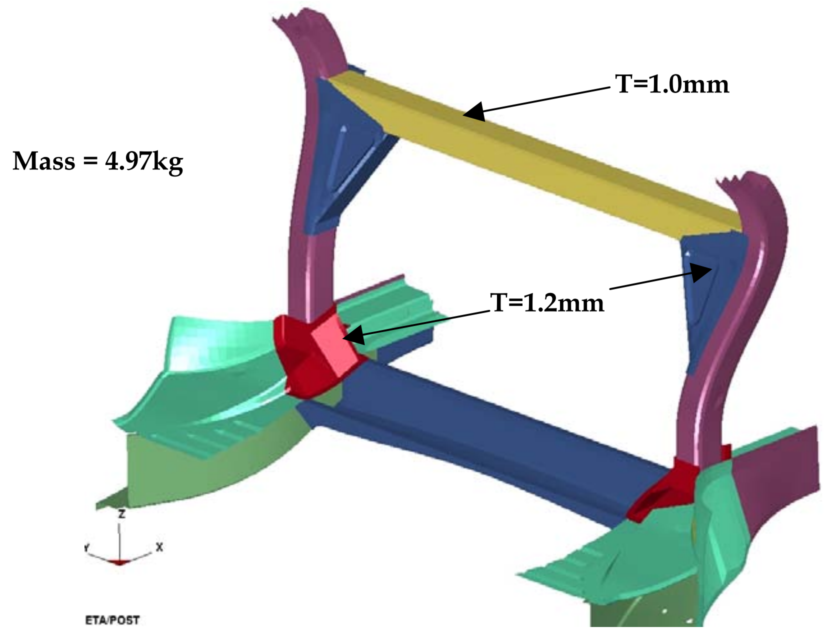

FIGURE 42: Package Tray FGPC-ACD Design

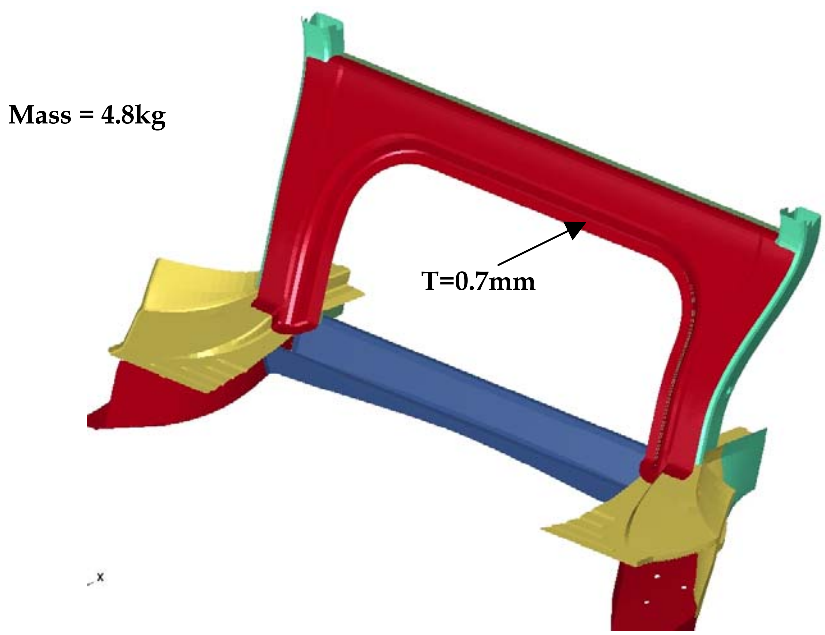

FIGURE 43: Package Tray FGPC-ACD Modified Design

The mode shapes for the revised Package Tray design are shown in the following figures, Figures 44 & 45 show the torsional mode at 55.3Hz and Figures 46 & 47 show the bending at 61Hz.

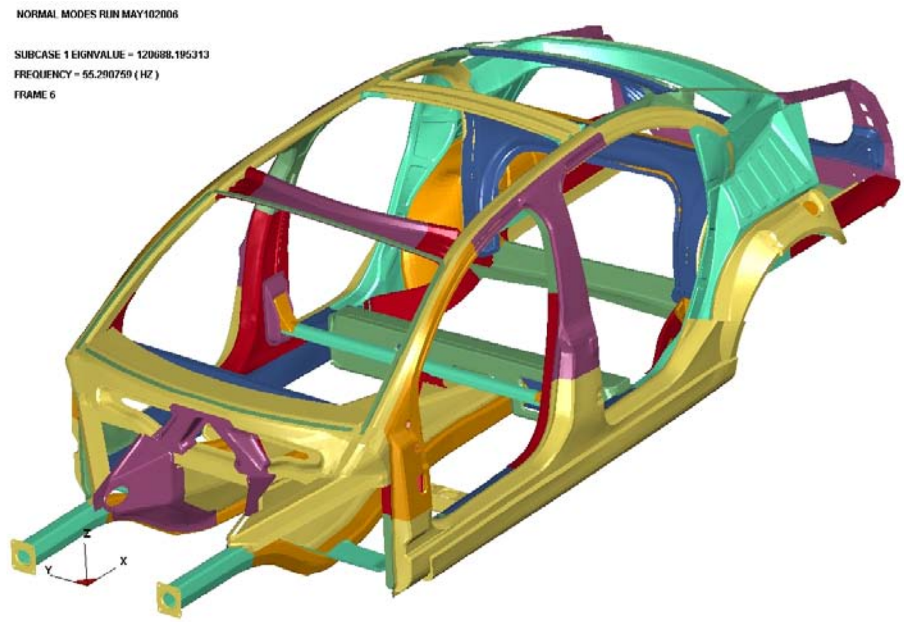

FIGURE 44: Torsion mode (ISO View)

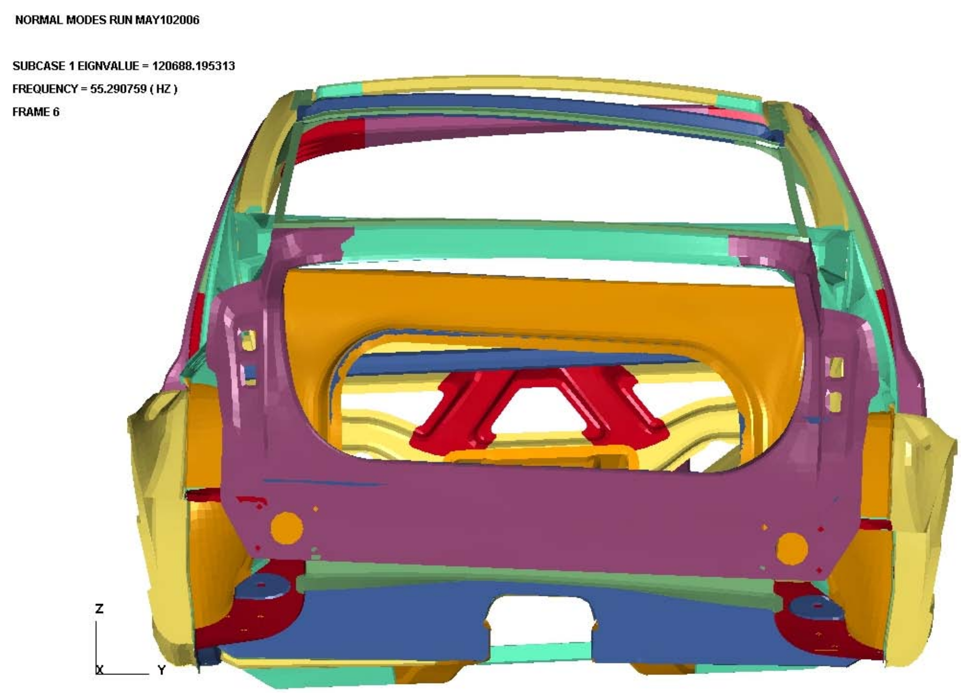

FIGURE 45: Torsion Mode (Rear View)

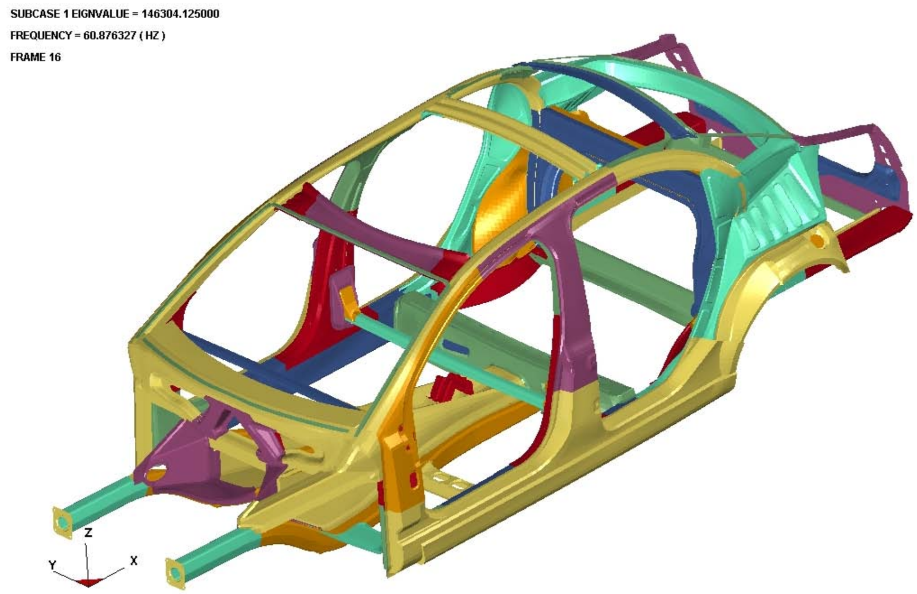

FIGURE 46: Bending Mode (ISO View)

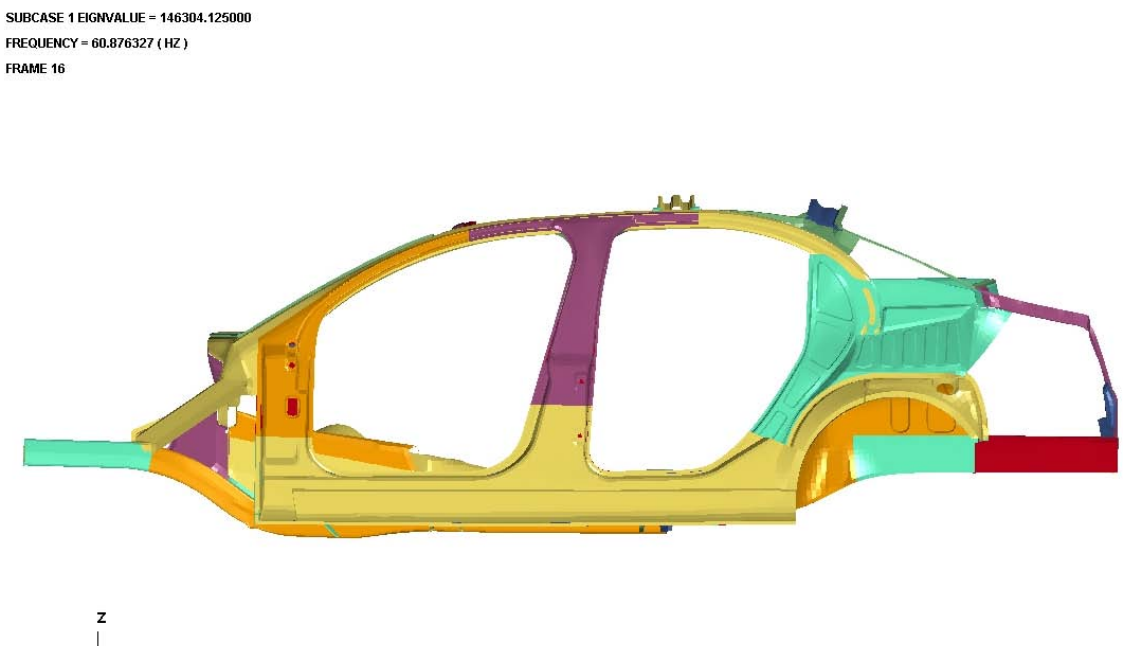

FIGURE 47: Bending Mode (Side View)

Figures 48 & 49 shows the strain energy plots for the revised Upper and Lower Package Tray joints.

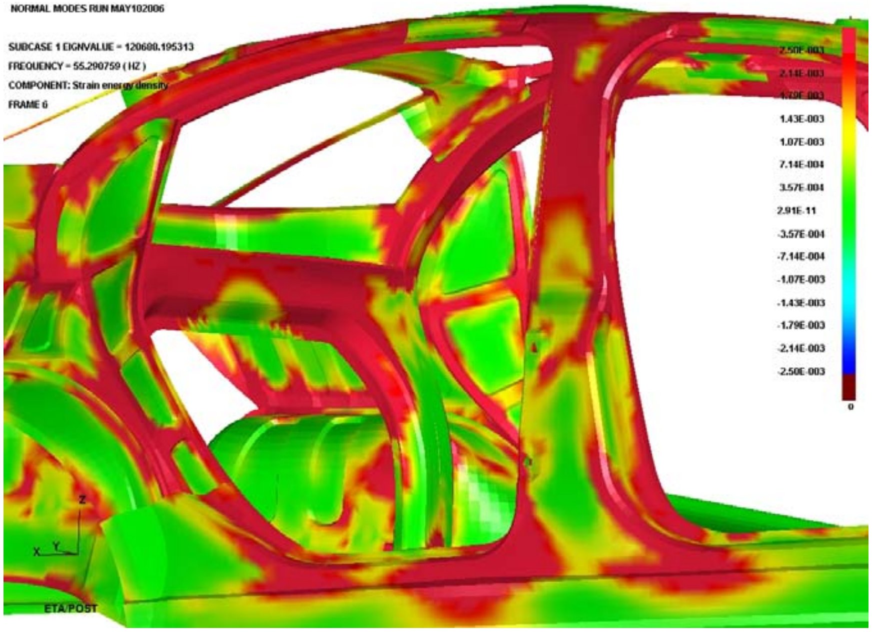

FIGURE 48: Torsion Mode Strain Energy Plot – Package Tray Area Upper Joint

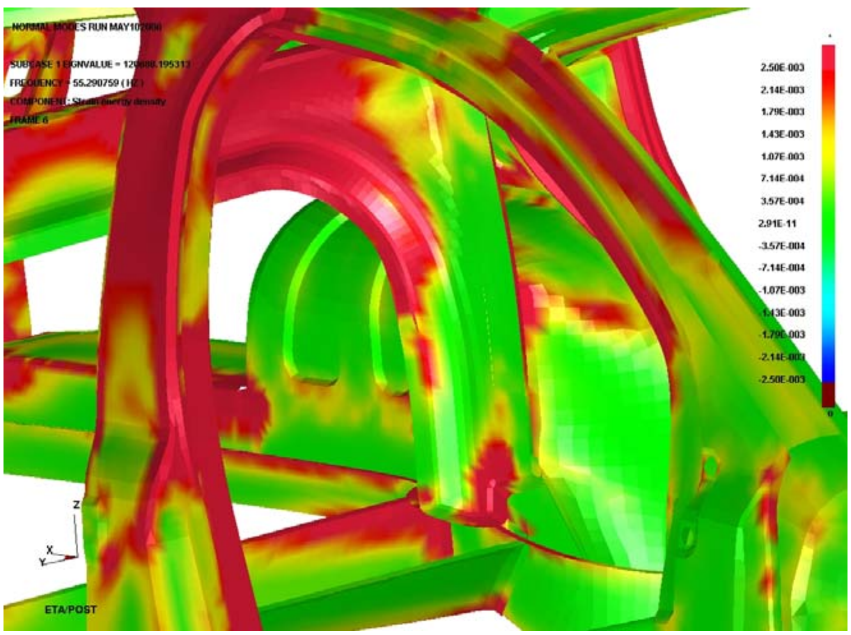

FIGURE 49: Torsion Mode Strain Energy Plot – Package Tray Area Lower Joint

Table 5 summarizes the complete results for the modal analysis.

NAME	TARGET (Hz)	FGPC-BO (Hz)	FGPC-AO (Hz)	FGPC-ACD (Hz)	Modified FGPC-ACD* (Hz)
Bending Frequency (BIP)	57	71	57	61	61
Torsion Frequency (BIP)	56	57	47	54	55.3

*Modified FGPC-ACD refers to the revised Package Tray design.

TABLE 5: Results for Modal Analysis

11.3. STATIC TORSION AND BENDING STIFFNESS

Static stiffness analysis was performed on the BIP model. The torsional and bending stiffnesses were compared to the target values. The deformed shapes are shown in Figures 50 & 51. Table 6 summarizes the complete results for the stiffness analysis.

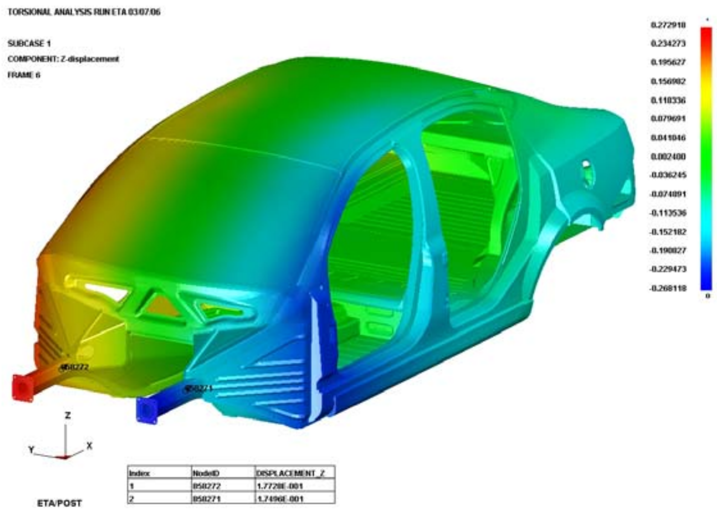

FIGURE 50: Static Torsional Stiffness – Deformed Shape

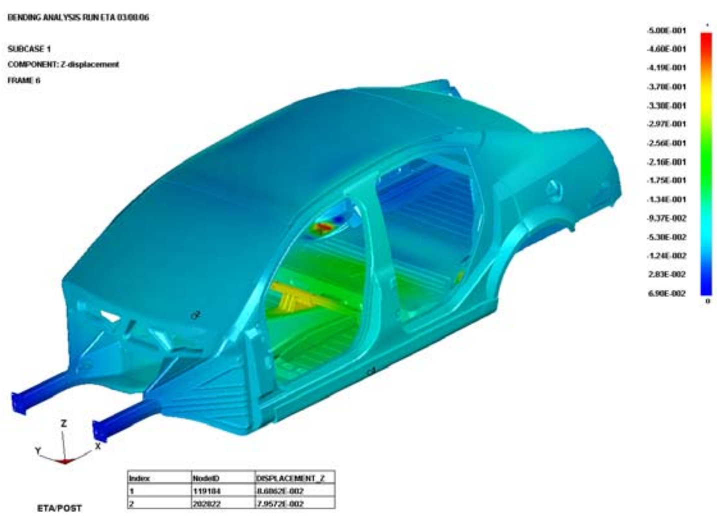

FIGURE 51: Static Bending Stiffness – Deformed Shape

NAME	TARGET	FGPC-BO	FGPC-AO	FGPC-ACD
Bending Stiffness	>12000N/mm	NA	8547N/mm	12500N/mm
Torsional Stiffness	>13000Nm/deg	NA	11192 Nm/deg	12496Nm/deg

TABLE 6: Results for the Static Bending and Torsional Stiffness

12. CONCLUSIONS

Table 7 summarizes the results of the Task 5.0: Concept Design Analysis Check loadcases. Note FGPC-ACD Final just missed the torsional modal and stiffness targets. These will be included as part of the design evaluation in the Task 6.0: Final Optimization.

LOADCASE	RESULT	NOTES
IIHS Front Crash 40% ODB	Not satisfied	Further analysis required to satisfy this regulation
FMVSS214 New Side Pole Impact	Not satisfied	Further analysis required to satisfy this regulation
IIHS Side Impact	Satisfied	
Roof Crush	Satisfied	
Door Intrusion	Satisfied	
Rear Crash	Satisfied	
Normal Modes (Free-Free)	Satisfied	Torsional mode just missed target, will be address as part of Task 6.0: Final Optimization
Bending/Torsional Stiffness	Satisfied	Torsional stiffness just missed target, will be address as part of Task 6.0: Final Optimization

TABLE 7: Task 5.0: Concept Design Analysis Check Results Summary

Table 8 summarizes the mass savings achieved by FGPC-ACD Final over the baseline FGPC-BO design. FGPC-AO is included for comparison.

ASSEMBLY	FGPC-BO (kg)	FGPC-AO (kg)	FGPC-ACD Final (kg)	Difference FGPC-BO to FGPC-AO		Difference FGPC-BO to FGPC-ACD Final	
				(kg)	(%)	(kg)	(%)
BIW (Body-In-White)	227.2	205.4	210.8	21.8	10	16.4	7
Door Beam	12.6	5.4	8.6	7.2	57	4.0	32
Total	239.8	210.8	219.4	29.0	12	20.4	9

TABLE 8: FGPC-ACD Final Mass Savings Over FGPC-BO (FGPC-AO Shown For Comparison)

APPENDIX A
IIHS FRONT CRASH 40% ODB REGULATIONS

Offset barrier crash tests are conducted at 40mph (64.4km/hr) with a 40% overlap. The test vehicle is aligned with the deformable barrier such that the right edge of the barrier face is offset to the left of the vehicle centerline by 10% of the vehicle's width. See Figure A1. The vehicle width is defined and measured as indicated in SAE J1100 – Motor Vehicle Dimensions, which states, "the maximum dimension measured between the widest part on the vehicle, excluding exterior mirrors, flexible mud flaps, and marker lamps, but including bumpers, moldings, sheet metal protrusions, or dual wheels, if standard equipment."

The vehicle is accelerated by the propulsion system at an average of 0.3g until it reaches the test speed and then is released from the propulsion system 25cm before the barrier. The onboard braking system, which applies the vehicle's service brakes on all four wheels, is activated 1.5sec after the vehicle is released from the propulsion system.

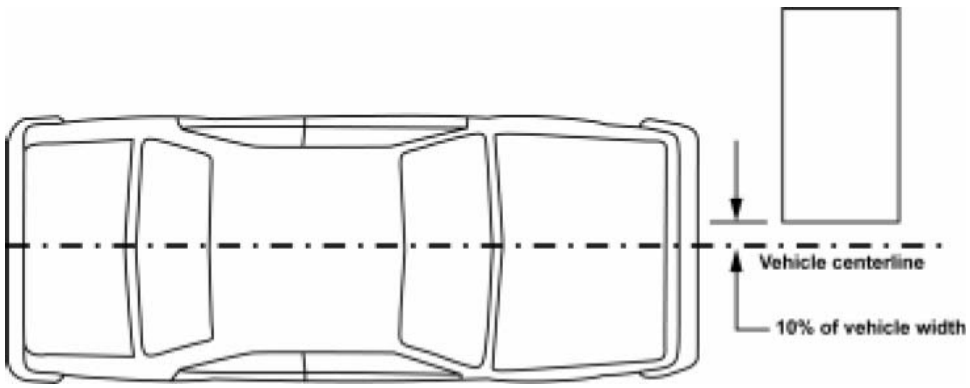

FIGURE A1: Vehicle Overlap with Deformable Barrier

MEASUREMENT POINT LOCATIONS

The following are the locations for measuring vehicle intrusion:

- **Steering column (one point)**
  The marked reference is the geometric center of the steering wheel, typically on the airbag door. After the crash, this point is measured by folding the airbag doors back into their undeployed position. In most cases, this measurement is probably less than the maximum intrusion into the compartment. However, if the steering column completely separates from the instrument panel (for example, due to shear module separation) during the crash, the steering column post-crash measurement is taken by placing and holding the wheel and column in its approximate maximum dynamic position as recorded on the high-speed film. The film may not always show clearly where the column was during the crash, and in such cases other clues would be needed to reposition the column for measurement. In rare instances, it may not be possible to obtain any meaningful post-crash measurement.
- **Lower instrument panel (two points)**
  The left and right lower instrument panel (knee bolster) lateral coordinates are defined by adding 15cm to and subtracting 15cm from the steering column reference lateral coordinate, respectively. The vertical coordinate is the same for both left and right references and is defined as 45cm above the height of the floor (without floormats). If the panel or knee bolster loosens or breaks away in the crash, the post-crash measurements are taken by pressing and holding the panel against the underlying structure.

- **Brake pedal (one point)**
  The geometric center of the brake pedal pad (top surface). If the brake pedal is constructed so that it dangles loosely after the crash, the brake pedal is pushed straight forward against the toepan/floorpan and held there to take the post-crash measurement. If the pedal drops away entirely, no post-crash measurement is taken.

- **Toepan (three points)**
  The vertical coordinate for all toepan measurement locations is the vertical coordinate of the brake pedal reference. The lateral coordinates of the left, center, and right toepan locations are obtained by adding 15cm to, adding 0cm to, and subtracting 15cm from the brake pedal reference lateral coordinate, respectively. The longitudinal coordinate is measured and a mark is temporarily placed at the locations on the toepan. A utility knife is used to cut a small “V” in the carpet and underlying padding at each point on the toepan. The point of the “V” is peeled back, and the exposed floor is marked and measured. The carpet and padding are then refitted prior to the crash.

- **Left footrest (one point)**
  The vertical coordinate for the footrest measurement location is the vertical coordinate of the brake pedal reference. The lateral coordinate of the footrest is obtained by adding 25cm to the brake pedal reference lateral coordinate. The same procedure described above for cutting the carpet is used to mark and measure the underlying structure. In cases where there is a specific footrest construct at the footrest measurement location, the construct is removed and the underlying structure is marked and measured. The construct is reinstalled prior to the crash.

- **Seat bolts (typically, four points)**
  Each of the four (or fewer) bolts that anchor the driver seat to the floor of the vehicle.

- **A-Pillar (one point)**
  The A-Pillar is marked on the outside of the vehicle at the same vertical coordinate as the base of the left front window.

- **B-Pillar (one point)**
  The B-Pillar is marked on the outside of the vehicle at the longitudinal center of the pillar at the same vertical coordinate as the lower A-Pillar mark.

APPENDIX B

SIDE POLE IMPACT (FMVSS214 NEW) REGULATIONS

The vehicle is propelled at 20mph into a 10in diameter pole at an angle of 75 degrees to its longitudinal axis, as shown in Figure B1. The pole is lined up with the center of the occupant's head. The occupant may be either a 50th percentile male at the mid-track seat position, or a 5th percentile female at the full forward seat position.

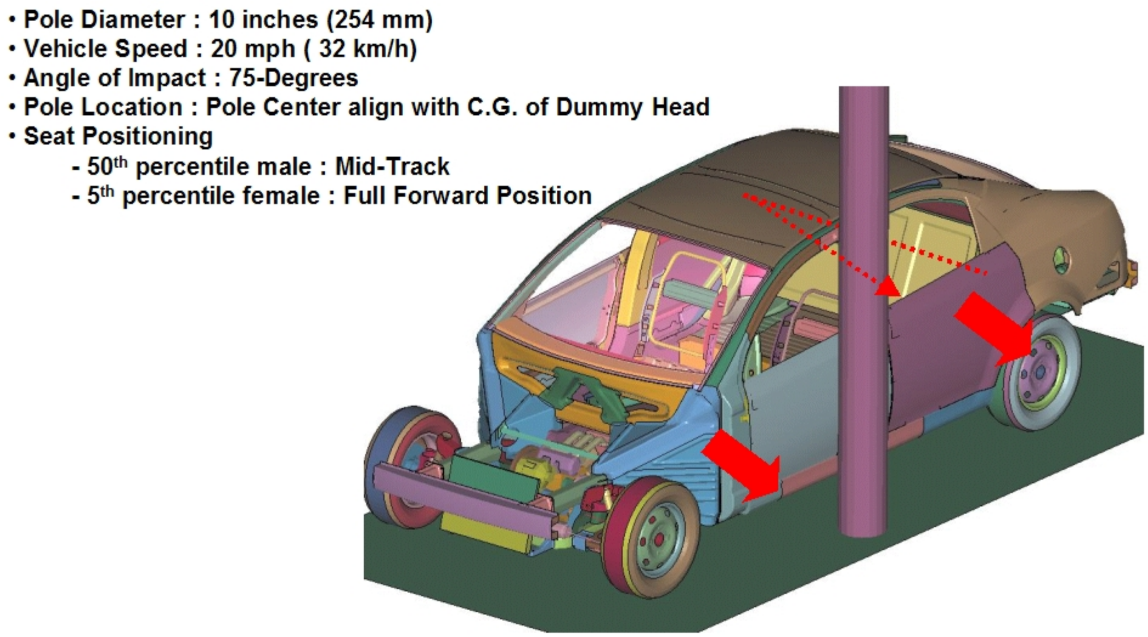

FIGURE B1: Pole Impact

APPENDIX C
IIHS SIDE IMPACT REGULATIONS

The IIHS Side Impact regulations state that a 1500kg MDB (Moving Deformable Barrier) strike the stationary test vehicle on the driver's side at a speed of 50km/hr and an angle of 90 degrees. The barrier block is made from aluminum honeycomb, and has 379mm ground clearance. The front aluminum mounting plate has been raised 100mm higher off the ground and has been extended 200mm taller than a standard FMVSS214 barrier. The longitudinal impact point of the barrier on the side of the test vehicle is dependent on the vehicle's wheelbase. The IRD (Impact Reference Distance) is defined as the distance rearward from the test vehicle's front axle to the closest edge of the deformable barrier when it first contacts the vehicle. See Figure C1.

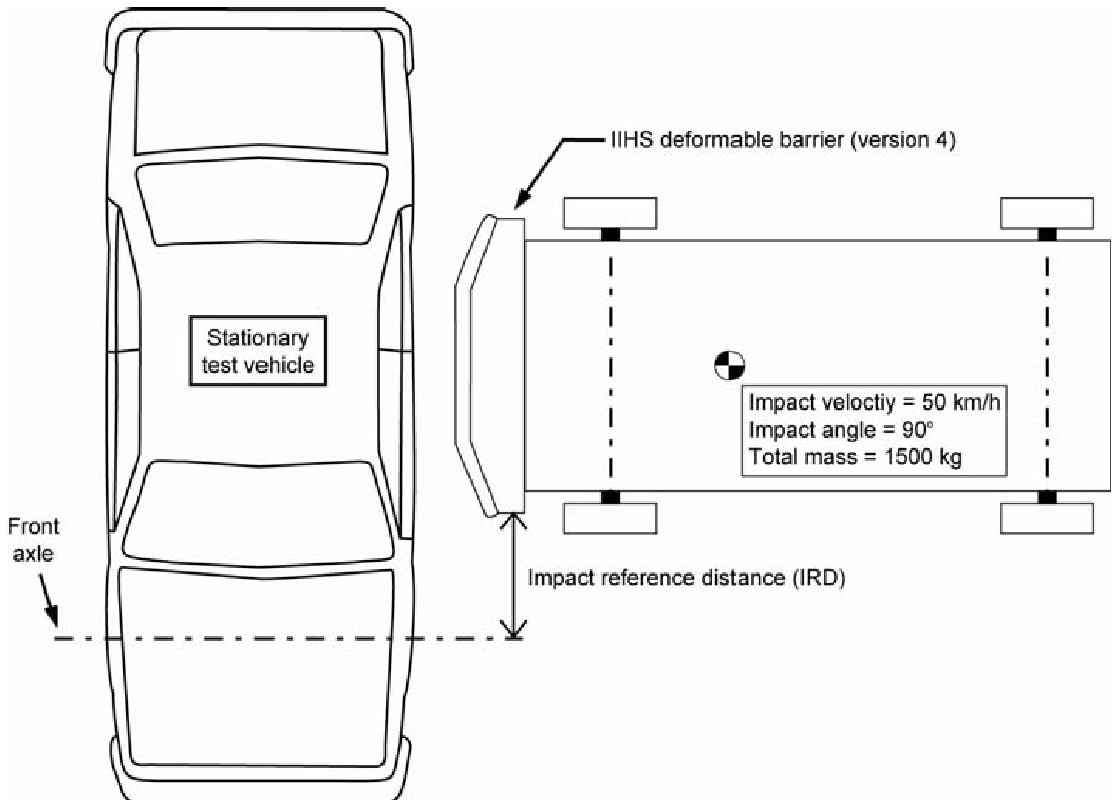

FIGURE C1: Moving Deformable Barrier Alignment with Test Vehicle

The structural rating requirements are shown in Figure C2.

Boundary line	Good	Acceptable	Marginal	Poor
B-pillar to driver seat centerline distance (cm)	12.5	5.0	0.0	
Structural failures	Downgrade structural rating by one category			

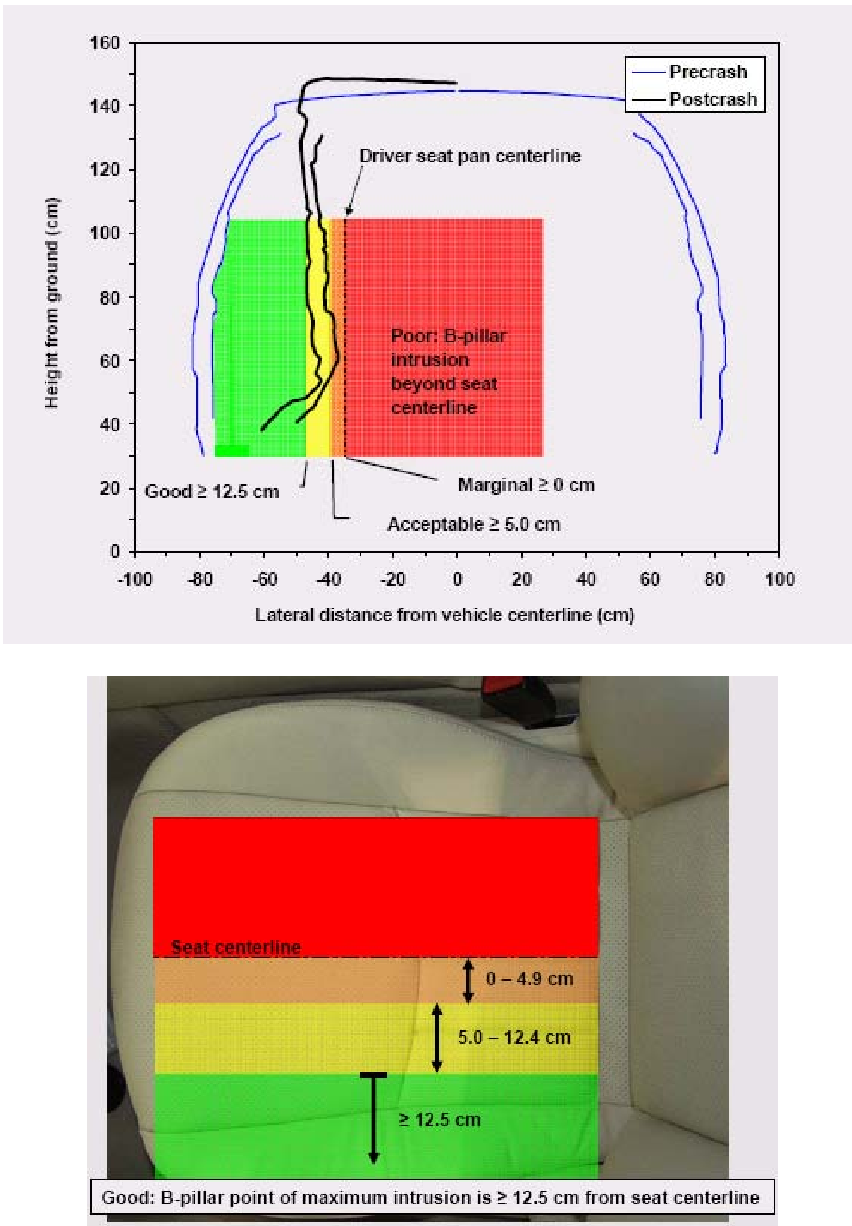

FIGURE C2: Structural Rating (B-Pillar Deformation)

APPENDIX D
ROOF CRUSH (FMVSS216) REGULATIONS
TEST DEVICE
The test device is a rigid unyielding block with its lower surface formed as a flat rectangle 30 x 72in.

TEST PROCEDURE
Place the sills or chassis frame of the vehicle on a rigid horizontal surface, fix the vehicle rigidly in position, close all windows, close and lock all doors, and secure any convertible top or removable roof structure in place over the passenger compartment.

Orient the test device as shown in Figure D1, so that

1. Its longitudinal axis is at a forward angle (side view) of 5 degrees below the horizontal and is parallel to the vertical plane through the vehicle's longitudinal centerline.
2. Its lateral axis is at a lateral outboard angle, in the front view projection, of 25 degrees below the horizontal.
3. Its lower surface is tangent to the surface of the vehicle.
4. The initial contact point, or center of the initial contact area, is on the longitudinal centerline of the lower surface of the test device and 10in from the forward most point of that centerline.

Apply force in a downward direction perpendicular to the lower of the test device at a rate of not more than 0.5in/sec until reaching a force of 1.5 x the unloaded vehicle weight of the tested vehicle or 5000lb, whichever is less. Complete the test within 120sec. Guide the test device so that throughout the test it moves, without rotation, in a straight line with its lower surface oriented as specified in 1 through 4.

A test device shall not move more than 5in, when it is used to apply a force of 1.5 x the unloaded vehicle weight or 5000lb, whichever is less, to either side of the forward edge of vehicle's roof in accordance with the procedure. Both the left and right front portions of the vehicle's roof structure shall be capable of meeting the requirements, but a particular vehicle need not meet further requirements after being tested at one location.

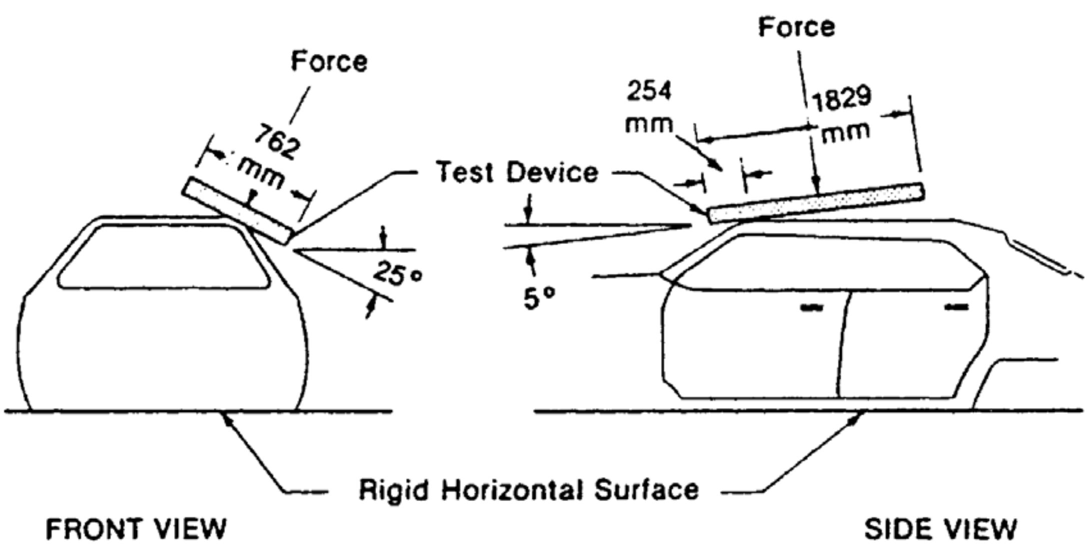

FIGURE D1: Test Device Location and Application To The Roof

APPENDIX E
DOOR INTRUSION (FMVSS214) REGULATIONS
BARRIER SPECIFICATION

The barrier is a rigid cylinder 12in in diameter and 25in overall height. See Figure E1.

BARRIER POSITION

The following applies to both front and rear doors:

- Longitudinal Position
  The central axis of cylindrical barrier is located at the middle of the line 5in (127mm) above the lowest point of the door system.
- Lateral Position
  The circumference of the cylindrical barrier is 5mm away from the outer most surface of the door system.
- Vertical Position
  The bottom of cylindrical barrier should be lined up with the line 5in (127mm) above the lowest point of the door system.

PERFORMANCE REQUIREMENTS

According to FMVSS 214 static regulation, there are three criteria based on the barrier forces

- Initial crush resistance is the average barrier force from 0 to 6in of barrier advancement and shall not be less than 2250lb. The average barrier force is obtained by integrating the barrier force with respect to the crush distance from 0 to 6in. and then dividing it by the crush distance of 6in.
- Intermediate crush resistance is the average barrier force from 0 to 12in of barrier advancement and shall not be less than 3500lb. The average barrier force is obtained by integrating the barrier force with respect to the crush distance from 0 to 12in and then dividing it by the crush distance of 12in.
- Peak crush resistance is the largest force recorded over the entire 18in. crush distance and shall not be less than 7000lb or 2 x the curb weight of the vehicle, whichever is less.

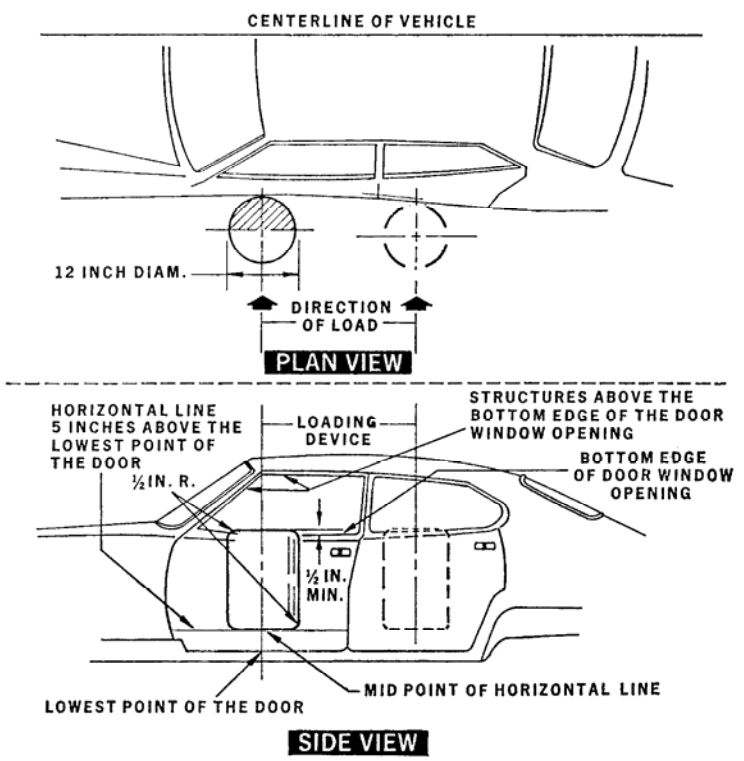

FIGURE E1: ***Loading Device Locations and Application To The Doors***

APPENDIX F
REAR CRASH (FMVSS301) REGULATIONS
TEST REQUIREMENTS

Each passenger car and each multipurpose passenger vehicle, truck and bus with a GVWR of 10000lb or less shall meet the requirements. When the vehicle is impacted from the rear by a barrier moving at 48 km/hr, fuel spillage shall not exceed the limits of the followings. Fuel spillage in any fixed or moving barrier crash test shall not exceed 28g from impact until motion of the vehicle has ceased, and shall not exceed a total of 142g in the 5min period following cessation of motion. For the subsequent 25min period, fuel spillage during any 1min interval shall not exceed 28g.

TEST CONDITIONS

Where a range is specified, the vehicle must be capable of meeting the requirements at all points within the range. The following conditions apply to all tests.

- The fuel tank is filled to any level from 90 to 95% of capacity with Stoddard solvent, having the physical and chemical properties of Type 1 solvent.
- The fuel system other than the fuel tank is filled with Stoddard solvent to its normal operating level.
- In meeting the requirements, if the vehicle has an electrically driven fuel pump that normally runs when the vehicle's electrical system is activated, it is operating at the time of the barrier crash.
- The parking brake is disengaged and the transmission is in neutral, except that in meeting the requirements of S6.5 the parking brake is set.
- Tires are inflated to manufacturer's specifications.
- The vehicle, including test devices and instrumentation.

REAR MOVING BARRIER TEST CONDITIONS

The rear moving barrier, see Figure F1, test conditions and the positioning of the barrier and the vehicle is as followings. The barrier and test vehicle are positioned so that at impact

- The vehicle is at rest in its normal attitude
- The barrier is traveling at 48 km/hr with its face perpendicular to the longitudinal centerline of the vehicle
- A vertical plane through the geometric center of the barrier impact surface and perpendicular to that surface coincides with the longitudinal centerline of the vehicle.

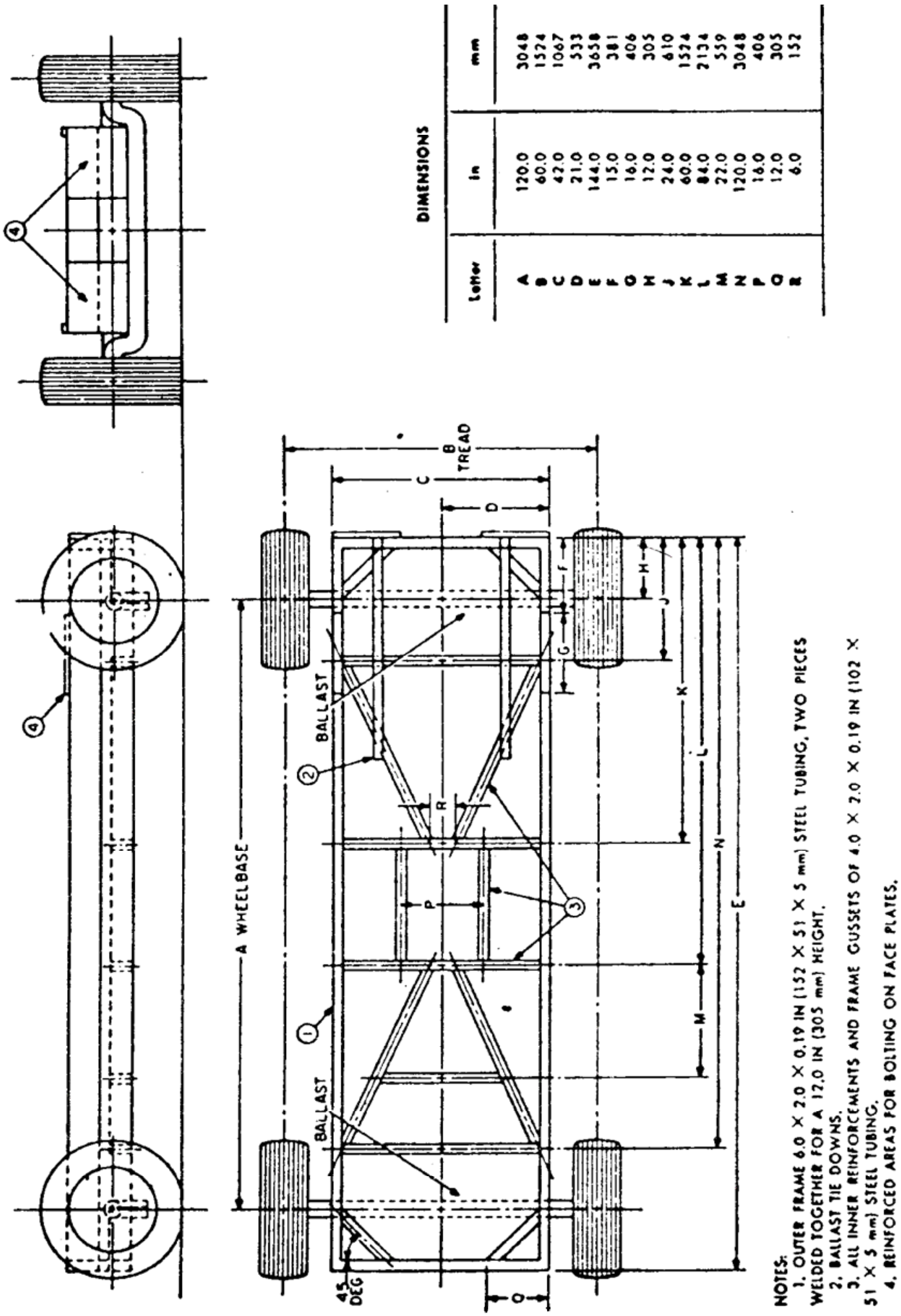

FIGURE F1: Common Carriage for Moving Barriers

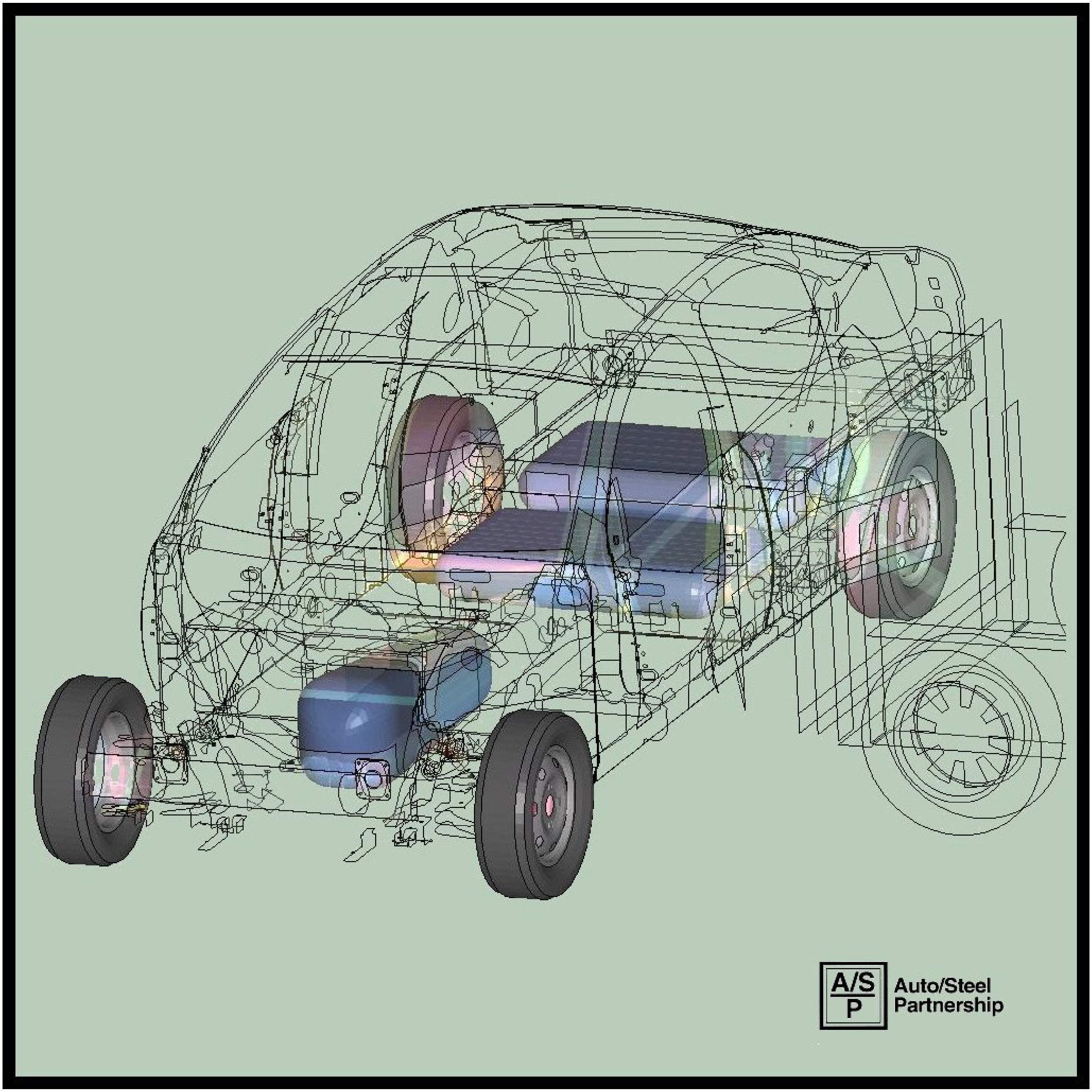

Future Generation Passenger Compartment
Task 5.5 - Concept Design Check Supplement

Design changes necessary to satisfy the requirements of IIHS Front Crash 40% ODB & Side Pole Impact (FMVSS 214 New)

Task 5.5 - Concept Design Check Supplement

Table of Contents

Task 5.5 - Concept Design Check Supplement

1. INTRODUCTION

This report completes Task 5.5: Concept Design Check Supplement of the FGPC (Future Generation Passenger Compartment) project. Its purpose is to document the design changes necessary to allow FGPC to satisfy the targets of IIHS Front Crash 40% ODB and Side Pole Impact (FMVSS 214 New).

The analysis performed under Task 5.0: Concept Design Analysis Check demonstrated that the FGPC could meet all the requirements relating to the safety cage. However, the structure was unable to satisfy the requirements of IIHS Front Crash 40% ODB and Side Pole Impact (FMVSS 214 New). Since these two requirements were not included as design constraints in the Task 3.0: Optimization. Upon review of the Task 5.0: Concept Design Analysis Check, A/SP decided that FGPC should satisfy both loadcases before beginning the Task 6.0: Final Optimization.

2. OBJECTIVE

The objective of this task is to improve the performance of the FGPC-ACD vehicle structure so that it meets or exceeds the performance of the pre-optimization FGPC-BO with respect to both IIHS Front Crash and FMVSS214 New Pole Impact loadcases. This will be achieved by,

- Developing new load paths to translate and dissipate loads as necessary
- Develop an intergraded solution that is both mass efficient and manufacturable

3. REGULATIONS

Detailed specifications are described in Appendices A & B.

4. IIHS FRONT CRASH 40% ODB

4.1. TARGET

- Rocker cross-sectional forces
  Section forces should meet or exceed those of the FGPC-BO.
- Door open-ability
  Doorframe deformation should not exceed FGPC-BO levels (minimal relative displacement with respect to the A & B-Pillars).

4.2. LOADS AND BOUNDARY CONDITIONS

The vehicle impacts a deformable barrier, offset 10% from centerline (40% overlap), at 40mph. See Figures 1 & 2.

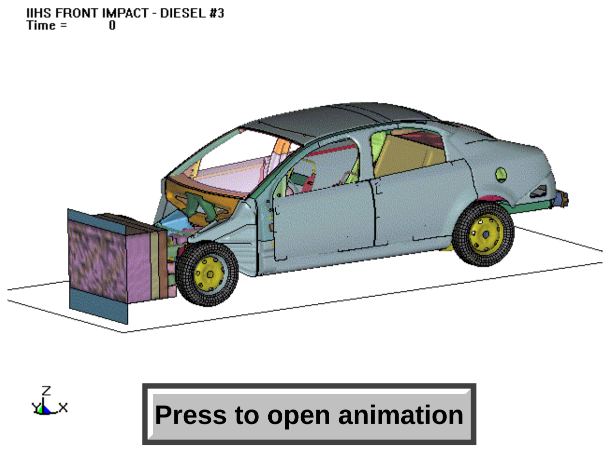

FIGURE 1: IIHS Side Impact Model (ISO View)

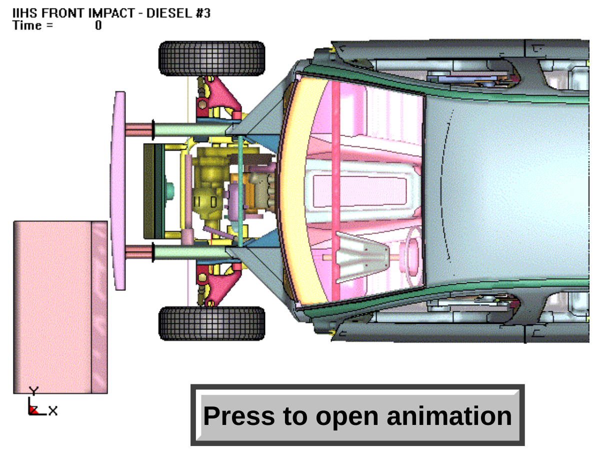

FIGURE 2: IIHS Side Impact Model (Top View)

Rocker cross-sectional forces and door open-ability were used to evaluate the vehicle's performance. The Door open-ability was measured in three locations: Top, Middle and Bottom. See Figure 3.

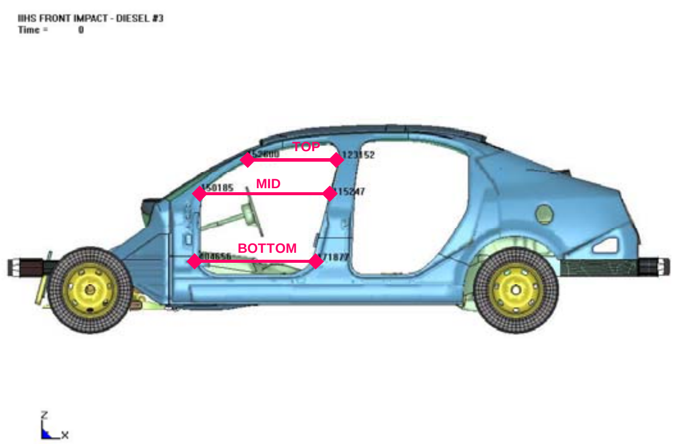

FIGURE 3: Door Open-Ability Measurement Points

4.3 BACKGROUND

The analysis performed for Task 5.0: Concept Design Check identified a weak performance of the FGPC-ACD structure under the IIHS Front Crash load condition. Table 1 and Figure 4 summarize the performance of both FGPC-BO and FGPC-ACD under this load condition.

MODELS	MASS (kg)	DOOR OPEN-ABILITY (mm)			ROCKER X-SECTIONAL FORCE (kN)
		TOP	MID	BOTTOM	
FGPC-BO	1351.1	2.5	8.2	17.0	121.5
FGPC-ACD	1327.3 (23.8 less)	15.1	126.7	169.0	41.7

Mass in brackets is normalized to FGPC-BO.

TABLE 1: IIHS Front Impact 40% ODB – FGPC-BO & FGPC-ACD

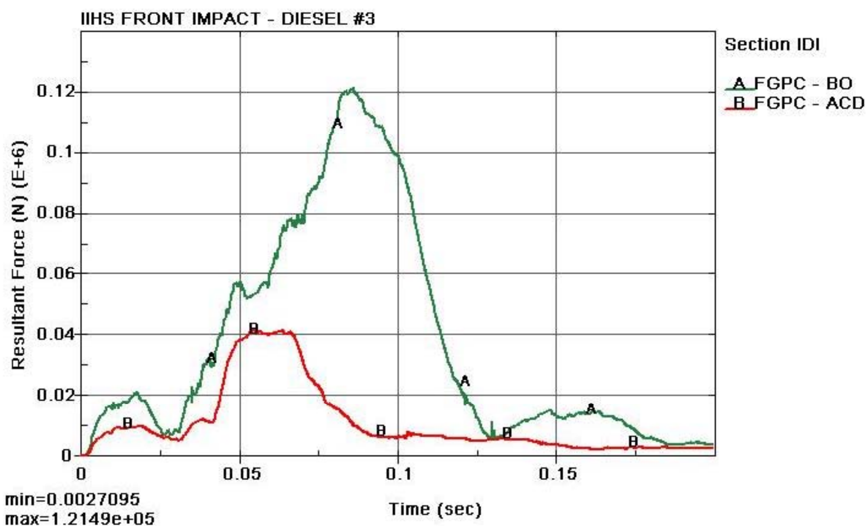

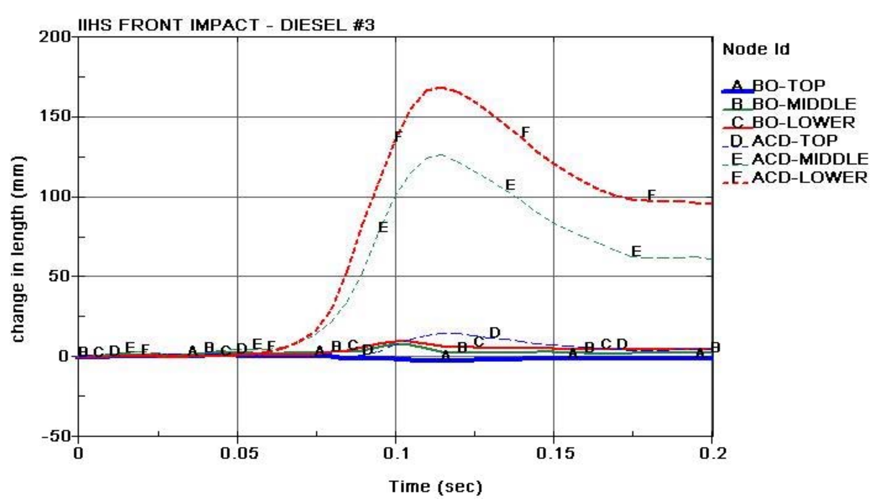

FIGURE 4: Rocker Cross-Sectional Forces & Door Open-Ability – FGPC-BO & FGPC-ACD

Figure 5 shows the deformation of the rocker and roof area for both FGPC-BO and FGPC-ACD.

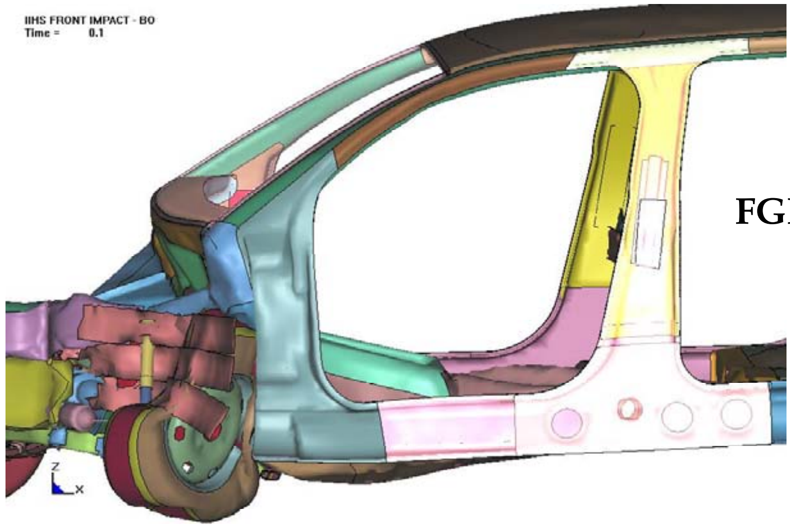

FGPC-BO

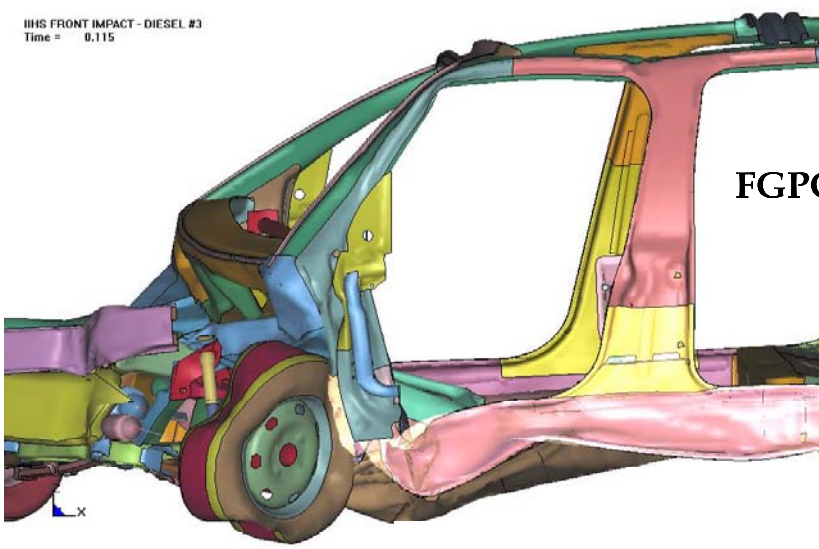

FGPC-ACD

FIGURE 5: IIHS 40% ODB – Rocker Deformation – FGPC-BO & FGPC-ACD

Press to open animation

4.4 RESULTS SUMMARY

Table 2 below summarizes the performance of all the analysis iterations completed. For comparison the results of the FGPC-BO and FGPC-ACD are included. Masses in brackets are normalized to FGPC-BO.

ITERATIONS	MASS (kg)*	DOOR OPEN-ABILITY (mm)			ROCKER X-SECTIONAL FORCE (kN)	NOTES
		TOP	MID	BOT		
FGPC-BO	1351.1	2.5	8.2	17.0	121.5	Before Optimization
FGPC-ACD	1327.3 (23.8 less)	15.1	126.7	169.0	41.7	After Concept Design
FGPC-ACD1a	1357.8 (6.7 more)	6.9	2.8	7.5	147.2	Tailored Rocker Inr (0.6/1.5), Roof Sd Rail (0.7/1.2)
FGPC-ACD2a	1354.4 (3.3 more)	6.1	57.0	53.0	79.2	Rocker (1.0/0.6)
FGPC-ACD3a	1352.4 (1.3 more)	12.4	90.7	99.9	41.3	Added Reinforcement to the Sub Frame
FGPC-ACD4a	1351.1 (0.0 more)	11.5	117.3	136.1	40.1	Changed Rocker Inr (31162) from Mart 1300 to Boron 1550. Change Rocker Otr (31470) from DP780 to Mart1300. Change B-Pillar Inr Lower (31208) from Boron 1550 to Mart 1330 Body Side Otr 31470 (1.0)
FGPC-ACD5a	1354.5 (3.4 more)	9.1	98.5	100.1	38.5	ACD4 /change Body Side OTR (1.0/1.25)
FGPC-ACD6a	1356.7 (5.6 more)	7.3	84.7	92.6	50.2	Rocker INR X-section change, Rocker Reinf1(0.6), holes X-mbr
FGPC-ACD7a	1361.5 (10.4 more)	5.6	47.0	39.3	83.4	Tailored Rocker INR (0.6/1.5/.08), Rocker REINF2 (1.5), holes X-mbr
FGPC-ACD8a	1363.9 (12.8 more)	10.0	29.9	18.2	129.0	Changes to ACD7: pid 11346 (0.7/1.5) & pid 31162 (0.6/1.5)
FGPC-ACD9a	1357.1 (6.0 more)	6.1	81.3	85.7	43.8	Rocker Tube (1.2)
FGPC-ACD10a	1359.7 (8.6 more)	6.1	37.9	32.5	161.2	Change the gauge of Rocker Inr & A-Pillar Inner TWB Lower" (1.5)
FGPC-ACD11a	1361.9 (10.8 more)	5.1	30.6	21.6	145.5	ACD10 + Body Side OTR (1.25) & A-Pillar Inr TWB Lower" (0.7 mm)
FGPC-ACD12a	1364 (12.9 more)	8.0	23.7	19.1		ACD11 + Rocker Reinf. A (0.6 mm between A & B-Pillar)
FGPC-ACD13a	1366 (14.9 more)	8.0	8.2	4.2	167.0	ACD11 + Rocker Reinf. A(1.2 mm between A & B-Pillar)
FGPC-ACD14a	1364.4 (13.3 more)	9.0	15.8	7.4	170.4	ACD11 + Rocker Reinf. B(1.2mm between A & B-Pillar)
FGPC-ACD15a	1365 (13.9 more)	6.5	9.1	3.1	180.6	ACD11 + Rocker 1.5/2.0/1.5 + Tube for side pole

* Masses in brackets are normalized to FGPC-BO.

TABLE 2: Iteration Summary

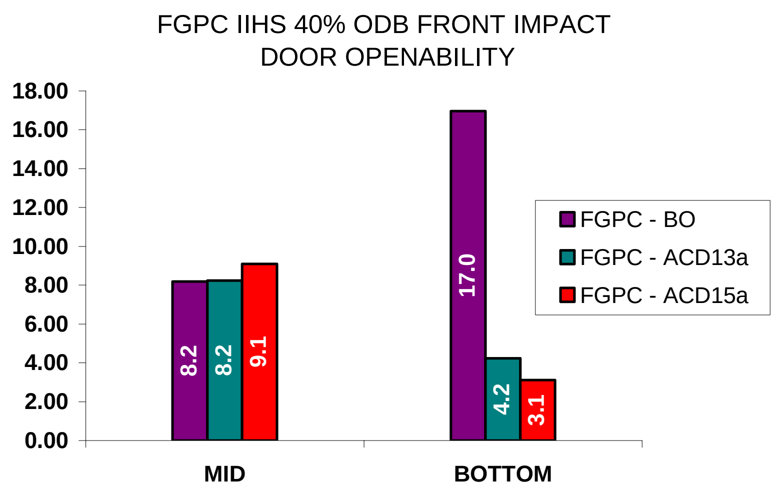

FIGURE 6: IIHS 40% ODB – Door Open-Ability

Figure 6 compares the door open-ability performance, at the Mid and Bottom positions, of FGPC-BO and the two most significant iterations FGPC-ACD13a and FGPC-ACD15a

4.5 DETAILED DISCUSSION OF KEY ITERATION RESULTS

In order to improve the IIHS Front Crash performance a variety of design variables were considered. The following is a detailed discussion of the key iterations.

Note, the IIHS Front Crash and Pole Impact iteration studies were executed in parallel and although they shared many key features, for simplicity they should be considered independently. IIHS Front Crash iterations have an "a" suffix, Pole Impact a "b."

4.5.1 FGPC-ACD1a

For the first iteration, FGPC-ACD1a, both the Rocker Inner and Member Body Side Inner were split into two pieces. The front half of each component was then up-gauged. See Figure 7. Comparison of the Rocker cross-sectional forces for FGPC-BO and FGPC-ACD1a are given in Figure 8.

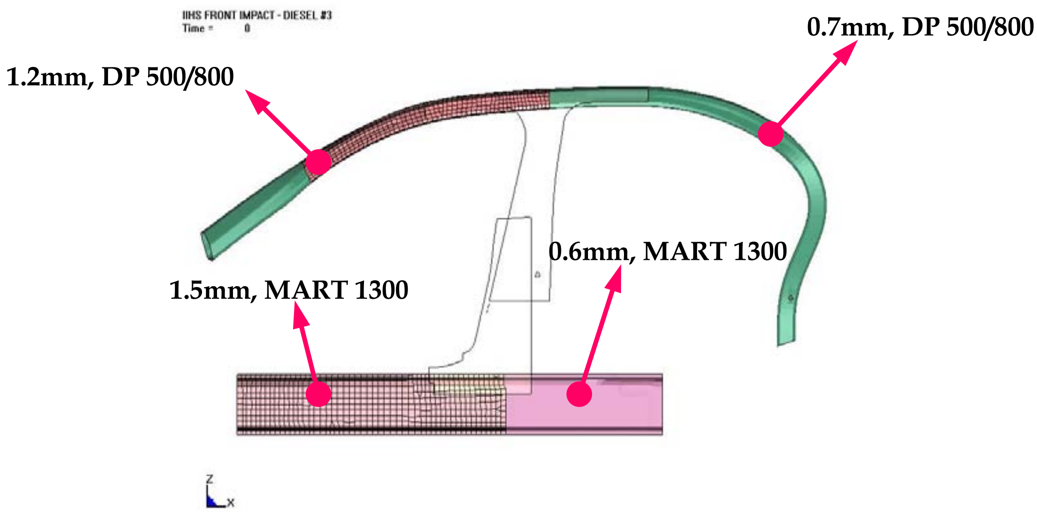

FIGURE 7: FGPC-ACD1a Geometry Revisions

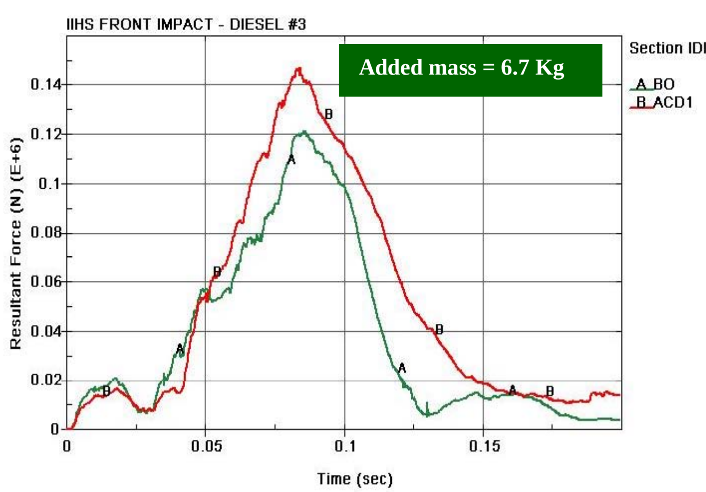

FIGURE 8: IIHS 40% ODB – FGPC-BO & FGPC-ACD1a Section Forces

Figure 9 shows the Rocker Inner deformation after the impact. Although the front portion of the Rocker Inner, between the A and B-Pillars, performs well, the deformation beyond the B-Pillar is very severe when compare to FGPC-BO. The result of this iteration confirms the need to improve the stiffness of the Rocker especially between the B and C-Pillars.

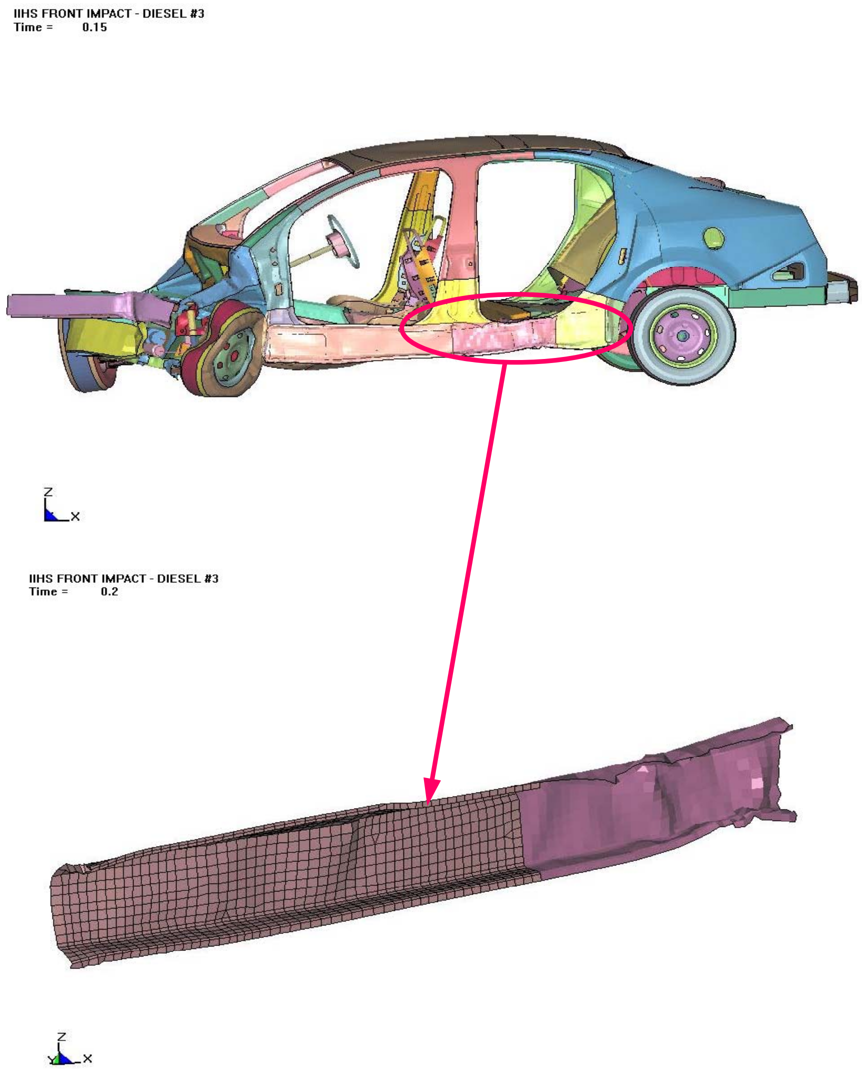

FIGURE 9: IIHS 40% ODB– FGPC-ACD1a Deformed Shape

Press to open animation **Press to open animation**

4.5.2 FGPC-ACD6a

For FGPC-ACD6a the Rocker Inner cross-section was locally refined and an additional inner reinforcement was added. See Figure 10. These modifications created Rocker Inner cross-section forces well below those of FGPC-BO resulting in major deformation of both the Rocker and Roof. See Figure 11.

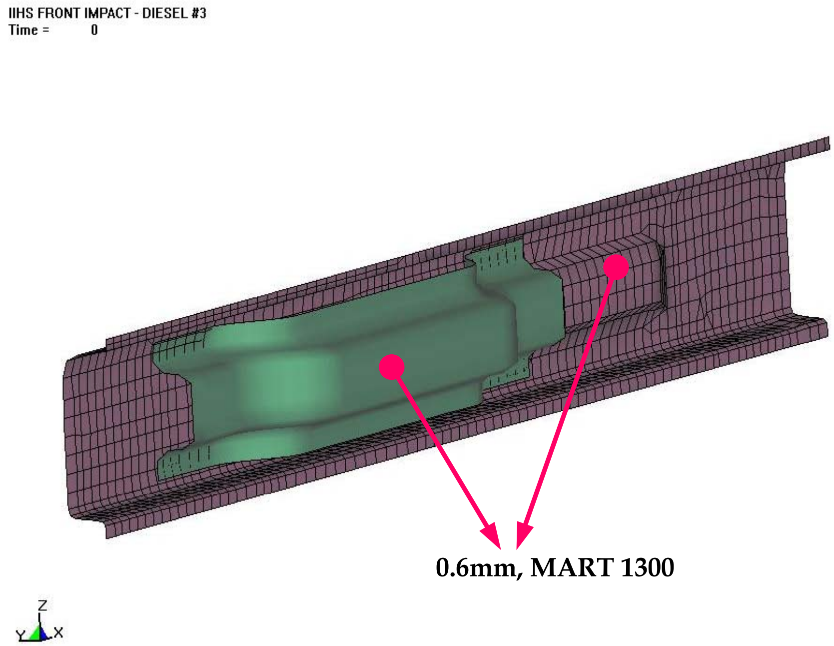

FIGURE 10: FGPC-ACD6a Geometry Revisions

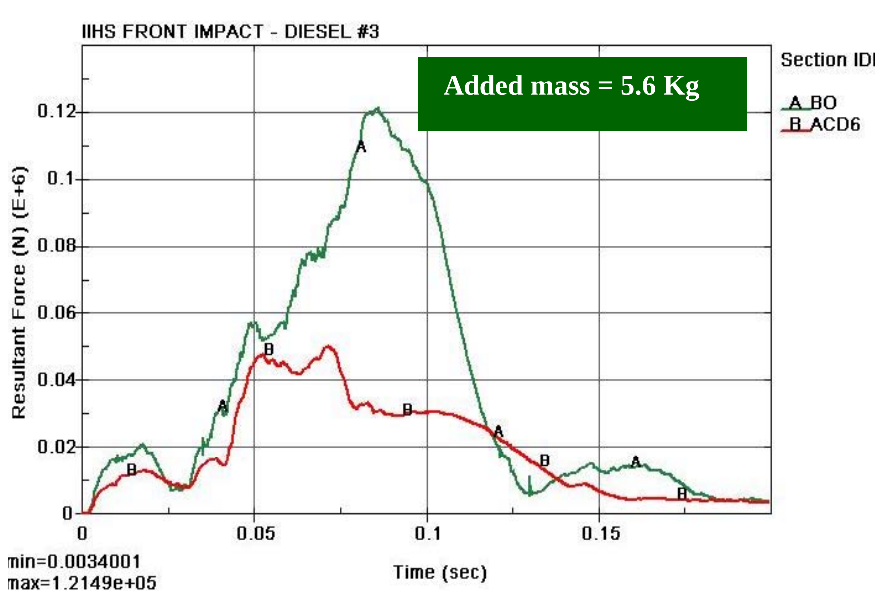

FIGURE 11: IIHS 40% ODB – FGPC-BO & FGPC-ACD6a Section Forces

Figure 12 shows a severe deformation in the lower A-Pillar, which not only affects the door open-ability but also caused the Roof Rail to buckle. Poor transition between the lower A-Pillar and the front of the new Rocker Inner Reinforcement was identified as the cause of the passenger compartment collapse.

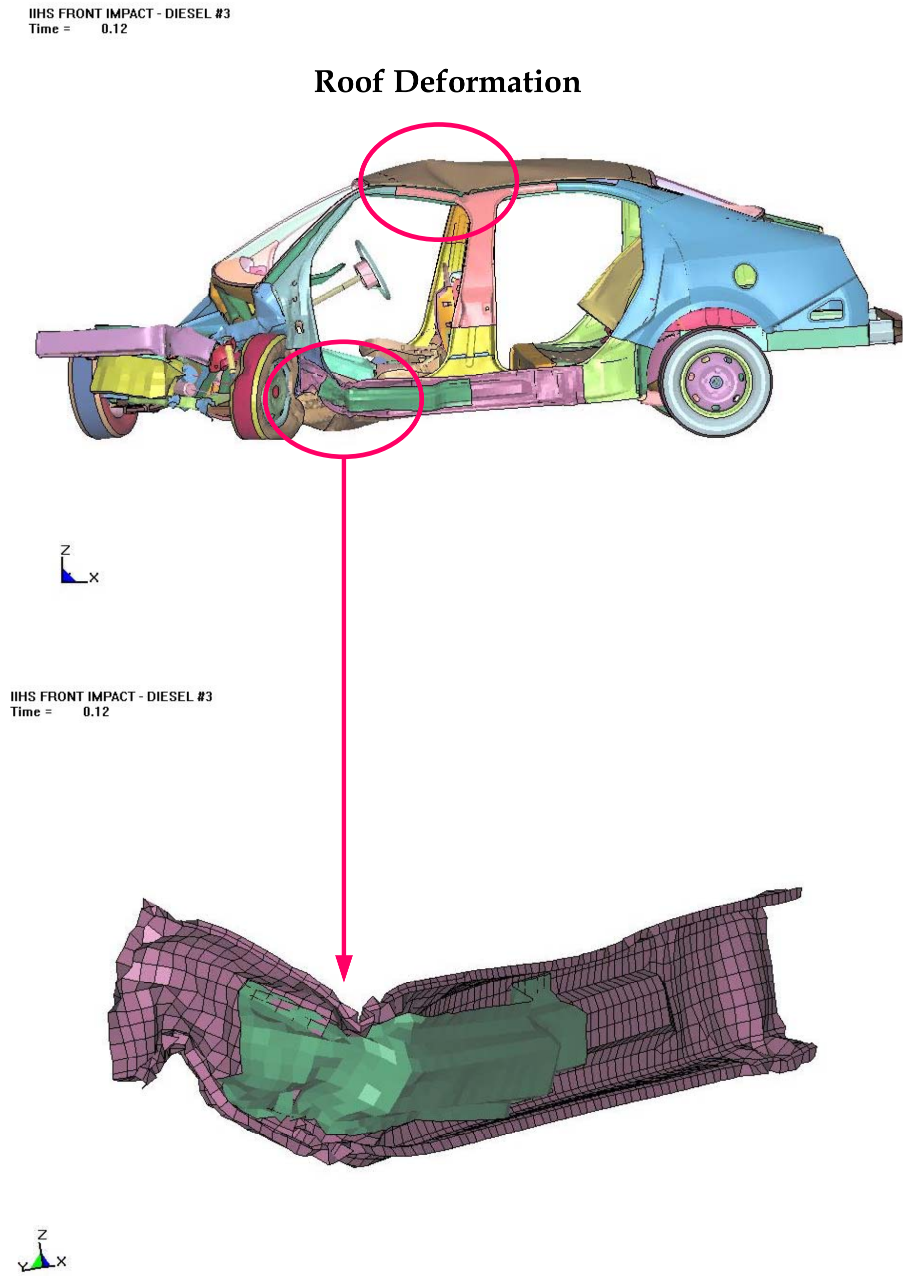

FIGURE 12: IIHS 40% ODB– FGPC-ACD6a Deformed Shape

Press to open animation

Press to open animation

4.5.3 FGPC-ACD7a

Iteration FGPC-ACD7a was set up based upon the results of the previous two iterations. The Rocker Inner was split into three different sections thus allowing a more uniform section change. The position and length of the Rocker Inner Reinforcement was also modified, adding additional stiffness to the Rocker. Figure 13 shows the design modifications and the Rocker Inner cross-section forces.

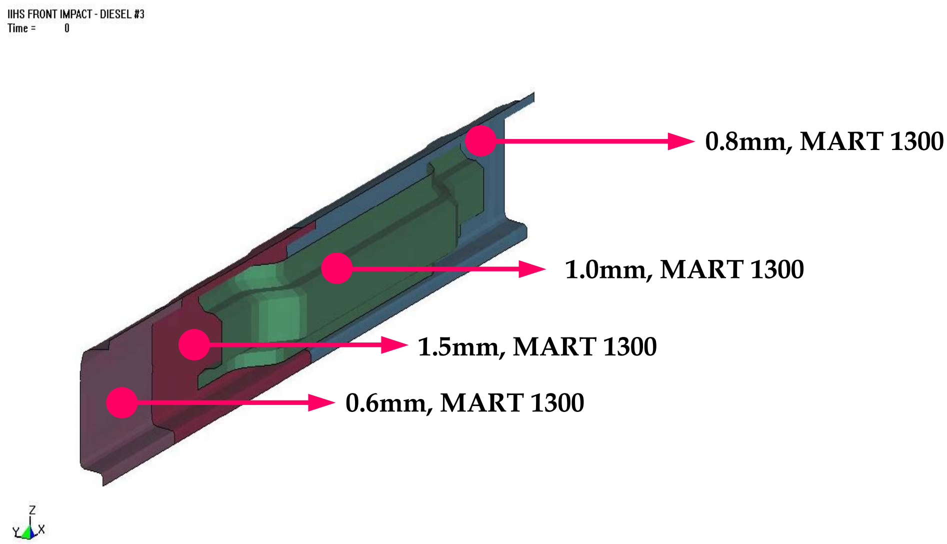

FIGURE 13: FGPC-ACD7a Geometry Revisions

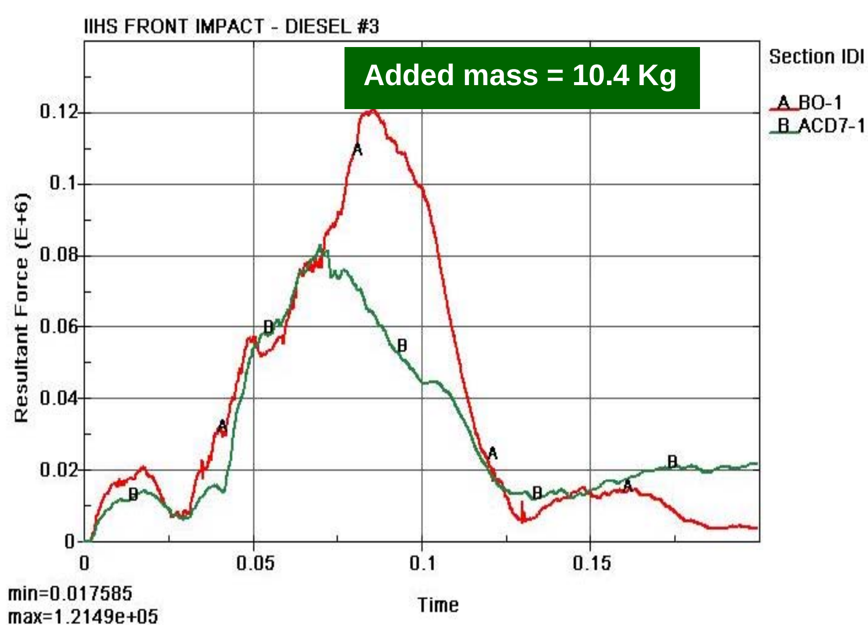

FIGURE 14: IIHS 40% ODB – FGPC-BO & FGPC-ACD7a Section Forces

Although the performance has improved over the previous iterations, there is still a sudden change in the structure's stiffness at the lower A-Pillar and the front portion of the Rocker Inner. This weakness allowed the structure to collapse. Figure 15 highlights both the Rocker and Roof Rail deformation.

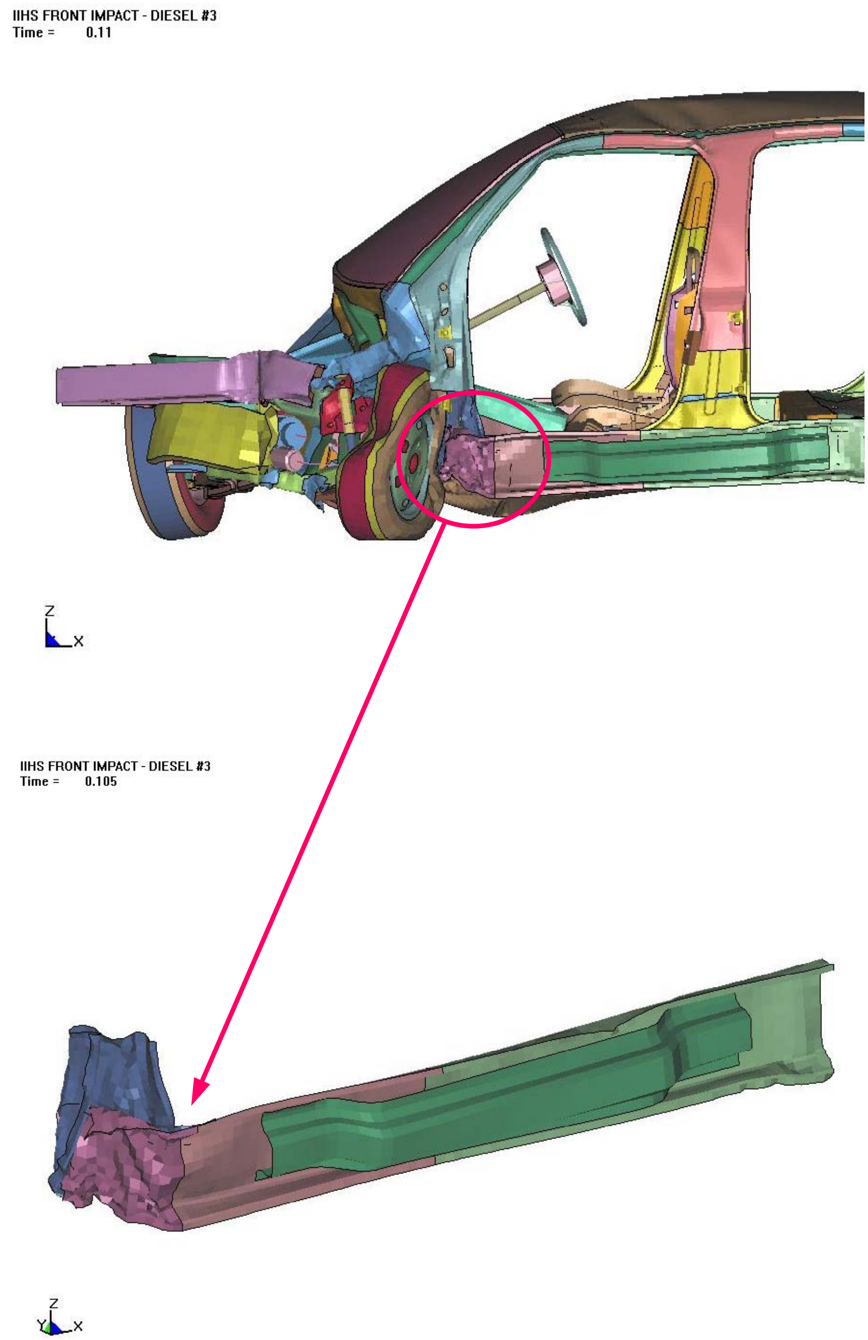

FIGURE 15: IIHS 40% ODB– FGPC-ACD7a Deformed Shape

Press to open animation

Press to open animation

4.5.4 FGPC-ACD13a

As Figure 16 illustrates, the Rocker Inner Reinforcement design was simplified from the previous iteration reviewed, FGPC-ACD7a. Its gauge was also increased to 1.2mm. The gauge of the Rocker Inner between the A and B-Pillars was also increased to 1.5mm. Although these modifications would add an additional 14.9kg to the FGPC-BO, the performance has been significantly improved. This iteration will be used as the baseline for further design iterations.

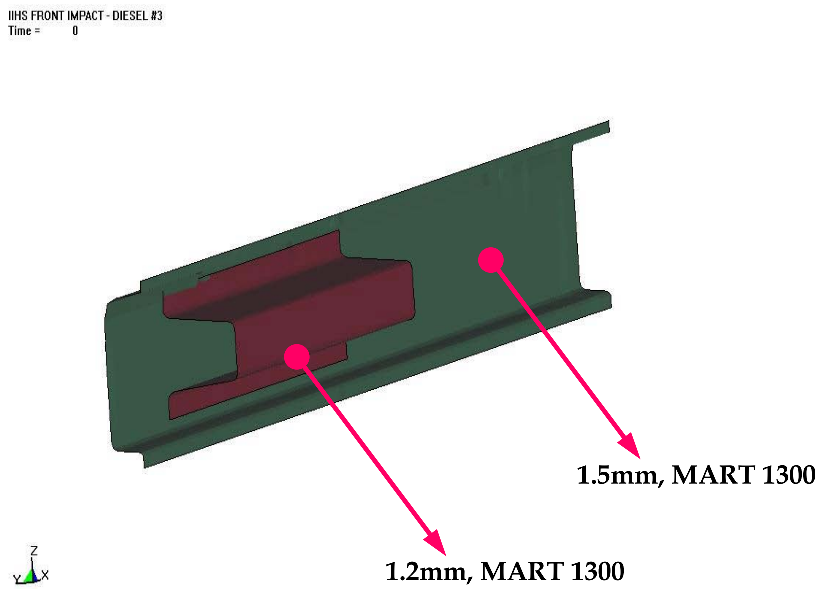

FIGURE 16: FGPC-ACD13a Geometry Revisions

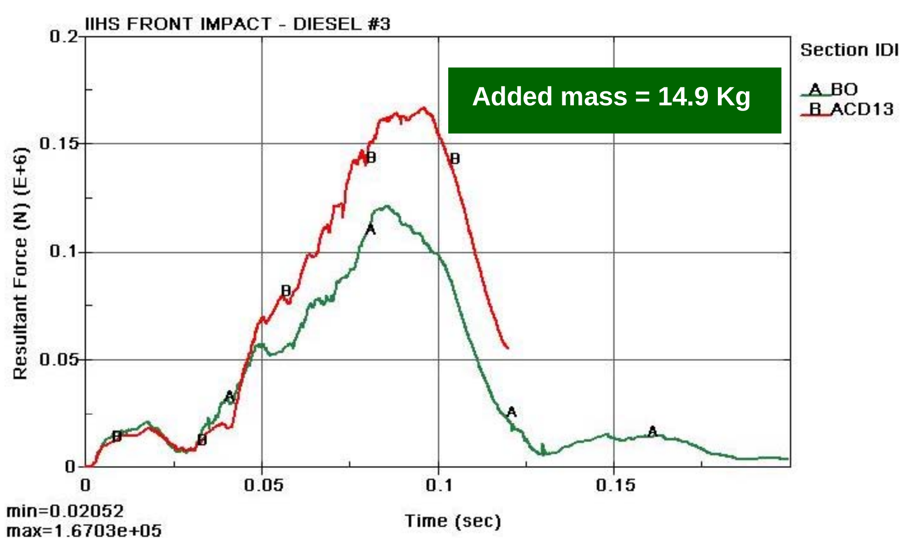

FIGURE 17: IIHS 40% ODB – FGPC-BO & FGPC-ACD13a Section Forces

Figure 18 shows the rocker deformation of FGPC-ACD13a.

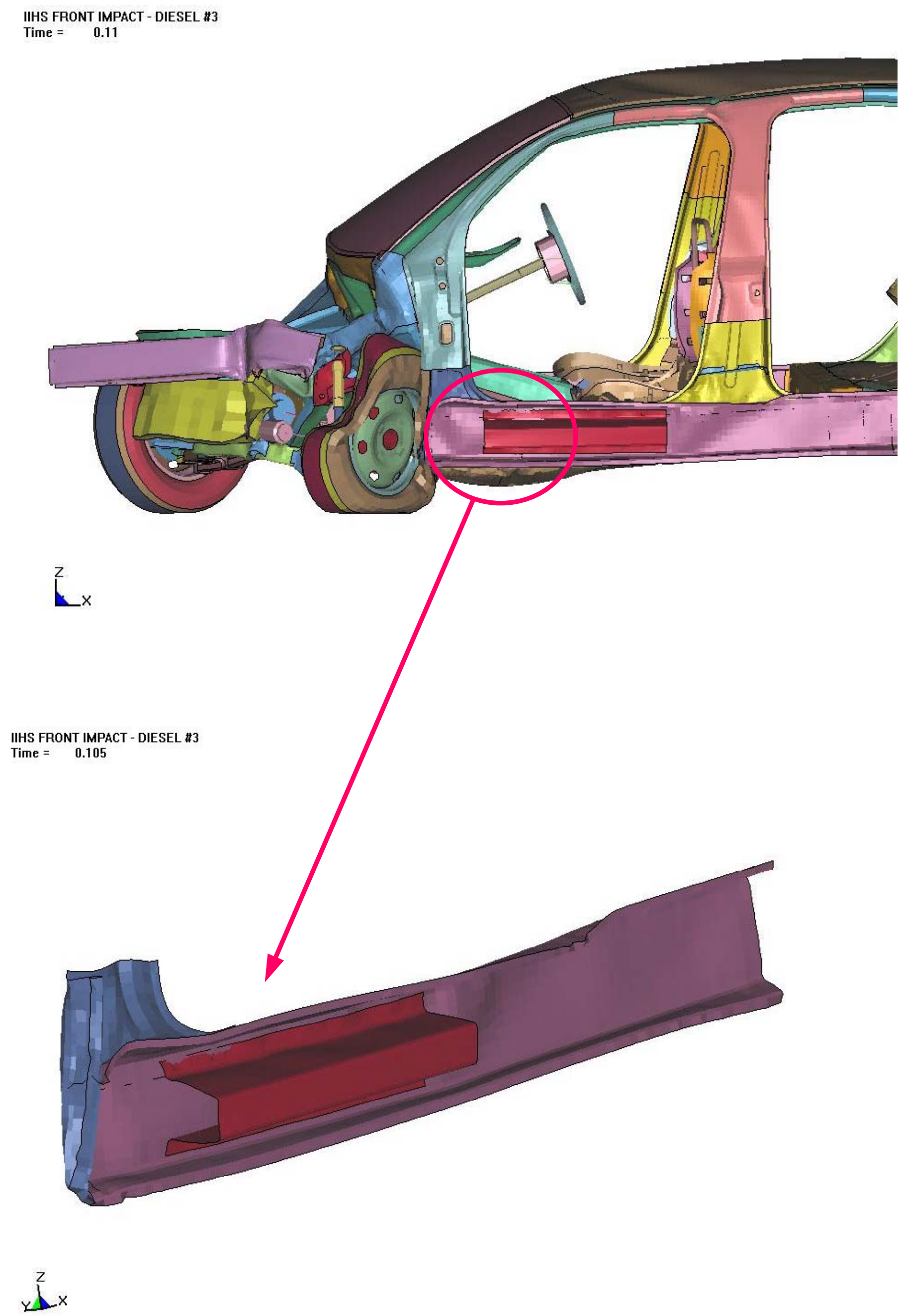

FIGURE 18: IIHS 40% ODB– FGPC-ACD13a Deformed Shape

Press to open animation

Press to open animation

4.5.5 FGPC-ACD15a

The final iteration aimed to determine the effect of increasing the Rocker stiffness without using any reinforcement but by increasing the gauge of the Rocker Inner alone. See Figures 19 & 20.

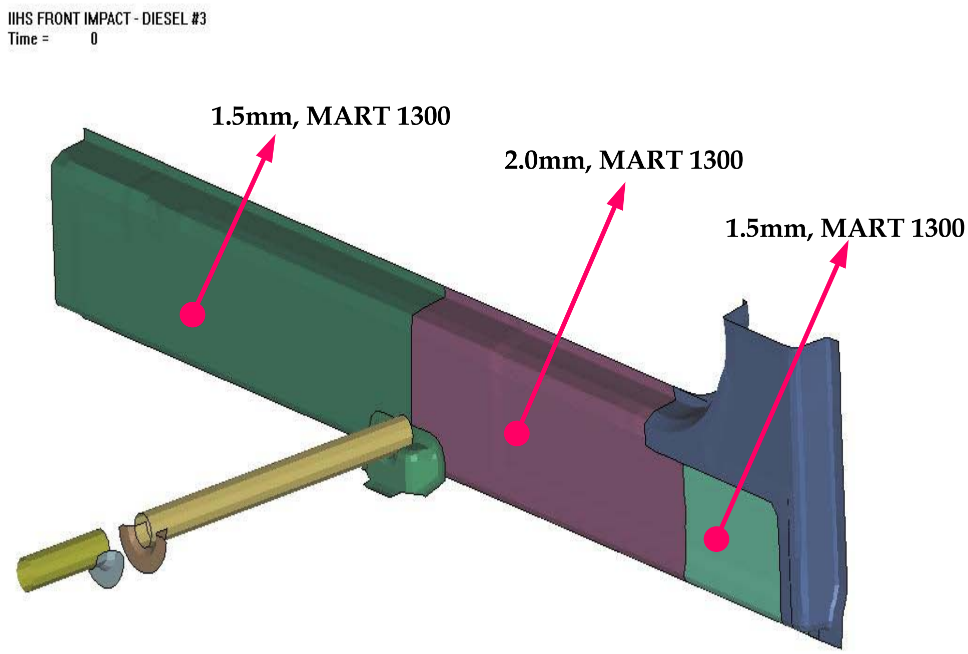

FIGURE 19: FGPC-ACD15a Geometry Revisions

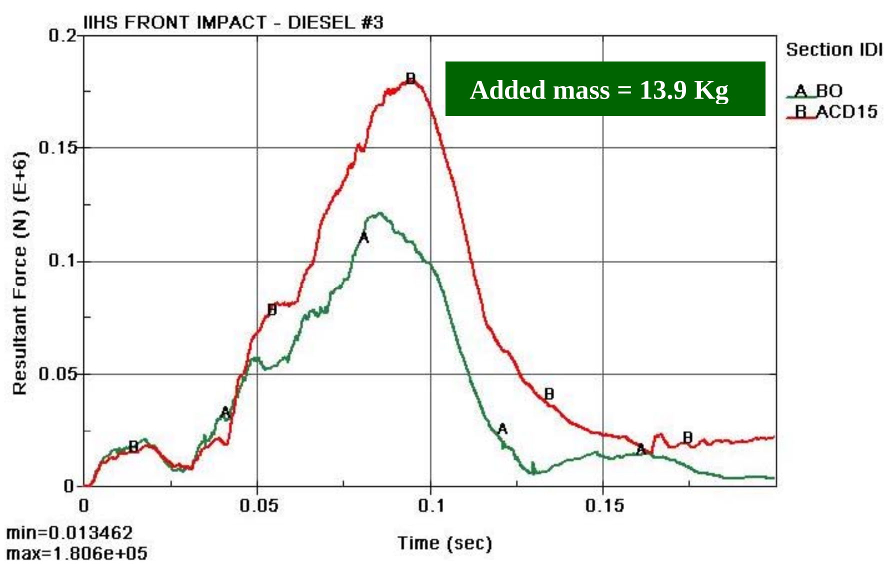

FIGURE 20: IIHS 40% ODB – FGPC-BO & FGPC-ACD15a Section Forces

The deformed shape of FGPC-ACD15a is shown in Figure 21. The Rocker Inner shows an increase in its stiffness, which does not allow the passenger compartment to collapse. This performance was achieved at a cost of 13.9kg over FGPC-BO.

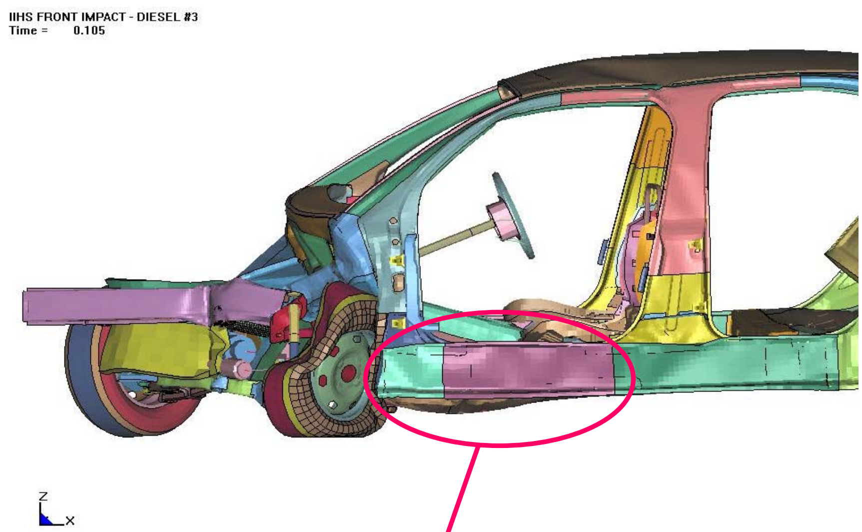

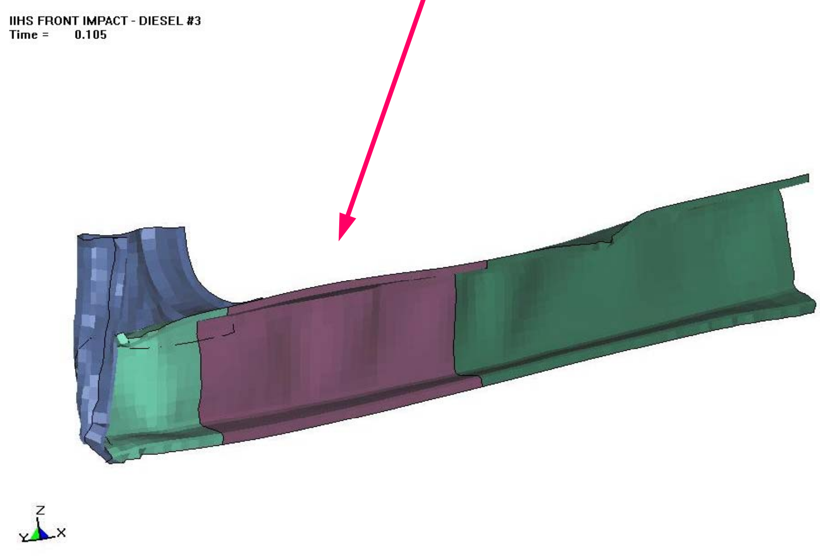

FIGURE 21: IIHS 40% ODB– FGPC-ACD15a Deformed Shape

Press to open animation

Press to open animation

4.6 IIHS FRONT CRASH 40% ODB CONCLUSION

This analysis has shown that the Rocker Inner plays an important role in the structure's performance under this loading condition. To improve its stiffness a number of different approaches were considered such as increasing the gauge, modifying its cross-section and adding additional reinforcement. FGPC-ACD13a satisfies the requirements of IIHS 40% ODB and will be used as the baseline for the final optimization performed in Task 6.0: Final Optimization. It should be noted that although FGPC-ACD15a performed well, it was not considered as strong a candidate for the final optimization as FGPC-ACD13a.

5. SIDE POLE IMPACT (FMVSS214 NEW)

5.1. TARGET

FMVSS214 New Pole Impact sets limits on occupant injury criteria, with no structural performance requirements. Since no occupant models are used in this study, the maximum structural intrusion into the passenger compartment was measured instead. This is similar to the IIHS Side Impact target. The maximum intrusion in the pole impact occurs on the Front Door Inner, while the side impact intrusion is measured at the B-Pillar.

Therefore the target is to meet or exceed the performance of the FGPC-BO, which had a maximum intrusion of 7mm inboard of the driver's seat centerline.

5.2. LOADS AND BOUNDARY CONDITIONS

The vehicle is propelled at 20mph into a 10in diameter pole at an angle of 75 degrees to its longitudinal axis, as shown in Figure 22. The pole is lined up with the center of the occupant's head. It should noted that the seats in the FGPC are designed to be stationary with adjustable driver controls and so the head position will remain constant regardless of occupant size.

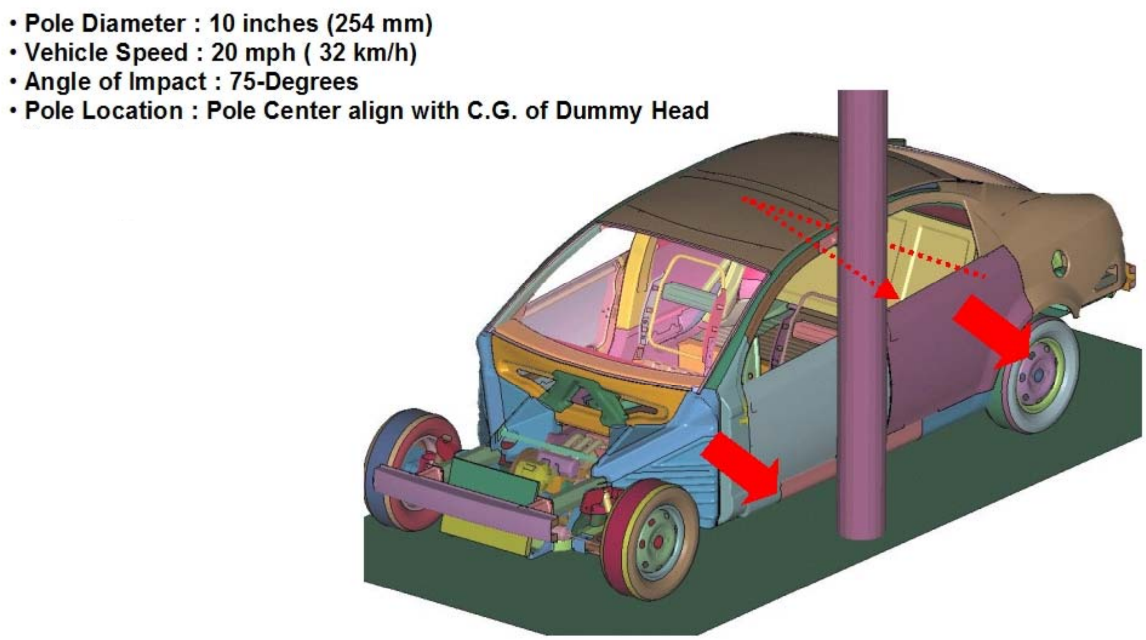

FIGURE 22: Pole Impact Set-Up

5.3. BACKGROUND

The analysis performed for Task 5.0: Concept Design Check identified a weak performance of the FGPC-ACD structure under the FMVSS214 New Pole Impact load condition. Changes to the vehicle structure made post optimization altered the loadpath, resulting in different deformation mode and decreased performance. See Figures 23 & 24.

Press to open animation

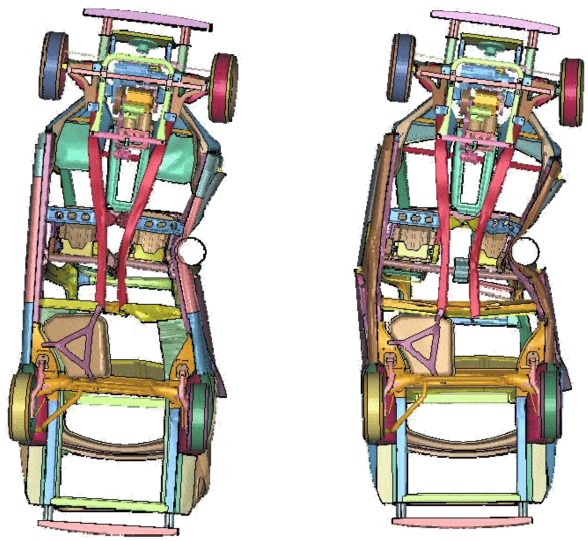

FIGURE 23: Global Deformation of FGPC-BO & FGPC-ACD Final at 100msec.

ITERATIONS	MASS (kg)	DISTANCE (mm)
FGPC-BO	1351.1	-7
FGPC-ACD Final*	1331.0	-120

*FGPC-ACD Final is the design resulting from the IIHS Side Impact iteration study performed in Task 5.0: Concept Design Analysis Check.

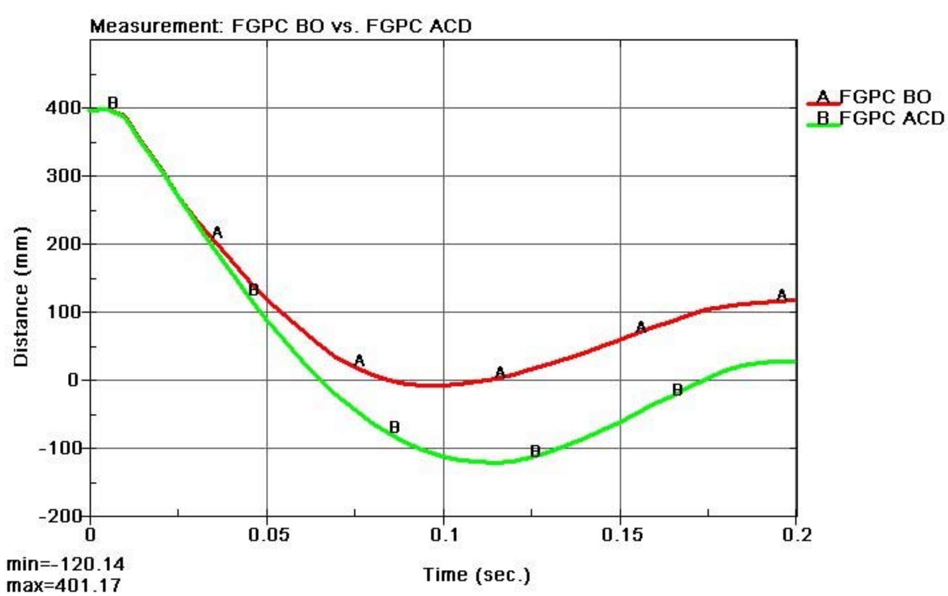

FIGURE 24: Performance Comparison of FGPC-BO & FGPC-ACD Final

5.4. RESULTS

The goal of this analysis was to match the performance of the FGPC-BO. Table 3 summarizes the results from the iteration study. The performance of FGPC-BO and FGPC-ACD Final are included for comparison. Masses in brackets are normalized to FGPC-BO.

ITERATIONS	MASS* (kg)	DISTANCE (mm)	NOTES
FGPC-BO	1351.1	-7	Before optimization
FGPC-ACD Final	1331 (20.1 less)	-120	After optimization
FGPC-ACD1b	1357.8 (6.7 more)	-74	Tailored Rocker Inner (1.5/0.6), Roof SD Rail (0.7/1.2)
FGPC-ACD2b	1351.1 (0.0 more)	-105	Rocker Inner (Mart1300 to Boron), OTR (DP780 to Mart 1300), B-Pillar LWR (Boron1550 to Mart 1300)
FGPC-ACD3b	1353.3 (2.2 more)	-94	Rocker INR change, Rocker Reinfor1(0.6), X-member W/O holes
FGPC-ACD4b	1358.0 (6.9 more)	-60	Tailored Rocker Inner (0.6/1.5/0.8), Rocker Reinf2 (1.0), X-member W/O holes
FGPC-ACD5b	1359.9 (8.8 more)	-43	Tailored Rocker Inner (0.6/1.5/0.8), Rocker Reinf2 (1.5), X-member W/O holes
FGPC-ACD6b	1352.8 (1.7 more)	-105	Tube X-member(2.0)
FGPC-ACD7b	1359.5 (8.4 more)	-42	Tube X-member(1.2),Rocker Inner (1.5)
FGPC-ACD8b	1357.1 (6.0 more)	-97	Rocker Tube(1.2)
FGPC-ACD9b	1358.1 (7.0 more)	-81	Rocker Tube(1.2), Tube X-member(1.2)
FGPC-ACD10b	1352.5 (1.4 more)	-87	No.2 Tube X-member (1.2), X-member W/O Holes
FGPC-ACD11b	1352.7 (1.6 more)	-65	No.2 Tube X-member (1.0), CTR tube X-member (1.2), X-member W/O Holes
FGPC-ACD12b	1360.0 (8.9 more)	5	ACD11+Rocker Inner (1.5)
FGPC-ACD13b	1362.1 (11.0 more)	-5	BO seat tube(1.2), tube X-member(1.2), Rocker Inner (1.5)
FGPC-ACD14b	1360.0 (8.9 more)	10	ACD11 solution2 + Rocker Inner (1.5)
FGPC-ACD15b	1364.2 (13.1 more)	26	ACD14 + Rocker reinfor(1.2)

* Masses in brackets are normalized to FGPC-BO.

TABLE 3: Iteration Summary

Figure 25 shows the relative performance of FGPC-ACD Final and the most successful iteration FGPC-ACD15b compared to the baseline FGPC-BO. FGPC-BO achieved an intrusion of –7mm whereas FGPC-ACD Final was –120mm and FGPC-ACD15b was +26mm respectively. This meant that FGPC-ACD Final's performance was –113mm poorer than FGPC-BO and FGPC-ACD15b was +33mm better.

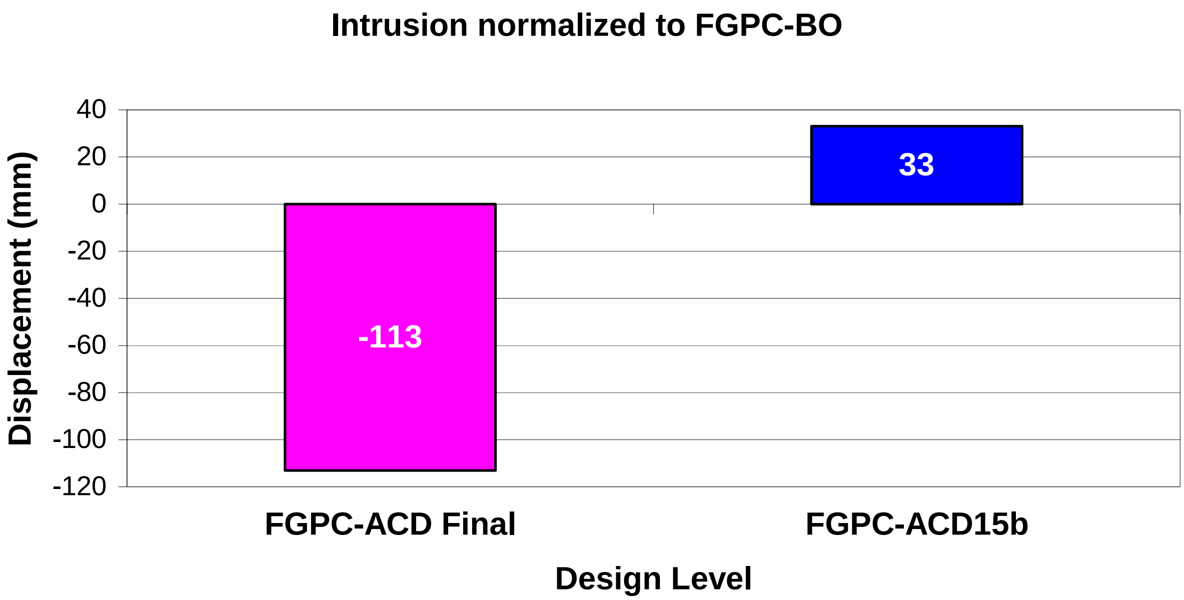

FIGURE 25: Intrusion of FGPC-ACD & FGPC-ACD15b normalized to the performance of FGPC-BO

5.5. DETAILED DISCUSSION OF KEY ITERATION RESULTS

In order to improve the Pole Impact performance a variety of design variables were considered. The following is a detailed discussion of the key iterations.

Note, the IIHS Front Crash and Pole Impact iteration studies were executed in parallel and although they shared many key features, for simplicity they should be considered independently. IIHS Front Crash iterations have an "a" suffix, Pole Impact a "b."

5.5.1 FGPC-ACD1b

For the first iteration, FGPC-ACD1b, both the Rocker Inner and Member Body Side Inner were split into two pieces. The front half of each component was then up-gauged. See Figure 26.

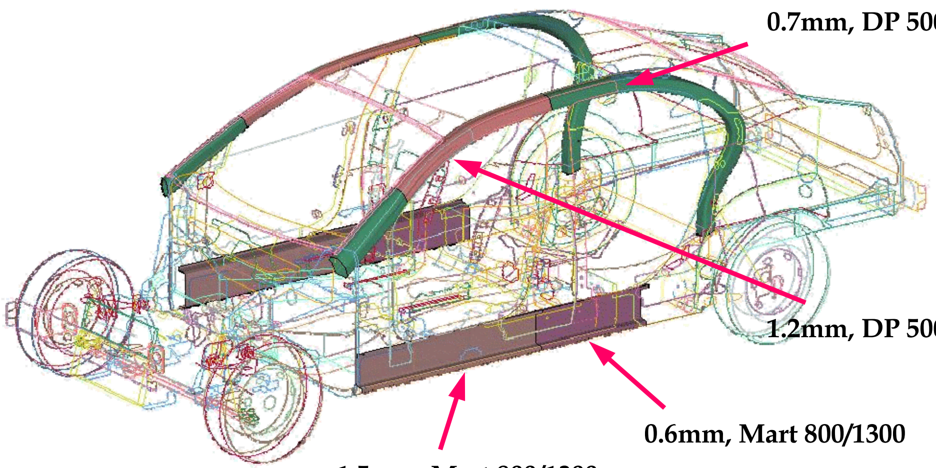

FIGURE 26: FGPC-ACD1b Highlighting Tailor-Welded Rocker Inner & Roof Side Rail Changes

Comparison of the plastic strain of FGPC-ACD Final and FGPC-ACD1b are given in Figure 27. Though the deformed shape of the two designs is similar, the intrusion was reduced by 46mm. The design changes were very modest and can easily be applied to the other iterations in this study.

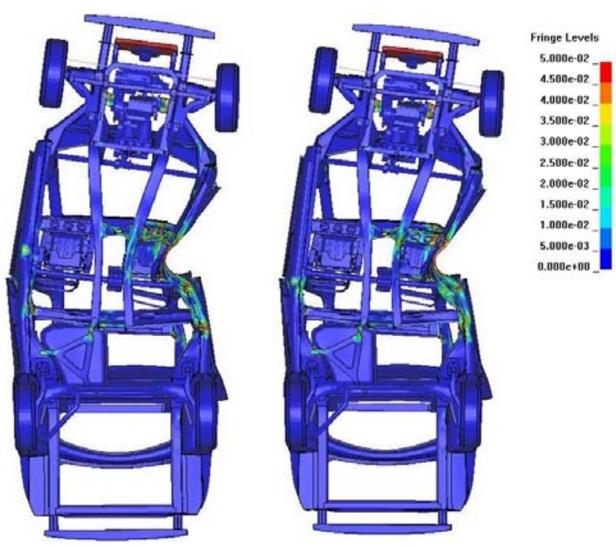

FIGURE 27: Plastic Strain Contours of FGPC-ACD & FGPC-ACD1b

5.5.2 FGPC-ACD3b

For FGPC-ACD3b the Rocker Inner cross-section was locally refined to increase its bending stiffness by including a U-shaped indentation. An additional Rocker Inner Reinforcement was welded to the Rocker Inner in the impact area and the holes in the Front Seat Cross-member were filled to increase its buckling strength. See Figure 28.

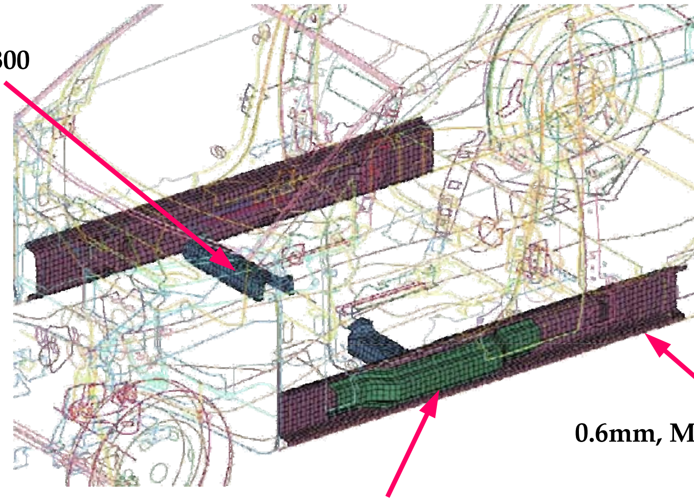

FIGURE 28: FGPC-ACD3b Highlighting Rocker Inner, Rocker Inner Reinforcement & Front Seat Cross-member Changes

Figure 29 shows plastic strain of FGPC-ACD Final and FGPC-ACD3b. Unfortunately the local solutions created a weak zone at the end of the Rocker Inner Reinforcement, gaining just a 26mm improvement over the baseline.

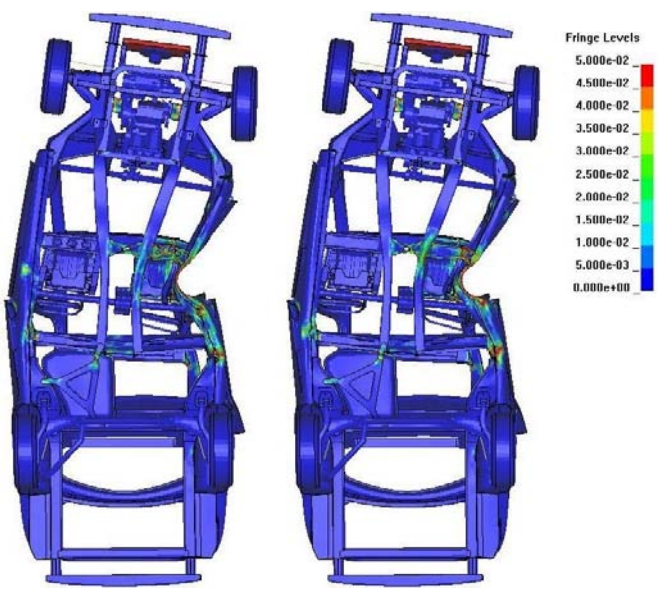

FIGURE 29: Plastic Strain Contours of FGPC-ACD & FGPC-ACD3b

5.5.3 FGPC-ACD9b

Figure 30 shows FGPC-ACD9b, which uses tube reinforcements in combination with the Front Seat Cross-member and the Rocker Inner. The purpose of the Rocker Inner tube reinforcement is to provide a multi-function solution for the IIHS Side and Front Crashes and the Pole Impact. The Front Seat Cross-member tube reinforcement will provide additional passenger compartment support.

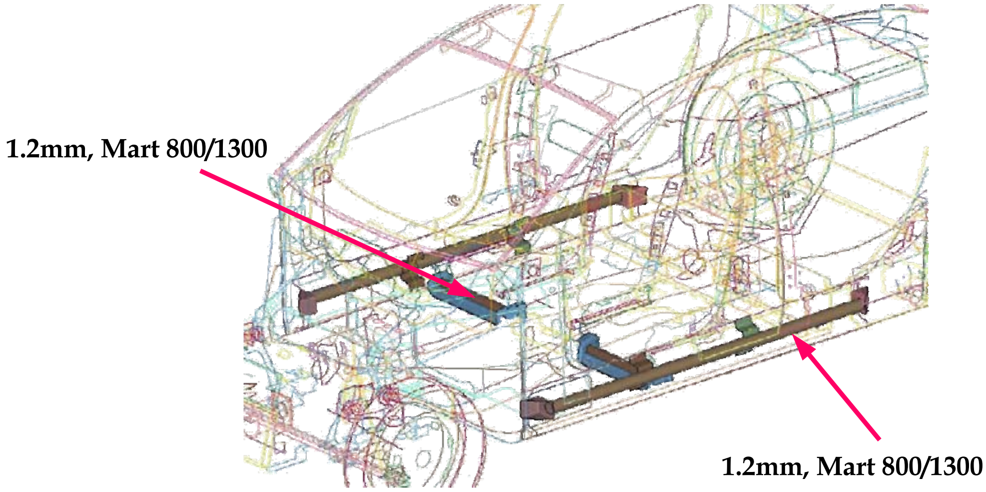

FIGURE 30: FGPC-ACD9b Highlighting Rocker Inner & Front Seat Cross-member Tube Reinforcements

Comparisons of the plastic strains, see Figure 31, shows that the Front Seat Cross-member reinforcement worked well. However, the Rocker Inner tube reinforcement did not have sufficient bending stiffness. This iteration gained a 39mm improvement.

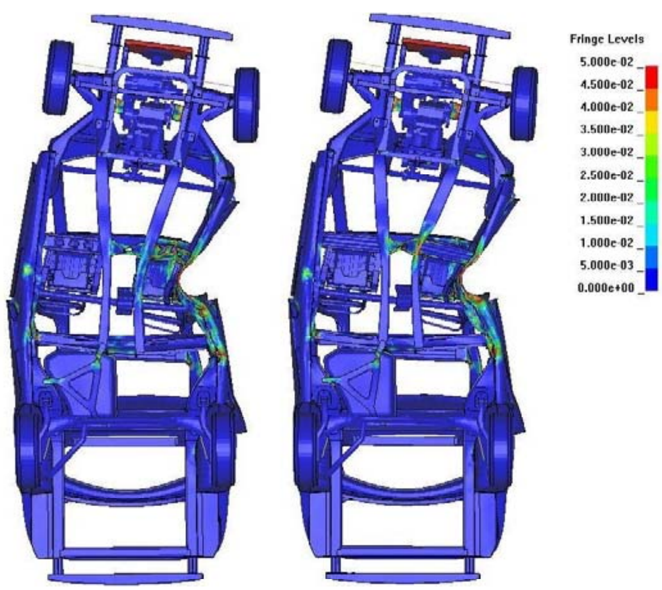

FIGURE 31: Plastic Strain Contours of FGPC-ACD & FGPC-ACD9b

5.5.4 FGPC-ACD11b

Though the Front Seat Cross-member tube reinforcement was useful because it was not aligned with the pole its effectiveness was limited. For FGPC-ACD11b the tube reinforcement was repositioned to improve its efficiency. See Figure 32.

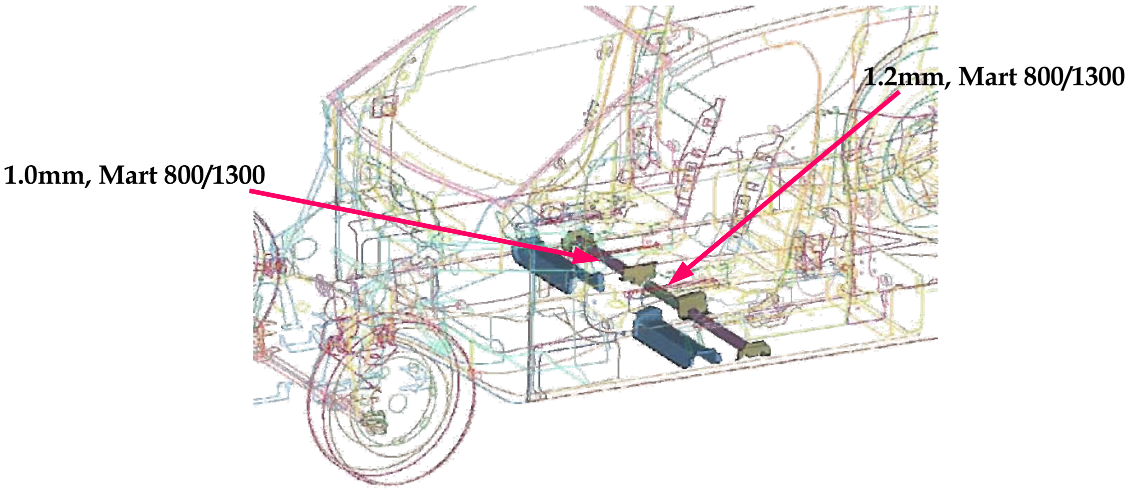

FIGURE 32: FGPC-ACD11b Highlighting Second Tube Cross-member & Center Support

FGPC-ACD11b achieved an improvement of 55mm. The effectiveness of the second tube reinforcement can be seen in Figure 33, which compares the plastic strains of FGPC-ACD Final and FGPC-ACD11b.

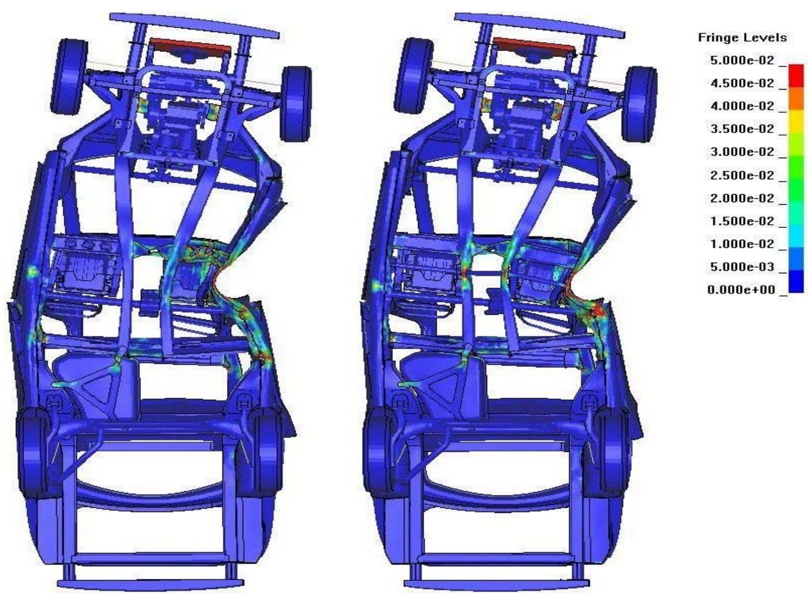

FIGURE 33: Plastic Strain Contours of FGPC-ACD & FGPC-ACD11b

5.5.5 FGPC-ACD12b

Iteration FGPC-ACD1b achieved a 46mm improvement with modifications that could easily be incorporated into the other iterations. FGPC-ACD12b combined the design changes of both FGPC-ACD1b and FGPC-ACD11b, achieving an intrusion of +5mm. This was a significant improvement over the baseline, FGPC-BO, which had a –7mm displacement.

5.5.6 FGPC-ACD13b

Figure 34 shows FGPC-ACD13b, which had a tube reinforcement on the Front Seat Cross-member and used the rear seat mount tube from the original FGPC-BO design. The purpose of this iteration was to consider the effect of relocating the center cross-member. FGPC-ACD12b used a cross-member that was directly aligned with the pole whereas for FGPC-ACD13b the pole impacted between the two cross-members.

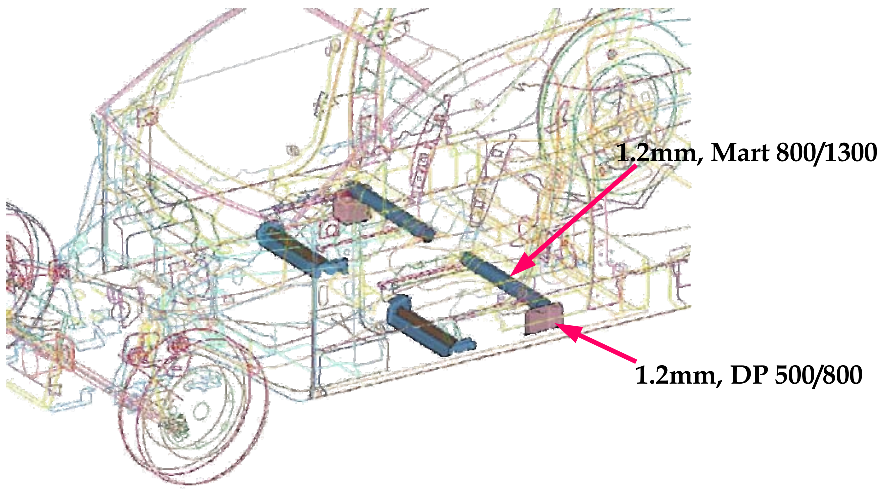

FIGURE 34: FGPC-ACD13 Highlights Seat Mounting Tube

Figure 35 shows the plastic strains of FGPC-ACD Final, FGPC-ACD12b and FGPC-ACD13b. FGPC-ACD13b achieved an intrusion of –5 mm, an improvement over FGPC-BO's performance but less than that achieved by FGPC-ACD12b.

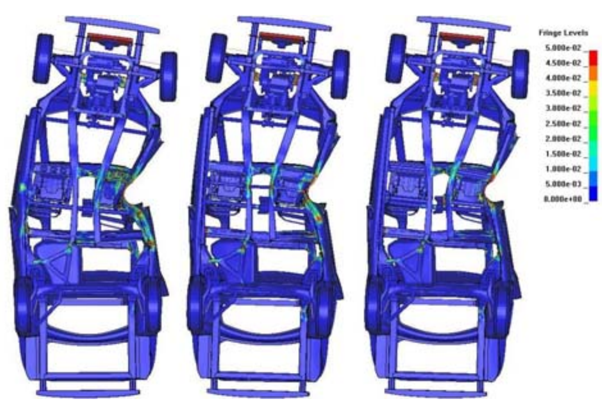

FIGURE 35: Plastic Strain Contours of FGPC-ACD Final, FGPC-ACD12b & FGPC-ACD13b

5.5.7 FGPC-ACD15b

FGPC-ACD15b was based upon FGPC-14b with the following modifications, a new center tube cross member design, tube cross member, rocker reinforcement, seat cross member and thicker rocker inner panel. The material properties and gauges are shown in Figure 36.

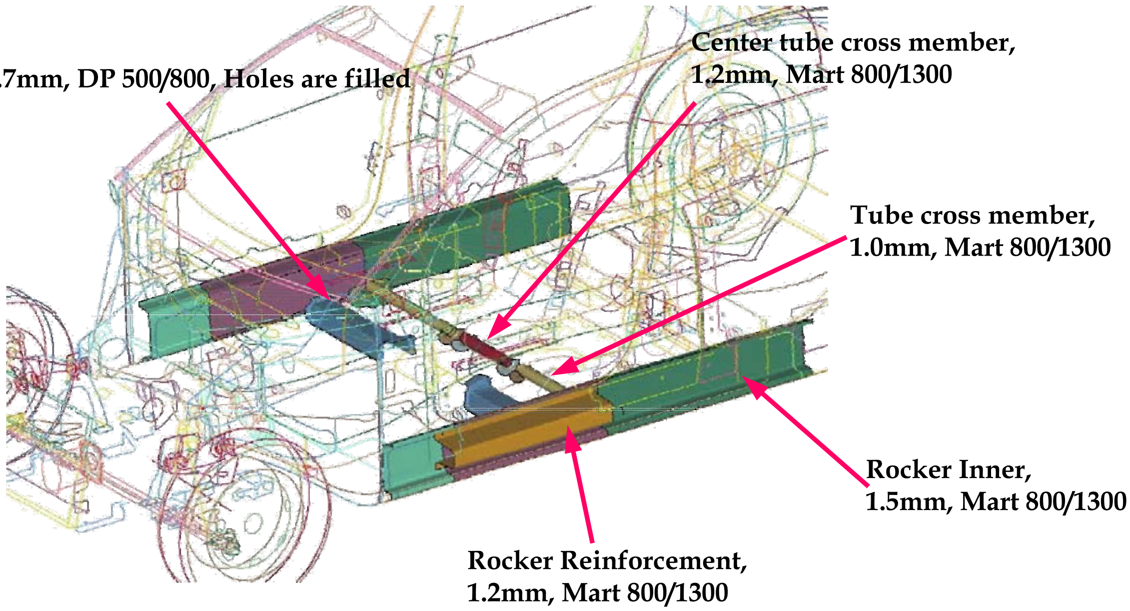

FIGURE 36: FGPC-ACD15 Description of Material Properties & Gauges

Figure 37 shows plastic strain of FGPC-ACD Final and FGPC-ACD15b. Referring to FGPC-ACD Final on the left. The driver's (impact) side Rocker bends globally while the high-positioned Seat Cross-member translates the load to the passenger's (non-struck) side Rocker without absorbing much of the impact energy. In contrast, FGPC-ACD15b allows more localized bending in the driver's side Rocker. It also uses an enhanced Rocker structure and an additional center cross-member. More force is absorbed without causing the passenger side Rocker to deform. An improvement of 146mm was created by these changes.

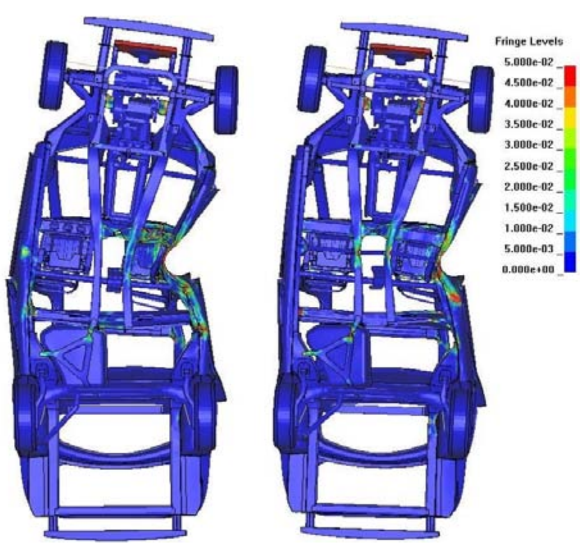

FIGURE 37: Plastic Strain Contours of FGPC-ACD & FGPC-ACD15

Press to open animation

5.6. SIDE POLE IMPACT (FMVSS214 NEW) CONCLUSION

FGPC-ACD15b satisfies the requirements of FMVSS214 NEW, exceeding the performance of FGPC-BO by 33mm. Figure 38 shows a comparison of the intrusions for FGPC-BO, FGPC-ACD Final and FGPC-ACD15b. Their minimum values were –7, -120 and +26mm respectively.

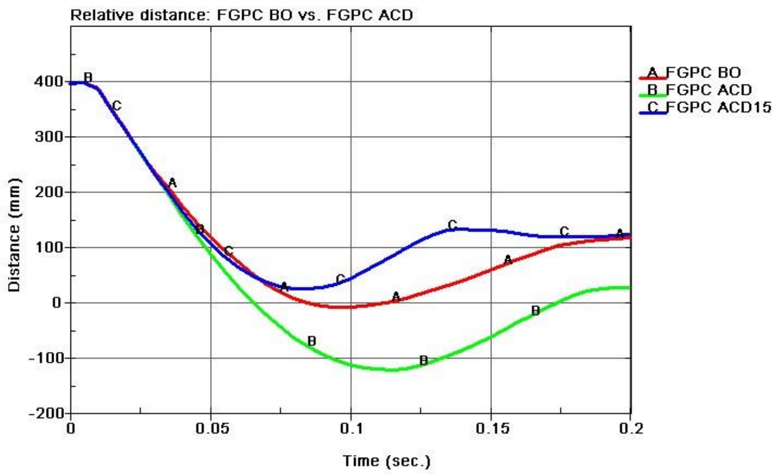

FIGURE 38: FGPC-BO, FGPC-ACD Final & FGPC-ACD15b Intrusion Comparisons

6. CONCLUSION

FGPC-ACD13a, the preferred iteration from the IIHS Front Crash 40% ODB and FGPC-ACD15b, the finalized iteration from the FMVSS214 NEW Side Pole Impact are in fact the same design. This model satisfied both requirements with a mass increase of 13.1kg over FGPC-BO. It will therefore be used as the baseline for the Task 6.0 Final Optimization.

Note, the masses listed in Tables 2 & 3 for both FGPC-ACD13a and FGPC-ACD15b were 1366 and 1364.2kg respectively. This disparity in mass is due to slightly different setups required by the two analyses. As stated previously the two models represent the same geometry.

APPENDIX A
IIHS FRONT CRASH 40% ODB REGULATIONS
Offset barrier crash tests are conducted at 40mph (64.4km/hr) with a 40% overlap. The test vehicle is aligned with the deformable barrier such that the right edge of the barrier face is offset to the left of the vehicle centerline by 10% of the vehicle's width. See Figure A1. The vehicle width is defined and measured as indicated in SAE J1100 – Motor Vehicle Dimensions, which states, "the maximum dimension measured between the widest part on the vehicle, excluding exterior mirrors, flexible mud flaps, and marker lamps, but including bumpers, moldings, sheet metal protrusions, or dual wheels, if standard equipment."

The vehicle is accelerated by the propulsion system at an average of 0.3g until it reaches the test speed and then is released from the propulsion system 25cm before the barrier. The onboard braking system, which applies the vehicle's service brakes on all four wheels, is activated 1.5sec after the vehicle is released from the propulsion system.

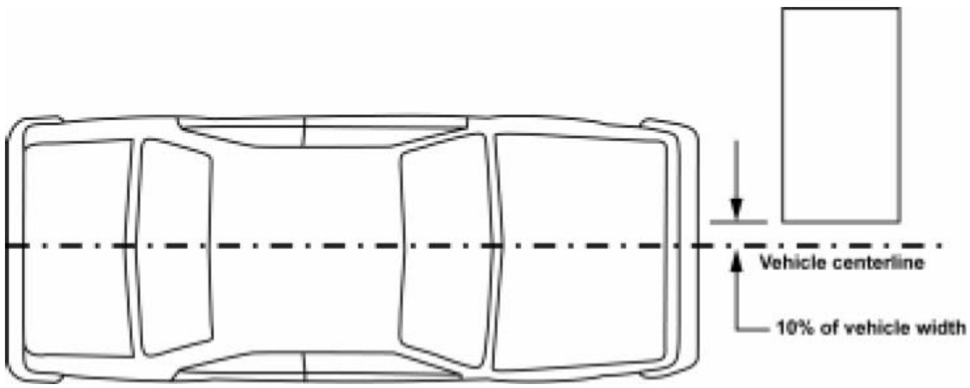

FIGURE A1: Vehicle Overlap with Deformable Barrier

MEASUREMENT POINT LOCATIONS
The following are the locations for measuring vehicle intrusion:

- **Steering column (one point)**
  The marked reference is the geometric center of the steering wheel, typically on the airbag door. After the crash, this point is measured by folding the airbag doors back into their undeployed position. In most cases, this measurement is probably less than the maximum intrusion into the compartment. However, if the steering column completely separates from the instrument panel (for example, due to shear module separation) during the crash, the steering column post-crash measurement is taken by placing and holding the wheel and column in its approximate maximum dynamic position as recorded on the high-speed film. The film may not always show clearly where the column was during the crash, and in such cases other clues would be needed to reposition the column for measurement. In rare instances, it may not be possible to obtain any meaningful post-crash measurement.
- **Lower instrument panel (two points)**
  The left and right lower instrument panel (knee bolster) lateral coordinates are defined by adding 15cm to and subtracting 15cm from the steering column reference lateral coordinate, respectively. The vertical coordinate is the same for both left and right references and is defined as 45cm above the height of the floor (without floormats). If the panel or knee bolster loosens or breaks away in the crash, the post-crash measurements are taken by pressing and holding the panel against the underlying structure.

- **Brake pedal (one point)**
  The geometric center of the brake pedal pad (top surface). If the brake pedal is constructed so that it dangles loosely after the crash, the brake pedal is pushed straight forward against the toepan/floorpan and held there to take the post-crash measurement. If the pedal drops away entirely, no post-crash measurement is taken.

- **Toepan (three points)**
  The vertical coordinate for all toepan measurement locations is the vertical coordinate of the brake pedal reference. The lateral coordinates of the left, center, and right toepan locations are obtained by adding 15cm to, adding 0cm to, and subtracting 15cm from the brake pedal reference lateral coordinate, respectively. The longitudinal coordinate is measured and a mark is temporarily placed at the locations on the toepan. A utility knife is used to cut a small "V" in the carpet and underlying padding at each point on the toepan. The point of the "V" is peeled back, and the exposed floor is marked and measured. The carpet and padding are then refitted prior to the crash.

- **Left footrest (one point)**
  The vertical coordinate for the footrest measurement location is the vertical coordinate of the brake pedal reference. The lateral coordinate of the footrest is obtained by adding 25cm to the brake pedal reference lateral coordinate. The same procedure described above for cutting the carpet is used to mark and measure the underlying structure. In cases where there is a specific footrest construct at the footrest measurement location, the construct is removed and the underlying structure is marked and measured. The construct is reinstalled prior to the crash.

- **Seat bolts (typically, four points)**
  Each of the four (or fewer) bolts that anchor the driver seat to the floor of the vehicle.

- **A-Pillar (one point)**
  The A-Pillar is marked on the outside of the vehicle at the same vertical coordinate as the base of the left front window.

- **B-Pillar (one point)**
  The B-Pillar is marked on the outside of the vehicle at the longitudinal center of the pillar at the same vertical coordinate as the lower A-Pillar mark.

APPENDIX B

SIDE POLE IMPACT (FMVSS214 NEW) REGULATIONS

The vehicle is propelled at 20mph into a 10in diameter pole at an angle of 75 degrees to its longitudinal axis, as shown in Figure B1. The pole is lined up with the center of the occupant's head. The occupant may be either a 50th percentile male at the mid-track seat position, or a 5th percentile female at the full forward seat position.

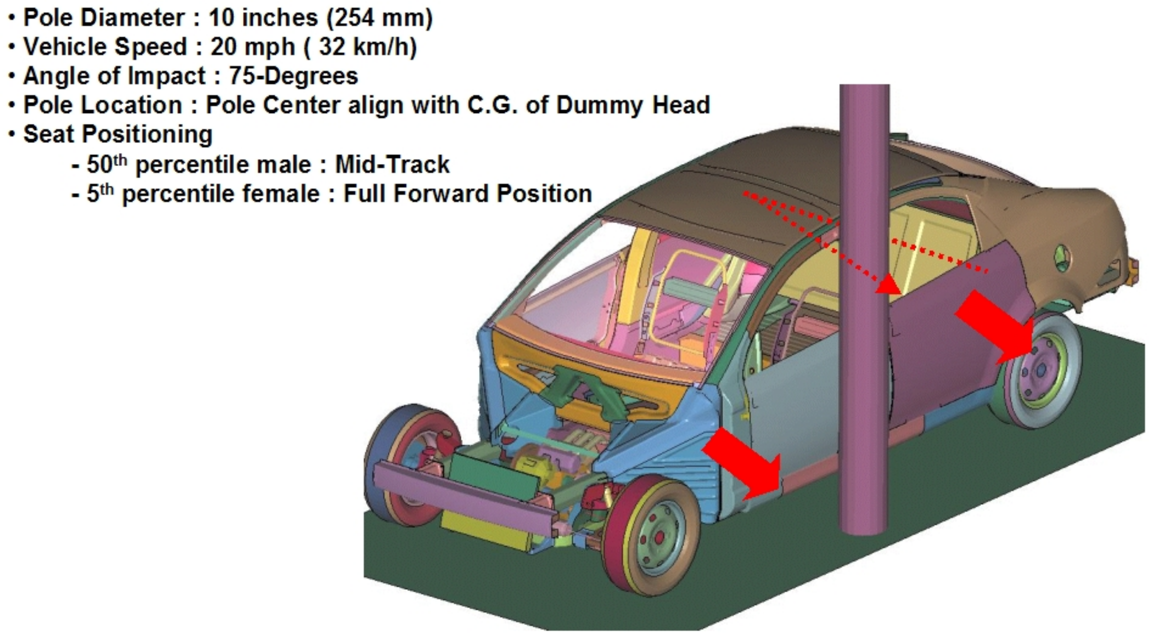

FIGURE B1: Pole Impact

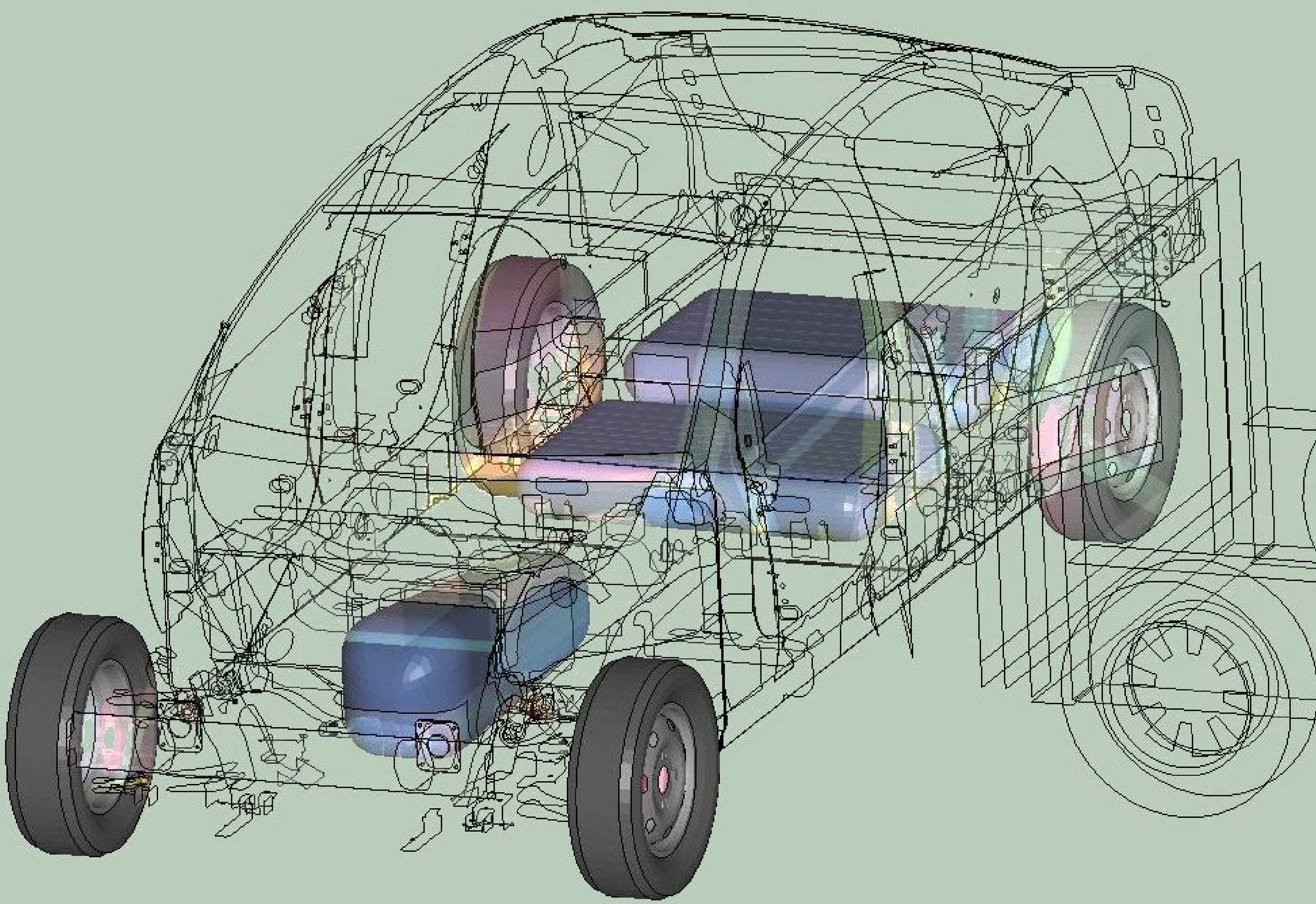

Final passenger

compartment

gauge optimization

Future Generation Passenger Compartment
Task 6.0 - Final Mass Optimization Report

Task 6.0 – Final Optimization

Table of Contents

Task 6.0 - Final Optimization

1. INTRODUCTION

This report completes Task 6.0: Final Optimization of the FGPC (Future Generation Passenger Compartment) project. Its purpose is to document the process used for identifying the final optimal mass design for thickness variables which satisfies the IIHS Side Impact, IIHS Front Crash 40% ODB, Pole Impact (FMVSS 214 NPRM-Notice of Proposed Rule Making), Torsional Stiffness, Front and Rear Side Door Intrusion and Roof Crush targets.

Task 6.0: Final Optimization consists of two sets of analysis. The first optimized the gauge of the passenger compartment structure for minimum mass subject to IIHS Side Impact, IIHS Front Crash ODB, and Torsional Stiffness (Modal) loadcases. The solution performance of these loadcases overlaps and so they must be considered together. The second series of analysis optimized the gauge of the front and rear side intrusion door beams independently. This was possible because they have little influence on the vehicle ‘s performance under the first set of loadcases. By separating them from the total number of design variables the duration of the optimization was reduced. From experience gained in Task 5.5: Concept Design Check Supplement, the IIHS Front Crash ODB was found to be a dominating loadcase, limiting the influence of the Pole Impact. To expedite the optimization the Pole Impact was performed individually.

For both optimization studies, the analysis used the diesel engine variant because its performance was the poorest baseline analysis.

2. OBJECTIVE

The objective of this task is to minimize the mass of the FGPC concept design while meeting the targets for the IIHS Side Impact, Pole Impact, IIHS Front Crash ODB, Torsional Stiffness (Bending and Torsion Modal Performance) and the Side Door Intrusion loadcases. The mass savings are to be achieved by changing the thickness of the passenger compartment components.

3. NAMING CONVENTION

Throughout this report the various FGPC design levels will be identified in the following manner:

- FGPC-BO (FGPC-Before Optimization)
  Task 2.0: Calibration Baseline - ULSAB-AVC PNGV modified to accommodate both Diesel and Fuel Cell powertrains. This is the FGPC Baseline.

- FGPC-AO (FGPC-After Optimization)
  Task 3.0: Optimization - the optimized FGPC Baseline.

- FGPC-ACD (FGPC-After Concept Design)
  Task 4.0: Concept Design - the optimization results integrated into a production viable vehicle.

- FGPC-ACDC (FGPC-After Concept Design Analysis Check)
  Task 5.0: Concept Design Analysis Check – check of FGPC-ACD performance after the optimization, manufacturability and assembly considerations had been integrated into the design

- FGPC-BFO (FGPC-Before Final Optimization)
  Task 5.5: Concept Design Check Supplement - Revisions made to FGPC-ACD in order to satisfy IIHS Front Crash and FMVSS214 New Pole Impact requirements

- FGPC-AFO (FGPC-After Final Optimization)
  Task 6.0: Final Optimization – final gauge optimization of FGPC-BFO

- FGPC-FCD (FGPC-Final Concept Design Check)
  Task 7.0: Final Concept Design Check - validation of FGPC-AFO performance after the optimization against all loadcases

4. FGPC-BFO - BASELINE DESIGN

All results from the optimization are compared to FGPC-BFO. This model represents the completion of Task 5.5: Concept Design Check Supplement and so it satisfied all FGPC loadcases. Unless noted otherwise, it is assumed that FGPC-BFO refers the diesel powertrain variant.

Results from Task 5.0: Concept Design Analysis Concept Check showed that the vehicle did not satisfy the requirements of IIHS Front Crash ODB or Pole Impact and was very close to meeting the FGPC targets for the torsional stiffness. Task 5.5: Concept Design Check Supplement was a supplemental analysis to ensure that the vehicle met all performance targets before proceeding with the Task 6.0: Final Optimization.

5. IIIHS SIDE IMPACT, IIHS FRONT CRASH 40% ODB & TORSIONAL STIFFNESS OPTIMIZATION

Fourteen (14) different part thickness variables were studied to find a minimum mass design that satisfies the design performance criteria for IIHS Side Impact, IIHS Front Crash ODB and Torsional Stiffness analyses. The material and shape of the parts were not varied in this optimization, as these values had been determined in the previous tasks. The IIHS Front Crash ODB was not used as one of the requirements in the previous optimization studies. The primary goal of this task was to reduce as much mass as possible, as a considerable amount of mass had to be added during Task 5.5: Concept Design Check Supplement to satisfy the Pole Impact and the IIHS Front Crash ODB requirements, which were not a part of the previous optimization setups.

5.1. DESIGN PERFORMANCE EVALUATION

The optimization creates a new design by assigning values to all design variables and then executing the analyses required to assess the performance of the design. Four responses were used to assess the performance of each design, as defined in the optimization statement: the mass, the survival space during IIHS Side Impact, the door open ability during IIHS Front Crash ODB and the Torsional Stiffness of the design. The discussion below describes how these measurements are calculated for each design.

5.2. MASS

The mass of only the parts being designed is used as a performance measure during all the optimization runs. The sum of the masses for all the designed parts is the value that is optimized during the optimization run.

5.3. SURVIVAL SPACE

The survival space measures the performance of the design for the IIHS Side Impact analysis. The survival space is measured as the normal distance between an XZ-plane passing through the middle of the driver seat to the closest point on the inner B-Pillar/Rocker. The measure is shown in Figure 1 & 2. A value greater than 125mm is considered good. This value will be used for the target survival space during the optimization run.

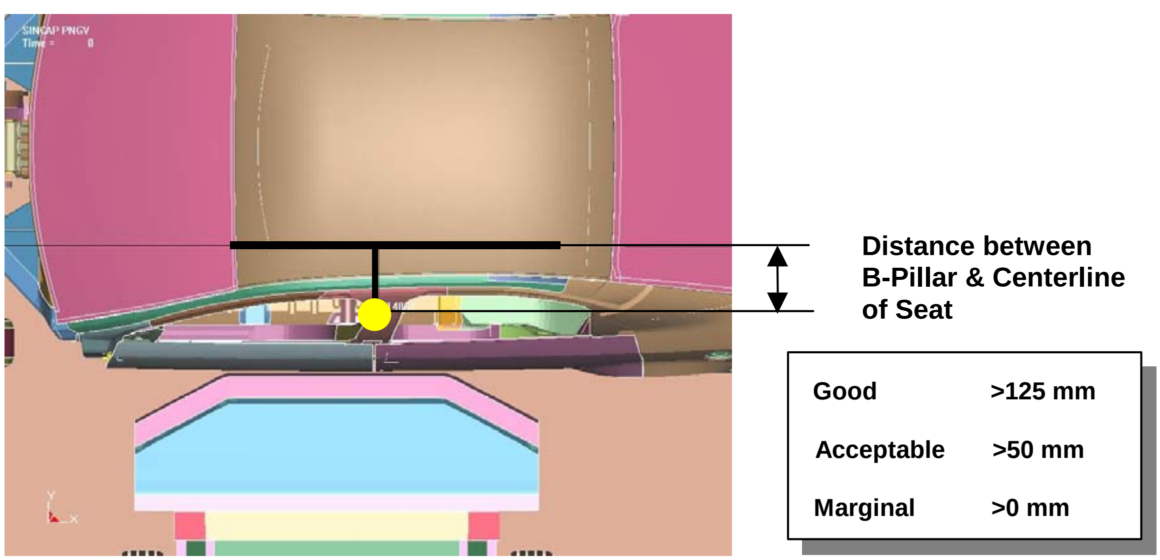

FIGURE 1: Survival Space – Final Distance Between B-Pillar & Seat Centerline

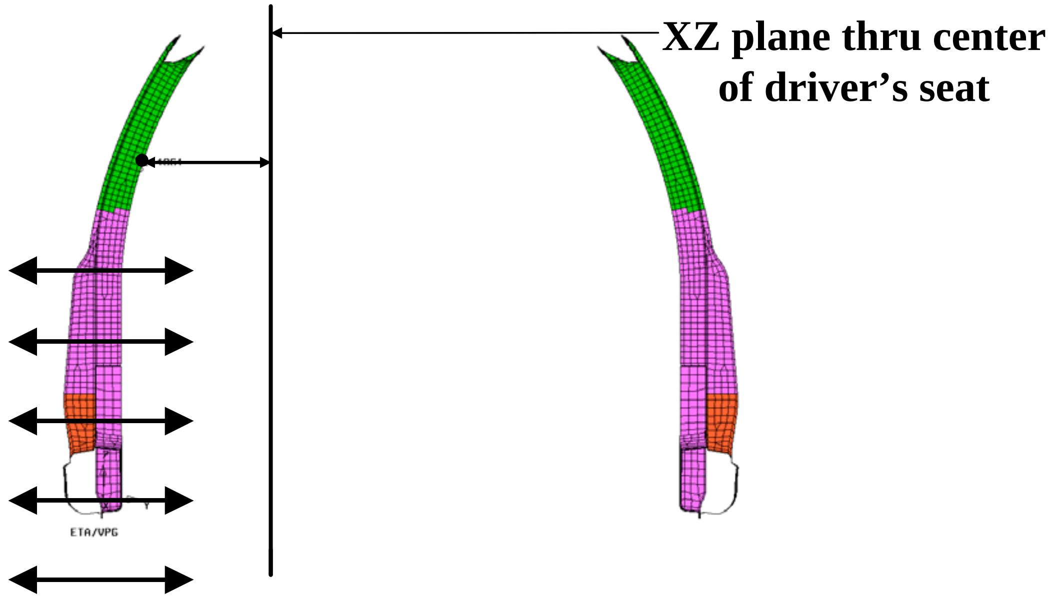

FIGURE 2: Survival Space - Measured At Multiple Locations,
Worst (Smallest) Quoted As Survival Space Value

5.4. DOOR OPEN-ABILITY

The door open ability check measures the ability of the driver to open the door in the event of an IIHS Front Crash ODB. The target is measures the relative change in distance at three different locations along the height of the front door as shown in Figure 3. The target requires a change in distance of less than 5.0mm at all three locations.

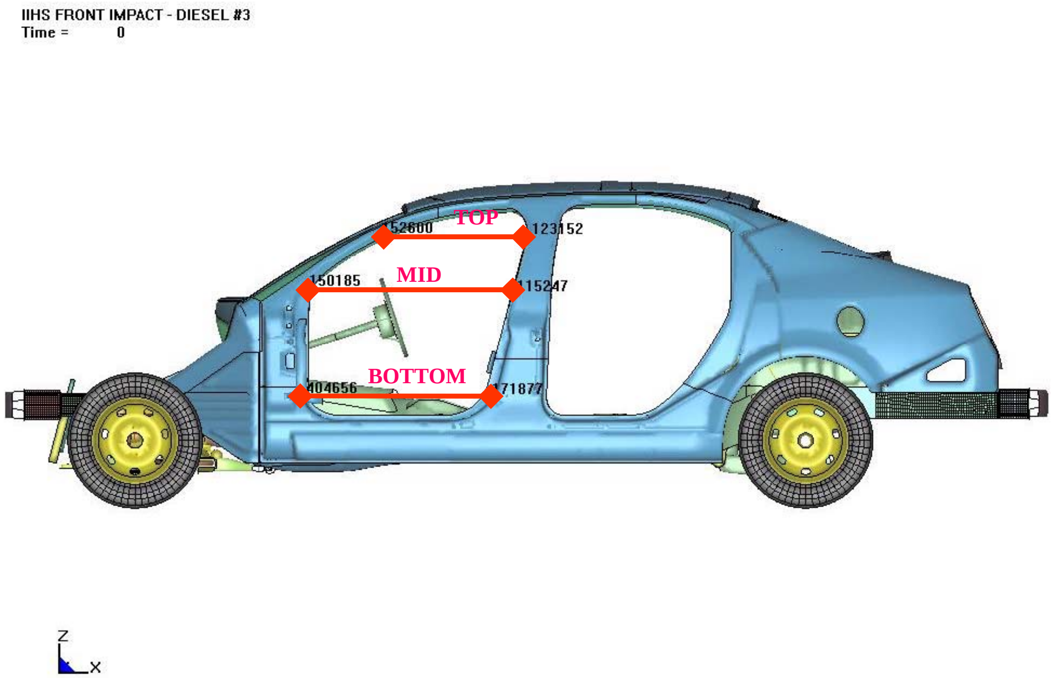

FIGURE 3: Door Open-Ability Measurement Points – Change In Length < 5mm

5.5. TORSIONAL STIFFNESS

The Torsional Stiffness was measured to ensure that the stiffness of the design is above the target of 14000 Nmm/deg. A higher torsional stiffness also will result in an increase in the frequency for the torsional mode of vibration, which was just below the target in the baseline design.

5.6. OPTMIZATION STATEMENT

The objective of this run is to optimize the thickness of the parts in the passenger compartment for a minimum mass design. The optimization statement for the run is:

Minimize:

Mass of the design

Subject to:

Survival space for IIHS side impact > 125mm
Door open ability constraint < 5mm @ three locations on front door
Torsional stiffness > 14000Nm/deg

By varying:

Size of the Roof Bow
Size of the Roof Rail
Size of the B-Pillar Upper Inner
Size of the B-Pillar Lower Inner
Size of the B-Pillar Outer
Size of the Inner Rocker Front
Size of the Inner Rocker Mid
Size of the Inner Rocker Rear
Size of the Rocker Outer
Size of the Rocker Reinforcement
Size of the B-Pillar Crossbar
Size of the Floor Kick-down Front
Size of the Floor Kick-down Back
Size of the A-Pillar

A total of 14 design variables were considered. All 14 variables are continuous. All the design variables are shown in Figure 4.

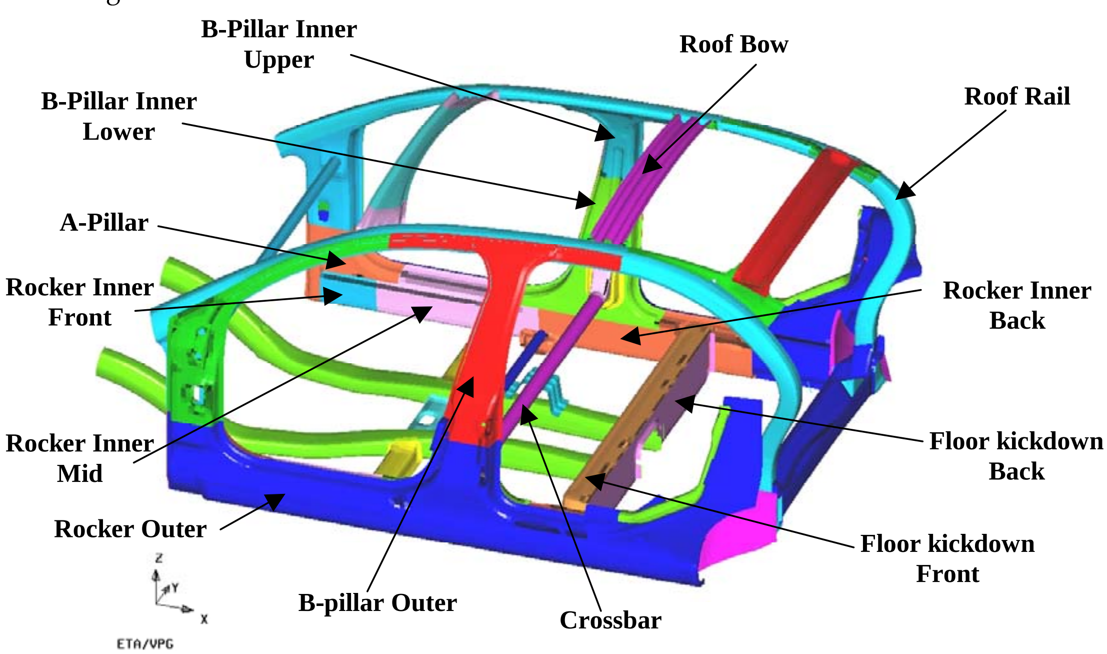

FIGURE 4. Run 1 Optimization - Design Variables

5.7. RESULTS

The final optimization reduced the mass of the designed parts by 12.0%, from 64.42 to 56.8kg. The results are shown in the Tables 1 & 2. The deformed plots of the optimized design for the IIHS Side Impact and the IIHS Front Crash ODB analyses are shown in Figures 5 & 6 respectively.

VARIABLE NAME	BASELINE (mm)	MINIMUIM mm)	MAXIMUM (mm)	OPTIMIZED (mm)
Roof Bow thickness	0.8	0.6	1.6	0.9
Roof Rail thickness	0.7	0.7	1.2	0.8
B-Pillar Inner lower thickness	0.7	0.8	1.3	0.8
B-Pillar Inner upper thickness	1.25	0.8	1.3	1.09
B-Pillar Outer thickness	1.0	0.8	1.3	1.1
Rocker Inner Front thickness	1.5	0.9	2.0	1.19
Rocker Inner Mid thickness	1.5	0.9	2.0	1.48
Rocker Inner Back thickness	1.5	0.8	1.3	1.01
Rocker Outer thickness	1.25	0.8	1.3	0.826
Rocker reinforcement thickness	1.2	0.6	2.0	0.9
Floor kick-down front thickness	0.8	0.7	1.5	0.9
Floor kick-down back thickness	1.2	0.7	1.3	1.1
Crossbar thickness	2.0	1.5	2.3	1.65
A-Pillar part thickness	0.7	0.6	1.6	0.915

TABLE 1: Optimal Design Variables - (Baseline & Range Shown For Comparison)

NAME	TYPE	DIRECTION	FGPC-BFO	FGPC-AFO	CHANGE
Mass	Objective	Minimize	64.42kg	56.8kg	-12%
Intrusion (measured IIHS side impact)	Constraint	>125mm	131.4mm	123.0mm	Almost Satisfied
Door integrity (measured for the ODB)	Constraint	<5.0mm @ three locations	6.54mm* 2.41mm* 6.88mm*	3.61mm 3.81mm 2.5mm	Satisfied
Torsional stiffness	Constraint	> 14000 Nm/deg	13779 Nm/deg	13771 Nm/deg	Almost Satisfied

*Task 5.5: Concept Design Check Supplement concludes that Iteration FGPC-ACD13a would be used as the baseline for the final optimization, FGPC-BFO. The report quotes the performance for FGPC-ACD13a as 8.0, 8.2 and 4.2mm. The difference in performance between FGPC-ACD13a and FGPC-BFO shown here is due to an analysis sensitivity created by running the same model with a different hardware/software combination.

TABLE 2: Response Values – Baseline & Optimized Design

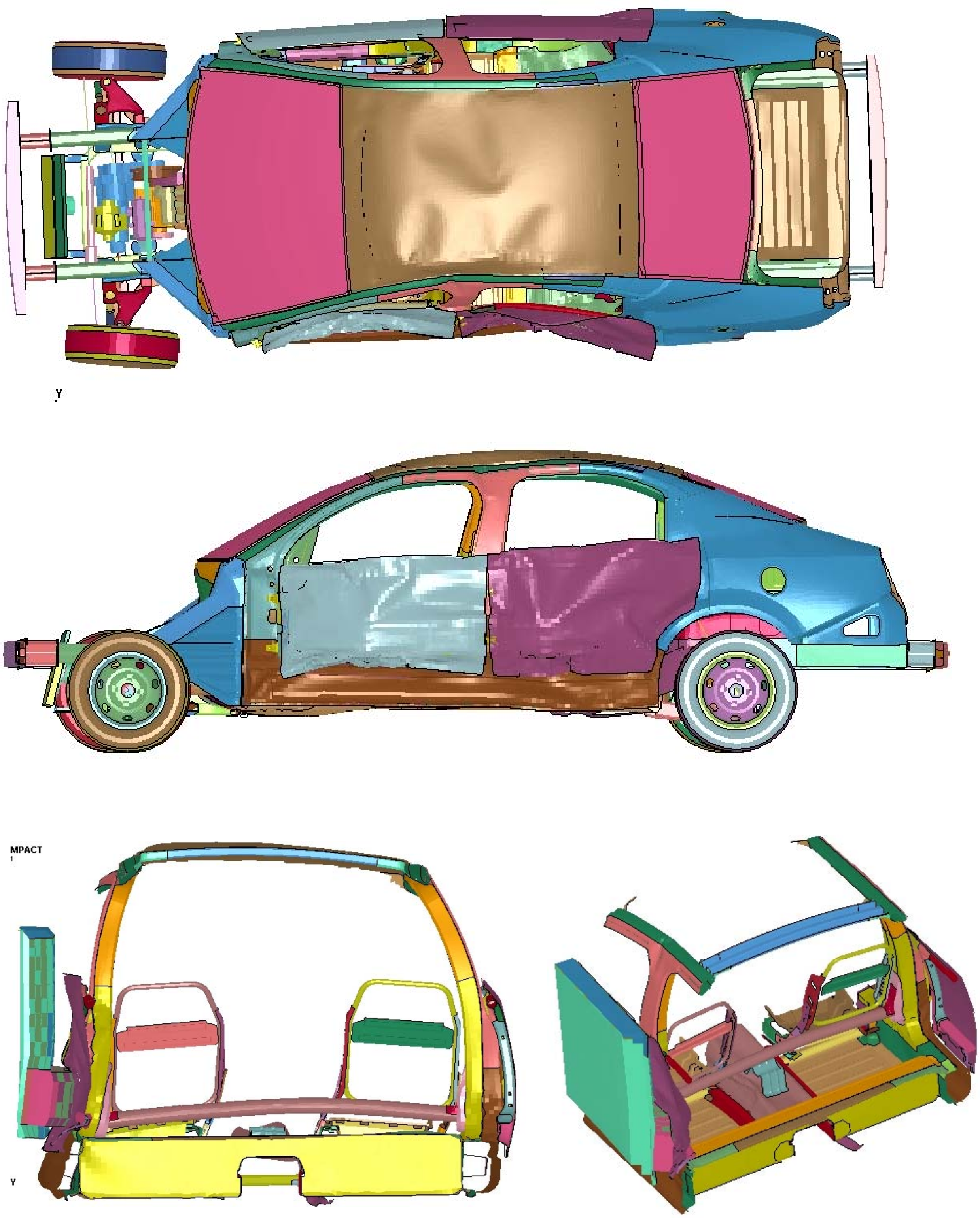

FIGURE 5: IIHS Side Impact Analysis – Optimized Design Deformed Shape

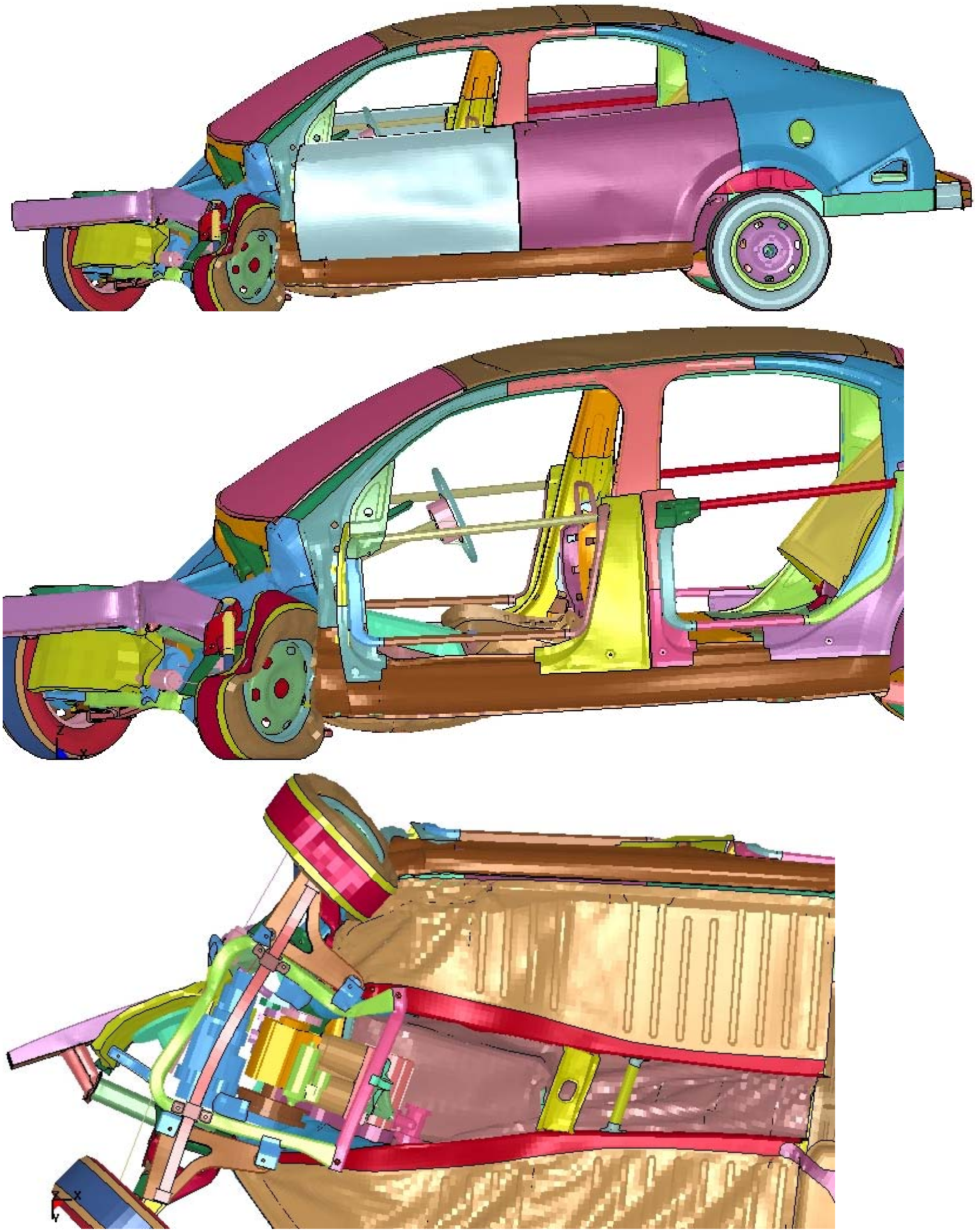

FIGURE 6: IIHS Front Crash ODB Analysis – Optimized Design Deformed Shape

6. FRONT DOOR BEAM OPTIMIZATION

A second optimization run was setup to find the minimum mass configuration of the front door beams, which meet the side door intrusion requirements. The target requirement force values for the optimization were set slightly higher than the actual FMVSS requirement. The objective is to be achieved by varying just the thickness of the four front door intrusion beams. The only requirements are the side door intrusion analysis average force values at 6in intrusion and 12in intrusion.

6.1. DESIGN PERFORMANCE EVALUATION

The optimization creates a new design by assigning values to all design variables and then executing the analyses required to assess the performance of the design. Three responses were used to assess the performance of each design, as defined in the optimization statement: the mass, the average force at 6in intrusion and the average force at 12in intrusion. The discussion below describes how these measurements are calculated for each design.

6.2. MASS

The mass of only the parts being designed (the four front door intrusion beams) is used as a performance measure during all the optimization. The sum of the masses for all the designed parts is the value that is optimized during the optimization run.

6.3. AVERAGE FORCE TARGETS

The other responses used in the performance evaluation of the design are the average force values at two different levels of intrusion. The force is measured in the rigid wall used for the intrusion analysis. Figure 7 shows a force-deflection plot for the side door intrusion analysis. The analysis is performed for a total intrusion of 12in. The first target is for the average force during the first 6in intrusion to be above 10.9kN. The second target is for the average force at 12in intrusion to be above 17.2kN.

6.4. OPTMIZATION STATEMENT

The objective of this run is to optimize the thickness of the front door side intrusion beams for a minimum mass design. The optimization statement for the run is:

Minimize:

Mass of the design

Subject to:

Average force @ 6in intrusion > 10.9kN
Average force @ 12in intrusion > 17.2kN

By varying:

Size of the Front door beam 1
Size of the Front door beam 2
Size of the Front door beam 3
Size of the Front door beam 4

The thickness values for all the beams parts are varied between 0.6 and 1.1mm. The material and shape of the door beams have not been changed in this optimization run. The optimization problem has 4 design variables, 2 constraints and one objective. Figure 8 shows the parts that are being designed for thickness during the optimization run.

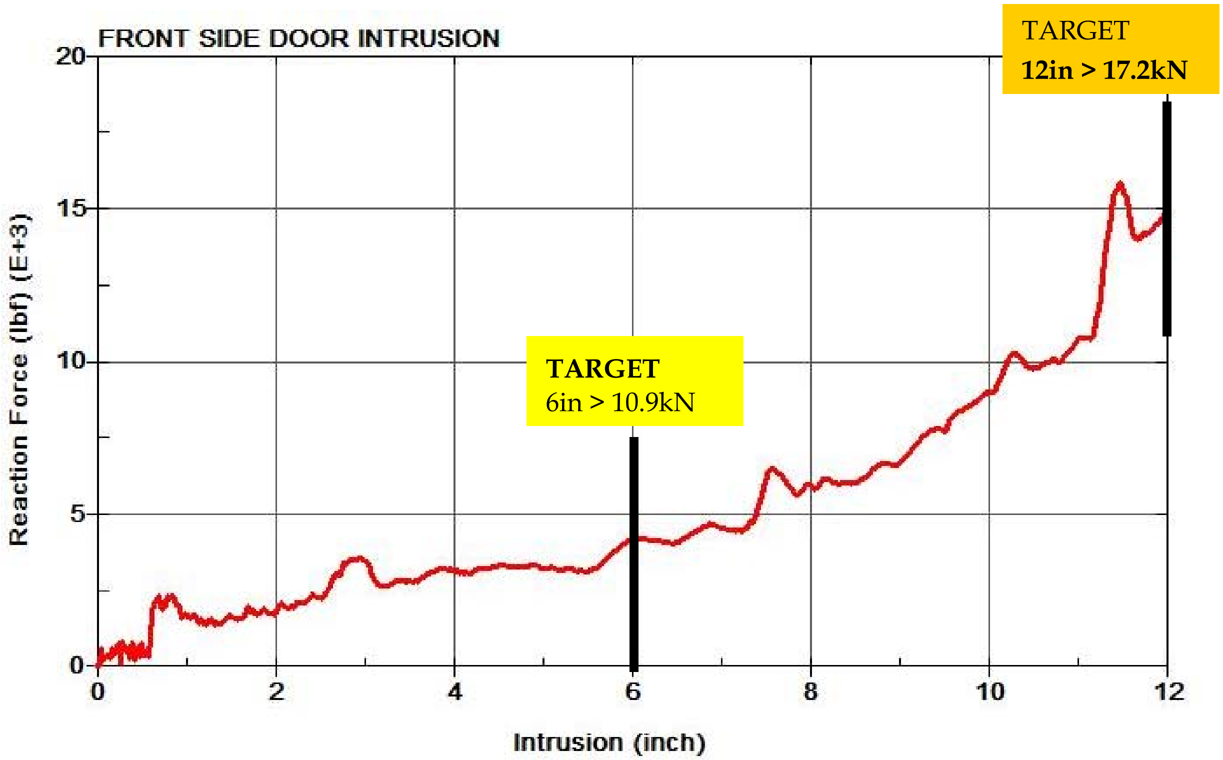

FIGURE 7: Rigid Wall Force Deflection – Front Side Door Intrusion

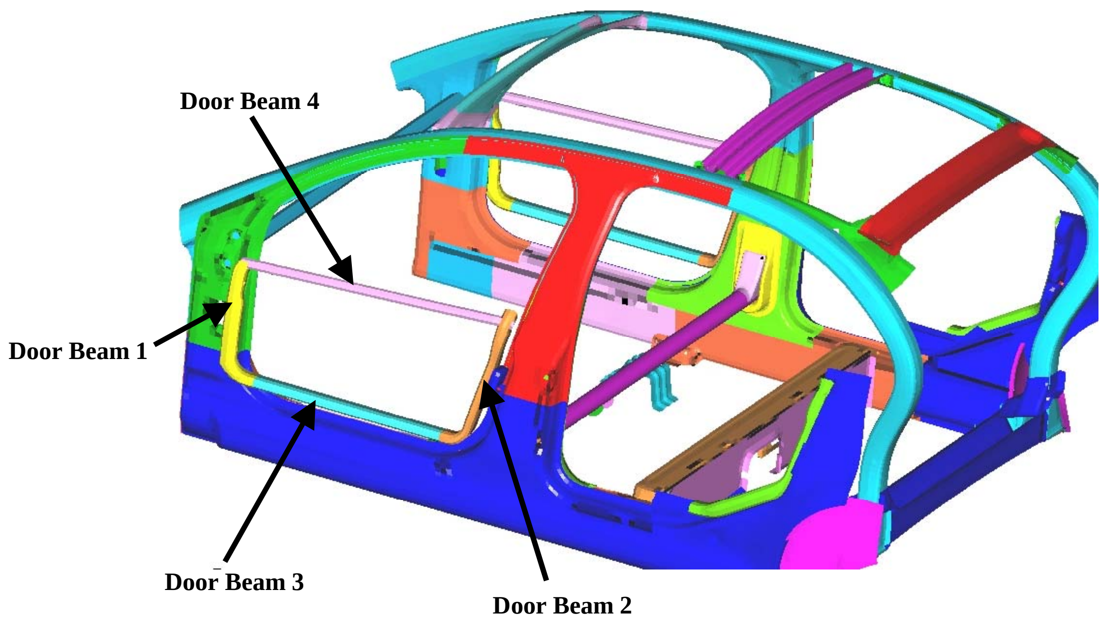

FIGURE 8: Front Door Beam Location

6.5. RESULTS

The optimized design is 29.3% lighter than the baseline design (a reduction of 1.54kg, from 5.256 to 3.714kg). It also meets both the force constraints. The results are shown in Tables 3 & 4. The thickness of 3 of the 4 door beams was reduced to the minimum allowed value of 0.6mm, while the final door beam thickness was set to 0.9mm. The thickness of the rear door beams was already at the minimum allowed value; as a result these were not optimized. Figures 9 shows the deformed plots of the optimized design after the front side door intrusion analysis.

VARIABLE	MINIMIUM GAUGE (mm)	BASELINE GAUGE (mm)	MAXIMUM GAUGE (mm)	OPTIMIZED GAUGE (mm)
Door Beam 1	0.6	0.8	1.1	0.6
Door Beam 2	0.6	0.8	1.1	0.6
Door Beam 3	0.6	0.8	1.1	0.9
Door Beam 4	0.6	0.8	1.1	0.6

TABLE 3: Optimal Design Variables (Baseline & Range Shown For Comparison)

RESPONSE	TYPE	TARGET	BASELINE	OPTIMIZED
Mass	Objective	Minimize	5.256kg	3.714kg
Avg. Force @ 6in	Constraint	>10.9kN		11.04kN
Avg. Force @12in	Constraint	>17.2kN		23.04kN

TABLE 4: Optimal Design Responses (Baseline & Targets Shown For Comparison)

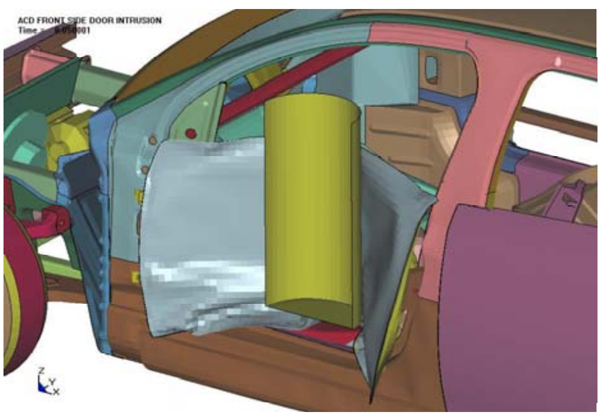

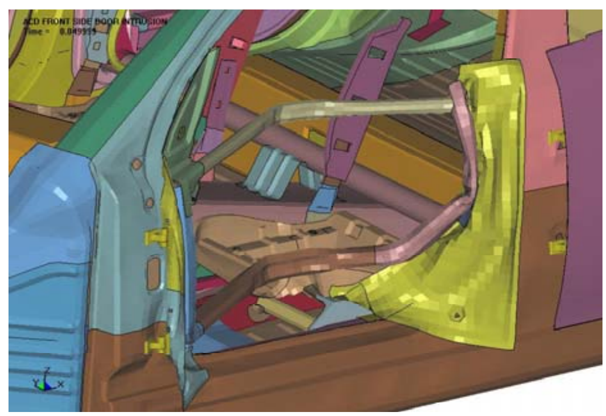

FIGURE 9: Front Door - 12in Intrusion Deformed Shape

Press to open animation

Press to open animation

7. REAR DOOR BEAM OPTIMIZATION

The rear door beam thicknesses were 0.6 and 0.8mm at the start of this task, which is near the lower limit of 0.6mm assumed for this program. Therefore, instead of performing a thickness optimization, the door beam geometry was modified to remove more mass while still meeting the targets.

The door beam sectional dimensions were reduced by approximately 20% and the door beam thicknesses were all made 0.6mm, as shown in Figure 10.

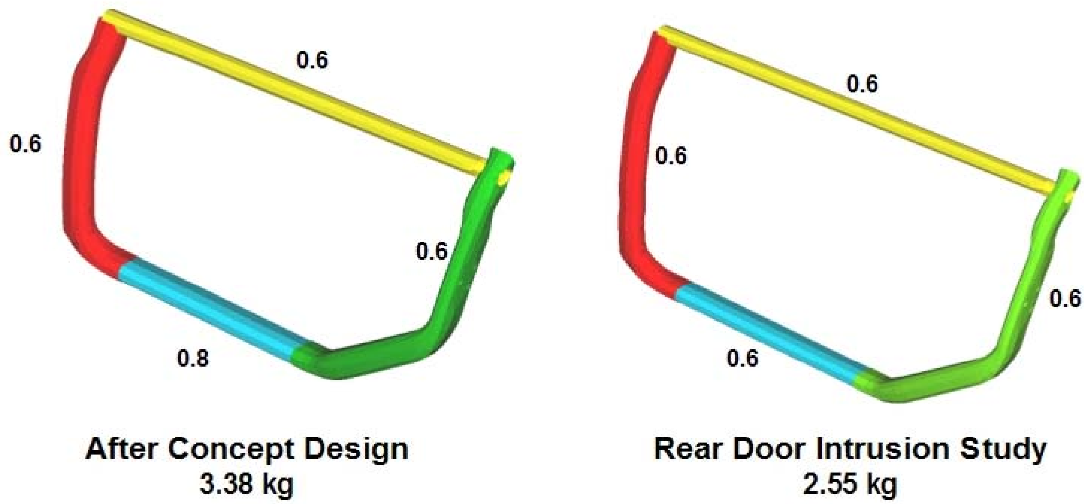

FIGURE 10: Modified Rear Door Beams

7.1. AVERAGE FORCE TARGETS

Figure 11 compares the rigid barrier force performance of both FGPC-ACD and FGPC-AFO. It also summarizes the average force at 6 and 12in deflections. The deformed shape is shown in Figure 12.

7.2. MASS

The updated door beam design is over 30% above the FMVSS 214 Static requirements, while providing a total mass savings of 0.83kg. Though the potential for even more weight savings still exits, it is bound by the manufacturing issues raised by using a minimum gauge of less than 0.6mm.

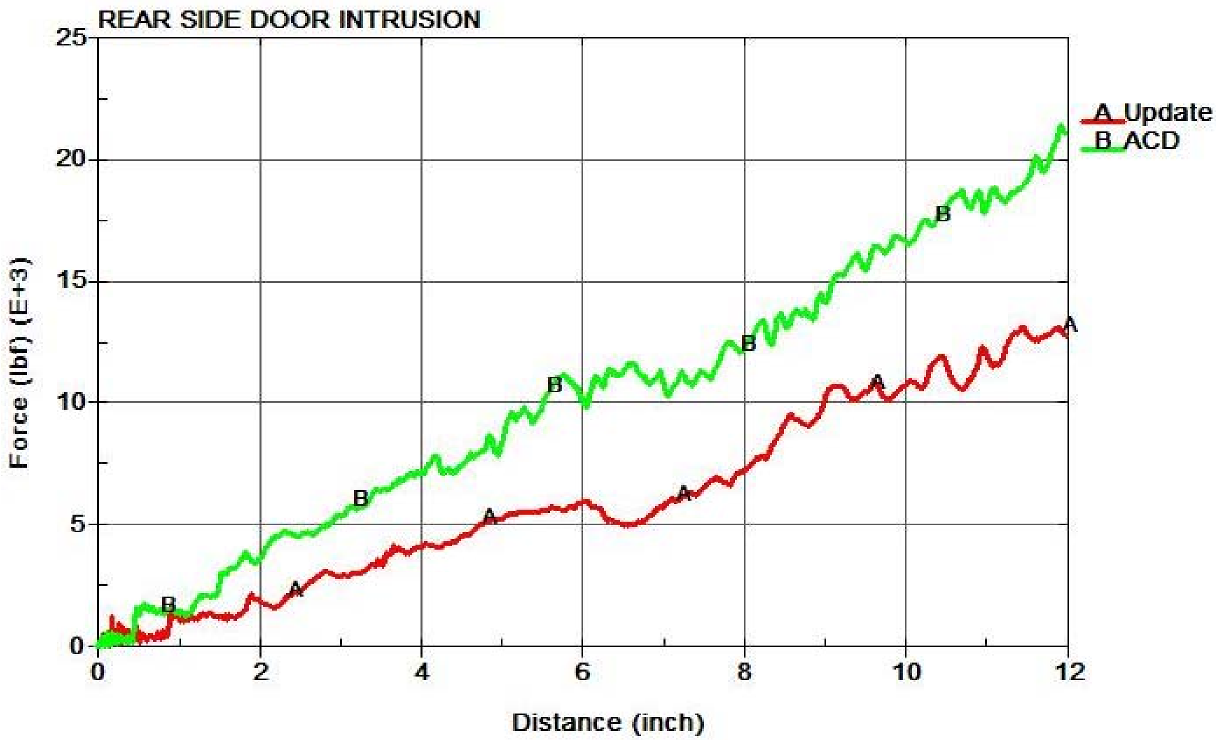

TARGET	FGPC-ACD (lbf)	FGPC-AFO (lbf)	FMVSS214 (lbf)
6 inch	3621	2987	2250
12inch	6822	6053	3500

FIGURE 11: Modified Rear Door Beams Force vs. Deflection

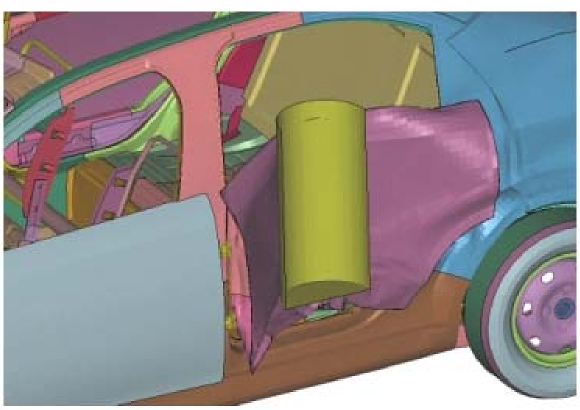

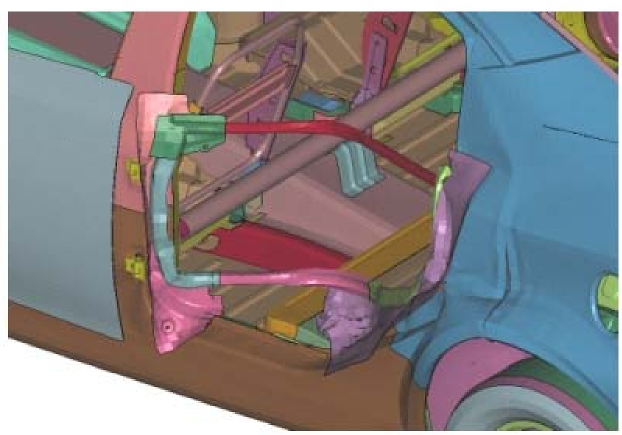

FIGURE 12: Modified Rear Door Beams –Deformed Shape At 12in Deflection

Press to open animation

Press to open animation

8. POLE IMPACT OPTIMIZATION

From experience gained in Task 5.5: Concept Design Check Supplement, the IIHS Front Crash ODB was found to be a dominating loadcase, limiting the influence of the Pole Impact. To expedite the optimization the Pole Impact was performed individually. The Pole impact simulation was performed on the optimized model from IIHS front and side impact. In Task 5.5 tubes were added under the front seats and across the tunnel to provide a load path for the pole impact, as shown in Figure 13. A small optimization minimized the mass of the tubes while still satisfying the pole impact criteria.

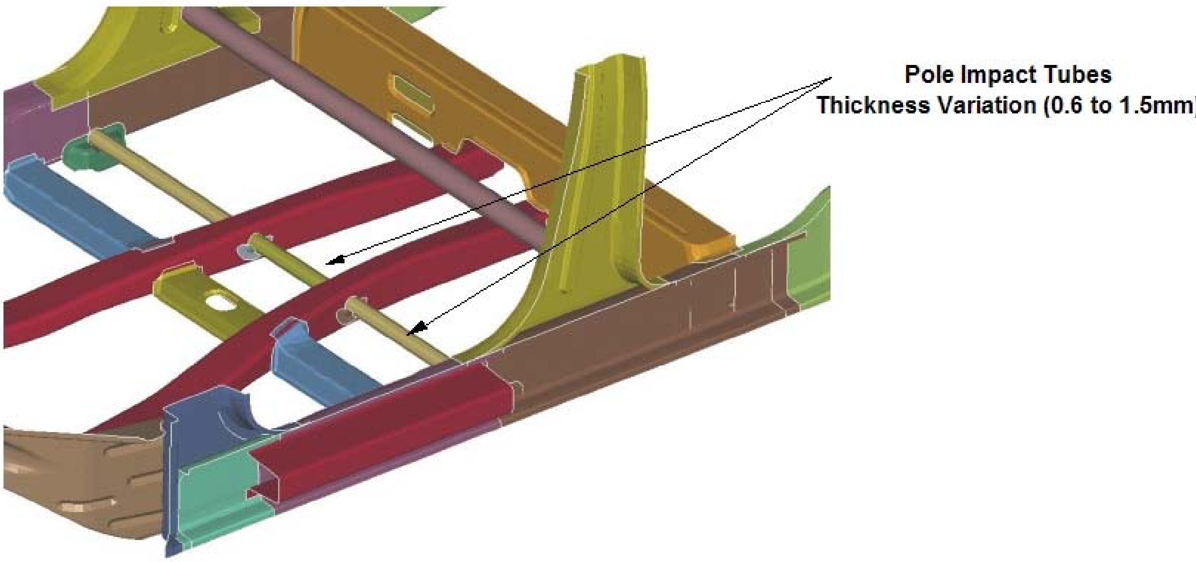

FIGURE 13: Pole Impact Optimization Setup

The optimization analysis showed that the pole impact target was not met over the tube thickness range 0.6 to 1.5mm. The Pole Impact requirement could not be met without modifying the thickness or design of parts other than the tubes.

A small sensitivity study was performed to determine which changes in thickness from the original design degraded the pole impact performance. The two major thickness changes in the impact zone were the IIHS Side Impact crossbar (2.0 to 1.65mm) and the Rear Rocker (1.5 to 1.0mm). Analyses were run with each of these parts back to their original thickness (Iterations #1 and #2 in Table 5). The results of these runs showed that restoring the IIHS Side Impact Tube thickness had no effect on the pole impact performance, but increasing the Rear Rocker thickness met the pole impact target (+2.8mm maximum seat to structure distance compared to –7mm target). The thicker Rear Rocker also increased the mass by 1.9kg.

Next, the Cross-member Support Rear Center Bracket and the Cross-member Reinforcement Tunnel Lower (Figure 14) were removed to save weight. The bracket across the tunnel was thought to be unnecessary since the pole impact tube reinforced the same area. The bracket beneath the IIHS Side Impact Tube was not thought to contribute to the structural performance since it was not connected to the tube. The pole impact tubes were also reduced from 1.2 to 0.6mm in the center and from 1.0 to 0.8mm between the Rocker and Tunnel. Removing the brackets and reducing the tube thickness saved 1.4kg weight while still meeting the pole impact target (-5mm seat to structure distance), as shown in Table 5.

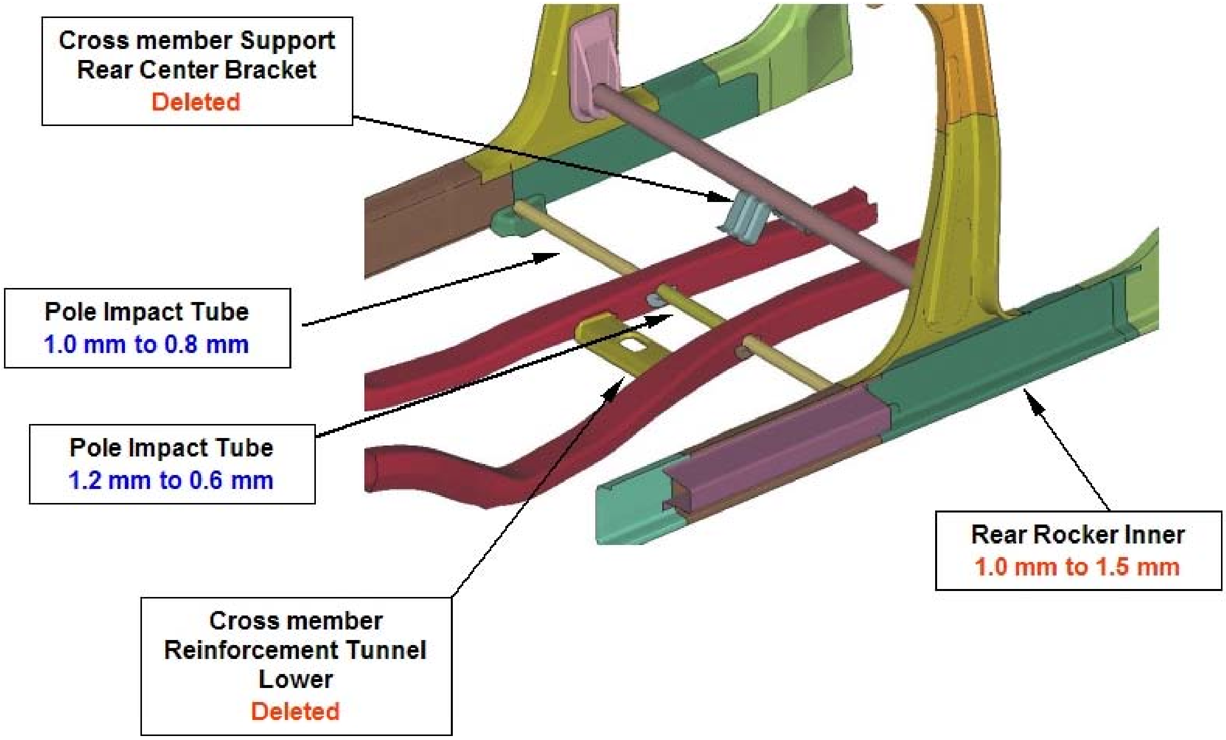

FIGURE 14: Pole Impact Sensitivity Study Results - Iteration #7

SIMULATION	CONFIGURATION	MINIMUM STRUCTURE TO SEAT DISTANCE (mm)
After Final Optimization	Base After Optimization Model	-33.4
Iteration #1	FGPC-AFO + Side Impact Tube thickness increased 1.65 to 2.0mm	-33.6
Iteration #2	FGPC-AFO + 1.5mm Rear Rocker Inner	2.8
Iteration #3	FGPC-AFO + 1.25mm Rear Rocker Inner	-16.3
Iteration #4	Iteration #2 + Under tunnel bracket	-2.1
Iteration #5	Iteration #2 + Side Impact Tube bracket	2.9
Iteration #6	Iteration #4 + 1.3mm Rear Rocker Inner	-18.7
Iteration #7	Iteration #2 + Under tunnel bracket - Over Tunnel Bracket + Reduced Pole Impact Tubes	-5.05
Iteration #8	Iteration #7 + Over Tunnel Bracket	-9.32
TARGET		>-7mm

TABLE 5: Pole Impact Sensitivity Study Results

9. OPTIMIZATION RESULT VARIATIONS

The optimal design satisfies both IIHS Side Impact and Front Crash ODB with a solution tolerance of approximately ± 1 to 2%. These small differences are a function of the explicit FEA method. To control this issue, ETA has minimized the variation in software and hardware architectures. The results quoted in this report are considered pessimistic. Task 7.0: Final Concept Design Analysis Check will resolve this variation.

10. CONCLUSION

The combined IIHS Side Impact, IIHS Front Crash ODB and Torsional Stiffness optimization reduced the BIW mass by 7.6kg. For Pole Impact optimization increased the Rear Rocker by 1.9kg, while removing 1.4kg in brackets and tubes for a net BIW reduction of 7.1kg. The Front Door optimization reduced the mass by an additional 1.5kg and changes to the rear door structure saved an additional 0.8kg. The total vehicle mass reduction for the BIW and doors achieved by this task was 9.4kg.

Table 6 summarizes the FGPC project to date comparing the mass of FGPC-BO, the project baseline design, to the results of Task 6.0: Final Optimization, FGPC-AFO. Task 7.0: Final Design Analysis Check will check this design against all loadcases.

STRUCTURE	FGPC-BO (kg)	FGPC-AFO (kg)	MASS SAVINGS (kg)	CHANGE (%)
BIW + IP BEAM	227.2	216.8	10.4	5

MODIFIED PARTS	FGPC-BO (kg)	FGPC-AFO (kg)	MASS SAVINGS (kg)	CHANGE (%)
BIW	130.6	120.2	10.4	8
Doors	12.6	6.3	6.3	50
TOTAL	**143.2**	**126.5**	**16.7**	**12**

STRUCTURE	INDUSTRY STANDARD (kg)	FGPC-AFO (kg)	MASS SAVINGS (kg)	CHANGE (%)
BIW + IP BEAM	310.0	216.8	93.2	30

TABLE 6: Current Mass Summary For FGPC Project

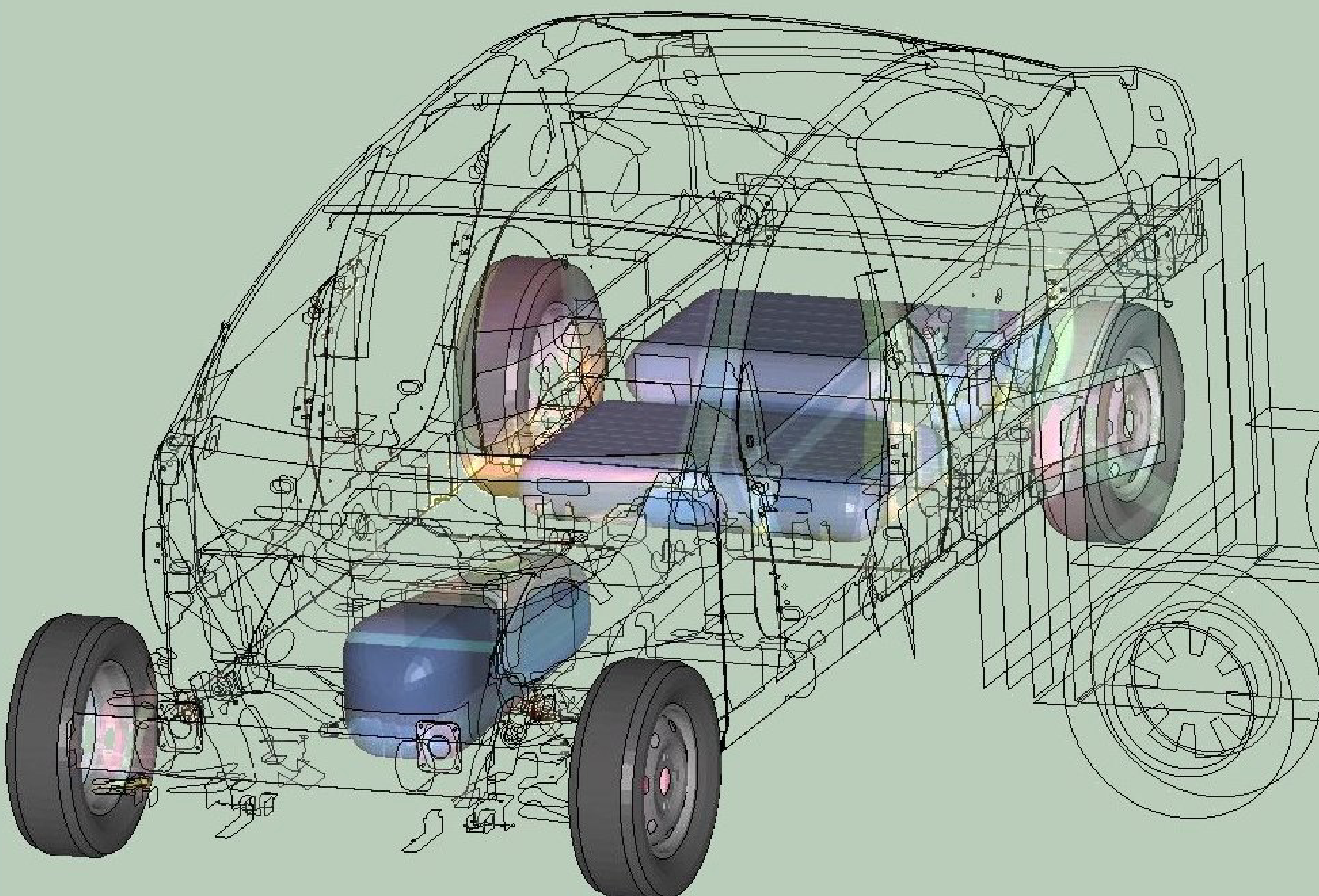

A/S P Auto/Steel Partnership

Future Generation Passenger Compartment
Task 7.0 - Final Concept Design Check

Final design concept's performance assessment under all loadcases considered

Task 7.0 - Final Concept Design Check

Table of Contents

Task 7.0 - Final Concept Design Check

1. INTRODUCTION

This report completes Task 7.0: Final Concept Design Check of the FGPC (Future Generation Passenger Compartment) project. Its purpose is to document the performance of the FGPC-AFO, the final optimization model, under the following loadcases:

1. US-Front crash NCAP (Flat Barrier zero degree impact)
2. IIHS Front Crash 40% ODB (Offset Deformable Barrier)
3. Side Pole Impact (FMVSS214 NEW)
4. IIHS Side Impact
5. Roof Crush
6. Door Intrusion
7. Rear Crash
8. Durability (VPG)
9. Stamping and Formability
10. Modal & Static Stiffness
    - Normal Modes (Free-Free)
    - Static Torsion & Bending Stiffness

2. NAMING CONVENTION

Throughout this report the various FGPC design levels will be identified in the following manner:

- FGPC-BO (FGPC-Before Optimization)
  Task 2.0: Calibration Baseline - ULSAB-AVC PNGV modified to accommodate both Diesel and Fuel Cell powertrains. This is the FGPC Baseline.

- FGPC-AO (FGPC-After Optimization)
  Task 3.0: Optimization - the optimized FGPC Baseline.

- FGPC-ACD (FGPC-After Concept Design)
  Task 4.0: Concept Design - the optimization results integrated into a production viable vehicle.

- FGPC-ACDC (FGPC-After Concept Design Analysis Check)
  Task 5.0: Concept Design Analysis Check – Check of FGPC performance after changes due to optimization, design and manufacturability constraints.

- FGPC-BFO (FGPC-Before Final Optimization)
  Task 5.5: Concept Design Check Supplement - Final design changes to meet IIHS Front Crash and Pole Impact by adding new load path and material gauge changes

- FGPC-AFO (FGPC-After Final Optimization)
  Task 6.0: Final Optimization - Gauge optimization performed on FGPC-BFO, the Task 5.5: Concept Design Analysis Check model.

- FGPC-FCD (FGPC-Final Concept Design)
  Task 7.0: Final Concept Design Check - All final design changes checked under all loadcases.

3. OBJECTIVE

The objective of this task is to compare the performance of the FGPC-AFO to FGPC-BO for each loadcase.

4. REGULATIONS

Detailed specifications are described in Appendices A through G.

Auto Steel Partnership

5. FGPC-FCD Model

The FE model for FGPC-FCD is based on the FGPC-AFO model. The major differences of this model are:

1. The material gauges were revised to more realistic values, for example 0.92mm was decreased to 0.9mm. See Figure 1.
2. The Rear door beams were modified after shape optimization to meet manufacturability considerations.
3. The joints were updated based on Task 4.0: Concept Design recommendations.
   - Reduction of cost and manufacturing effort by replacing laser welding with spot welds and structural adhesive. Adhesives were only proposed in areas that would not degrade the vehicle performance integrity. See Figure 2.
   - Henkel Terokal 4555B structure adhesive was used in the areas that would increase BIW stiffness (10% increase based on ETA experience). Its properties are listed in Table 1 and a stress/strain curve is shown in Figure 3.

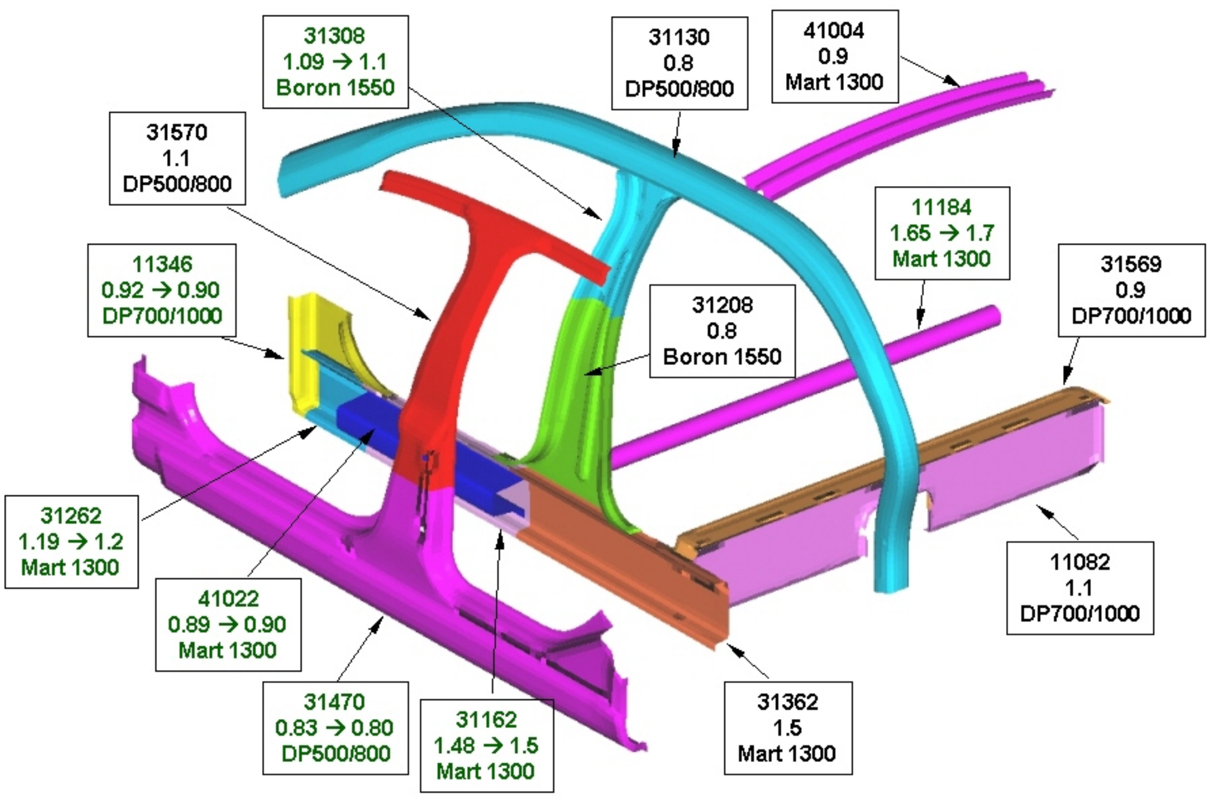

FIGURE 1: Finalized BIW Gauges & Materials

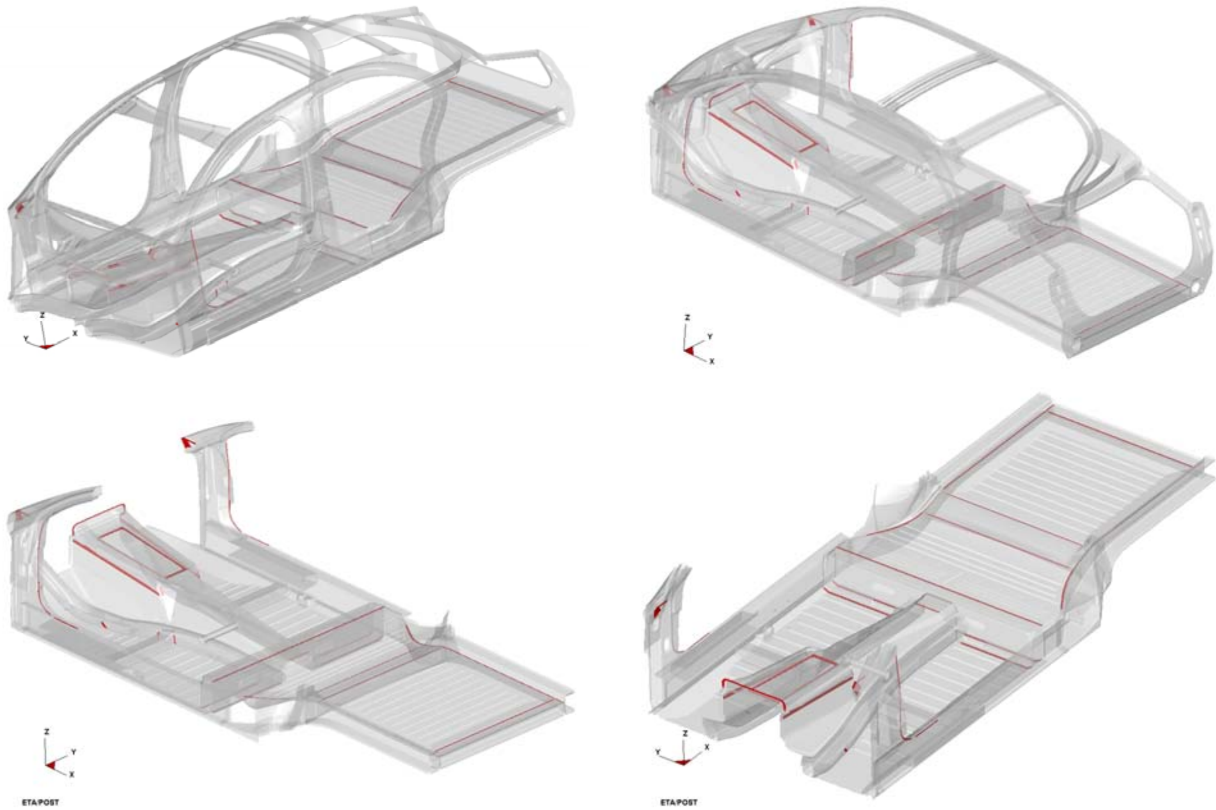

FIGURE 2: Adhesive Locations

PROPERTIES	TEROKAL 4555B
Density (ASTM D792)	1.07g/cm^3
Hardness (ASTM D2240)	80.8 Type D
Glass Transition (ASTM D4065)	107.7 C
Coefficient of Thermal Expansion	69.5m/m/^{o}C
Elongation (ASTM D638)	2.45%
Tensile Strength (ASTM 638)	28711kPa
Poisson's Ratio (ASTM 638)	.417
Young's Modulus (ASTM 638)	1887MPa

TABLE 1: Henkel 9982281 TEROKAL 4555B Properties

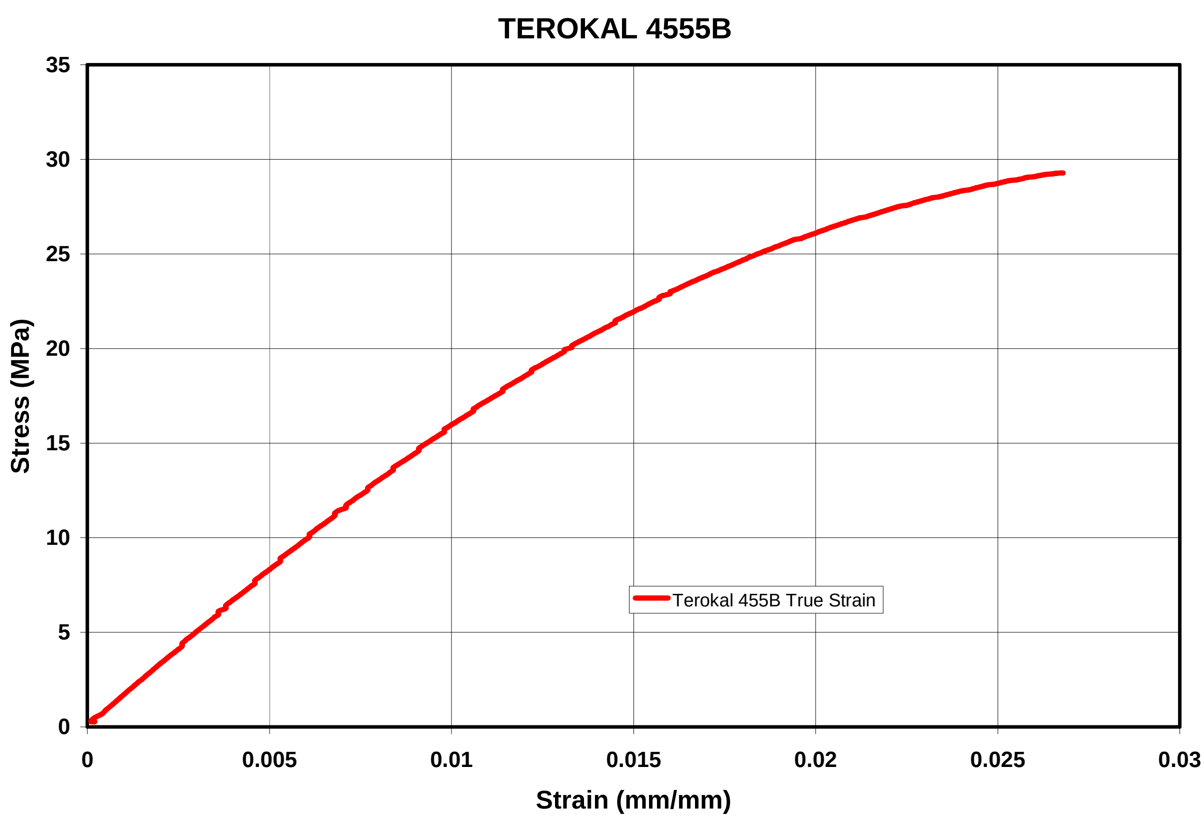

FIGURE 3: Henkel 9982281 TEROKAL 4555B Adhesive Stress/Strain Curve

6. ZERO DEGREE FRONT CRASH -US-NCAP

This analysis is intended to assess the structural performance for the frontal impact (NCAP). The 35 miles per hour zero degree barrier impact simulation is based on National Highway Transportation safety Administration (NHTSA) new car assessment program (NCAP) test.

6.1. TARGET

Based on NCAP FMVSS 208 requirements the following targets have been set:

- Crush distance
- Vehicle pulse

6.2. LOADS AND BOUNDARY CONDITIONS

The impact barrier is represented as a fixed rigid wall positioned so that it almost contacts the front tip of the front bumper at the start of the simulation. The ground is also represented as a rigid wall positioned at the very lowest points of the tires. Initial velocity of 35 mph in X direction is applied to all the nodes. The performance of the vehicle structure was verified under NCAP loading; the vehicle is impacted into a rigid wall at a speed of 35 mph. The results are compared to the FGPC-BO. Figures 4 & 5 show the vehicle structure before impact as well as after impact for both FGPC-BO and FGPC-FCD.

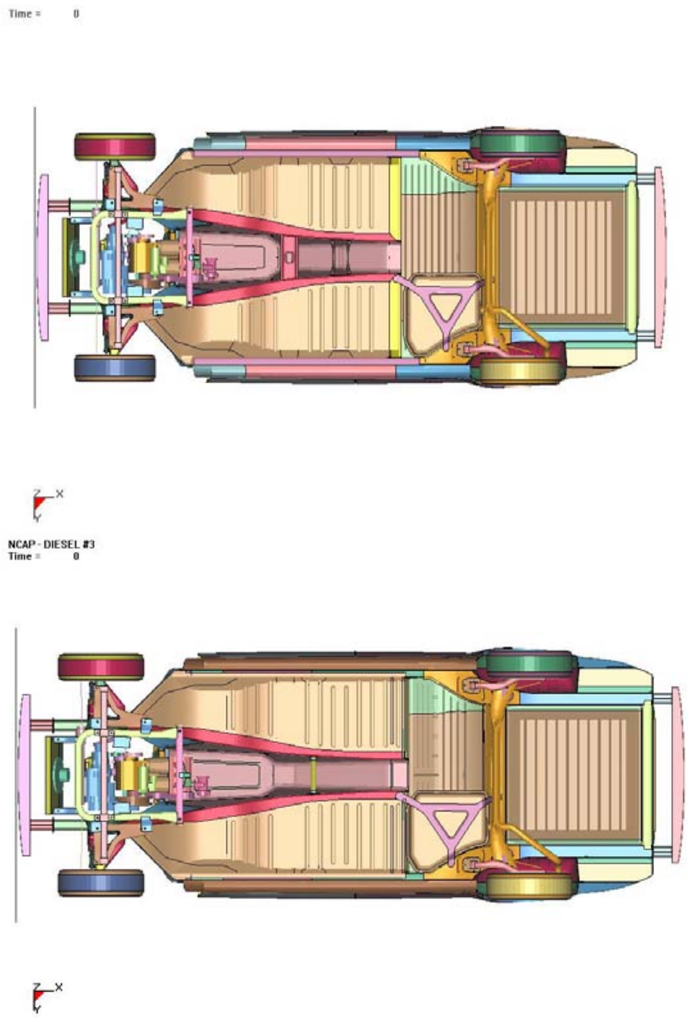

FIGURE 4: NCAP Bottom View Of Undeformed Vehicle Structure (FGPC-BO vs. FGPC-FCD)

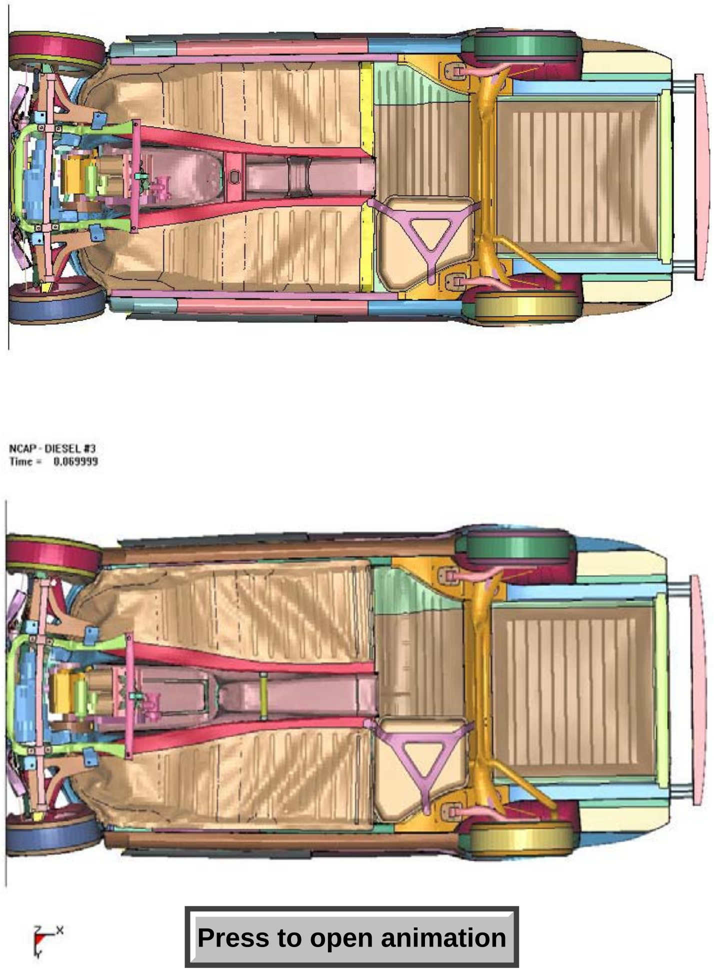

FIGURE 5: NCAP Bottom View Of Deformed Vehicle Structure (FGPC-BO vs. FGPC-FCD)

6.3. RESULTS

Displacement and velocity measurements in key areas and critical locations are compared to identify whether or not the new design performs as well as or even better than FGPC-BO. Figure 6 shows the comparison between the buckling modes of the front longitudinal member. It indicates that the changes incorporated to the structure are not affecting the longitudinal performance.

FGPC-BO

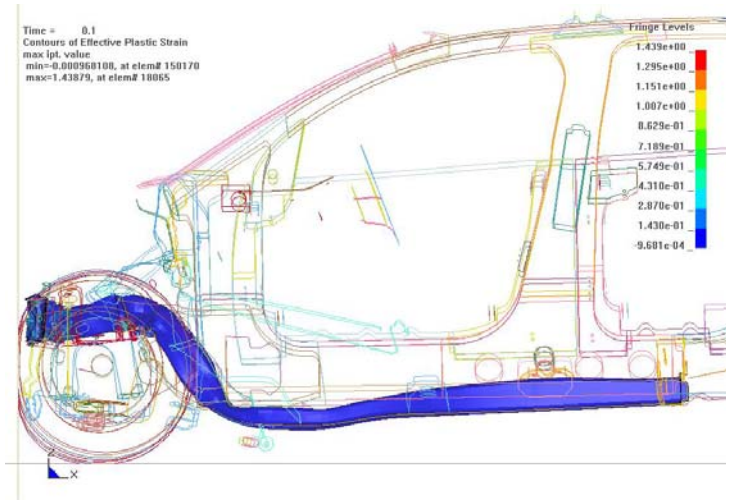

FGPC-FCD

Press to open animation

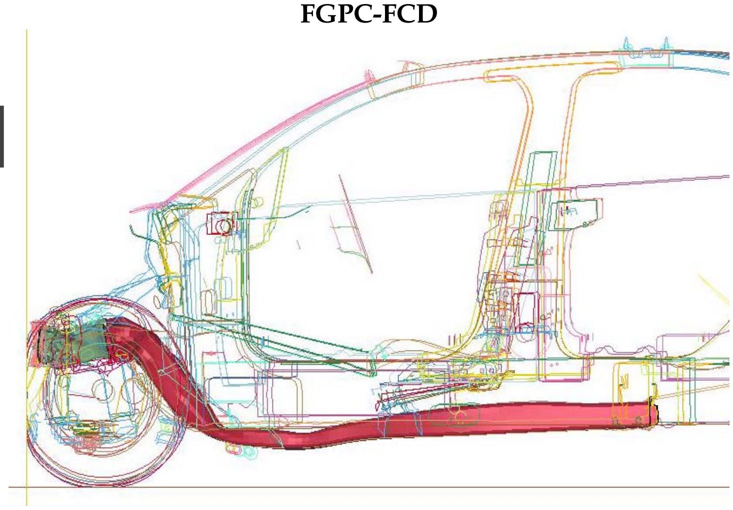

FIGURE 6. Front Longitudinal Member Buckling Mode Comparison (FGPC-BO vs. FGPC-FCD)

The displacement, velocity, and deceleration for the lower B-Pillar are shown in Figures 7 & 8, respectively. The results show that the FGPC-FCD has similar performance with respect to the FGPC-BO

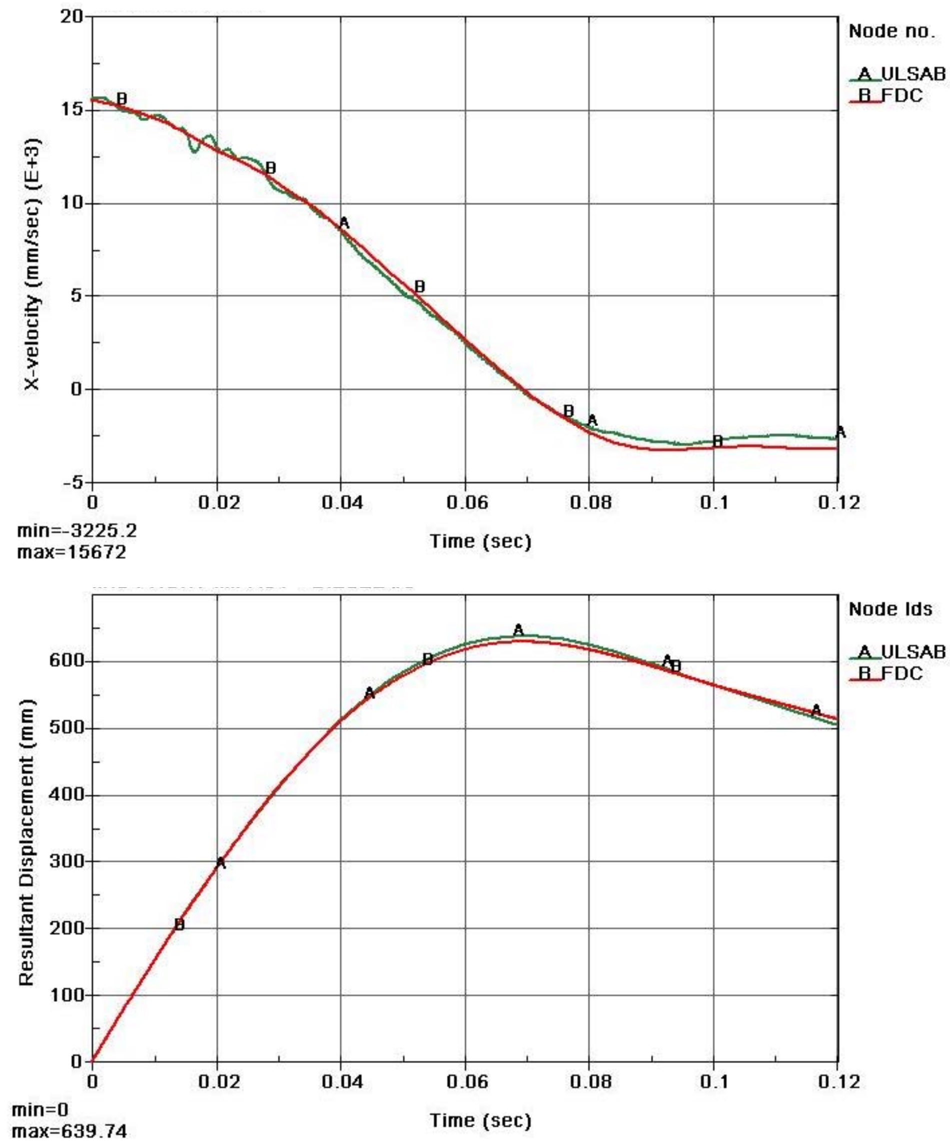

FIGURE 7: Lower B-Pillar Displacement & Velocity Comparison (Displacement & Velocity vs. Time)

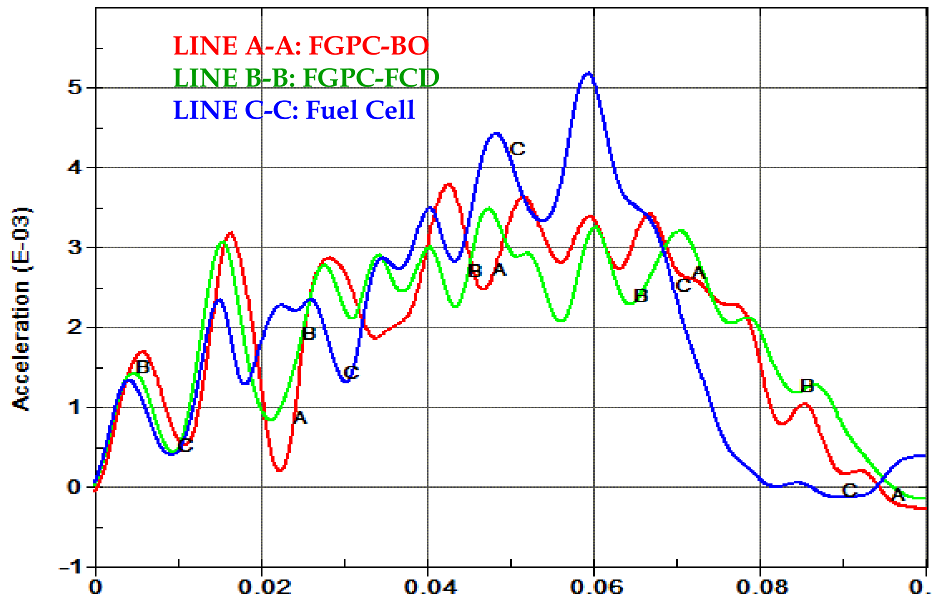

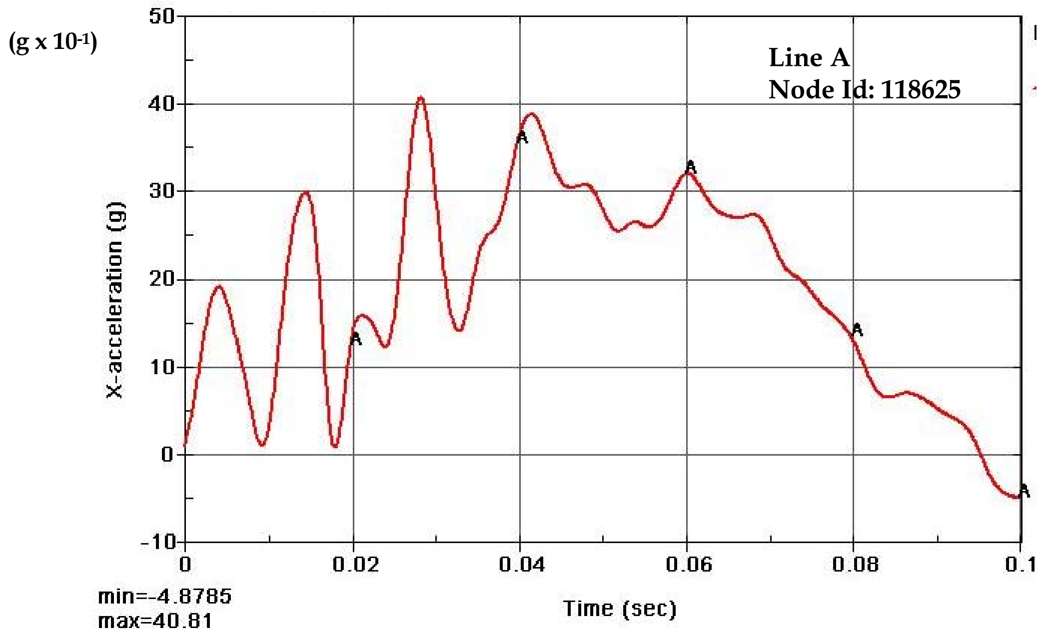

FIGURE 8: Lower B-Pillar Pulse (Deceleration vs. Time)

Absorption of kinetic (impact) energy of the vehicle structure, acceleration pulse, dynamic crush and time to zero velocity were measured to compare the updated vehicle structure with the FGPC-BO structure. The new optimized structure shows similar performance, (TTZV is the time to zero velocity), as shown in Table 2 and Figure 9.

	PEAK ACCEL. (g)	DYNAMIC CRUSH (mm)	TTZV (ms)
FGPC-BO	37.36	639.7	69.9
FGPC-FCD	40.81	630.2	69.2

TABLE 2:Vehicle Pulse & Crush Distance Performance (FGPC-BO vs. FGPC-FCD)

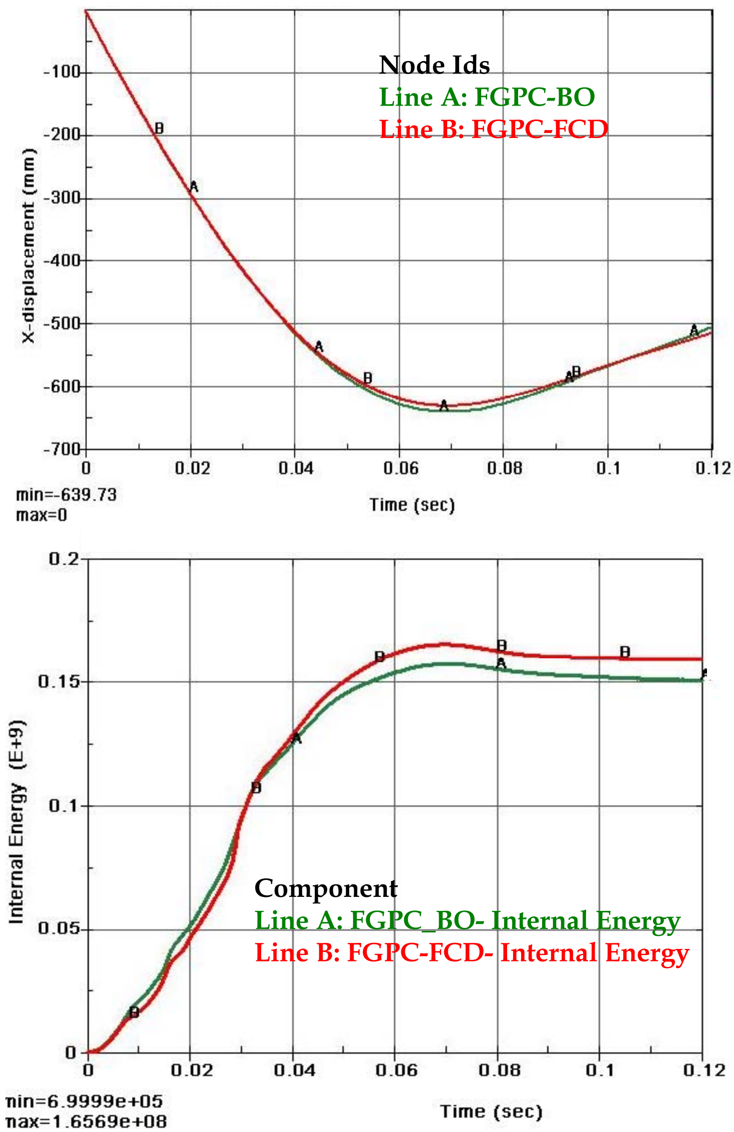

FIGURE 9: X-Displacement Of Lower B-Pillar & Vehicle Internal Energy

6.4. CONCLUSION

The results of FGPC-FCD analysis show no major changes in the vehicle performance after final design change and weight optimization compared to the vehicle performance before optimization. The vehicle structure performs well, satisfying the target.

7. IIHS FRONT CRASH 40% ODB

7.1. TARGETS

IIHS Front Crash 40% ODB impact is an analysis check loading case. The full regulations are in Appendix A. The target, established here by the FGPC team, considers design changes that may affect the safety cage structural integrity such as door operability and body structure deformation. Based on this strategy the following targets have been set for this loadcase:

- Rocker cross-sectional forces
  Section forces should meet or exceed those of the FGPC-BO.
- Door open-ability
  Doorframe deformation should not exceed FGPC-BO levels.

7.2. LOADS AND BOUNDARY CONDITIONS

The vehicle impacts a deformable barrier, offset 10% from centerline (40% overlap), at 40mph. See Figures 10 & 11.

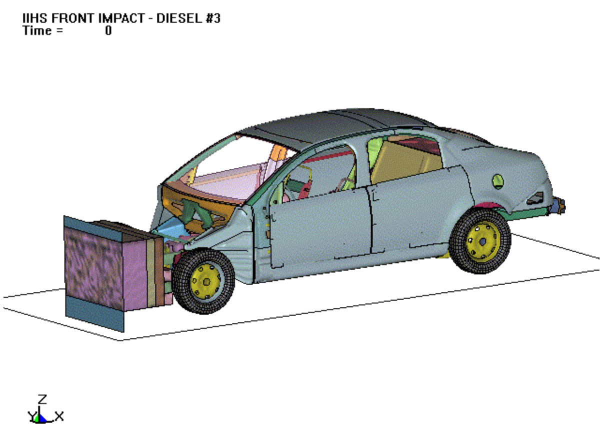

FIGURE 10: IIHS Side Impact Model (ISO View)

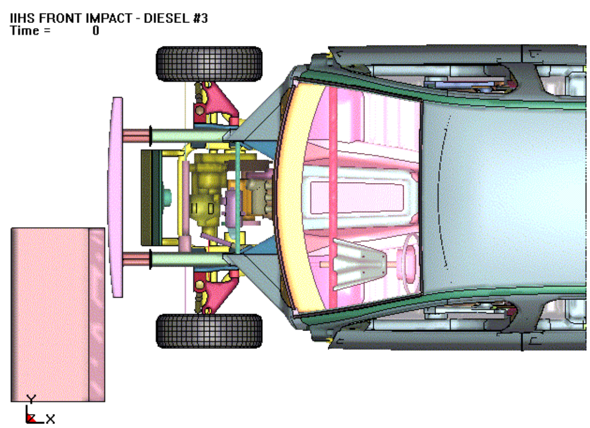

FIGURE 11: IIHS Side Impact Model (Top View)

Rocker cross-sectional forces and door open-ability were used to evaluate the vehicle's performance. The Door open-ability was measured in three locations: Top, Middle and Bottom. See Figure 12.

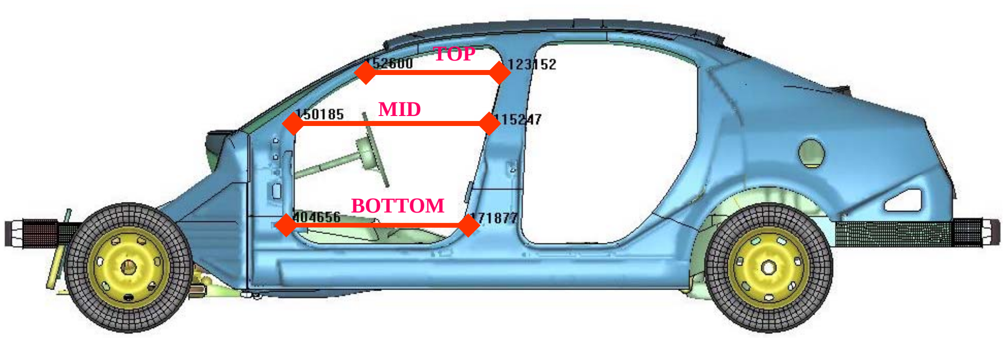

FIGURE 12: Door Open-Ability Measurement Points

7.3. RESULTS

The analysis was performed to make sure the design changes did not have a negative effect on the performance of the vehicle under the IIHS Front Impact load. Figure 13 shows the design changes in the rocker area.

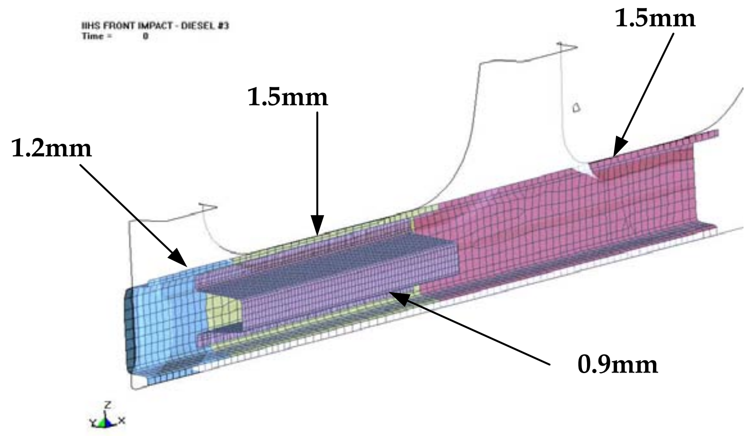

FIGURE 13: Rocker Design Changes

Table 3 and Figure 14 show the results for rocker cross-section force and door openability both for the FGPC-BO and FGPC-FCD.

RUNS	CURB WEIGHT	DOOR OPENABILITY (CHANGE IN LENGTH)			X-SECTION FORCE	NOTE
		TOP	MID	BOTTOM	ROCKER	
FGPC-BO	1102.1	0.3	4.2	3.3	121.5	Before Optimization
FGPC-FCD	1086.3	0.2	4.2	4.9	134.7	Final Concept Design

TABLE 3: IIHS Front Impact 40% ODB – FGPC-BO & FGPC-FCD

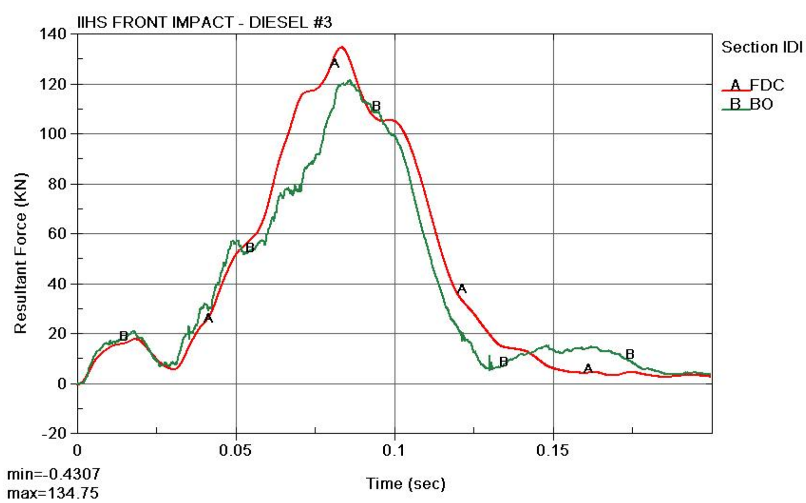

FIGURE 14: Rocker Cross-Section Forces – FGPC-BO & FGPC-FCD

Figure 15 shows the design change in the rocker area for the FGPC-FCD.

FGPC-BO

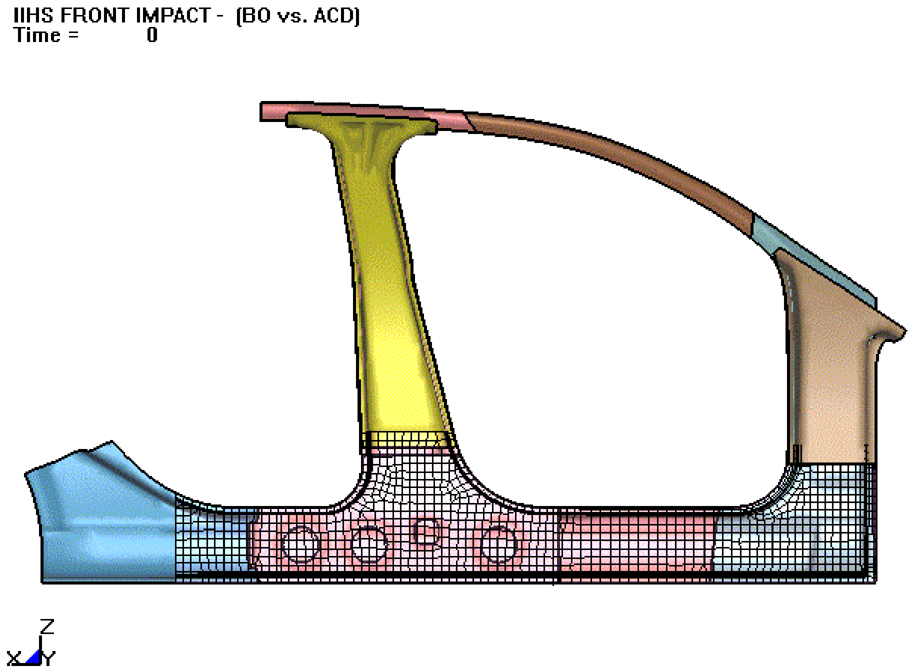

FGPC-FCD

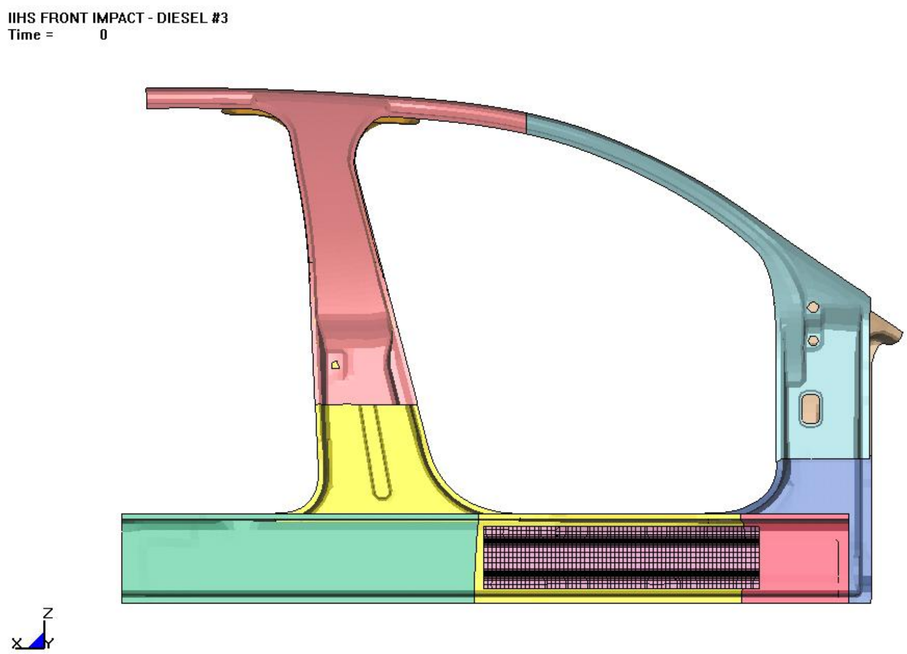

FIGURE 15: Rocker Design Changes - Before & After Optimization

Press to open animation

Figure 16 shows a comparison between the change in length for FGPC-FCD and the vehicle structure before optimization: at the top, middle, and lower of the front door, respectively.

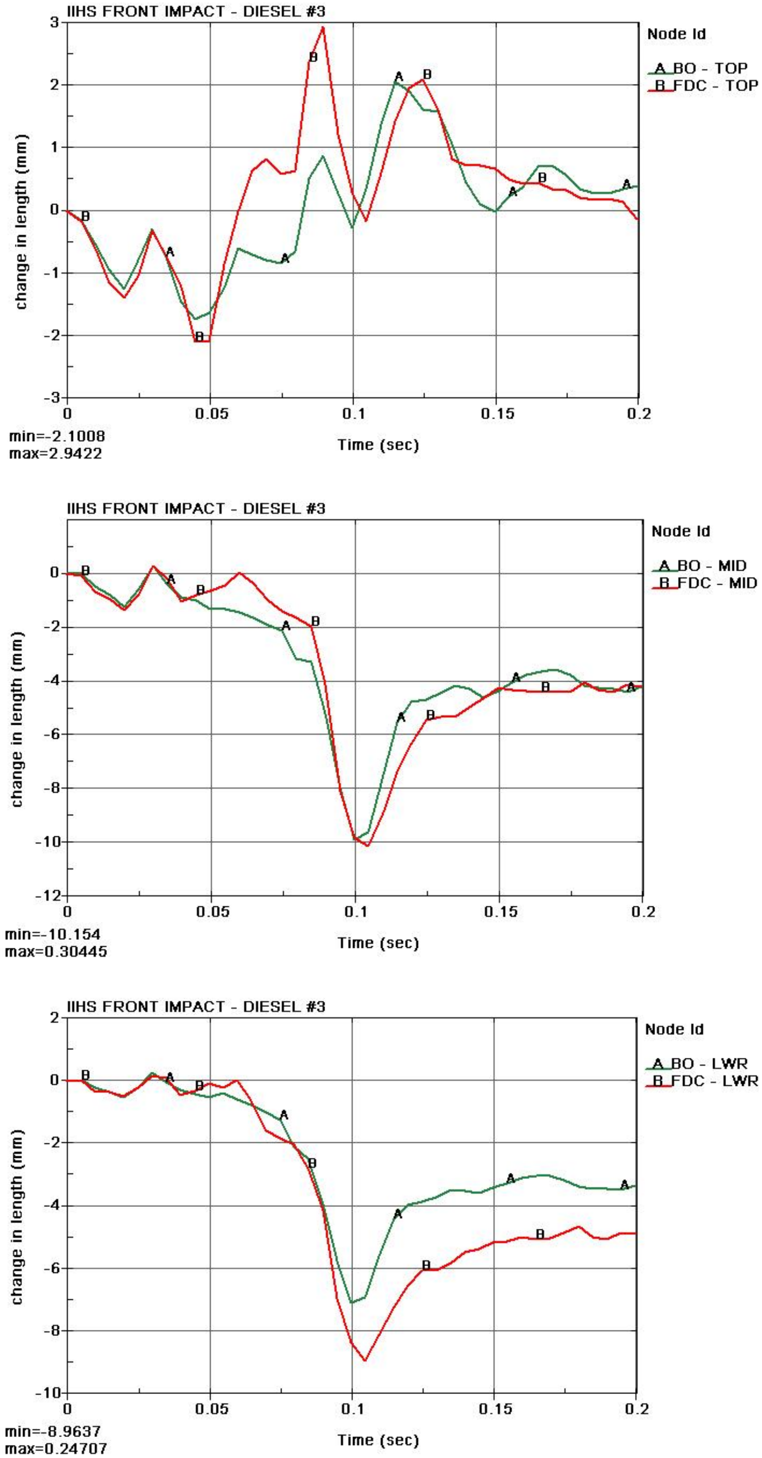

FIGURE 16: IIHS 40% ODB, FGPC-FCD (TOP, MID & BOTTOM)

Figure 17 shows the chart representation of the "change in length" (upper, middle, and lower position) of the front door for FGPC-BO and FGPC-FCD.

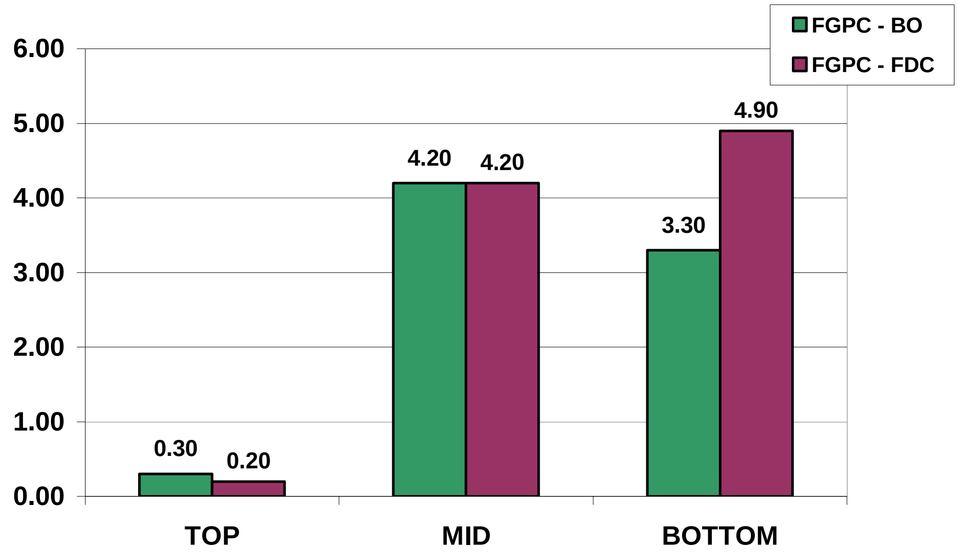

FIGURE 17: IIHS 40% ODB – Door Openability

Figure 18 shows the rocker inner deformation after the impact.

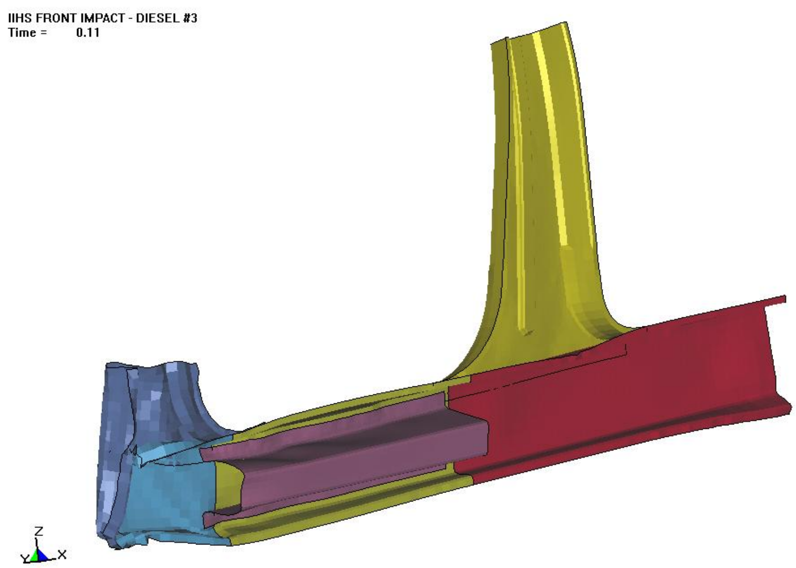

FIGURE 18: IIHS 40% ODB– FGPC-FCD (Lower)

7.4. CONCLUSION

The new FGPC-FCD structure vehicle with the proposed design change does satisfy the requirements of IIHS 40% ODB. The change in length for the lower position of the door is slightly higher than the FGPC-BO. This difference is based on the allowed tolerance used in the final optimization.

8. SIDE POLE IMPACT (FMVSS214 NEW)

8.1. TARGET

FMVSS214 New Pole Impact sets limits on occupant injury criteria, with no structural performance requirements. Since no occupant models are used in this study, the maximum structural intrusion into the passenger compartment was measured instead. This is similar to the IIHS Side Impact target. The maximum intrusion in the pole impact occurs on the Front Door Inner, while the side impact intrusion is measured at the B-Pillar.

Therefore the target is to meet or exceed the performance of the FGPC-BO, which had a maximum intrusion of 7mm inboard of the driver's seat centerline.

8.2. LOADS AND BOUNDARY CONDITIONS

The vehicle is propelled at 20mph into a 10in diameter pole at an angle of 75 degrees to its longitudinal axis, as shown in Figure 19. The pole is lined up with the center of the occupant's head. It should be noted that the seats in the FGPC are designed to be stationary with adjustable driver controls, so the head position will remain constant regardless of occupant size.

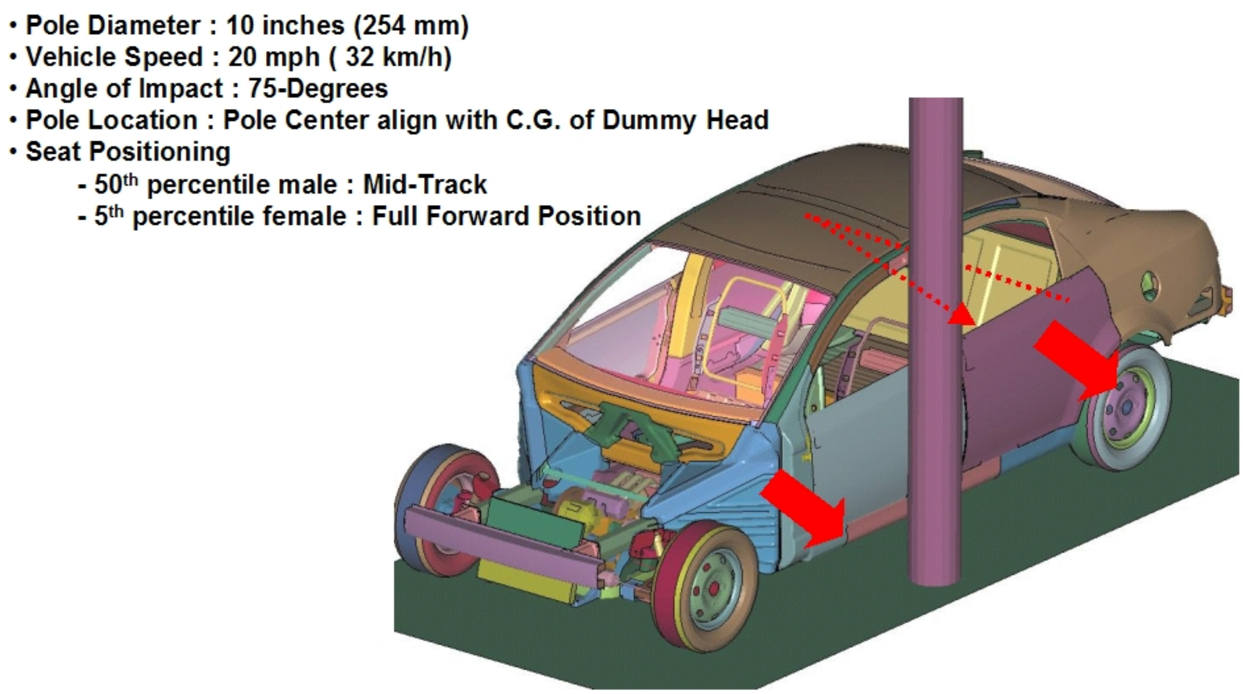

FIGURE 19: Pole Impact Set-Up

8.3. RESULTS

Figure 20 shows the intrusion of the front door relative to the center of the driver's seat. The minimum distance between the door beam and the centerline of seat for the FGPC-ACD model was -120mm, compared to -7mm for FGPC-BO. It is improved to +26 mm through 15 iterations and FGPC-FCD has +2 mm. The objective to meet or exceed FGPC-BO structural performance is fulfilled.

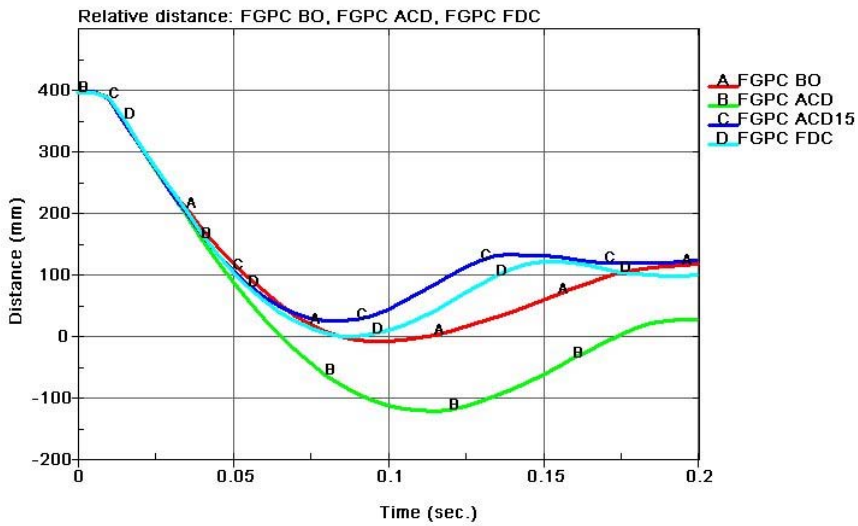

	MIN DISTANCE (mm)
FGCP-BO	-7
FGCP-ACD	-120
FGPC-ACD15b	26
FGCP-FCD	2

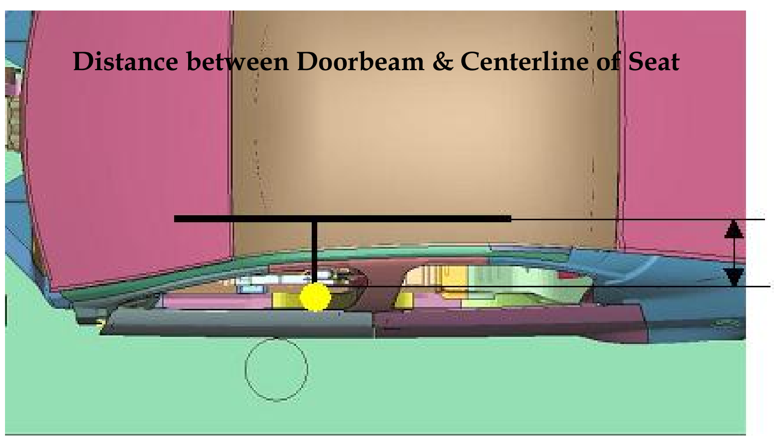

FIGURE 20: Intrusion of Front Door Into Passenger Compartment

Future Generation Passenger Compartment (FGPC)

Figures 21 & 22 compare the deformed shapes for both the FGPC-BO and FGPC-FCD vehicles.

FGPC-BO

Press to open animation

FGPC-FCD

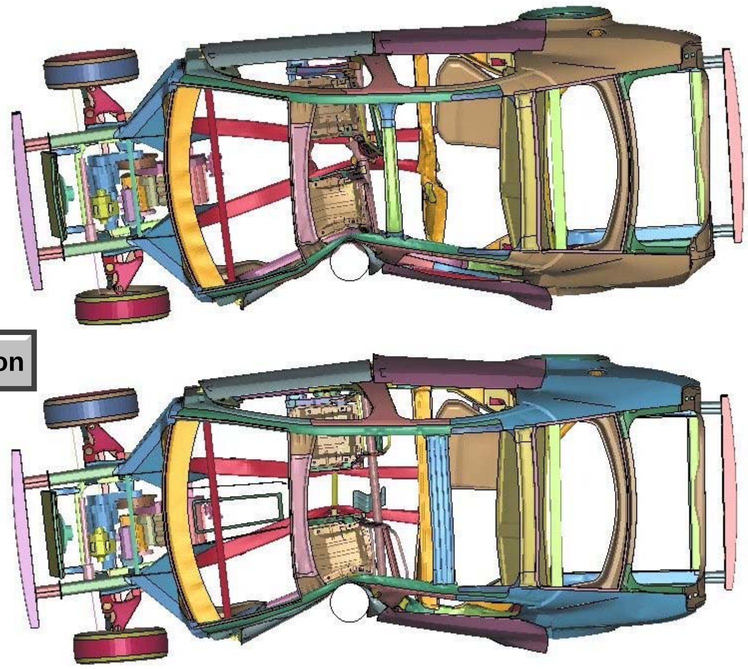

FIGURE 21: Deformed Shape FGPC-BO vs. FGPC-FCD (Top View)

FGPC-BO

Press to open animation

FGPC-FCD

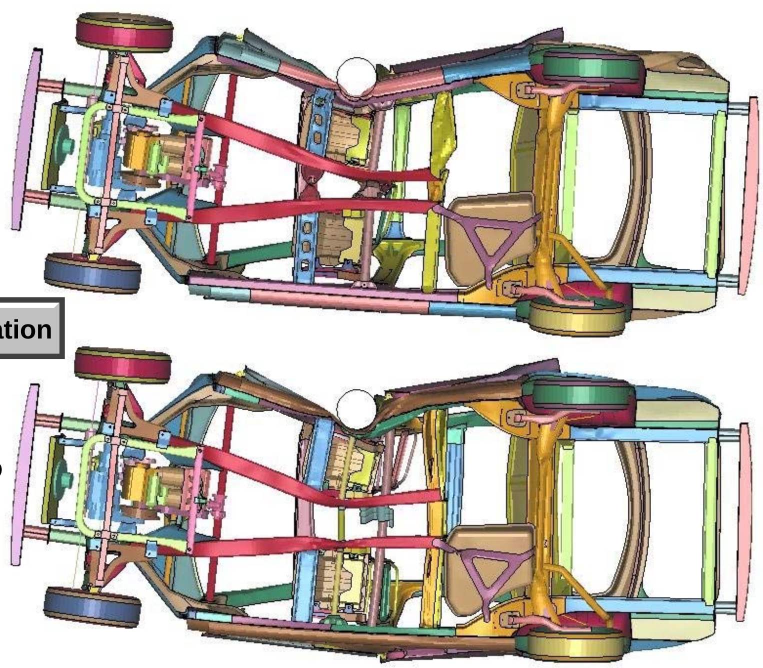

FIGURE 22: Deformed Shape FGPC-BO vs. FGPC-FCD (Bottom View)

The previous figures show that for the FGPC-BO, the Seat Cross-member transfers the load from the Rocker to the Tunnel. However, for the FGPC-ACD design, the Seat Cross-member is above the Rocker, so it transfers the load directly to the non-struck side of the vehicle. The Rocker therefore has less support between the Kick-down Cross-member and the Front Seat Cross-member. FGPC-FCD has a cross member at the impact location, which provides more support to the Rocker.

8.4. CONCLUSION

The results of the FGPC-FCD analysis shows no major change in the vehicle performance after design changes compared to the vehicle performance before optimization. The vehicle structure does perform well and meets the acceptance criteria.

9. IIHS SIDE IMPACT

9.1. TARGET

The regulations for IIHS Side Impact include occupant injury criteria. However, the FGPC project is only concerned with the vehicle structure. Therefore the FGPC team used a target that maintains the IIHS survival space requirement of not less than 125mm. See Figure 25.

9.2. LOADS AND BOUNDARY CONDITIONS

A 1500kg MDB (Moving Deformable Barrier) is positioned so that there is 379mm of ground clearance. The rearward distance from the test vehicle's front axle to the closest edge of the deformable barrier, known as the IRD (Impact Reference Distance), is 810 mm. The barrier impacts the vehicle with an initial velocity of 50kph. See Figure 23.

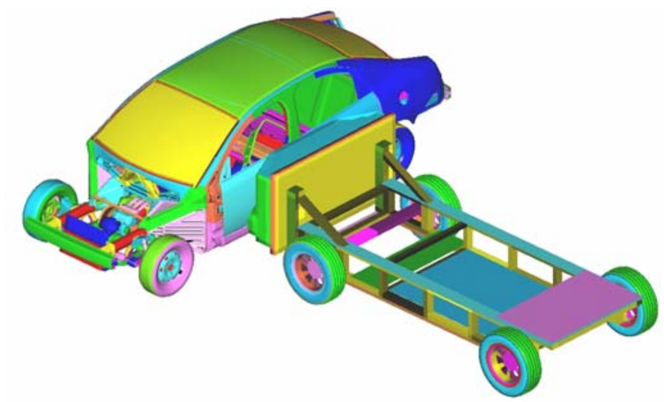

FIGURE 23: IIHS Side Impact Analysis

9.3. RESULTS

9.3.1 FGPC-AFO

Comparisons of the B-Pillar and Seat Cross-member deformations for FGPC-ACD Final and the FGPC-AFO are shown in Figure 24.

The FGPC-AFO Seat Cross-member kinks on the driver's side, resulting in increased B-Pillar deformation compared to FGPC-ACD Final. The B-Pillar intrusion (survival space) measurements are shown in Figure 25. The survival space is reduced to 107 mm, which is below the target of 125mm.

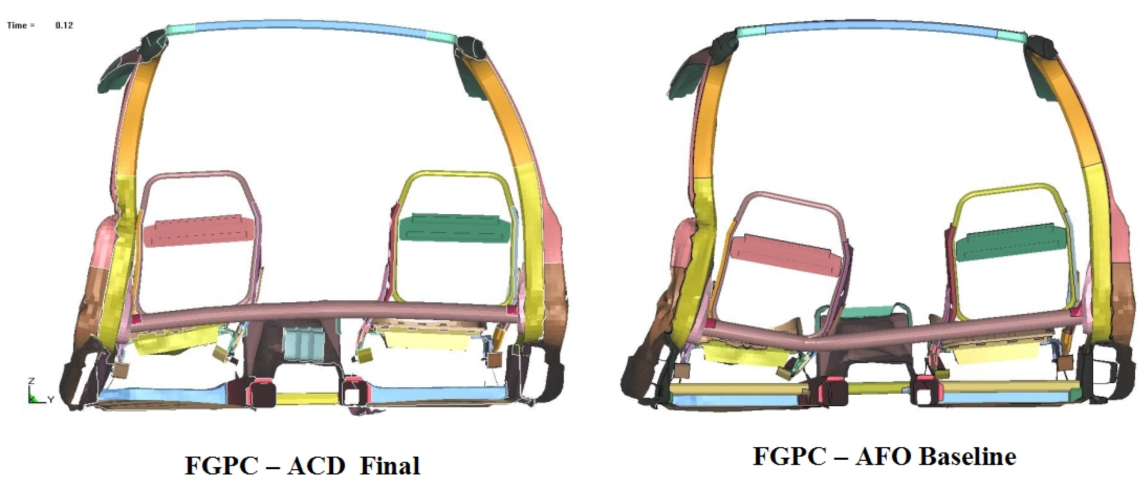

FIGURE 24: B-Pillar & Seat Cross-Member Deformation Comparison

B-Pillar Intrusion

FGPC – ACD Final:	124.7 mm
FGPC – AFO Baseline:	107.0 mm
FGPC – AFO Final:	134.5 mm

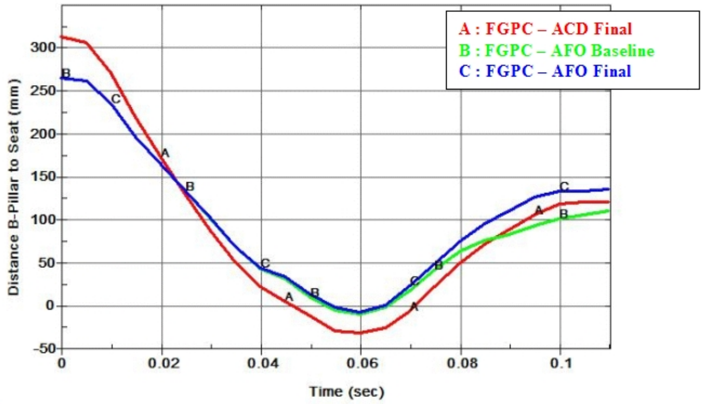

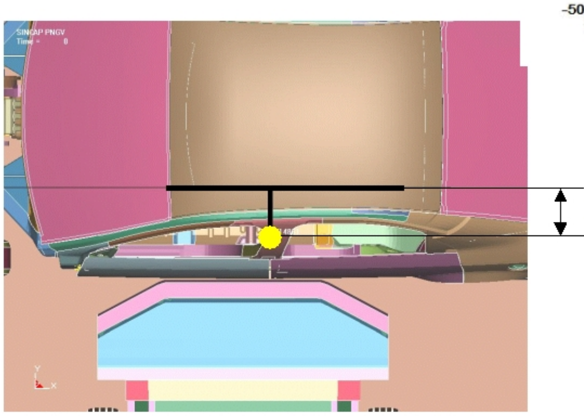

Distance between B-Pillar and Centerline of Seat

Good	>	125 mm
Acceptable	>	50 mm
Marginal	>	0 mm

FIGURE 25: IIHS Side Impact B-Pillar Intrusion

9.3.2 FGPC-AFO Iteration Study

A small iteration study was performed to determine why the IIHS Side Impact performance of the FGPC-AFO was inferior to the FGPC-ACD final model.

The Cross-member Support Rear Center Bracket, which is directly beneath the Side Impact Cross-member, was removed in the Task 6.0 Pole Impact optimization to save weight. It is suspected that the removal of this bracket changed the deformation mode of the cross-member.

The bracket was replaced for the first and only iteration. The deformed shape for this analysis is shown in Figure 26. The bracket, light blue in the figure, prevented the cross-member from bending downward, which allowed it to bend without kinking. The resulting side impact performance exceeded the target, yielding a B-Pillar intrusion of 134.5 mm.

The mass penalty for adding the bracket back into the vehicle is 0.5 kg.

The deformed shape of the FGPC-AFO final model is shown in Figure 27.

Press to open animation

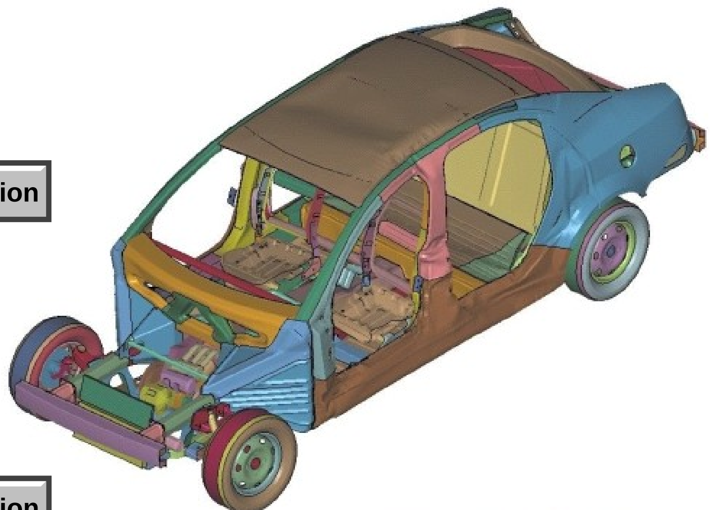

Press to open animation

Press to open animation

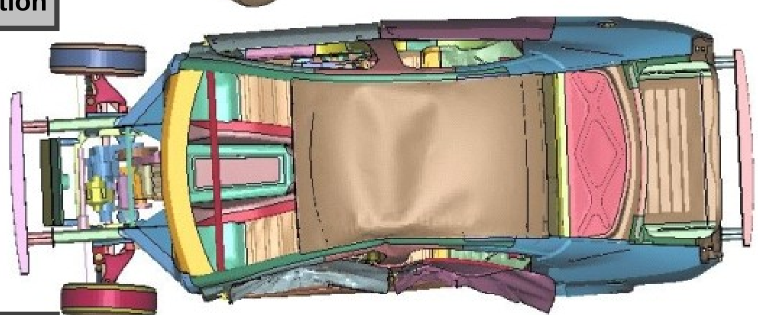

Press to open animation

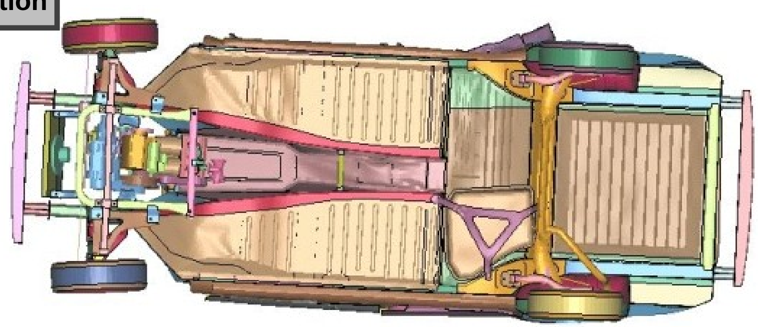

FIGURE 26: Deformed Shape of FGPC-AFO Final

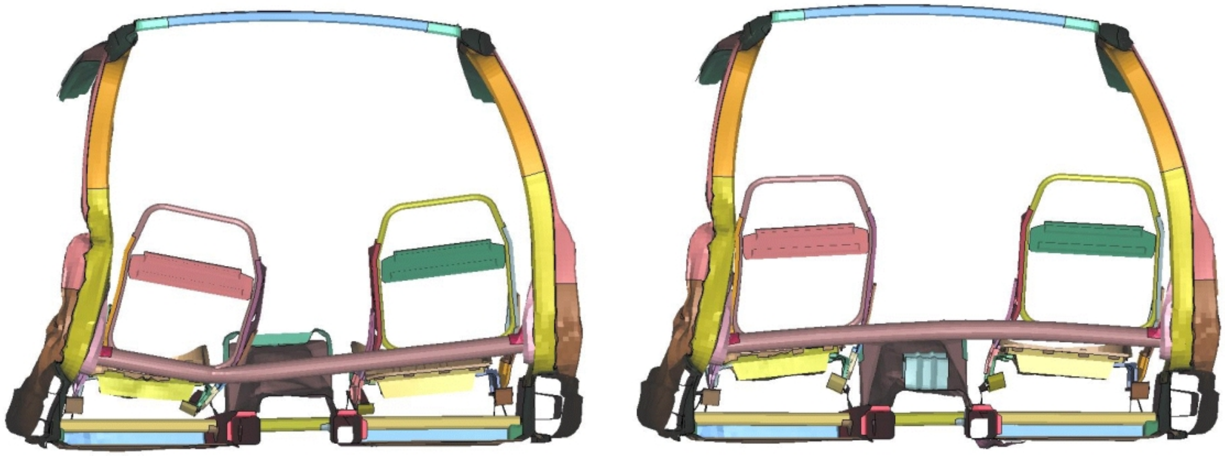

FIGURE 27: FGPC-AFO Baseline & FGPC-AFO Final
B-Pillar Deformation Comparison

9.4. CONCLUSION

FGPC-AFO model did not meet the IIHS Side Impact target. A small iteration study showed that, by replacing the bracket on the tunnel beneath the Seat Cross-member, the performance is restored. The bracket added 0.5 kg back into the design.

10. ROOF CRUSH

10.1. TARGET

The FGPC team set the Roof crush resistance target as a deflection of 127mm or less under a loading of 2.75 x the unloaded vehicle weight. Note this target exceeds the loading set by FMVSS216, which requires the same deflection for a loading of 1.5 x the unloaded vehicle weight.

10.2. LOADS AND BOUNDARY CONDITIONS

A rigid plate (1829 x 762mm) is pushed onto the A-Pillar at a velocity of 50in/sec (5in over the 100msec analysis time). Note the analysis speed of 50in/sec is higher than the regulation's 5in/120sec. This was done to reduce the computation time to a more reasonable length of time. The higher velocity does introduce a slight inertial effect into the analysis, which is known to increase the reaction force by a small, but nearly negligible amount. Both Rockers were fixed in all degrees of freedom (translations in and rotations about x, y and z). See Figure 28.

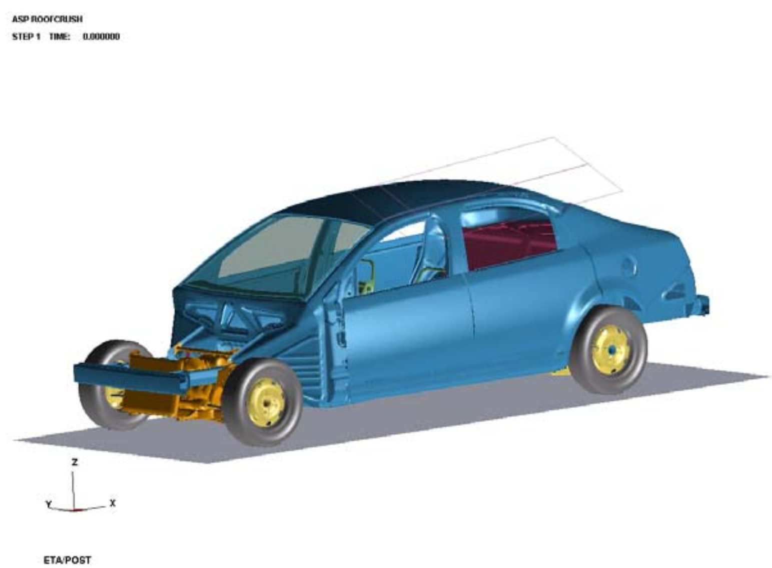

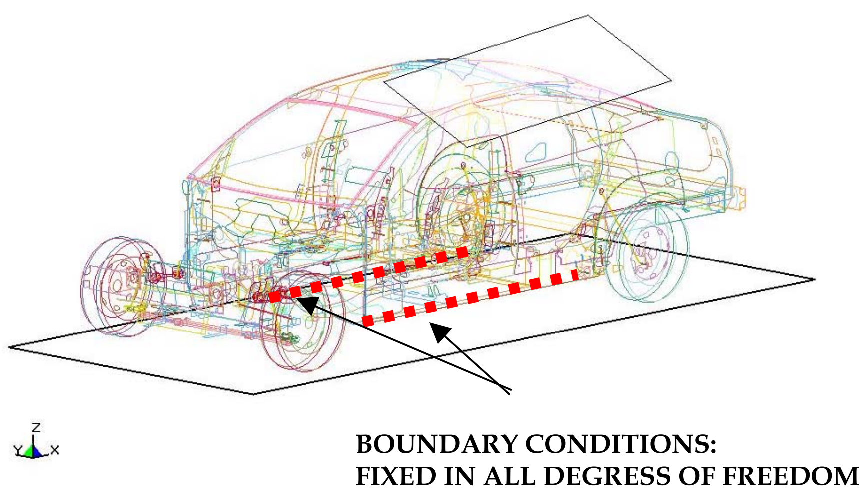

FIGURE 28: Roof Crush Model & Boundary Conditions

10.3. RESULTS

FGPC-FCD performs well under the FMVSS216 load case. Results are shown in Figure 29.

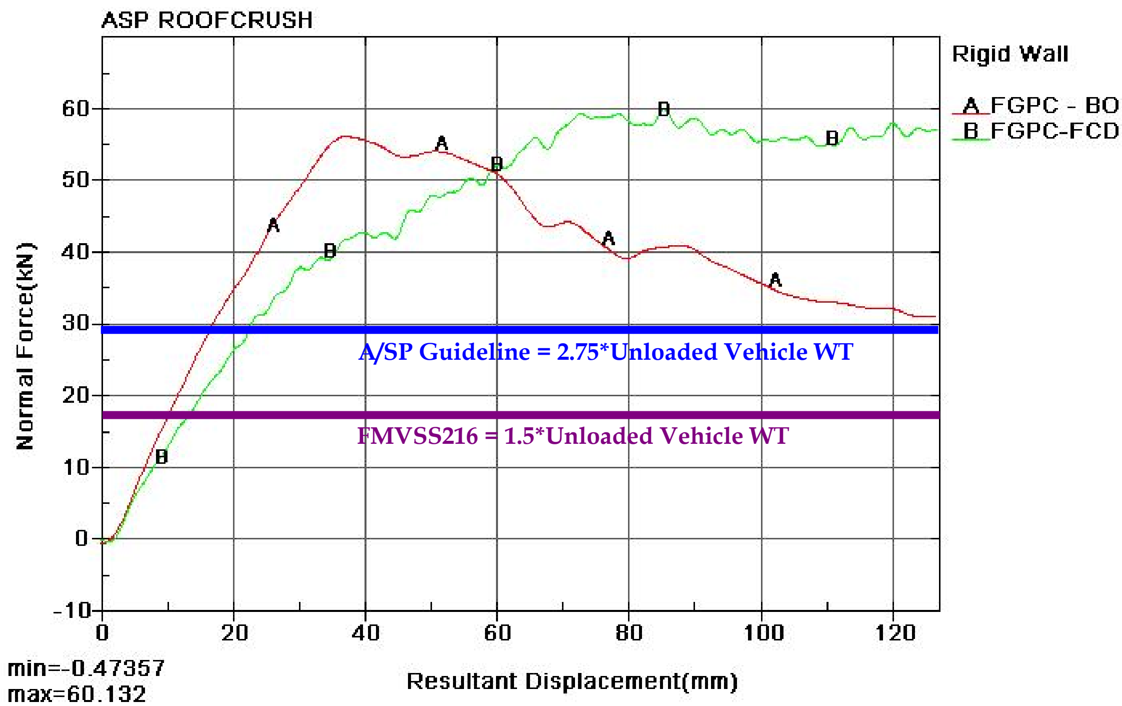

FIGURE 29: Roof Crush Results For FGPC-BO & FGPC-FCD

Press to open animation

Press to open animation

Figure 30 shows the plastic strain of the FGPC-FCD. The deformation mode is similar to the FGPC-BO. Buckling at the B-Pillar reinforcement causes the body side crumpling at the A-pillar.

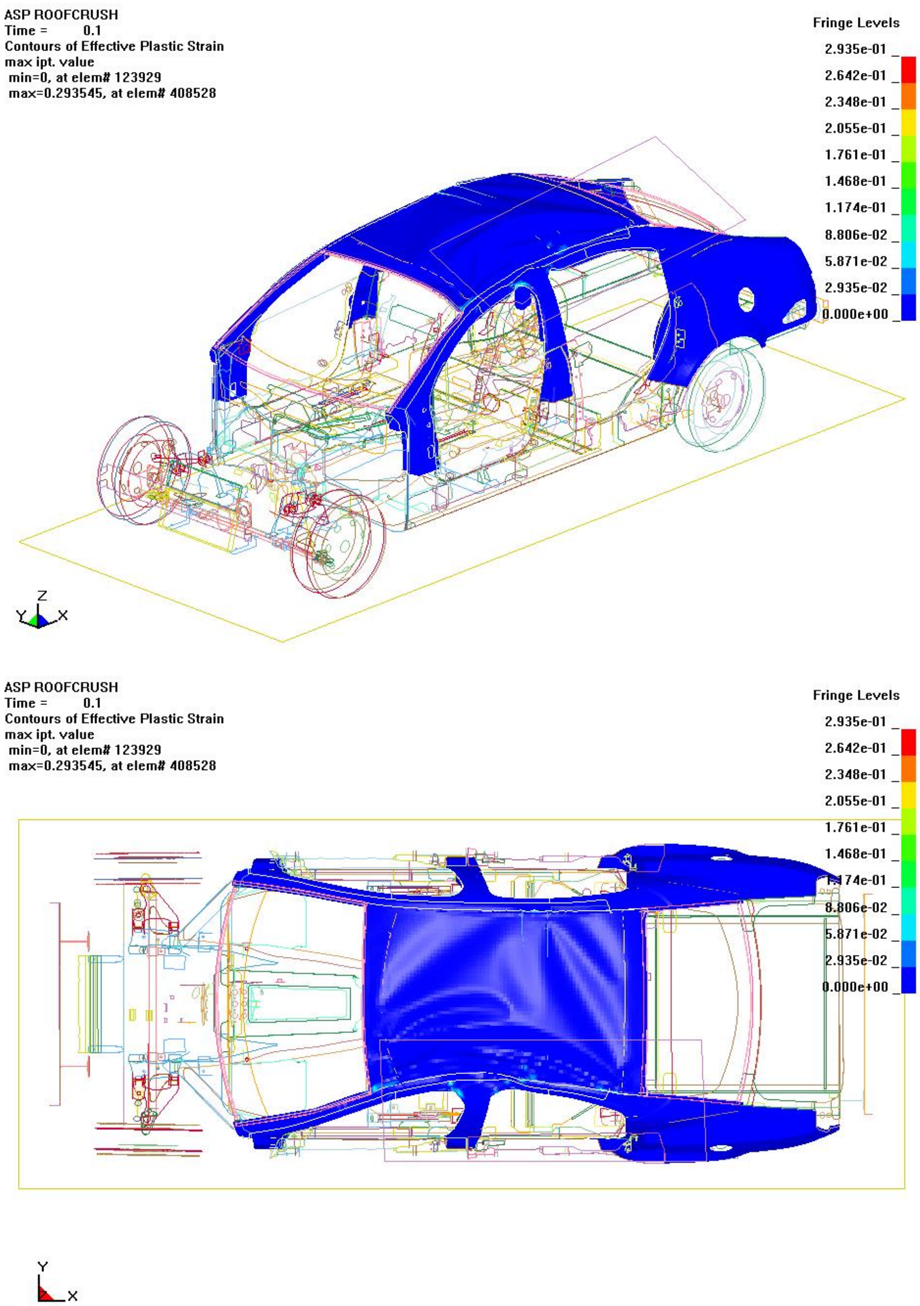

FIGURE 30: Plastic Strain – Deformed Shape

10.4. CONCLUSION

FGPC-FCD satisfies the FMVSS216 requirements. The structure also meets the A/SP (Auto/Steel Partnership) recommendation of 2.75 x the unloaded vehicle weight.

11. DOOR INTRUSION

11.1. TARGET

FGPC team set the target at 10% above FMVSS214 requirements, listed below:

- Initial crush resistance: The average force required to deform the door shall not be less than 2250lb over the first 6in of barrier displacement.
- Intermediate crush resistance: The average force required to deform the door shall not be less than 3500lb over the first 12in of barrier displacement.

11.2. LOADS AND BOUNDARY CONDITIONS

The barrier is a rigid cylinder 12in diameter and 25in high. The longitudinal axis of the cylinder is positioned vertically at the mid-point of the line 5in (127mm) above the lowest point on the door. The bottom of the barrier is inline with this point. The external circumference of the cylindrical barrier is spaced 5mm from the outer door skin. See Figure 31.

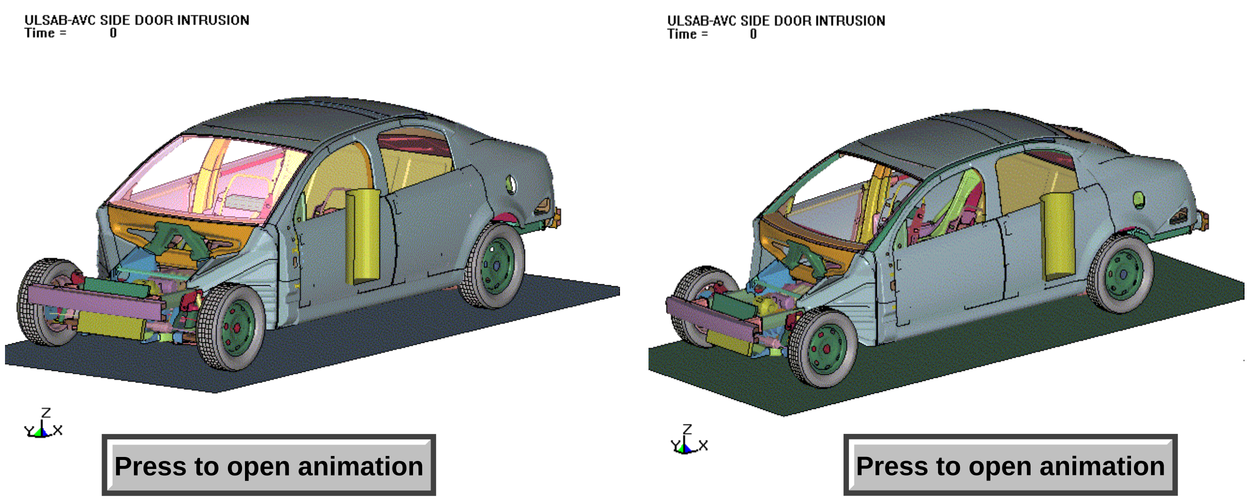

FIGURE 31: Door Intrusion Models (Front & Rear Door)

The front and rear of both Rockers are fixed in all directions. The bottom of the non-impacted Rocker is also fixed in all directions. See Figure 32.

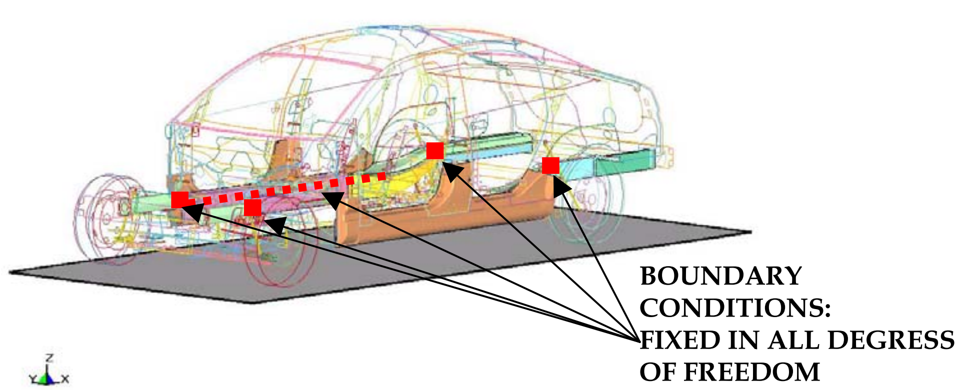

FIGURE 32: Side Door Intrusion – Boundary Conditions

11.3. RESULTS

The side door intrusion analysis was run after updating the vehicle structure based on the work of optimization. The new structure does perform well under the FMVSS214 load case for both the front and rear doors.

Figure 33 shows the Barrier force vs. barrier displacement, before optimization and after final concept design, for both front and rear doors. The energy vs. barrier displacement is obtained from the integration of the force plot (Figure 34). While the average forces at 6 and 12-inch displacements are calculated from energy vs. displacement plot. Figure 35 and Tables 4 & 5 give the average forces for both front and rear doors.

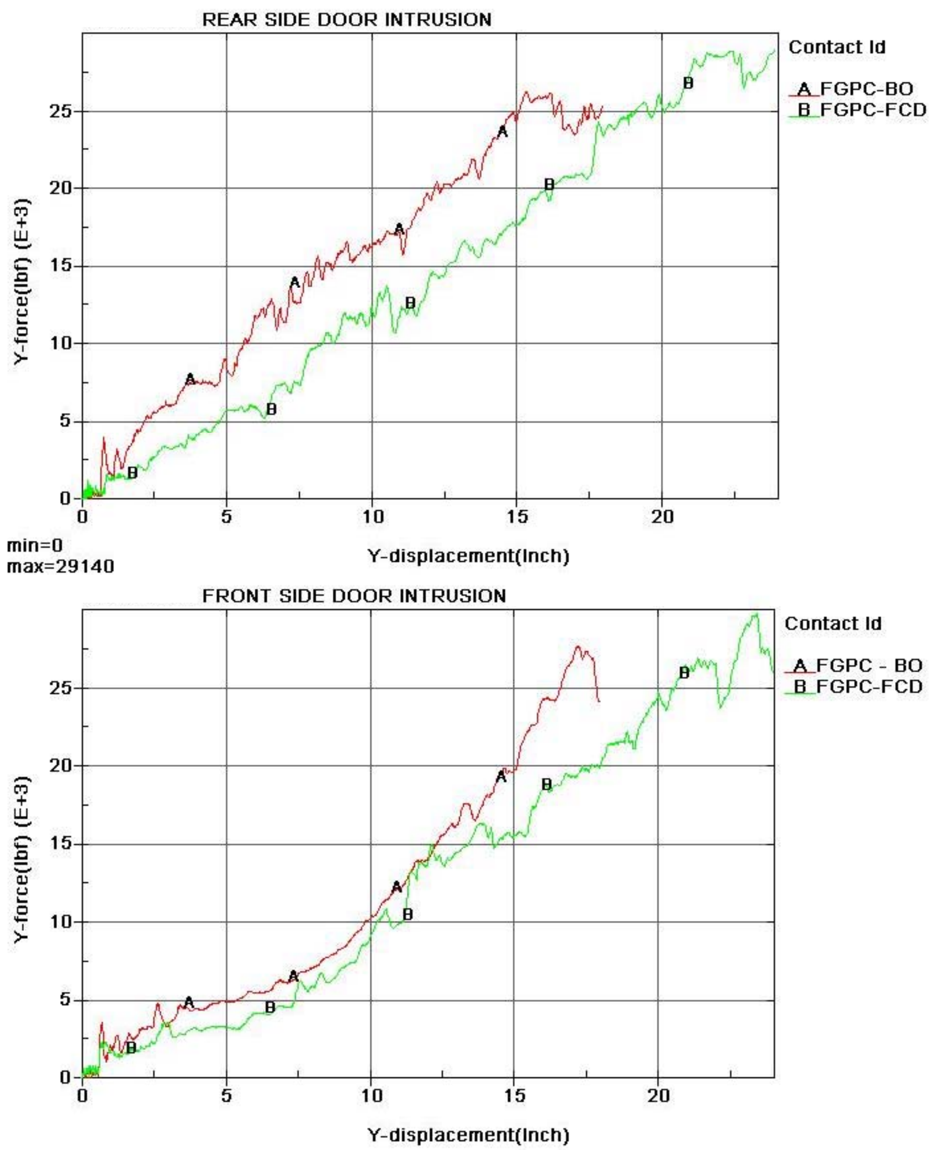

FIGURE 33: Front & Rear Door - Barrier Force (lbf) vs. Barrier Displacement (inch) For FGPC-BO & FGPC-FCD

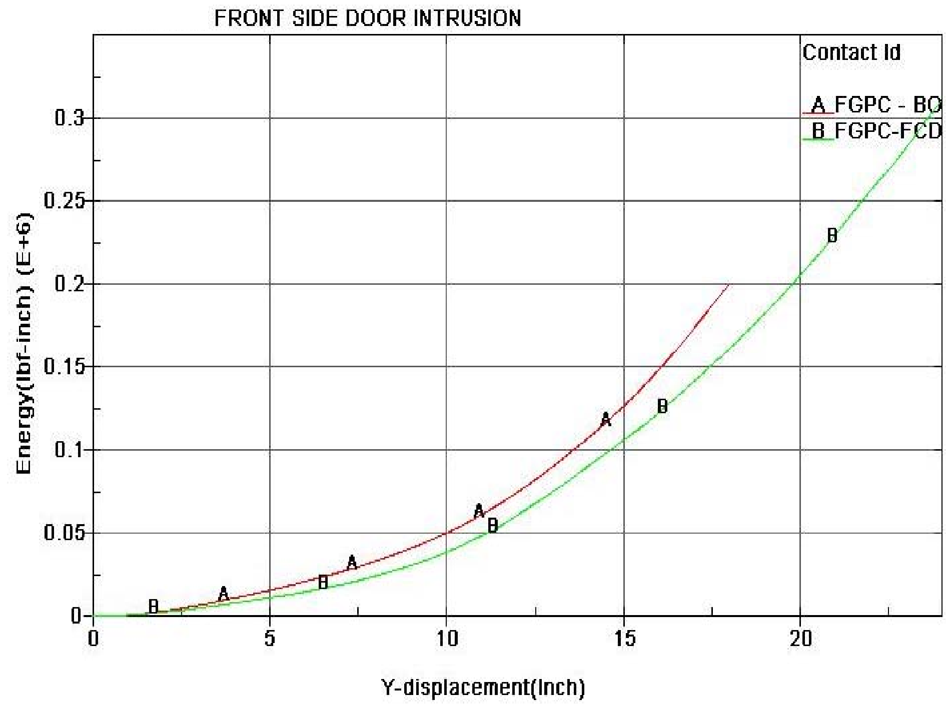

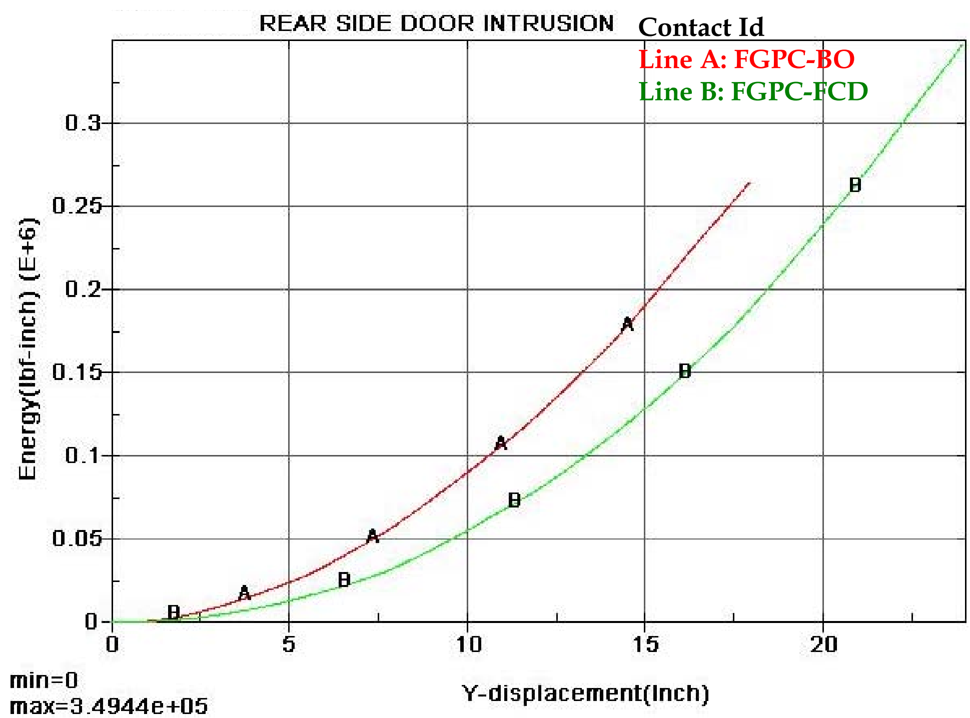

FIGURE 34: Front & Rear Door - Energy (lbf-inch) vs. Barrier Displacement (inch) for FGPC-BO & FGPC-FCD

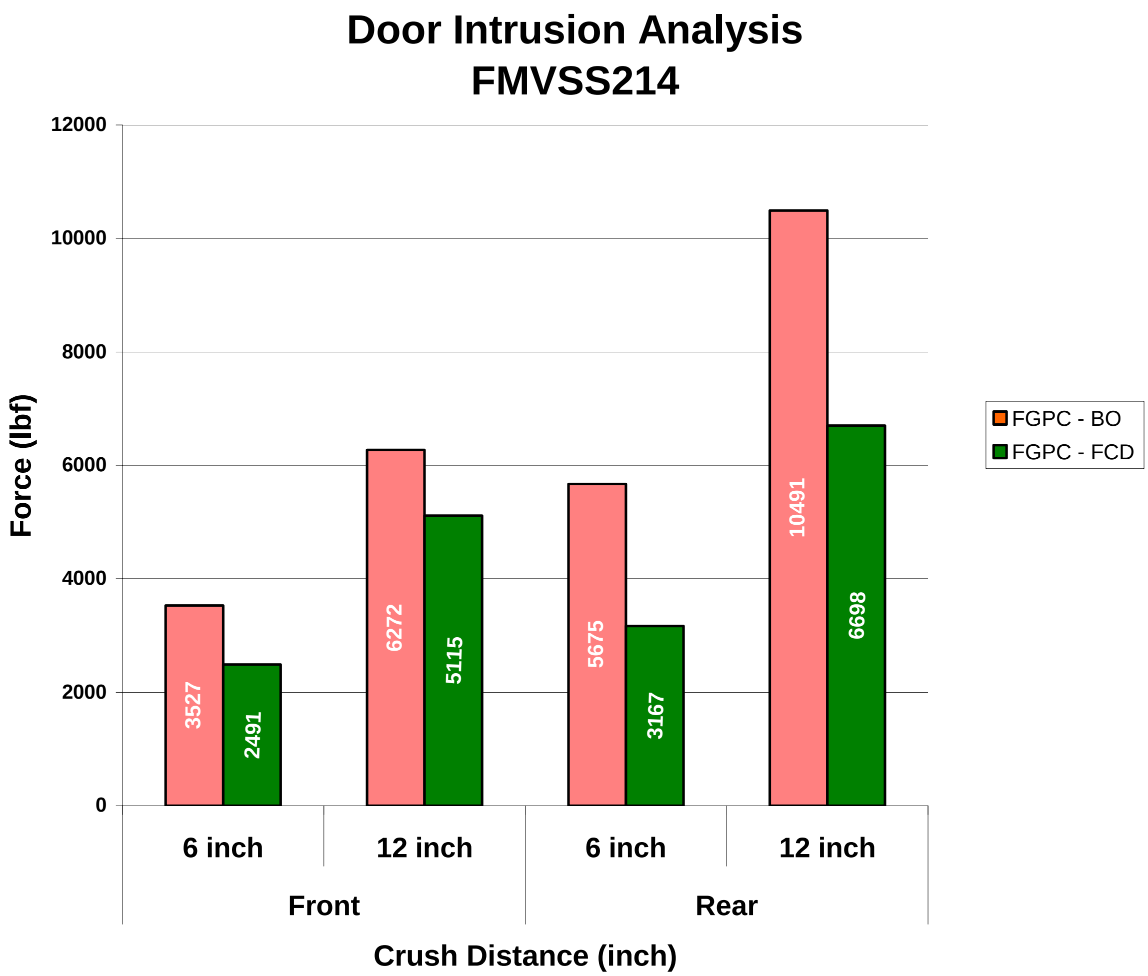

FIGURE 35: Door Intrusion For FGCP-BO & FGPC-FCD

BARRIER SIZE	FGPC-BO (lbf)	FGPC-FCD (lbf)	FMVSS214 (lbf)
6 inch	3527	2491	2250
12 inch	6272	5115	3500

TABLE 4: Front Door Performance

BARRIER SIZE	FGPC-BO (lbf)	FGPC-FCD (lbf)	FMVSS214 (lbf)
6 inch	5675	3167	2250
12 inch	10491	6698	3500

TABLE 5: Rear Door

11.4. DOOR INTRUSION CONCLUSION

FGPC–FCD satisfies the requirements of FMVSS214 and ASP internal targets (10% above FMVSS 214).

12. REAR CRASH

12.1. TARGET

The same target as FMVSS301, which requires maintenance of fuel tank integrity.

12.2. LOADS AND BOUNDARY CONDITIONS

A rigid wall impacts the rear of the vehicle at a constant velocity of 35mph. The vehicle is free to move upon impact. See Figure 36.

FIGURE 36: Rear Crash Model

12.3. RESULTS

No major design changes were made to the rear of the vehicle. As a result, the FGPC-FCD performed as well as the FGPC-BO. Figure 37 shows the deformed shape of the FGPC-FCD at 0.12s, and the maximum deformation of FGPC-ACD and FGPC-BO.

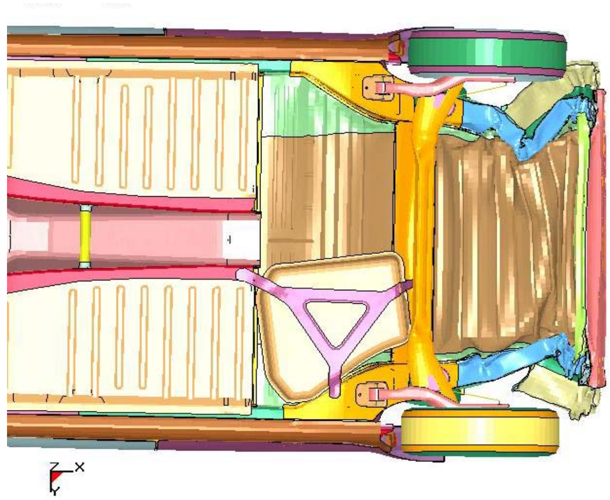

Press to open animation

FGPC-FCD (Bottom View)

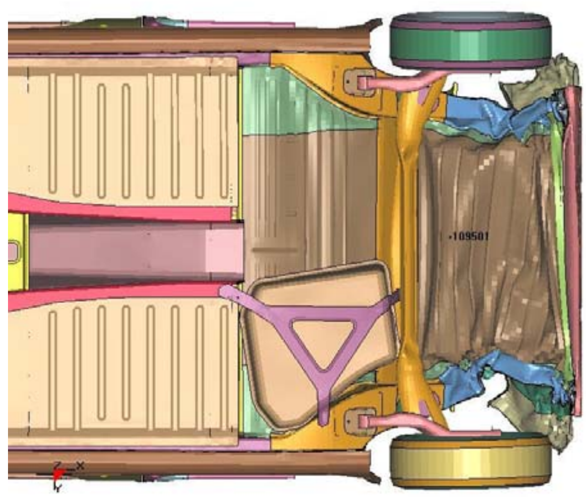

Press to open animation

FGPC-ACD (Bottom View)

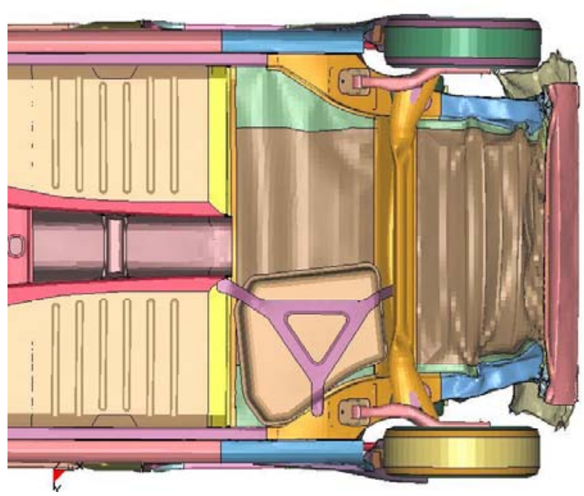

Press to open animation

FGPC-BO (Bottom View)

FIGURE 37: Rear Crash Deformed Shape

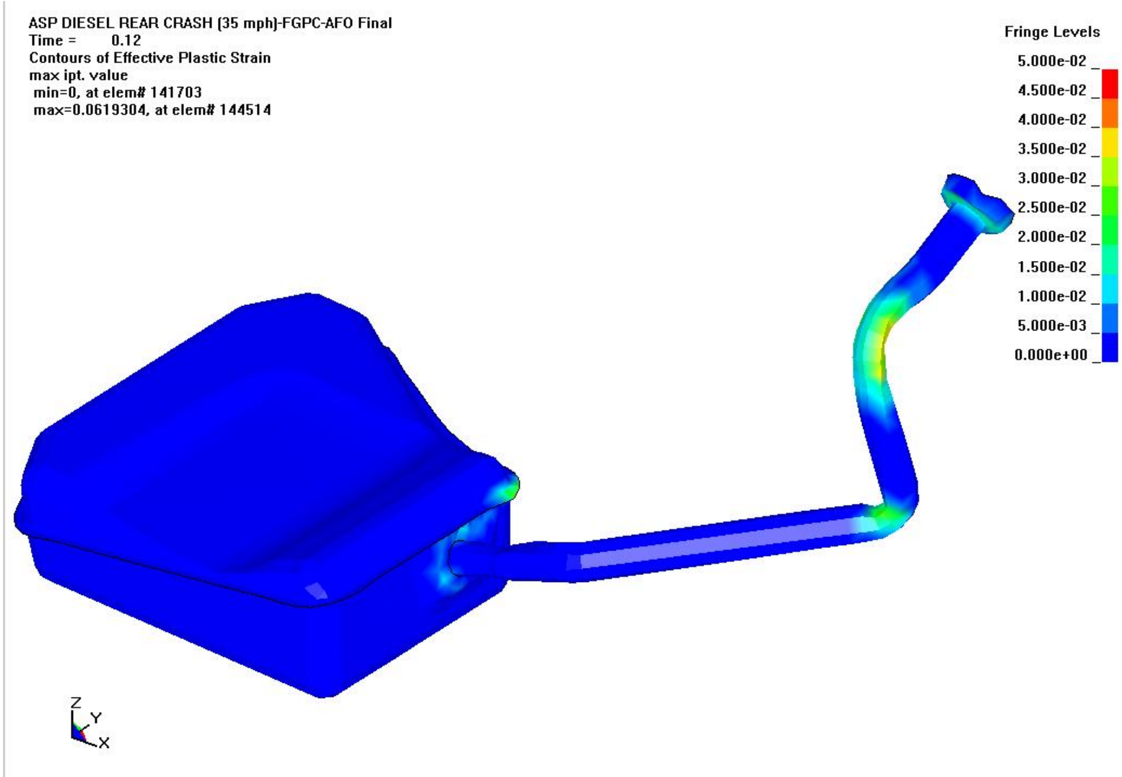

FIGURE 38: Fuel Tank At 5% Plastic Strain

12.4. CONCLUSION

The rear longitudinal buckling mode has changed for the three designs. The rear deformation changes from FGPC-BO to FGPC-ACD are due to small changes in the rear floor geometry in design stage, FGPC-ACD shows more deformation in floor and left hand side longitudinal. See Figure 37. In the FGPC-FCD model, as a part of near-term strategy, laser weld connections of the longitudinal and floor were replaced by structural adhesives and spot-welds. This change made the rear structure stiffer and caused the buckling mode to change.

Figure 38 shows a plastic strain value of 6.2% on the fuel tank filler tube while the FGPC-ACD model had a 13.3% plastic strain. This high value is a localized deformation around the bent areas of the filler tube. The maximum plastic strain value of the tank is 3.5%, which is below the allowable values.

13. VPG FULL VEHICLE SYSTEM DURABILITY ANALYSIS

13.1. BACKGROUND

Vehicle development relies greatly on the validation of the design through testing of vehicles, whether it is in the crash test facility or the proving ground. These validation tests are typically performed on the complete vehicle, as a system.

In order to achieve a higher degree of confidence in the vehicle design, there is a need to simulate the vehicle performance as a system. It is expected that a component reacts differently when tested individually than when it is integrated into the vehicle system under impact loads. It should also be expected that the durability performance of a vehicle's components is dependent upon the other components within the system. Therefore, as a validation of the vehicle design established for the FGPC, a vehicle system model was developed for the simulation of vehicle proving ground durability events.

This type of analysis is ideal for projects such as the FGPC for several reasons. First, using the basic vehicle suspension parameters developed very early in a program and some reasonable assumptions for tire size, and vehicle mass and CG, it's possible to predict road loads for specific durability road surfaces. This early load information can be obtained without the costly and time-consuming production of a "mule" vehicle, and is vital for the initial development and robust design of vehicle suspension and chassis components.

Second, VPG Full Vehicle System Durability Analysis is an excellent tool for enhancing the development of suspension, chassis, and body components that are important for the long-term durability of a vehicle. The non-linear explicit code is ideal for evaluating load paths, identifying key suspension and component interactions, and understanding the root cause for potential durability issues within a vehicle system.

13.2. SUSPENSION SYSTEMS

The suspension sub-system models used for this analysis were basically unchanged relative to the FGPC-BO model, with only minor changes to create a more realistic loading condition for the vehicle as it passes over three-dimensional road surfaces.

Front Suspension **Rear Suspension**

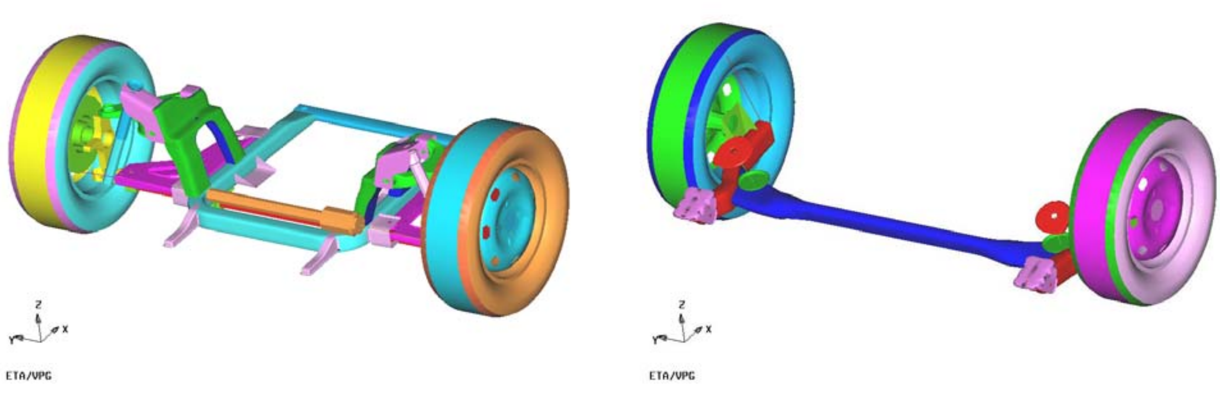

FIGURE 39: Suspension Systems Used For eta/VPG analysis

The front suspension for this vehicle is a conventional double-wishbone design, sprung by a slightly unconventional transverse leaf spring setup. It was left primarily unchanged from the original ULSAB-AVC, using the original bushing, spring, and damper rates. The tire stiffness parameters were adjusted to provide a more realistic response of the contact interaction with the road surface. The major revision was to the transverse leaf spring model, which was modified to more accurately transfer load through the suspension sub-system. The leaf spring material parameters were tuned to provide the correct spring rate and a discrete spring with pre-load was added to the system to account for the installation load on the spring.

The rear suspension, an H-beam or twist-beam setup with separate coil springs and suspension dampers remained identical to the original ULSAB-AVC model. The bushing, coil spring, and suspension damper rates were unmodified. Again the stiffness parameters of the rear tires were adjusted to provide a more realistic response of the contact interaction with the road surface.

13.3. LOADS AND BOUNDARY CONDITIONS

One VPG durability road was chosen to perform this study: Ripple Track. This road is a sinusoidal profile and includes a diagonal component that is at the nominal road height. The road profile is developed from the Ripple Track road surface at the MGA Proving Grounds, in Burlington, Wisconsin, and is used with the permission of MGA Research Corporation. The full vehicle FE crash model was modified to include tire models compatible with predicting durability road loads via contact with a fixed 3-D road surface. As in the actual test specification the vehicle model is given an initial vehicle speed of 35mph. In order to allow the vehicle model to reach an equilibrium condition, an approach to the road surface was included, as shown in Figure 40. The total event simulation time was 1.5sec, which allows the complete vehicle to exit the Ripple Track surface.

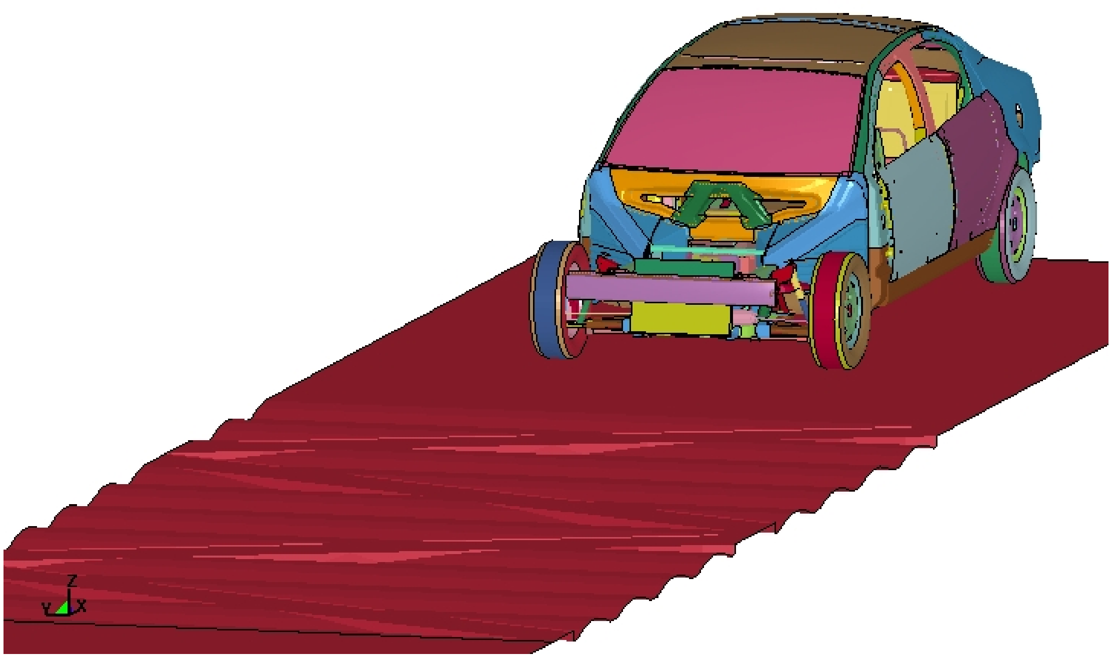

FIGURE 40: VPG Full Vehicle System Analysis Of Ripple Track

Press to open animation

13.4. RESULTS

Initial results for the FGPC Full Vehicle System Durability Analysis show that with one exception, the vehicle's suspension and chassis components perform very well on the Ripple Track road surface. Figure 41 shows a plot of the effective plastic strain (eps) in the underbody. This indicates that only localized areas of the underbody may undergo minimal amounts of plastic strain under this loading condition. To completely evaluate the plastic strain distribution under durability loading, additional road surfaces, including potholes, would need to be included.

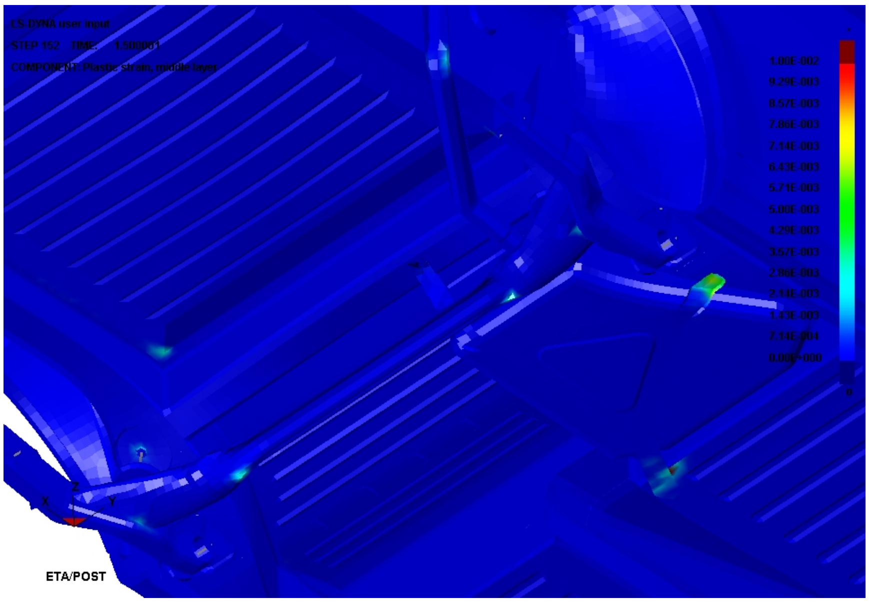

Press to open animation

FIGURE 41: Underbody Effective Plastic Strain

The rear suspension does an excellent job of isolating the road loads and limits the components exceeding yield to a small region of the twist beam, the attachment of the twist beam to the trailing arms, and the attachment of the spring cup to the body. None of these hot spots exceeds 0.4% effective plastic strain, well below the critical plastic strain (See Figure 42).

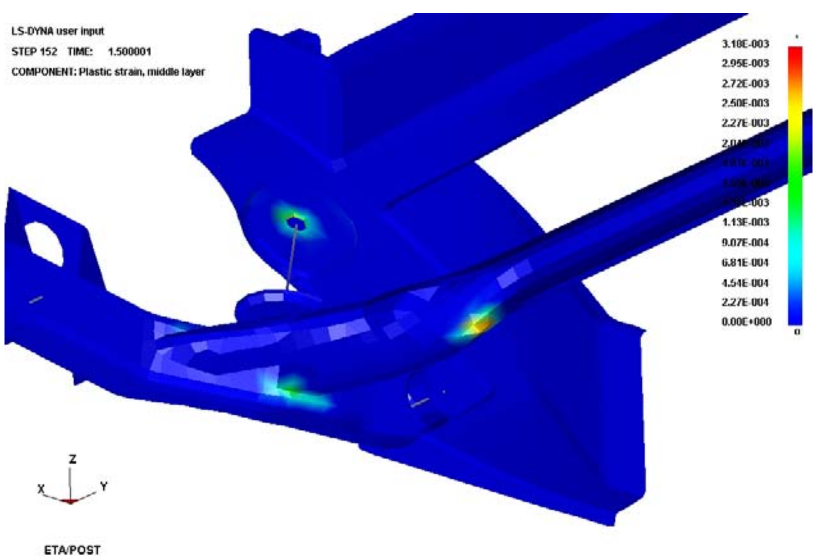

FIGURE 42: Rear Suspension Effective Plastic Strain

The results also show two minor hotspots on the fuel tank strap and on the floor pan just in front of the fuel tank (less than 0.3% eps). Their presence is most likely related to the absence of preload on this sub-system. The FE model does not assume that there is tension on the tank strap. This allows the tank to float around a little bit, which will signficantly increase the deformation of the strap and allow the tank to make contact with the floor pan. See Figure 43.

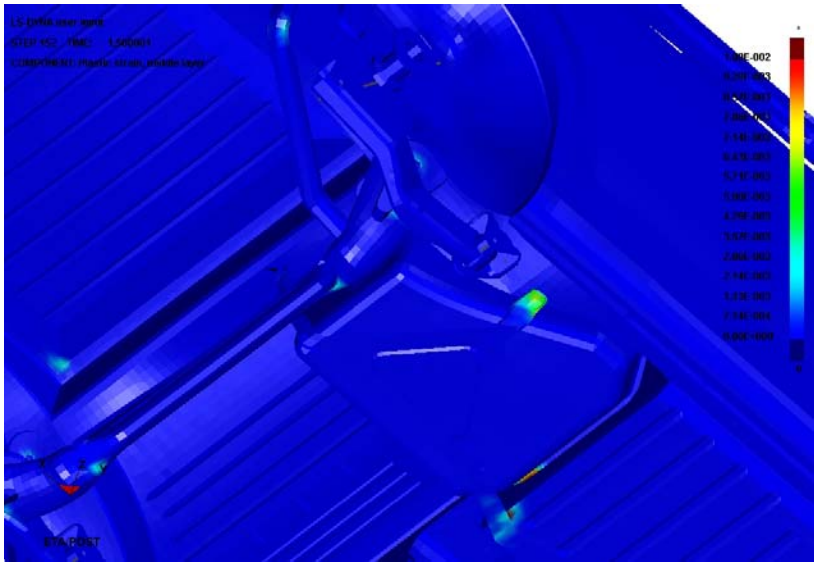

FIGURE 43: Fuel Tank effective Plastic Strain

The only region of signficant concern, based on this analysis is the front shock tower region. This component shows significant plastic strain at its attachment to the front longitudinal, as seen in Figure 44. This hot spot occurs at the smallest cross-section of the tower, and a review of the results shows that the flexibility of the shock tower at this location is very high, resulting in a significant amount of relative motion between the tower and the longitudinal and almost 14% effective plastic strain at this critical location.

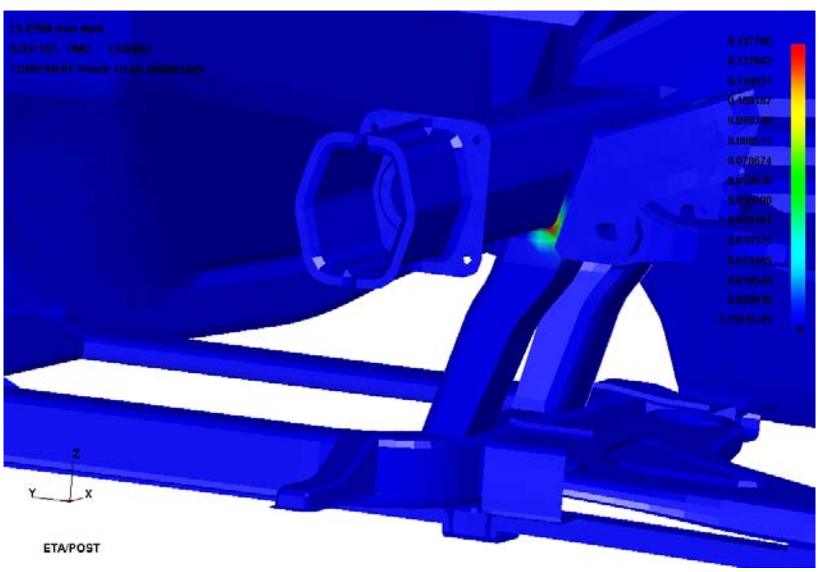

Press to open animation *FIGURE 44: Front Shock Tower Effective Plastic Strain*

13.5. CONCLUSION

This VPG Full Vehicle System Durability Analysis has been completed to highlight the potential of this type of analysis, not as a requirement of the customer. As a result, the specific durability requirements and targets have not been established. Instead, the following basic guideline has been used to highlight potential durability issues in the FGPC: no component shall exhibit effective plastic strain above 0%, i.e. stresses above yield. As highlighted in the Results section, several components, including the rear suspension twist beam and trailing arm, as well as the fuel tank strap and floor pan at the fuel tank, were shown to marginally exceed this target.

A detail modeling for boundary conditions of the fuel tank is necessary, it is believed that the tank strap and floor pan durability performance are underestimated, and therefore not a significant issue.

In order to address the durability concern found in the rear suspension twist beam/trailing arm sub-system, a very simple solution could be presented. The damping characteristics of the suspension dampers defined for this FE model are not adequate from a durability standpoint. The suspension damper definition in this model assumes a simple linear force-velocity relationship, while in reality, this relationship is typically very non-linear for damper velocities exceeding one meter per second. Treatment of this suspension characteristic is very important when considering vehicle durability. A more realistic suspension damper curve would help to further reduce the loads seen by the rear suspension, and thus lower stresses and plastic strain.

The results for the front shock tower show a potential region of concern that would need to be studied further. It is believed that the addition of a bracket to reinforce the joint between the tower and the longitudinal would serve to limit the deformation of the shock tower and improve its durability performance significantly.

It should be noted that these results are entirely dependent on several vehicle suspension tuning parameters, such as bushing stiffness, suspension damping and spring rates, and tire tuning parameters such as radial and lateral stiffness. In order to complete a thorough and more realistic VPG Full Vehicle System Durability assessment of the FGPC vehicle, these parameters should be developed beyond their current level, and additional road surfaces should be included in the assessment of the vehicle system durability.

14. FORMING SIMULATION

14.1. BACKGROUND

In today's forming industry there are two methods of forming analysis, one-step and incremental simulations.

- One-step simulation is efficient for product design stage evaluation
    - Don't need binder and addendum to run the simulation.
    - Fast results, only good for feasibility studies.
    - The results accuracy is only to provide direction
    - Incremental simulation is effective for the tooling stage evaluation
    - Requires a binder and addendum to run the simulation.
    - Detailed, accurate and reliable results for tooling design

One step forming analysis was performed in order to identify the safety cage parts that have potential problems in forming using the HSLA materials. Although one step forming analysis is an approximate simulation, it still can identify the major issues. ETA/DYNAFORM was used for the simulations.

14.2. TARGETS

The objective of this study was to measure the thinning of the formed parts and identify any potential problems. Table 6 lists the maximum allowable percentage thinning targets for each part considered.

14.3. RESULTS

The following analysis only considers the parts that have been modified in the FGPC safety cage, see Figure 45.

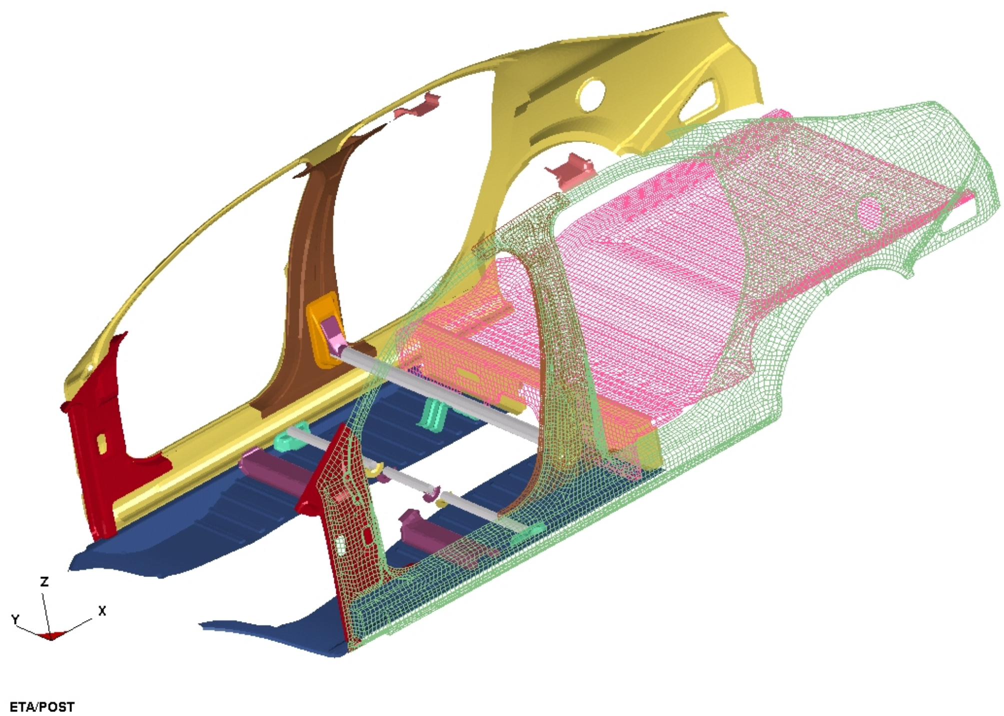

FIGURE 45: Redesigned Parts

Table 6 gives the original part thickness, the actual predicted minimum thickness after stamping and the target thickness values in mm and percentage thinning. Each part's material individually defined its thinning target. The row in red highlights severe thinning, the orange critical thinning and the yellow rows parts of concern. The rest meet their targets. Figures 46 through 58 show the thinning plots for each part.

PART NAME	ORIGINAL THICKNESS (mm)	MINIMUM THICKNESS (mm)	TARGET THICKNESS (mm)	MAXIMUIM ALLOWABLE PERCENTAGE THINNING
A-Post Inner	0.91	0.75	0.83	10
Body-Side-Outer	0.94	0.78	0.8	15
B-Pillar-Inner	1.05	0.96	0.94	10
Cross Member-Support-Rear-Outer Bracket	1.2	0.86	1.02	15
Cross-Member-Support-Rear-Center-Bracket	1.4	1.25	1.19	15
Front-Floor	0.6	0.59	0.42	30
Cross-Member-Support-Front-Seat	0.7	0.58	0.59	15
Cross-Member-Kick up	1.16	1.09	1.04	10
Rear-Floor	0.84	0.74	0.76	10
Cross-Member-Roof-Bracket	0.7	0.65	0.56	20
Pole-Cross-Member-Support-Inner-Bracket	0.7	0.66	0.59	15
Pole-Cross-Member-Support-Outer-Bracket	0.7	0.59	0.59	15
Cross-Member-Support-Rear-Outer-Upper-Bracket	1	0.91	0.85	15

TABLE 6: Forming Results

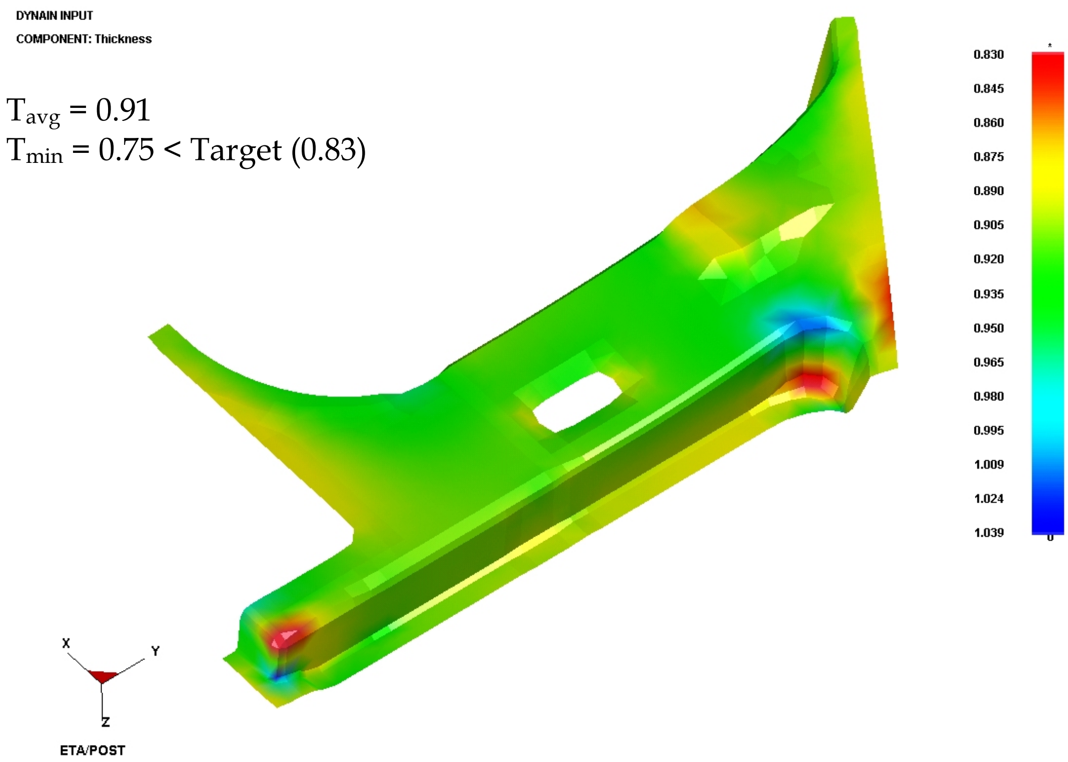

FIGURE 46: A-Post Inner Thickness Plot

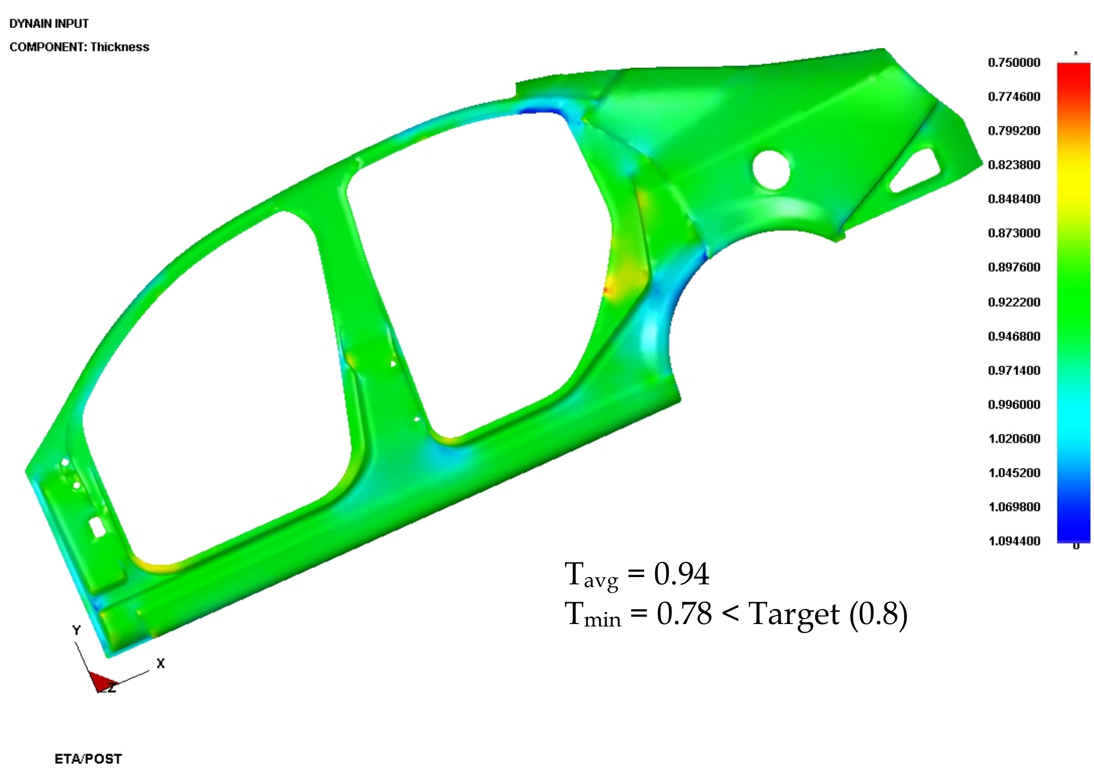

FIGURE 47: Body-Side-Outer Thickness Plot

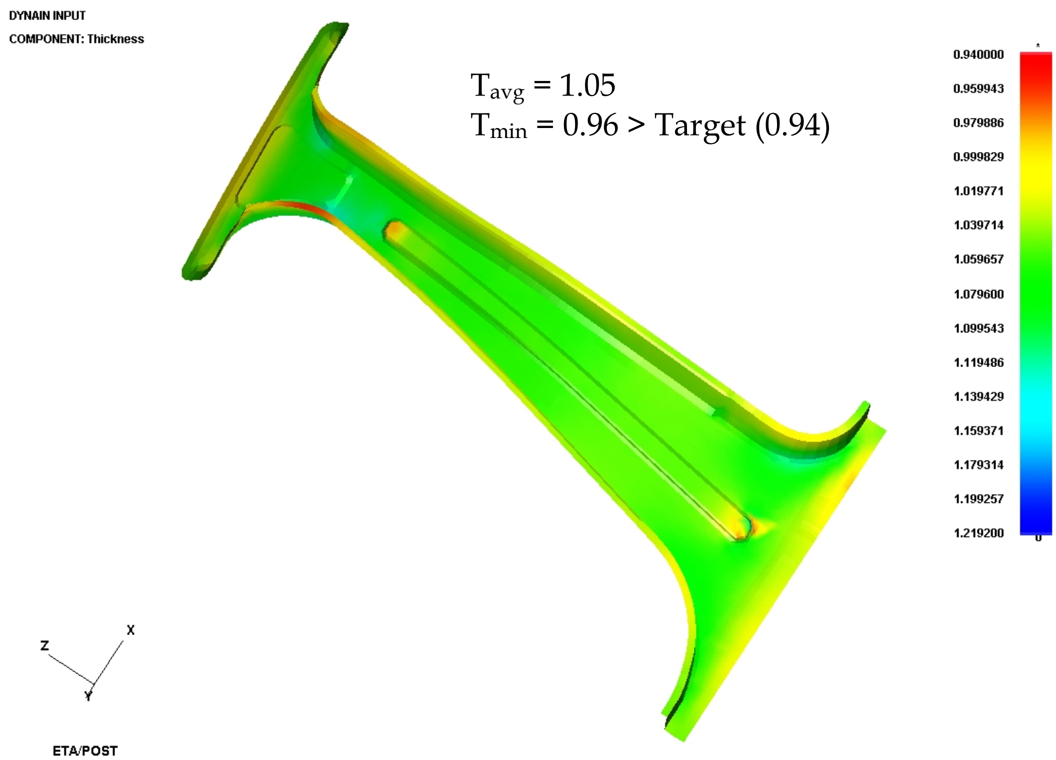

FIGURE 48: B-Pillar-Inner-Thickness Plot

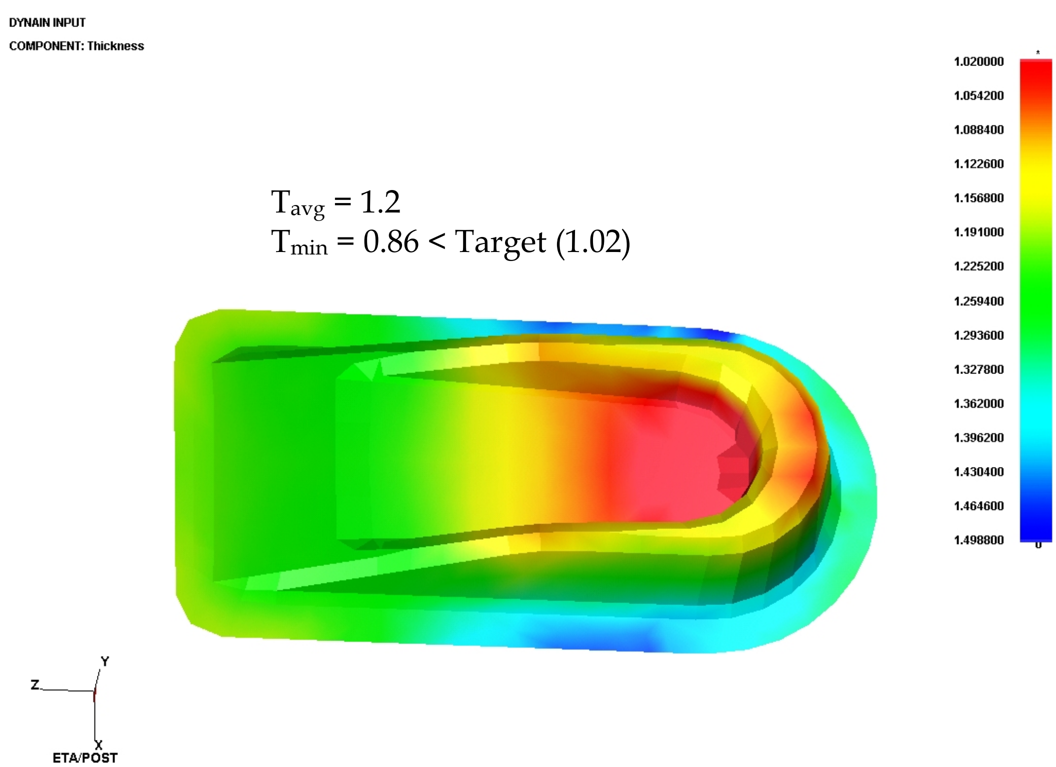

FIGURE 49: Cross-Member-Support-Rear-Outer-Bracket Thickness Plot

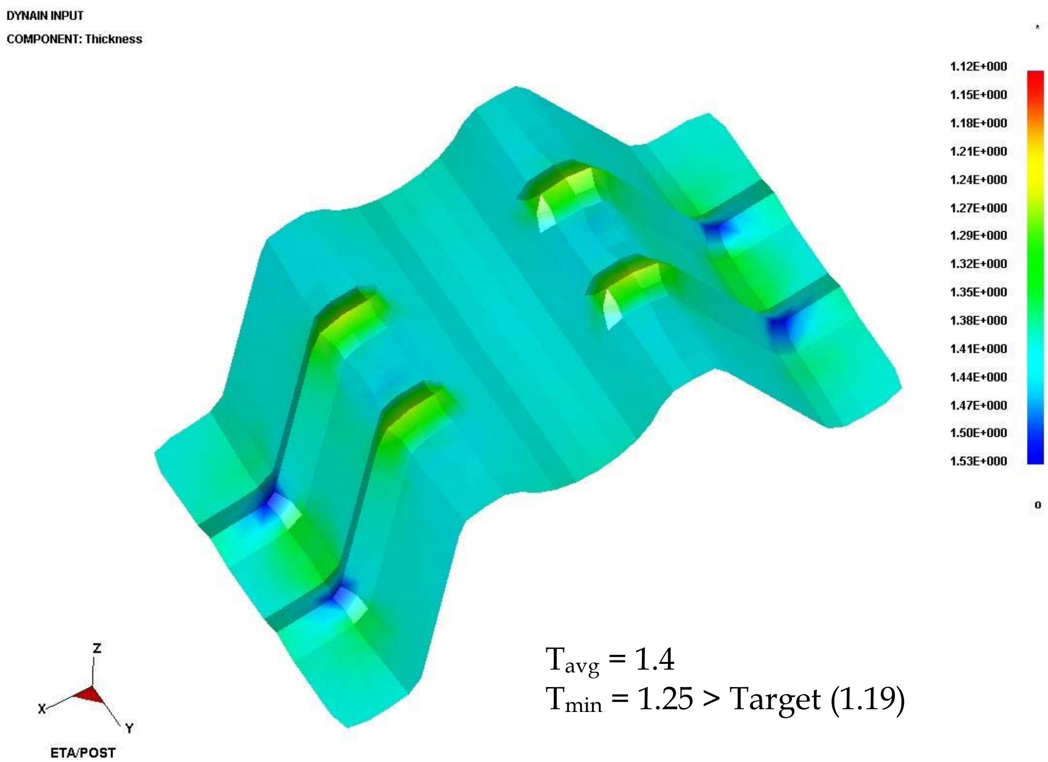

FIGURE 50: Cross-Member-Support-Rear-Center-Bracket Thickness Plot

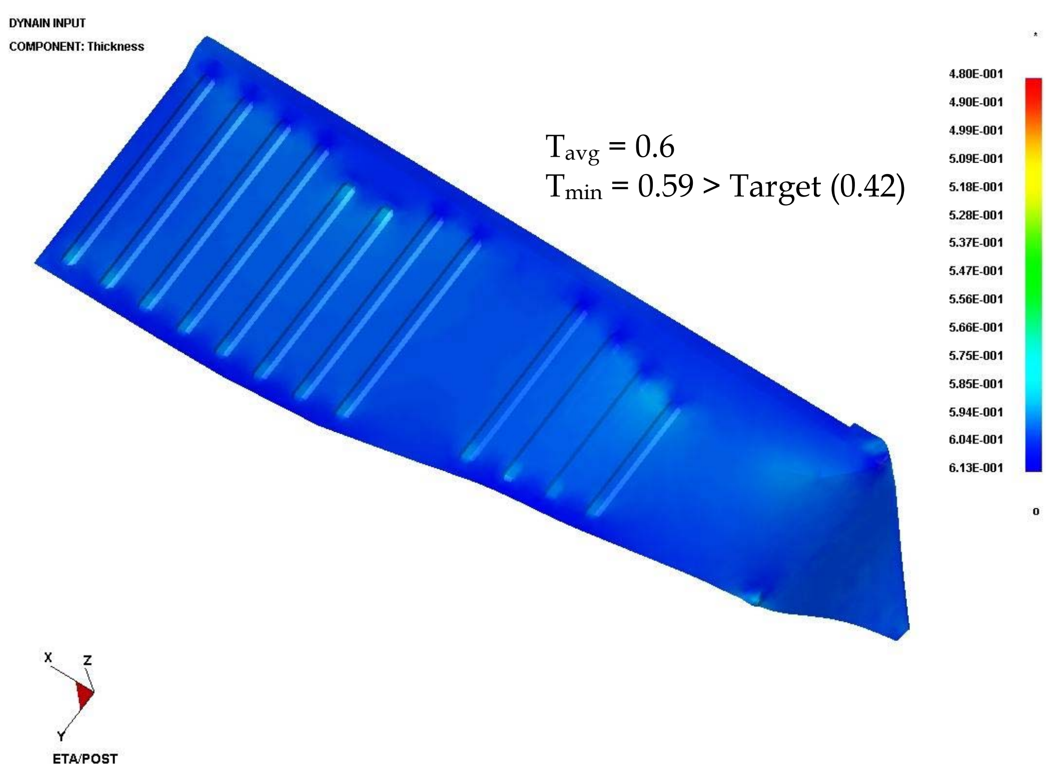

FIGURE 51: Front-Floor Thickness Plot

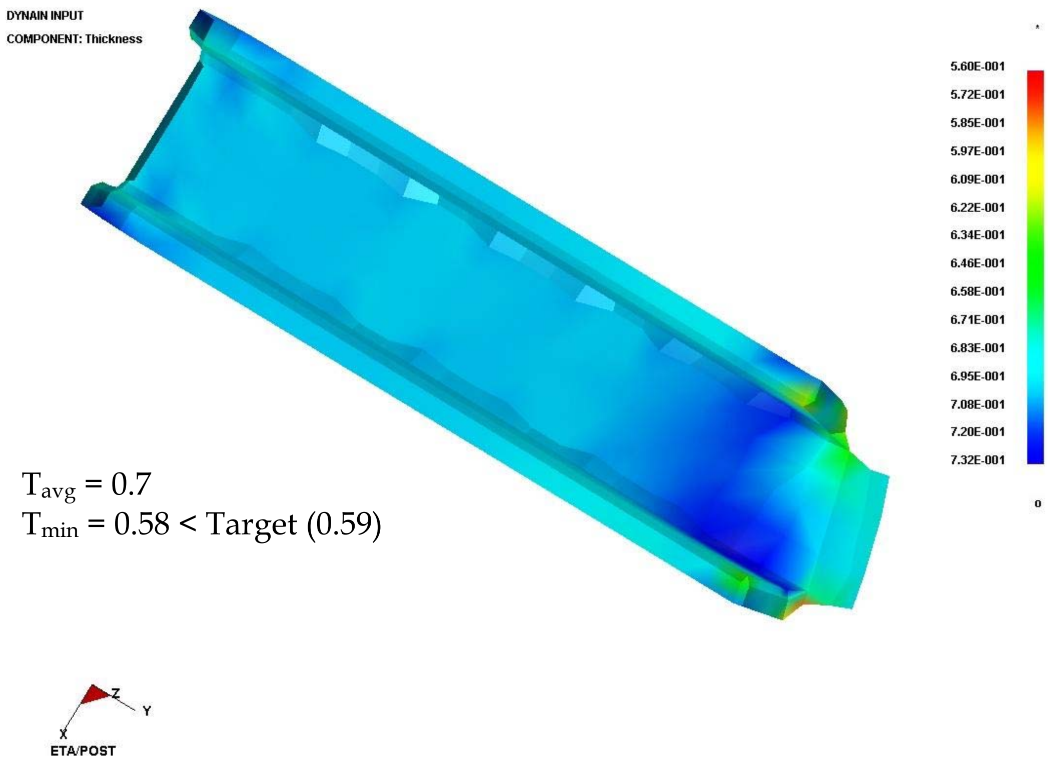

FIGURE 52: Cross-Member-Support-Front-Seat Thickness Plot

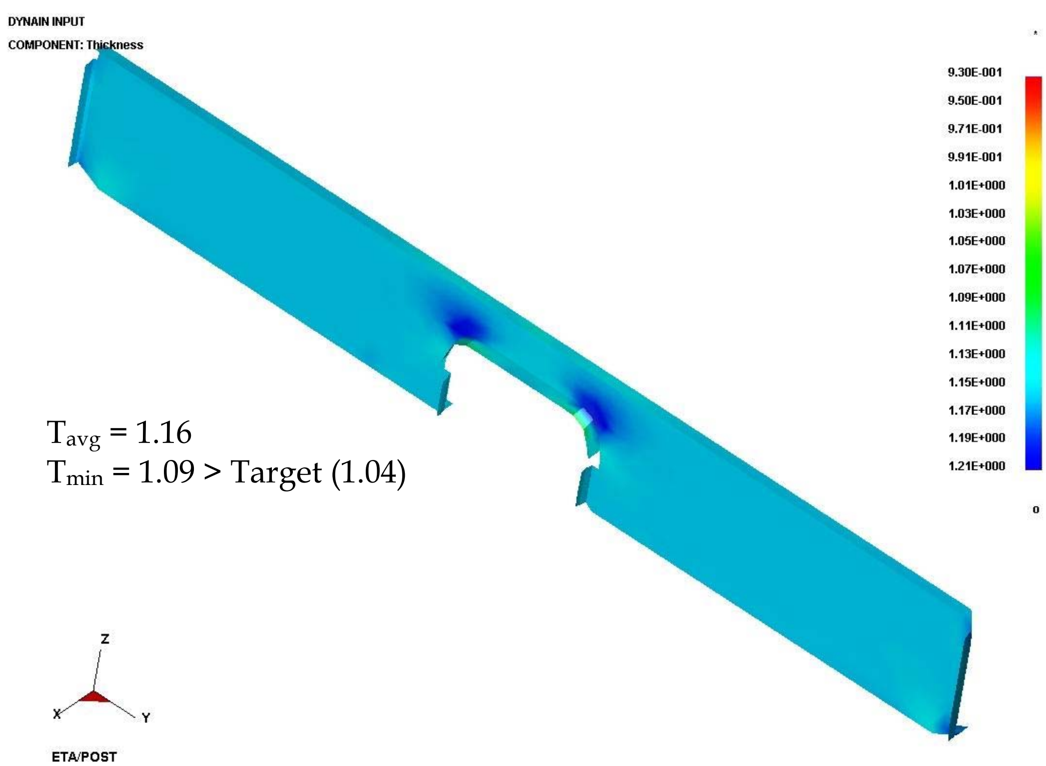

FIGURE 53: Cross-Member-Kick up Thickness Plot

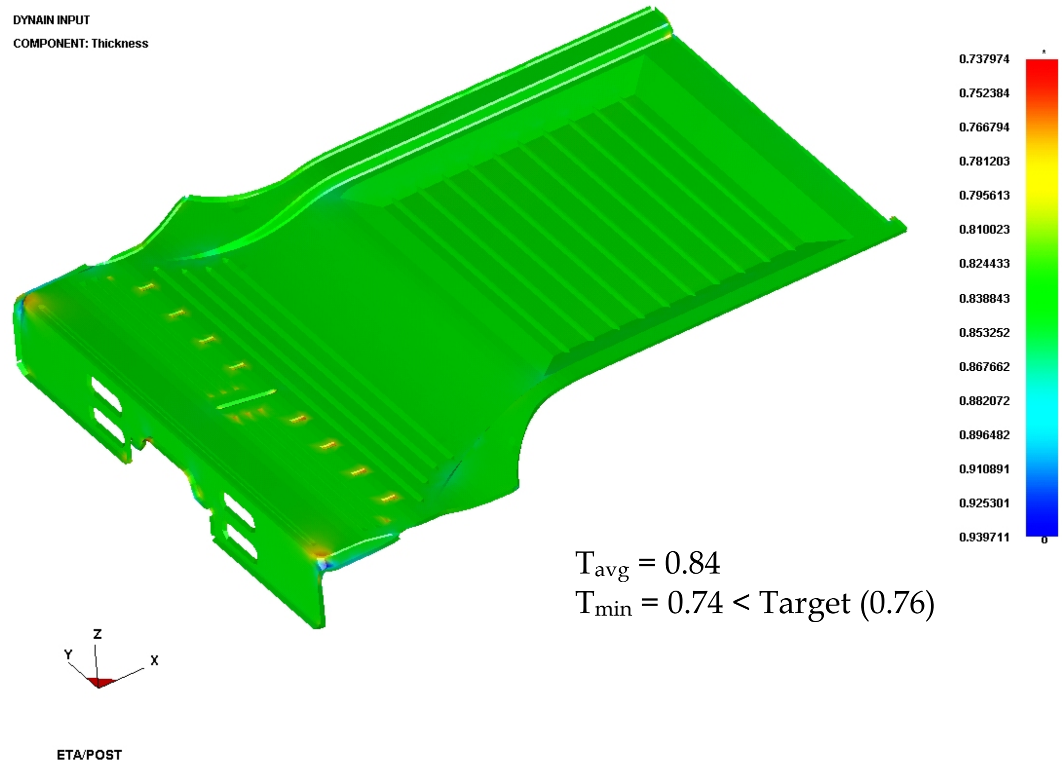

FIGURE 54: Rear-Floor Thickness Plot

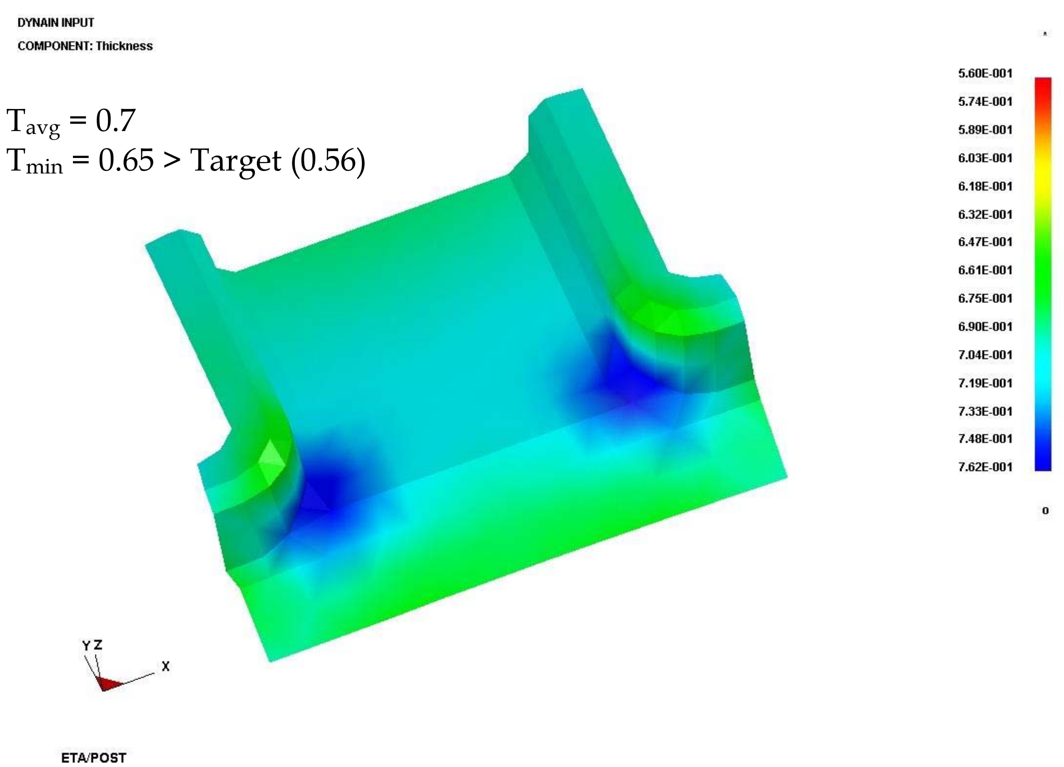

FIGURE 55: Cross-Member-Roof-Bracket Thickness Plot

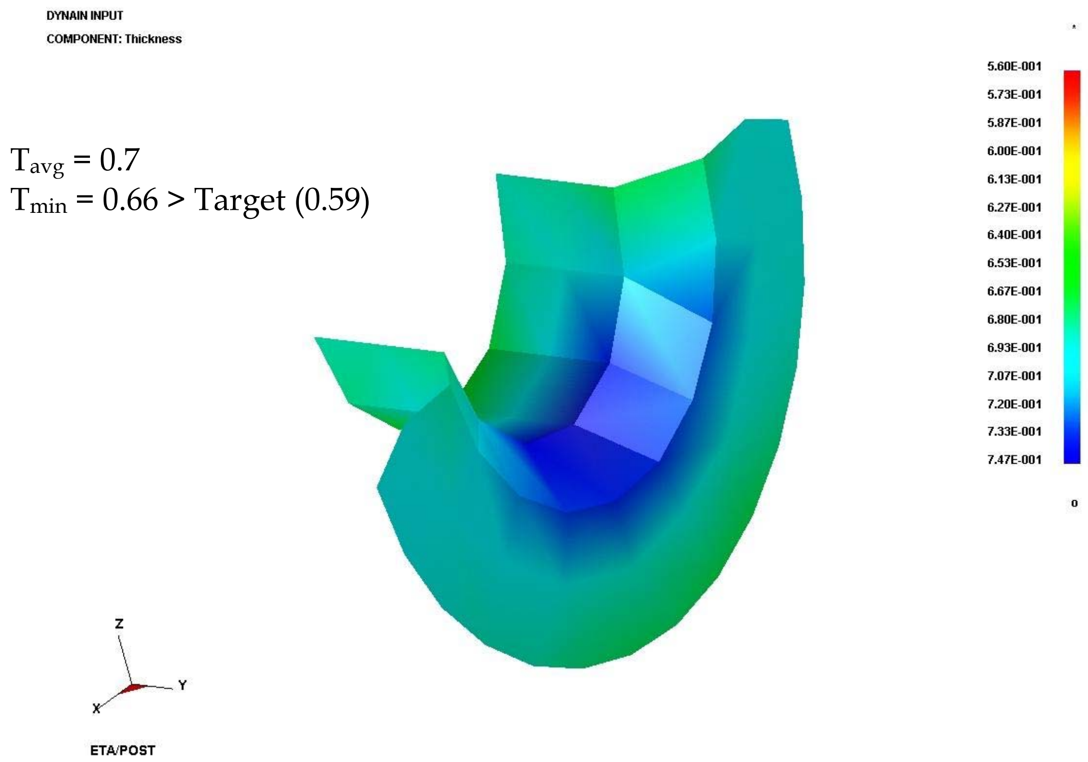

FIGURE 56: Pole-Cross-Member-Support-Inner-Bracket Thickness Plot

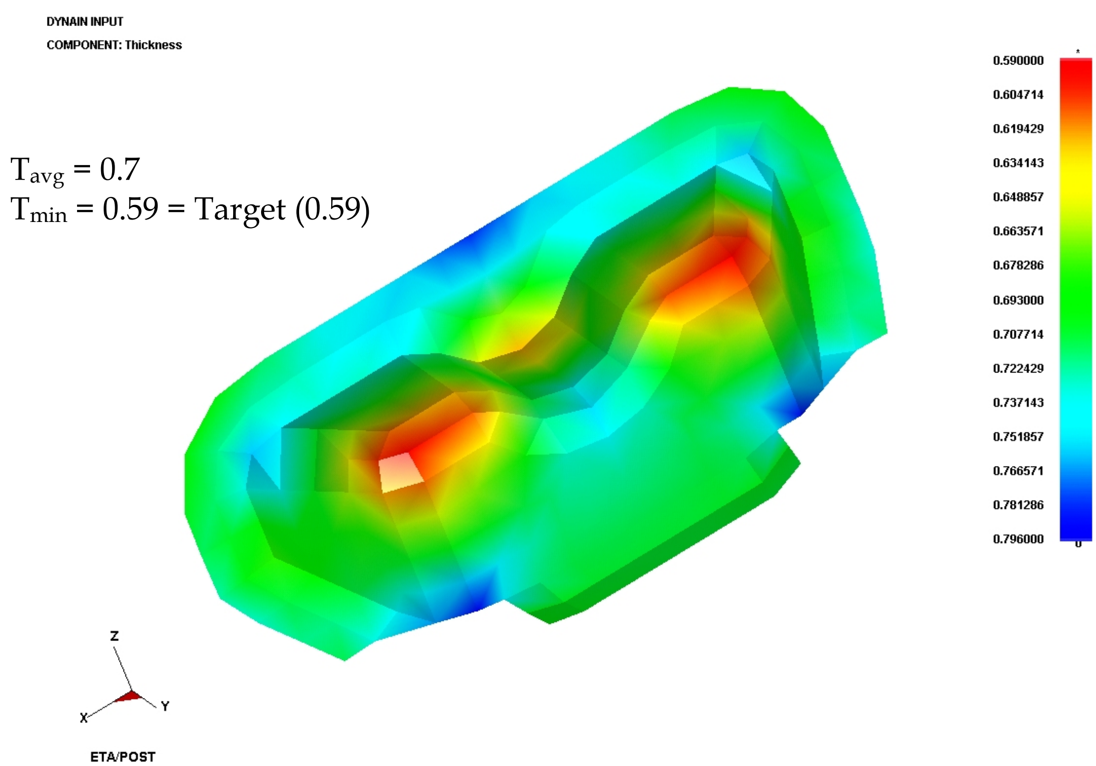

FIGURE 57: Pole-Cross-Member-Support-Outer-Bracket Thickness Plot

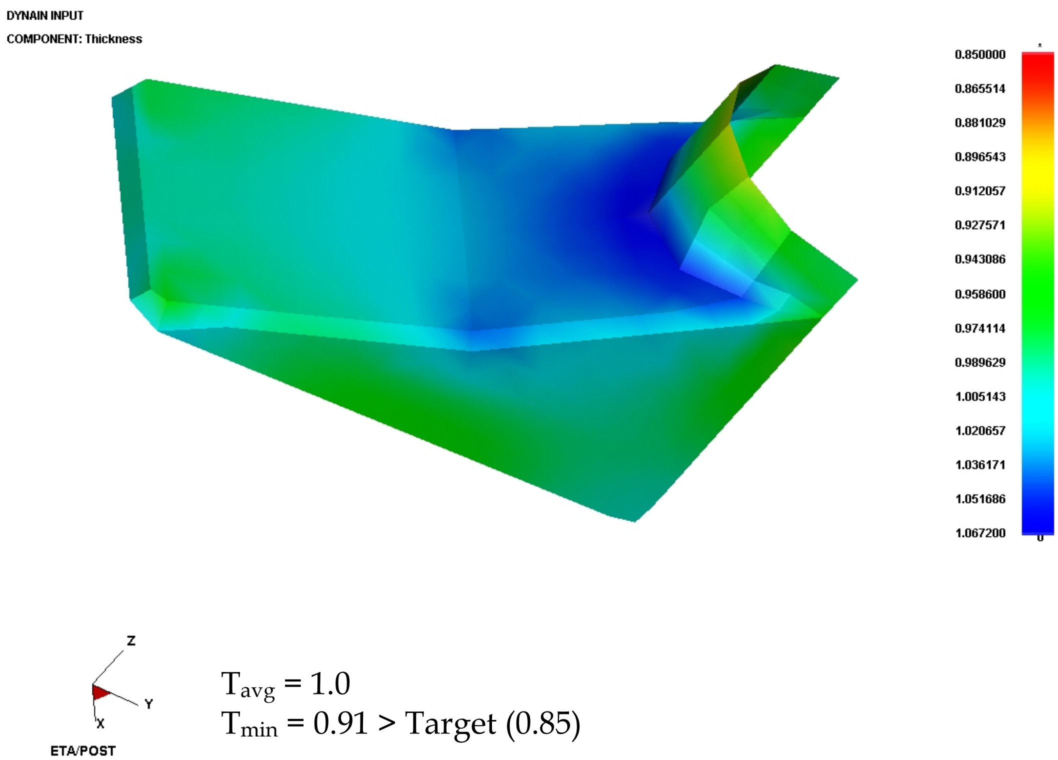

$T_{avg} = 1.0$
$T_{min} = 0.91 > \text{Target } (0.85)$

FIGURE 58: Cross-Member Support Rear Outer Upper Bracket Thickness Plot

14.4. CONCLUSION

Only two parts significantly exceeded their individual targets. The maximum thinning predicted for the A-Post Inner was 18% (target 10%) and for the Cross-Member-Support-Rear-Outer-Bracket, 28% (target 15%). The highlighted parts shown in Table 6 would require an incremental analysis in order to more accurately predict their stamping behavior.

15. MODAL AND STATIC STIFFNESS

15.1. TARGET

The target for a trimmed BIW vehicle was 40Hz but since the trimmed body mass and CG was not fully defined the FGPC team decided to use targets for the BIW based upon the ULSAB-AVC performance.

- Modal Modes — Bending – 57Hz; Torsion – 56Hz
- Stiffness — Bending – greater than 12000N/mm; Torsion – greater than 13000Nm/deg

15.2. NORMAL MODES (FREE-FREE)

A normal modes analysis was performed on the BIP (Body-In-Prime) model. The torsional and bending modes were extracted and compared to the target values, see Table 7. The mode shapes are shown in the following figures. Figures 59 & 60 show the torsional mode at 56 Hz, while Figures 61 & 62 show the bending mode at 63Hz.

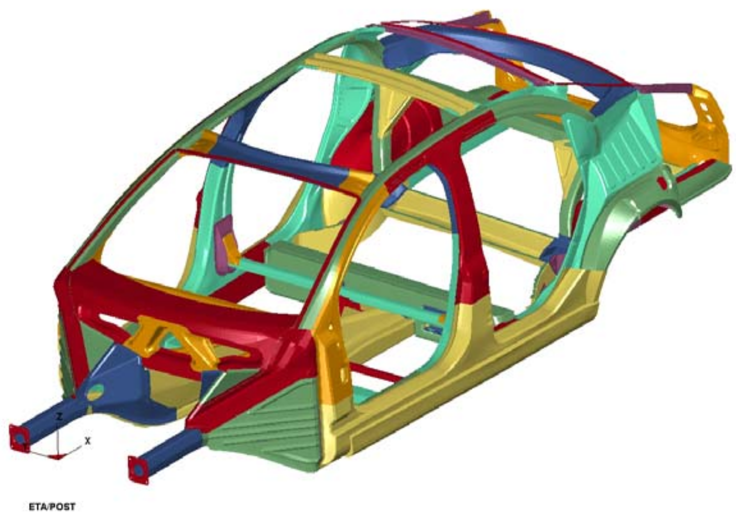

Press to open animation

FIGURE 59: Torsion Mode (ISO View)

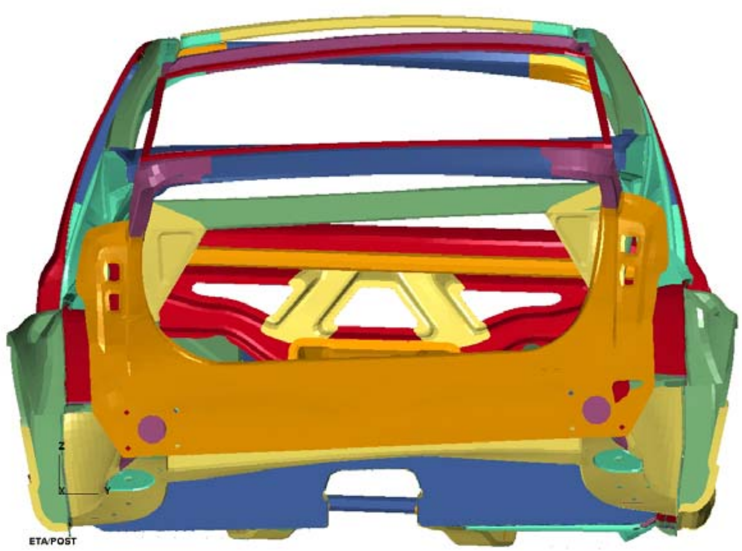

Press to open animation

FIGURE 60: Torsion Mode (Rear View)

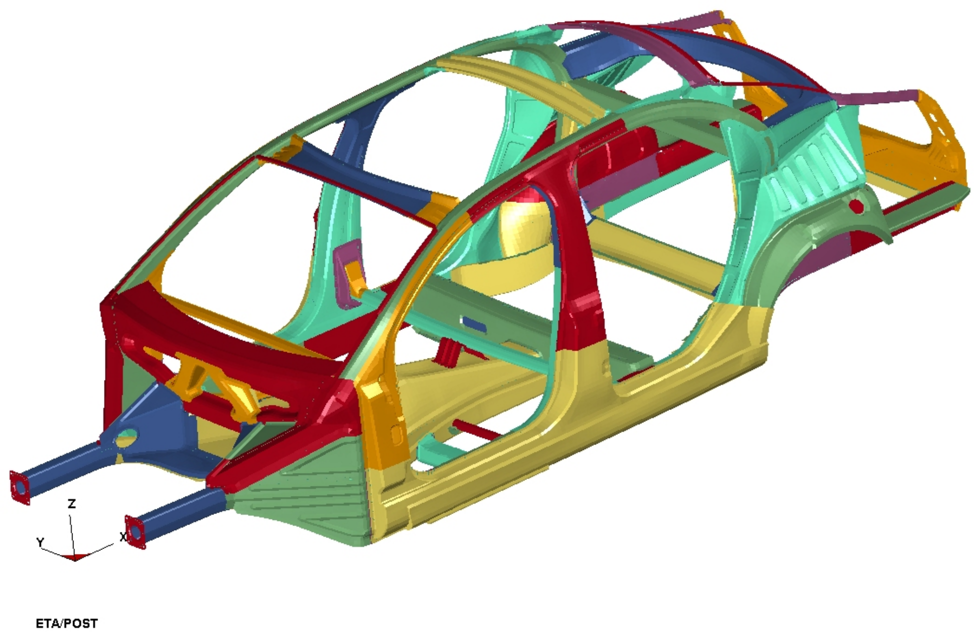

Press to open animation

FIGURE 61: Bending Mode (ISO View)

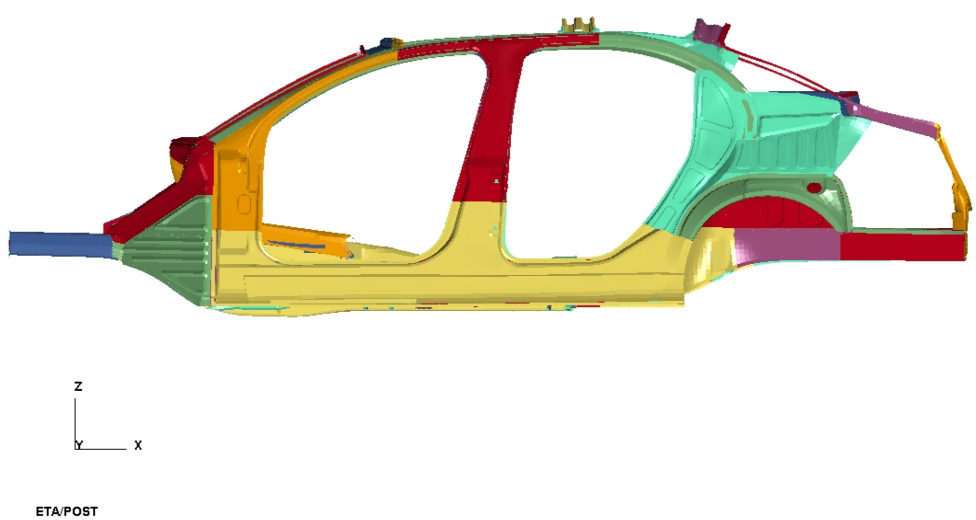

Press to open animation

FIGURE 62: Bending Mode (Side View)

Figures 63 & 64 show the strain energy plots for the Upper and Lower Package Tray joints, indicating a potential for improvement.

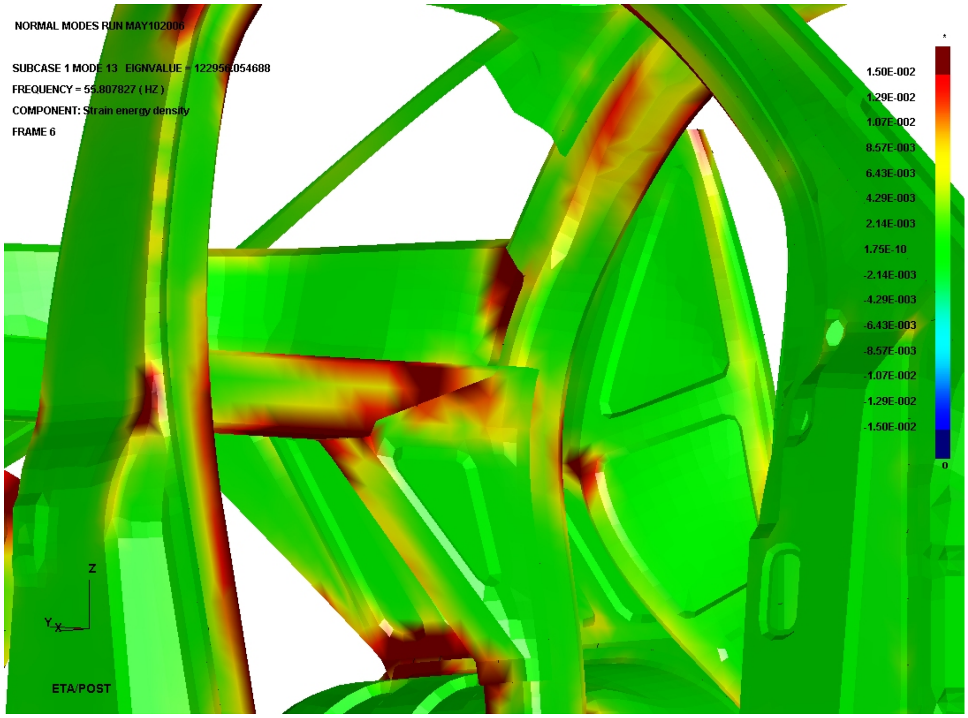

FIGURE 63: Torsion Mode Strain Energy Plot – Package Tray Area Upper Joint

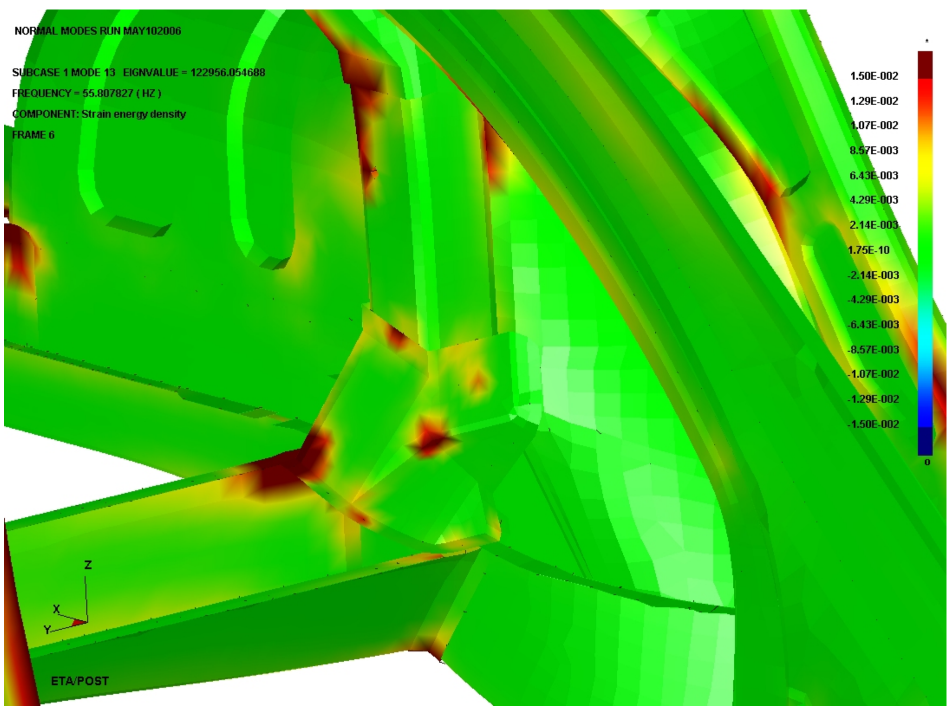

FIGURE 64: Torsion Mode Strain Energy Plot – Package Tray Area Lower Joint

NAME	TARGET (Hz)	FGPC-BO (Hz)	FGPC-AO (Hz)	FGPC-ACD (Hz)	FGPC-FCD (Hz)
Bending Frequency (BIW)	57	71	57	61	63
Torsion Frequency (BIW)	56	57	47	54	56

TABLE 7: Results For Modal Analysis

15.3. RESULTS OF STATIC TORSION AND BENDING STIFFNESS

Static stiffness analysis was performed on the BIP model. The torsional and bending stiffness values were compared to the target values in Table 8. The FGPC-ACD bending and torsional stiffnesses are above set targets. The deformed shapes are shown in Figures 65 & 66.

NAME	TARGET	FGPC-BO	FGPC-AO	FGPC-FCD
Bending Stiffness	>12000N/mm	NA	8547N/mm	**12988 N/mm**
Torsional Stiffness	>13000Nm/deg	NA	11192 Nm/deg	**13290 Nm/dg**

TABLE 8: Results For The Static Bending & Torsional Stiffness

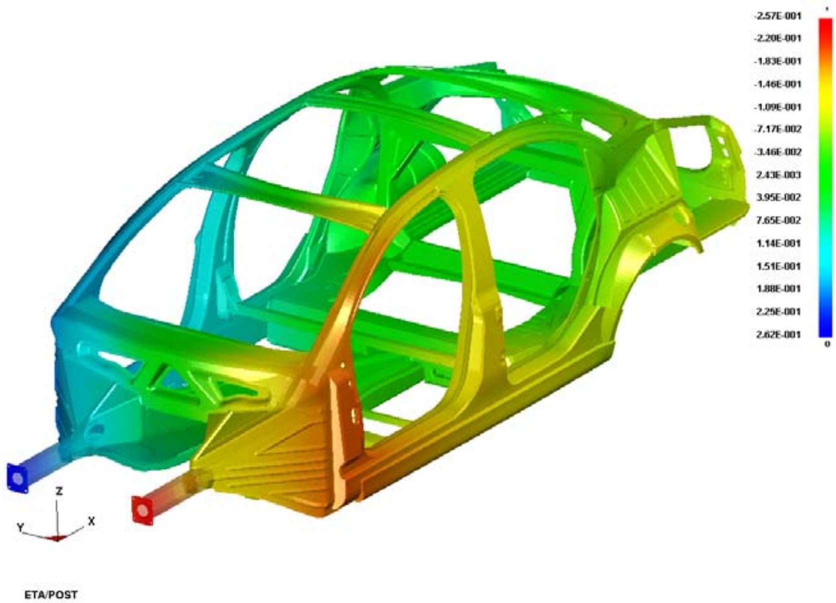

FIGURE 65: Static Torsional Stiffness – Deformed Shape

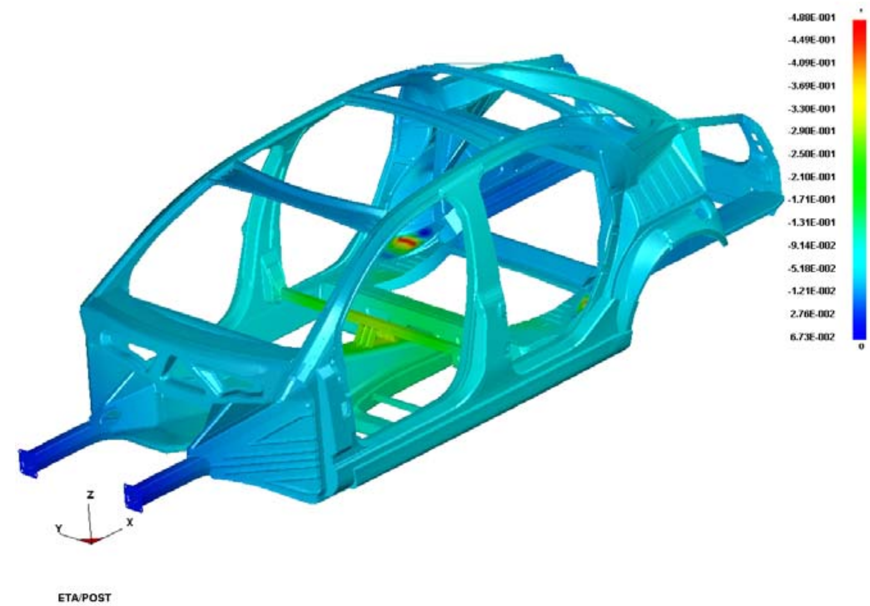

FIGURE 66: Static Bending Stiffness – Deformed Shape

15.4. CONCLUSION

FGPC modal frequencies and static stiffness satisfies the program targets.

16. TASK 7.0 CONCEPT DESIGN ANALYSIS CHECK CONCLUSIONS

Table 9 summarizes the results of the Task 7.0 loadcases.

LOADCASE	Met FGPC Targets	NOTES
US-NCAP Front Crash (0 Degree)	Yes	Final optimization results satisfied FGPC targets
IIHS Front Crash 40% ODB	Yes	Final optimization results satisfied FGPC targets
FMVSS 214 New -Side Pole Impact	Yes	Further analysis was required to satisfy the targets
IIHS Side Impact	Yes	Further analysis was required to satisfy the targets
Roof Crush	Yes	Final optimization results satisfied FGPC targets
Door Intrusion	Yes	Final optimization results satisfied FGPC targets
Rear Crash	Yes	Final optimization results satisfied FGPC targets
Durability (VPG)	Yes	No clear target was set
Stamping and Formability	Yes	Final optimization results satisfied FGPC targets
Normal Modes (Free-Free)	Yes	Final optimization results satisfied FGPC targets
Bending/Torsional Stiffness	Yes	Final optimization results satisfied FGPC targets

TABLE 9: Task 7.0 Concept Design Analysis Check Results Summary

Table 10 summarizes the mass savings achieved by FGPC-FCD over the baseline design, FGPC-BO.

STRUCTURE	FGPC-BO (kg)	FGPC-FCD (kg)	MASS SAVINGS (kg)	CHANGE (%)
BIW + IP BEAM	227.2	217.6	9.6	4

MODIFIED PARTS	FGPC-BO (kg)	FGPC-FCD (kg)	MASS SAVINGS (kg)	CHANGE (%)
BIW	130.6	121.0	9.6	7
Doors	12.6	6.4	6.2	49
TOTAL	**143.2**	**127.4**	**15.8**	**11**

STRUCTURE	INDUSTRY STANDARD (kg)	FGPC-FCD (kg)	MASS SAVINGS (kg)	CHANGE (%)
BIW + IP BEAM	310.0	217.6	92.4	30

TABLE 10: FGPC-FCD Final Mass Savings Over FGPC-BO

Figure 67 & Table 11 compare the FGPC-FCD to an "In-Class Vehicle," the comparison is based upon data taken from a currently produced 4-Door Mid Size Sedan of similar dimensions.

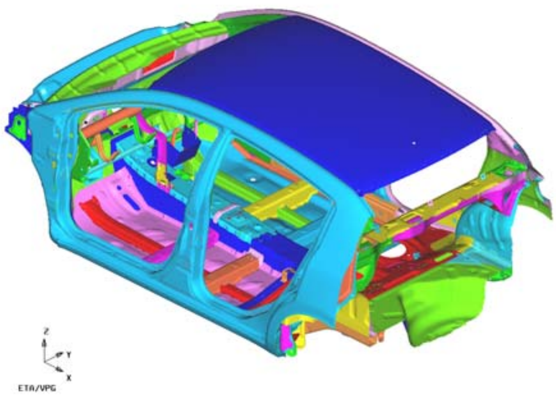

In-Class Vehicle

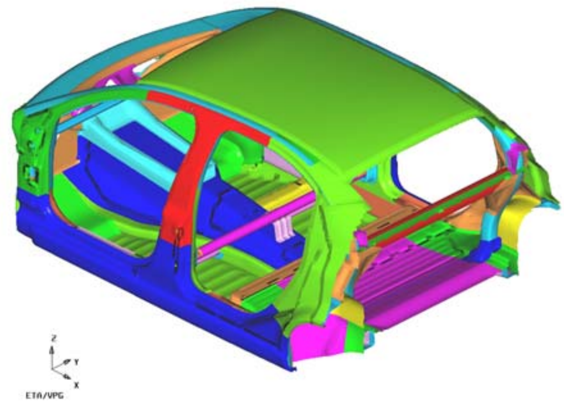

FGPC-FCD

FIGURE 67: Safety Cage Comparison – In-Class Vehicle vs FGPC-FCD

	IN-CLASS VEHICLE* (kg)	FGPC-FCD (kg)	CHANGE (%)
BIW+IP	314.7	217.6	31
Safety Cage	246.8	169.3	31

*Based upon historic data, a 4-Door Mid Size Sedan with similar dimensions to the FGPC vehicle

TABLE 11: In-Class Vehicle vs FGPC-FCD Comparison

APPENDIX A
FRONT CRASH REGULATIONS, NCAP
Scope and Purpose:
This standard specifies performance requirements for the protection of vehicle occupants in crashes. The purpose of this standard is to reduce the number of deaths of vehicle occupants, and the severity of injuries, by specifying vehicle crashworthiness requirements in terms of forces and accelerations measured on a variety of anthropomorphic dummies in test crashes, and static airbag deployment tests. This standard also specifies equipment requirements for active and passive restraint systems.

Application:
Passenger cars, trucks, buses, and multipurpose passenger vehicles with a GVWR of 3,855 kg (8,500 lb) or less and an UVW of 2,495 kg (5,500 lb) or less, except for walk-in van-type trucks or vehicles designed to be sold exclusively to the U. S. Postal Service

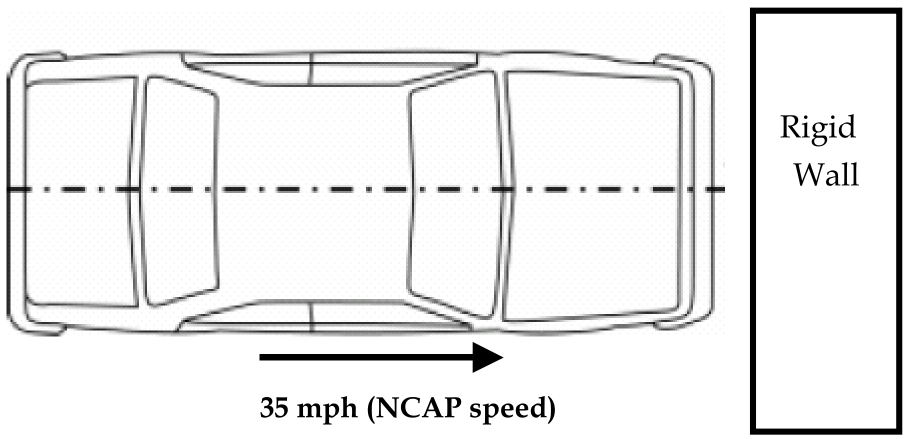

FIGURE A1: Vehicle Overlap With Deformable Barrier

APPENDIX B

IIHS FRONT CRASH REGULATIONS, 40% ODB

Offset barrier crash tests are conducted at 40mph (64.4km/hr) with a 40% overlap. The test vehicle is aligned with the deformable barrier such that the right edge of the barrier face is offset to the left of the vehicle centerline by 10% of the vehicle's width. See Figure B1. The vehicle width is defined and measured as indicated in SAE J1100 – Motor Vehicle Dimensions, which states, "the maximum dimension measured between the widest part on the vehicle, excluding exterior mirrors, flexible mud flaps, and marker lamps, but including bumpers, moldings, sheet metal protrusions, or dual wheels, if standard equipment."

The vehicle is accelerated by the propulsion system at an average of 0.3g until it reaches the test speed and then is released from the propulsion system 25cm before the barrier. The onboard braking system, which applies the vehicle's service brakes on all four wheels, is activated 1.5sec after the vehicle is released from the propulsion system.

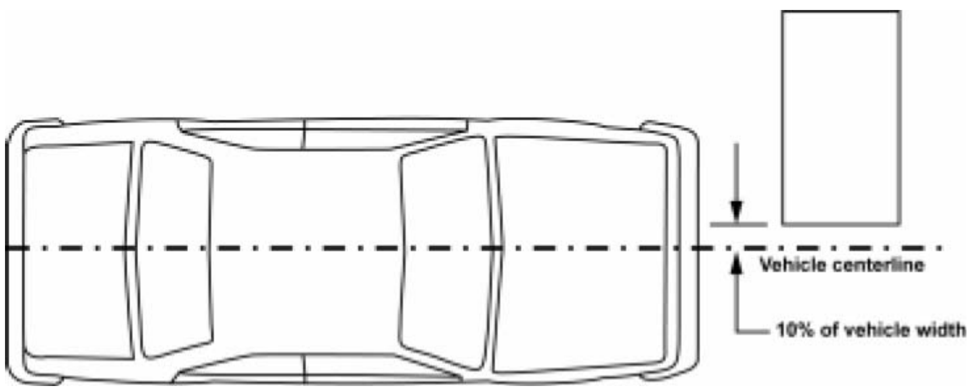

FIGURE B1: Vehicle Overlap With Deformable Barrier

MEASUREMENT POINT LOCATIONS

The following are the locations for measuring vehicle intrusion:

- **Steering column (one point)**
  The marked reference is the geometric center of the steering wheel, typically on the airbag door. After the crash, this point is measured by folding the airbag doors back into their undeployed position. In most cases, this measurement is probably less than the maximum intrusion into the compartment. However, if the steering column completely separates from the instrument panel (for example, due to shear module separation) during the crash, the steering column post-crash measurement is taken by placing and holding the wheel and column in its approximate maximum dynamic position as recorded on the high-speed film. The film may not always show clearly where the column was during the crash, and in such cases other clues would be needed to reposition the column for measurement. In rare instances, it may not be possible to obtain any meaningful post-crash measurement.
- **Lower instrument panel (two points)**
  The left and right lower instrument panel (knee bolster) lateral coordinates are defined by adding 15cm to and subtracting 15cm from the steering column reference lateral coordinate, respectively. The vertical coordinate is the same for both left and right references and is defined as 45cm above the height of the floor (without floormats). If the panel or knee bolster loosens or breaks away in the crash, the post-crash measurements are taken by pressing and holding the panel against the underlying structure.

- **Brake pedal (one point)**
  The geometric center of the brake pedal pad (top surface). If the brake pedal is constructed so that it dangles loosely after the crash, the brake pedal is pushed straight forward against the toepan/floorpan and held there to take the post-crash measurement. If the pedal drops away entirely, no post-crash measurement is taken.

- **Toepan (three points)**
  The vertical coordinate for all toepan measurement locations is the vertical coordinate of the brake pedal reference. The lateral coordinates of the left, center, and right toepan locations are obtained by adding 15cm to, adding 0cm to, and subtracting 15cm from the brake pedal reference lateral coordinate, respectively. The longitudinal coordinate is measured and a mark is temporarily placed at the locations on the toepan. A utility knife is used to cut a small "V" in the carpet and underlying padding at each point on the toepan. The point of the "V" is peeled back, and the exposed floor is marked and measured. The carpet and padding are then refitted prior to the crash.

- **Left footrest (one point)**
  The vertical coordinate for the footrest measurement location is the vertical coordinate of the brake pedal reference. The lateral coordinate of the footrest is obtained by adding 25cm to the brake pedal reference lateral coordinate. The same procedure described above for cutting the carpet is used to mark and measure the underlying structure. In cases where there is a specific footrest construct at the footrest measurement location, the construct is removed and the underlying structure is marked and measured. The construct is reinstalled prior to the crash.

- **Seat bolts (typically, four points)**
  Each of the four (or fewer) bolts that anchor the driver seat to the floor of the vehicle.

- **A-Pillar (one point)**
  The A-Pillar is marked on the outside of the vehicle at the same vertical coordinate as the base of the left front window.

- **B-Pillar (one point)**
  The B-Pillar is marked on the outside of the vehicle at the longitudinal center of the pillar at the same vertical coordinate as the lower A-Pillar mark.

APPENDIX C

SIDE POLE IMPACT (FMVSS214 NEW) REGULATIONS

The vehicle is propelled at 20mph into a 10in diameter pole at an angle of 75 degrees to its longitudinal axis, as shown in Figure B1. The pole is lined up with the center of the occupant's head. The occupant may be either a 50th percentile male at the mid-track seat position, or a 5th percentile female at the full forward seat position.

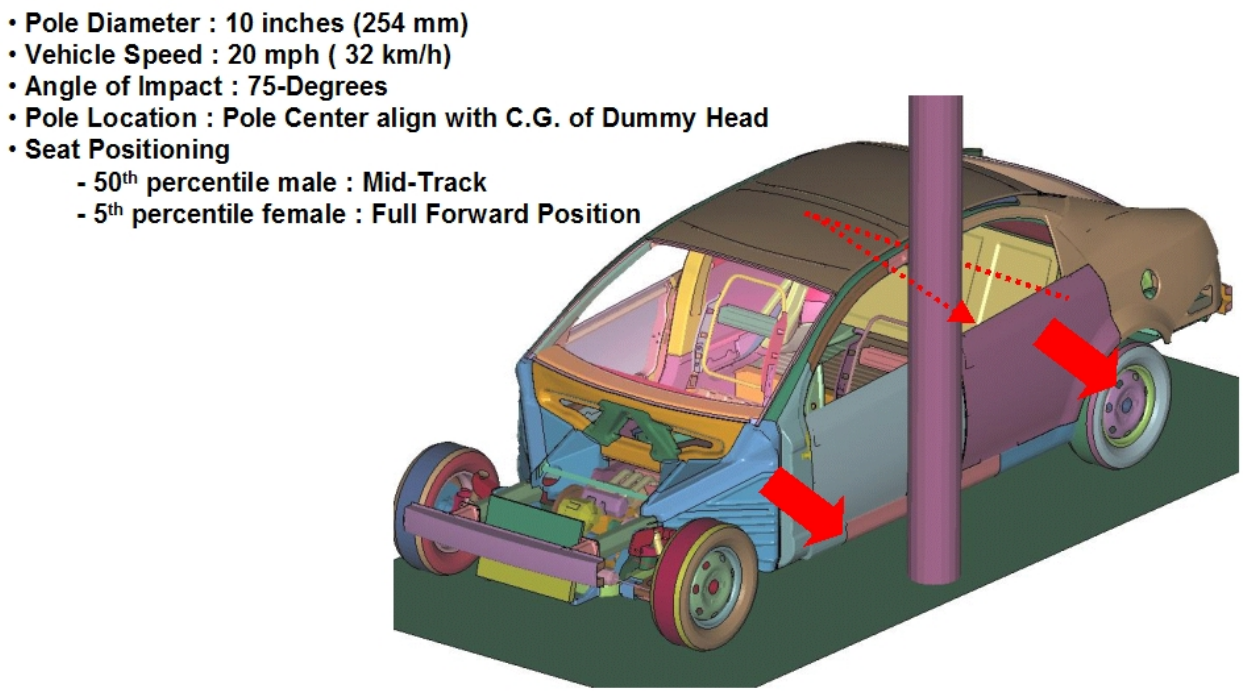

FIGURE C1: Pole Impact

APPENDIX D
IIHS SIDE IMPACT REGULATIONS

The IIHS Side Impact regulations state that a 1500kg MDB (Moving Deformable Barrier) strike the stationary test vehicle on the driver's side at a speed of 50km/hr and an angle of 90 degrees. The barrier block is made from aluminum honeycomb, and has 379mm ground clearance. The front aluminum mounting plate has been raised 100mm higher off the ground and has been extended 200mm taller than a standard FMVSS214 barrier. The longitudinal impact point of the barrier on the side of the test vehicle is dependent on the vehicle's wheelbase. The IRD (Impact Reference Distance) is defined as the distance rearward from the test vehicle's front axle to the closest edge of the deformable barrier when it first contacts the vehicle. See Figure D1.

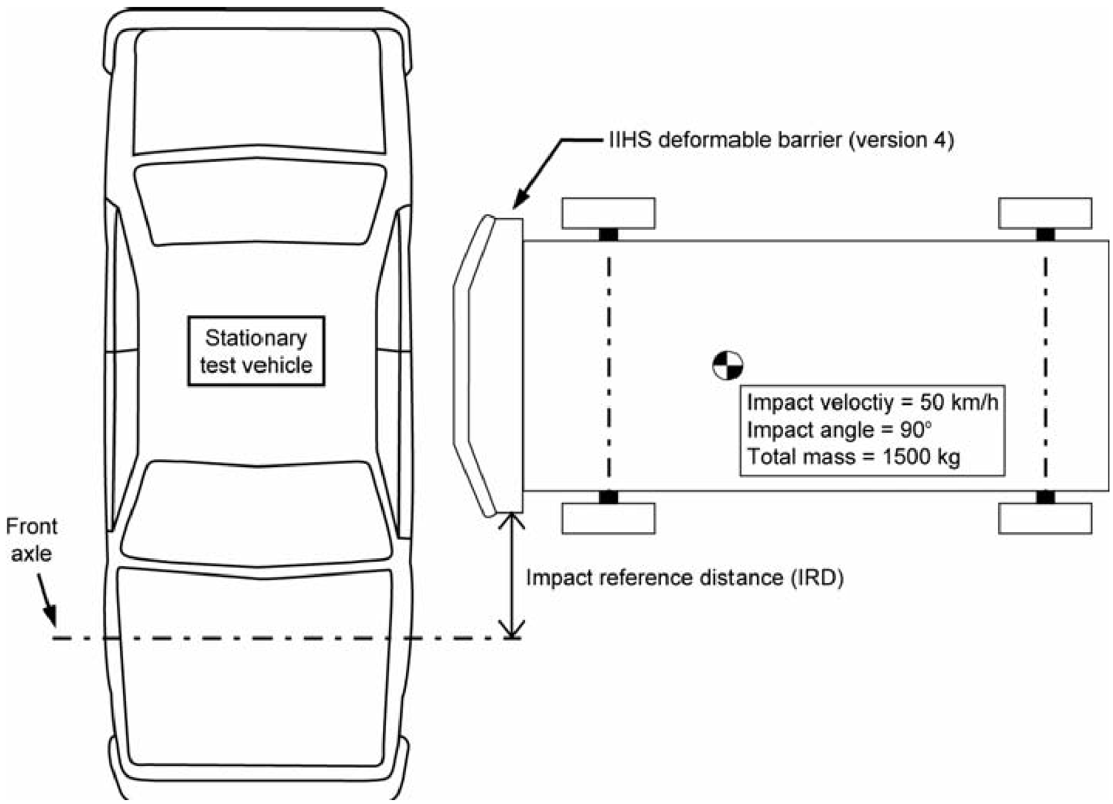

FIGURE D1: Moving Deformable Barrier Alignment With Test Vehicle

The structural rating requirements are shown in Figure D2.

Boundary line	Good	Acceptable	Marginal	Poor
B-pillar to driver seat centerline distance (cm)	12.5	5.0	0.0	
Structural failures	Downgrade structural rating by one category			

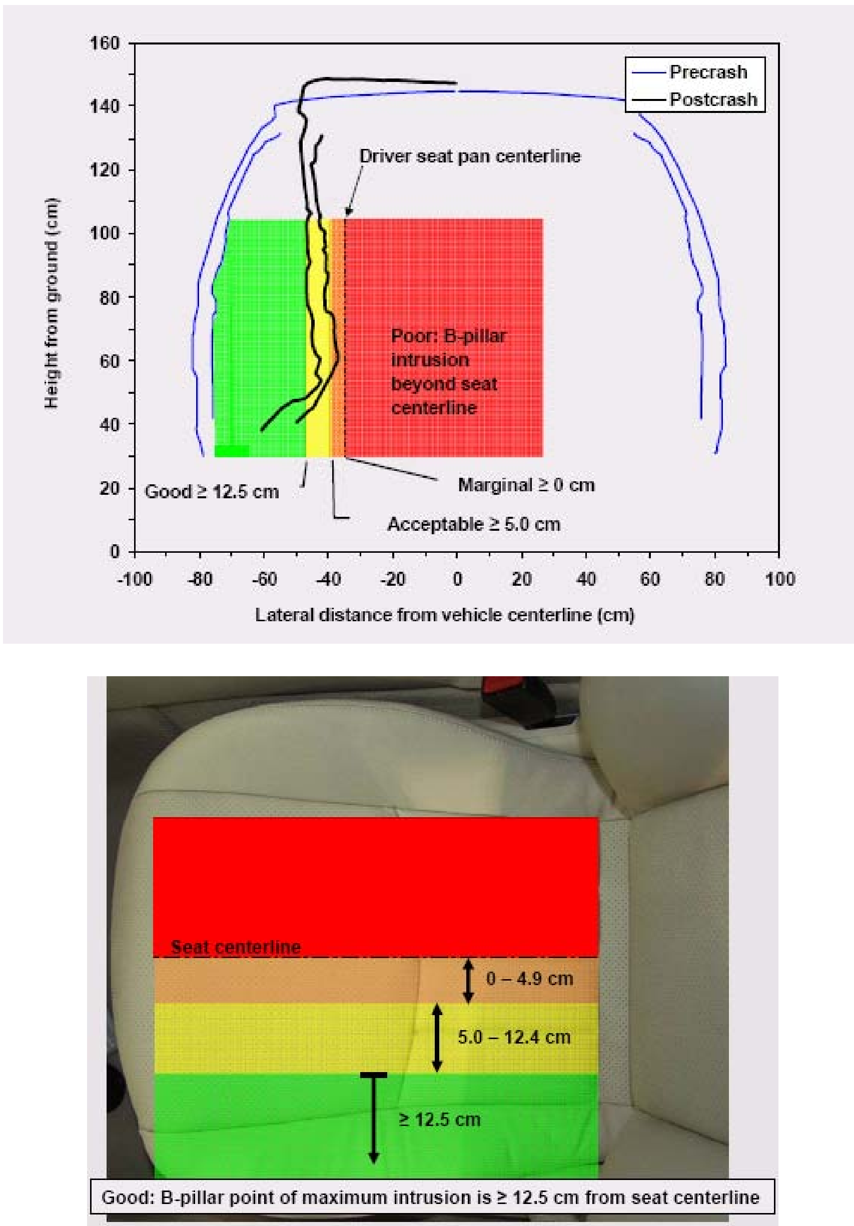

FIGURE D2: Structural Rating (B-Pillar Deformation)

APPENDIX E
ROOF CRUSH (FMVSS216) REGULATIONS
TEST DEVICE
The test device is a rigid unyielding block with its lower surface formed as a flat rectangle 30in x 72in.

TEST PROCEDURE
Place the sills or chassis frame of the vehicle on a rigid horizontal surface, fix the vehicle rigidly in position, close all windows, close and lock all doors, and secure any convertible top or removable roof structure in place over the passenger compartment.

Orient the test device as shown in Figure E1, so that:

1. Its longitudinal axis is at a forward angle (side view) of 5 degrees below the horizontal and is parallel to the vertical plane through the vehicle's longitudinal centerline.
2. Its lateral axis is at a lateral outboard angle, in the front view projection, of 25 degrees below the horizontal.
3. Its lower surface is tangent to the surface of the vehicle.
4. The initial contact point, or center of the initial contact area, is on the longitudinal centerline of the lower surface of the test device and 10in from the forward most point of that centerline.

Apply force in a downward direction perpendicular to the lower of the test device at a rate of not more than 0.5in/sec until reaching a force of 1.5 x the unloaded vehicle weight of the tested vehicle or 5000lb, whichever is less. Complete the test within 120sec. Guide the test device so that throughout the test it moves, without rotation, in a straight line with its lower surface oriented as specified in 1 through 4.

A test device shall not move more than 5in, when it is used to apply a force of 1.5 x the unloaded vehicle weight or 5000lb, whichever is less, to either side of the forward edge of vehicle's roof in accordance with the procedure. Both the left and right front portions of the vehicle's roof structure shall be capable of meeting the requirements, but a particular vehicle need not meet further requirements after being tested at one location.

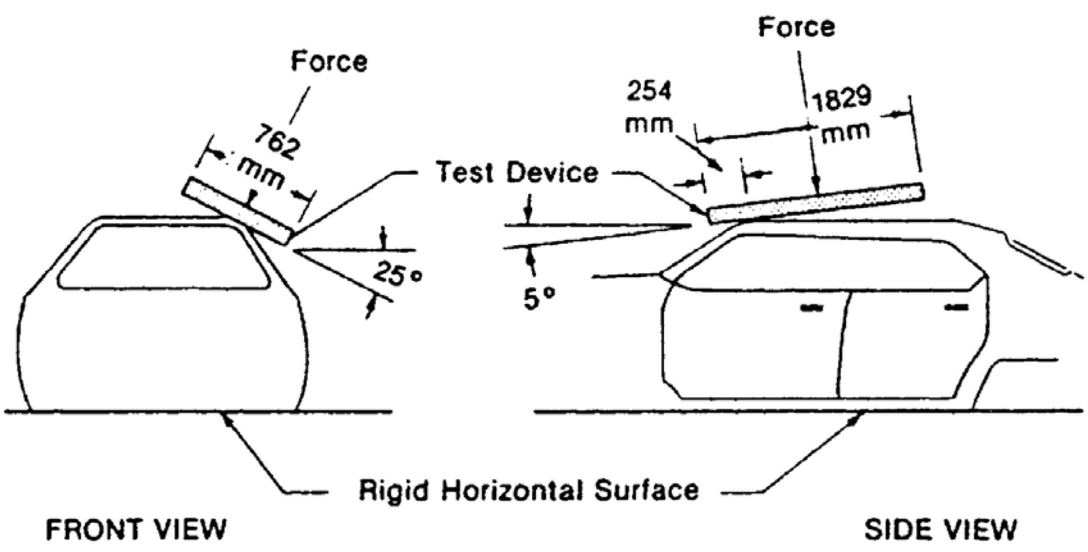

FIGURE E1: Test Device Location & Application To The Roof

APPENDIX F
DOOR INTRUSION (FMVSS214) REGULATIONS
BARRIER SPECIFICATION

The barrier is a rigid cylinder 12in in diameter and 25in overall height. See Figure F1.

BARRIER POSITION

The following applies to both front and rear doors:

- Longitudinal Position
  The central axis of cylindrical barrier is located at the middle of the line 5in (127mm) above the lowest point of the door system.
- Lateral Position
  The circumference of the cylindrical barrier is 5mm away from the outer most surface of the door system.
- Vertical Position
  The bottom of cylindrical barrier should be lined up with the line 5in (127mm) above the lowest point of the door system.

PERFORMANCE REQUIREMENTS

According to FMVSS 214 static regulation, there are three criteria based on the barrier forces

- Initial crush resistance is the average barrier force from 0 to 6in of barrier advancement and shall not be less than 2250lb. The average barrier force is obtained by integrating the barrier force with respect to the crush distance from 0 to 6in. and then dividing it by the crush distance of 6in.
- Intermediate crush resistance is the average barrier force from 0 to 12in of barrier advancement and shall not be less than 3500lb. The average barrier force is obtained by integrating the barrier force with respect to the crush distance from 0 to 12in and then dividing it by the crush distance of 12in.
- Peak crush resistance is the largest force recorded over the entire 18in. crush distance and shall not be less than 7000lb or 2 x the curb weight of the vehicle, whichever is less.

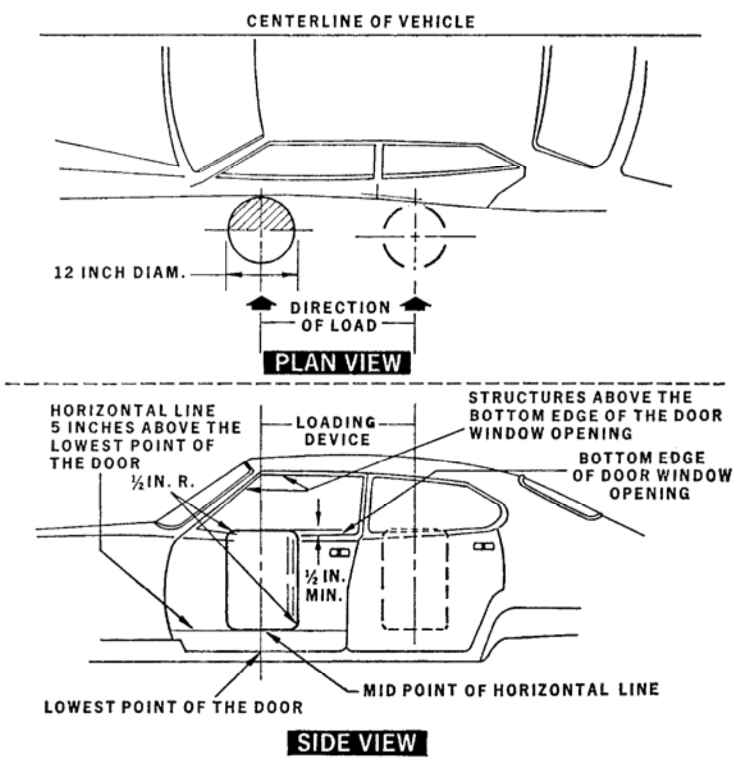

FIGURE F1: Loading Device Locations & Application To The Doors

APPENDIX G
REAR CRASH (FMVSS301) REGULATIONS
TEST REQUIREMENTS

Each passenger car and each multipurpose passenger vehicle, truck and bus with a GVWR of 10000lb or less shall meet the requirements. When the vehicle is impacted from the rear by a barrier moving at 48 km/hr, fuel spillage shall not exceed the limits of the followings. Fuel spillage in any fixed or moving barrier crash test shall not exceed 28g from impact until motion of the vehicle has ceased, and shall not exceed a total of 142g in the 5min period following cessation of motion. For the subsequent 25min period, fuel spillage during any 1min interval shall not exceed 28g.

TEST CONDITIONS

Where a range is specified, the vehicle must be capable of meeting the requirements at all points within the range. The following conditions apply to all tests.

- The fuel tank is filled to any level from 90 to 95% of capacity with Stoddard solvent, having the physical and chemical properties of Type 1 solvent.
- The fuel system other than the fuel tank is filled with Stoddard solvent to its normal operating level.
- In meeting the requirements, if the vehicle has an electrically driven fuel pump that normally runs when the vehicle's electrical system is activated, it is operating at the time of the barrier crash.
- The parking brake is disengaged and the transmission is in neutral, except that in meeting the requirements of S6.5 the parking brake is set.
- Tires are inflated to manufacturer's specifications.
- The vehicle, including test devices and instrumentation.

REAR MOVING BARRIER TEST CONDITIONS

The rear moving barrier, see Figure G1, test conditions and the positioning of the barrier and the vehicle is as followings. The barrier and test vehicle are positioned so that at impact

- The vehicle is at rest in its normal attitude
- The barrier is traveling at 48 km/hr with its face perpendicular to the longitudinal centerline of the vehicle
- A vertical plane through the geometric center of the barrier impact surface and perpendicular to that surface coincides with the longitudinal centerline of the vehicle.

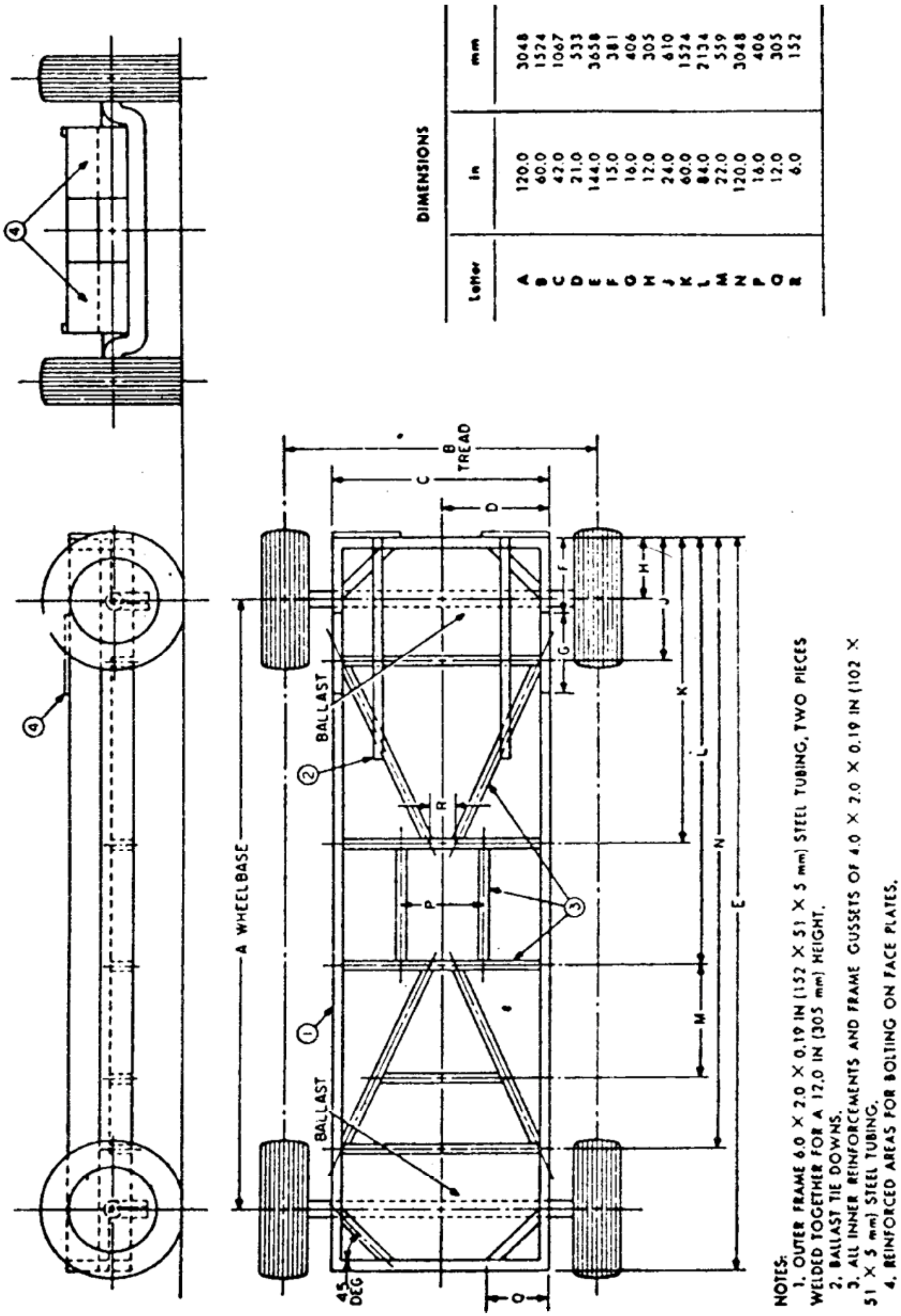

Letter	in	mm
A	120.0	3048
B	60.0	1524
C	42.0	1067
D	21.0	533
E	144.0	3658
F	15.0	381
G	16.0	406
H	12.0	305
J	24.0	610
K	60.0	1524
L	84.0	2134
M	22.0	559
N	120.0	3048
P	16.0	406
Q	12.0	305
R	6.0	152

FIGURE G1: Common Carriage For Moving Barriers

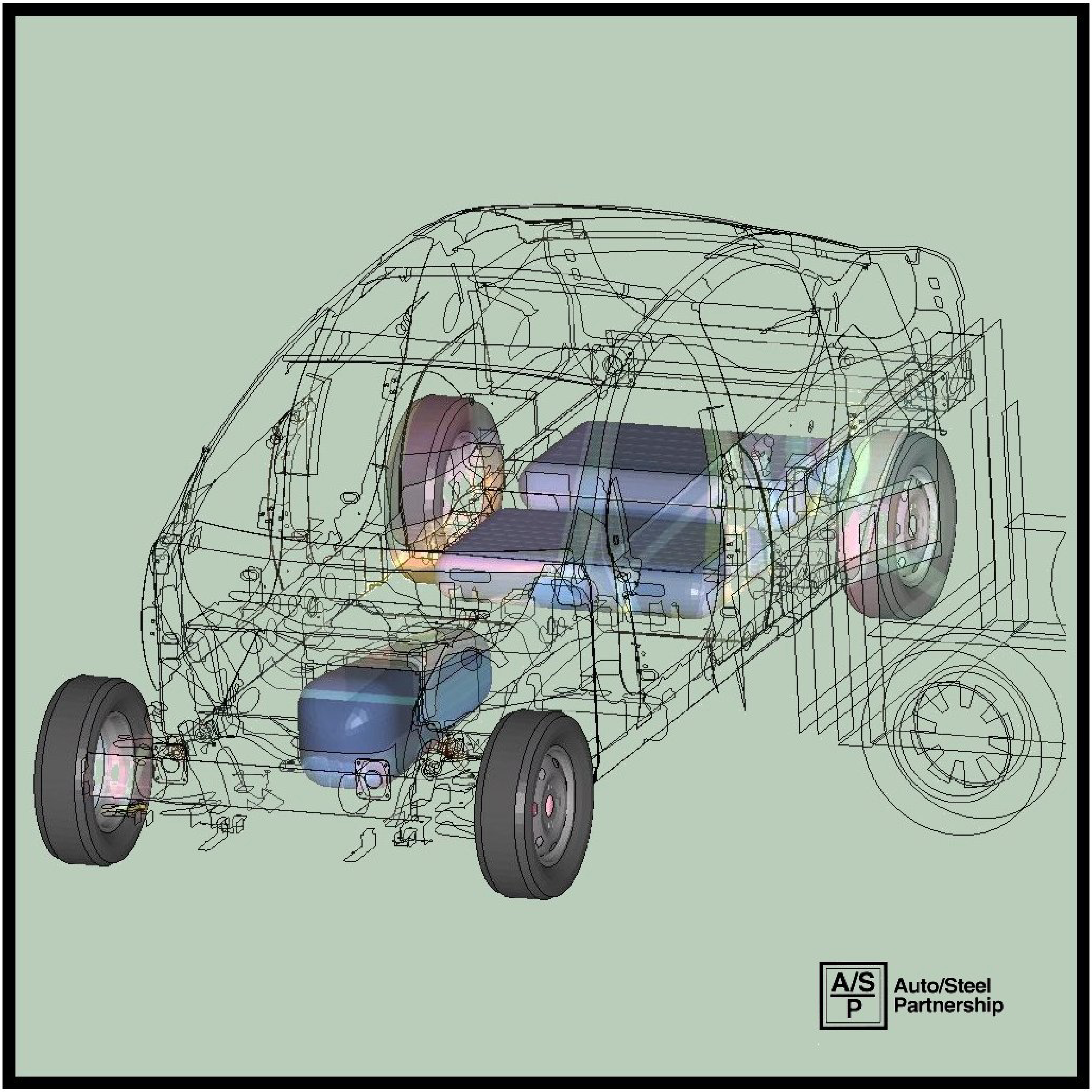

Future Generation Passenger Compartment
Task 7.5 - Barrier Height & Curb Weight Sensitivity

Barrier height & FGPC curb weight sensitivity analysis

Task 7.5 - Barrier Height & Curb Weight Sensitivity

Table of Contents

Task 7.5 - Barrier Height & Curb Weight Sensitivity

1. INTRODUCTION

This report completes Task 7.5: Barrier Height & Curb Weight Sensitivity Study. Its purpose is to determine the effect of varying curb weight and barrier height on the IIHS Side Impact performance of the FGPC vehicle.

2. OBJECTIVE

The objective of this task is to evaluate the effect on IIHS Side Impact performance of varying barrier height and vehicle mass. These will be modified as follows:

- Increasing the curb weight in 50kg increments from 0 to 350kg.
- Moving the IIHS Side Impact barrier ±1in from its baseline position.

3. BACKGROUND

The ULSAB-AVC vehicle was the starting point for the FGPC project. In Task 2.0: Calibration Baseline of the project, the vehicle passenger compartment was modified and packaged to allow the vehicle to be capable of having 2 different types of drive trains: rear wheel drive diesel engine and fuel cell power. The vehicle was evaluated for Front Crash, Rear Crash, Roof Crush and IIHS Side Impact.

The vehicle was optimized for IIHS Side Impact and Roof Crush strength by varying shape, material and thickness of critical parts in Task 3.0: Optimization. The design was modified in Task 4.0: Concept Design of the project to reflect the optimization results as closely as possible. This new FGPC design was then checked once again for Front Crash, Rear Crash and Side Impact in Task 5.0: Concept Design Check and further modified to meet the requirements in Task 5.5: Concept Design Check Supplement. The new design was then once again optimized for mass based on IIHS Side Impact, IIHS Offset Frontal Crash, Torsional Stiffness and Pole Impact by varying thickness only in Task 6.0: Final Optimization. A final design check was then made in Task 7.0: Final Concept Design Check by analyzing all load cases once again.

The mass of the vehicle was closely tracked throughout the program. The judgment criterion for IIHS Side Impact in this program is based on the intrusion of the B-Pillar relative to the Driver Seat centerline. The B-Pillar intrusion in Side Impact is sensitive to vehicle mass because it affects how much energy is transferred from the moving deformable barrier. A lighter vehicle will be pushed sideways more easily by the barrier and therefore deform less than a heavier vehicle.

The height of the IIHS Side Impact barrier will also affect the B-Pillar intrusion. As the barrier impact point gets closer to the Rocker, more load is transferred to the Underbody and less to the B-Pillar, which improves the structural response.

Auto Steel Partnership

4. MASS SENSITIVITY STUDY

4.1. ANALYSIS PLAN

This study determined the effect of increasing the vehicle mass on IIHS Side Impact performance. The baseline curb weight is 1092.8kg. Seven iterations were performed with 50kg increments up to a curb weight of 1442.8kg.

4.2. LOADS AND BOUNDARY CONDITIONS

A 1500kg MDB (Moving Deformable Barrier) was positioned so that there was 379mm of ground clearance. The rearward distance from the test vehicle's front axle to the closest edge of the deformable barrier, known as the IRD (Impact Reference Distance), was 810mm. The barrier impacted the vehicle with an initial velocity of 50kph. The vehicle and barrier are shown in Figure 1.

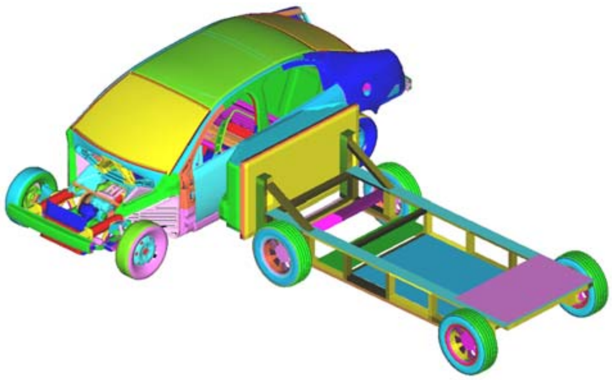

FIGURE 1: IIHS Side Impact Analysis

4.3. MASS DISTRIBUTION

Each 50kg mass increment is distributed across 15 items in the same ratio. Table 1 shows mass increase and vehicle curb weight used in each iteration.

	BASELINE	IT #1	IT #2	IT #3	IT #4	IT #5	IT #6	IT #7
Mass Increment (kg)	0	50	100	150	200	250	300	350
Vehicle Curb Weight (kg)	1092.8	1142.8	1192.8	1242.8	1292.8	1342.8	1392.8	1442.8
Mass Increase (%)	0	4.58	9.15	13.73	18.30	22.88	27.45	32.03

TABLE 1: Curb Weight Increase Summary

The AS/P team decided how the added mass would be distributed throughout the vehicle in order to reach the required weight. Figure 2 shows where concentrated masses were added and what they represent. Table 2 shows the amount added for each iteration. The mass of the engine and transmission were specified in a part inertia definition in the model and mass was added to those components by changing the mass value directly in the LS-Dyna deck.

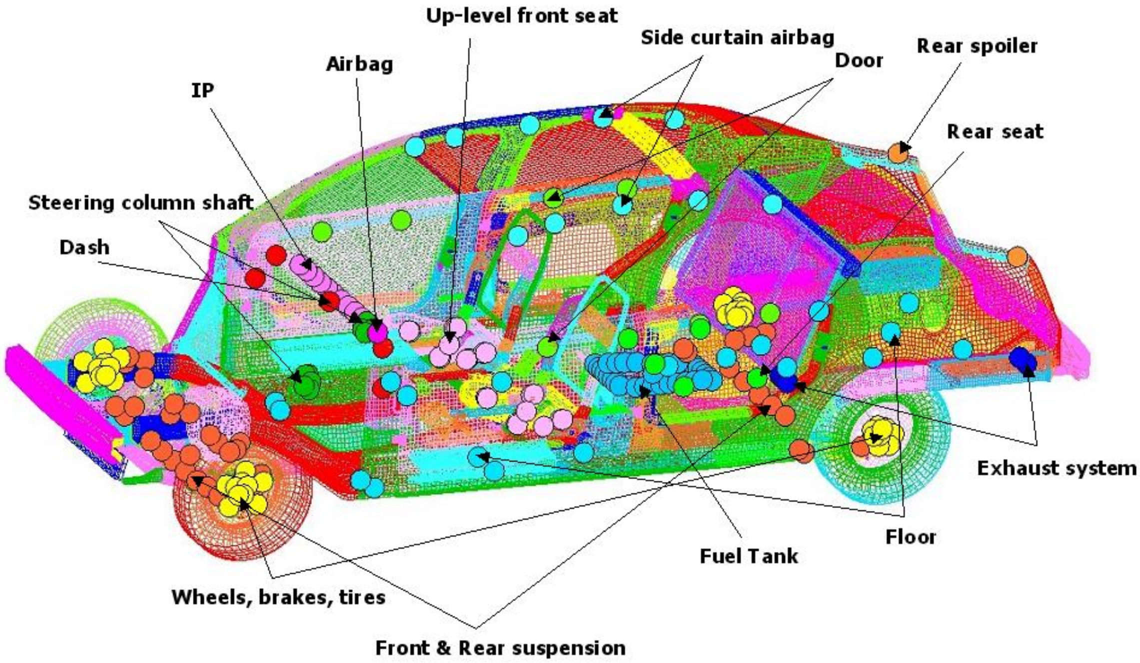

FIGURE 2: Mass Distribution

	BASELINE (kg)	IT #1 (kg)	IT #2 (kg)	IT #3 (kg)	IT #4 (kg)	IT #5 (kg)	IT #6 (kg)	IT #7 (kg)
Engine/Trans	0	12.22	24.44	36.65	48.87	61.09	73.31	85.53
Fuel Tank	0	6.02	12.03	18.05	24.06	30.08	36.09	42.11
Front & Rear suspension	0	7.52	15.04	22.56	30.08	37.59	45.11	52.63
IP	0	1.88	3.76	5.64	7.52	9.40	11.28	13.16
Steering column shaft	0	1.88	3.76	5.64	7.52	9.40	11.28	13.16
Exhaust system	0	1.88	3.76	5.64	7.52	9.40	11.28	13.16
Dash	0	0.94	1.88	2.82	3.76	4.70	5.64	6.58
Door	0	0.94	1.88	2.82	3.76	4.70	5.64	6.58
Floor	0	1.88	3.76	5.64	7.52	9.40	11.28	13.16
Wheels, brakes & tires	0	7.52	15.04	22.56	30.08	37.59	45.11	52.63
Up-level Front seat	0	3.76	7.52	11.28	15.04	18.80	22.56	26.32
Up-level Rear seat	0	0.94	1.88	2.82	3.76	4.70	5.64	6.58
Airbag	0	0.38	0.75	1.13	1.50	1.88	2.26	2.63
Side curtain airbag	0	1.88	3.76	5.64	7.52	9.40	11.28	13.16
Rear spoiler	0	0.38	0.75	1.13	1.50	1.88	2.26	2.63

TABLE 2: Mass Distribution By Part Summary

4.4. RESULTS

Figure 3 shows the IIHS Side Impact structural performance for the baseline and iterations. The distance from the B-Pillar to the centerline of the Seat is measured and should be greater than 125mm to achieve a rating of Good.

The baseline response is in the Good range at 130.2mm. Increasing the mass in 50kg increments produces a nearly linear change in response. Adding 350kg reduces the B-Pillar to centerline distance to 112.0mm, which is in the acceptable range. There is a very slight improvement (~3mm) in intrusion from 150kg to 200kg due to slight oscillations in the B-Pillar to Seat center distance after the impact.

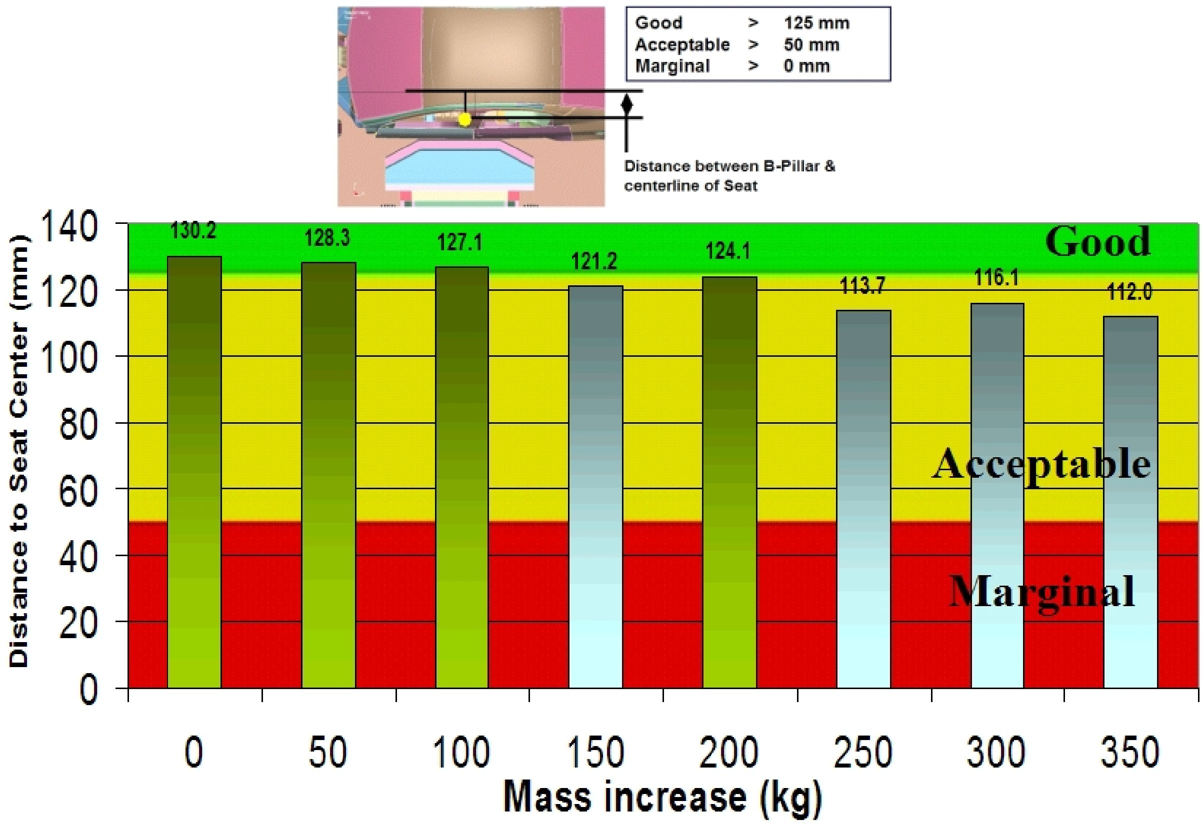

FIGURE 3: IIHS Side Impact Performance Comparison – Mass Sensitivity

Figure 4 shows the relationship between the percentage mass and percentage intrusion increase. Increasing the curb weight of the vehicle by 32% without adding reinforcement or changing the structure is shown to cause only a 10% degradation in B-Pillar to Seat centerline distance.

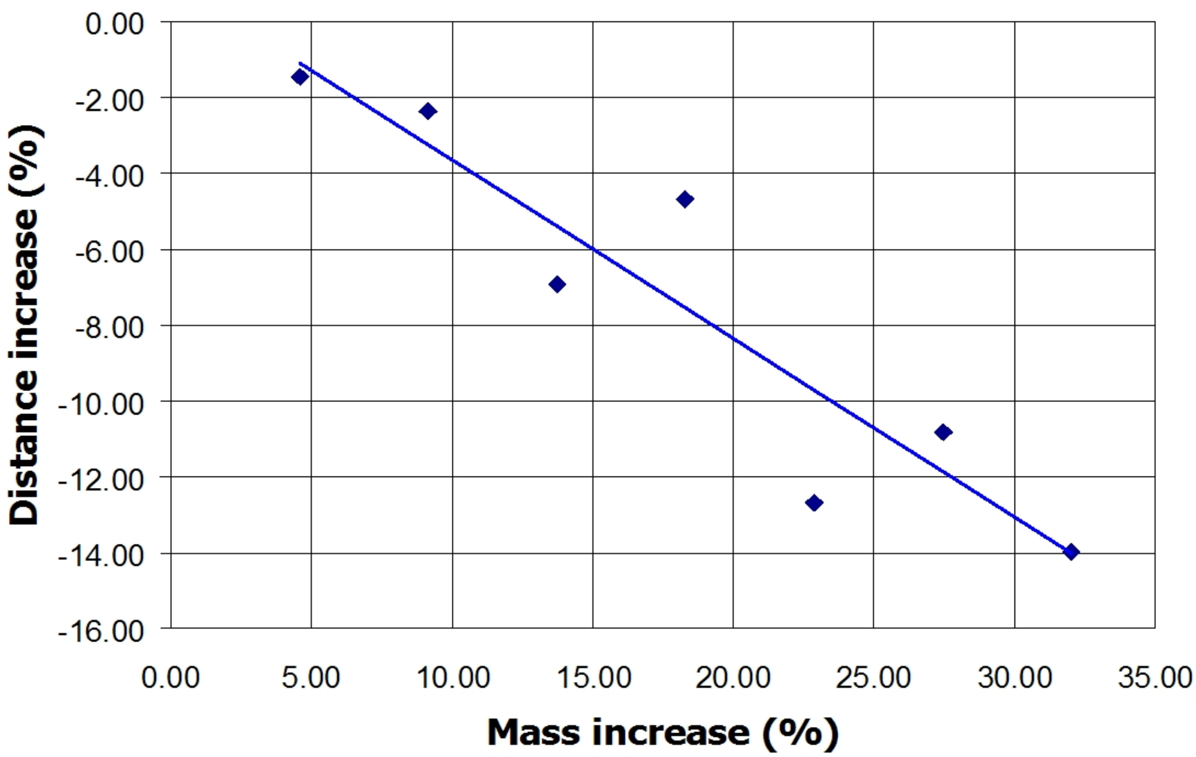

FIGURE 4: IIHS Side Impact Mass Sensitivity

The deformed shape of the vehicle at the B-Pillar is shown in Figure 5. In each iteration, the Side Impact Tube connected to the B-Pillar at the height of the barrier bumper bends without kinking, transferring load to the non-struck side of the vehicle. The B-Pillar remains nearly straight with little bending, so that its maximum intrusion occurs at the roof. A vehicle without such a load path between the B-Pillars may be more sensitive to mass increases.

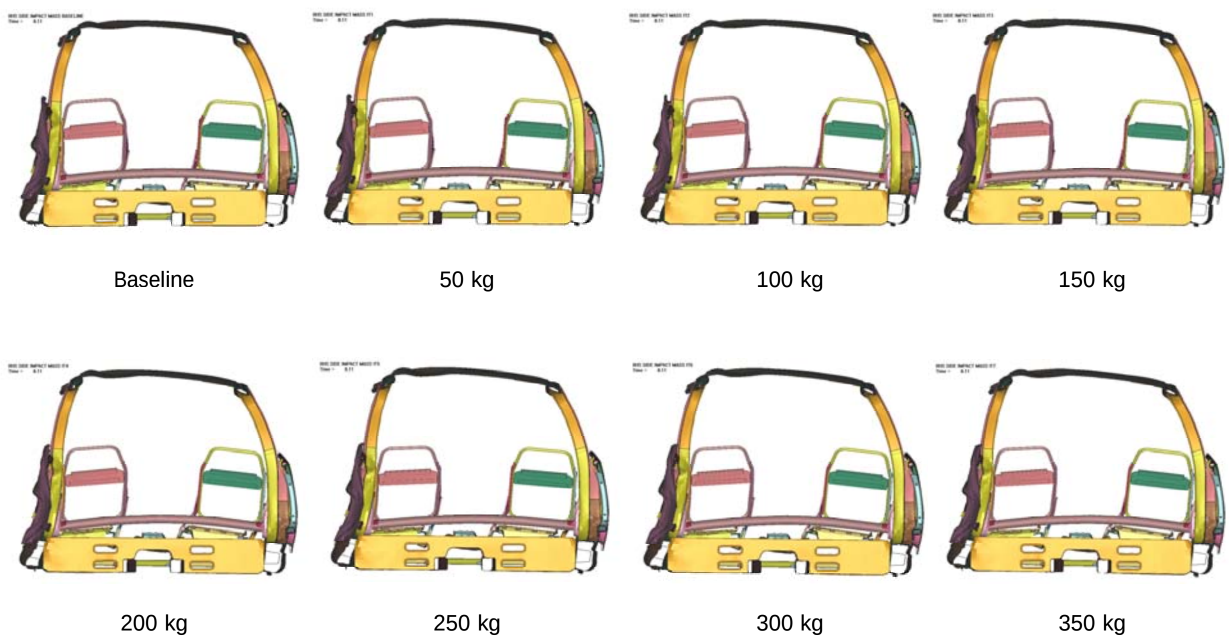

FIGURE 5: Deformation Shape Comparison – Baseline & Iterations

4.5. MASS SENSITIVITY CONCLUSION

Increasing the mass of the FGPC vehicle in 50kg increments produces a nearly linear increase in B-Pillar intrusion into the passenger compartment. A 350kg mass increase results in only 18.2mm degradation in the intrusion, which demonstrates that the design is very robust for IIHS Side Impact. The Side Impact Tube very effectively transfers load at the lower B-Pillar to the non-struck side, which keeps the B-Pillar deformation mode the same through the range of mass additions. If the mass were to be increased enough to cause a kink in the Side Impact Tube, the effect of added mass may not remain linear and the design would become more sensitive to mass addition. The sensitivity would also be expected to be greater in the absence of a Side Impact Tube.

5. BARRIER HEIGHT SENSITIVITY STUDY

5.1. ANALYSIS PLAN

This study determined the effect of barrier height variations on IIHS Side Impact performance. The barrier is moved ±1in and the results are compared to the baseline height.

5.2. LOADS AND BOUNDARY CONDITIONS

The baseline for this study was the same as the Mass Sensitivity Study baseline, which is shown in Figure 1. Iterations were performed by moving the barrier up 1in from the baseline and down 1in from the baseline.

5.3. RESULTS

Figure 6 shows the IIHS Side Impact structural performance for the baseline and iterations. The distance from the B-Pillar to the centerline of the Seat is measured and should be greater than 125mm for a Good rating. Figure 7 shows the deformed shapes for the 3 runs.

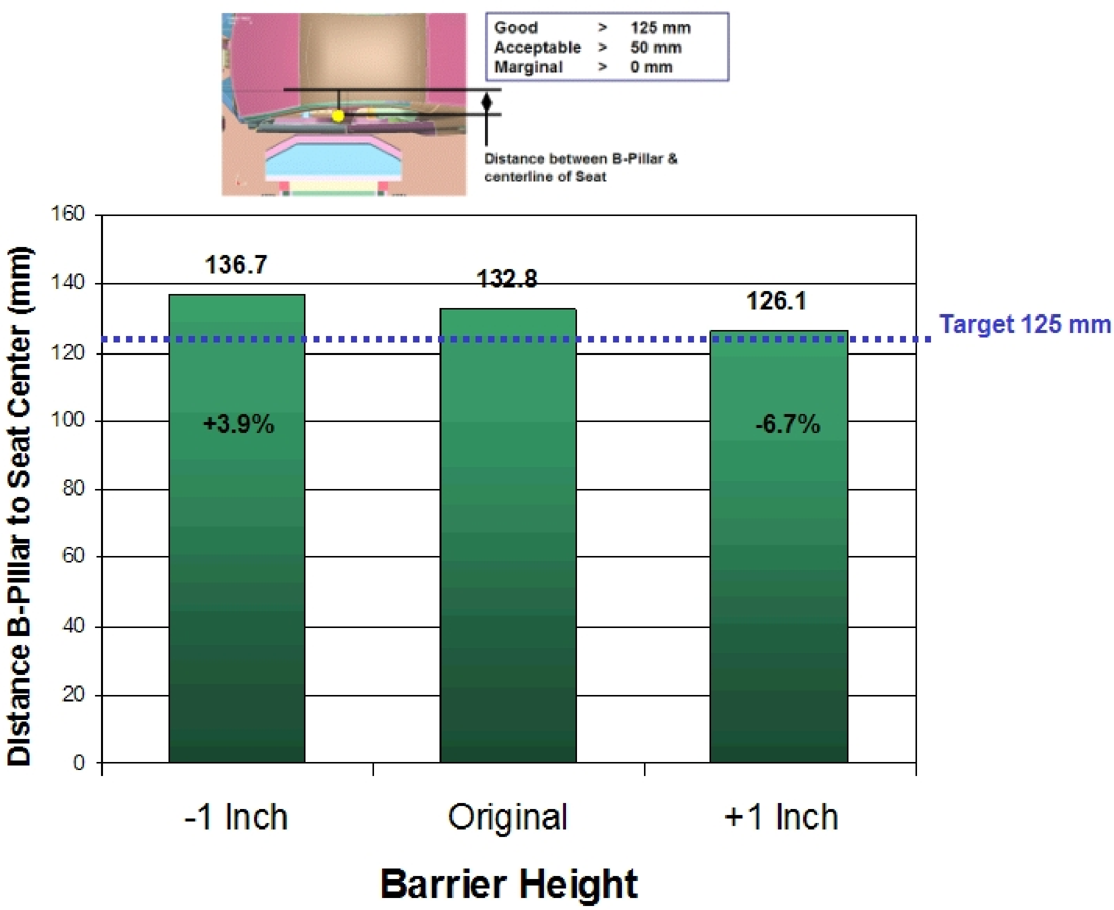

FIGURE 6: IIHS Side Impact Performance Comparison – Barrier Height Sensitivity

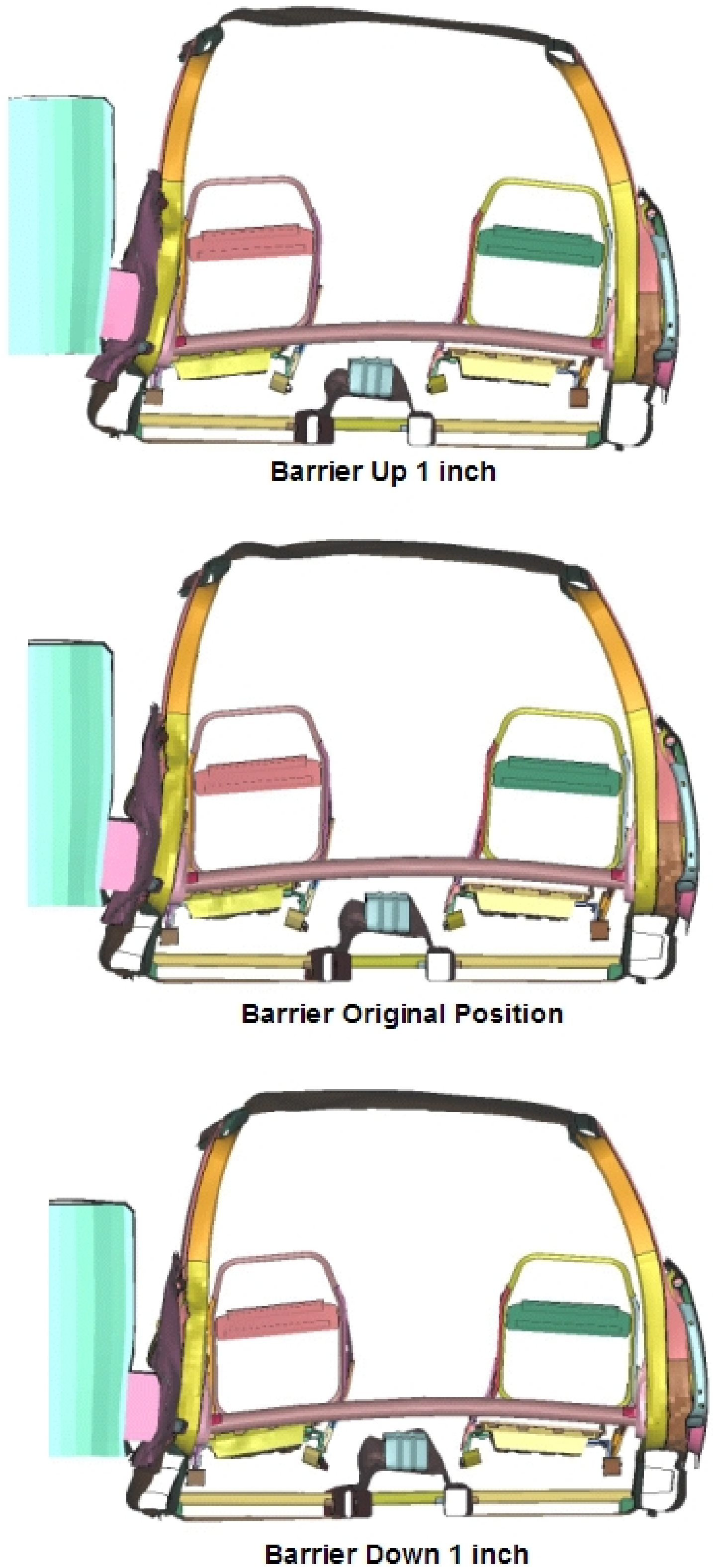

FIGURE 7: Deformation Shape Comparison – Baseline & Iterations

The baseline IIHS Side Impact response of 132.8mm is above the target of 125mm. Although the baseline model is the same as that of the mass sensitivity study, the IIHS response differs slightly because they were analyzed using different hardware.

The results show that moving the barrier downward has less of an effect on the B-Pillar to Seat center distance (+3.9%) than moving it upward (-6.7%). The deformed shapes show that moving the barrier downward allows it to more fully engage the Side Impact Tube, which provides an efficient load path to the non-struck side. The Rocker is also more fully engaged. Moving the barrier upward 1in allows it to slide slightly above the height of the Side Impact Tube, making it less effective at transferring load and leading to more B-Pillar deformation.

5.4. BARRIER HEIGHT SENSITIVITY CONCLUSION

The FGPC vehicle is slightly more sensitive to a movement 1in upward of the IIHS Side Impact barrier than a 1in downward movement. Moving the barrier upward increased the intrusion by 6.7mm, while moving it downward decreased the intrusion by 3.9mm. The target intrusion of 125mm was still met for all of the runs.

The Side Impact Tube of the FGPC plays a large role in the IIHS Side Impact response because it is at the height of the barrier bumper and is a very effective load path to the non-struck side. Moving the barrier upward reduces the effectiveness of the tube because the barrier bumper is not fully engaged by it. Moving the barrier downward allows the rocker to play more of a role while still engaging the tube, which improves the response. As is the case with the mass sensitivity study, the barrier height sensitivity would be expected to be greater in the absence of a Side Impact Tube.

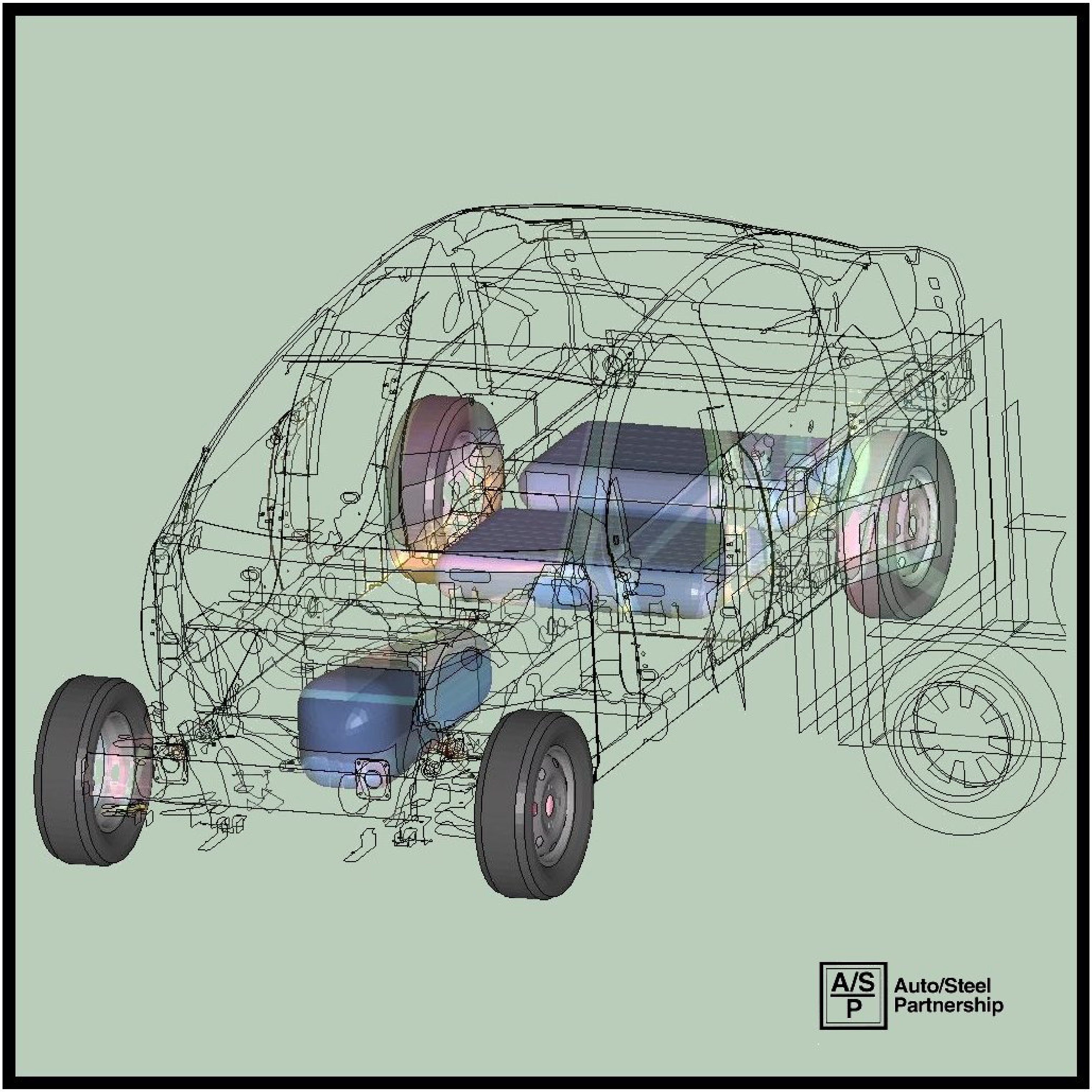

Future Generation Passenger Compartment
Task 8.0 - Final Concept Design Report

Details of the finalized

Concept design

Task 8.0 - Final Concept Design

Table of Contents

Task 8.0 - Final Concept Design

1. INTRODUCTION

This report completes Task 8.0: Final Concept Design of the FGPC (Future Generation Passenger Compartment) project. Its purpose is to document the choices made to best integrate the Task 6.0: Final Optimization results into a production viable design concept. The design changes were executed on the Task 5.5: Concept Design Check Supplement version of the FGPC, which had previously modified the Task 3.0: Optimization version of FGPC to satisfy the requirements of all the loading conditions considered.

2. OBJECTIVE

To integrate the design directions and recommendations from the Task 6.0: Final Optimization into the current concept design stage.

Task 8.0: Final Concept Design will take the Task 5.5: Concept Design Check Supplement design and while considering manufacturability, joining strategy, assembly process and cost reduction incorporate as many of the Task 6.0: Final Optimization's mass reduction suggestions as possible.

3. DETAILED REVIEW OF FINAL OPTIMIZATION COMPONENTS

3.1 ROCKER INNER (31162/3)

To satisfy the requirements of the IIHS Side and FMVSS214 New Pole Impacts the following changes were made to the Rocker Inner. The design was revised from a one-piece roll formed component to a two-piece TWB (Tailor Welded Blank) roll form. The gauge of the front section of the TWB was increased from 0.6 to 1.2mm and the rear section from 0.6 to 1.5mm. No changes were made to either the cross-sectional shape or length.

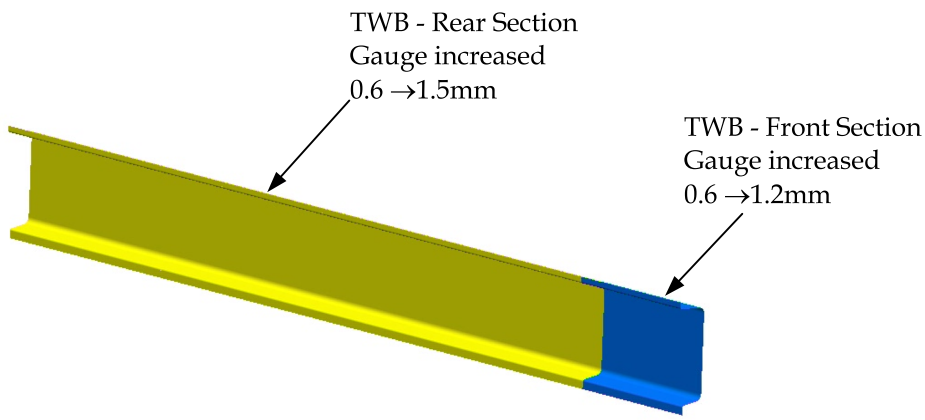

FIGURE 1: Revised Rocker Inner - Roll formed TWB (Tailor Welded Blank)

3.2 A-POST INNER (11146/7)

Task 6.0: Final Optimization revised the A-Post Inner from a TWB to a one-piece component. The original TWB was built-up from 0.7 and 0.9mm thick pieces, the revised design is 0.9mm thick. This change did not require any alteration to the manufacturing or assembly processes.

3.3 REAR FLOOR (31069)

Task 3.0: Optimization had previously simplified the TWB from a three to two piece design. Task 6.0: Final Optimization was, however, allowed to reconsider the Rear Floor as a three-piece TWB. The optimization increased the front portion of the rear floor pan from 0.8 to 0.9mm. This modification did not affect any manufacturability or assembly considerations of this component.

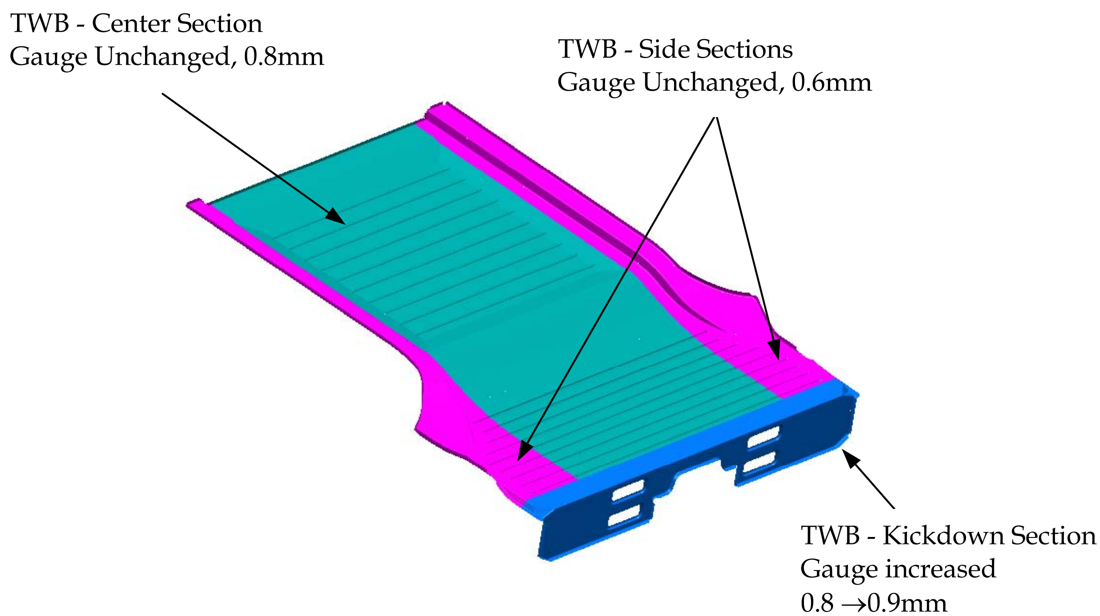

FIGURE 2: Revised Rear Floor TWB (31069)

3.4 BODY SIDE OUTER (31170/1)

The gauges of the central Body Side Outer TWB were revised. These changes had no impact on the manufacturing or assembly processes.

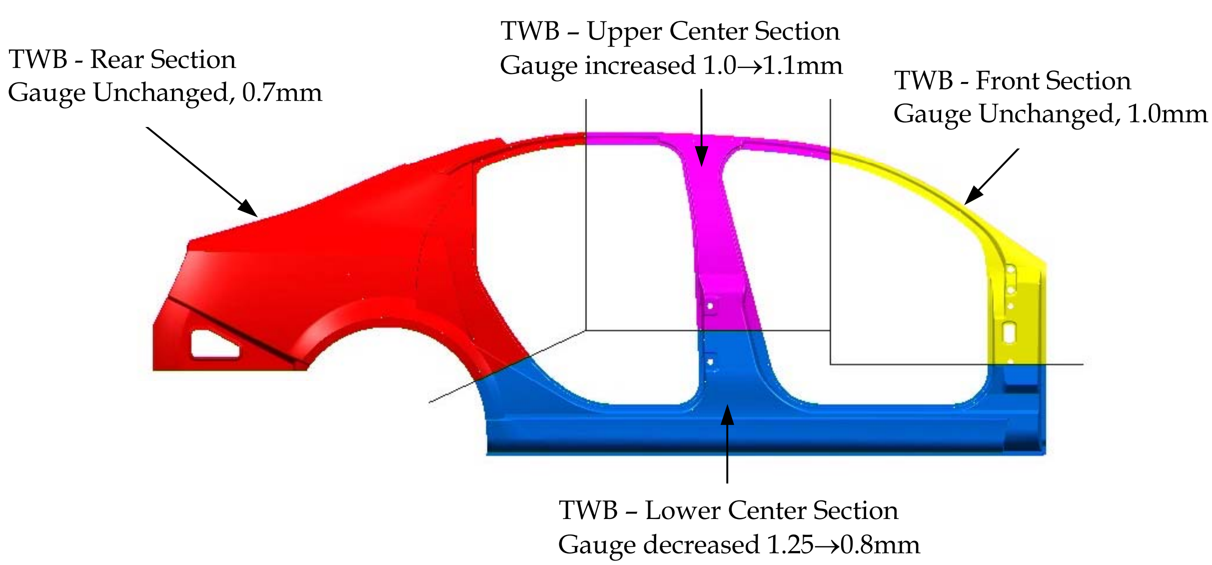

FIGURE 3: Revised Body Side Outer TWB (31170/1)

3.5 DOOR CLOSURES

3.5.1 HYDROFORMED DOOR REINFORCEMENTS

The Door Reinforcements were modified to accept the recommendations of the Task 6.0: Final Optimization. Though the basic shape of the Rear Door Reinforcements remained consistent with the original design, the tubes were reduced by a normal offset of 4mm per side and down gauged to 0.6mm. The Front Door Reinforcements cross-sections were maintained but their gauges were reduced to 0.6mm. The only exception was the lower tube, which was decreased to 0.9mm.

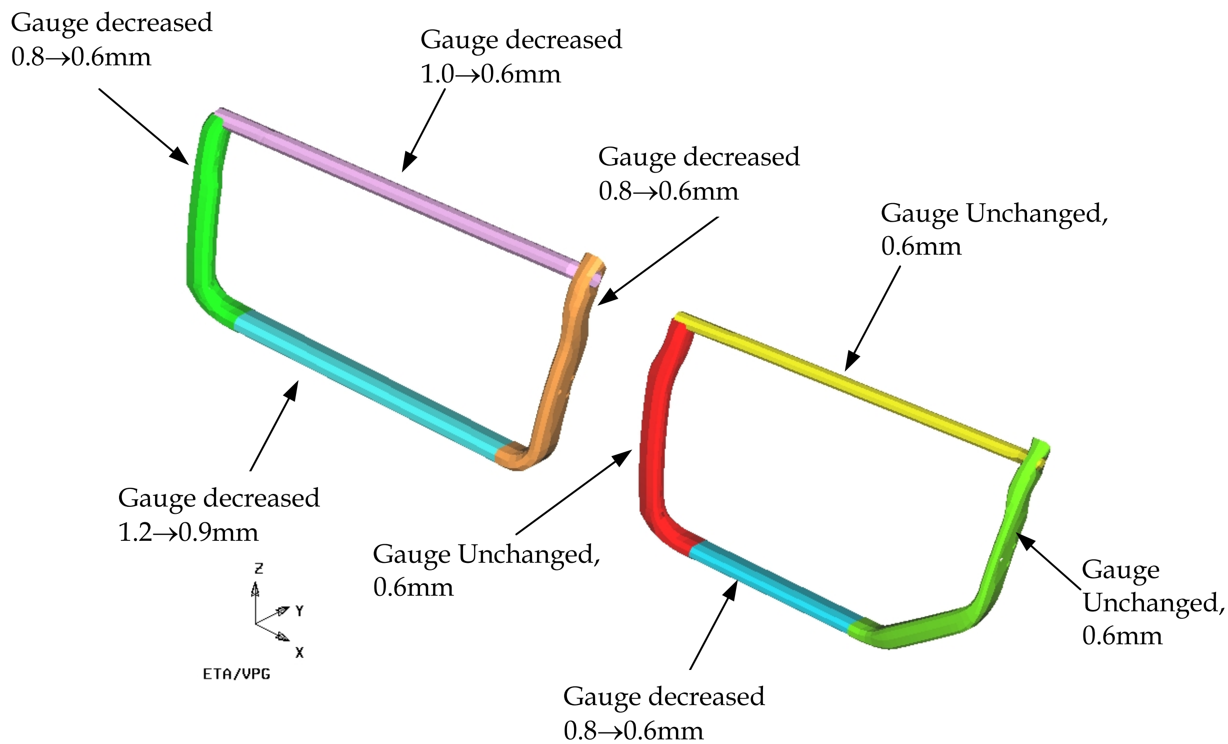

FIGURE 4: Front & Rear Door Reinforcements

3.6 CHANGES TO OTHER PARTS

The majority of FGPC parts are not TWB but made from a single gauge. Table 1 summarizes the revisions made to a number of parts where the gauge was revised. These modifications had no impact on the manufacturing or assembly processes.

PART	FGPC-ACD GAUGE (mm)		FGPC-FCD GAUGE (mm)	
Cross-member Kick-down (11082)		1.2		1.1
B-Pillar Inner (31208/9)	Upper	1.25	Upper	1.1
	Mid	0.7	Mid	0.8
Cross-member Roof (41004)		0.8		0.9

TABLE 1: Gauge Revisions Summary

3.7 NEW COMPONENTS

During the course of the Task 6.0: Final Optimization a number of components were added to the structure. These were primarily aimed at improving the vehicle's IIHS Side and FMVSS214 New Pole Impact performance. Changes to the production process were limited to the addition of the components themselves and re-sequencing of the sub-assemblies. Refer to Section 4 for further discussion. The additional welding requirements are summarized in Table 4.

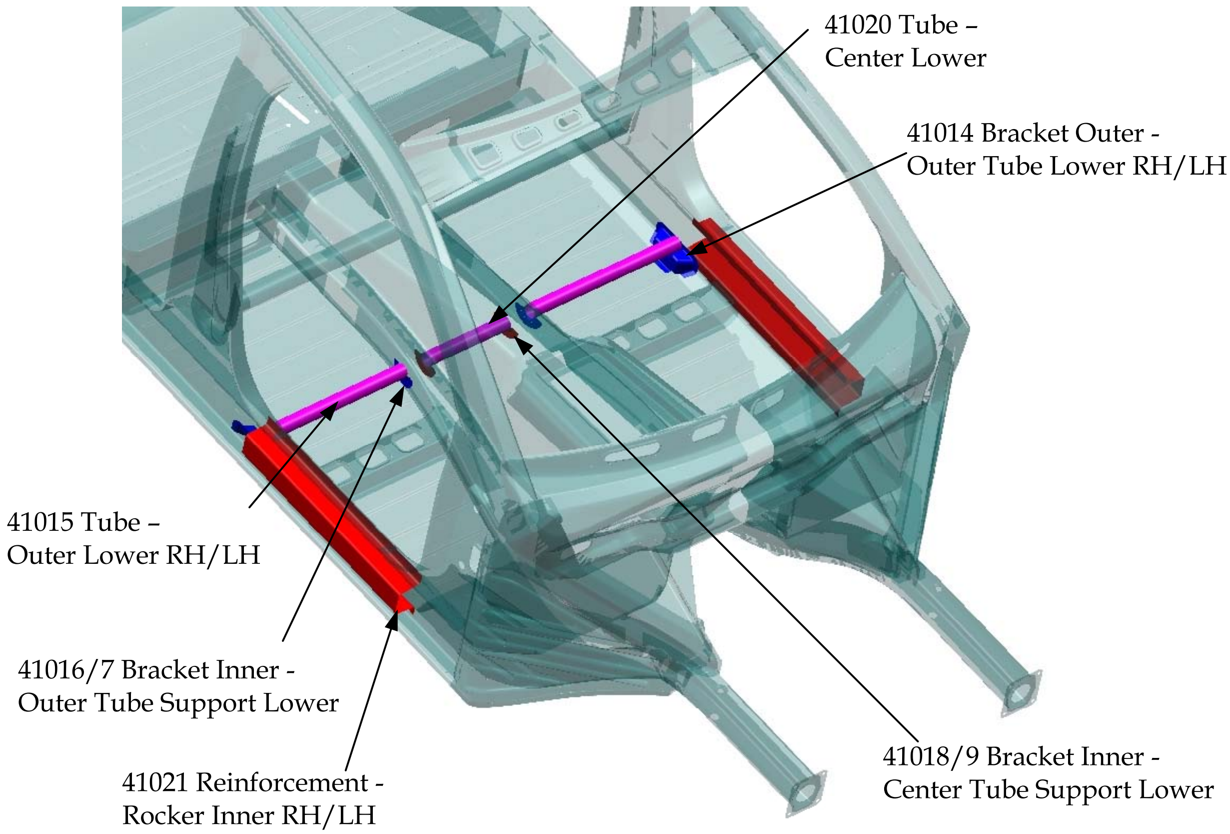

FIGURE 5: New Components

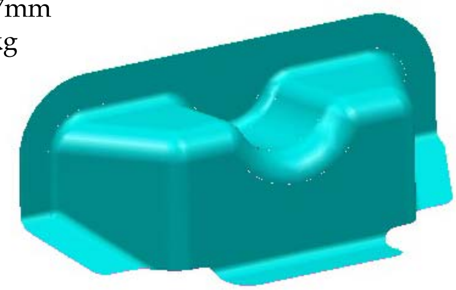

FIGURE 6: Bracket Outer - Outer Tube Support Lower (41014)

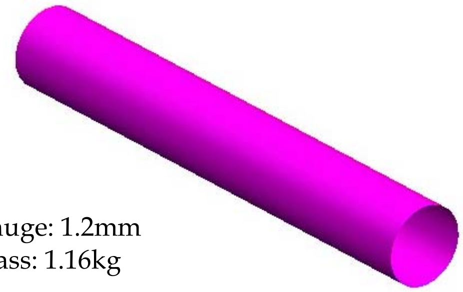

FIGURE 7: Tube- Outer Lower (41015)

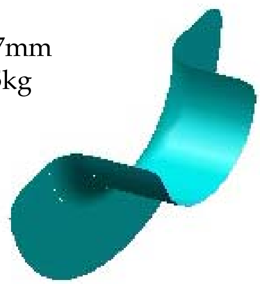

FIGURE 8: Bracket Inner - Outer Tube Support Lower (41016/7)

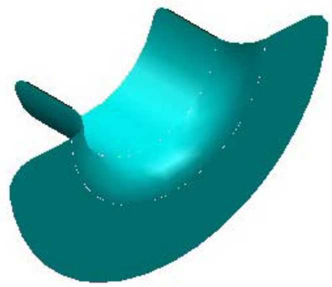

FIGURE 9: Bracket Outer - Center Tube Support Lower (41018/9)

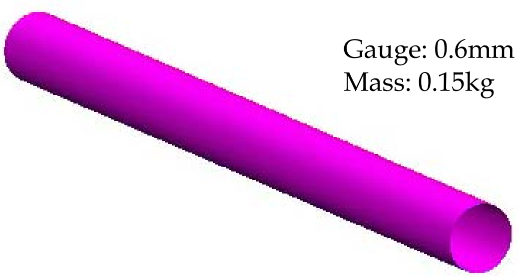

FIGURE 10: Tube - Center Lower (41020)

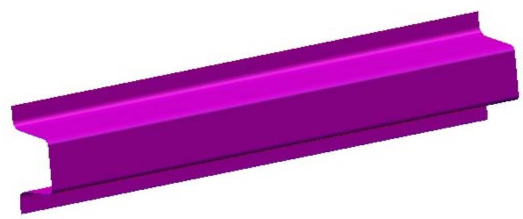

FIGURE 11: Reinforcement - Rocker Inner (41021/2)

4. ASSEMBLY PROCESS REVISION – NEW COMPONENTS

4.1 Assembly Rail Front (37130/1)

Note there are left and right handed versions of Assembly Rail Front (37130/1). Bracket Inner - Outer Tube Support Lower (41016/7) was added to the Assembly Rail Front (37130/1) as Items #5 and #6 of the assembly. The brackets are laser welded to the outside, relative to the transmission tunnel, vertical sidewall of the left and right Member Rail Front (31050/1) respectively. The laser welding uses 6 stitches and adds 126mm of new laser welds.

Bracket Inner - Center Tube Support Lower (41018/9) was added to the Assembly Rail Front (37130/1) as Items #7 and #8 of the assembly. The brackets are laser welded to the inside, relative to the transmission tunnel, vertical sidewall of the left and right Member Rail Front (31050/1) respectively. The laser welding uses 6 stitches and adds 126mm of new laser welds.

Bracket Inner – Outer Tube Support Lower (41016/7)
Added as part of Assembly Rail Front (37130/1) in two places

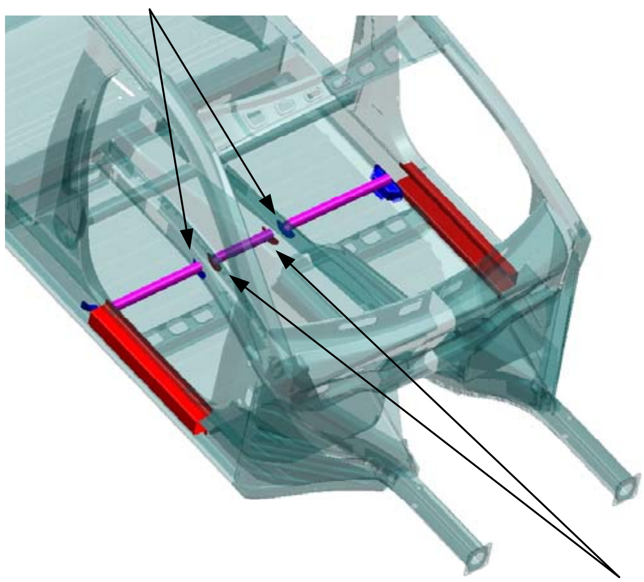

Bracket Inner – Center Tube Support Lower (41018/9)
Added as part of Assembly Rail Front (37130/1) in two places

FIGURE 12: Assembly Rail Front (37130/1)

4.2 Assembly Underbody Ladder (37128)

Tube – Center Lower (41020) was added to the Assembly Underbody Ladder (37128) as Item#11 of the assembly. It is MIG welded to the left and right hand Bracket Inner - Center Tube Support Lower (41018/9). To allow adequate access for MIG welding this process must be performed before Item #9, Assembly Tunnel (37129), is added. The brackets are part of Items #5, the Assembly Rail Front RH (37130) and Item #6, the Assembly Rail Front LH (37131) respectively.

Tube - Center Lower (41020)
Added as part of Assembly Underbody Ladder (37128)

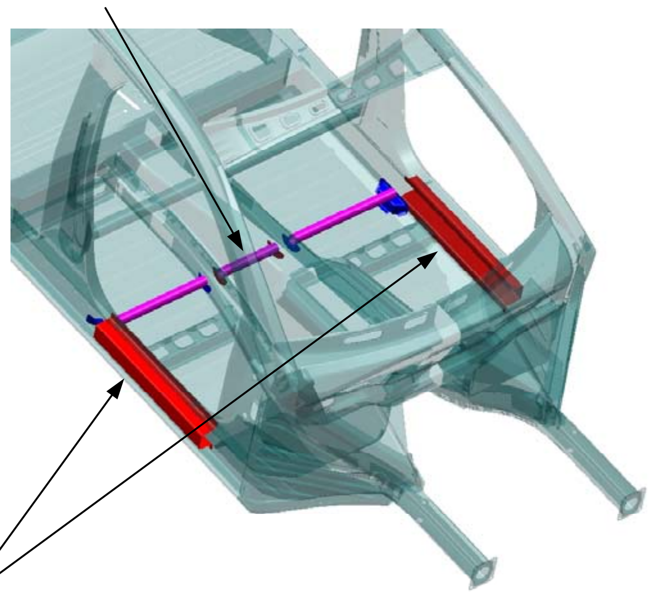

Reinforcement – Rocker Inner (41021/2)
Added as part of Assembly Body Side Inner (37126) in two places

FIGURE 13: Assembly Underbody Ladder (37128) & Assembly Body Side Inner (37126)

4.3 Assembly Body Side Inner (37126)

Reinforcement - Rocker Inner (41021) was added to the Assembly Body Side Inner (37126) as Item#15 of the assembly. It is laser welded to Item#9, the Rocker Inner (31162), using 30-laser stitch welds. This process added 630mm of new laser welds.

4.4 Assembly Body Side Structure Stage 1 (37120A)

Bracket Outer - Outer Tube Support Lower (41014) was added to the Assembly Body Side Structure Stage 1 (37120A) as Items #11 and #12. The brackets are welded to the Front Floor (31016/7), previously included in Assembly Underbody Stage 3 (37124) and glued to the inside vertical sidewall of the Rocker Inner (31162/3), previously included in Assembly Body Side Inner (37126). Laser welding the brackets to the vertical side of the Rocker Inner is not possible due to accessibility problems. As mentioned previously, see Section 5.0 of the Task 4.0: Concept Design, the laser's PFO (Primary Focusing Optics) must be held within ±2mm and within 6° of normal to the material. This requirement cannot be met because the Front Floor would obstruct the PFO. Due to concerns with weld spatter, current practice also limits the PFO to 30° from horizontal, which means that PFO could not be angled sufficiently to compensate for the floor. The joint between the bracket and the floor uses 12-laser stitch welds, adding 252mm of new laser welds. Two beads of structural adhesive, 180mm long, are used to joint the bracket to the sidewall of the rocker.

Tube - Outer Lower (41015) was added to the Assembly Body Side Structure Stage 1 (37120A) as Items #16 and #17. The tubes are MIG welded to the Bracket Inner - Outer Tube Support Lower (41016/7) and the Bracket Outer - Outer Tube Support Lower (41014). The MIG welding uses 8 welds and adds 120mm of new MIG welds.

Bracket Outer - Outer Tube Support Lower (41014)
Added as part of Assembly Body Side Structure Stage 1 (37120A) in two places

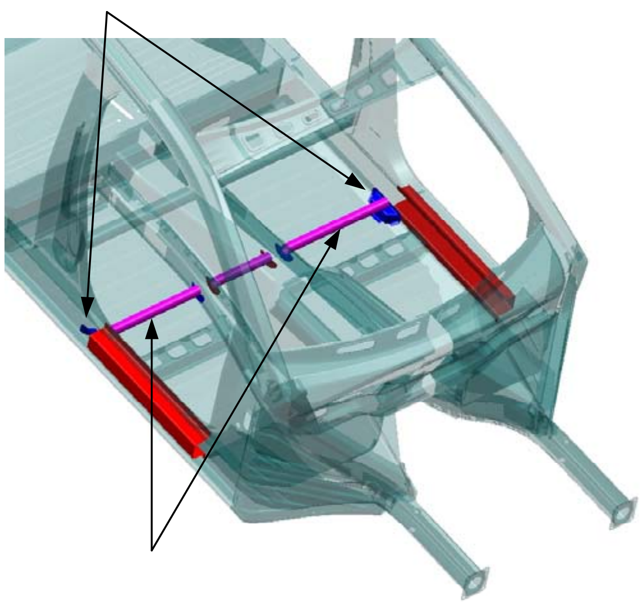

Tube - Outer Lower (41015)
Added as part of Assembly Body Side Structure Stage 1 (37120A) in two places

FIGURE 14: Assembly Body Side Structure Stage 1 (37120A)

5. GAUGE AND MASS PARTS LIST

Table 2 summarizes the gauge and mass of all revised and new components.

PART NUMBER	NAME	FGPC-ACD OPTIMIZED GAUGE (mm)	FGPC-ACD CONCEPT D MASS (kg)	FGPC-FCD OPTIMIZED GAUGE (mm)	FGPC-FCD OPTIMIZED MASS (kg)
11082	Crossmember Kick-up	1.20	3.22	1.10	2.97
11146/7	A-Post Inner R&L	0.90(Upr)	2.06	0.90	3.50
		0.70(Lwr)	1.1		
11182/3	Reinf Rail Rear Suspension	1.50	1.54	1.50	1.54
31069	Floor Rear	0.60	3.46	0.60(Sides)	3.46
		0.80(Mid)(Frt)	13.26	0.80(Middle)	10.67
				0.90 (Frt)	2.93
31162/3	Rocker Inner R&L	0.60	4.88	1.20 (Frt)	1.40
				1.50(Rear)	10.50
31170	Body Side Outer RH	1.0 Ctr Upr	1.71	1.10	1.88
		1.25 Ctr Lwr	8.757	0.80	5.60
		0.7 Rear	5.601		5.601
		1.0 Frt	1.371		1.371
31171	Body Side Outer LH	1.0 Ctr Upr	1.71	1.10	1.88
		1.25 Ctr Lwr	8.757	0.80	5.60
		0.7 Rear	5.662		5.662
		1.0 Frt	1.371		1.371
31208/9	B-Pillar Inner R&L	1.25(Upr)	2.78	1.10	2.46
		0.70(mid)	2.78	0.80	3.20
41004	Crossmember Roof	0.80	1.4	0.90	1.58
41008/9	B-Pillar Bulkhead	0.80	0.24	0.80	0.24
ADDED PARTS					
41014	Brkt Otr - Otr Tube Support Lwr R&L			0.70	0.20
41015	Tube Otr - Lwr R&L			1.20	1.16
41016/7	Brkt Inr - Otr Tube Support Lwr			0.70	0.05
41018/9	Brkt Otr - Ctr Tube Support Lwr			0.70	0.05
41020	Tube Ctr - Lwr			0.60	0.15
41021	Reinf - Rocker Inner R&L			0.90	3.18
FRONT DOOR TUBULAR STRUCTURE					
11204/5	Hinge TubeFront Door R&L	0.80	0.858	0.60	0.64
32006/7	Latch Tube Front Door R&L	0.80	0.992	0.60	0.74
32008/9	Lower Tube Front Door R&L	1.20	2.002	0.90	1.50
32010/1	Outer Belt Reinforcement - Front Door	1.00	1.572	0.60	0.94
REAR DOOR TUBULAR STRUCTURE					
32040/1	Hinge TubeRear Door R&L	0.60	0.75	0.60	0.64
32042/3	Latch Tube Rear Door R&L	0.60	1.026	0.60	0.86
32044/5	Lower Tube Rear Door R&L	0.80	0.822	0.60	0.52
32046/7	Outer Belt Reinforcement - Rear Door	0.60	0.884	0.60	0.72

TABLE 2: Gauge & Mass Summary - Revised & New Components

6. MATERIAL TYPE PARTS LIST

Table 3 summarizes the material grade of all new components.

PART No	NAME	MATERIAL
41014	Brkt Otr – Otr Tube Support Lwr R&L	DP500/800
41015	Tube Otr – Lwr R&L	MART800/1300
41016/7	Brkt Inr – Otr Tube Support Lwr	DP500/800
41018/9	Brkt Otr – Ctr Tube Support Lwr	DP500/800
41020	Tube Ctr - Lwr	MART800/1300
41021/2	Reinf – Rocker Inner R&L	MART800/1300

TABLE 3: Materials Summary - New Components

7. WELDS AND ADHESIVES

Table 4 summarizes all the joints used in the vehicle by type. It includes details of the number and length of new ones.

ASSEMBLY	JOINT METHOD	TOTAL LENGTH (mm)	No Of NEW JOINTS	NEW JOINT LENGTH (mm)
17136	25 Laser welds	525		
17137	31 Laser welds	651		
37119	222 Laser welds	4662		
	306 Spot welds	-		
	2 Adhesive patches	1800		
37120A	372 Laser welds	7812	+12	252
	62 Spot welds	-		
	2 Adhesive patches	506		
	26 MIG welds	450	+8	120
73120B	32 Laser welds	672		
37121	68 Spot welds	-		
37122	24 Spot welds	-		
37124	184 Laser welds	3864		
37125	136 Laser welds	2856		
	195 Spot weld	-		
	9 Adhesive patches	8180		
37126	384 Laser welds	8064	+30	630
37128	76 Laser welds	1596		
	76 Spot welds	-		
	6 Adhesive patches	1670		
	4 MIG Welds	60	+4	60
37129	22 Spot welds	-		
	3 Adhesive patches	3070		
37130	140 Laser welds	2940	+12	252
37132	54 Spot welds	-		

JOINT TYPE	ULSAB-AVC PNGV		FGPC-FCD	
	TOTAL	LENGTH (mm)	TOTAL	LENGTH (mm)
Laser welds		99735	1570	32970
Spot welds	814	-	807	-
Adhesive patches		1606	22	15220
MIG welds	-	-	30	510

TABLE 4: Joint Summary

8. CONCLUSION

Table 5 summarizes the mass reductions for the major stages of the project. It then compares the before optimization to completion of the final concept design, identifying the mass saving for the complete project. Finally it compares the final concept design to an industry standard.

	FGPC-BO (kg)	FGPC-ACD (kg)	FGPC-BFO (kg)	FGPC-AFO (kg)	FGPC-FCD (kg)
BIW + IP BEAM	227.2	210.8	223.9	216.8	217.6

MODIFIED PARTS	FGPC-BO (kg)	FGPC-ACD (kg)	FGPC-BFO (kg)	FGPC-AFO (kg)	FGPC-FCD (kg)
BIW	130.6	114.2	127.3	120.2	121.0
Doors	12.6	8.6	8.6	6.3	6.4
TOTAL	**143.2**	**122.8**	**135.9**	**126.5**	**127.4**

	FGPC-BO (kg)	FGPC-FCD (kg)	MASS SAVINGS (kg)	CHANGE (%)
BIW + IP BEAM	227.2	217.6	9.6	4

MODIFIED PARTS	FGPC-BO (kg)	FGPC-FCD (kg)	MASS SAVINGS (kg)	CHANGE (%)
BIW	130.6	121.0	9.6	7
Doors	12.6	6.4	6.2	49
TOTAL	**143.2**	**127.4**	**15.8**	**11**

STRUCTURE	INDUSTRY STANDARD (kg)	FGPC-FCD (kg)	MASS SAVINGS (kg)	CHANGE (%)
BIW + IP BEAM	310.0	217.6	92.4	30

TABLE 5: Final Mass Summary For FGPC Project

Figure 15 & Table 6 compare the FGPC-FCD to an "In-Class Vehicle," the comparison is based upon data taken from a currently produced 4-Door Mid Size Sedan of similar dimensions.

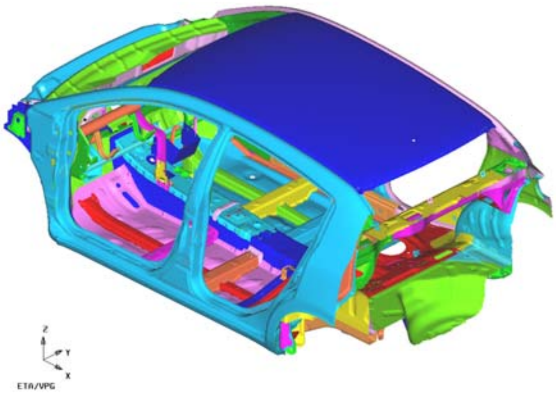

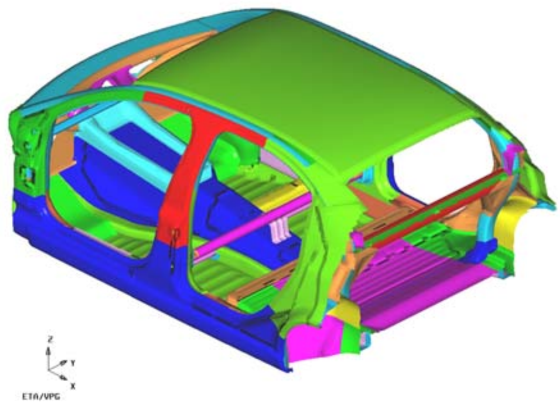

In-Class Vehicle **FGPC-FCD**

FIGURE 15: Safety Cage Comparison – In-Class Vehicle vs FGPC-FCD

	IN-CLASS VEHICLE* (kg)	FGPC-FCD (kg)	CHANGE (%)
BIW+IP	314.7	217.6	31
Safety Cage	246.8	169.3	31

*Based upon historic data, a 4-Door Mid Size Sedan with similar dimensions to the FGPC vehicle

TABLE 6: In-Class Vehicle vs FGPC-FCD Comparison